NVE

RAPPORT NR. 8 / 2023

Climate change impacts on runoff and hydropower production in Georgia

SKREVET AV Elin Langsholt

NVE Rapport nr. 8/2023:
Climate change impacts on runoff and hydropower production in Georgia

Published by:	Norwegian Water Resources and Energy Directorate
Author:	Elin Langsholt
Cover photo:	Borjomi, Georgia. Photo: Elin Langsholt/NVE

ISBN:	978-82-410-2309-5
ISSN:	2704-0305
Case number:	201835977

Abstract: The analysis presented in this report, estimates the effect of climate change on the hydro power potential of Georgia. A theoretical hydro power potential under the prevailing climate conditions has been calculated in an earlier study, and is the reference potential. Three climate projections and two emission scenarios has been used to span possible future climate realizations. A hydrological model estimates the response of a changed climate on the hydrological regime. The effects have been studied with a focus on the near future (2031-2060) and the end of the century (2071-2100), relative to the control period 1961-1990. There is a tendency common to all projections, and amplified for the high emission scenario, that the power potential increases along the Greater Caucasus. In the other regions of Georgia, the power potential decreases or has minor changes.

Key words: Georgia, hydro power potential, climate change, hydrology

Norwegian Water Resources and Energy Directorate
Middelthuns gate 29
P.O. Box 5091 Majorstuen
N-0301 Oslo
Norway

Telephone: +47 22 95 95 95
E-mail: nve@nve.no
Internet: www.nve.no

April, 2023

Contents

Preface

Georgia has an increasing electricity demand. Hydropower currently accounts for the majority of the electricity production, and there are plans to develop the renewable energy sources to avoid a deficit and for generating electricity for export. In realizing these plans, one factor to consider is the likely impacts of climate change on the hydropower system.

An assessment of the hydropower potential in Georgia was one of the final products from the first phase of the institutional cooperation between the Ministry of Energy and Natural Resources of Georgia and NVE. That study was based on data that represent the prevailing climate. There is a need to include scenarios for climate change in the analysis of hydrological data and, in turn, for planning and decision making about the hydropower potential and other utilizations of the water resources.

This report presents the results of a study that assesses the impact of climate change on the future hydropower potential in Georgia. The present hydrological regime, as well as the hydrological regime for two future periods are described by a spatially distributed hydrological model. Simulations of the future hydrological regimes are made by using forcing data from climate models, operating under two different emission scenarios. Characteristic changes from the present to the future hydrological regimes, indicate probable impacts of climate change on the hydropower potential.

Oslo, April 2023

Hege Hisdal
Director
Hydrology Department

Ivar Berthling
Head of Section
Section for Hydrological Modelling

This document is sent without signature. The content is approved according to internal routines.

Summary

In the institutional cooperation between Ministry of Energy and Natural Resources (MENR) and the National Environmental Agency (NEA) of Georgia and Norwegian Water Resources and Energy Directorate (NVE), an assessment of the hydropower potential in Georgia has been made (Arnesen et al. 2021). The study is based on the prevailing climate conditions. A question that arises is how climate change will affect the hydropower potential. In this study, we have applied three projections and two emission scenarios to span possible future climate realizations. A hydrological model estimates the response of a changed climate on the hydrological regime. The effects have been studied with a focus on the near future (2031-2060) and the end of the century (2071-2100), relative to the control period 1961-1990.

Regionally, the annual mean temperature will increase by 1.9-3.3 degrees in the near future and by 4.5-6.5 degrees by the end of the century, when applying the high emission scenario. Climate change will also have a marked effect on the hydrological regime and the water balance. The effect varies regionally. When it comes to precipitation, the different projections show no general trend. The evapotranspiration, on the other hand, increases, as a result of higher temperature and more available energy. For the regions where no external sources of water are available, this implies decreasing streamflow, for the water balance to add up consistently. The occurrence of glaciers in the Greater Caucasus, however, represent an external deposit of water, which acts as a net source of water in a warming climate. This has a considerable and positive effect on streamflow from the Greater Caucasus. Common to all regions, is the tendency that a reduced snow cover will bring about higher stream flow in the winter and earlier spring floods.

The future changes in the amount of discharge, as well as in the variability of the discharge, has direct implications on the potential hydropower production in a hydropower system that is adapted for the present climate. A method that applies the cumulative frequency curve for stream flow on stream flow series for the three time periods studied, is used to estimate typical impacts of climate change on the hydropower potential, assuming that the hydropower system is made up by of run-of-river hydropower plants at the outlet of representative catchments. There is a tendency common to all projections, and amplified for the high emission scenario, that the power potential increases along the Greater Caucasus. In the other regions of Georgia, the power potential decreases or has minor changes. Comparing the hydropower changes due to climate change with the distribution of the hydropower potential between the 14 zones that represent Georgia's geographical variation, used by Arnesen et al (2021), we notice that the zones with a positive change in hydropower potential coincides with the zones with the highest estimated hydropower potential. The overall result when estimating the future hydropower potential, as a result, tends to increase from the present level.

The conclusions made in this study are subject to some degree of uncertainty. A handful of error sources are discussed.

1 Introduction

An institutional cooperation between Ministry of Energy and Natural Resources (MENR) and the National Environmental Agency (NEA) of Georgia and Norwegian Water Resources and Energy Directorate (NVE) has taken place since 2013. One aim of the project is to provide a basis for further development of renewable energy sources, through mapping and analysis of hydrological data, which is essential for hydropower development. Today, hydropower stations of Georgia produce between 80 and 85 % of the electricity utilized within the country. There is, however, a potential for a considerable growth in hydropower production. Therefore, MENR has a strategy for further hydropower development, to sustain economic growth in Georgia.

In the first phase of the project, a runoff map for Georgia was developed (Beldring et al., 2017). This map is the basis for an assessment of the hydropower potential of Georgia (Arnesen et al., 2021). In that study, data that represent the prevailing climate are used. Global climate change, however, will have effects on the hydrological processes that are of decisive importance for development of a hydropower-based energy system.

Numerous studies, that indicate trends towards a warmer climate and subsequent effects on river discharge, have been published for the region. Glacier degradation may give increased water input to river discharge for a period, until a peak is reached, when the balance between high melting rate and shrinking glaciated area reaches a tipping point. Rivers from the Caucasus region, representing the highest hydropower potential in Georgia, are partly fed by glacier melt water. A study presented by Kordzakhia et al. (2021), estimated a decline in the glaciated area in the Rioni catchment in the Greater Caucasus of 70% over the past 50 years. Kordzakhia, G. (2021) gives an overall presentation of glacier's degradation due to climate change impact in the Fourth National Communication of Georgia to the Framework Convention on Climate Change, a topic that also was presented at COP26 in Glasgow in 2021. There, it is concluded that both small and large glaciers have retreated during the last decades, the retreat has accelerated during the period studied, and the glacier degradation process in Eastern Georgia is more intensive than in Western Georgia. Kordzakhia, M. (2021) refers to a study that indicates negative effects of climate change on river discharge, in rivers partially fed by glacier melt water, specifically the Rioni river. The decreasing discharge is partly associated with the shrinking glacier area. This is consistent with Rets et al. (2020), who claim that the peak water of glacial runoff, as a consequence of deglaciation, has already been passed in the central North Caucasus, and is now decreasing as glacier extents are reduced. Megrelidze (2021) refers to a study of extreme hydrometeorological events, among them floods and flash floods, phenomena that show an increasing frequency in Georgia during the last decades. The tendency towards more flood forming wet days is, however, not as evident in the climate scenarios as in the observation series, so, applied to the long-term development of extreme hydrological events, the study does not conclude. In Khelidze et al. (2019), trends in water discharge and hydropower potential in the rivers, where current observations are available, are assessed. They conclude that substantial changes in water discharges and hydropower potential can be observed

over the past decades and recommend further studies of the hydropower potential of the Georgian rivers.

The objective of the present study is to assess the impact of climate change on the future hydropower potential in Georgia. A spatially distributed hydrological model, has been used to describe the hydrological regime of today, as well as for two future periods, the “near future”, 2031-2060, and “the end of the century”, 2071-2100. Simulations of the future hydrological regimes are made by using forcing data from climate models. Data from three different climate models, operating under two different emission scenarios, are applied, to span some of the realisations a changing climate may give rise to. Characteristic changes from the present to the future hydrological regimes, indicate probable impacts of climate change on the hydropower potential.

2 Study area

Georgia has a total area of 69 700 km^2, with a topography ranging from the sea level up to above 5000 masl. The country is located in the Caucasus region, and is bordered by Russia to the north, Azerbaijan to the southeast, Armenia and Turkey to the south and the Black Sea to the west. Climate zones varies from humid subtropical and semiarid climate to alpine climate. The alpine zone contains mountain massifs included in the Greater Caucasus, covered with permanent snow and glaciers, the height of which is more than 5000 metres above sea level. Some 400 glaciers with total area of 380 km2 are currently registered on the territory of the country (Kordzakhia, G. (2021).

Georgia has about 26 000 rivers with a total length of 60 000 km. Drainage is into the Black Sea to the west and through Azerbaijan to the Caspian Sea to the east. The largest river is the Kura River, which flows from northeast Turkey across the plains of eastern Georgia, through the capital, Tbilisi, and into the Caspian Sea. The Rioni River, the largest river in Western Georgia, rises in the Greater Caucasus and empties into the Black Sea. In the subtropical agricultural district along the Black Sea coast, many stretches of rivers have been turned into an extensive system of canals.

In order to make a realistic hydropower potential estimate, Arnesen et al. (2021) divided the country into 14 geographical zones, based on a suggestion from the National Environmental Agency of Georgia. To describe the inflow variation over the country, each zone was represented by one hydrological series. Figure 2-1 shows a map of the 14 zones, and table 2-1 lists the hydrological station selected to represent each zone.

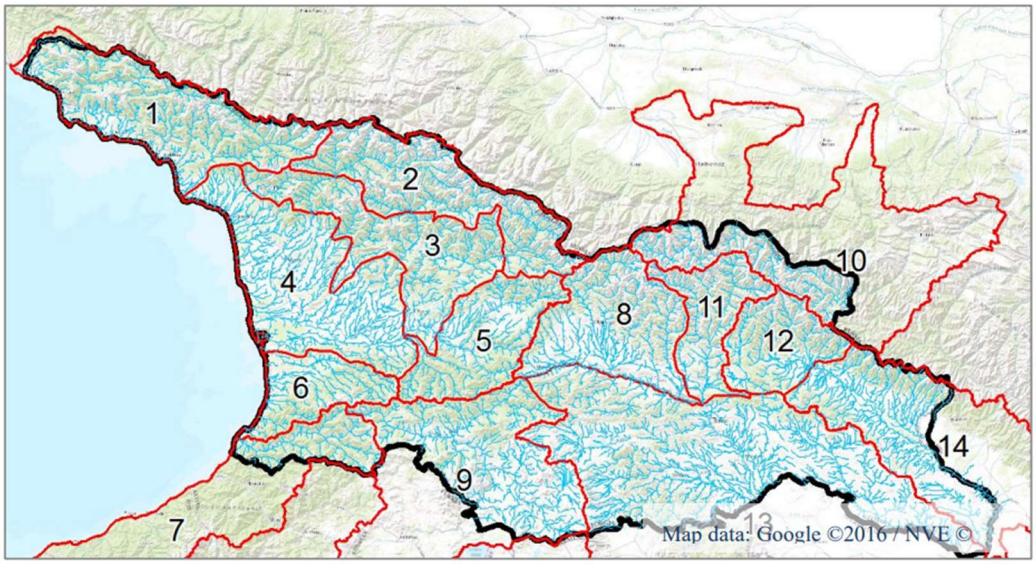

Figure 2-1. Georgia is divided into 14 hydrological zones, each represented by one hydrological station.

Zone		Station number	Metering station	Gross hydropower potential (TWh/year	Area (km2)
1		21	Gumista – V. Aachadara	13.9	556
2		128	Rioni - C. Oni	11.9	1060
3		131	Rioni V. Alpana	7.7	2830
4		231	Texuri - V. Naqlaquevi	3.1	558
5		174	Kvirila – C. Zestaponi	1.3	2490
6		242	Supsa - D. Chokhatauri	2.9	316
7		278	Achhristskali - D. Qeda	2.8	1360
8		355	Didi-Liakhvi - V. Kekhvi	1.6	924
9		296	Mtkvari (Kura) – V. Khertvisi	1.8	4980
10		289	Chkheri – D. Stefantsminda	4.0	27.3
11		382	Gudamakris-Aragvi (Black Aragvi) – At the mouth	2.0	235
12		424	Iori – V. Lelovani	1.2	494
13		419	Mashavera – D. Kazreti	1.5	570
14		441	Alazani – V. Heretiskari (Heretiskari)	0.7	4530

Table 2-1. The metering stations representing each of the 14 zones, the total technical hydropower potential in the zone according to Arnesen et al. (2021) and catchment area for the station.

Calculations of the amount of water that typically might be available for hydropower production under the present and the future hydrological regimes are made for these 14 stations. For the study of characteristic impacts of climate change on the

hydrological regimes and the water balance elements, the 14 zones are grouped into 4 regions, each represented by one or two stations. Table 2-2 lists the stations used for climate impact studies. The region of the greater Caucasus is represented by the large Rioni river, which shows a more moderate response than the smaller and highly alpine river Chkheri. The other three regions are represented by one station each.

region	station used	zone
The Greater Caucasus	Rioni - C. Oni	2
The Greater Caucasus	Chkheri – D. Stefantsminda	10
The Black Sea Region	Texuri - V. Naqlaquevi	4
The Lesser Caucasus	Mtkvari (Kura) – V. Khertvisi	9
Eastern Plains	Alazani – V. Heretiskari (Heretiskari)	14

Table 2-2. The regions and stations used for the study of climate change impact on the hydrological regimes and the water balance elements.

3 Model simulations and data

3.1 The hydrological model

To assess the effects of climate change on hydrology and, in turn, on the hydropower production potential, a spatially distributed hydrological model has been used to describe the hydrological processes and states. The model is a rainfall – runoff model and has a time resolution of one day. It is a conceptual, HBV type model (Beldring et al. 2003) that simplifies the physical processes and replace them by a set of equations, that describe the essential characteristics of the precipitation-runoff processesk, see fig. 3-1. The spatial variation of the properties of the land surface is represented by data characterizing elevation, soil type, geology, vegetation, lakes, wetlands, and glaciers. The model describes accumulation, distribution and ablation of snow, the interception storage, distribution of soil moisture storage, evapotranspiration, groundwater storage, lake evaporation and runoff. Potential evaporation and snow melt rates are functions of air temperature. Glacier response is calculated for glacier covered areas of the model grid cells. Glacier balance dynamics, as a response to climate change, is not represented in the model, and the glaciers, thus, represent an inexhaustible reservoir of ice. This is a fact to have in mind when explaining the hydrological response to climate change for

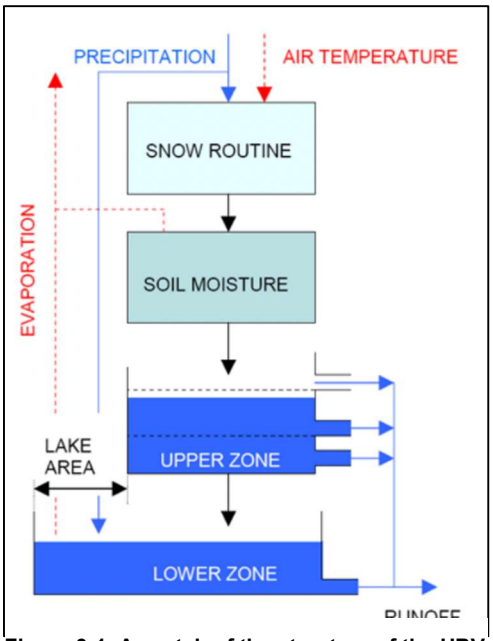

Figure 3-1. A scetch of the structure of the HBV model.

the partly glacier meltwater fed rivers of the Greater Caucasus region.

Observed precipitation, temperature and streamflow from the station network were used for calibrating and running the hydrological model for the period 1961-1990, called the control period. Climate data representing future periods, affected by climate change, are obtained from three global climate model simulations with two greenhouse gas emission scenarios for two future periods. The precipitation and temperature time series obtained, were used as input to the hydrological model, and the corresponding hydrological model results are assumed to represent future hydrological regimes.

The hydrological model used in this study was adapted for the entire land surface of Georgia and upstream areas in neighbouring countries, draining to Georgia. Observed meteorological and hydrological data from the period 1961-1990 was used for model set-up and for production of the runoff map. Data from 249 precipitation stations and 119 temperature stations were used as input data for a system of 160 watersheds, each represented by one hydrological station, all over Georgia. The model was calibrated by minimizing the residuals between simulated and observed daily runoff for the 160 hydrological stations simultaneously. For details about the model and the model set-up, see Beldring et al. (2017).

A map of mean annual runoff for the period 1961-1990 for Georgia is a major result of the first phase of the cooperation project between MENR and NEA of Georgia, and NVE (2013-2016). In this study, the same model set-up has been used and applied on catchment scale, to simulate the hydrological processes and states in the catchments selected, for different forcing data sets.

3.2 The control period

Meteorological and hydrological observations in Georgia dates back to the mid-20th century. The collapse of the Soviet Union around 1990 entailed setbacks to Georgia's hydrometeorological services, leading to degradation of the observation networks. Only parts of the network are re-established. To have sufficient data for setting up and running the hydrological model, it was decided to use data from the period 1961 - 1990 for the map of mean annual runoff for Georgia. The same considerations apply for this study, and the period 1961 – 1990 is taken as the reference time period, i.e. the control period, to which future regime changes are related. Figure 3-2 shows the runoff map developed in the first phase of the cooperation project.

The river catchments studied are approximated by the 1 km^2 grid cells covering the catchments. Precipitation and temperature values for the catchment grid cells were determined by inverse distance interpolation of observations from the closest precipitation and temperature stations. Elevation adjustments of the precipitation and temperature were made by precipitation elevation gradients and temperature lapse rates. Meteorological data were subject to quality control by visual inspection and comparison with neighbouring stations, to ensure that the data were representative for the model domain areas, had continuous records for most of the model period, and had minimum sampling and measurement errors. Some watersheds drain to Georgia from upstream areas in Turkey and Armenia. Data from

Turkish State Meteorological Service and Turkish General Directorate of State Hydraulic Works were obtained to cover these areas.

A similar quality control was applied to the streamflow stations. Data from 160 stations were accepted for use for calibration and validation of the hydrological model. The 14 stations used in this study are among these 160 stations.

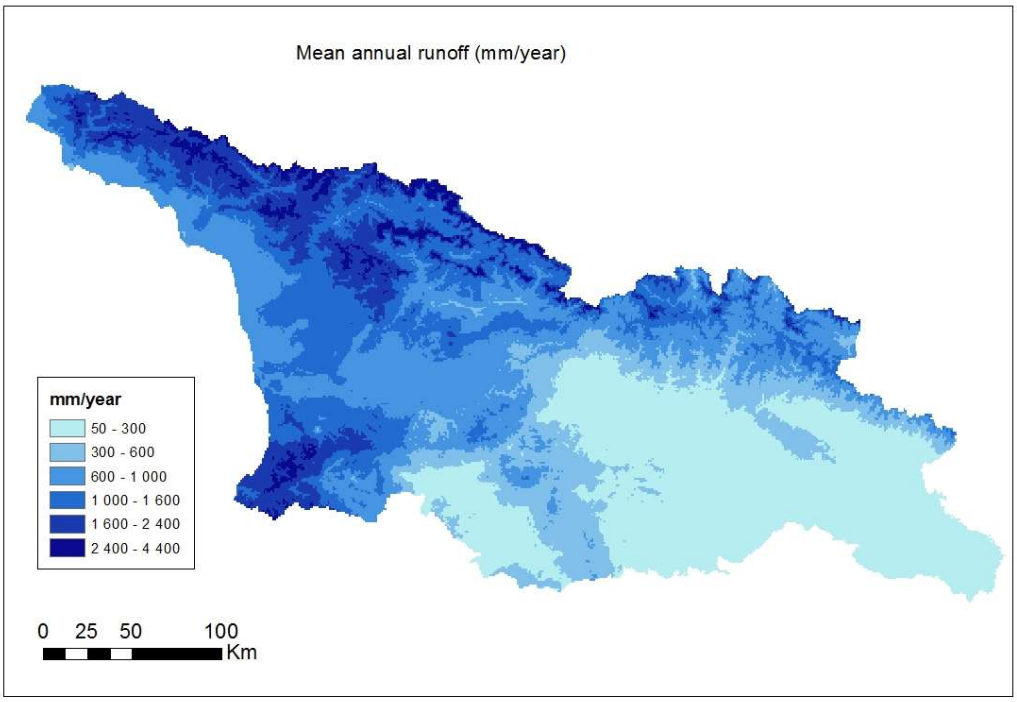

Figure 3-2. The map of mean annual runoff for the period 1961-1990 for Georgia (Beldring et al. 2017).

3.3 Climate projections

Climate projections, representing best guesses to our future climate, are provided by the World Climate Research Programme, Coupled Model Inter-comparison Project Phase 5 (CMIP5) and Coordinated Regional Climate Down¬scaling Experiment (CORDEX) Central Asia domain (https://cordex.org/domains/region-8-central-asia). Results from coarse-gridded global circulation models (GCMs) are dynamically downscaled to a spatial resolution of approximately 25 km by 25 km by a regional circulation model (RCM). Three combinations of GCM/RCMs are available for the project. The GCMs applied are HadGEM2-ES (HAD), a GCM developed by the Hadley Centre in Great Britain, MPI-ESM-LR (MPI), a GCM developed by the Max Planck Institute in Germany, and NorESM1-M (NOR), which is a Norwegian product from the Norwegian Climate Centre. The RCM use for downscaling is REMO2015, maintained by the Climate Service Centre Germany. See Figure 3-3 for a visualisation of the concepts.

The spatial resolution of GCMs and RCMs are too coarse to reproduce regional and local details of the climate at spatial scales that are necessary for hydrological impact studies. Thus, to obtain reliable estimates of temperature and precipitation projections, the RCM model results have been bias-adjusted and downscaled to meteorological station sites using the quantile perturbation method (Willems and Vrac, 2011; Sunyer et al., 2015). This procedure reproduces changes in monthly

temperature and precipitation quantiles from the control period to the projection periods, based on RCM outputs, while preserving the details of local meteorological observations from the control period. Two climate gas emission scenarios, RCPs (Representative Concentration Pathway), are applied: a low emission scenario, RCP2.6, and a high emission scenario, RCP8.5. Finally, two future periods are emphasised, 'Near future', 2031-2060, and 'End of century', 2071-2100. This provides a total of twelve datasets for possible future precipitation and temperature scenarios at the meteorological station sites in Georgia and Turkey.

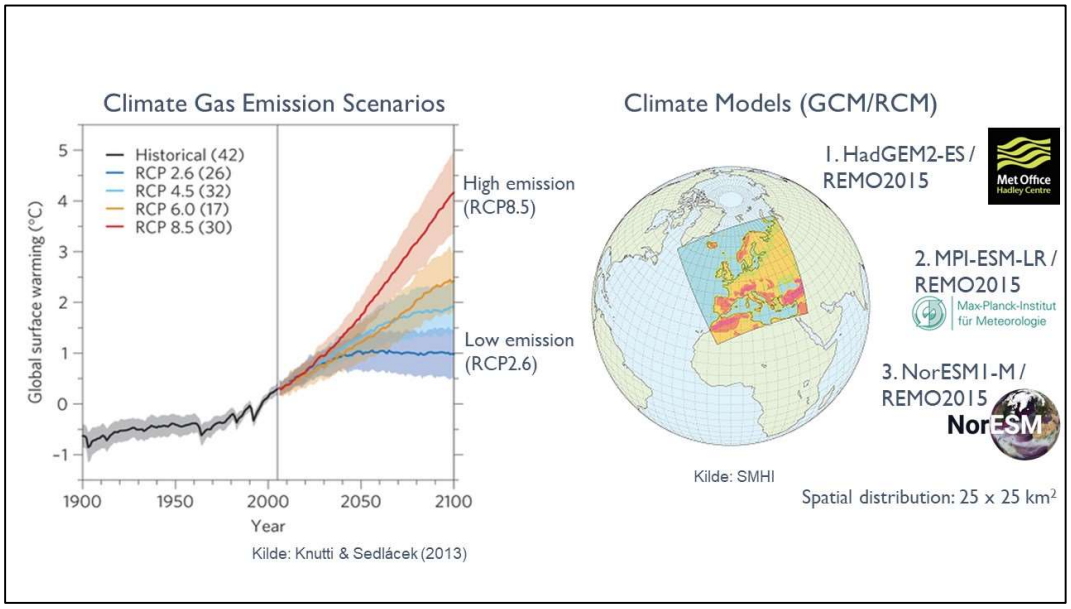

Figure 3-3. Visualisation of the concepts of emission scenarios and climate models.

4 Climate change impacts on hydrology

The observed meteorological data in the control period 1961 – 1990 and the downscaled global climate model results for the near future, 2031 – 2060, and the end of the century, 2071 – 2100, were used for driving the spatially distributed version of the HBV hydrological model (Beldring et al. 2003), to estimate hydrological variables and fluxes for the present and future climate conditions. For this study, we have focused on 5 catchments, representing 4 climatic regions in Georgia. The catchments are represented by the following gauging stations:

- 128 Rioni - C. Oni, zone 2 and 289 Chkheri - D. Stefantsminda, zone 10, representing the Greater Caucasus region
- 296 Mtkvari (Kura) – V. Khertvisi, zone 9, representing the Lesser Caucasus region. The analysis for this station is based on monthly data. Therefore, the curves for this station have a step-wise appearance.
- 231 Texuri - V. Naqlaquevi, zone 4, representing the Black Sea region

- 441 Alazani – V. Heretiskari, zone 14, representing the plains of eastern Georgia.

To reduce the outcome to a manageable amount of data, we have only studied the impacts according to two projections, HAD and MPI, applying the high emission scenario, RCP85. Graphs of streamflow represent the lumped streamflow at the catchment outlet, whereas the temperature, precipitation, evapotranspiration and snow water equivalent data presented, are averages over the catchment's grid cells. The impacts of the selected climate projections on the meteorological and hydrological processes in the near future and by the end of the century are graphed and shown in appendix A.

4.1 Temperature

Figure 4-1 shows the temperature change in the five catchments, which is an effect of increased concentrations of greenhouse gases in the atmosphere, according to the two projections and the high emission scenario. Monthly mean temperature for the 5 catchments, as well as catchment-average annual mean temperature, are shown. The catchments represent different temperature regimes, from continental climate with relatively cold winters in the mountains to the mild coastal climate along the Black Sea coast and on the western plains. The annual variation spans more than 20 degrees, and a shift of approximately 15 degrees separates the warmest from the coldest catchment.

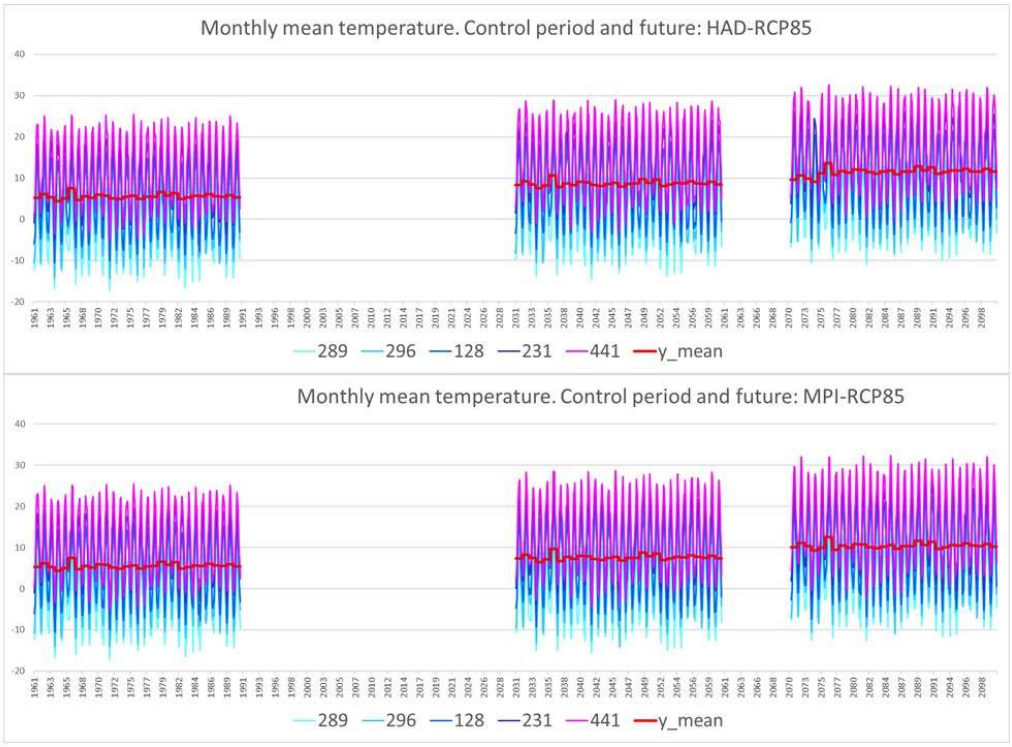

Figure 4-1. Monthly mean temperature for 5 catchments. Three periods are shown: the control period 1961-1990, near future 2031-2060 and the end of the century 2071-2100. Data according to the HAD projection are shown at the top, and to the MPI projection at the bottom. The high emission scenario RCP85 is used in both cases. Annual mean temperatures averaged over the 5 catchments are shown as bold, red lines.

The average annual temperature, shown as a bold, red curve, clearly visualise the temperature increase over the century. According to HAD-RCP85, an average temperature increase of 3.2 degrees can be expected in the near future, and an average increase of as much as 6 degrees by the end of the century. Similar estimates using the MPI-RCP85 projection are 2.1 and 4.9 degrees. Thus, the HAD projection gives the most pronounced temperature effect of increased greenhouse gas concentrations in the atmosphere of the two. The annual average temperature increase in the coldest (289 Chkheri) and warmest (441 Alazani) catchment is similar: 3.3/6.5 degrees and 3.1/6.0 degrees, respectively, according to HAD-RCP85, and 2.2/5.3 degrees and 2.0/4.8 degrees, respectively, according to MPI-RCP85.

The temperature change in terms of daily mean, season mean and annual mean for all the five stations is shown in appendix A. Table 4-1 sums up some key numbers of temperature change for the five stations. There is a tendency that the summer temperatures increase more than the winter temperatures. Average temperature increase in August from the control period to the near future and the end of the century for the catchments 289 and 441 is 3.1/6.6 degrees and 3.5/7.8 degrees, respectively, according to HAD-RCP85 and 3.3/6.3 degrees and 3.3/6.5 degrees, respectively, according to MPI-RCP85, whereas the temperature increase in February is 2.4/5.7 degrees and 2.0/4.3 degrees, respectively, according to HAD-RCP85 and 1.7/3.8 degrees and 1.4/4.0 degrees, respectively, according to MPI-RCP85. The tendency is more pronounced for the MPI projection. Comparing corresponding temperature differences, we notice that the temperature increase in August exceeds the one in February by up to more than 3 degrees. This interannual variation in temperature increase can be kept in mind when discussing the effects of climate change on evapotranspiration and water balance below.

Temperature increase will be accompanied by changes in cloud cover, precipitation, air humidity, radiation, wind and other meteorological elements. These changes will lead to changes in the land phase of the hydrological cycle with impacts on the water balance. An important factor for the water balance, which is strongly influenced by the

	Annual mean T in the control period		T change, HAD-RCP85				T change, MPI-RCP85			
			2031-2060		2071-2100		2031-2060		2071-2100	
	August	February	August	February	August	February	August	February	August	February
128 Rioni	4.9		3.2		6.2		2.1		4.9	
	14.8	-4.4	3.7	2.4	7.4	4.9	3.7	1.2	7.0	3.4
289 Chkheri	-2.1		3.3		6.5		2.2		5.3	
	7.3	-11.3	3.1	2.4	6.6	5.7	3.3	1.3	6.3	4.4
296 Mtkvari	3.6		3.1		6.1		2.1		5.0	
	14.7	-8.1	3.6	2.6	7.2	5.1	3.6	1.4	7.0	4.1
231 Texuri	9.5		3.1		6.0		1.9		4.5	
	18.5	0.9	4.1	2.3	7.8	4.3	3.5	1.2	6.4	3.1
441 Alazani	11.6		3.1		6.0		2.0		4.8	
	22.1	1.4	3.5	2.0	7.8	4.3	3.3	1.7	6.5	3.8
station average	***5.5***		***3.2***		***6.0***		***2.1***		***4.9***	
	15.5	***-4.3***	***3.6***	***2.3***	***7.4***	***4.9***	***3.5***	***1.4***	***6.6***	***3.8***

Table 4-1. The table summarizes the effect of the two climate projections HAD and MPI, combined with the high emission scenario RPC85, on the temperature in the five catchments studied. Temperature in the control period is shown to the left. In addition, the table shows average temperature increase in the near future and by the end of the century as well as in August and February. At the bottom of the table, the station averages of these characteristics are given.

temperature increase, is the glacier mass balance. The effect of climate change on glacier mass balance is not explicitly modelled in this study, but this aspect is qualitatively considered in the discussion below.

4.2 Precipitation

Figures A-36 to A-65 in appendix A show the effect of the two projections selected on precipitation amounts and interannual distribution of precipitation for the five catchments. The characteristics shown for the three periods 1960 – 1991 (control period), 2031 – 2060 (near future) and 271 – 2199 (the end of the century) are the daily, monthly and seasonal mean, as well as the annual sums over the three periods. Although there is no clear picture, there is a tendency that HAD increases the annual precipitation, whereas MPI makes no difference or a slight decrease in the annual precipitation. The exception is station 441 Alazani in the eastern plains, where HAD makes a reduction in the precipitation and MPI increases it. As a rule, the precipitation increase with respect to HAD is most pronounced in the spring-summer period. For MPI, there is a tendency that the summer period has the strongest decrease.

A summary of the annual precipitation change for the five stations is given in table 4-2.

		% change in precipitation HAD-RCP85		*% change in precipitation MPI-RCP85*	
Station	*Annual mean precipitation in the control period (mm)*	*2031 - 2060*	*2071 - 2100*	*2031 - 2060*	*2071 - 2100*
128 Rioni	1688	13	15	0	1
289 Chkheri	1551	3	5	0	1
296 Mtkvari	727	6	14	1	-3
231 Texuri	2451	13	15	0	3
441 Alazani	1078	-3	-4	3	1

Table 4-2. A summary of how the two projections HAD and MPI, along with the high emission scenario rcp85, changes the annual precipitation amount for the five stations studied. The annual precipitation is given in column 2.

4.3 Evapotranspiration

Evapotranspiration, as it is simulated by the HBV model, combines evaporation and transpiration, and calculates actual evapotranspiration. Actual evapotranspiration is typically influenced by availability of energy and water. The temperature is one statement of available energy, and in section 4.1 we saw a clear increase in that variable in all regions of Georgia towards the end of the century, an inevitable consequence of global warming. Consequently, we observe a general increase in evapotranspiration over the catchments. Appendix A, figures A-66 to A-95 show the effect of the two projections selected on evapotranspiration for the five regions. Table 4-3 gives a summary of the increase in evapotranspiration, and we notice that the average annual increase in evapotranspiration by the end of the century is 235 mm according to the HAD projection and 194 mm according to the MPI projection, peaking in 231 Texuri at the Black sea coast. The effect is most pronounced for the HAD regime, which is also the case for the temperature.

Interannually, we see that the spring-summer season has the highest increase in evapotranspiration in the regions where snow plays a significant role, i.e. in all regions except the eastern plains. In this aspect, the effect of water availability plays an important role. Referring to section 4.5, the future snow cover will become substantially less than today. Bare ground will appear earlier, and the growing season will start ahead of today's normal. Observing the effect of climate change on the streamflow, the positive change typically peaks in the spring. The combined effect of less snow cover, more plants, and more water in the rivers, will fuel the evapotranspiration more in the spring than in the other seasons. Moreover, the temperature increase is most pronounced in the summer, which is a factor that pushes the maximum evapotranspiration increase to the same season.

			Evapotranspiration change (mm) HAD-RCP85				Evapotranspiration change (mm) MPI-RCP85			
Station	Annual mean evapotranspiration in the control period		2031 - 2060		2071 - 2100		2031 - 2060		2071 - 2100	
	spring-summer	autumn-winter	spring-summer	autumn-winter	spring-summer	autumn-winter	spring-summer	autumn-winter	spring-summer	autumn-winter
128 Rioni	530		192		371		119		258	
	394	136	123	69	243	128	86	33	180	79
289 Chkheri	162		112				76		181	
	123	40	75	37			57	19	132	49
296 Mtkvari	559		121		214		79		99	
	438	121	86	34	156	58	65	14	72	27
231 Texuri	909		265		490		144		321	
	609	300	156	109	293	197	98	46	198	123
441 Alazani	848		60		103		71		110	
	617	230	25	35	48	54	39	32	41	69
station average	***602***		***150***		***235***		***98***		***194***	
	436	***165***	***93***	***57***	***148***	***88***	***69***	***29***	***125***	***69***

Table 4-3. The table summarizes the effect of the two climate projections HAD and MPI, combined with the high emission scenario RPC85, on the evapotranspiration in the five catchments studied. Evapotranspiration in the control period is shown to the left. In addition, the table shows average evapotranspiration increase in the near future and by the end of the century, as well as in the spring-summer season and in the autumn-winter season. At the bottom of the table, the station averages of these characteristics are given.

4.4 Streamflow and water balance

In appendix A, figures A-96 to A-135, different aspects of the effect of climate change on the streamflow are shown. The changing streamflow is shown as daily mean, maximum and minimum, season mean, monthly mean and annual mean. Table 4-4 gives a summary of the annual average change in streamflow for the selected stations and projections.

Together with precipitation and evapotranspiration, the specific streamflow, i.e., the runoff, makes up the long-term water balance, disregarding temporary storages, in a catchment. The water balance is seen in figures A-166 to A-185. The simplified annual water balance can be stated as follows:

$$\mathbf{P = E + Q},$$

where **P** is the annual precipitation, **E** is the annual evapotranspiration and **Q** is the annual runoff. However, when we look at the water balance bars in the appendix, it

appears that the water balance does not add up completely. One important component that is not accounted for in this simplified expression, is glacial melting, a diminishing storage which makes up a substantial amount of the water balance in the Greater Caucasus region, i. e. stations 128 and 189. This component is not accounted for here, because the hydrological model used does not model glacier dynamics explicitly. Glaciers as a land cover component is constant, acting as an inexhaustible storage of ice, with increasing melting because of increased temperature. The contribution of glacial melting to future streamflow is, therefore, a component fraught with great uncertainty. Nevertheless, the model results, combined with the knowledge of significant glacial cover in the area, indicates that glaciers are important contributors to future streamflow. In light of the conservative handling of the glacial coverage, not taking into account that the glaciers are getting smaller as the mass balance gets more negative as the temperature increases, it is, however, reasonable to believe that we overestimate future streamflow by some amount. The studies of effects of glacier melting on streamflow referred to in section 1, not least the studies of Kordzakhia, M. (2021) and Rets et al. (2020), substantiates the claim that the present calculations overestimate the future streamflow.

In the Lesser Caucasus region, the Black Sea region and the plains of eastern Georgia, glaciers have no, or only minor impact on the regional water balance. The slight inconsistency that we can observe in the water balance for these catchments, is due to double counting of water in the model, because of internal redistribution of water after a rainfall.

Looking at the figures in appendix A, we observe that a striking feature in the Greater Caucasus region is increased autumn, winter and early spring streamflow. Rain takes over for snow in increasingly more of the precipitation events, the snow cover melts earlier, as can be seen in section 4.5 which entails an earlier spring flood. Towards the summer, the tendency is that the streamflow decreases as a result of reduced snow cover and increased evapotranspiration in catchment 128 Rioni, whereas in catchment 289 Chkheri, in the high mountains, highly influenced by glaciers, a persisting snow cover and glacial melting makes the summer streamflow increase as well.

In catchment 296 Mtkvari in the Lesser Caucasus, we observe a diminishing streamflow, as evapotranspiration takes an ever-increasing share of the available water in this dry area and dominates the tendency of precipitation increase.

A similar trend can be seen in the coastal climate at the Black Sea, station 231 Texuri, but here, possible scenarios, represented by HAD, give increased precipitation in the near future, entailing increased streamflow, until evapotranspiration takes over and the streamflow decreases towards the end of the century.

The tendency in catchment 441 Alazani in the dry, eastern plains is similar to what we can see in the Lesser Caucasus: the streamflow decreases as evapotranspiration takes an increasing share of the water budget.

In the Greater Caucasus and towards the Black Sea, there’s a tendency that the streamflow pattern gets more vivid with climate change, with higher peaks all the year around, even when the average is reduced. The reason for this is probably heavier rainfall events, even in the winter, a well-known effect of a warmer atmosphere.

Appendix A shows how the minimum and maximum streamflow change, as well as the average streamflow. Where glacial melting compensates for decreased precipitation and higher evapotranspiration, reduced streamflow does not necessarily include the minimum flow, which, on the contrary, can increase.

In the dryer Lesser Caucasus and the eastern plains, decreasing streamflow includes minimum and maximum streamflow as well as average streamflow.

		Streamflow change (m3/s) HAD-RCP85		Streamflow change (m3/s) MPI-RCP85	
Station	Annual mean streamflow in the control period (m3/s)	2031 - 2060	2071 - 2100	2031 - 2060	2071 - 2100
128 Rioni	49.1	9.7	9.7	2.2	6.3
289 Chkheri	1.4	0.5	1.0	0.3	0.7
296 Mtkvari	30.5	-14.3	-20.4	-13.7	-22.5
231 Texuri	32.9	1.7	-2.3	-2.9	-5.3
441 Alazani	49.8	-13.8	-25.0	-7.6	-21.5
station average	***32.7***	***-3.2***	***-7.4***	***-4.3***	***-8.4***

Table 4-4. A summary of how the two projections HAD and MPI, along with the high emission scenario rcp85, changes the mean annual streamflow relative to the control period for the five stations studied. The annual mean streamflow observed in the control period is given in column 2.

4.5 Snow water equivalent

Climate change and temperature increase, inevitably bring about reduced snow water equivalent and shorter winter season in all regions. When discussing streamflow in section 4.4, we saw the consequences of this adaption in the form of earlier spring floods and higher streamflow in the winter.

Table 4-5 sums up the snow water equivalent in the control period, in the near future and by the end of the century, applying the HAD and MPI projections and the high emission scenario. Graphs showing the changing snow water equivalent can be seen in appendix A, figures A-136 to A-165. The hydrological model for the catchment 289 Chkheri, a small catchment high up in the Caucasus mountains, is badly tuned on snow. We can observe how the snow storage persists through the summer, accumulating year by year (figures A-146 and A-147). The tendency towards a drastic reduction in the snow cover is, nevertheless, clear.

In the eastern plains, the snow cover plays a minor role in the water balance. Snow only occasionally appear in the present climate, and will show up even less frequent in the future.

		Annual mean SWE (mm) HAD-RCP85		Annual mean SWE (mm) MPI-RCP85	
Station	Annual mean SWE in the control period (mm)	2031-2060	2071-2100	2031-2060	2071-2100
128 Rioni	164	103	39	125	66
289 Chkheri	6322	1538	208	2431	381
296 Mtkvari	41	29	20	32	21
231 Texuri	107	54	15	76	35
441 Alazani	6	3	1	4	1

Table 4-5. Annual mean snow water equivalent (SWE) in the control period and as a result of the two projections HAD and MPI, along with the high emission scenario rcp85, for the five stations studied.

5 Climate change impacts on hydropower production

The previous chapter shows how climate change may increase the streamflow in some regions of Georgia, while the streamflow decreases in other. The objective of the present chapter is to estimate what impact this change in hydrology will have on potential hydropower production in a hydropower system that is adapted for the present climate. In addition to the amount of discharge, the variability of the discharge will affect the impact.

5.1 Calculating hydropower potential

Representing the hydropower system by run-of-river hydropower plants at the outlet of representative catchments, estimates of typical impacts of climate change on the hydropower potential can be made by applying the flow duration curve of streamflow time series, and compare present and projected periods. The flow duration curve is a cumulative frequency curve for streamflow. Streamflow, on the vertical axis, is plotted against exceedance probability. The steeper the curve, the higher the temporal variability of the streamflow data series.

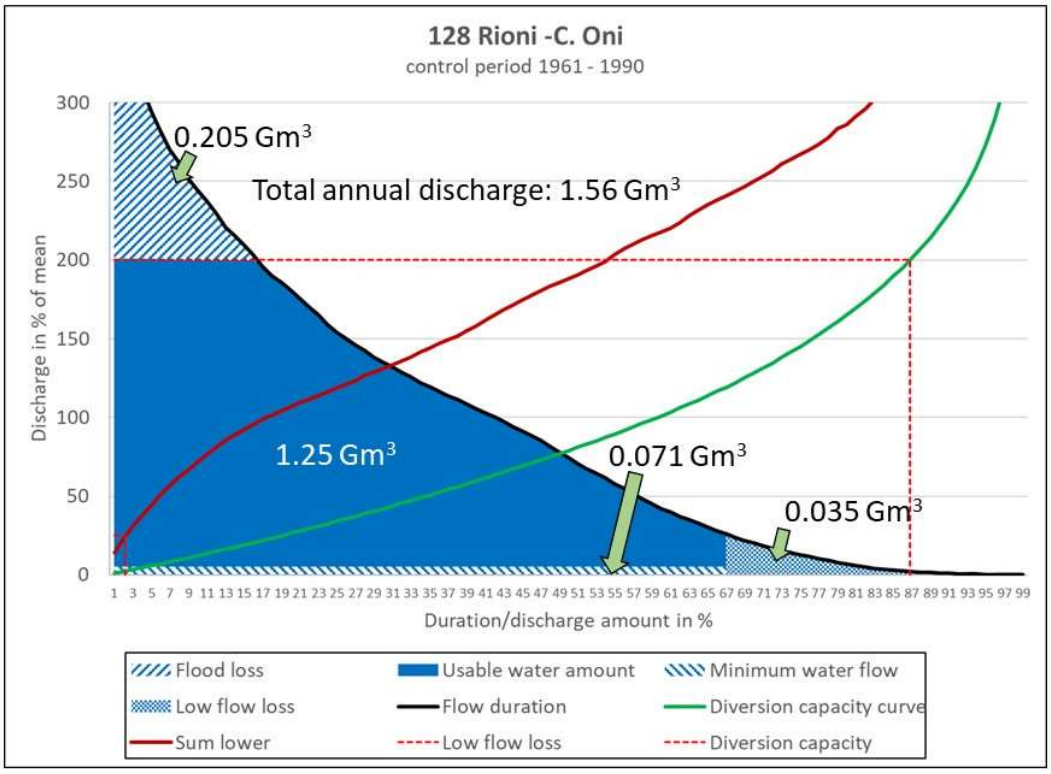

Figure 5-1. Flow duration curve (black), sum lower (red) and diversion capacity curve (green) for catchment 128 Rioni - C. Oni, based on hydrological model results for streamflow with observed precipitation and temperature for the control period 1961 - 1990. The annual discharge volumes that goes to flood loss, hydropower production potential, minimum water flow and low flow loss are shown as areal fractions below the flow duration curve.

Figure 5-1 shows the flow duration curve (in black) for the catchment 128 Rioni-C. Oni in region 2 (see figure 2-1), a Greater Caucasian region, for the period 1961 – 1990. The curve is based on hydrological simulations with observed input data. The streamflow values are given in percent of the mean streamflow, and the x-axis shows the duration of streamflow exceeding the corresponding value. The red curve (sum lower) integrates the volume of streamflow below a given value. The x-axis here shows the integrated fraction of total streamflow. The green curve (diversion capacity curve) shows the fraction of the streamflow (x-axis) that can be diverted by a construction as a function of installed capacity (y-axis).

The mean streamflow at 128 Rioni-C. Oni is 49.3 m^3/s. On average, the annual discharge volume passing through the station is 1.56 Gm^3. The operational range of a hydropower plant can be defined by a minimum and a maximum turbine discharge. Given a minimum turbine discharge of 20% of the mean streamflow, the low flow loss amounts to 0.035 Gm^3. A maximum turbine discharge of 200% of mean streamflow gives a flood loss of 0.205 Gm^3. Always ensuring a low flow of 5% of the mean, in respect of the ecology takes another 0.071 Gm^3, leaving 1.25 Gm^3 available for energy production. The red dotted lines show how the numbers are found, and the volumes are visualized as areal fractions below the flow duration curve.

Climate change will alter the flow regime, see section 4.4. Different climate models and emission scenarios give a wide range of possible climate change impacts. For the

present example, the climate scenario described by HadGEM2-ES / REMO2015 (HAD) and the high emission scenario RCP85 is used. In the mountainous Rioni catchment, climate change will give more precipitation, and higher temperatures will cause net glacier melting, which will make the streamflow increase, see section 4.4. Figure 5-2 shows how this projected streamflow regime will affect the volumes associated with the hydropower potential. For comparison, the y-axis is re-scaled according to the mean flow in the control period. Similar curves, without volume estimates, are given in appendix B for representative hydrological stations. In figure 5-2, notice how the total discharge in the river has increased, particularly within the operational range of the hydropower plant. This makes 1.71 Gm^3 available for production. The flood loss is about the same, 0.21 Gm^3, despite the increased total streamflow. Less snow and more moderate spring floods can explain this pattern. The low flow loss has decreased to 0.026 Gm^3, while the environmental low flow is the same, assuming that environmental requirements are constant, with only a minor adjustment related to the reduced low flow loss.

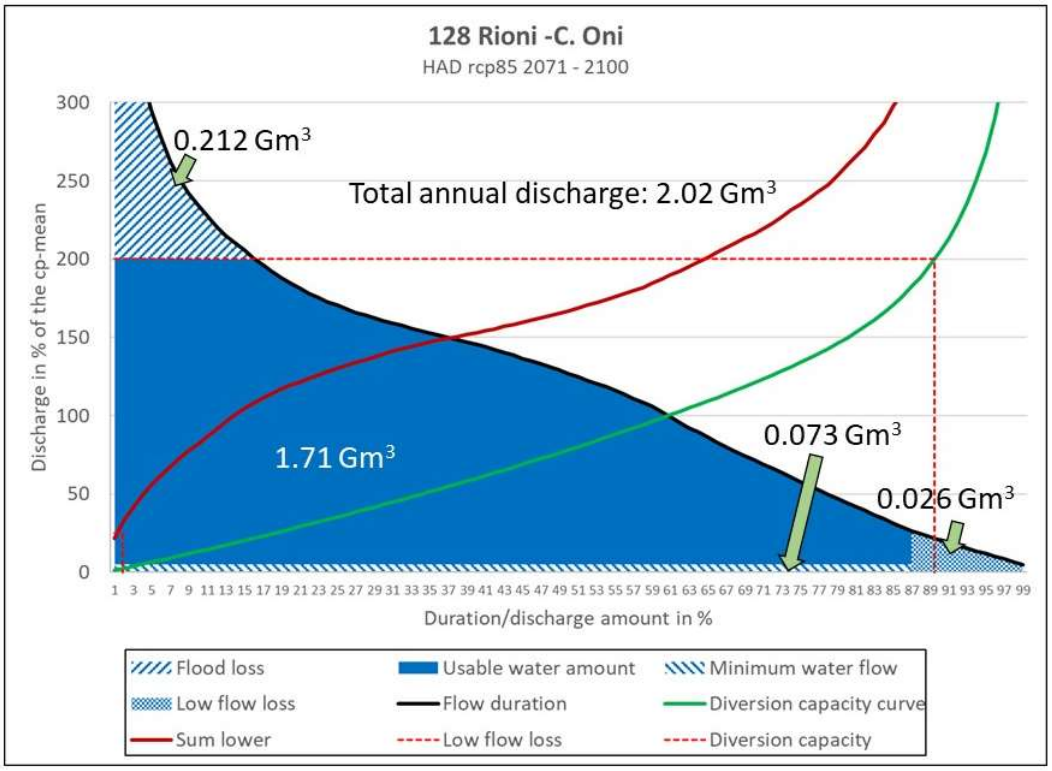

Figure 5-2. Flow duration curve, sum lower and diversion capacity curve for catchment 128 Rioni - C. Oni, based on hydrological model results for streamflow with precipitation and temperature input from climate projection HAD RCP85 for the period 2071 - 2100.

In the plains in southeast, the effect of climate change on the hydropower potential is turned around. Figure 5-3 shows the flow duration curve, the sum lower and the diversion capacity curve for the catchment 441 Alazani - V. Heretiskari in region 14, a river catchment draining towards Azerbaijan, for the period 1961 – 1990.

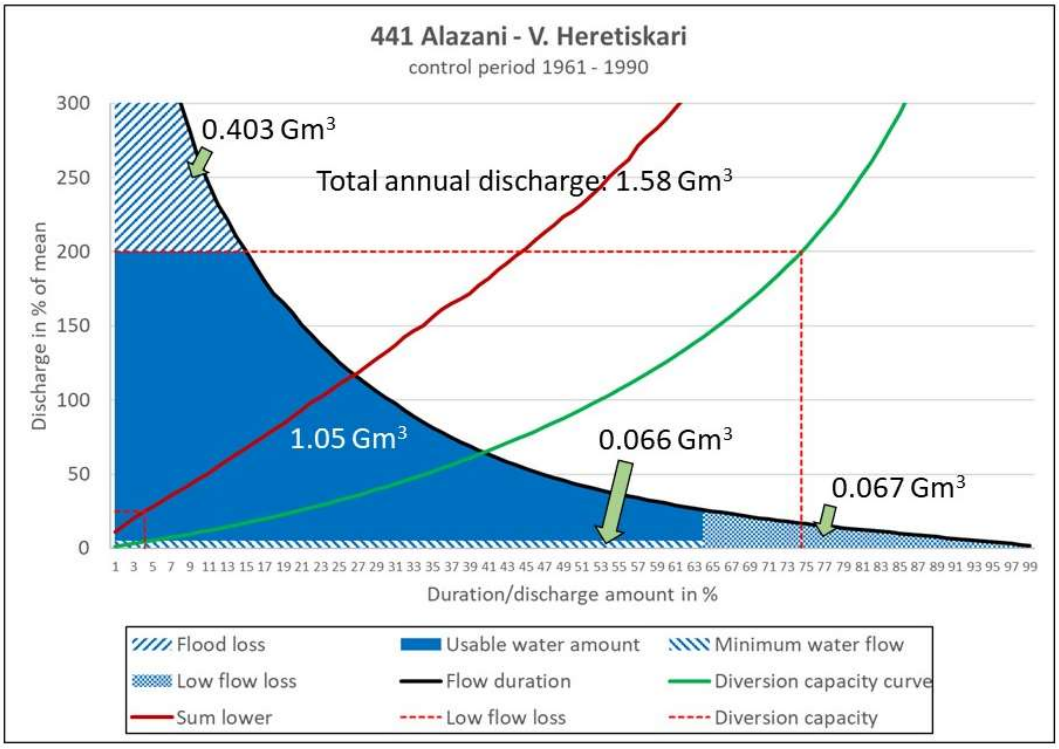

Figure 5-3. Flow duration curve, sum lower and diversion capacity curve for catchment 441 Alazani – V. Heretiskari, based on hydrological model results for streamflow with observed precipitation and temperature input for the control period 1961 – 1990.

In this region, increased evapotranspiration in the projected periods, caused by increased temperatures, makes the water amount left for streamflow decrease. Figure 5-4 shows how the total annual discharge is reduced from 1.58 Gm^3 to 0.79 Gm^3 when comparing the control period with the climate scenario described by HAD/RCP85. The flood loss is also reduced, but the low flow loss in this new regime is increased. All in all, the annual volume available for hydropower production ends up at 0.54 Gm^3, compared to the control period's 1.05 Gm^3.

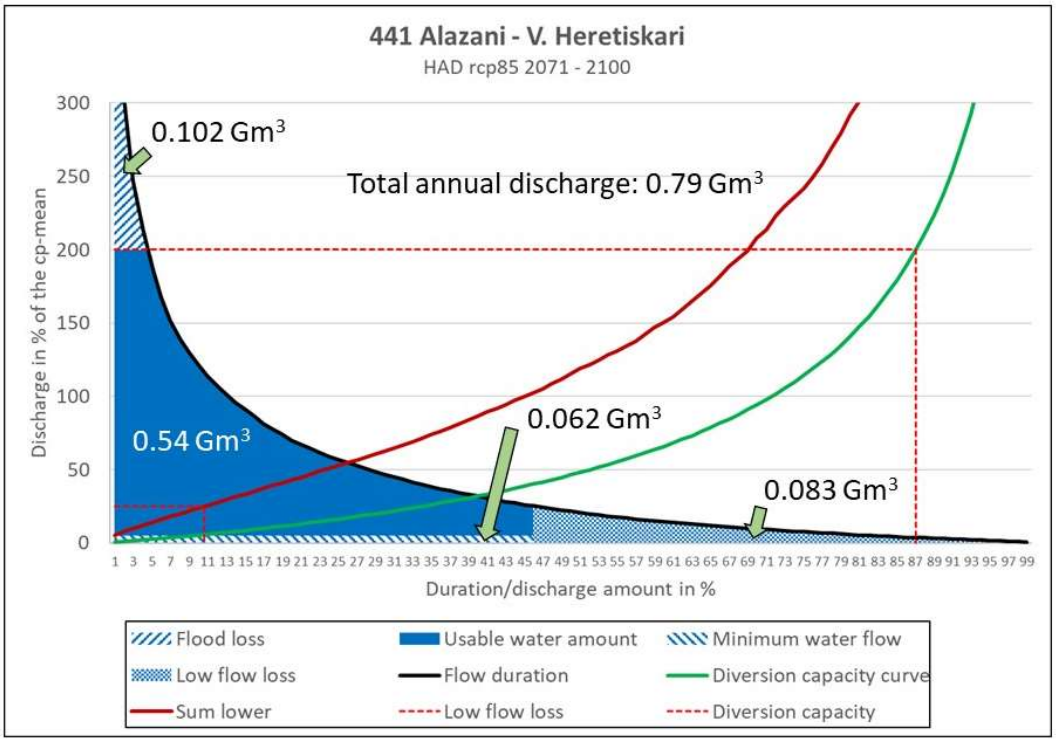

Figure 5-4. Flow duration curve, sum lower and diversion capacity curve for catchment 441 Alazani – V. Heretiskari, based on hydrological model results for streamflow with precipitation and temperature input from climate projection HAD RCP85 for the period 2071 - 2100.

5.2 Results

Similar estimates of available hydropower potential have been made for all the 14 catchments that represent the 14 hydrological zones in Georgia (figure 2-1). Assuming that the hydropower plants have an operational range spanning 20 – 200% of the mean catchment streamflow in the control period, the effect of climate change on the hydropower potential, according to the three climate projections and the two emission scenarios used, applied to the near future (2031-2060) and to the end of the century (2071 – 2100), is calculated. The result is shown in table 5-1 and visualised in figure 5-5.

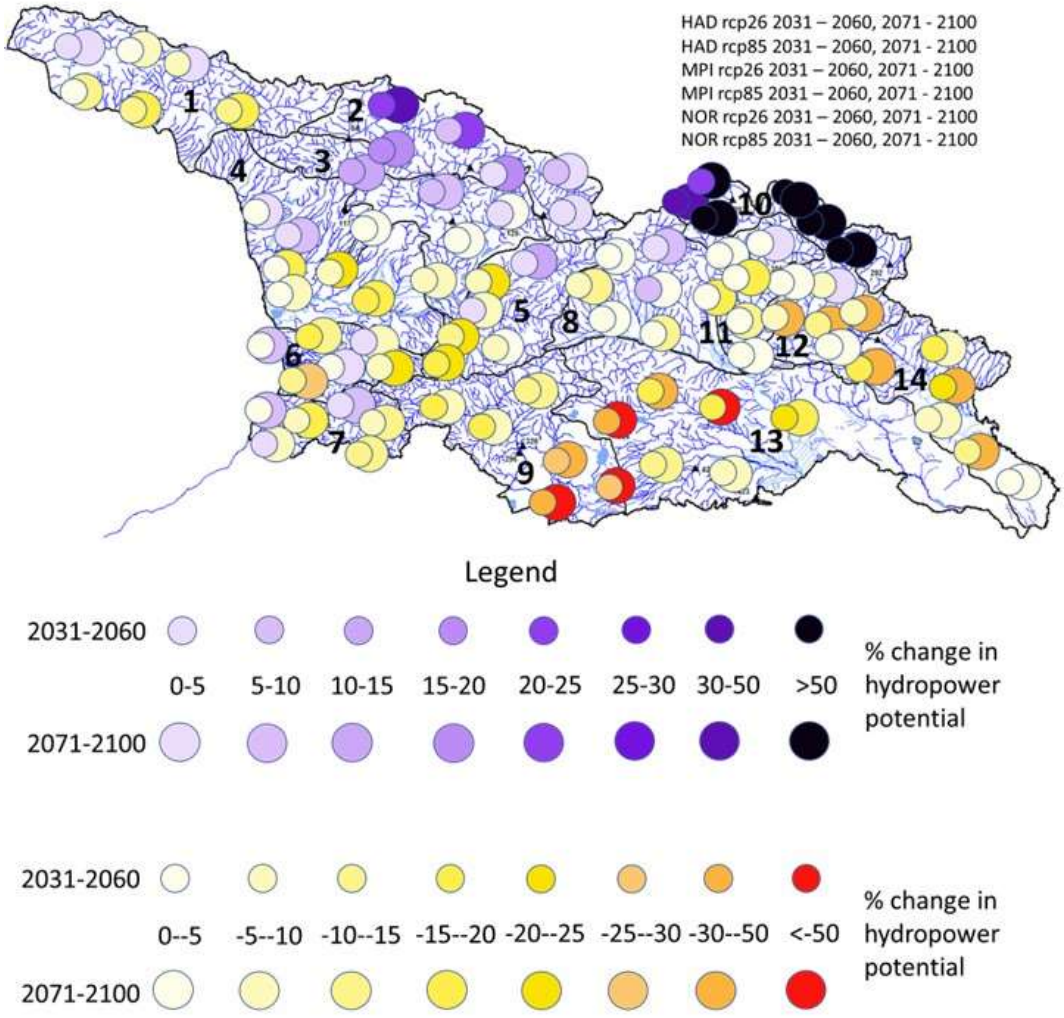

Figure 5-5. Estimated change in hydropower potential in the 14 hydrological zones in Georgia, according to the three climate projections and the two emission scenarios used. The small circles represent the near future, 2031 - 2060. The large circles represent the end of the century, 2071 - 2100. Blue colors indicate an increase in hydropower potential, while yellow-red colors indicate a reduction in hydropower potential, see the legend. All the indicators are connected to the same catchment within the zone, and the positioning within the zone is random.

		Control period	HAD rcp26		HAD rcp85		MPI rcp26		MPI rcp85		NOR rcp26		NOR rcp85	
		1961-1990	2031-2060	2071-2100	2031-2060	2071-2100	2031-2060	2071-2100	2031-2060	2071-2100	2031-2060	2071-2100	2031-2060	2071-2100
		Mean annual discharge available for hydropower production	% change from control period											
st. numbe	st. name													
21	Gumista – V. Aachadara	7.96E+08	3.53	1.80	-2.22	-12.56	-2.30	-5.01	-10.50	-18.62	-7.48	0.66	-11.77	-19.56
128	Rioni - C. Oni	1.32E+09	16.45	17.99	20.88	35.30	6.56	4.23	7.45	20.03	2.99	2.44	3.40	15.84
131	Rioni V. Alpana	3.09E+09	10.02	13.10	9.75	8.33	2.06	-2.26	-2.64	-1.92	-2.04	-2.50	-8.75	-5.24
231	Texuri - V. Naqlaquevi	9.00E+08	1.91	6.52	-1.24	-16.91	-1.70	-5.94	-9.73	-20.92	-1.38	0.43	-16.24	-19.27
174	Kvirila – C. Zestaponi	1.31E+09	4.69	10.41	-6.27	-20.75	0.52	-7.85	-10.32	-20.46	-7.79	-4.10	-18.07	-22.42
242	Supsa - D. Chokhatauri	3.49E+08	-2.96	3.16	-13.29	-26.04	0.82	-6.13	-9.32	-21.02	-4.83	5.48	-16.12	-14.49
278	Achhristskali - D. Qeda	1.32E+09	1.70	6.59	-8.47	-18.41	2.27	-5.04	-8.46	-14.38	-4.50	6.71	-12.60	-11.86
355	Didi-Liakhvi - V. Kekhvi	7.18E+08	4.53	7.51	5.11	1.77	-0.22	-2.67	-4.83	-10.67	-3.03	-3.70	-6.08	-13.45
296	Mtkvari (Kura) – V. Khertvisi	4.84E+08	-19.51	-8.57	-31.64	-56.31	-10.77	-14.43	-29.49	-63.78	-16.52	-9.24	-26.99	-49.46
289	Chkheri – D. Stefantsminda	1.48E+07	80.63	90.33	116.06	242.31	46.60	45.92	78.51	209.97	23.12	56.55	60.37	171.90
382	Gudamakris-Aragvi (Black Aragvi) – At the mouth	1.72E+08	-1.99	2.69	-0.84	-14.04	-1.69	-0.98	-3.69	-16.37	-3.18	-1.62	-2.44	-18.18
424	Iori – V. Lelovani	2.00E+08	-5.80	1.30	-11.49	-36.69	-1.02	-2.38	-6.68	-30.20	-4.78	-1.31	-9.20	-32.42
419	Mashavera – D. Kazreti	1.02E+08	-24.73	-19.85	-37.40	-56.71	-13.55	-12.91	-16.03	-50.00	-9.38	-17.32	-17.99	-48.54
441	Alazani – V. Heretiskari (Heretiskari)	1.11E+09	-19.41	-6.65	-22.09	-45.87	-5.26	-7.52	-10.93	-37.29	-4.60	-4.79	-17.90	-37.27

Table 5-1. Estimated annual discharge available for hydropower production in the control period and % change in the 14 hydrological zones in Georgia, according to the three climate projections and the two emission scenarios used.

In Figure 5-5, the results for all the different cases are presented together. In Figure 5-6, the two emission scenarios are presented separately, and we see a clear tendency towards a more pronounced response to the high emission scenario, RCP85, compared with the low one. Along the Greater Caucasus, the increased power potential brought about by RCP26-emission, is further intensified by the emission scenario RCP85. In this alpine area, glacier melting dominates the effect of increased evapotranspiration. The opposite effect is seen along the southern border to Armenia and towards the south-east, where reduced precipitation and increased evapotranspiration make the discharge go down. The low emission scenario gives rise to a reduced power potential, which is amplified by the high emission scenario. In the central and western Georgia, there are cases where the low emission scenario makes a slight change in the power potential to the lower or to the higher side, while the high emission scenario makes the scale turn upside down. In these cases, a balance between the effect of higher precipitation and higher evapotranspiration is tipped around. A similar tendency may be seen when passing from the near future towards the end of the century in many cases. Referring to Table 2-1, the zones with the highest power potential coincides with the regions where an increased power potential can be expected.

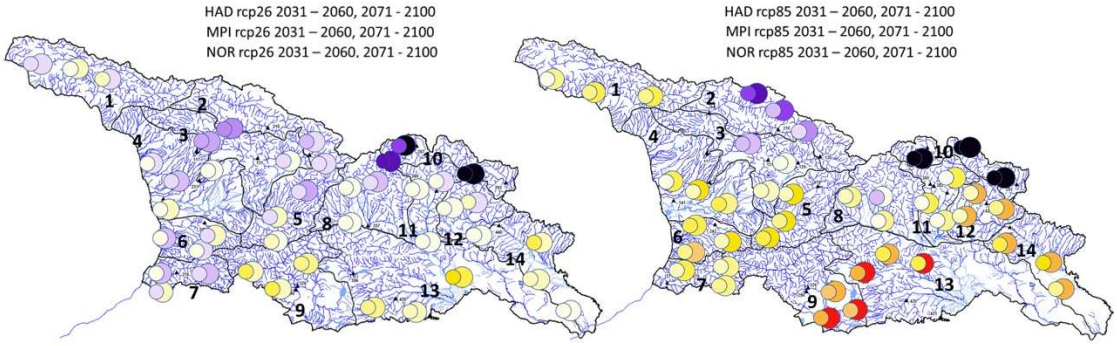

Figure 5-6. Estimated change in hydropower potential in the 14 hydrological zones in Georgia. To the left, the change accordig to the three climate projections and the low emission scenario RCP26 is shown. To the right, similar change for the high emission scenario RCP85 is shown. For a legend, see figure 5-5.

As can be seen in figures 5-7 and 5-8, the different projections used in the study will also influence the results. There's a slight tendency that the Hadley model gives a stronger impact of climate change on the power potential than the MPI model, and even more than the NorESM model. The different projections and scenarios studied, show a probable range of possible effects of climate change on the power potential.

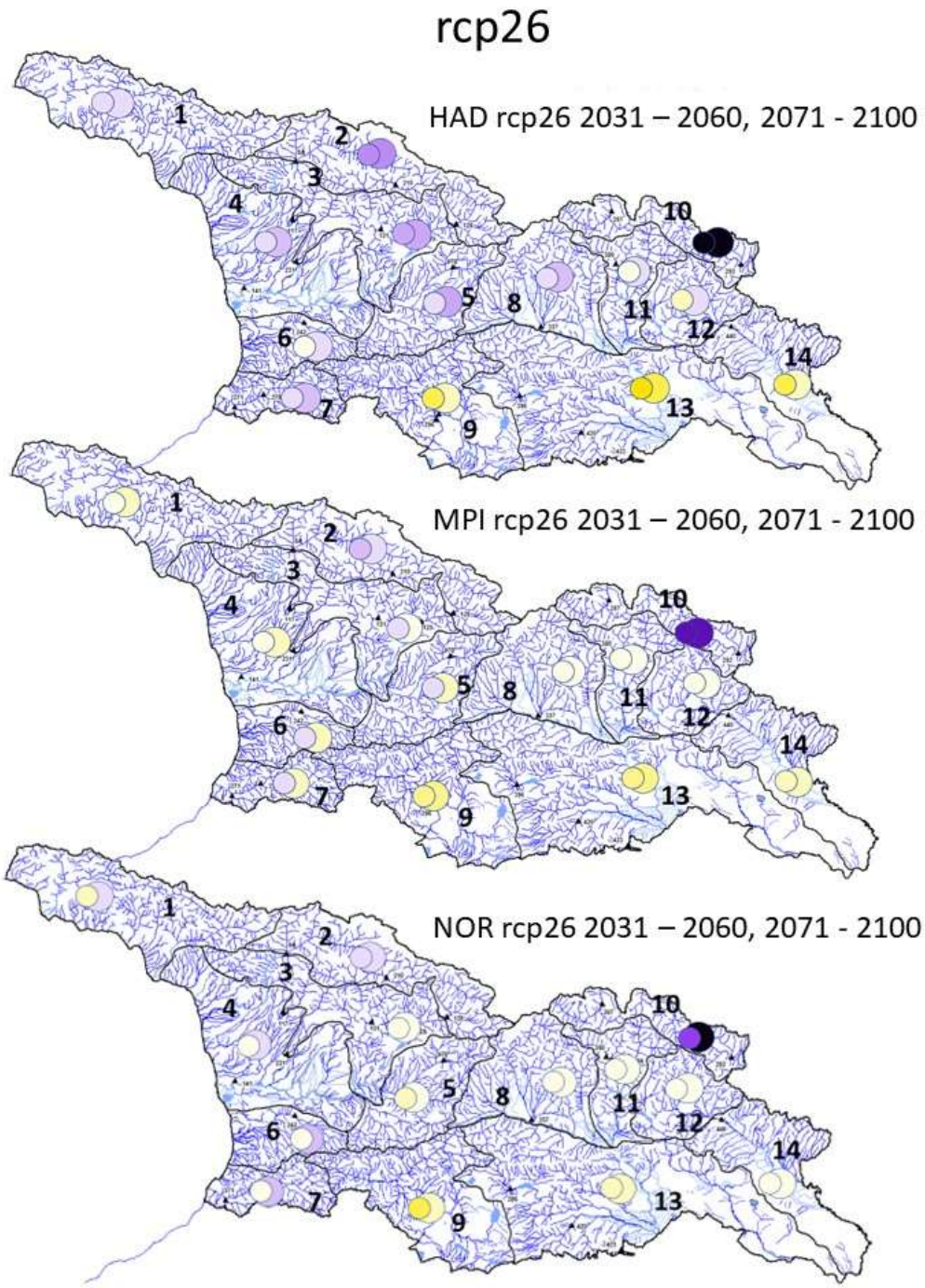

Figure 5-7. Estimated change in hydropower potential in the 14 hydrological zones in Georgia. Results from the three climate projections presented separately for the low emission scenario RPC26. For a legend, see figure 5-5.

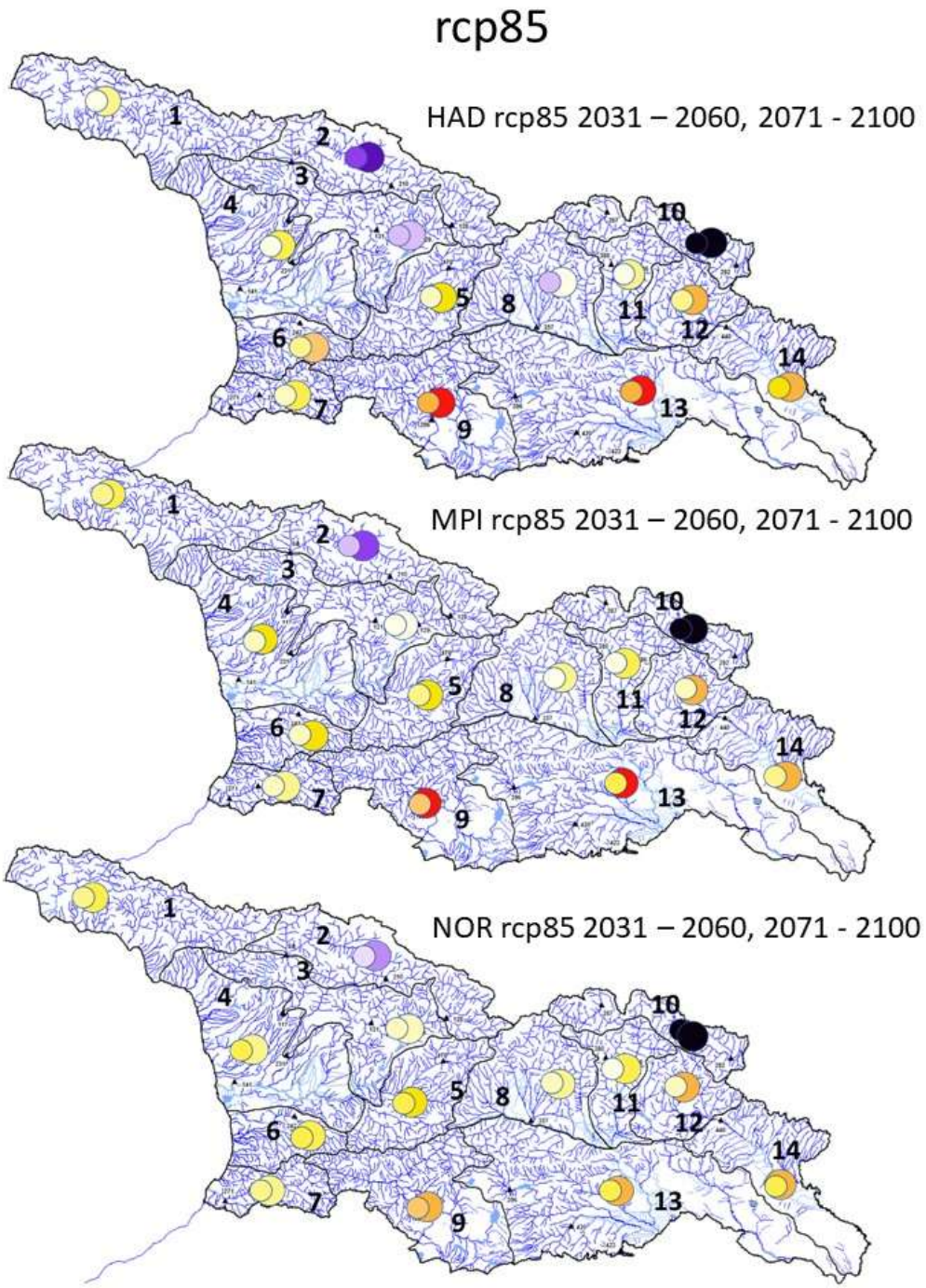

Figure 5-8. Estimated change in hydropower potential in the 14 hydrological zones in Georgia. Results from the three climate projections presented separately for the high emission scenario RPC85. For a legend, see figure 5-5.

6 Conclusions

We can put these results together with the estimates made of the hydropower potential from Arnesen et al. (2021). Arnesen et al. estimated the zonal hydropower potential for the 14 zones selected. In table 6-1, the zonal hydropower potential is adjusted according to the effect of climate change on the hydropower potential in the catchments representing the different zones. The effect on the total hydropower potential for Georgia is seen at the bottom of the table. The zones with the highest hydropower potential according to Arnesen et al., corresponds to the zones with a positive change in the hydropower potential as an effect of climate change. Consequently, most of the climate scenarios used increases the total hydropower potential of Georgia. The exceptions from this tendency, are NOR rcp25 and NOR rcp85 in the near future. This is an interesting result that might indicate a future trend in the hydropower potential of Georgia.

However, a handful of sources of uncertainty can be mentioned:

- The estimations rely on model simulations made by a hydrological model that is calibrated for the present climate. This may lead to suboptimal operation for other climate regimes. One particular aspect to bear in mind, is that the model does not consider glacier dynamics, i.e., the glacier areal coverage is not adjusted according to the glacier mass balance. This balance will obviously be negative through the present centennial, and the subsequent decreasing amount of glacier melt water expected, is not accounted for.
- Another source of error is the selection of stations representing the 14 geographical zones of Georgia. The one station selected per zone is not necessarily fully representative of the hydrological regime of the zone.
- A simplified run-of-river hydropower plant system is applied to calculate the impact of the changed hydrological regime on the hydropower potential.
- A good portion of uncertainty is also associated with how the future climate will look like. Here, we have assumed that by applying three different climate projections along with one low and one high emission scenario, we have spanned a reasonable width of realizations.

Zone	Net zonal hydropower potential (TWh/year)	Zonal hydropower potential adjusted according to effect of climate change on hydropower potential in the representative catchment											
		HAD rcp26		HAD rcp85		MPI rcp26		MPI rcp85		NOR rcp26		NOR rcp85	
		2031-2060	2071-2100	2031-2060	2071-2100	2031-2060	2071-2100	2031-2060	2071-2100	2031-2060	2071-2100	2031-2060	2071-2100
1	7.5	7.7	7.6	7.3	6.5	7.3	7.1	6.7	6.1	6.9	7.5	6.6	6.0
2	6.4	7.5	7.6	7.7	8.7	6.8	6.7	6.9	7.7	6.6	6.6	6.6	7.4
3	4.1	4.6	4.7	4.5	4.5	4.2	4.0	4.0	4.1	4.1	4.0	3.8	3.9
4	1.7	1.7	1.8	1.6	1.4	1.6	1.6	1.5	1.3	1.6	1.7	1.4	1.3
5	0.7	0.7	0.8	0.7	0.6	0.7	0.6	0.6	0.6	0.6	0.7	0.6	0.5
6	1.6	1.5	1.6	1.4	1.2	1.6	1.5	1.4	1.2	1.5	1.6	1.3	1.3
7	1.5	1.5	1.6	1.4	1.2	1.5	1.4	1.4	1.3	1.4	1.6	1.3	1.3
8	0.9	0.9	0.9	0.9	0.9	0.9	0.8	0.8	0.8	0.8	0.8	0.8	0.7
9	1.0	0.8	0.9	0.7	0.4	0.9	0.8	0.7	0.4	0.8	0.9	0.7	0.5
10	2.2	3.9	4.1	4.7	7.4	3.2	3.1	3.8	6.7	2.6	3.4	3.5	5.9
11	1.1	1.1	1.1	1.1	0.9	1.1	1.1	1.0	0.9	1.0	1.1	1.0	0.9
12	0.6	0.6	0.7	0.6	0.4	0.6	0.6	0.6	0.5	0.6	0.6	0.6	0.4
13	0.8	0.6	0.6	0.5	0.3	0.7	0.7	0.7	0.4	0.7	0.7	0.7	0.4
14	0.4	0.3	0.4	0.3	0.2	0.4	0.3	0.3	0.2	0.4	0.4	0.3	0.2
total	**30.3**	**33.4**	**34.3**	**33.3**	**34.6**	**31.4**	**30.5**	**30.5**	**32.0**	**29.8**	**31.5**	**29.2**	**31.0**

Table 6-1. The effect of climate change on the hydropower potential in the 14 zones of Georgia, assuming that the stations used are representative for the respective zone.

7 Acknowledgements

This work was funded by the Norwegian Ministry of Foreign Affairs, project Institutional Cooperation between Georgian public energy institutions and NVE of Norway for the period 2017-2023, Project: 32574, Cooperation Area: 32574-04 Climate Change Impact. Thanks to kind assistance in NVE in providing the data needed and help to interpret the results. The model simulations were performed by Dr. Stein Beldring. The downscaled climate projections were obtained by Dr. Wai Kwok Wong. Eva Klausen helped in organizing the data used in the analysis and Erik Holmqvist introduced me to useful functionality in the Hydra2 toolbox.

References

Arnesen, F., Kristensen, S. E., Shukakidze, G., Koestler, V., Geladze, V., Taksdal, E. and Eide, A. W. 2021. Hydro Power Potential in Georgia. NVE Report 5/2021.

Beldring, S., Engeland, K., Roald, L.A., Sælthun, N.R., Voksø, A. 2003. Estimation of parameters in a distributed precipitation-runoff model for Norway. Hydrology and Earth System Sciences 7, 304-316.

Beldring, S., Kordzakhia, M., Kristensen, S.E. 2017. Runoff map of Georgia. Norwegian Water Resources and Energy Directorate, Report no. 27/2017, 60 pp. https://publikasjoner.nve.no/rapport/2017/rapport2017_27.pdf

Elizbarashvili, N., Meladze, G., Sandodze, G. and Grigolia, L. 2022. Climate change and mountain landscapes of Georgia. … pp. 34-42. Proceedings from the International Eurasia Climate Change Congress Euracli'22.

Megrelidze, I. 2021. Fourth National Communication of Georgia, Under the United Nations Framework Convention on Climate Change, 4.8 Extreme Hydrometeorological Events, pp. 271-278. Tbilisi, Georgia

Khelidze, G., Shatakishvili, L., and Pipia, B. 2019. Quantitative assessment of hydropower potential by the impacts of climate transformation on the example of the rivers of Georgia. World Science. 10(50), Vol.1. doi: 10.31435/rsglobal_ws/31102019/67122.

Kordzakhia, G., Shengelia, L., Tvauri, G. and Dzadzamia, M. 2021. Climate change impact on the glaciers of the Rioni river basin (Georgia). Acta Horticulturae et Regiotecturae – Special Issue. Nitra, Slovaca Universitas Agriculturae Nitriae, 2021, pp. 27–30. DOI: 10.2478/ahr-2021-0006.

Kordzakhia, G. 2021. Fourth National Communication of Georgia, Under the United Nations Framework Convention on Climate Change, 4.4 Glaciers, pp. 241-250. Tbilisi, Georgia

Kordzakhia, M. 2021, Fourth National Communication of Georgia, Under the United Nations Framework Convention on Climate Change, 4.5 Water resources, pp. 250-258. Tbilisi, Georgia

Rets, E.P., Durmanov, I.N., Kireeva, M.B. et al. 2020. Past 'peak water' in the North Caucasus: deglaciation drives a reduction in glacial runoff impacting summer river runoff and peak discharges. *Climatic Change* **163**, 2135–2151 (2020). https://doi.org/10.1007/s10584-020-02931-y

Sunyer, M. A., Hundecha, Y., Lawrence, D., Madsen, H., Willems, P., Martinkova, M., Vormoor, K., Bürger, G., Hanel, M., Kriaučiūnienė, J., Loukas, A., Osuch, M., and Yücel, I. 2015. Inter-comparison of statistical downscaling methods for projection of extreme precipitation in Europe. Hydrol. Earth Syst. Sci., 19, 1827–1847. https://doi.org/10.5194/hess-19-1827-2015

Willems, P., and Vrac, M. 2011. Statistical precipitation downscaling for small-scale hydrological impact investigations of climate change. J. Hydrol., 402, 193–205. https://doi.org/10.1016/j.jhydrol.2011.02.030

Appendix A. Effects of climate change on hydrological and meteoro-logical processes for selected climate projections, climate gas emission scenarios and stations.

Climate projections:

- HadGEM2-ES (HAD)
- MPI-ESM-LR (MPI)

Emission scenario:

- the high emission scenario, RCP8.5.

Stations:

- 128 Rioni - C. Oni, zone 2, representing the Greater Caucasus region
- 289 Chkheri - D. Stefantsminda, zone 10, representing the Greater Caucasus region
- 296 Mtkvari (Kura) – V. Khertvisi, zone 9, representing the Lesser Caucasus region
- 231 Texuri - V. Naqlaquevi, zone 4, representing the Black Sea region
- 441 Alazani – V. Heretiskari, zone 14, representing the plains of eastern Georgia

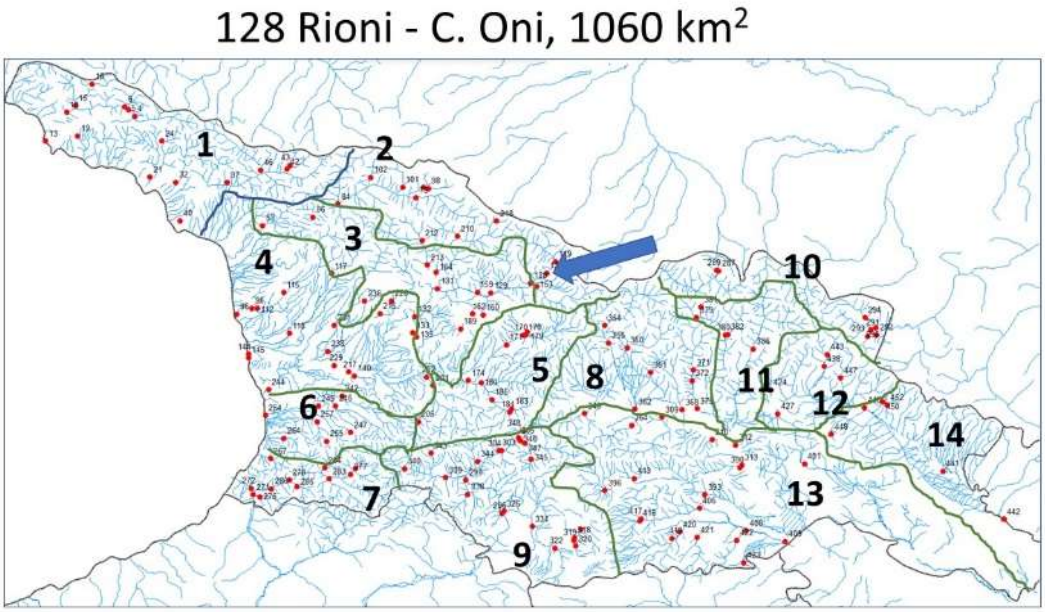

Figure A-1. Map of Georgia, where the 14 hydrological zones are drawn with green lines. The station representing zone 2, 128 Rioni – C. Oni, is marked by a blue arrow.

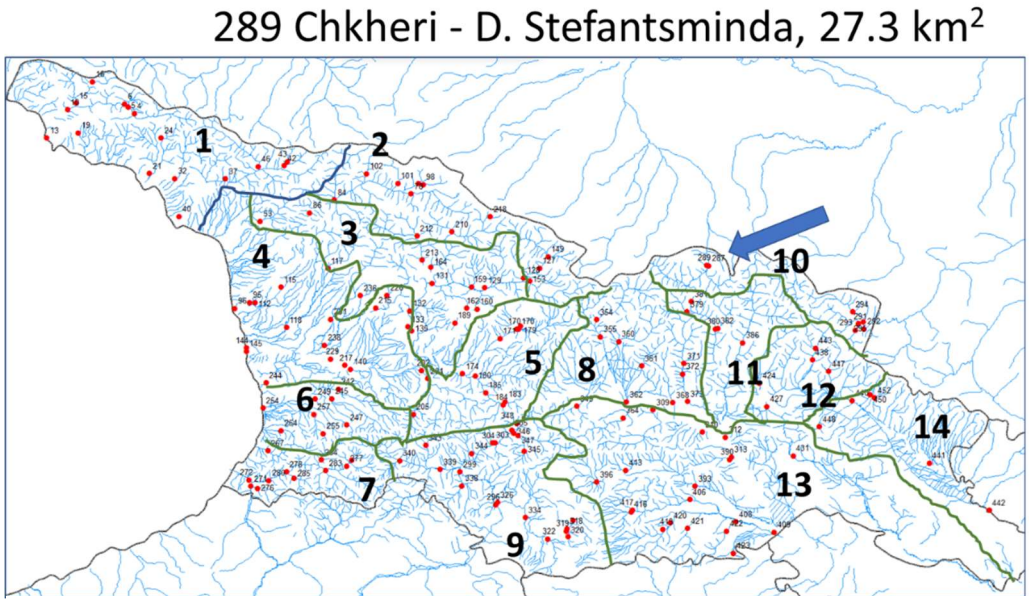

Figure A-2. Map of Georgia, where the 14 hydrological zones are drawn with green lines. The station representing zone 10, 289 Chkheri - D. Stefantsminda, is marked by a blue arrow.

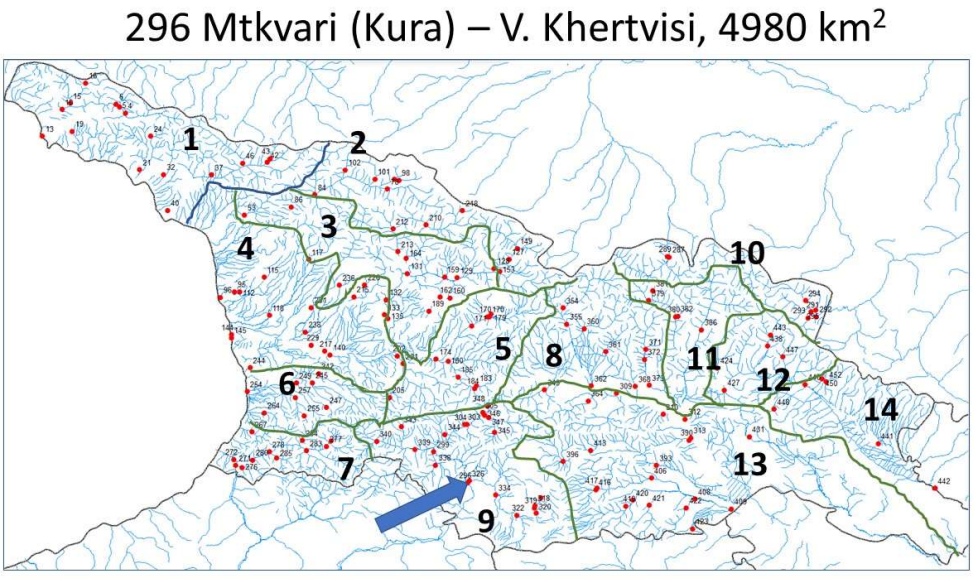

Figure A-3. Map of Georgia, where the 14 hydrological zones are drawn with green lines. The station representant zone 10, 296 Mtkvari (Kura) – V. Khertvisi, is marked by a blue arrow.

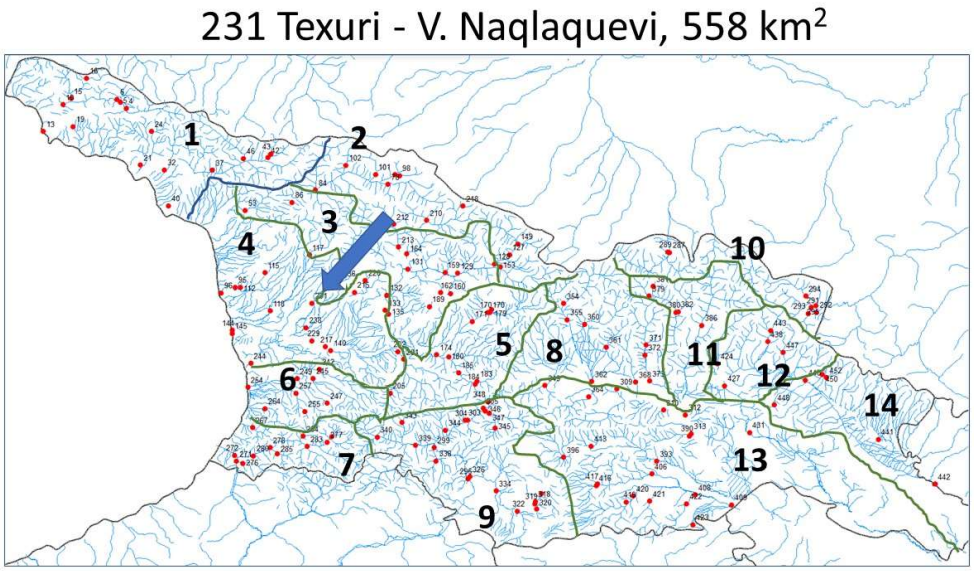

Figure A-4. Map of Georgia, where the 14 hydrological zones are drawn with green lines. The station representing zone 10, 231 Texuri - V. Naqlaquevi, is marked by a blue arrow.

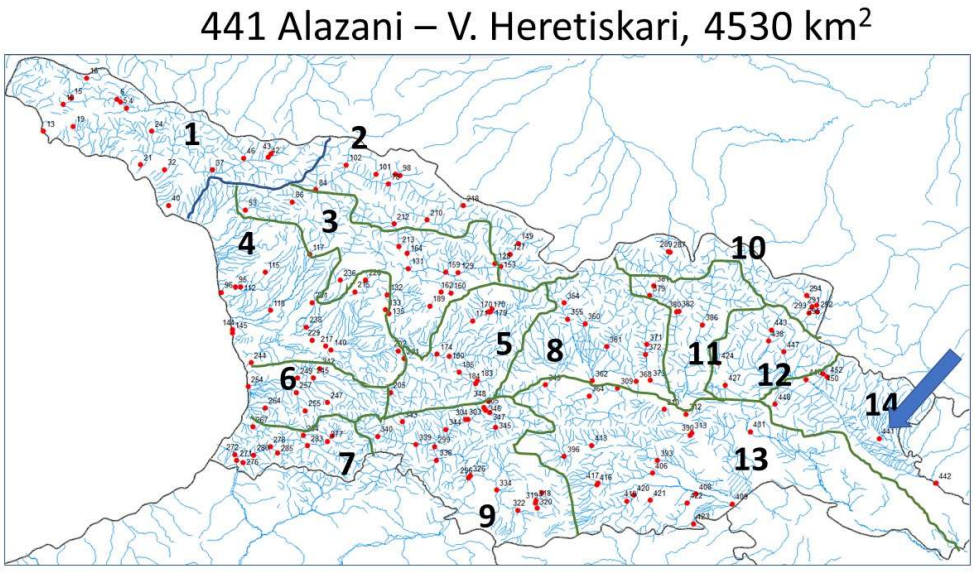

Figure A-5. Map of Georgia, where the 14 hydrological zones are drawn with green lines. The station representing zone 10, 441 Alazani – V. Heretiskari, is marked by a blue arrow.

Temperature

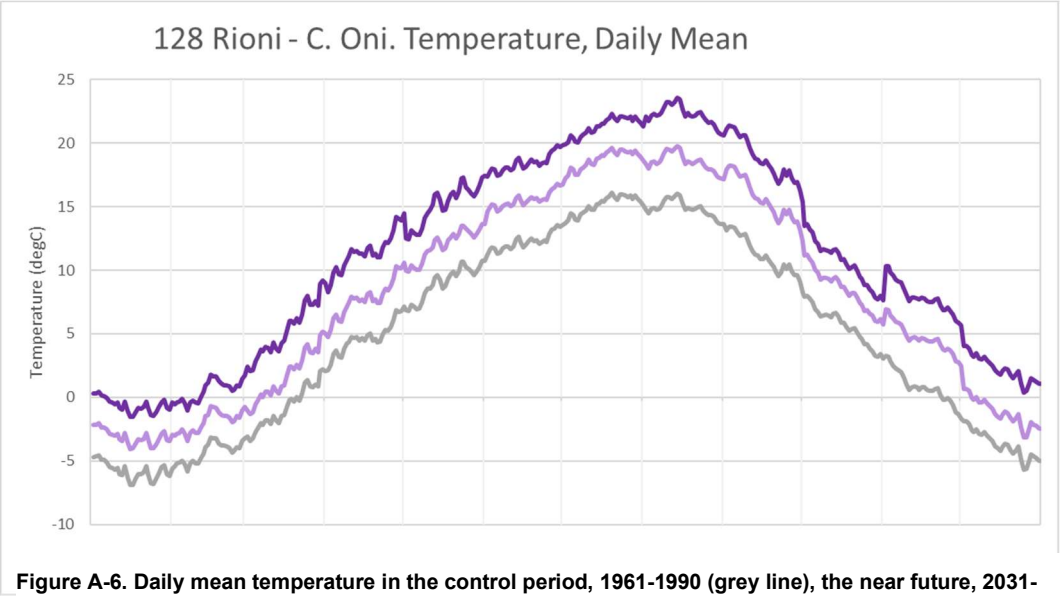

Figure A-6. Daily mean temperature in the control period, 1961-1990 (grey line), the near future, 2031-2060 (light purple line) and the end of the century, 2071-2100 (dark purple line), according to the climate projection HAD, for the station 128 Rioni – C. Oni.

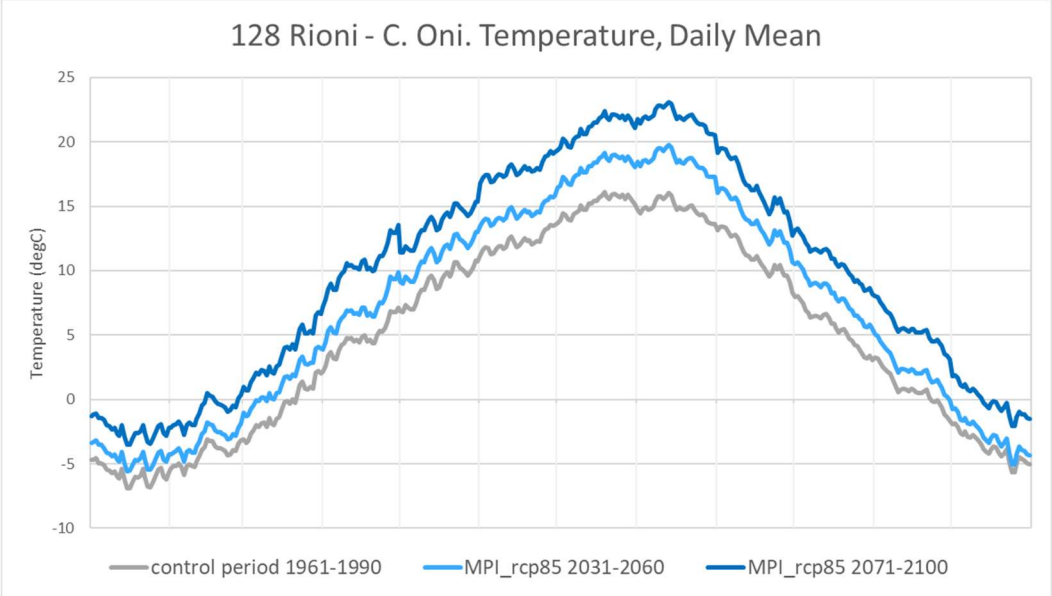

Figure A-7. Daily mean temperature in the control period, 1961-1990 (grey line), the near future, 2031-2060 (light blue line) and the end of the century, 2071-2100 (dark blue line), according to the climate projection MPI, for the station 128 Rioni – C. Oni.

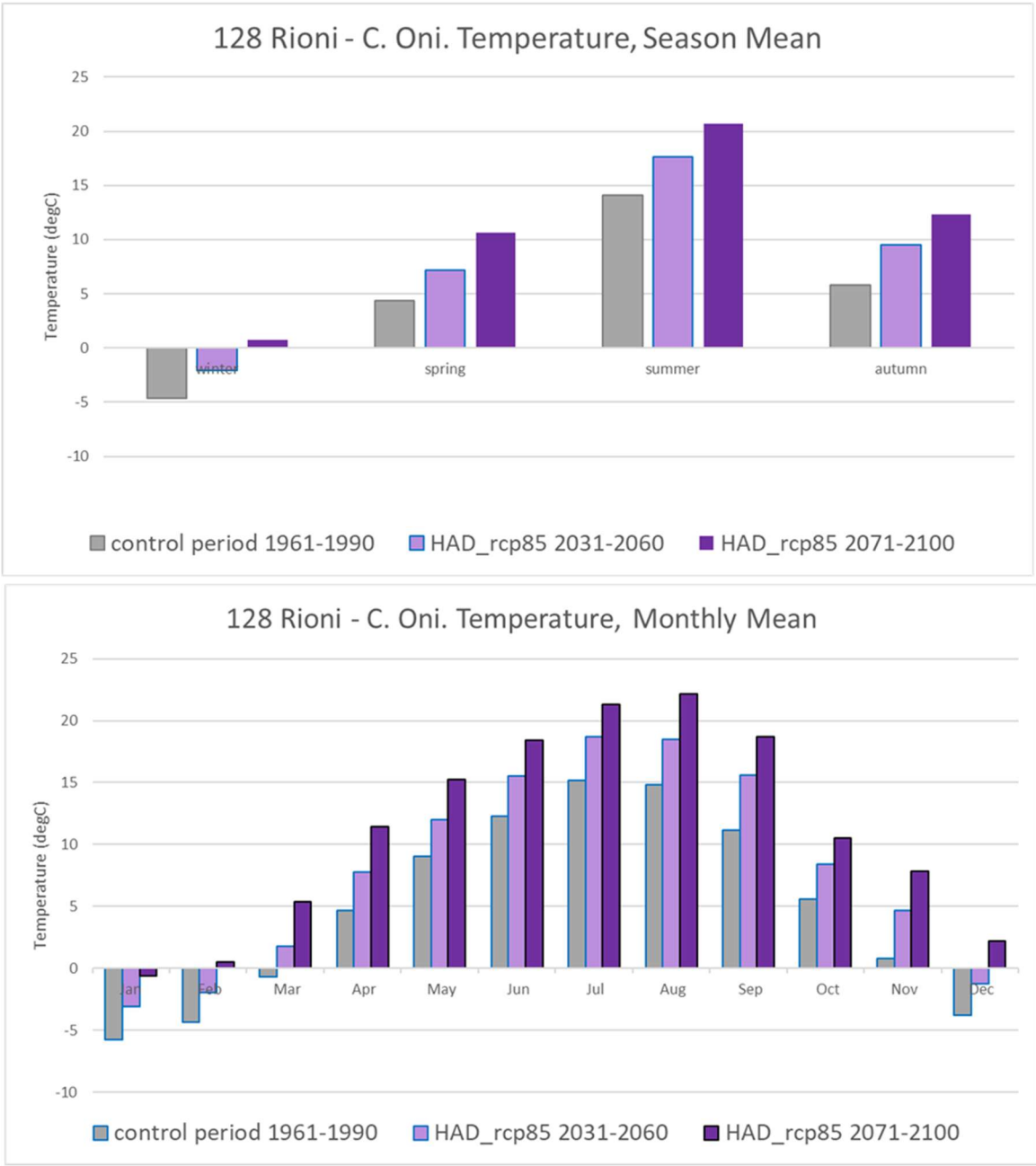

Figure A-8. Season mean (top) and monthly mean (bottom) temperature in the control period, 1961-1990 (grey bars), the near future, 2031-2060 (light purple bars) and the end of the century, 2071-2100 (dark purple bars), according to the climate projection HAD, for the station 128 Rioni – C. Oni.

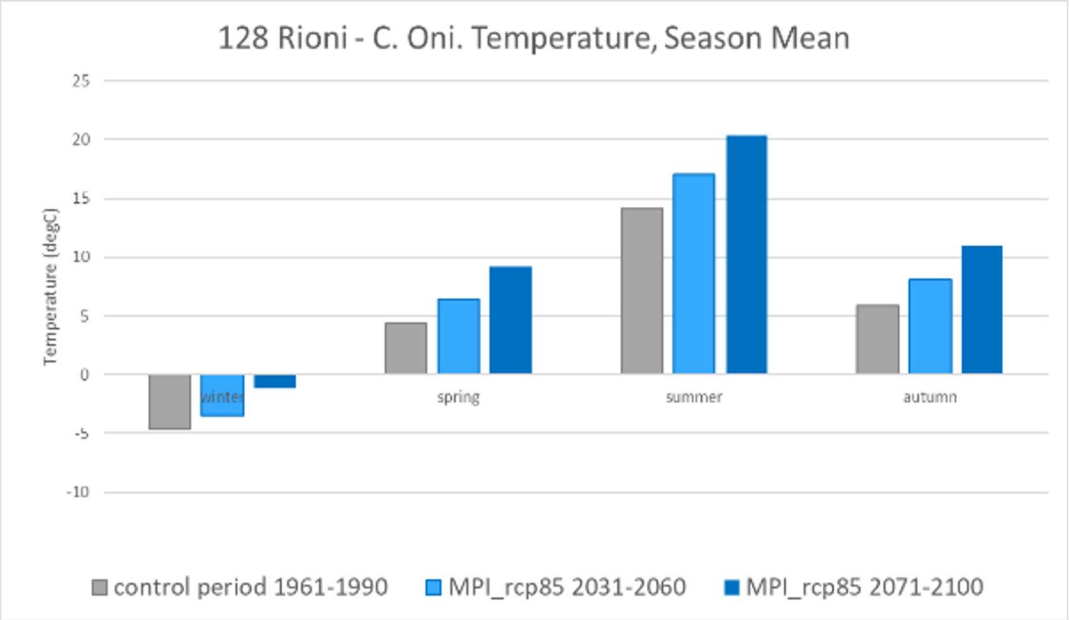

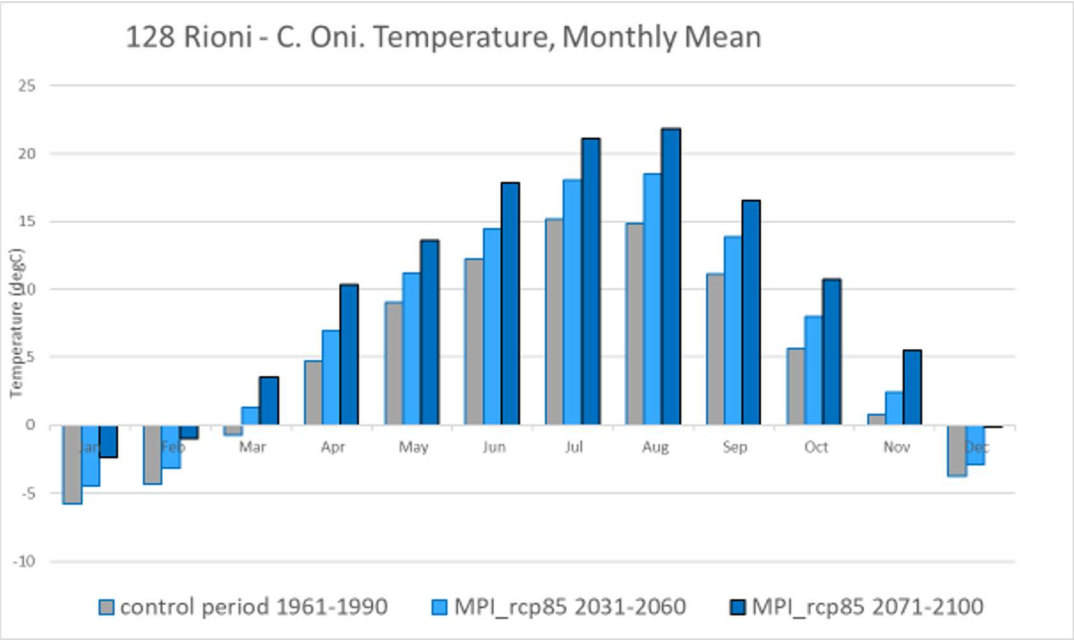

Figure A-9. Season mean (top) and monthly mean (bottom) temperature in the control period, 1961-1990 (grey bars), the near future, 2031-2060 (light blue bars) and the end of the century, 2071-2100 (dark blue bars), according to the climate projection MPI, for the station 128 Rioni – C. Oni.

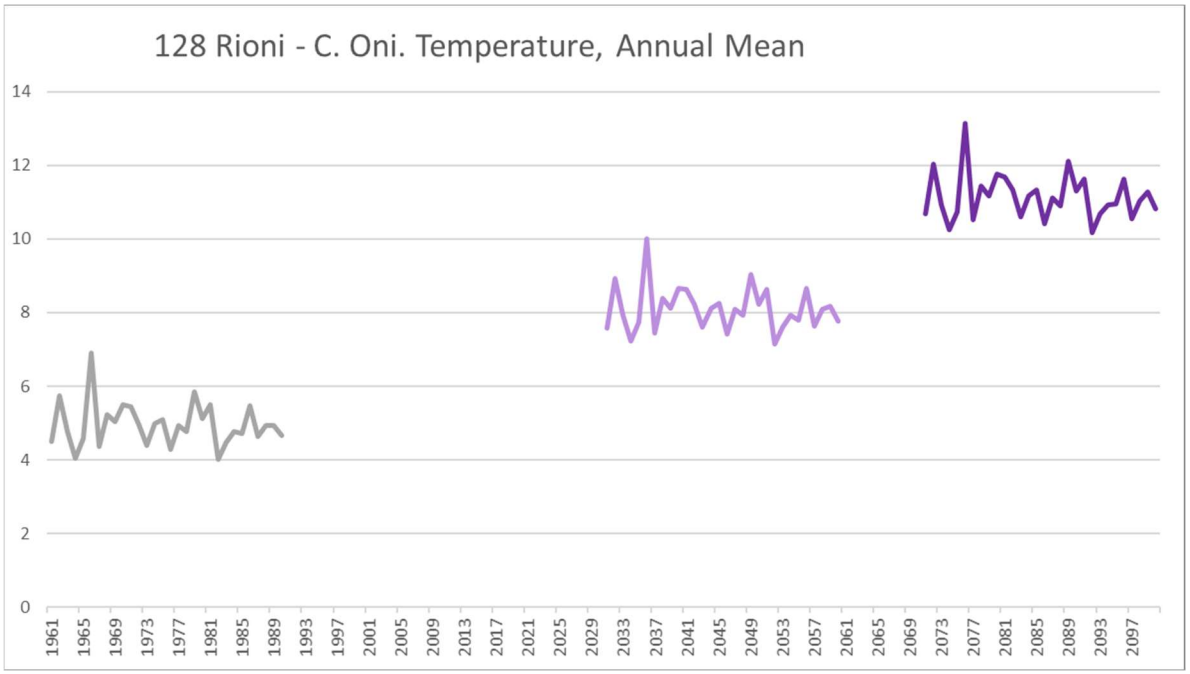

Figure A-10. Annual mean temperatures in the control period, 1961-1990 (grey line), the near future, 2031-2060 (light purple line) and the end of the century, 2071-2100 (dark purple line), according to the climate projection HAD, for the station 128 Rioni – C. Oni.

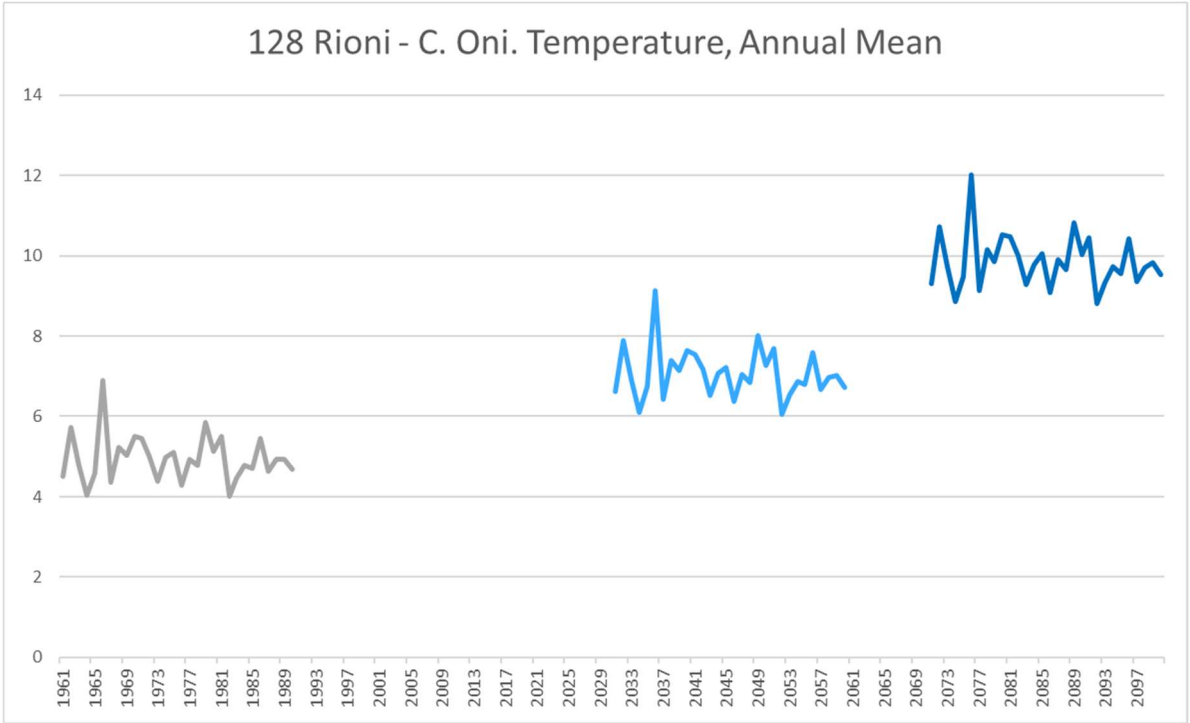

Figure A-11. Annual mean temperatures in the control period, 1961-1990 (grey line), the near future, 2031-2060 (light purple line) and the end of the century, 2071-2100 (dark purple line), according to the climate projection MPI, for the station 128 Rioni – C. Oni.

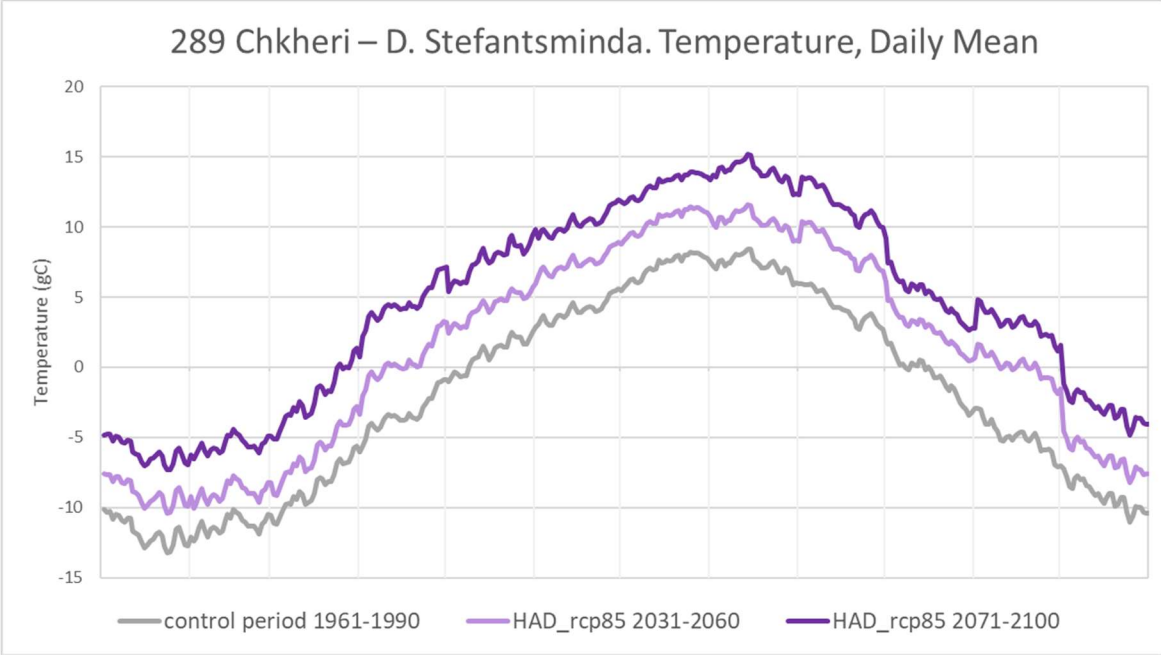

Figure A-12. Daily mean temperature in the control period, 1961-1990 (grey line), the near future, 2031-2060 (light purple line) and the end of the century, 2071-2100 (dark purple line), according to the climate projection HAD, for the station 289 Chkheri - D. Stefantsminda.

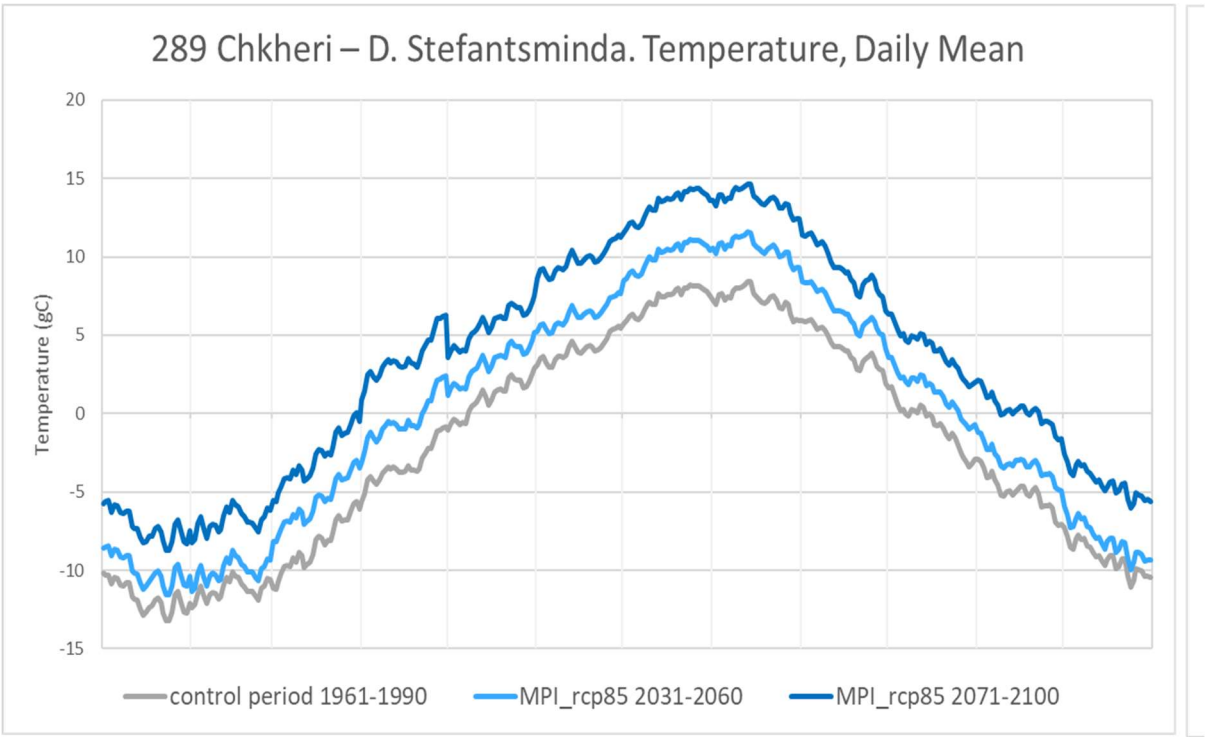

Figure A-13. Daily mean temperature in the control period, 1961-1990 (grey line), the near future, 2031-2060 (light blue line) and the end of the century, 2071-2100 (dark blue line), according to the climate projection MPI, for the station 289 Chkheri - D. Stefantsminda.

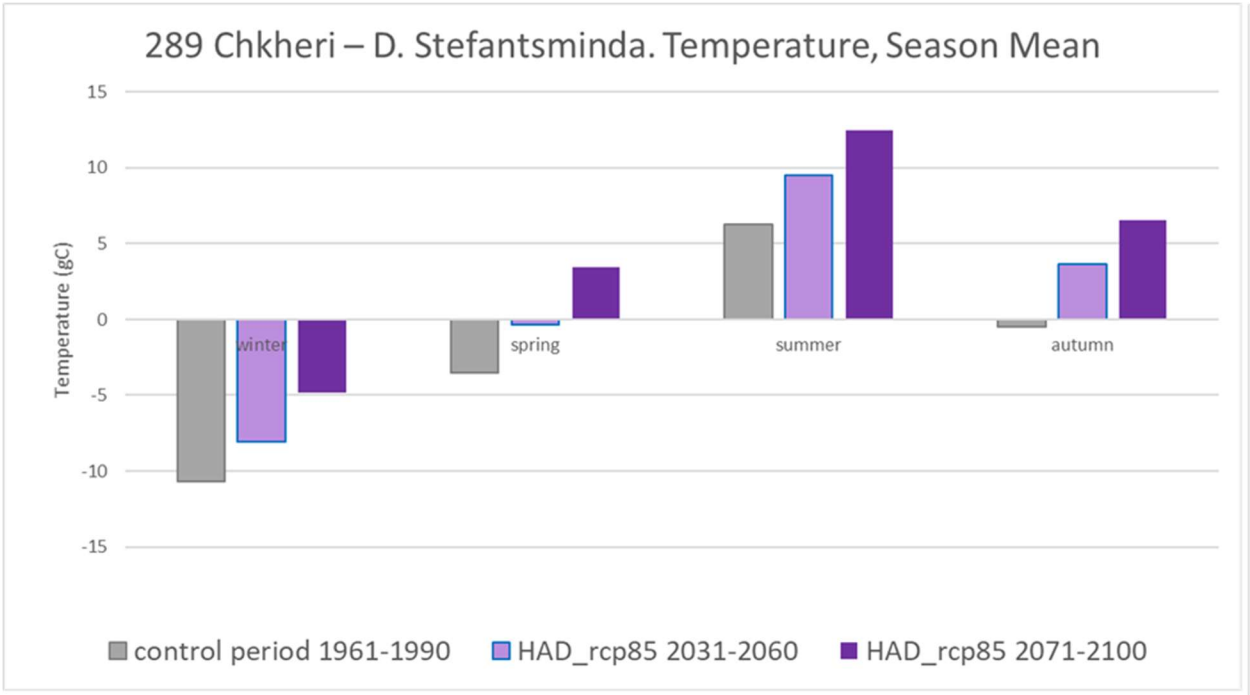

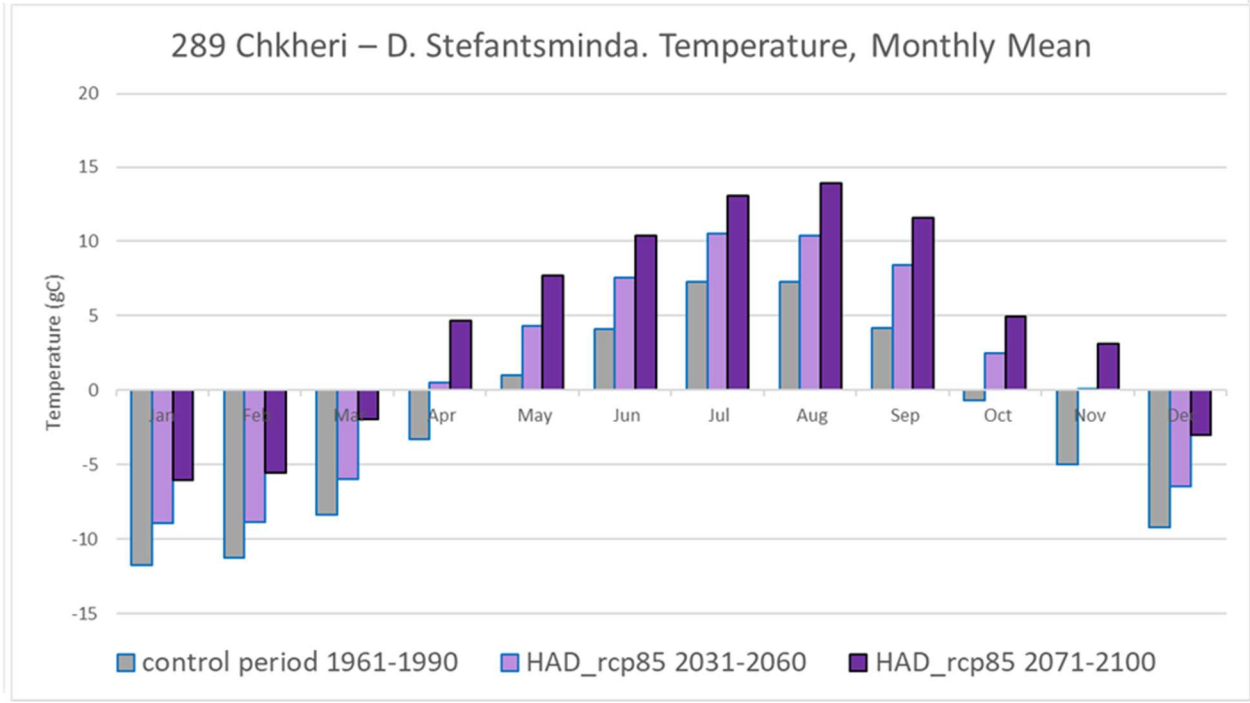

Figure A-14. Season mean (top) and monthly mean (bottom) temperature in the control period, 1961-1990 (grey bars), the near future, 2031-2060 (light purple bars) and the end of the century, 2071-2100 (dark purple bars), according to the climate projection HAD, for the station 289 Chkheri - D. Stefantsminda.

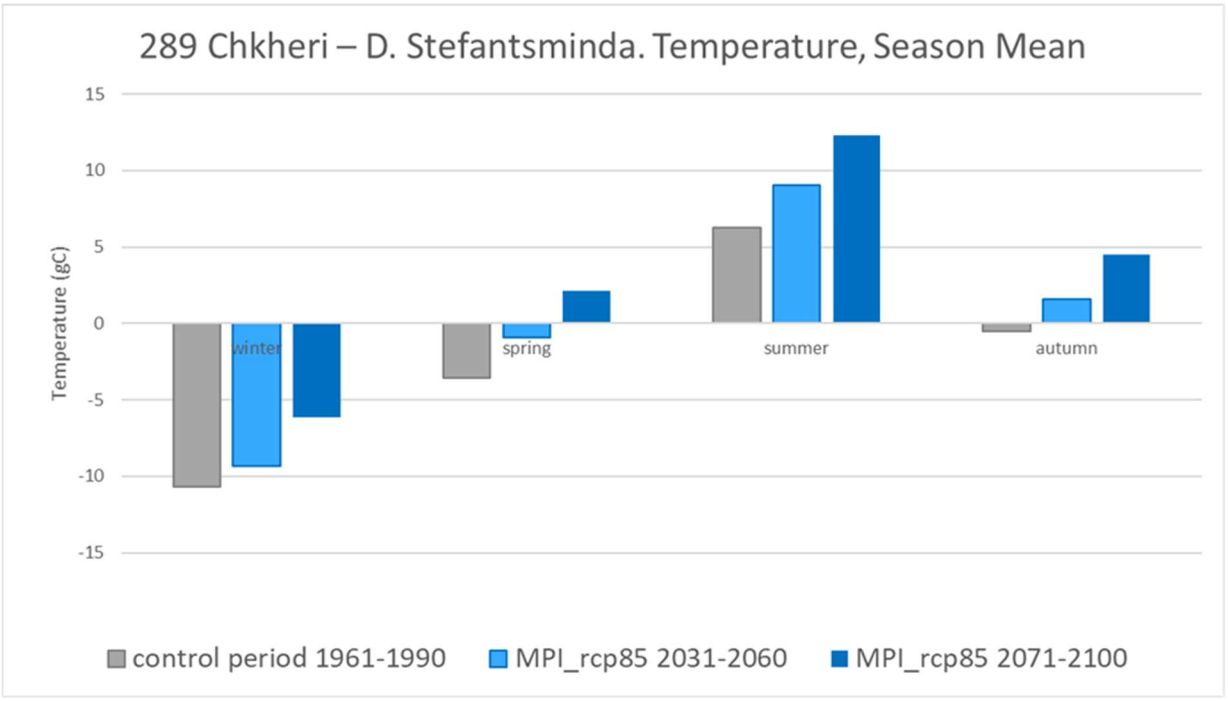

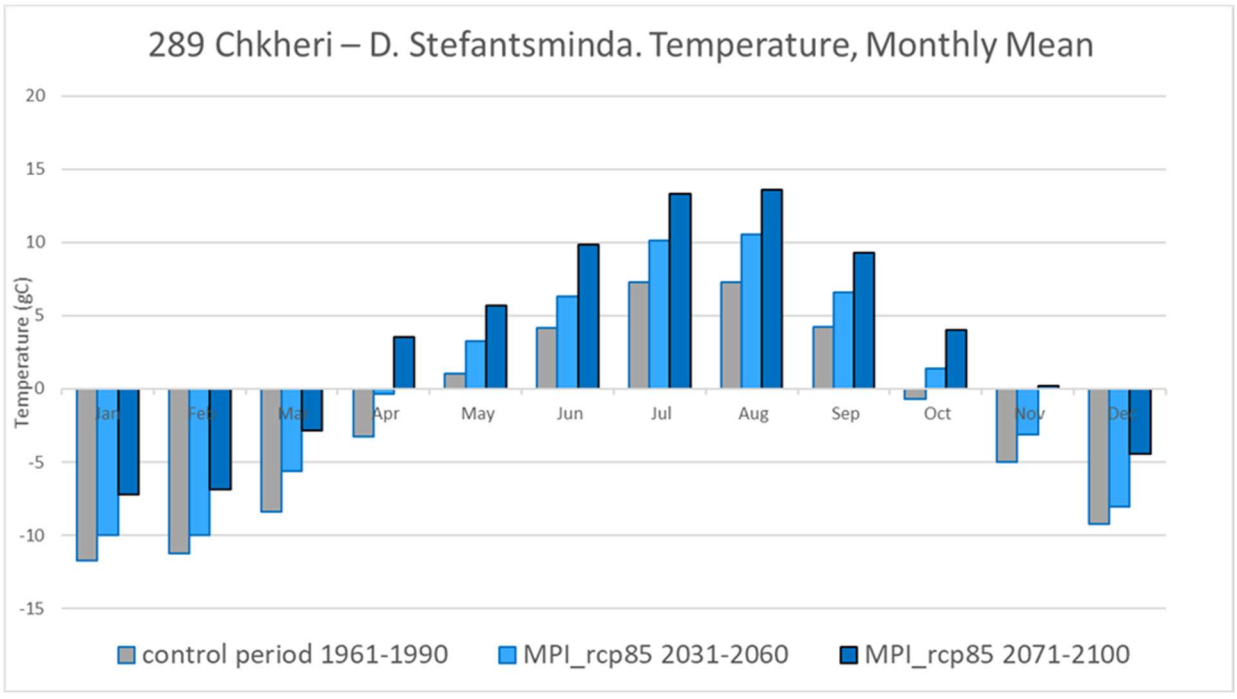

Figure A-15. Season mean (top) and monthly mean (bottom) temperature in the control period, 1961-1990 (grey l bars, the near future, 2031-2060 (light blue bars) and the end of the century, 2071-2100 (dark blue bars), according to the climate projection MPI, for the station 289 Chkheri - D. Stefantsminda.

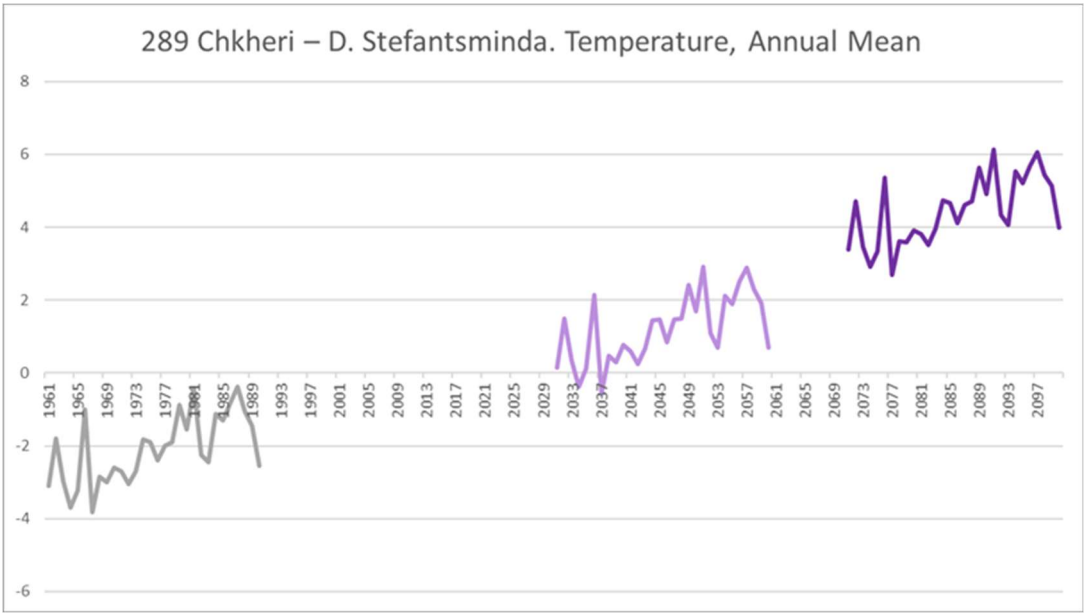

Figure A-16. Annual mean temperatures in the control period, 1961-1990 (grey line), the near future, 2031-2060 (light purple line) and the end of the century, 2071-2100 (dark purple line), according to the climate projection HAD, for the station 289 Chkheri - D. Stefantsminda.

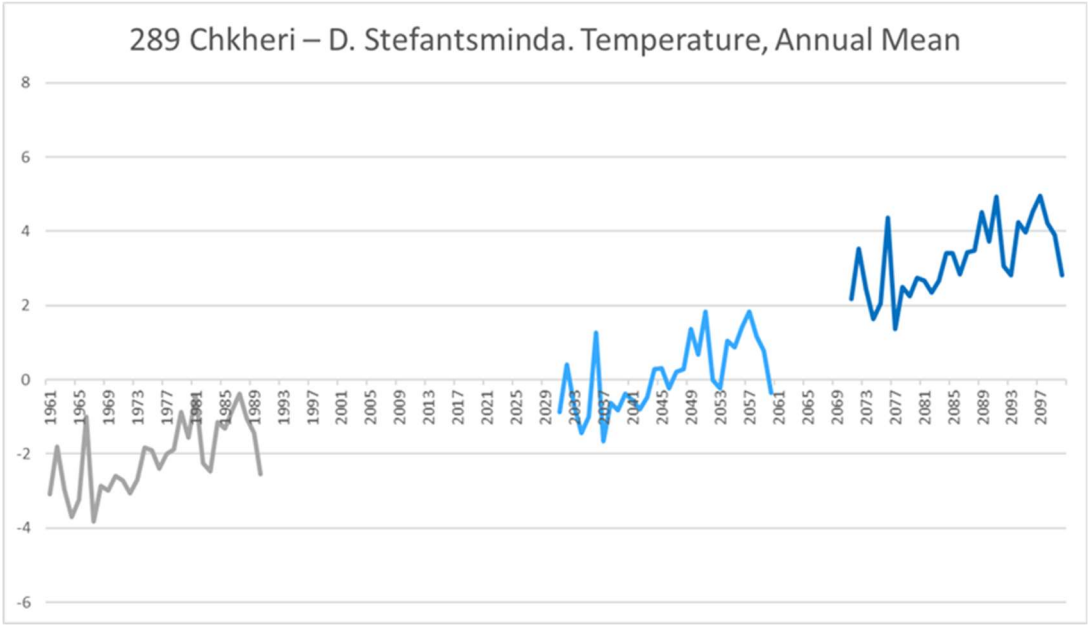

Figure A-17. Annual mean temperatures in the control period, 1961-1990 (grey line), the near future, 2031-2060 (light blue line) and the end of the century, 2071-2100 (dark blue line), according to the climate projection MPI, for the station 289 Chkheri - D. Stefantsminda.

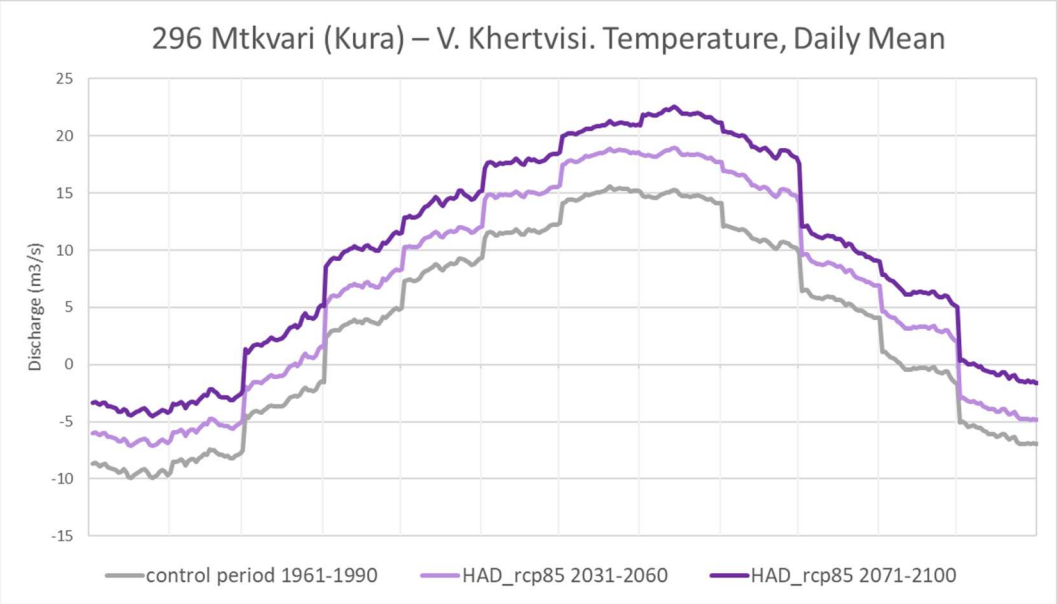

Figure A-18. Daily mean temperaure in the control period, 1961-1990 (grey line), the near future, 2031-2060 (light purple line) and the end of the century, 2071-2100 (dark purple line), according to the climate projection HAD, for the station 296 Mtkvari (Kura) – V. Khertvisi.

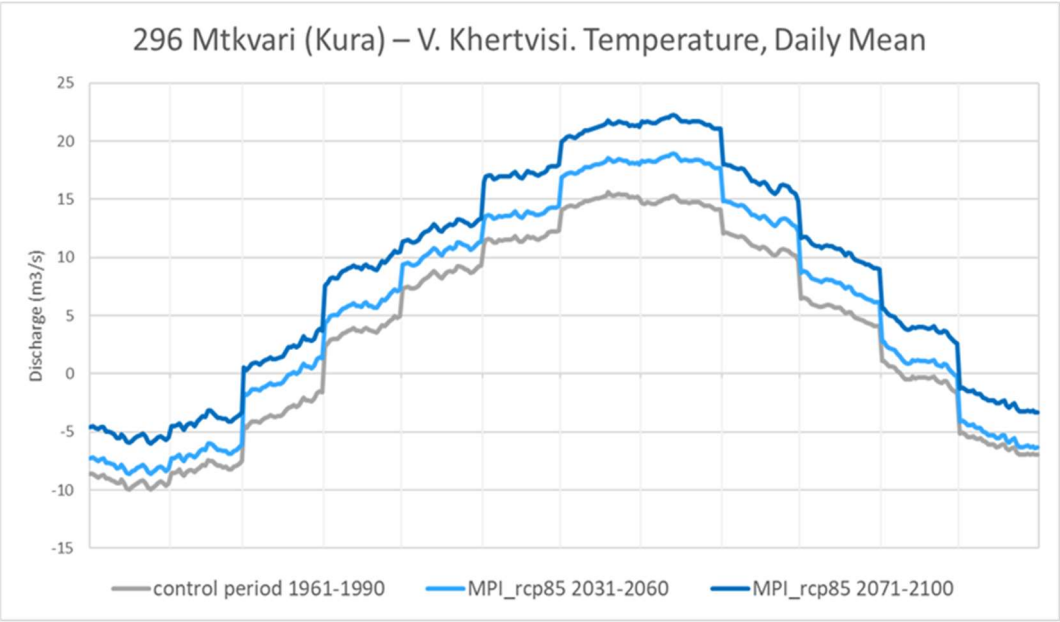

Figure A-19. Daily mean temperaure in the control period, 1961-1990 (grey line), the near future, 2031-2060 (light blue line) and the end of the century, 2071-2100 (dark blue line), according to the climate projection MPI, for the station 296 Mtkvari (Kura) – V. Khertvisi.

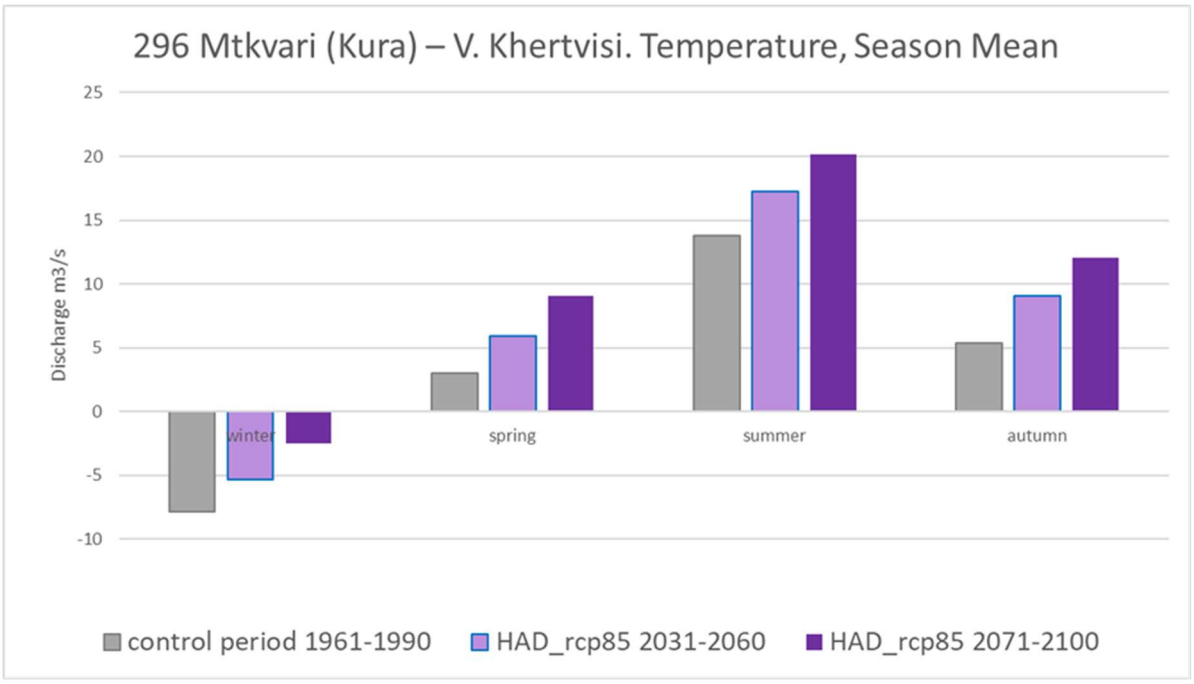

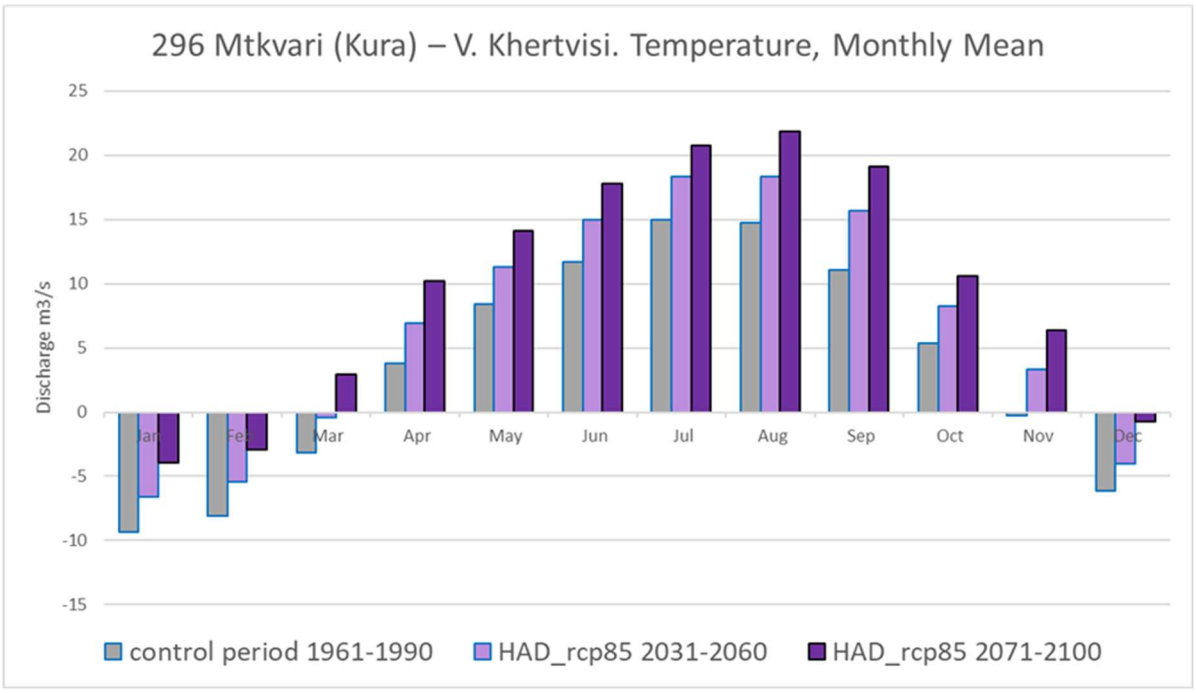

Figure A-20, Season mean (top) and monthly mean (bottom) temperature in the control period, 1961-1990 (grey bars), the near future, 2031-2060 (light purple bars) and the end of the century, 2071-2100 (dark purple bars), according to the climate projection HAD, for 296 Mtkvari (Kura) – V. Khertvisi.

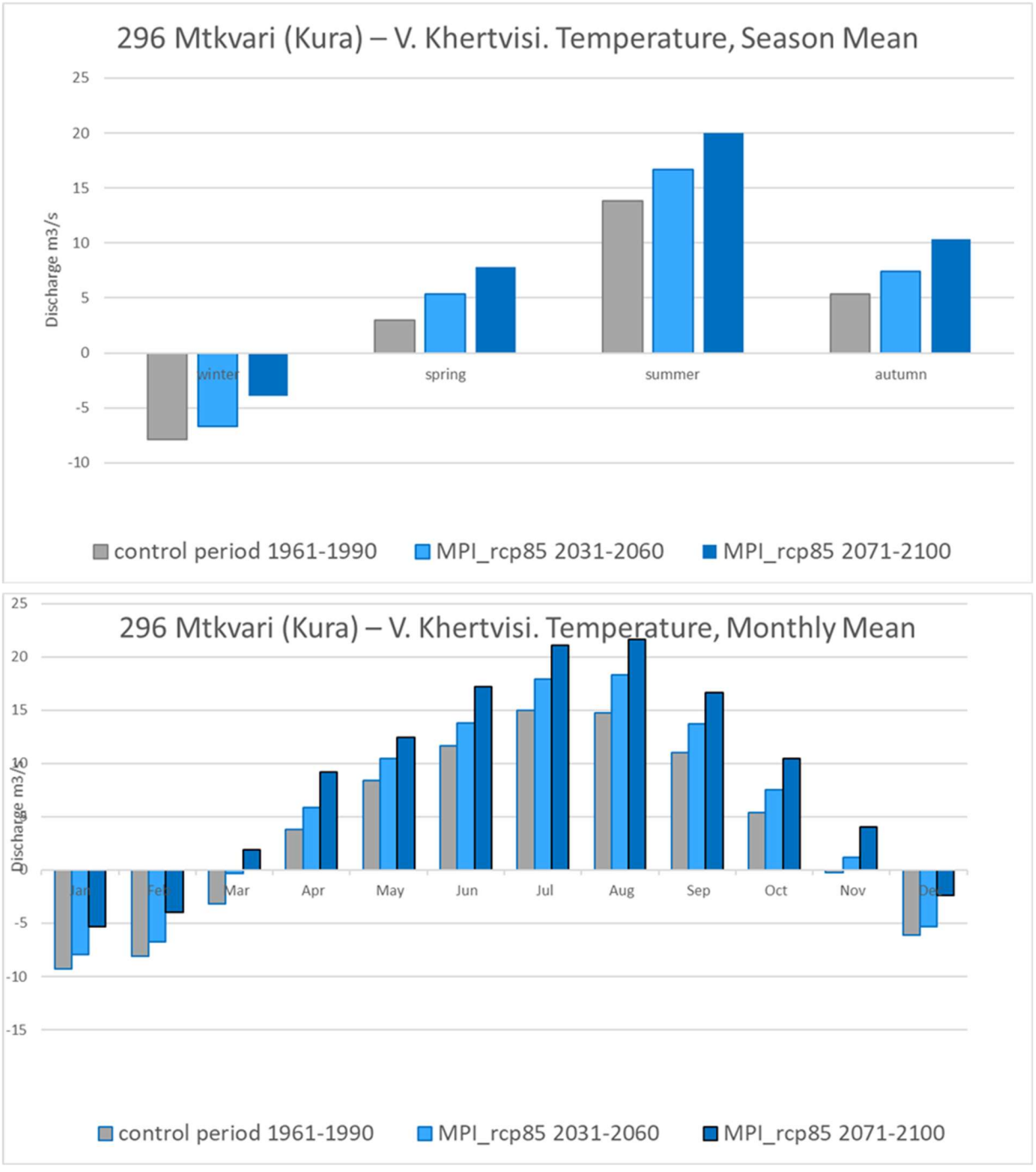

Figure A-21. Season mean (top) and monthly mean (bottom) temperature in the control period, 1961-1990 (grey bars), the near future, 2031-2060 (light blue bars) and the end of the century, 2071-2100 (dark blue bars), according to the climate projection MPI, for 296 Mtkvari (Kura) – V. Khertvisi.

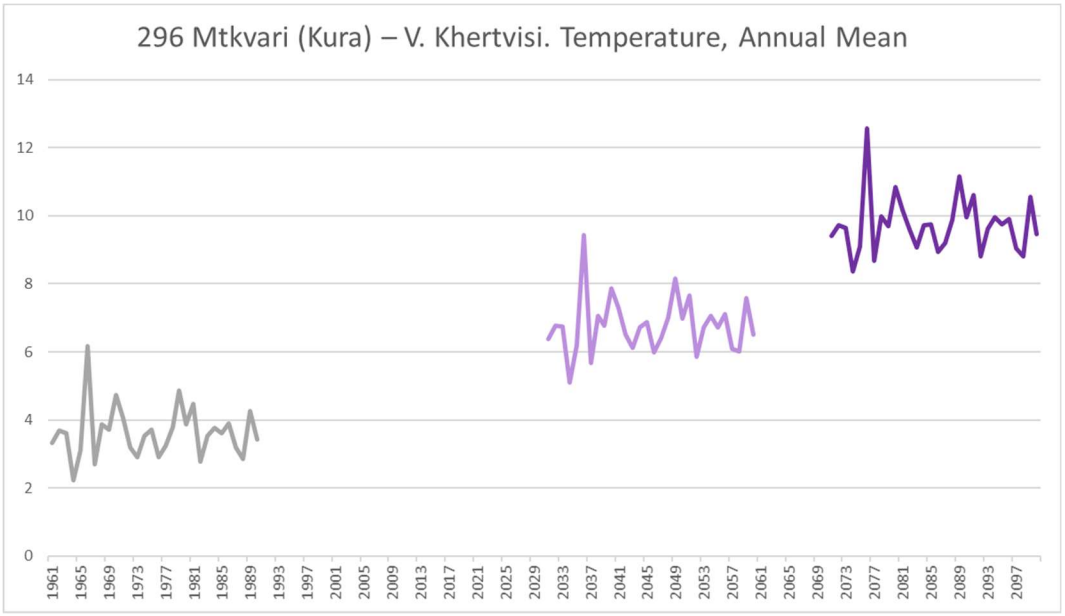

Figure A-22. Annual mean temperatures in the control period, 1961-1990 (grey line), the near future, 2031-2060 (light purple line) and the end of the century, 2071-2100 (dark purple line), according to the climate projection HAD, for the station 296 Mtkvari (Kura) – V. Khertvisi.

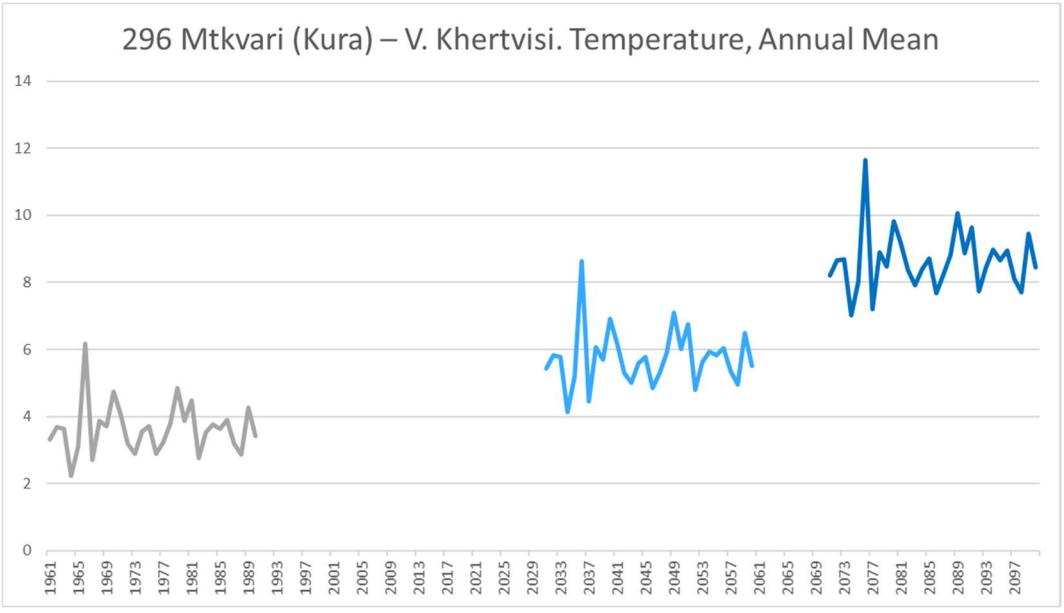

Figure A-23. Annual mean temperatures in the control period, 1961-1990 (grey line), the near future, 2031-2060 (light blue line) and the end of the century, 2071-2100 (dark blue line), according to the climate projection MPI, for the station 296 Mtkvari (Kura) – V. Khertvisi.

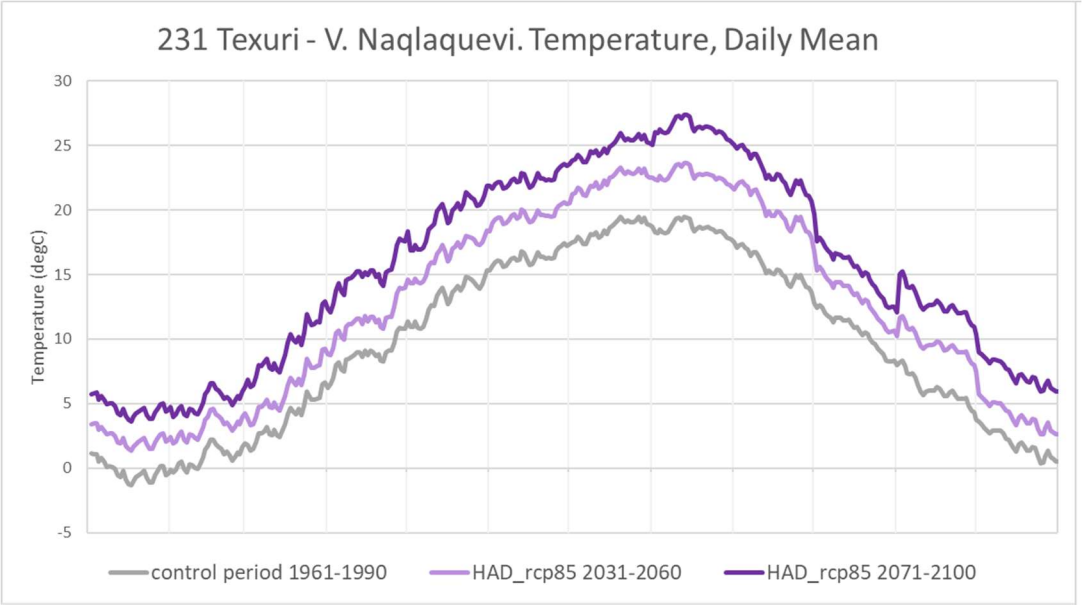

Figure A-24. Daily mean temperature in the control period, 1961-1990 (grey line), the near future, 2031-2060 (light purple line) and the end of the century, 2071-2100 (dark purple line), according to the climate projection HAD, for the station 231 Texuri - V. Naqlaquevi.

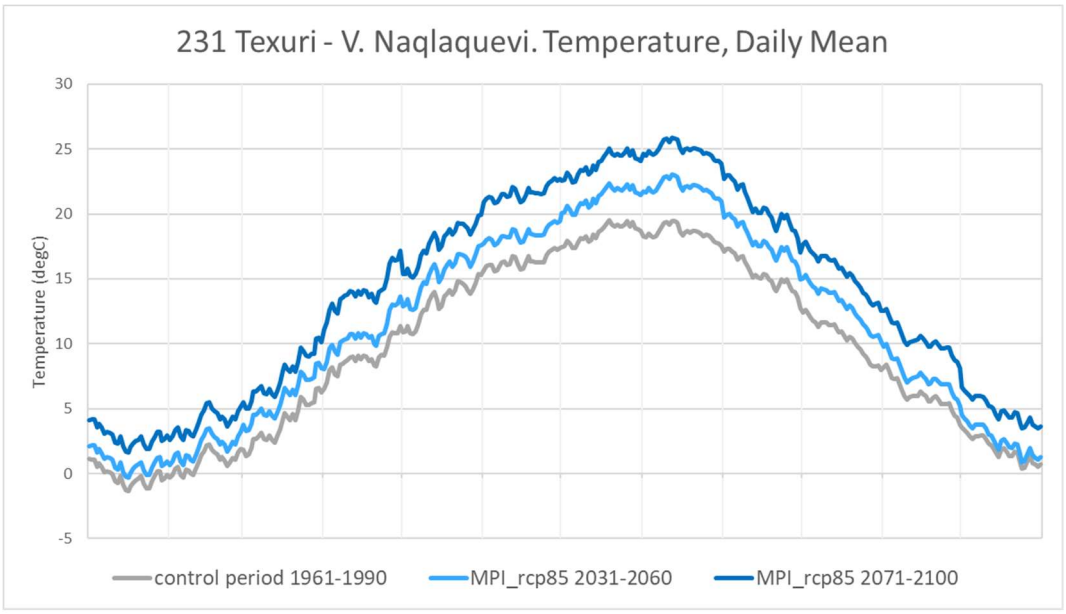

Figure A-25. Daily mean temperature in the control period, 1961-1990 (grey line), the near future, 2031-2060 (light blue line) and the end of the century, 2071-2100 (dark blue line), according to the climate projection MPI, for the station 231 Texuri - V. Naqlaquevi.

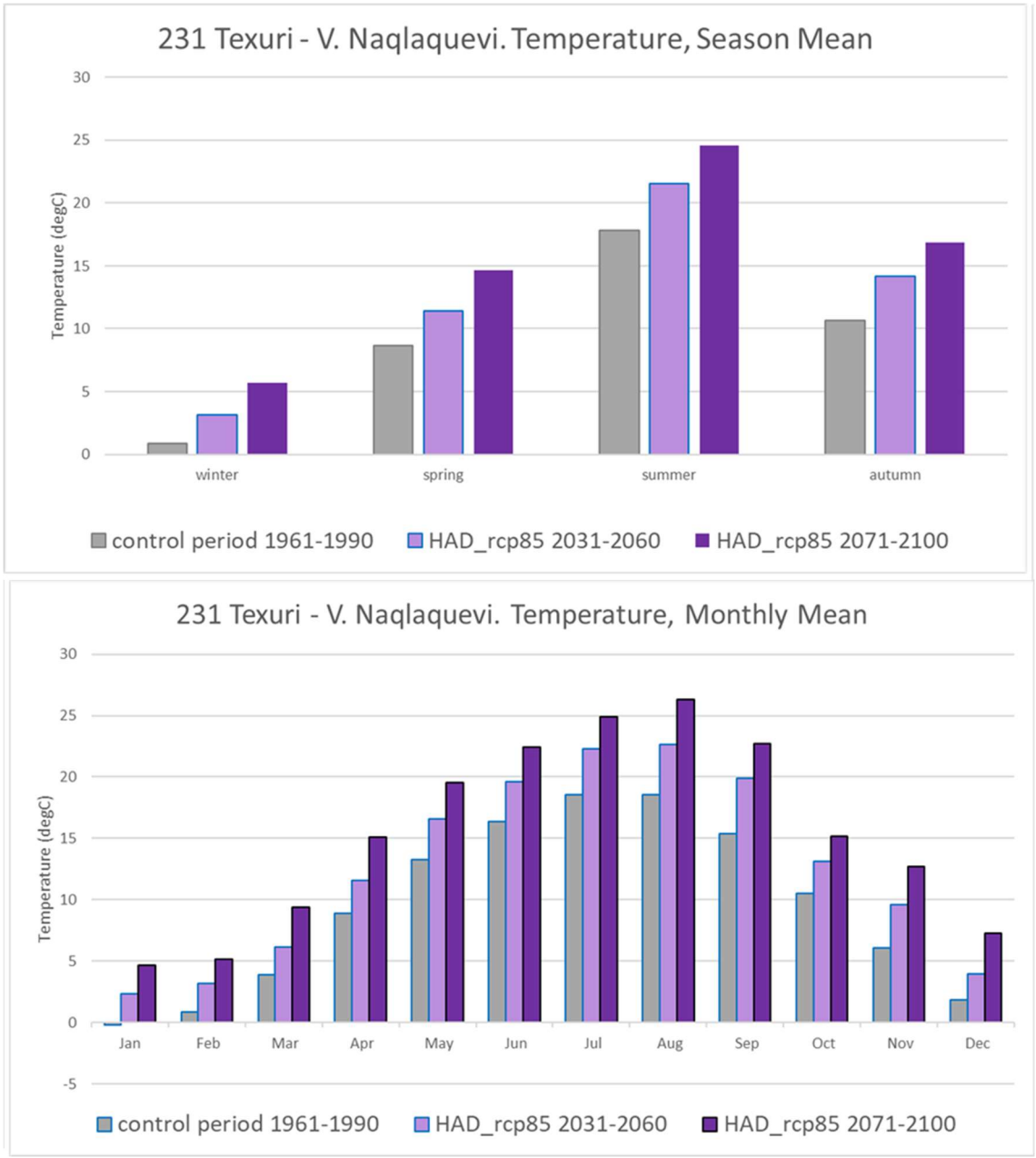

Figure A-26. Season mean (top) and monthly mean (bottom) temperature in the control period, 1961-1990 (grey bars), the near future, 2031-2060 (light purple bars) and the end of the century, 2071-2100 (dark purple bars), according to the climate projection HAD, for 231 Texuri - V. Naqlaquevi.

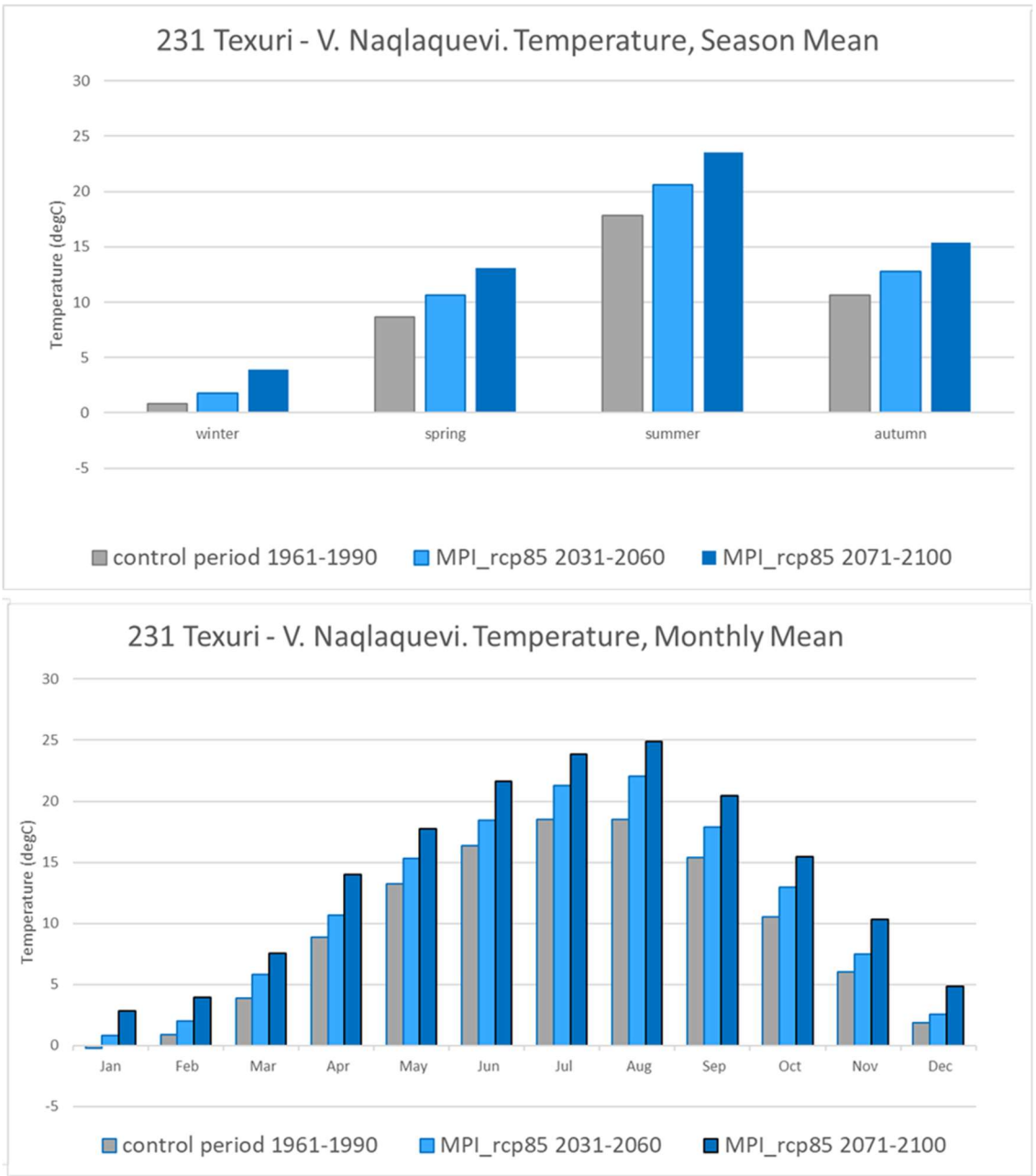

Figure A-27. Season mean (top) and monthly mean (bottom) temperature in the control period, 1961-1990 (grey line), the near future, 2031-2060 (light blue line) and the end of the century, 2071-2100 (dark blue line), according to the climate projection HAD, for 231 Texuri - V. Naqlaquevi.

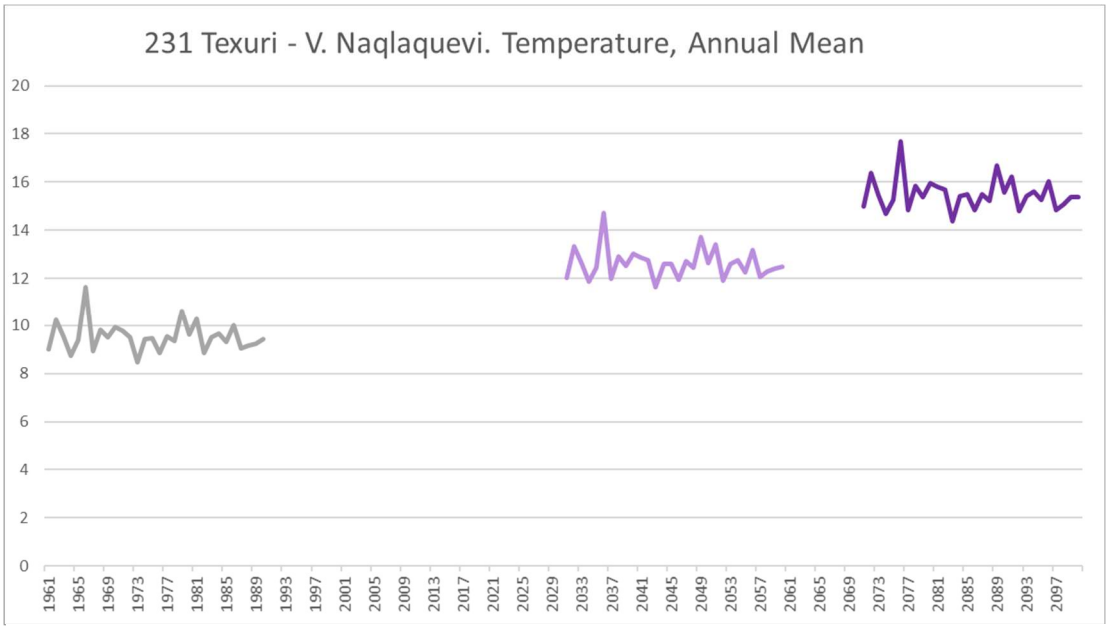

Figure A-28. Annual mean temperatures in the control period, 1961-1990 (grey line), the near future, 2031-2060 (light purple line) and the end of the century, 2071-2100 (dark purple line), according to the climate projection HAD, for the station 231 Texuri - V. Naqlaquevi.

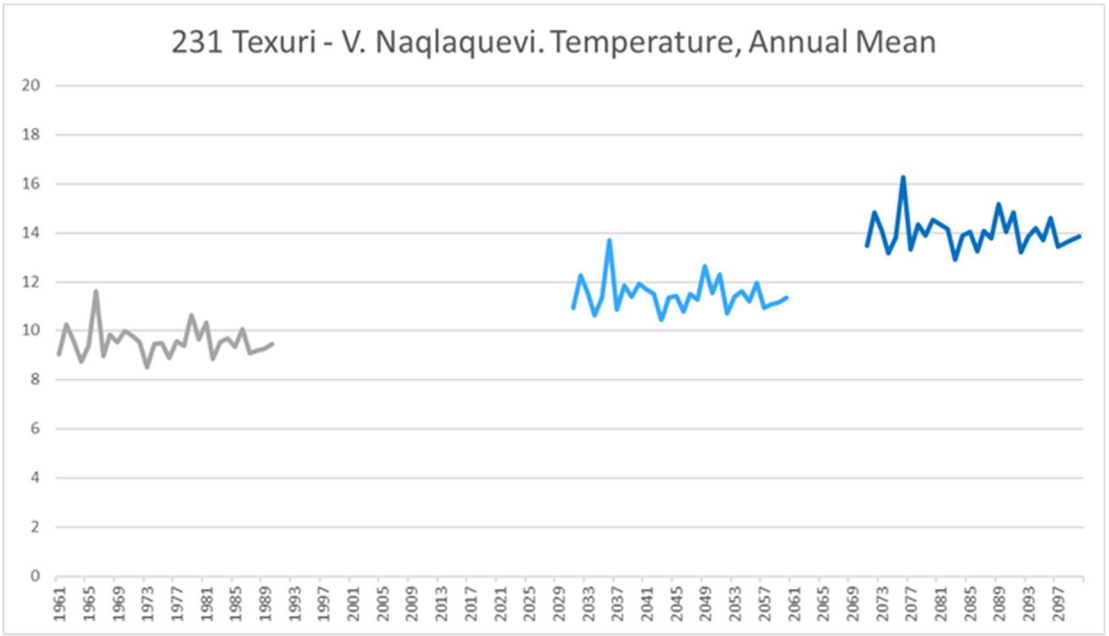

Figure A-29. Annual mean temperatures in the control period, 1961-1990 (grey line), the near future, 2031-2060 (light blue line) and the end of the century, 2071-2100 (dark blue line), according to the climate projection MPI, for the station 231 Texuri - V. Naqlaquevi.

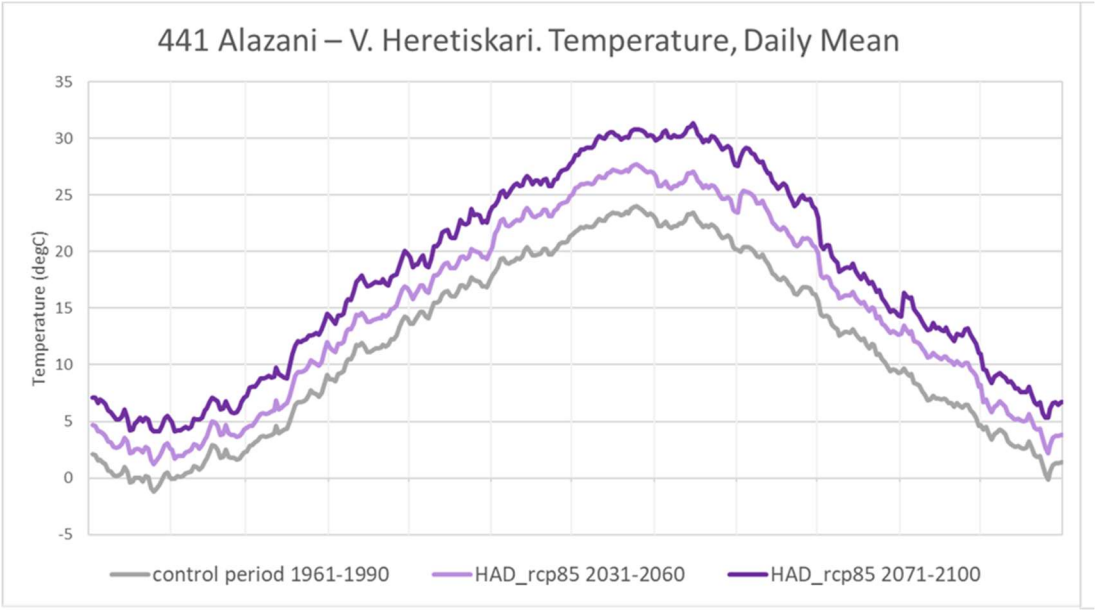

Figure A-30. Daily mean temperature in the control period, 1961-1990 (grey line), the near future, 2031-2060 (light purple line) and the end of the century, 2071-2100 (dark purple line), according to the climate projection HAD, for the station 441 Alazani – V. Heretiskari.

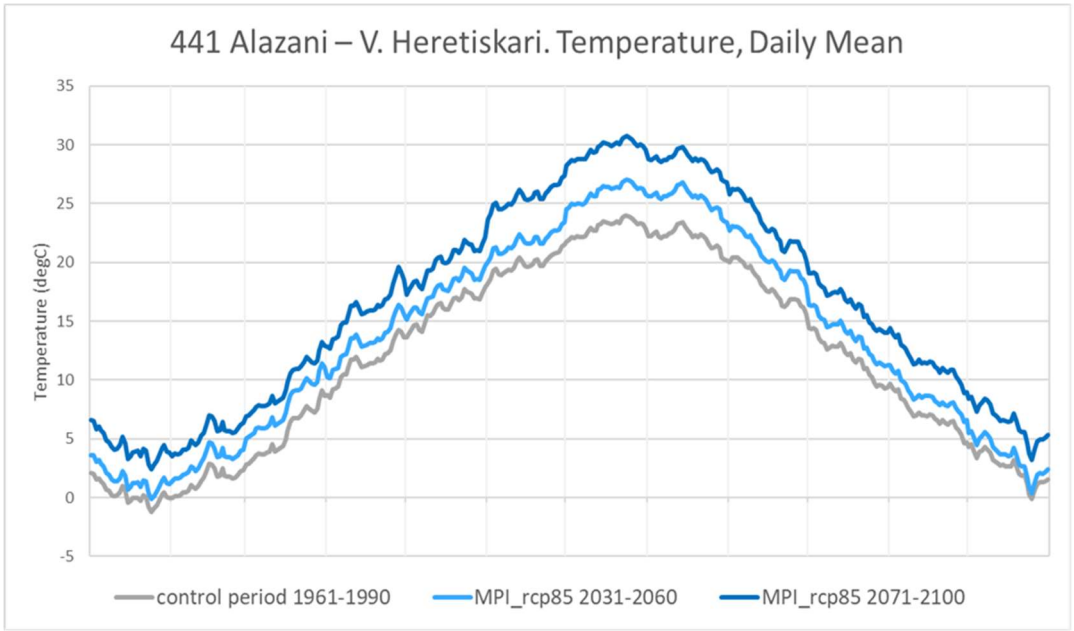

Figure A-31. Daily mean temperature in the control period, 1961-1990 (grey line), the near future, 2031-2060 (light blue line) and the end of the century, 2071-2100 (dark blue line), according to the climate projection MPI, for the station 441 Alazani – V. Heretiskari.

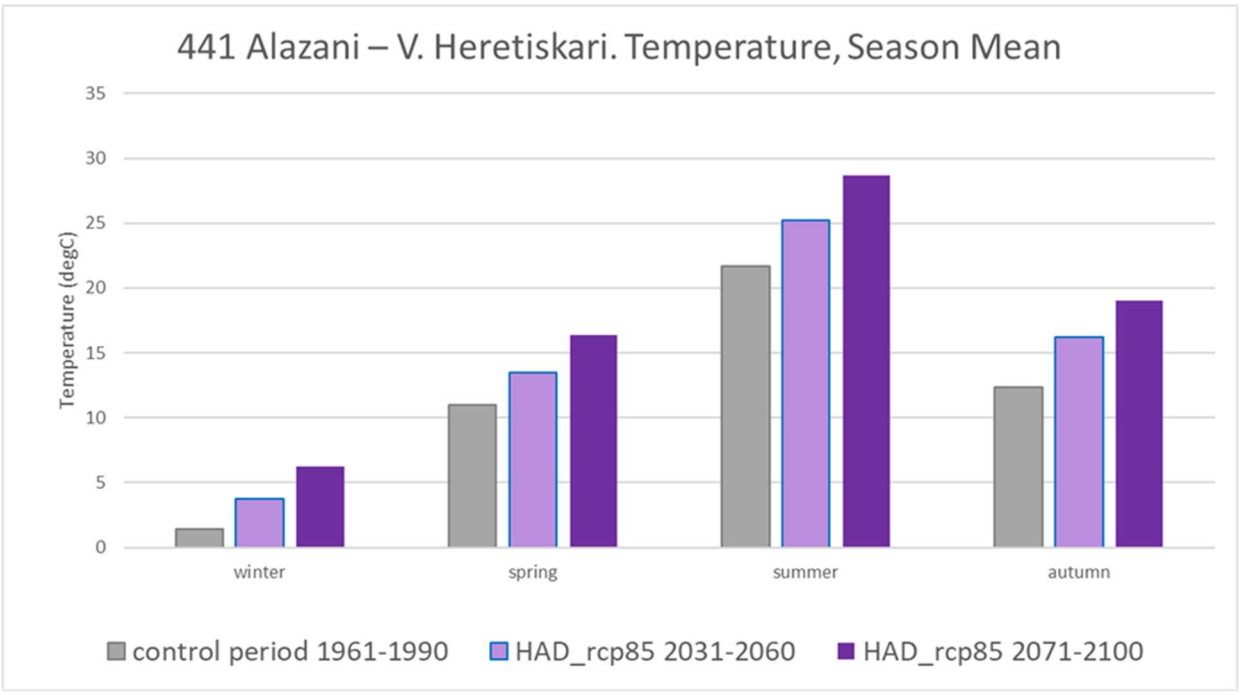

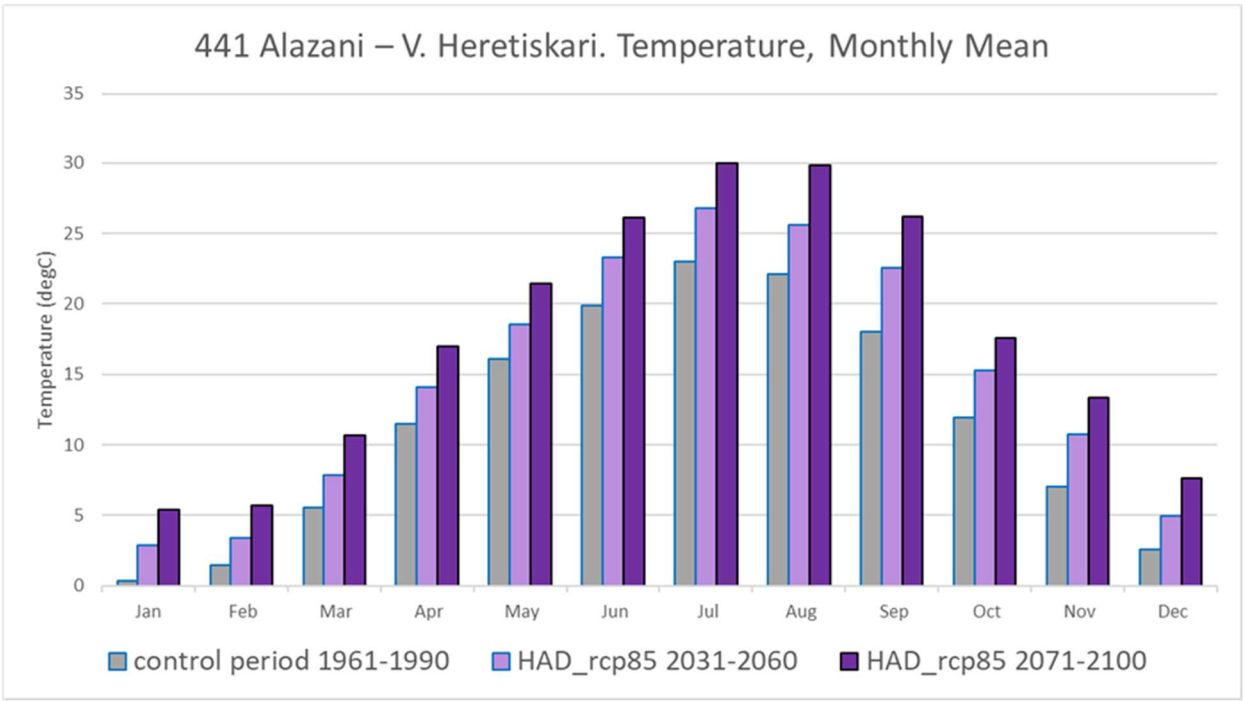

Figure A-32. Season mean (top) and monthly mean (bottom) temperature in the control period, 1961-1990 (grey bars), the near future, 2031-2060 (light purple bars) and the end of the century, 2071-2100 (dark purple bars), according to the climate projection HAD, for 441 Alazani – V. Heretiskari.

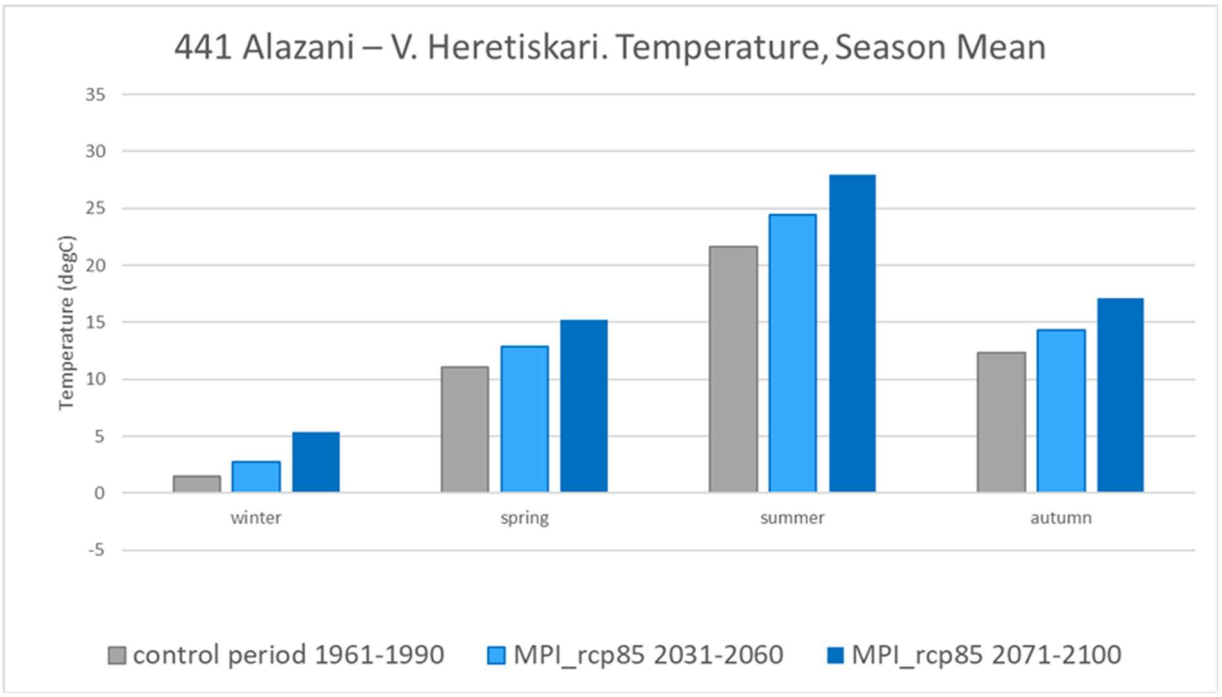

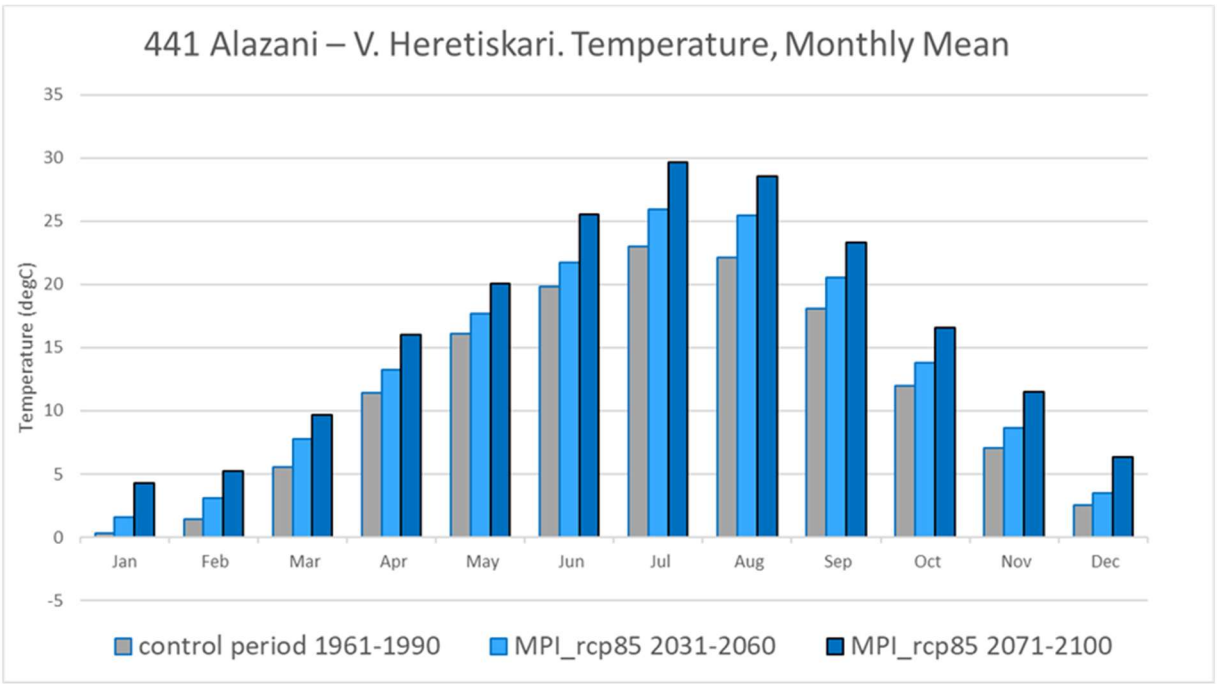

Figure A-33. Season mean (top) and monthly mean (bottom) temperature in the control period, 1961-1990 (grey bars), the near future, 2031-2060 (light blue bars) and the end of the century, 2071-2100 (dark blue bars), according to the climate projection MPI, for 441 Alazani – V. Heretiskari.

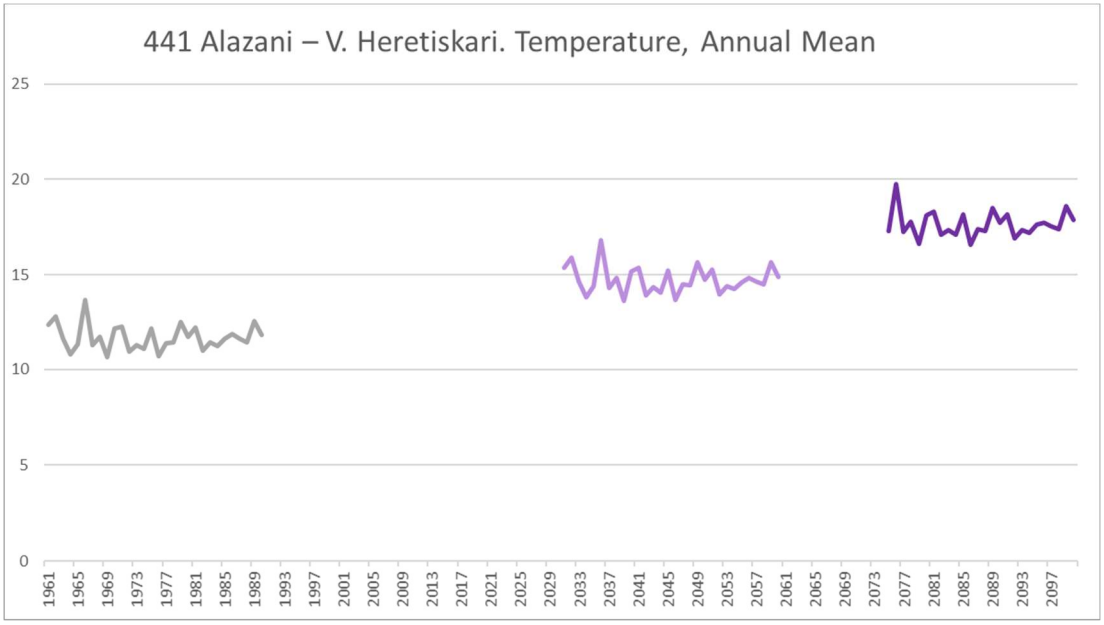

Figure A-34. Annual mean temperatures in the control period, 1961-1990 (grey line), the near future, 2031-2060 (light purple line) and the end of the century, 2071-2100 (dark purple line), according to the climate projection HAD, for the station 441 Alazani – V. Heretiskari.

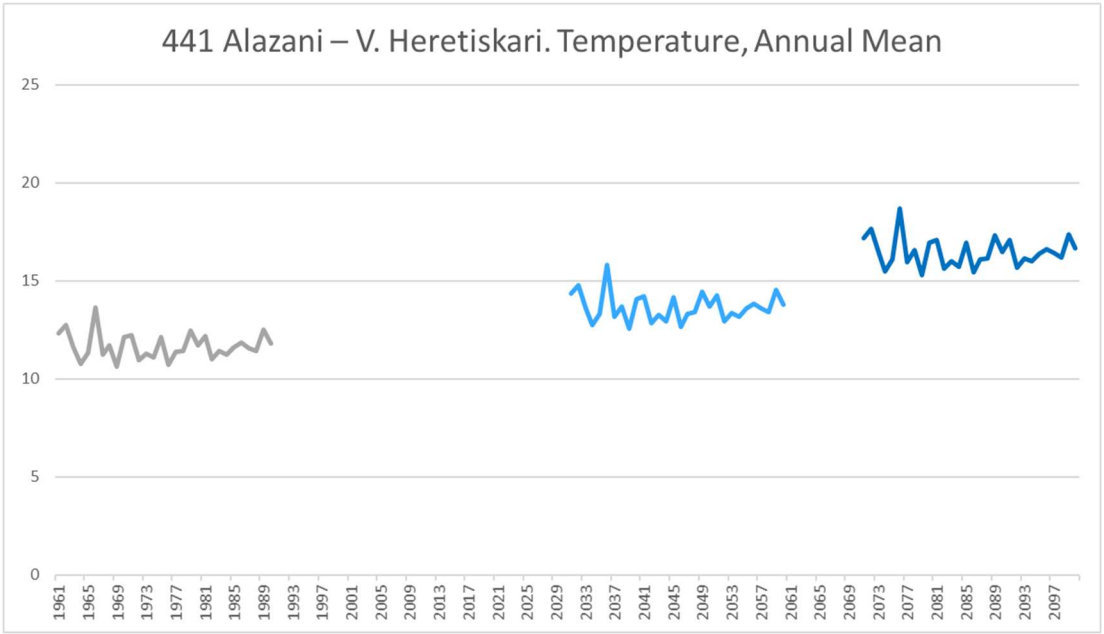

Figure A-35 Annual mean temperatures in the control period, 1961-1990 (grey line), the near future, 2031-2060 (light blue line) and the end of the century, 2071-2100 (dark blue line), according to the climate projection MPI, for the station 441 Alazani – V. Heretiskari.

Precipitation

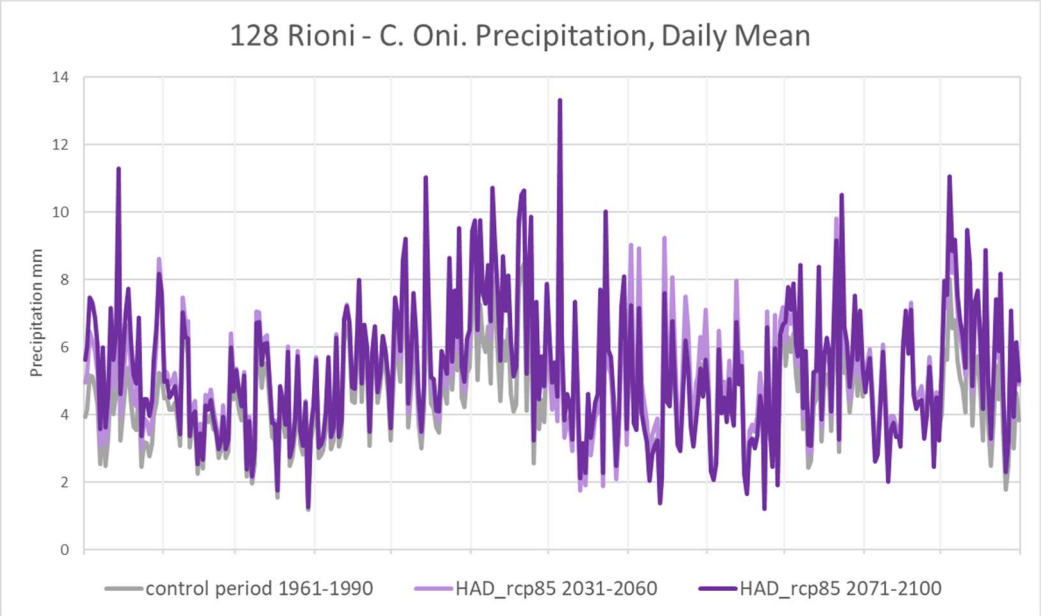

Figure A-36. Daily mean precipitation in the control period, 1961-1990 (grey line), the near future, 2031-2060 (light purple line) and the end of the century, 2071-2100 (dark purple line), according to the climate projection HAD, for the station 128 Rioni - C. Oni.

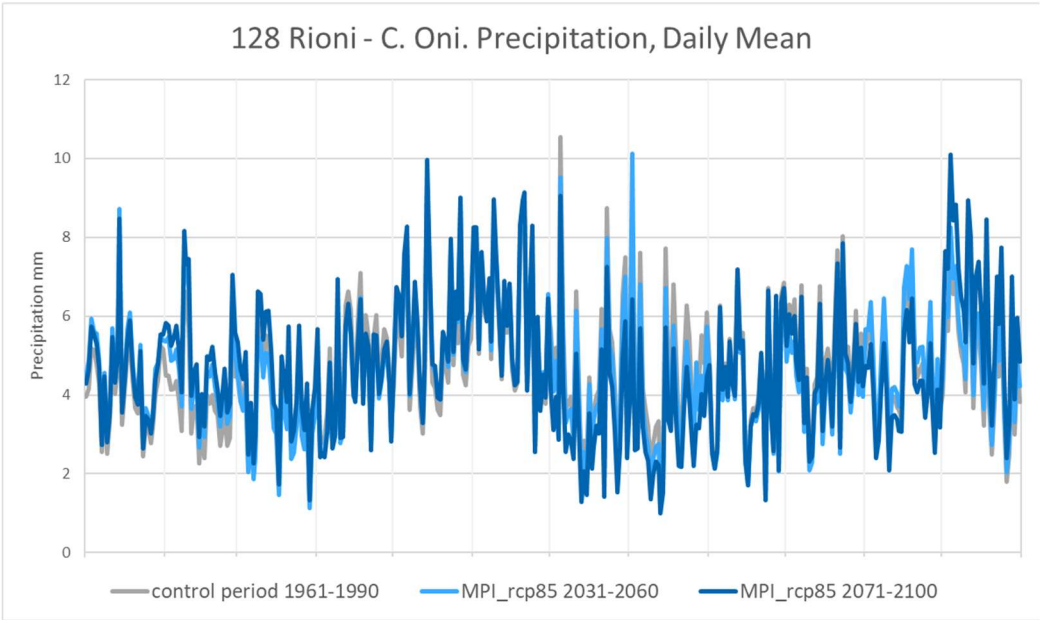

Figure A-37. Daily mean precipitation in the control period, 1961-1990 (grey line), the near future, 2031-2060 (light blue line) and the end of the century, 2071-2100 (dark blue line), according to the climate projection MPI, for the station 128 Rioni - C. Oni.

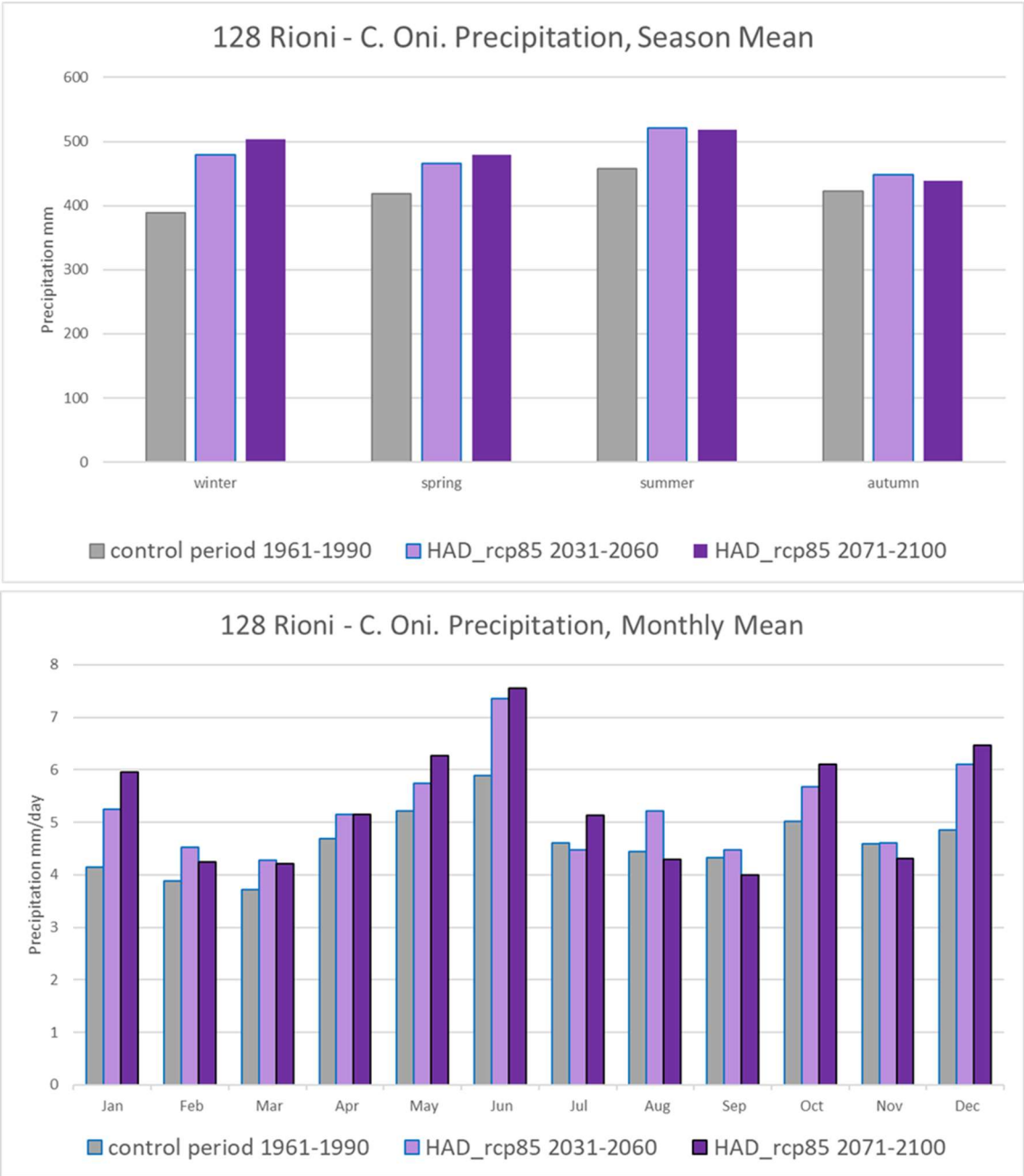

Figure A-38. Season mean (top) and monthly mean (bottom) precipitation in the control period, 1961-1990 (grey bars), the near future, 2031-2060 (light purple bars) and the end of the century, 2071-2100 (dark purple bars), according to the climate projection HAD, for the station 128 Rioni - C. Oni.

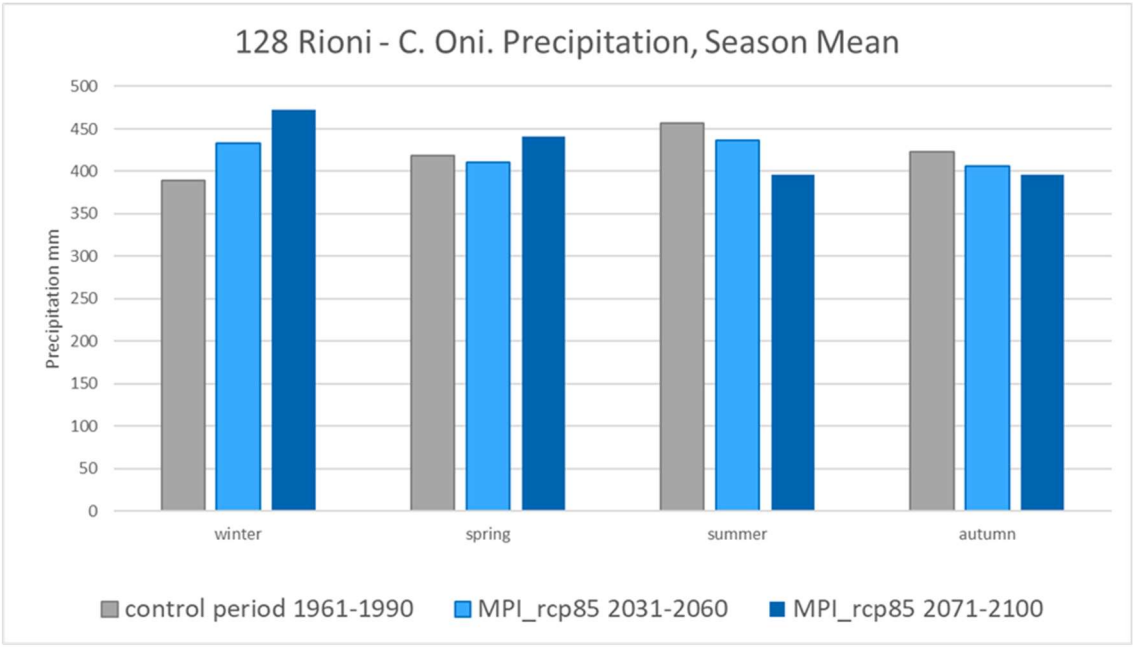

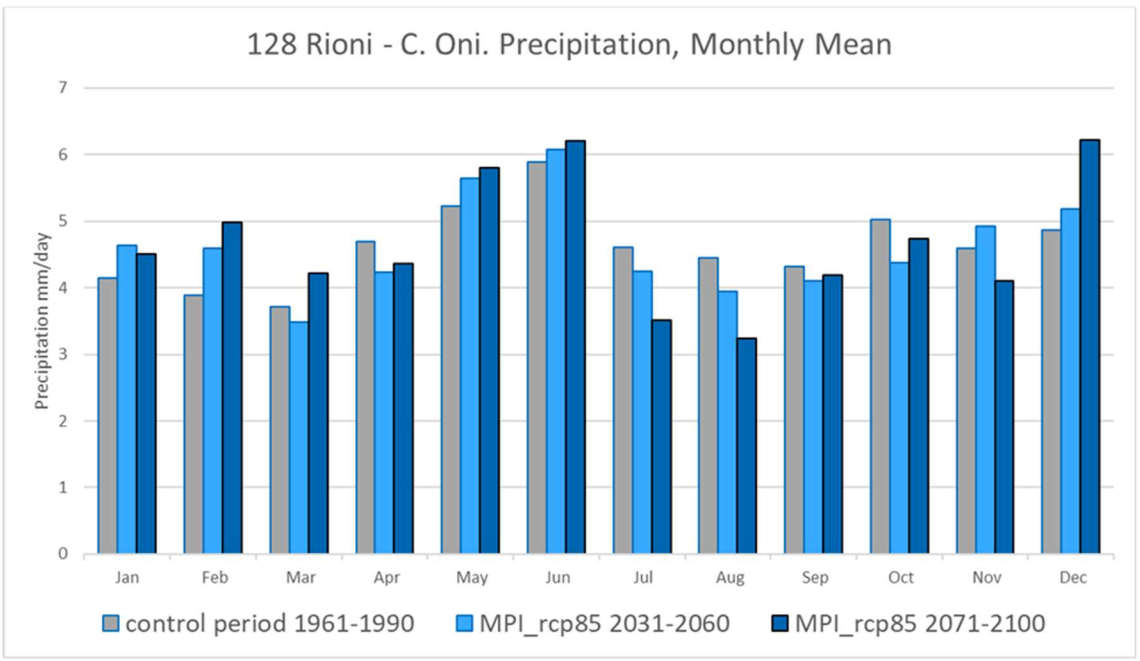

Figure A-39. Season mean (top) and monthly mean (bottom) precipitation in the control period, 1961-1990 (grey bars), the near future, 2031-2060 (light blue bars) and the end of the century, 2071-2100 (dark blue bars), according to the climate projection MPI, for the station 128 Rioni - C. Oni.

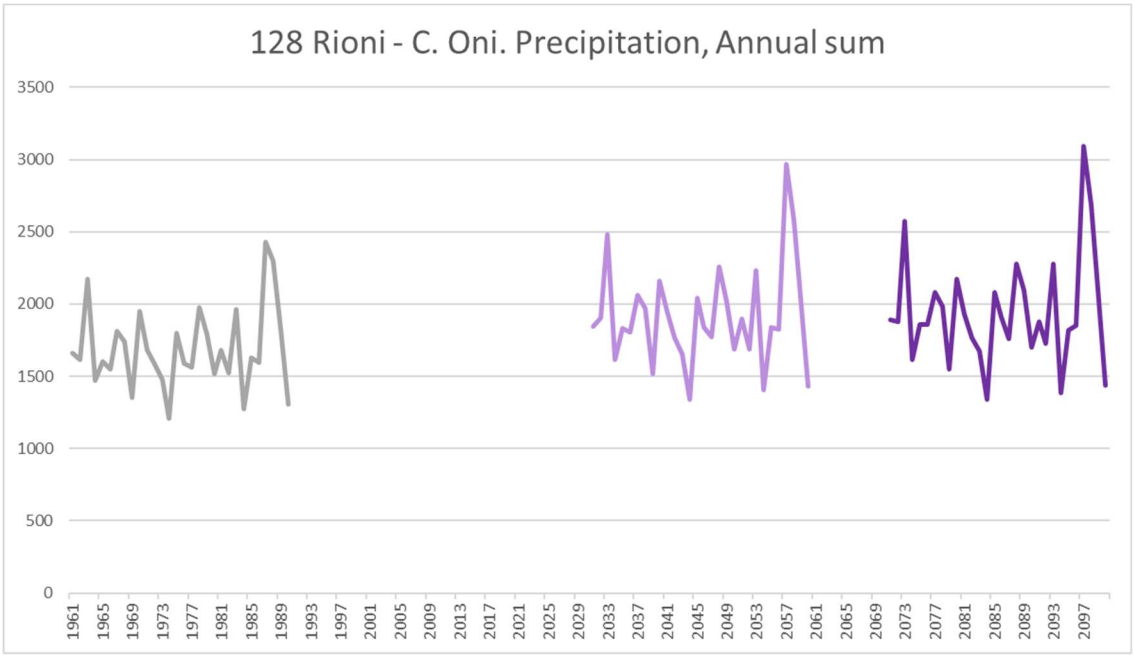

Figure A-40. Annual precipitation in the control period, 1961-1990 (grey line), the near future, 2031-2060 (light purple line) and the end of the century, 2071-2100 (dark purple line), according to the climate projection HAD, for the station 128 Rioni - C. Oni.

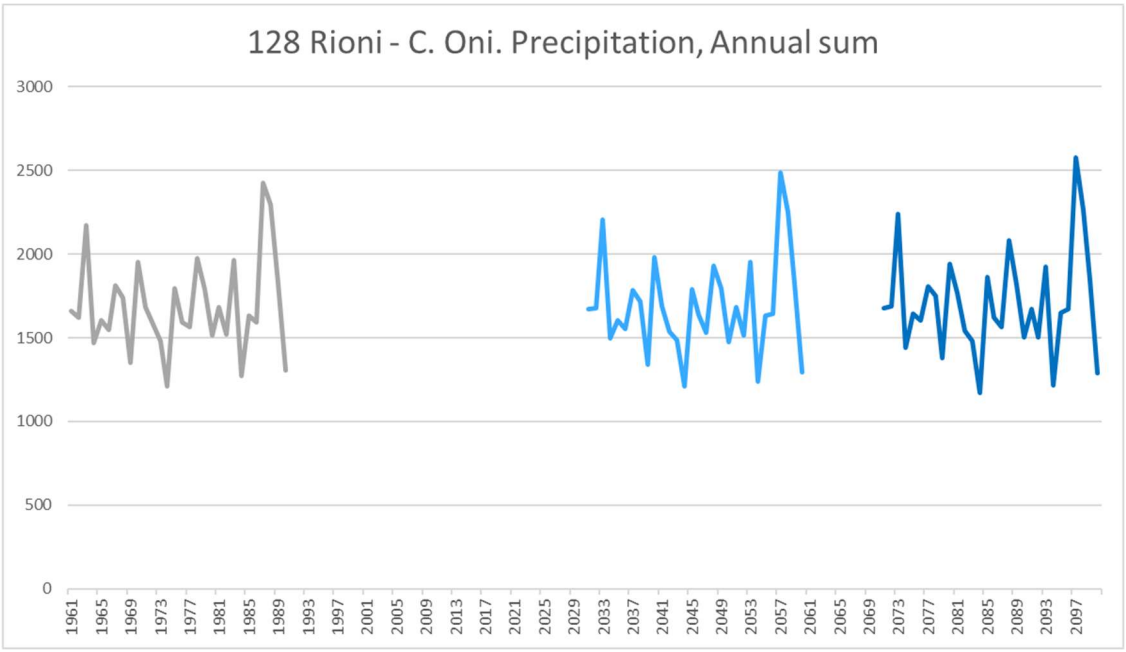

Figure A-41. Annual precipitation in the control period, 1961-1990 (grey line), the near future, 2031-2060 (light blue line) and the end of the century, 2071-2100 (dark blue line), according to the climate projection MPI, for the station 128 Rioni - C. Oni.

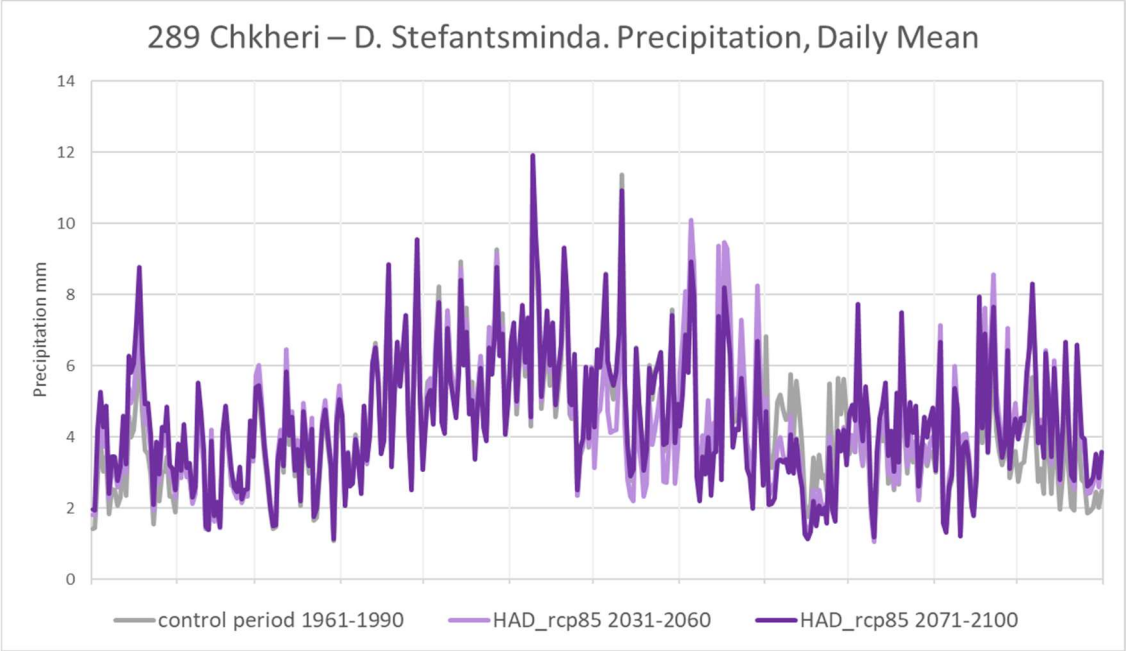

Figure A-42. Daily mean precipitation in the control period, 1961-1990 (grey line), the near future, 2031-2060 (light purple line) and the end of the century, 2071-2100 (dark purple line), according to the climate projection HAD, for the station 289 Chkheri – D. Stefantsminda.

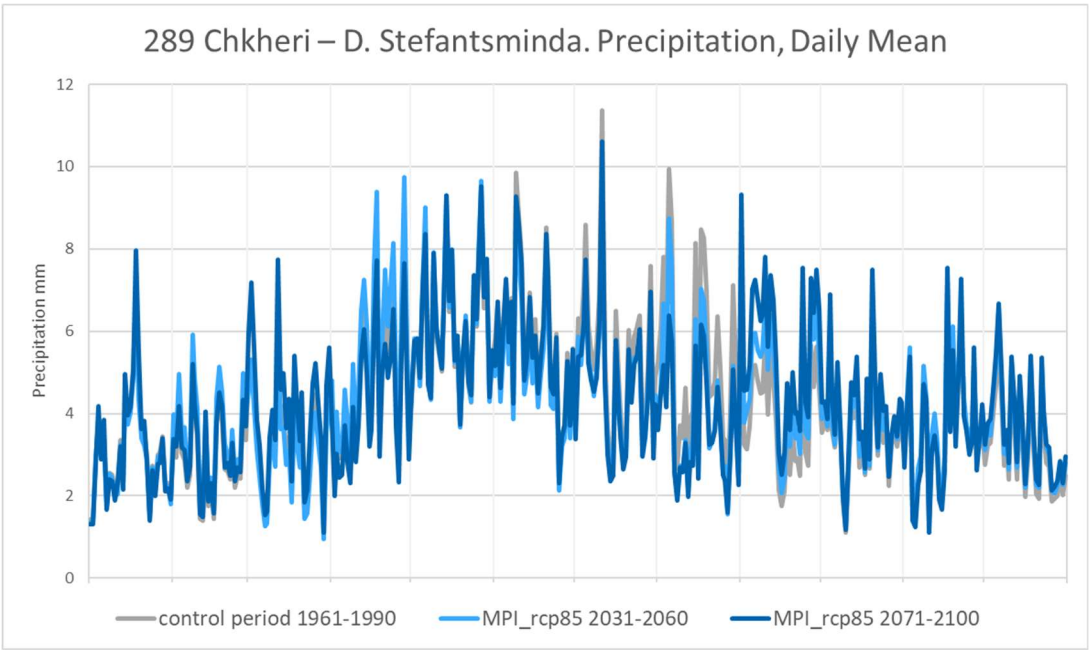

Figure A-43. Daily mean precipitation in the control period, 1961-1990 (grey line), the near future, 2031-2060 (light blue line) and the end of the century, 2071-2100 (dark blue line), according to the climate projection MPI, for the station 289 Chkheri – D. Stefantsminda.

Figure A-44. Season mean (top) and monthly mean (bottom) precipitation in the control period, 1961-1990 (grey bars), the near future, 2031-2060 (light purple bars) and the end of the century, 2071-2100 (dark purple bars), according to the climate projection HAD, for the station 289 Chkheri – D. Stefantsminda.

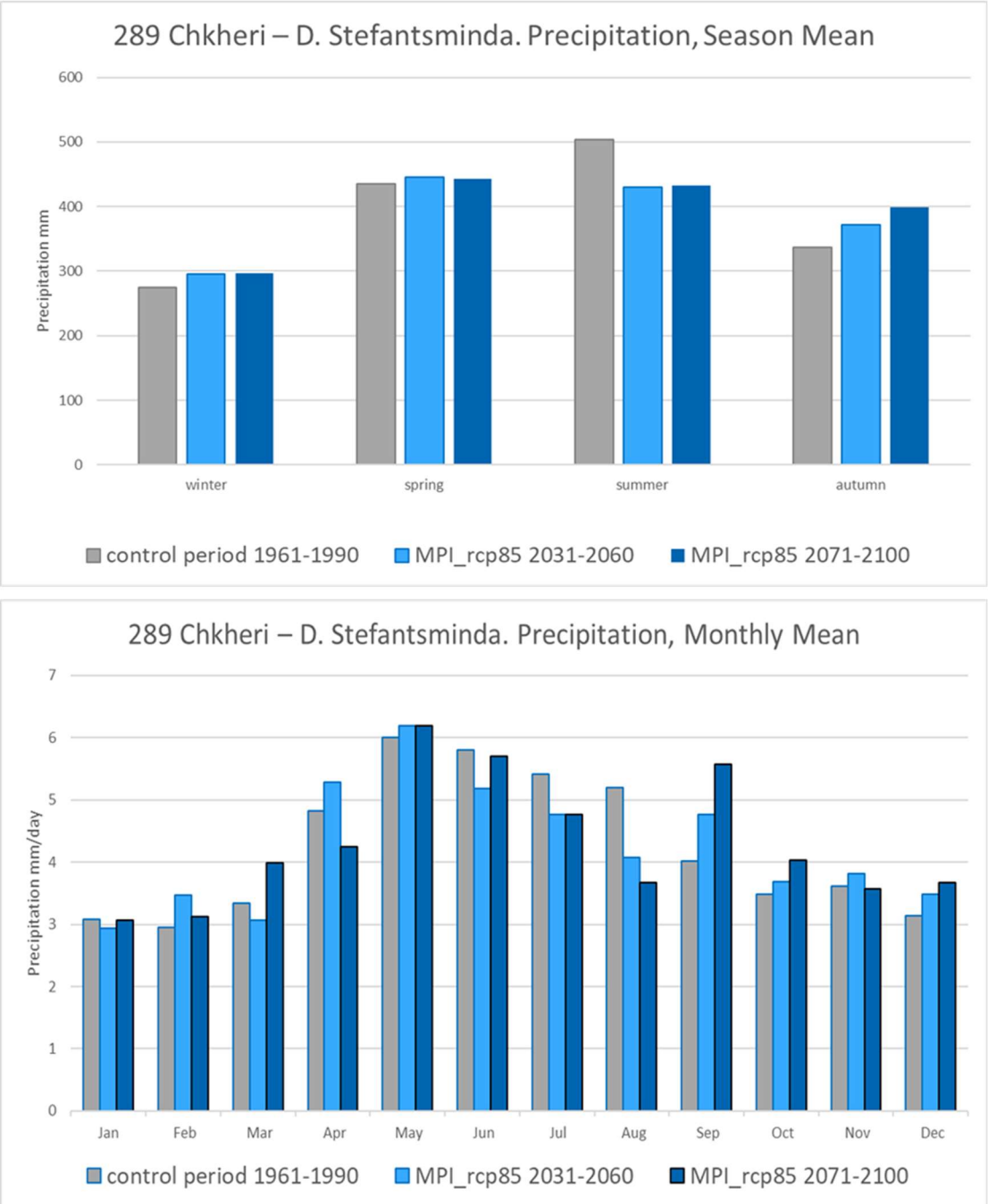

Figure A-45. Season mean (top) and monthly mean (bottom) precipitation in the control period, 1961-1990 (grey bars), the near future, 2031-2060 (light blue bars) and the end of the century, 2071-2100 (dark blue bars), according to the climate projection MPI, for the station 289 Chkheri – D. Stefantsminda.

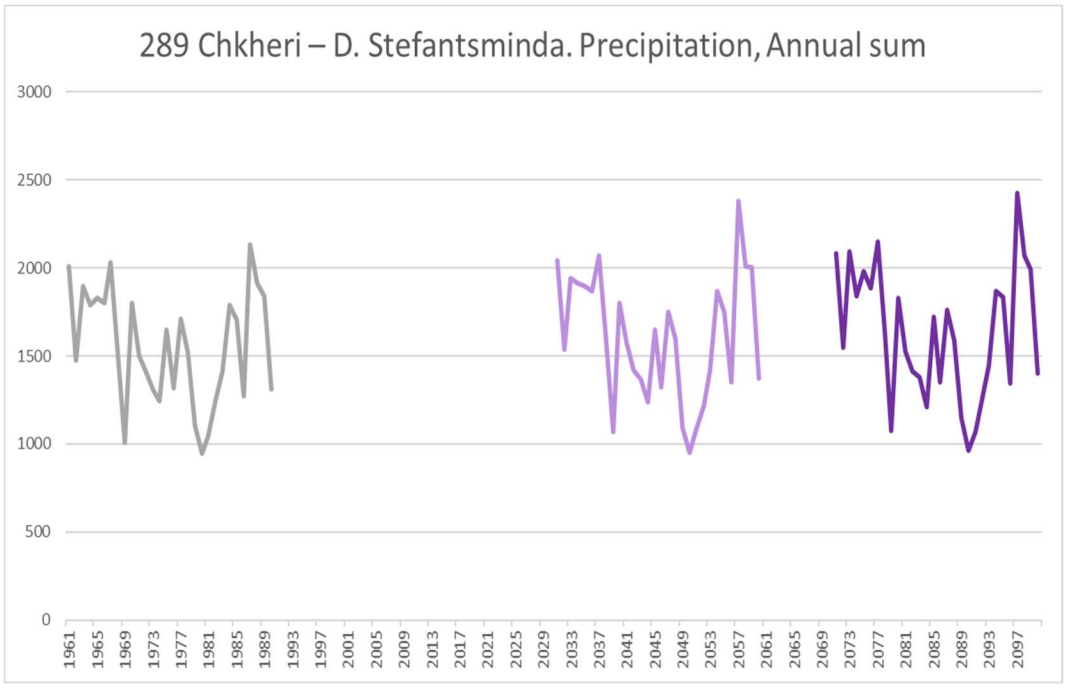

Figure A-46. Annual precipitation in the control period, 1961-1990 (grey line), the near future, 2031-2060 (light purple line) and the end of the century, 2071-2100 (dark purple line), according to the climate projection HAD, for the station 289 Chkheri – D. Stefantsminda.

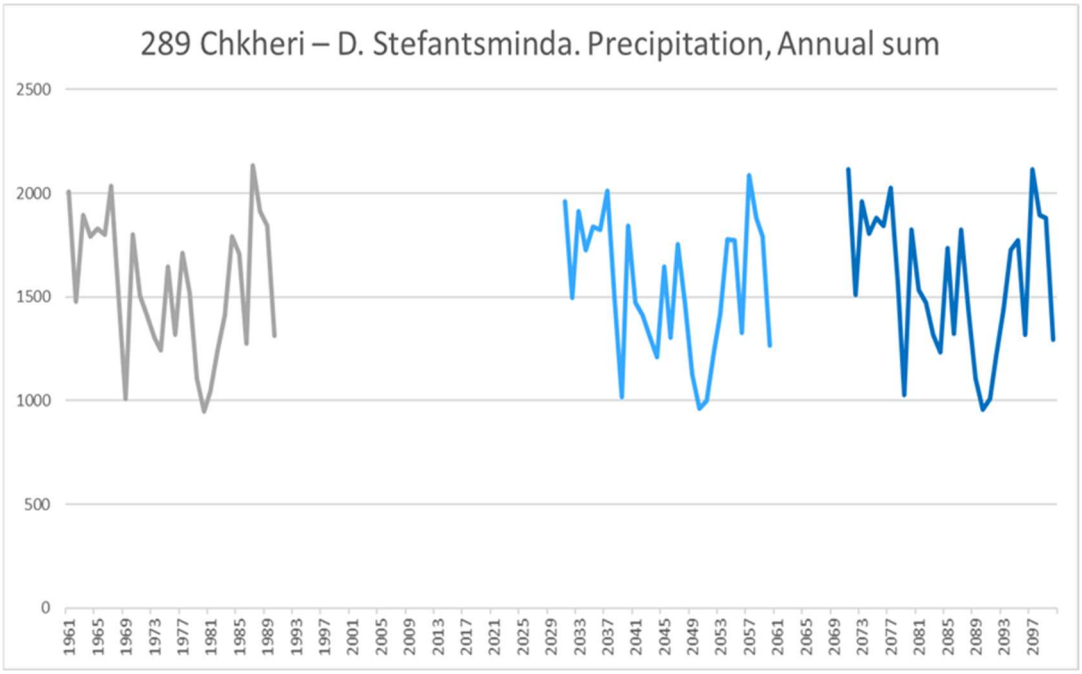

Figure A-47. Annual precipitation in the control period, 1961-1990 (grey line), the near future, 2031-2060 (light blue line) and the end of the century, 2071-2100 (dark blue line), according to the climate projection MPI, for the station 289 Chkheri – D. Stefantsminda.

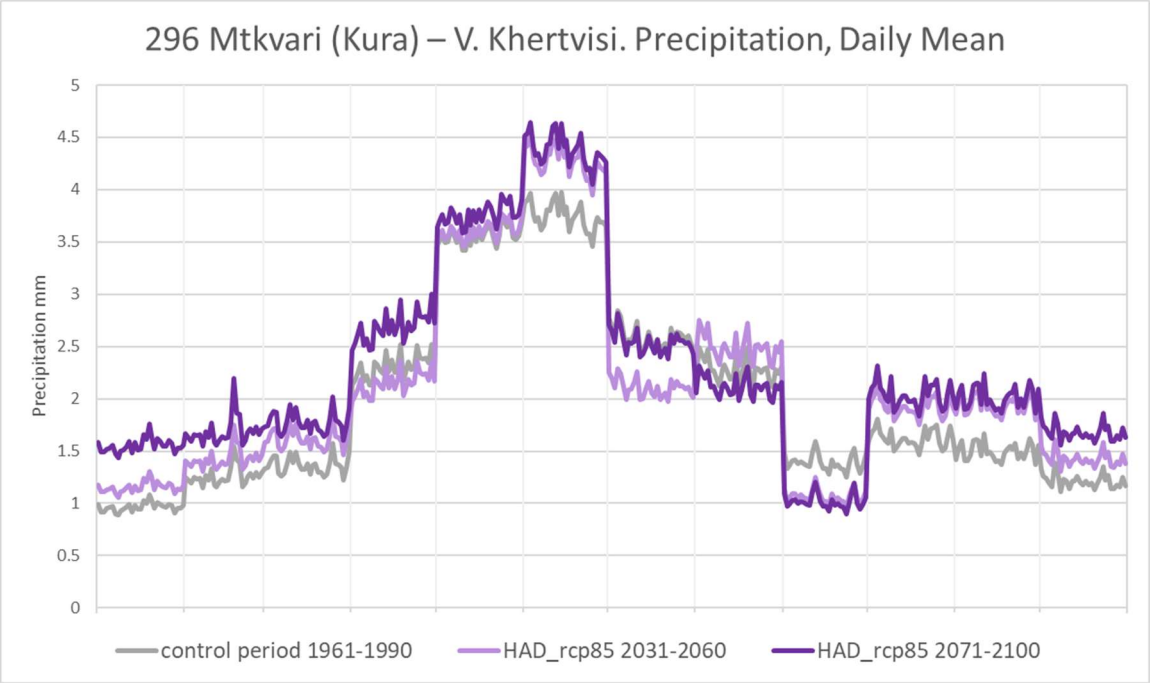

Figure A-48. Daily mean precipitation in the control period, 1961-1990 (grey line), the near future, 2031-2060 (light purple line) and the end of the century, 2071-2100 (dark purple line), according to the climate projection HAD, for the station 296 Mtkvari (Kura) – V. Khertvisi,

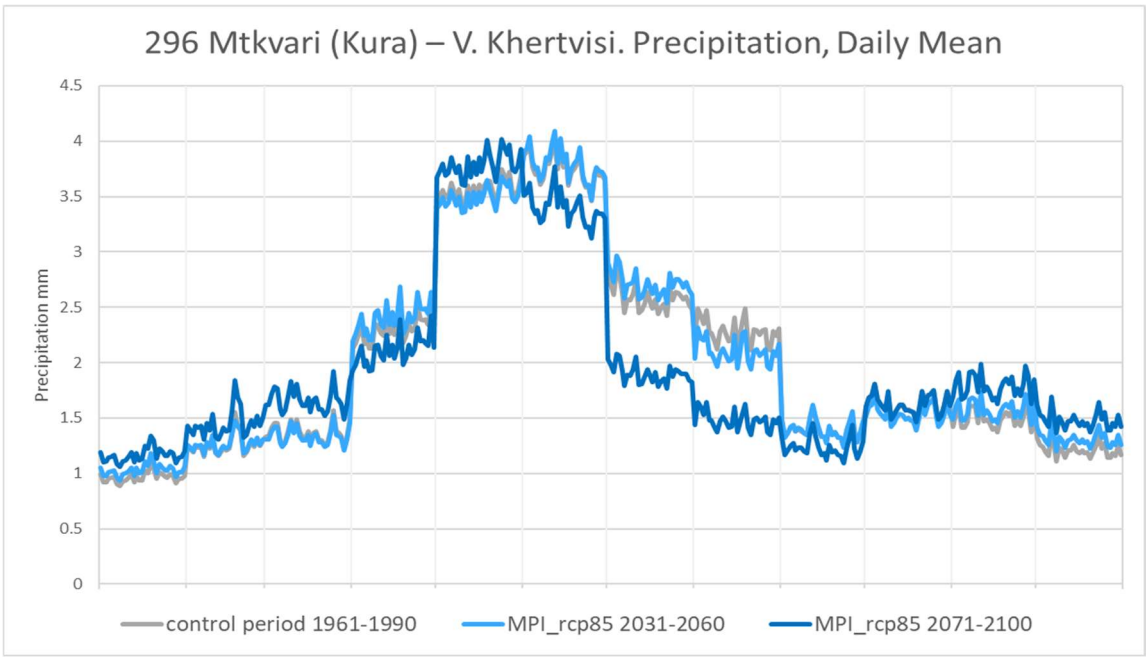

Figure A-49. Daily mean precipitation in the control period, 1961-1990 (grey line), the near future, 2031-2060 (light blue line) and the end of the century, 2071-2100 (dark blue line), according to the climate projection MPI, for the station 296 Mtkvari (Kura) – V. Khertvisi,

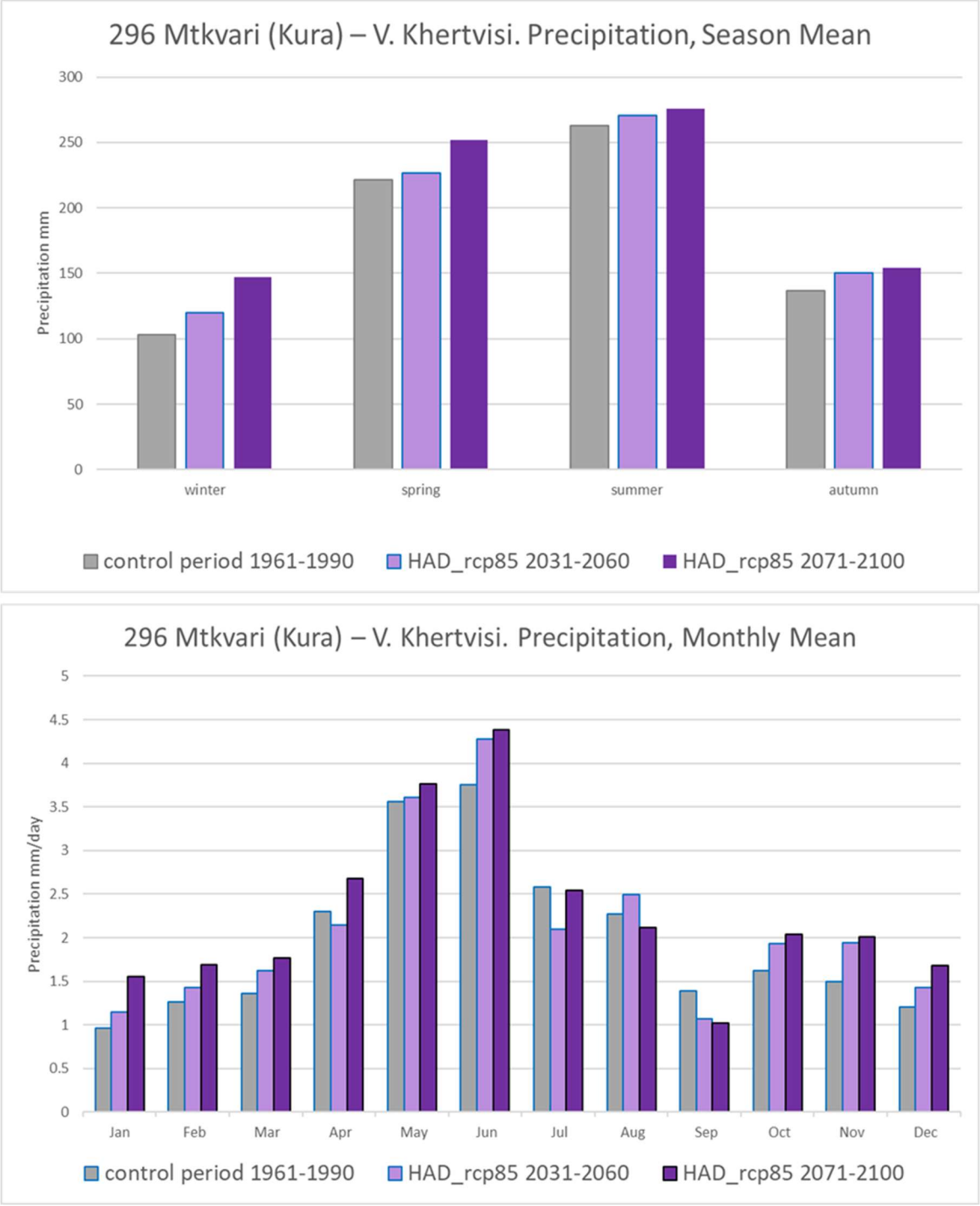

Figure A-50. Season mean (top) and monthly mean (bottom) precipitation in the control period, 1961-1990 (grey bars), the near future, 2031-2060 (light purple bars) and the end of the century, 2071-2100 (dark purple bars), according to the climate projection HAD, for the station 296 Mtkvari (Kura) – V. Khertvisi.

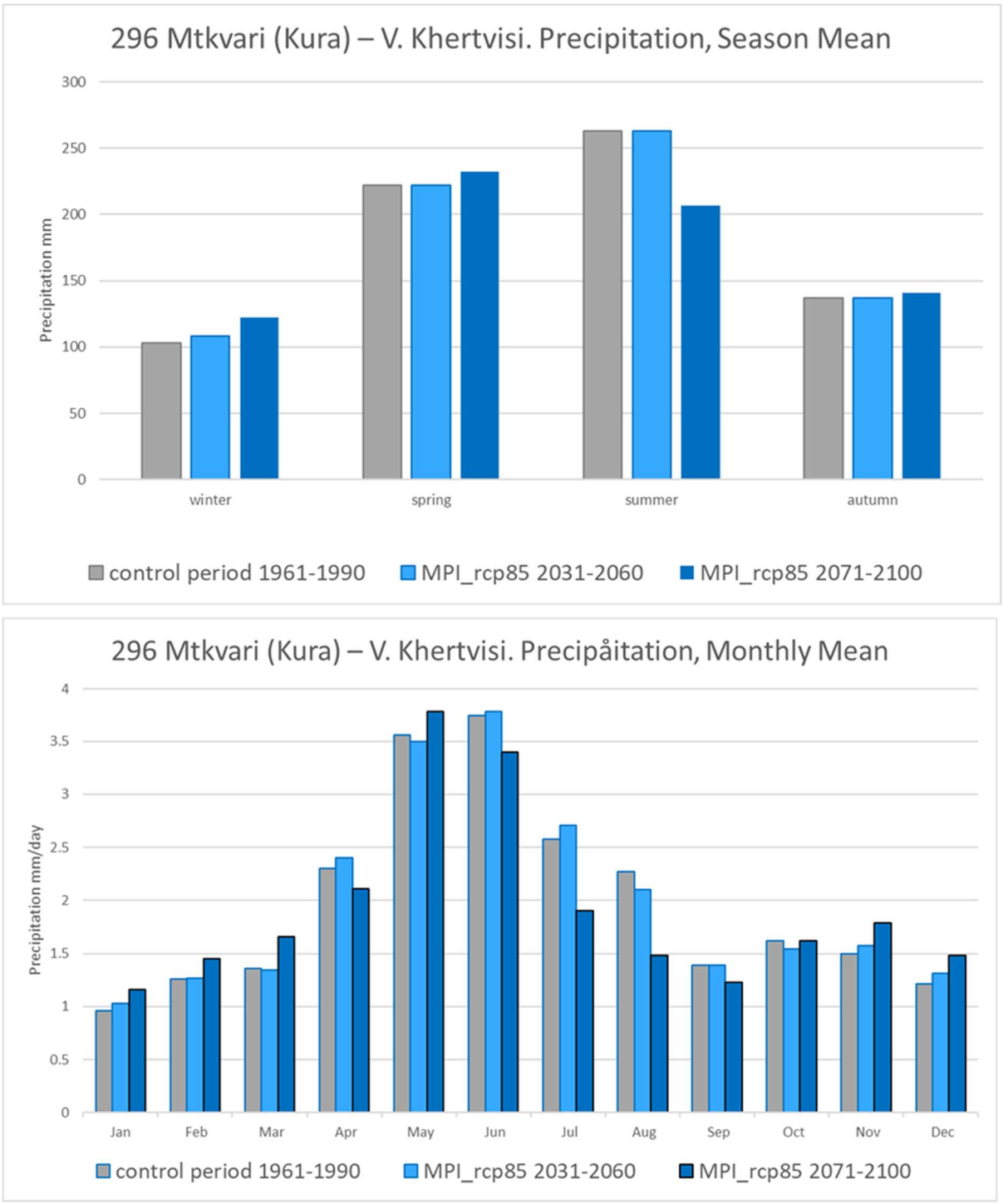

Figure A-51. Season mean (top) and monthly mean (bottom) precipitation in the control period, 1961-1990 (grey bars), the near future, 2031-2060 (light blue bars) and the end of the century, 2071-2100 (dark blue bars), according to the climate projection MPI, for the station 296 Mtkvari (Kura) – V. Khertvisi.

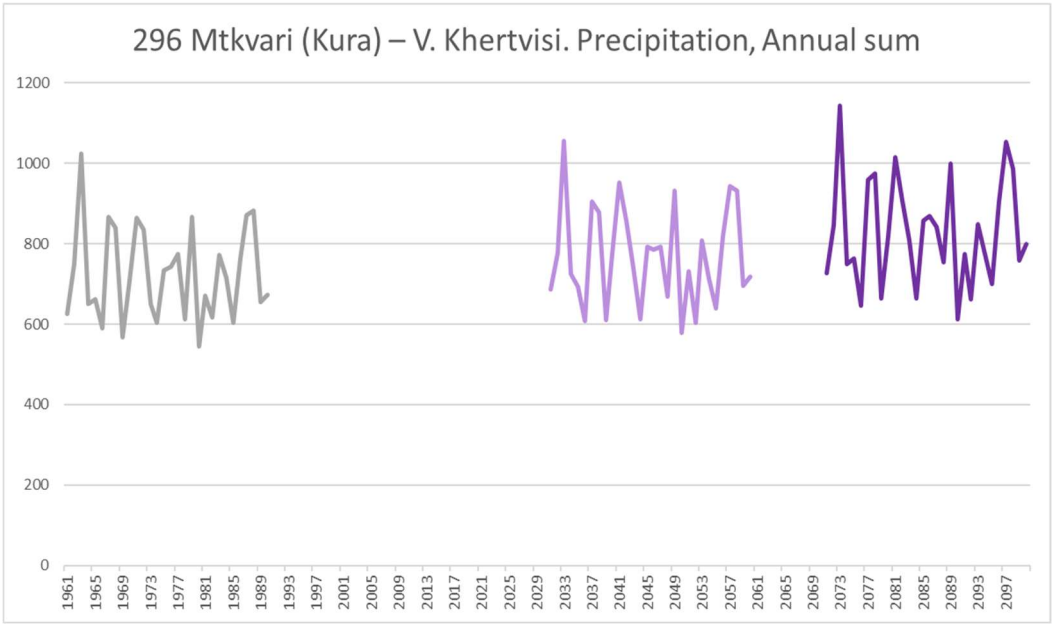

Figure A-52. Annual precipitation in the control period, 1961-1990 (grey line), the near future, 2031-2060 (light purple line) and the end of the century, 2071-2100 (dark purple line), according to the climate projection HAD, for the station 296 Mtkvari (Kura) – V. Khertvisi

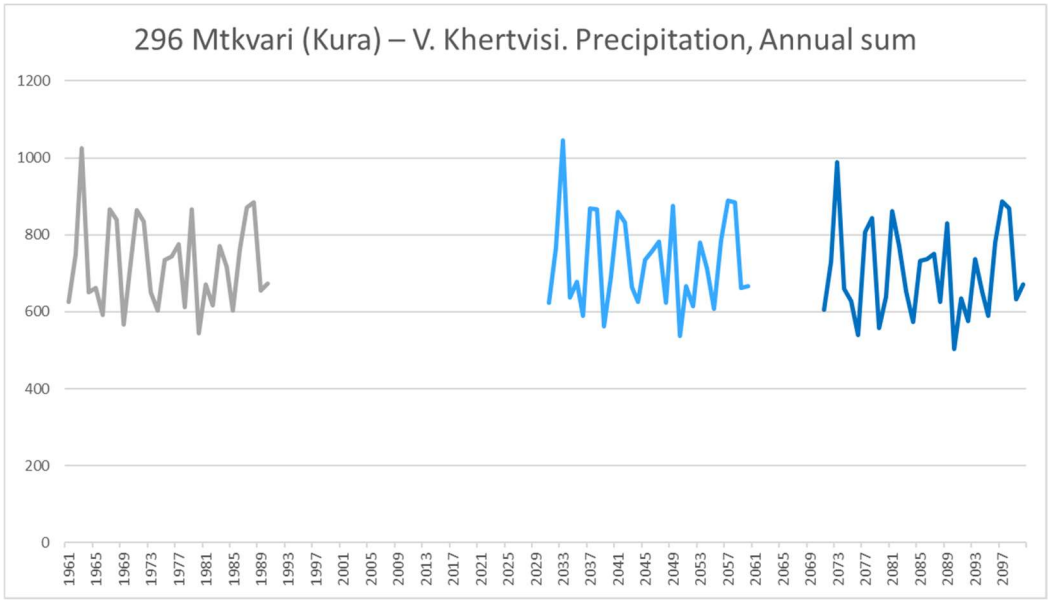

Figure A-53. Annual precipitation in the control period, 1961-1990 (grey line), the near future, 2031-2060 (light blue line) and the end of the century, 2071-2100 (dark blue line), according to the climate projection MPI, for the station 296 Mtkvari (Kura) – V. Khertvisi.

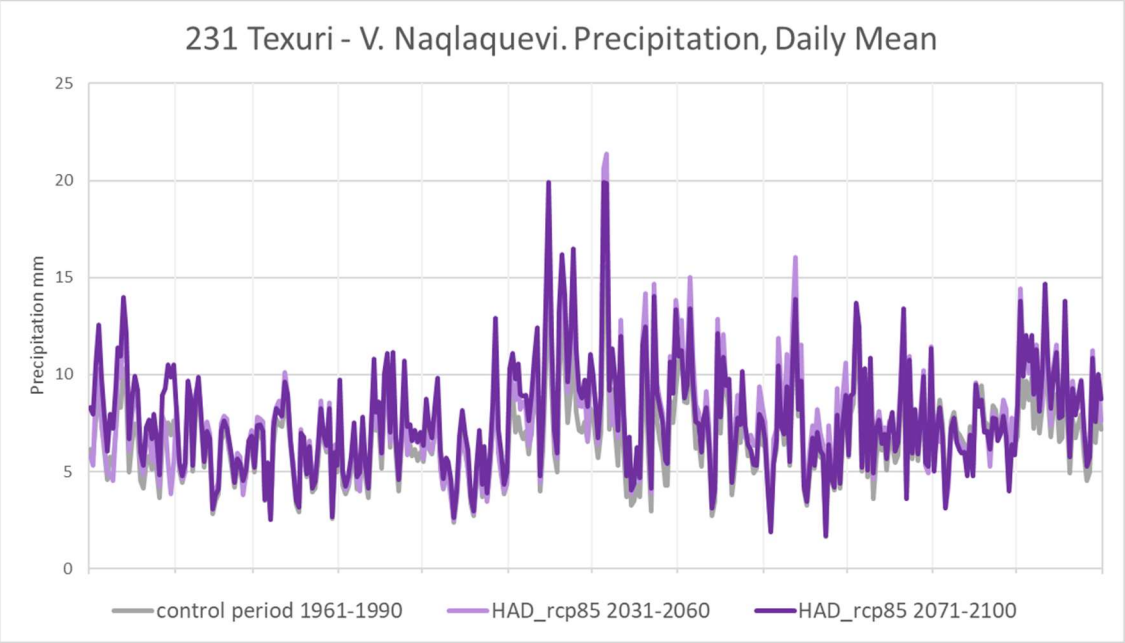

Figure A-54. Daily mean precipitation in the control period, 1961-1990 (grey line), the near future, 2031-2060 (light purple line) and the end of the century, 2071-2100 (dark purple line), according to the climate projection HAD, for the station 231 Texuri - V. Naqlaquevi.

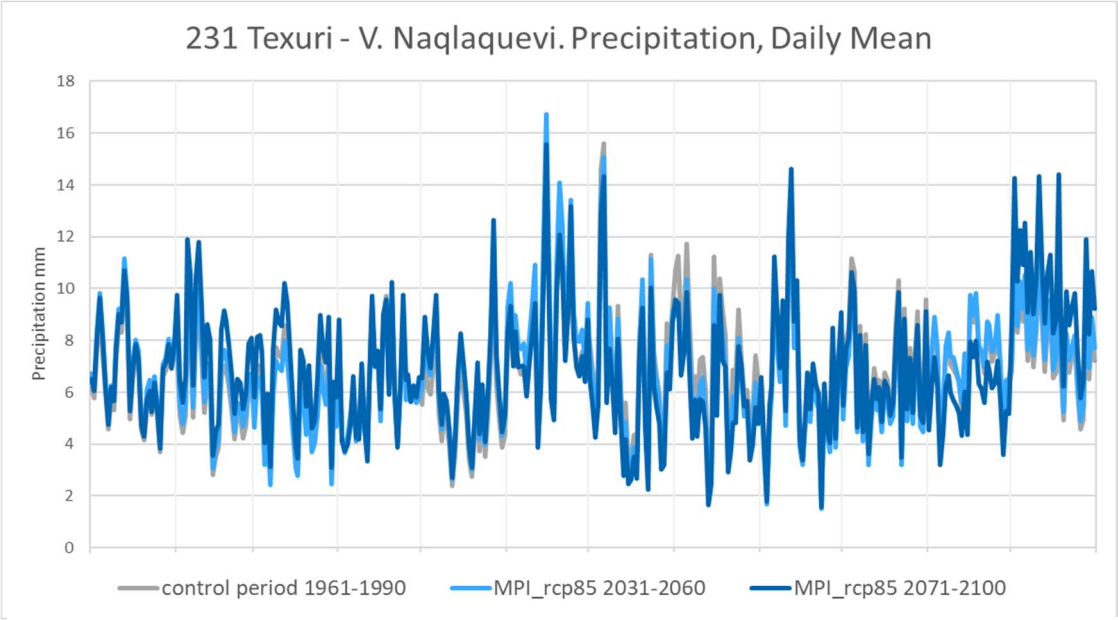

Figure A-55. Daily mean precipitation in the control period, 1961-1990 (grey line), the near future, 2031-2060 (light blue line) and the end of the century, 2071-2100 (dark blue line), according to the climate projection MPI, for the station 29 231 Texuri - V. Naqlaquevi.

Figure A-56. Season mean (top) and monthly mean (bottom) precipitation in the control period, 1961-1990 (grey bars), the near future, 2031-2060 (light purple bars) and the end of the century, 2071-2100 (dark purple bars), according to the climate projection HAD, for the station 231 Texuri - V. Naqlaquevi.

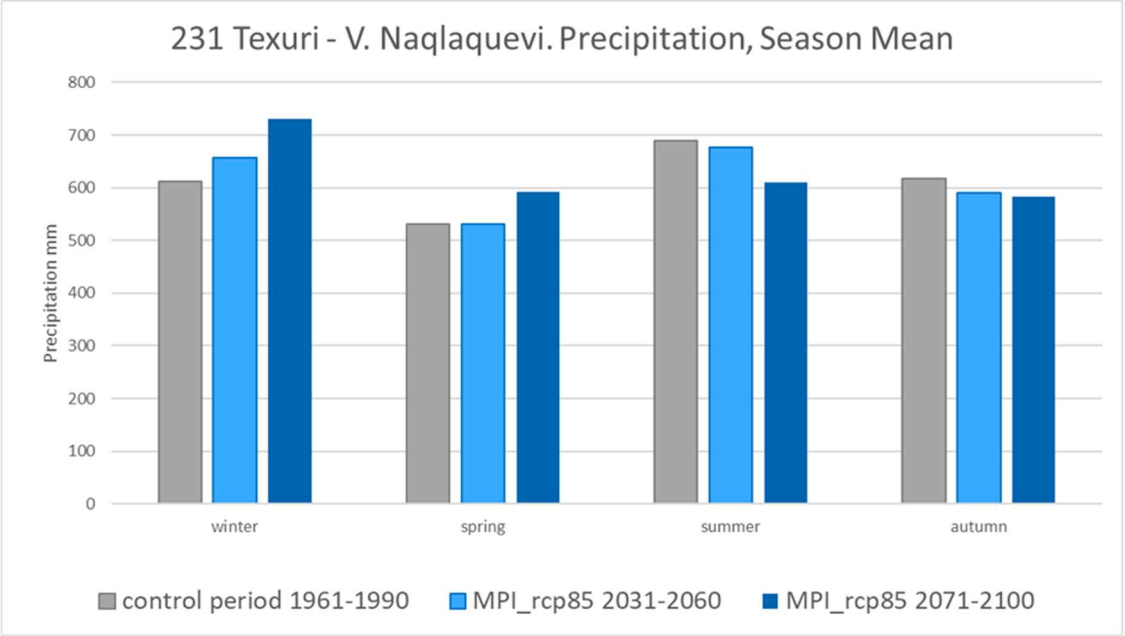

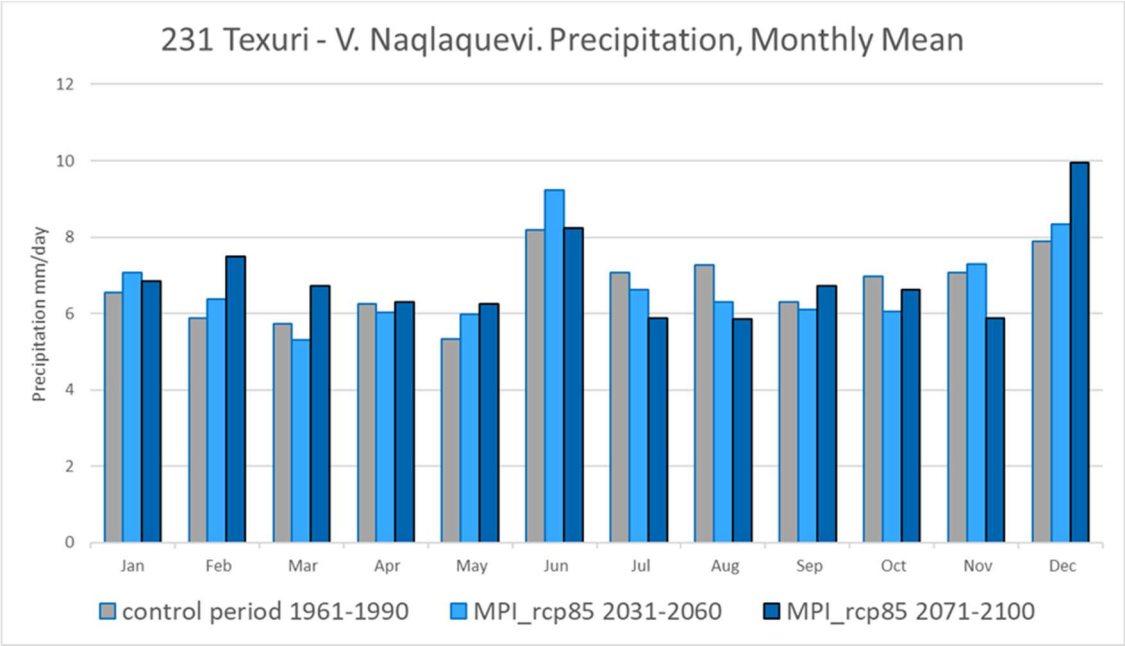

Figure A-57. Season mean (top) and monthly mean (bottom) precipitation in the control period, 1961-1990 (grey bars), the near future, 2031-2060 (light blue bars) and the end of the century, 2071-2100 (dark blue bars), according to the climate projection MPI, for the tation 231 Texuri - V. Naqlaquevi.

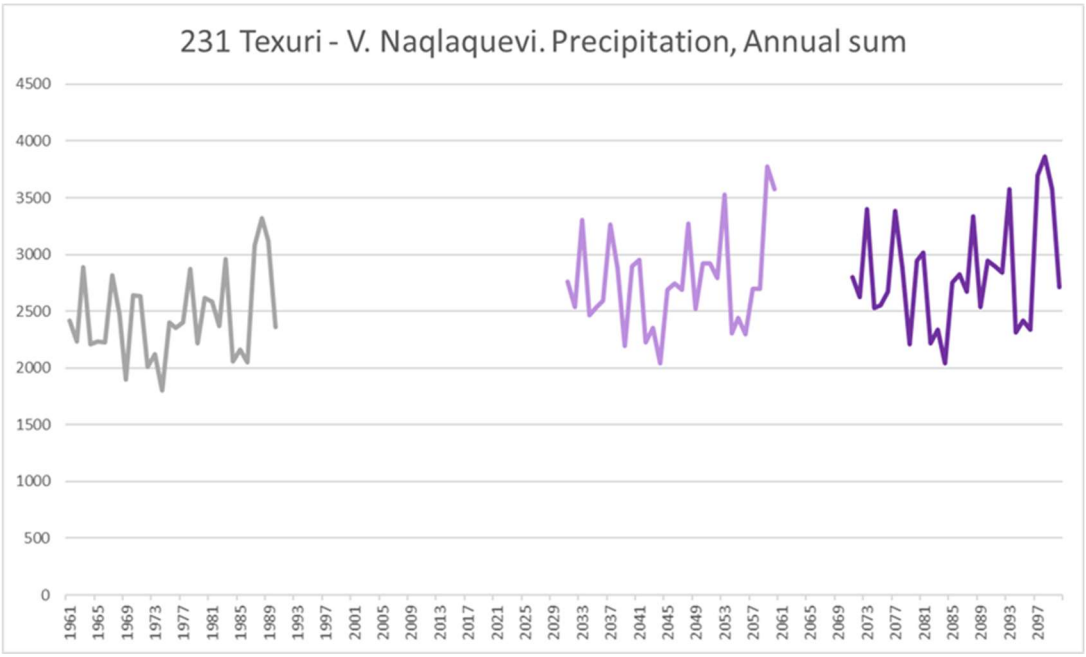

Figure A-58. Annual precipitation in the control period, 1961-1990 (grey line), the near future, 2031-2060 (light purple line) and the end of the century, 2071-2100 (dark purple line), according to the climate projection HAD, for the station 231 Texuri - V. Naqlaquevi.

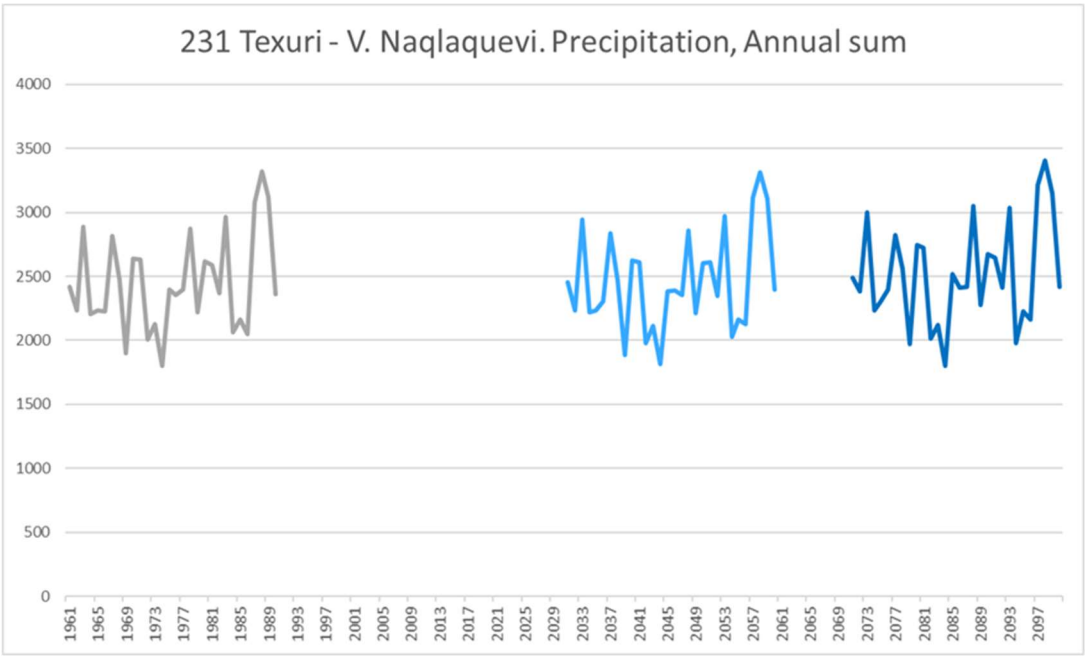

Figure A-59. Annual precipitation in the control period, 1961-1990(grey line), the near future, 2031-2060 (light blue line) and the end of the century, 2071-2100 (dark blue line), according to the climate projection MPI, for the station 231 Texuri - V. Naqlaquevi.

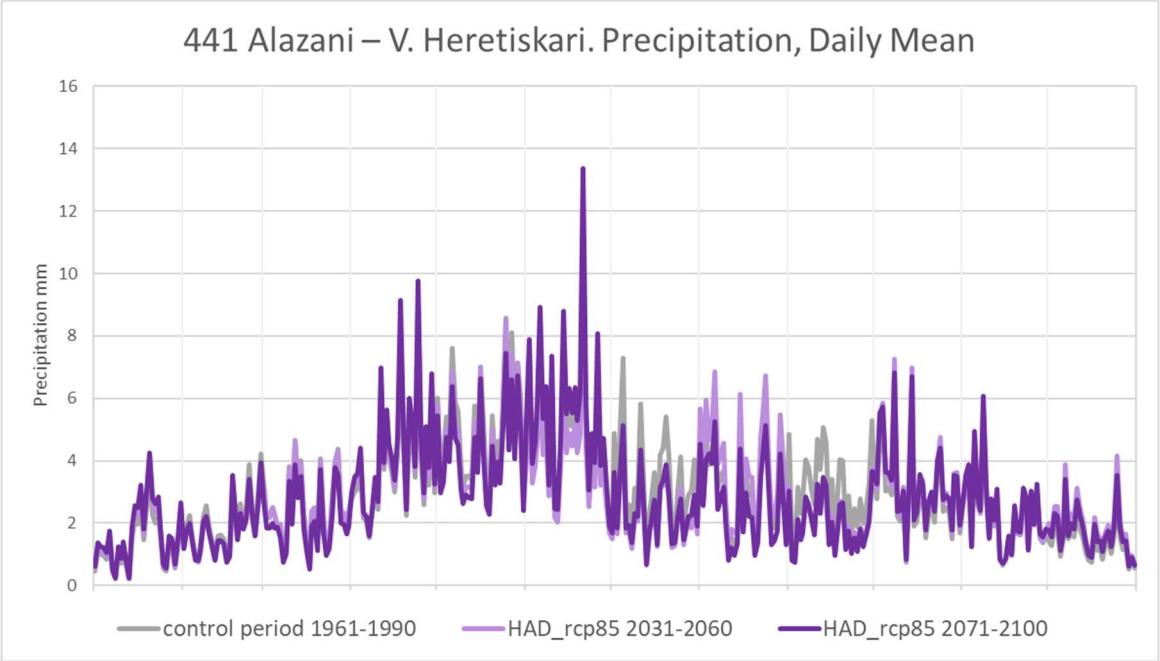

Figure A-60. Daily mean precipitation in the control period, 1961-1990 (grey line), the near future, 2031-2060 (light purple line) and the end of the century, 2071-2100 (dark purple line), according to the climate projection HAD, for the station 441 Alazani – V. Heretiskari.

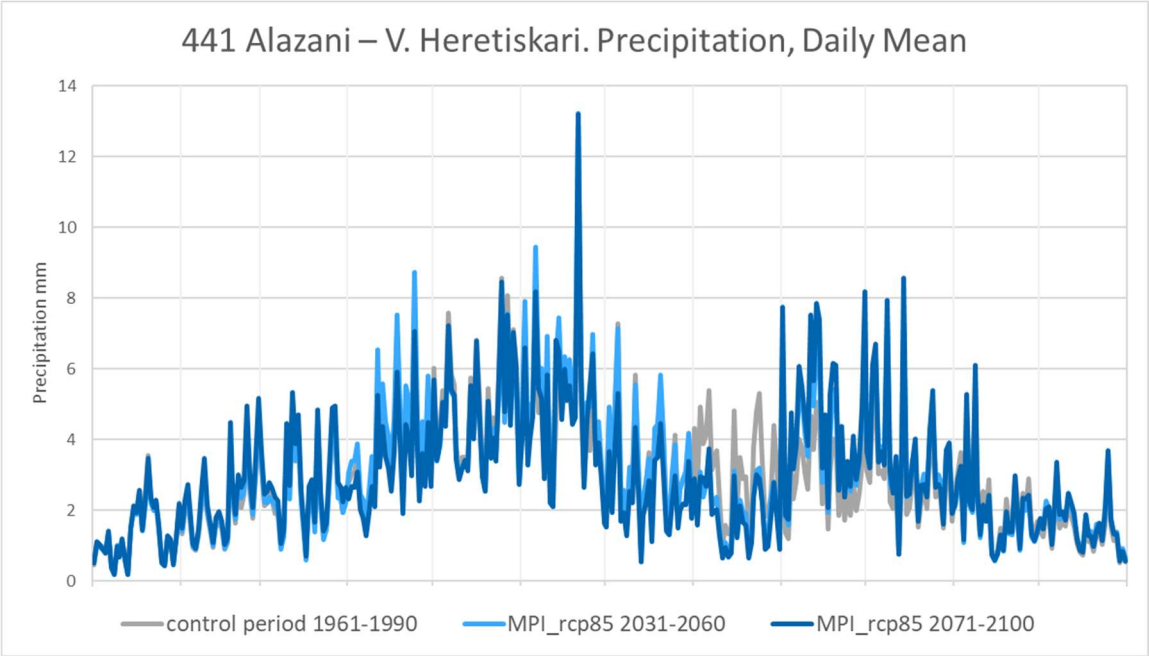

Figure A-61. Daily mean precipitation in the control period, 1961-1990 (grey line), the near future, 2031-2060 (light blue line) and the end of the century, 2071-2100 (dark blue line), according to the climate projection MPI, for the station 441 Alazani – V. Heretiskari.

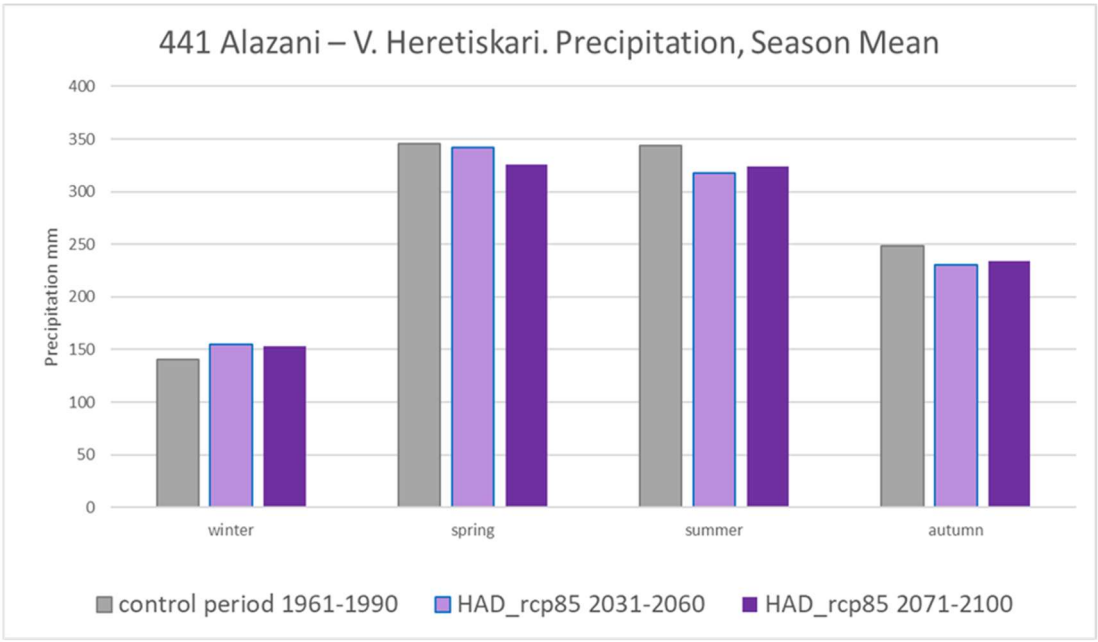

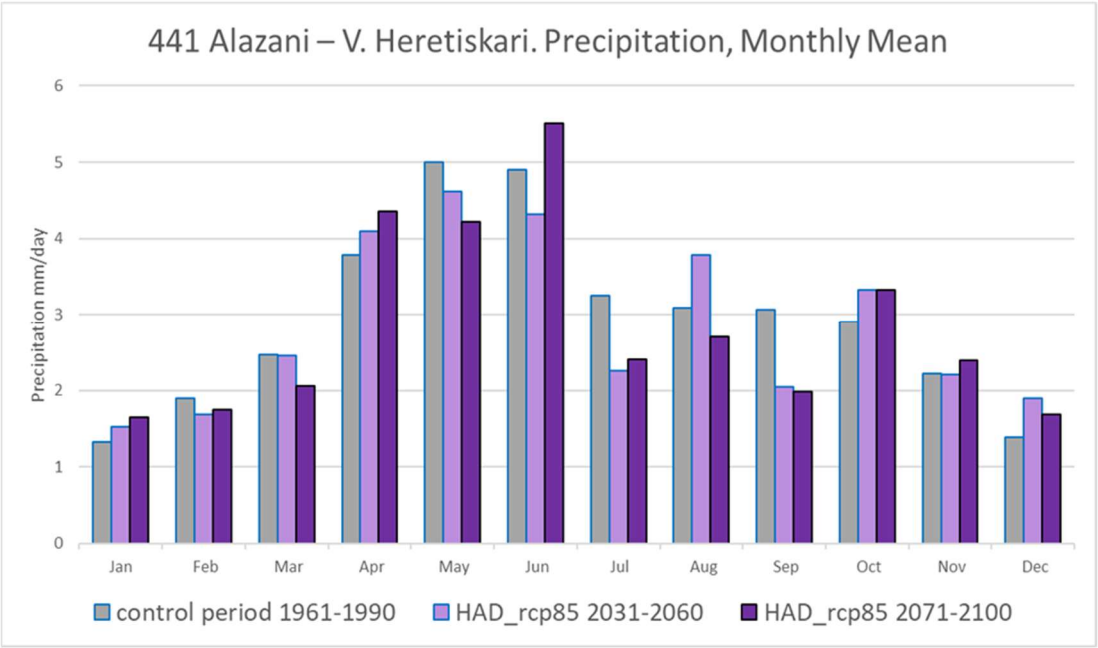

Figure A-62. Season mean (top) and monthly mean (bottom) precipitation in the control period, 1961-1990 (grey bars), the near future, 2031-2060 (light purple bars) and the end of the century, 2071-2100 (dark purple bars), according to the climate projection HAD, for the station 441 Alazani – V. Heretiskari.

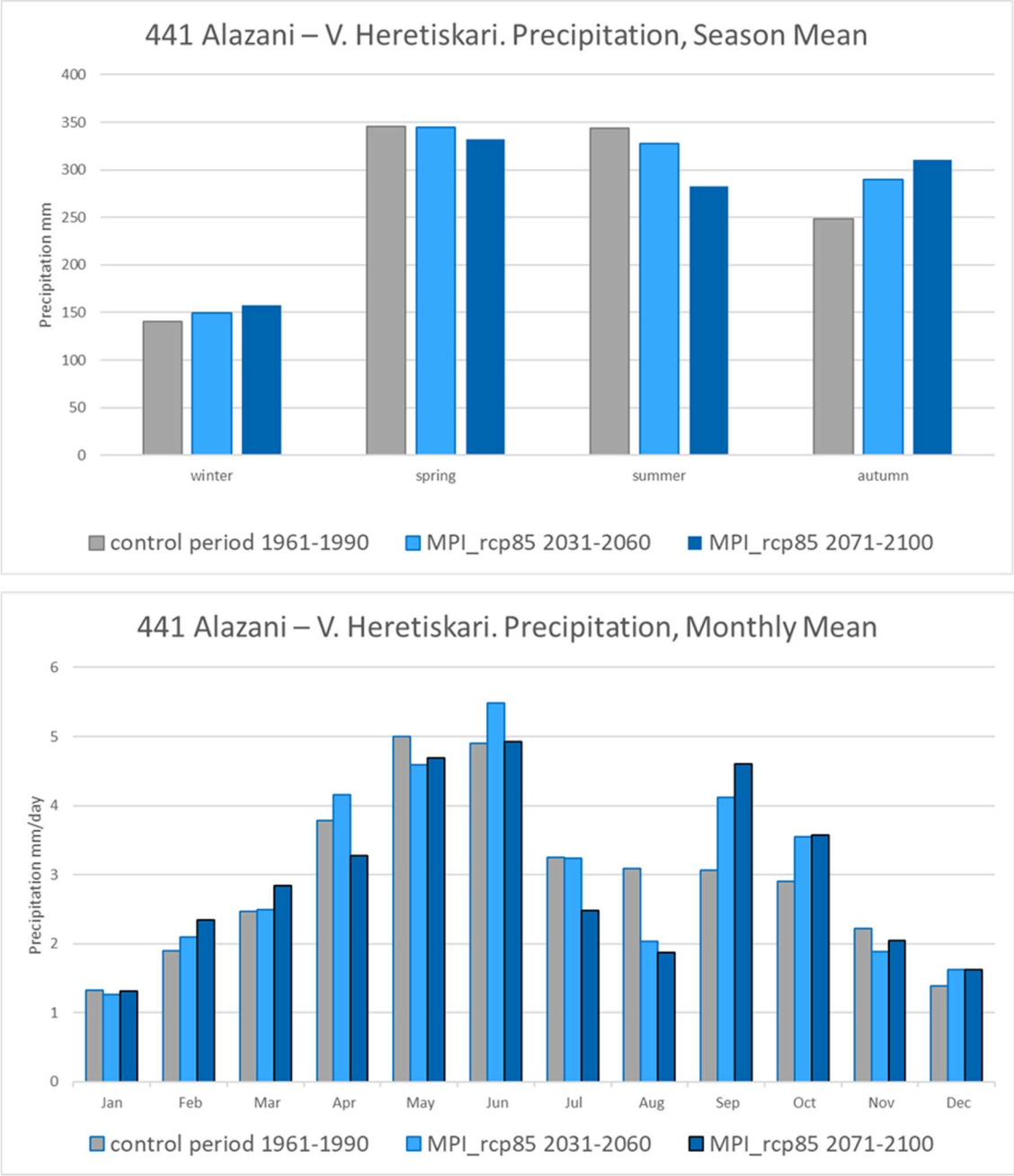

Figure A-63. Season mean (top) and monthly mean (bottom) precipitation in the control period, 1961-1990 (grey bars), the near future, 2031-2060 (light blue bars) and the end of the century, 2071-2100 (dark blue bars), according to the climate projection MPI, for the station 441 Alazani – V. Heretiskari.

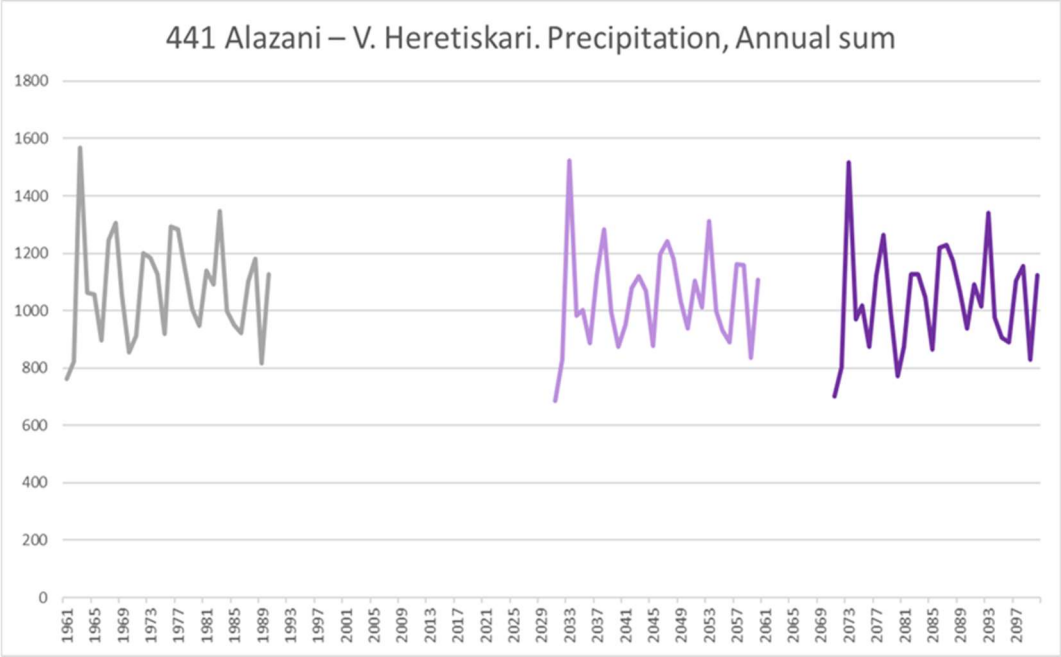

Figure A-64. Annual precipitation in the control period, 1961-1990 (grey line), the near future, 2031-2060 (light purple line) and the end of the century, 2071-2100 (dark purple line), according to the climate projection HAD, for the station 441 Alazani – V. Heretiskari.

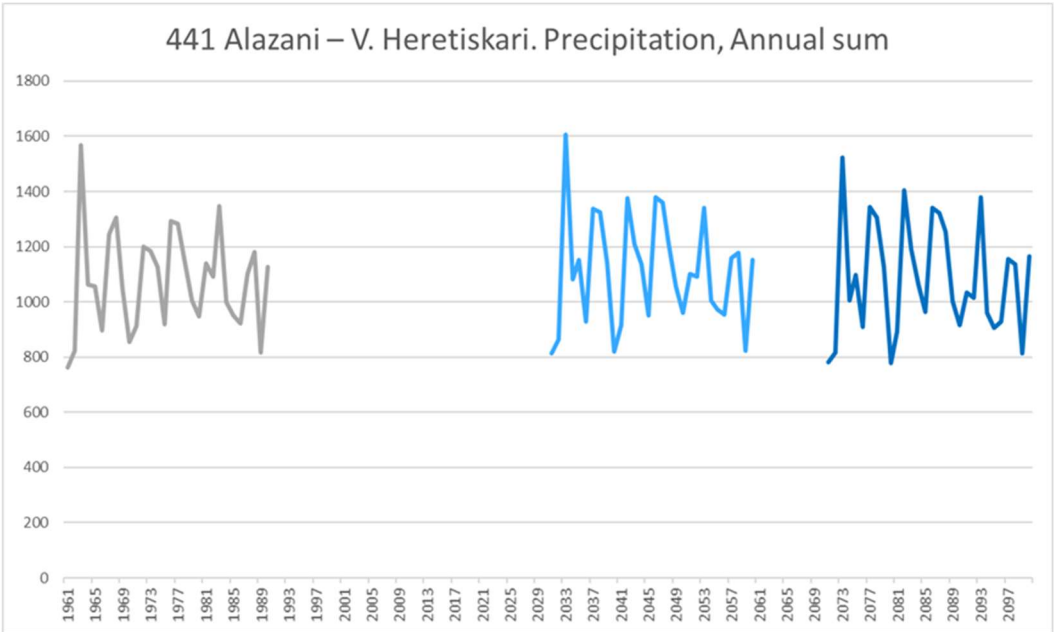

Figure A-65. Annual precipitation in the control period, 1961-1990 (grey line), the near future, 2031-2060 (light blue line) and the end of the century, 2071-2100 (dark blue line), according to the climate projection MPI, for the station 289 Chkheri – D. Stefantsmi.

Evapotranspiration

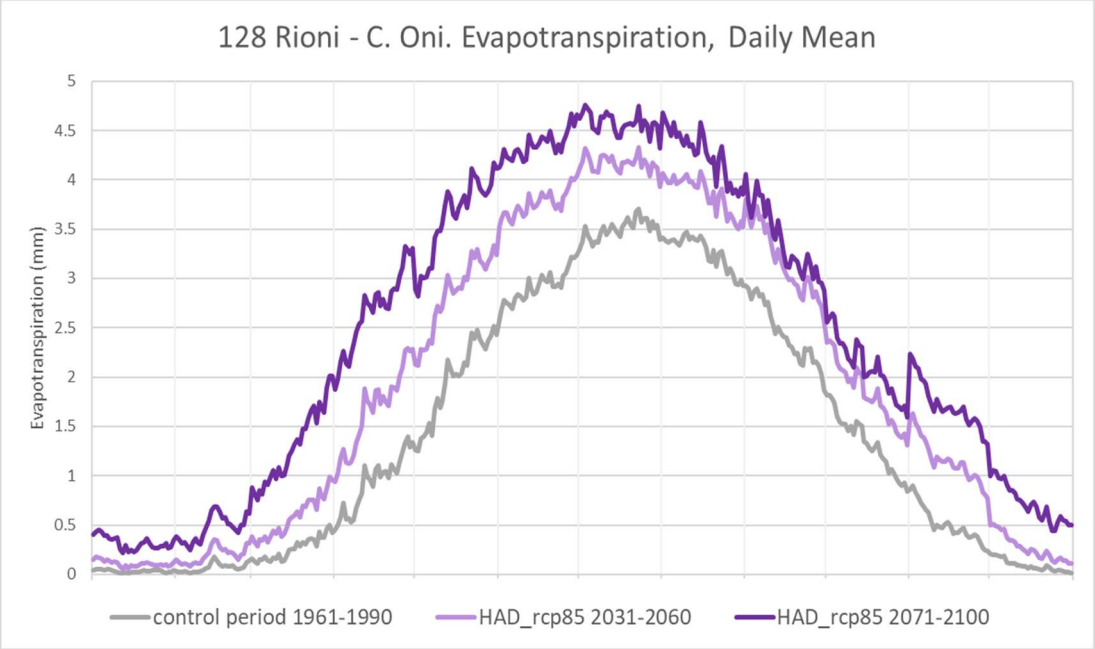

Figure A-66. Simulated daily mean evapotranspiration in the control period, 1961-1990 (grey line), the near future, 2031-2060 (light purple line) and the end of the century, 2071-2100 (dark purple line), according to the climate projection HAD, for the station 128 Rioni - C. Oni.

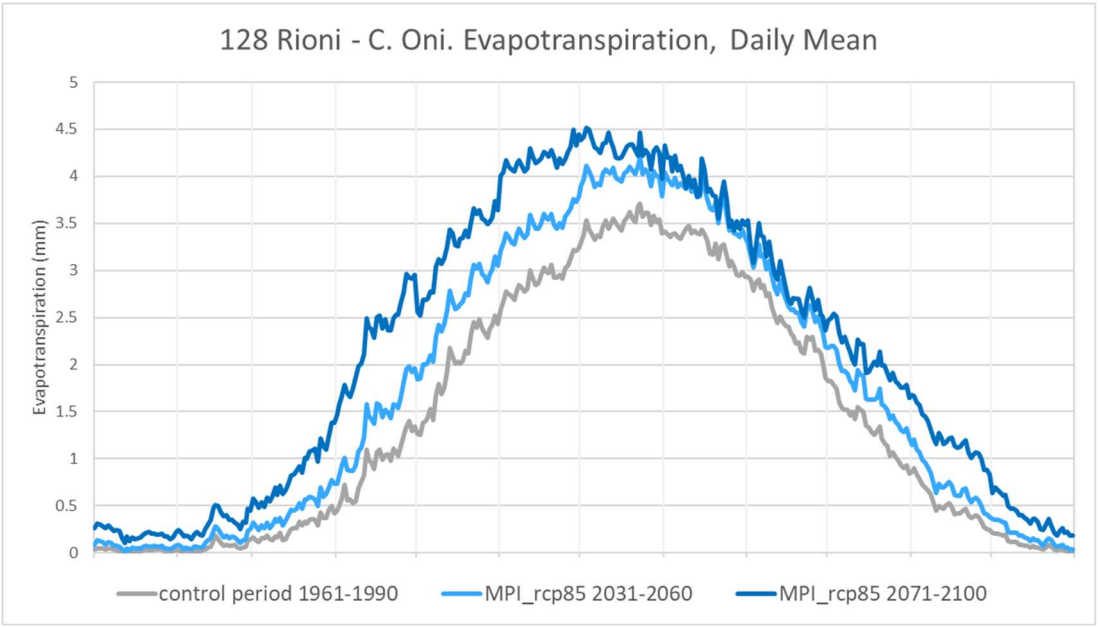

Figure A-67. Simulated daily mean evapotranspiration in the control period, 1961-1990 (grey line), the near future, 2031-2060 (light blue line) and the end of the century, 2071-2100 (dark blue line), according to the climate projection MPI, for the station 128 Rioni - C. Oni.

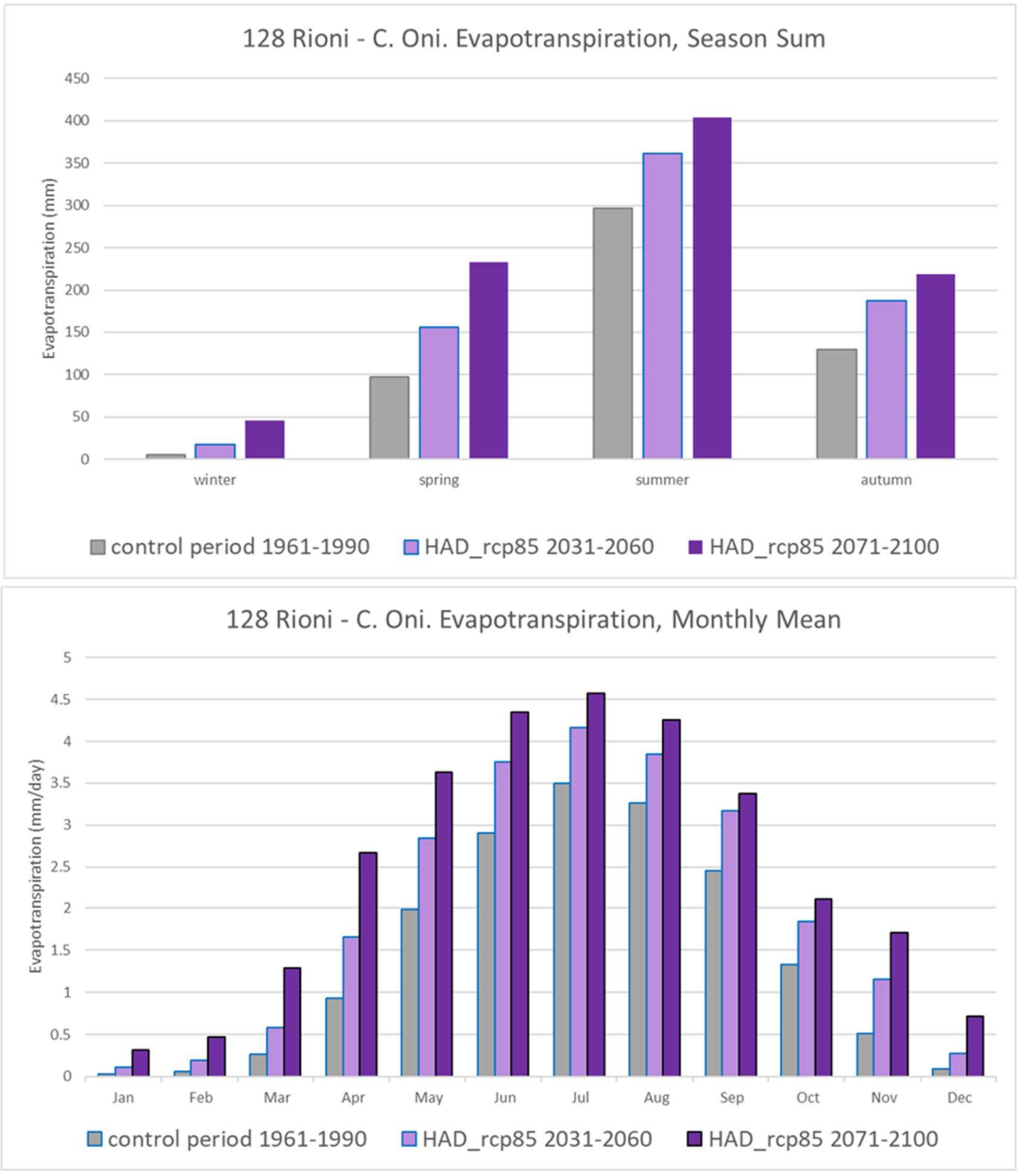

Figure A-68. Simulated season mean (top) and monthly mean (bottom) evapotranspiration in the control period, 1961-1990 (grey bars), the near future, 2031-2060 (light purple bars) and the end of the century, 2071-2100 (dark purple bars), according to the climate projection HAD, for the station 128 Rioni - C. Oni.

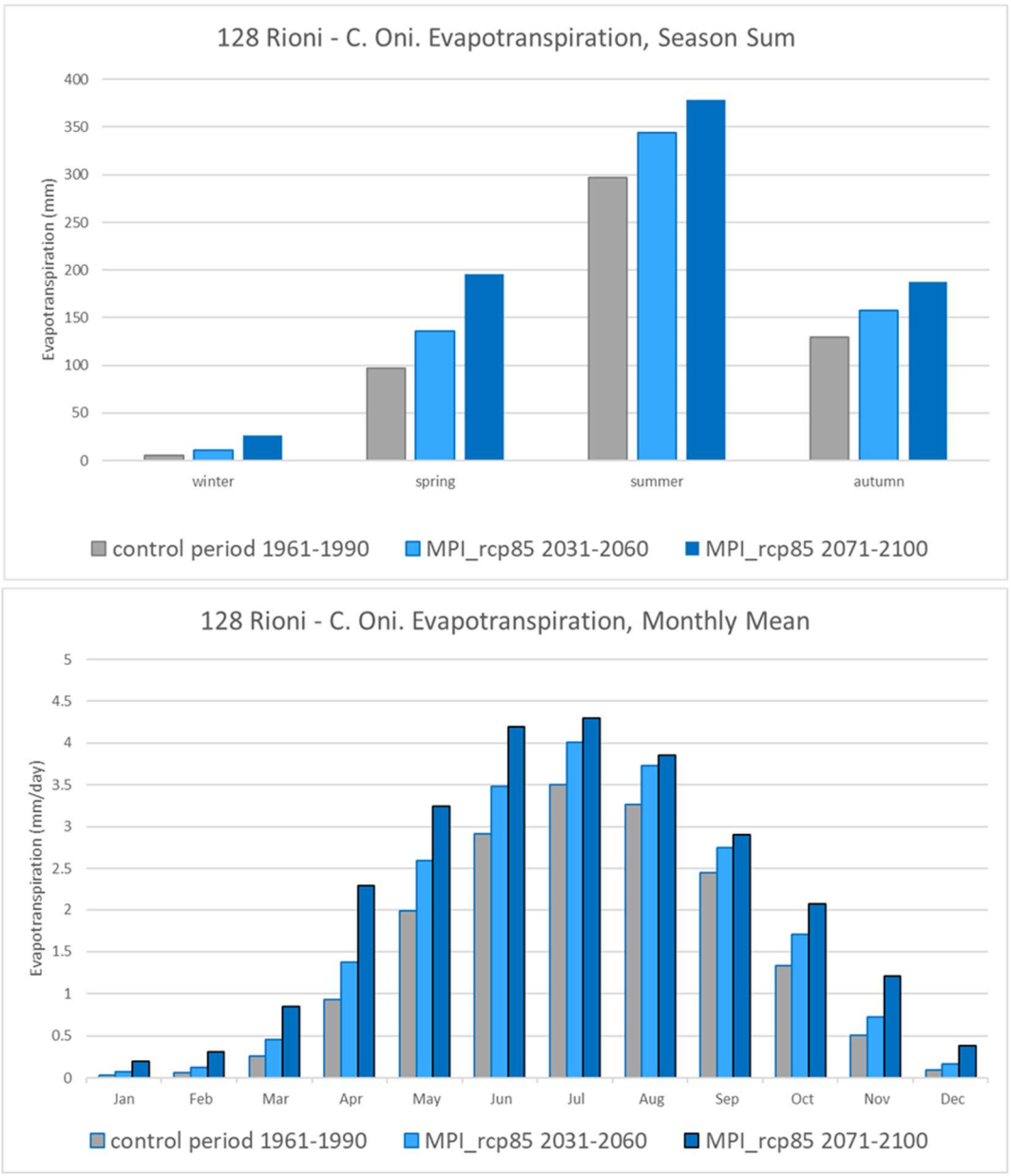

Figure A-69. Simulated season mean (top) and monthly mean (bottom) evapotranspiration in the control period, 1961-1990 (grey bars), the near future, 2031-2060 (light blue bars) and the end of the century, 2071-2100 (dark blue bars), according to the climate projection MPI, for the station 128 Rioni - C. Oni.

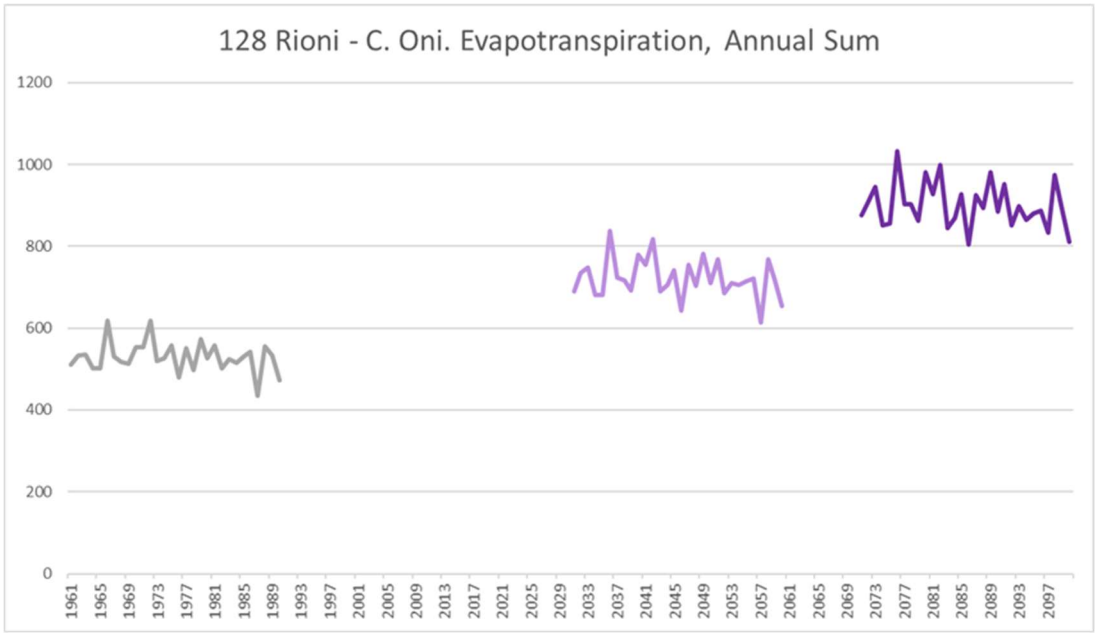

Figure A-70. Simulated annual evapotranspiration in the control period, 1961-1990 (grey line), the near future, 2031-2060 (light purple line) and the end of the century, 2071-2100 (dark purple line), according to the climate projection HAD, for the station 128 Rioni - C. Oni.

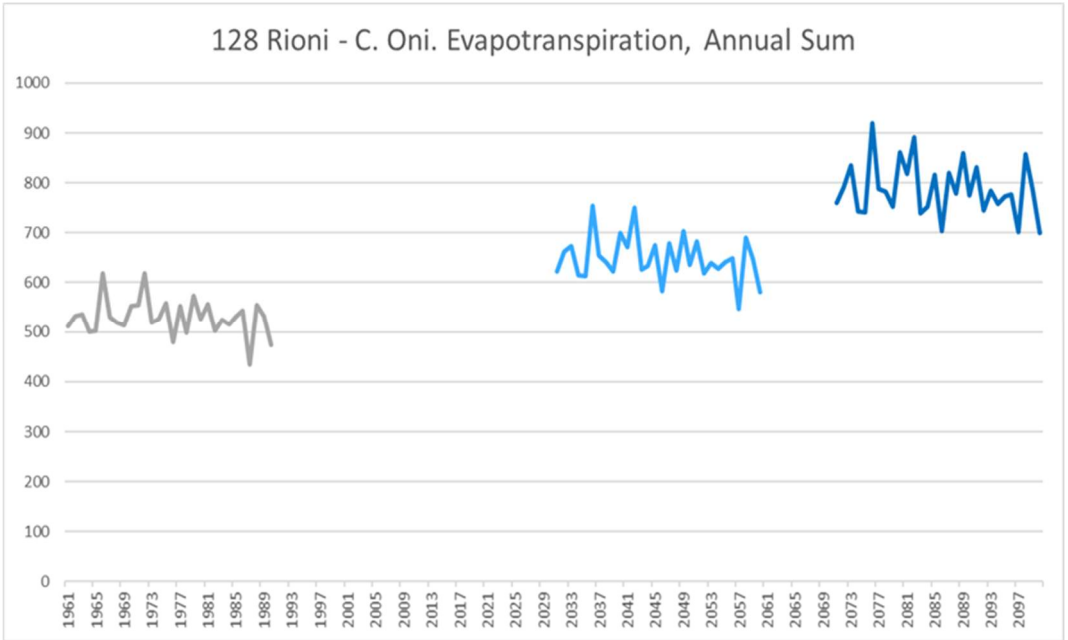

Figure A-71. Simulated annual evapotranspiration in the control period, 1961-1990 (grey line), the near future, 2031-2060 (light blue line) and the end of the century, 2071-2100 (dark blue line), according to the climate projection MPI, for the station 128 Rioni - C. Oni.

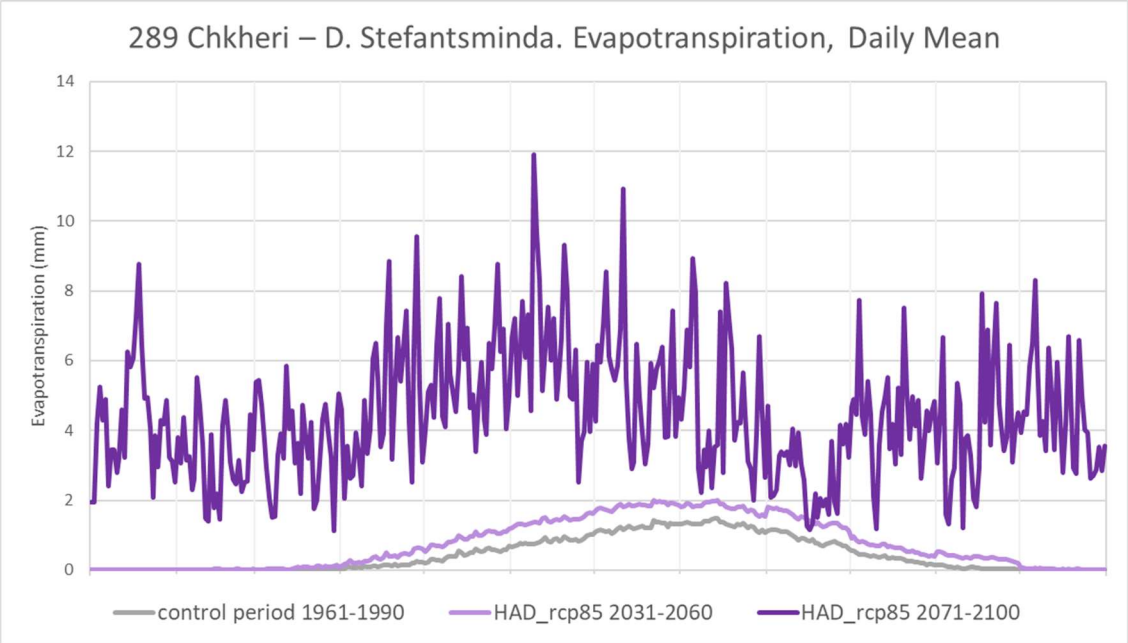

Figure A-72. Simulated daily mean evapotranspiration in the control period, 1961-1990 (grey line), the near future, 2031-2060 (light purple line) and the end of the century, 2071-2100 (dark purple line), according to the climate projection HAD, for the station 289 Chkheri – D. Stefantsminda.

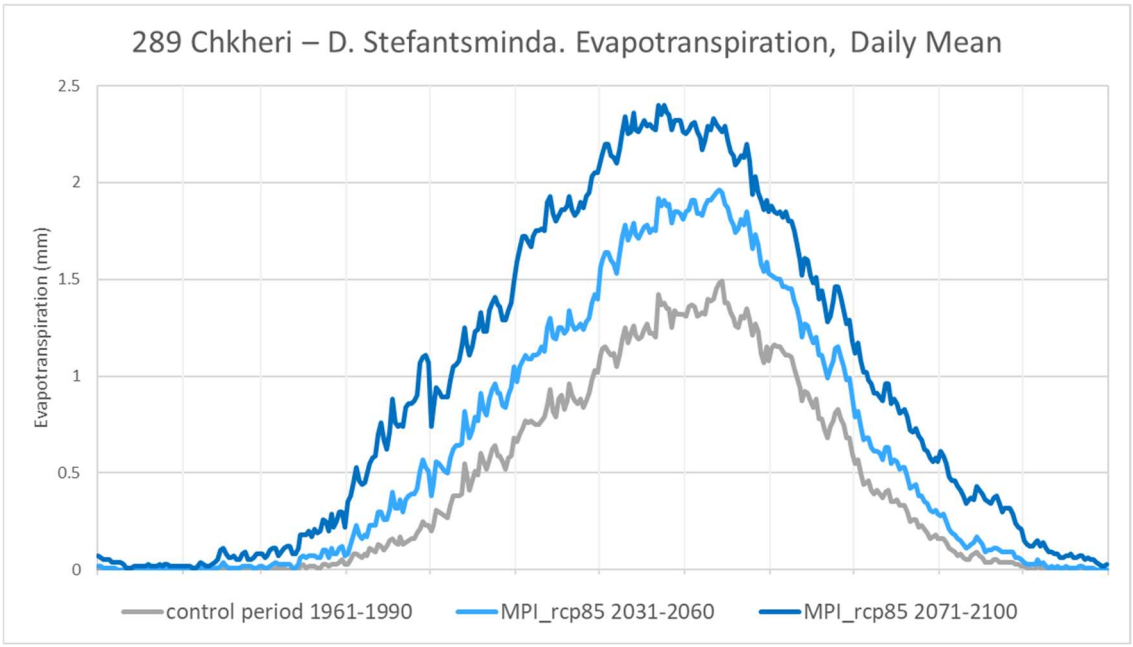

Figure A-73. Simulated daily mean evapotranspiration in the control period, 1961-1990 (grey line), the near future, 2031-2060 (light blue line) and the end of the century, 2071-2100 (dark blue line), according to the climate projection MPI, for the station 289 Chkheri – D. Stefantsminda.

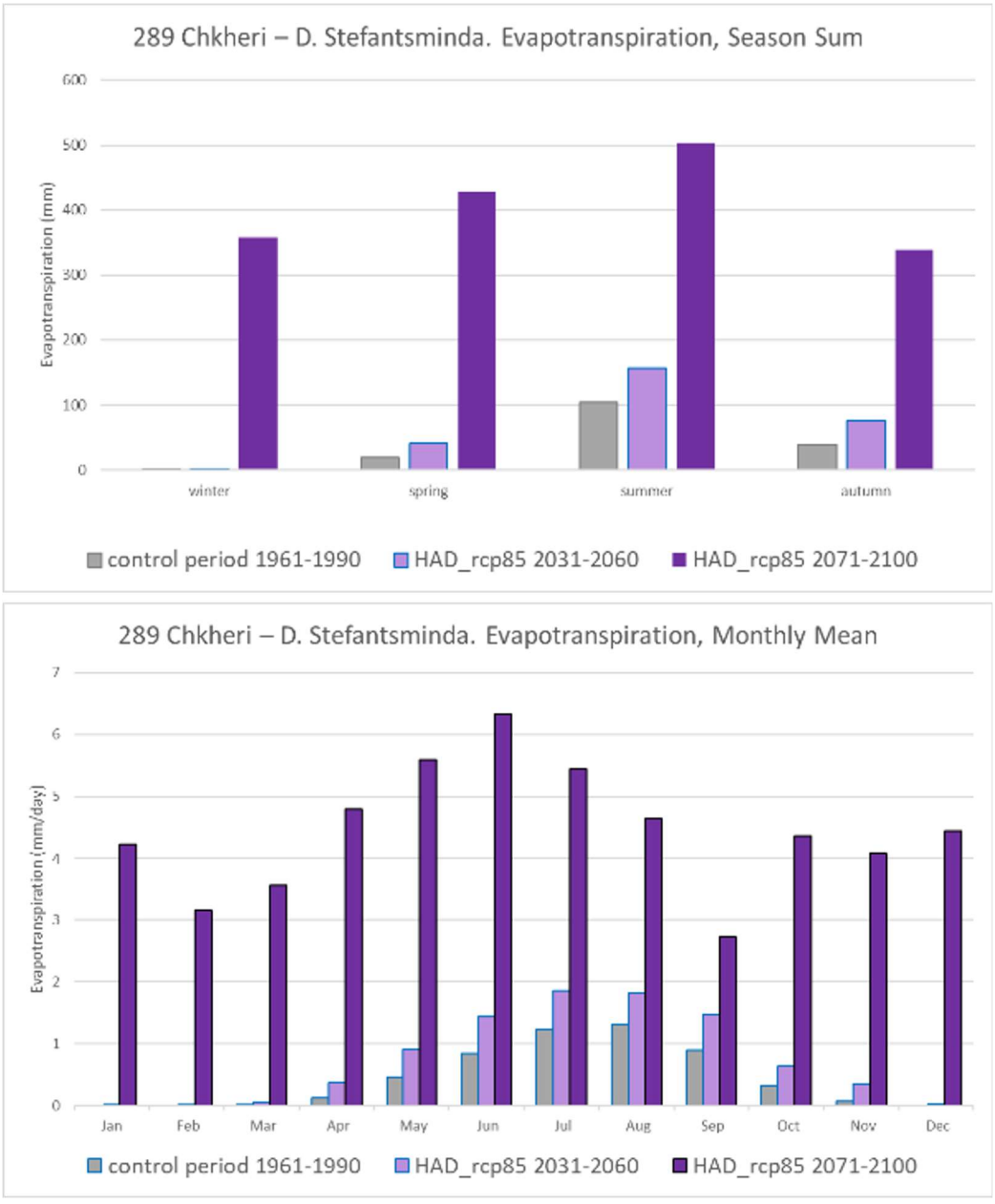

Figure A-74. Simulated season mean (top) and monthly mean (bottom) evapotranspiration in the control period, 1961-1990 (grey bars), the near future, 2031-2060 (light purple bars) and the end of the century, 2071-2100 (dark purple bars), according to the climate projection HAD, for the station 289 Chkheri – D. Stefantsminda

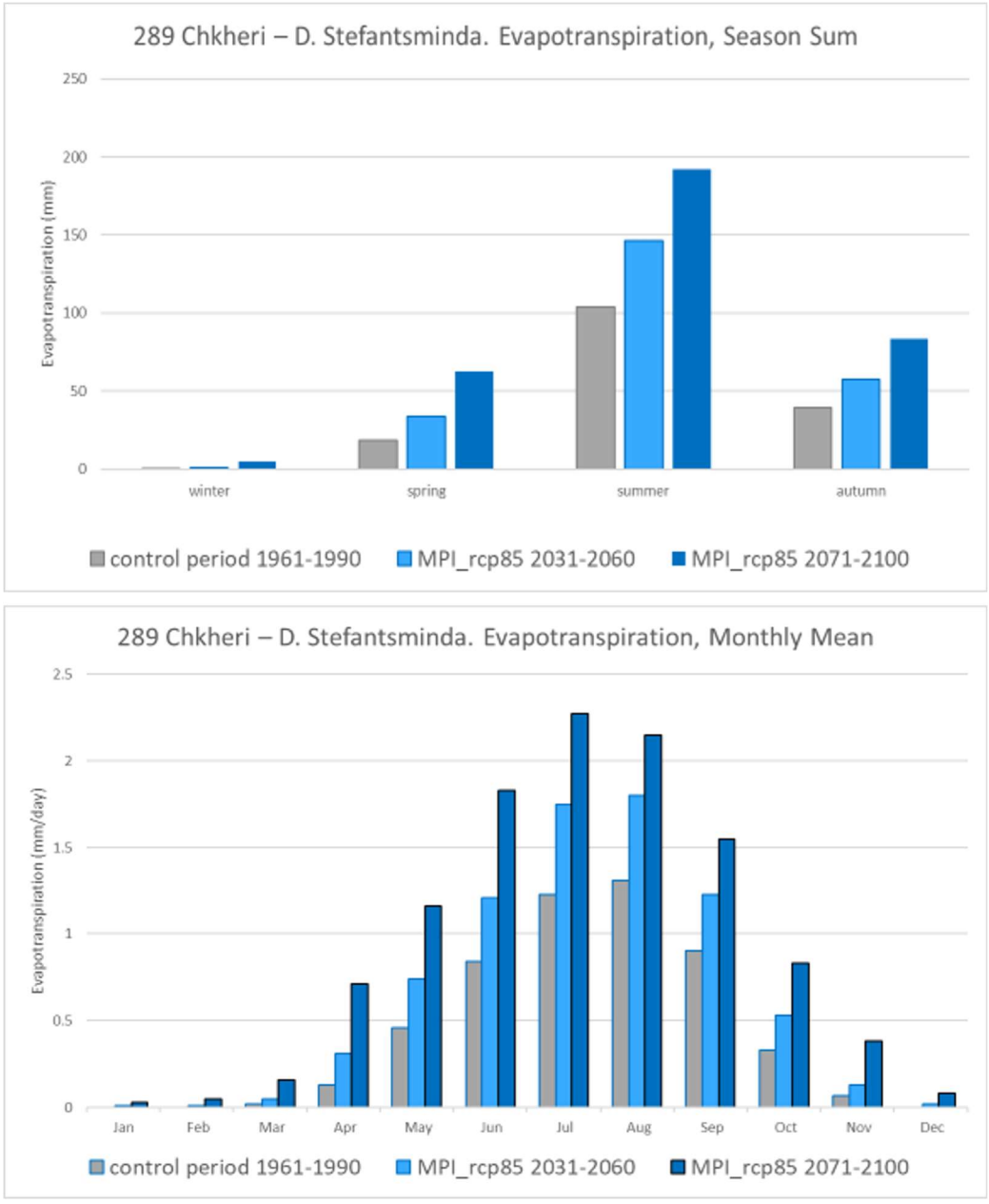

Figure A-75. Simulated season mean (top) and monthly mean (bottom) evapotranspiration in the control period, 1961-1990 (grey bars), the near future, 2031-2060 (light blue bars) and the end of the century, 2071-2100 (dark blue bars), according to the climate projection MPI, for the station 289 Chkheri – D. Stefantsminda.

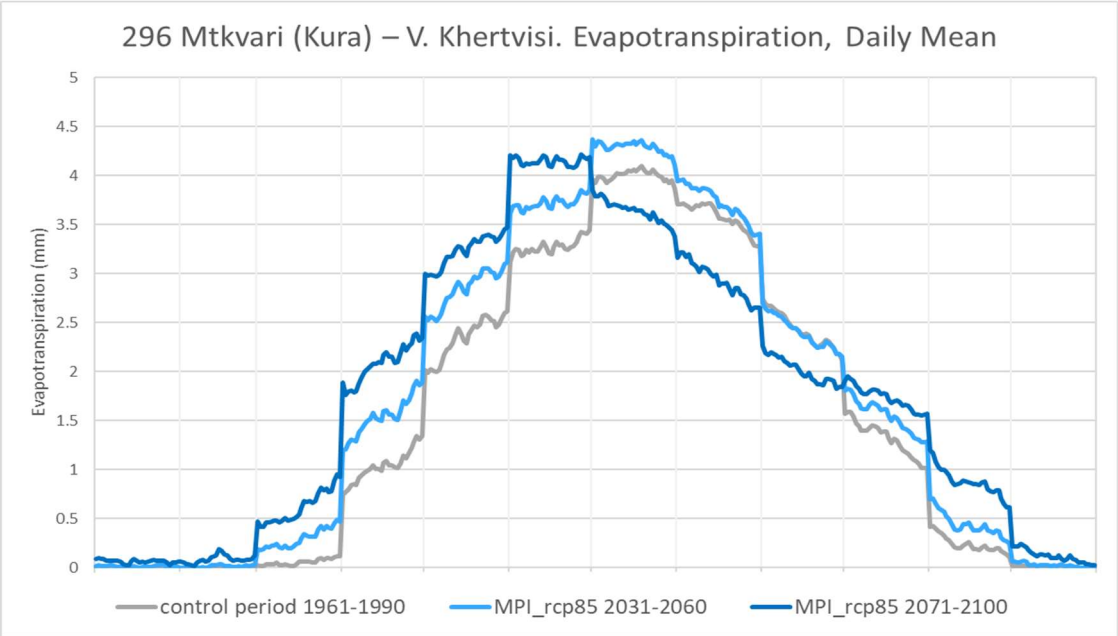

Figure A-76. Simulated annual evapotranspiration in the control period, 1961-1990 (grey line), the near future, 2031-2060 (light purple line) and the end of the century, 2071-2100 (dark purple line), according to the climate projection HAD, for the station 289 Chkheri – D. Stefantsminda.

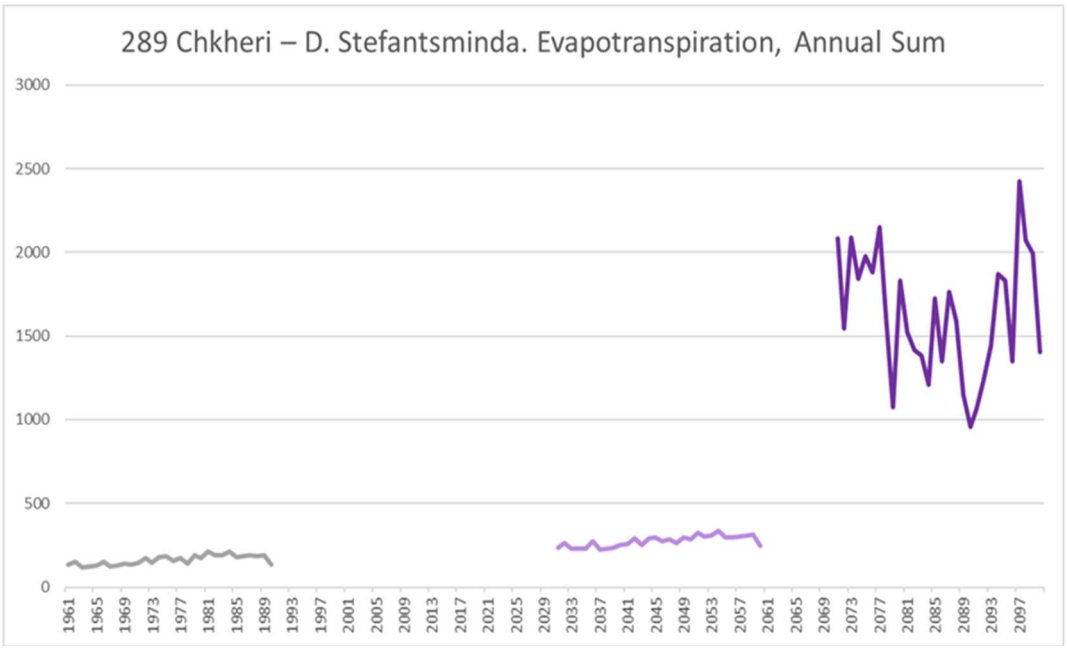

Figure A-77. Simulated annual evapotranspiration in the control period, 1961-1990 (grey line), the near future, 2031-2060 (light blue line) and the end of the century, 2071-2100 (dark blue line), according to the climate projection MPI, for the station 289 Chkheri – D. Stefantsminda.

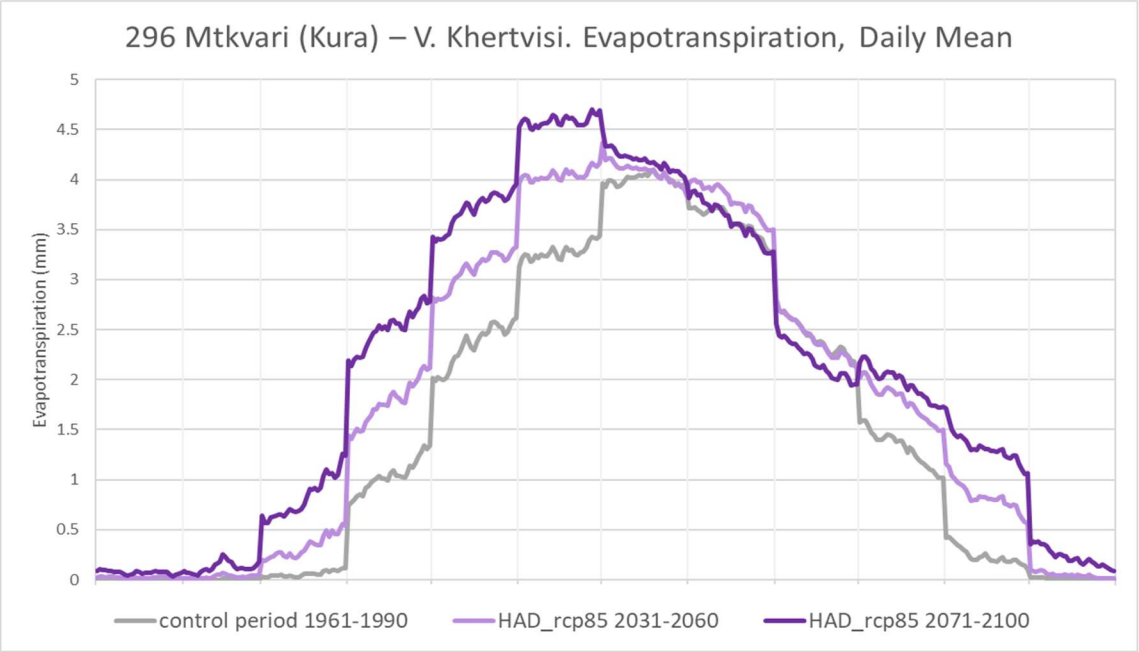

Figure A-78. Simulated daily mean evapotranspiration in the control period, 1961-1990 (grey line), the near future, 2031-2060 (light purple line) and the end of the century, 2071-2100 (dark purple line), according to the climate projection HAD, for the station 296 Mtkvari (Kura) – V. Khertvisi.

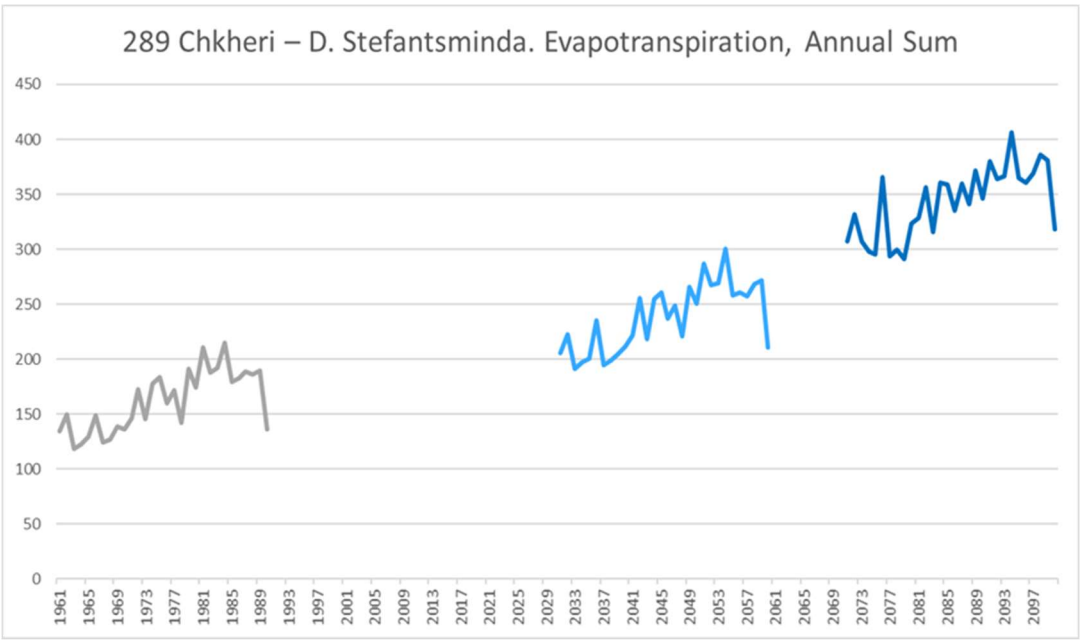

Figure A-79. Simulated daily mean evapotranspiration in the control period, 1961-1990 (grey line), the near future, 2031-2060 (light blue line) and the end of the century, 2071-2100 (dark blue line), according to the climate projection MPI, for the station 296 Mtkvari (Kura) – V. Khertvisi.

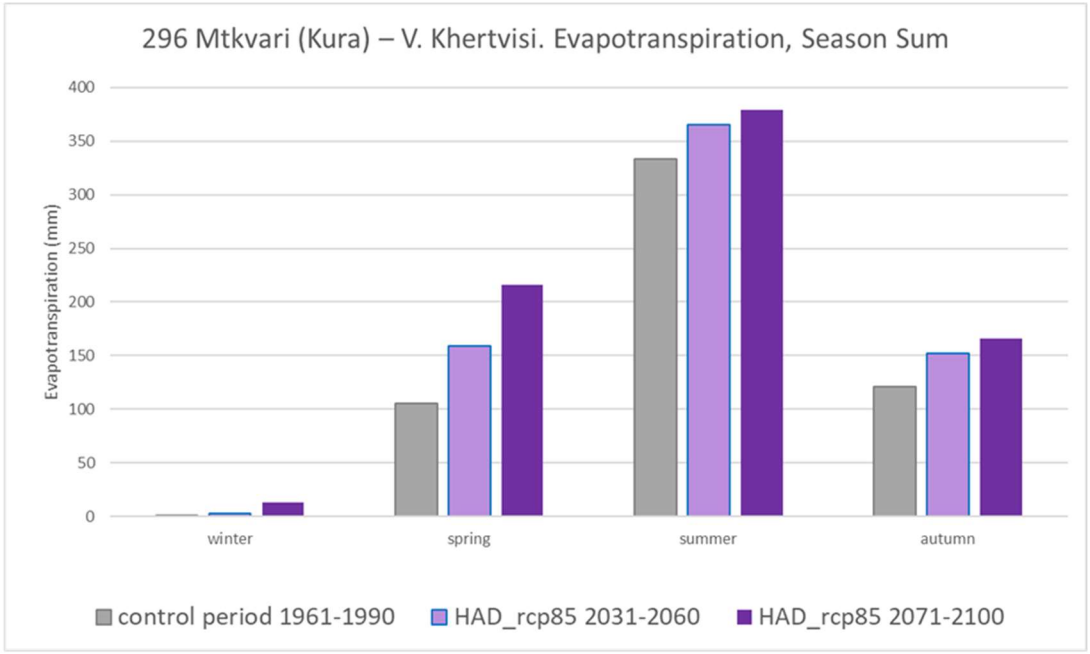

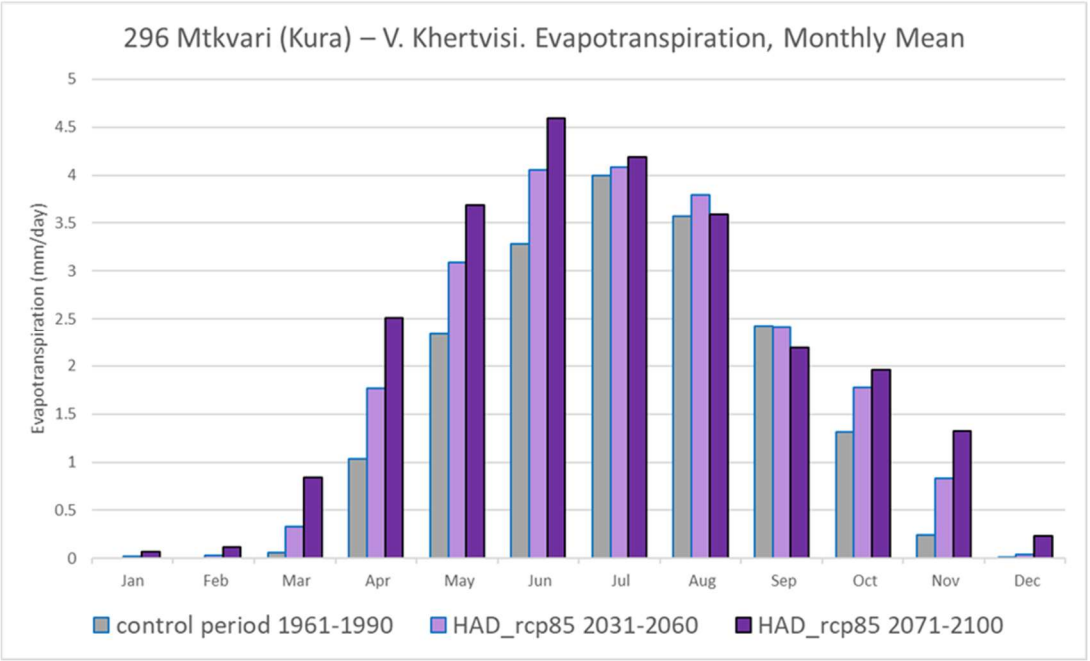

Figure A-80. Simulated season mean (top) and monthly mean (bottom) evapotranspiration in the control period, 1961-1990 (grey bars), the near future, 2031-2060 (light purple bars) and the end of the century, 2071-2100 (dark purple bars), according to the climate projection HAD, for the station 296 Mtkvari (Kura) – V. Khertvisi.

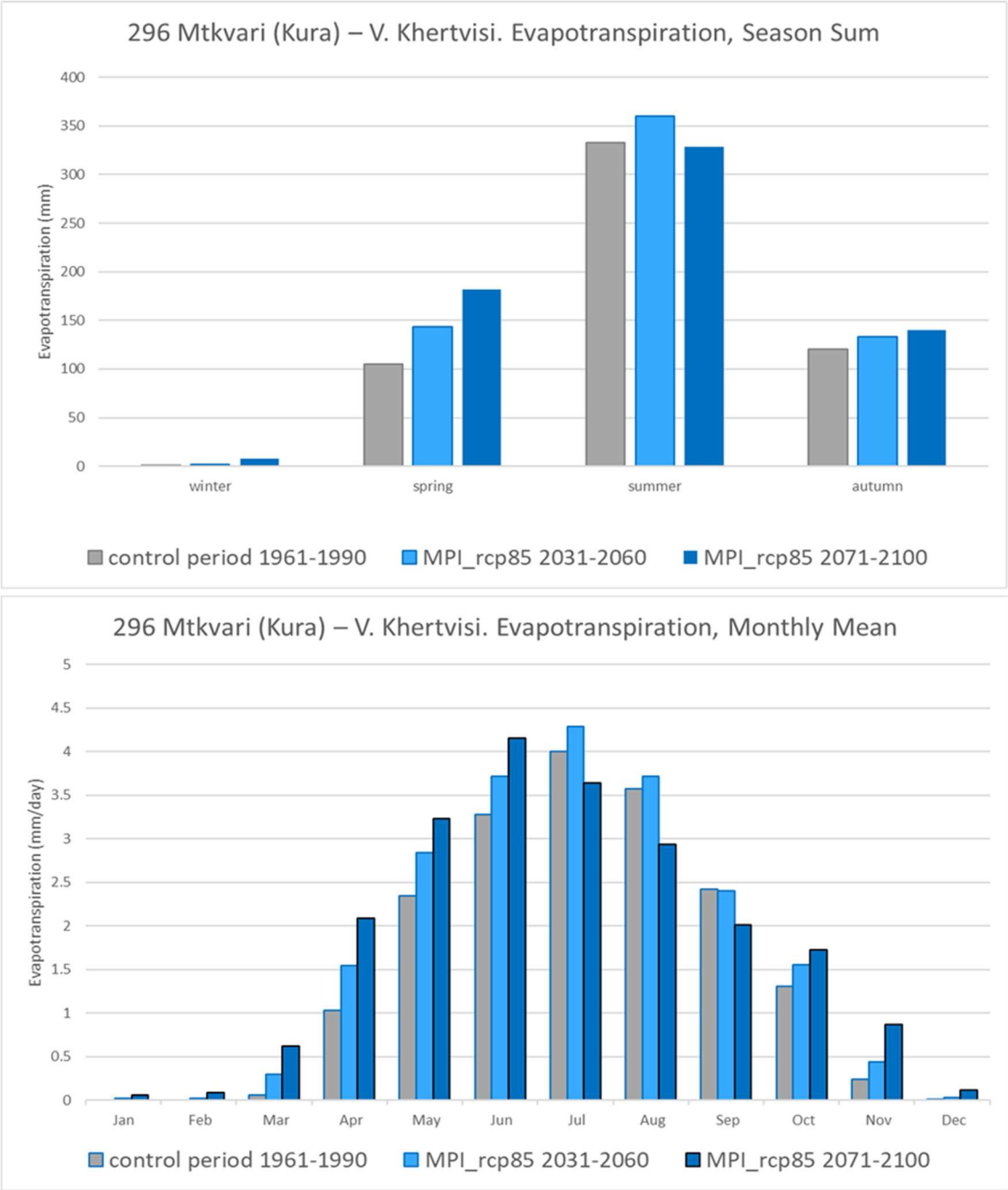

Figure A-81. Simulated season mean (top) and monthly mean (bottom) evapotranspiration in the control period, 1961-1990 (grey bars), the near future, 2031-2060 (light blue bars) and the end of the century, 2071-2100 (dark blue bars), according to the climate projection MPI, for the station 296 Mtkvari (Kura) – V. Khertvisi.

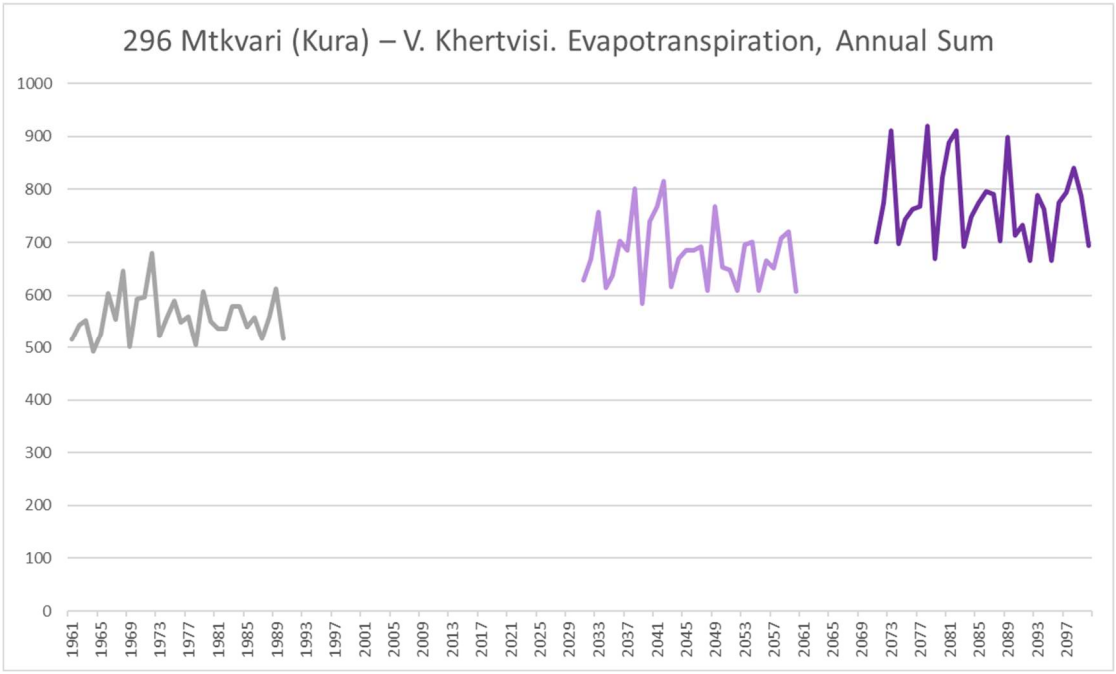

Figure A-82. Simulated annual evapotranspiration in the control period, 1961-1990 (grey line), the near future, 2031-2060 (light purple line) and the end of the century, 2071-2100 (dark purple line), according to the climate projection HAD, for the station 296 Mtkvari (Kura) – V. Khertvisi.

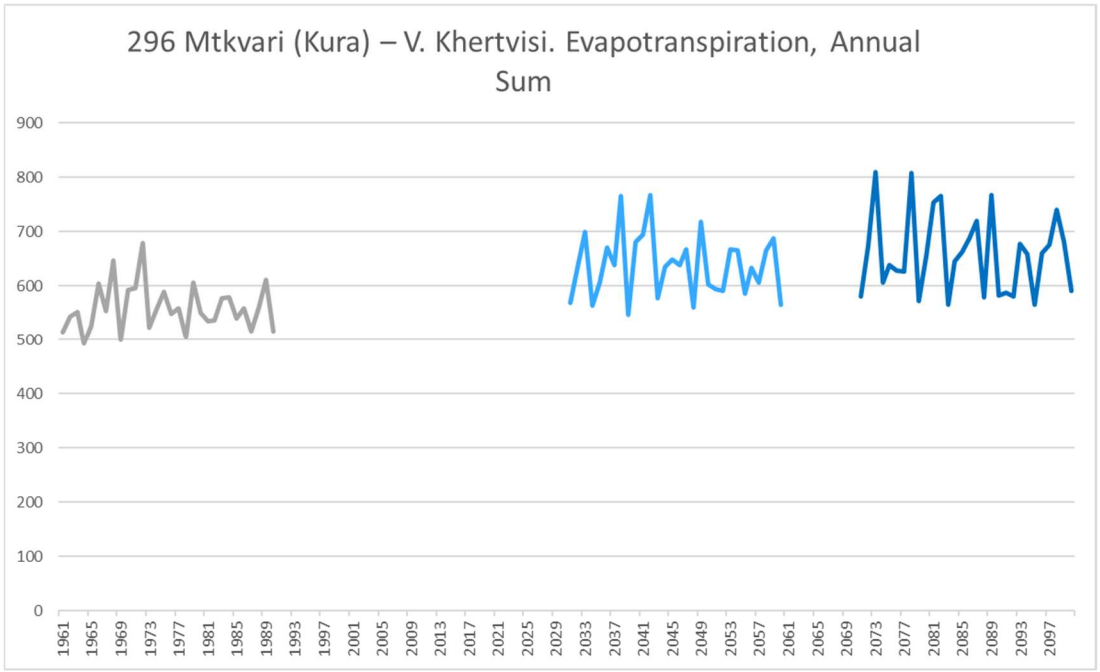

Figure A-83. Simulated annual evapotranspiration in the control period, 1961-1990 (grey line), the near future, 2031-2060 (light blue line) and the end of the century, 2071-2100 (dark blue line), according to the climate projection MPI, for the station 296 Mtkvari (Kura) – V. Khertvisi

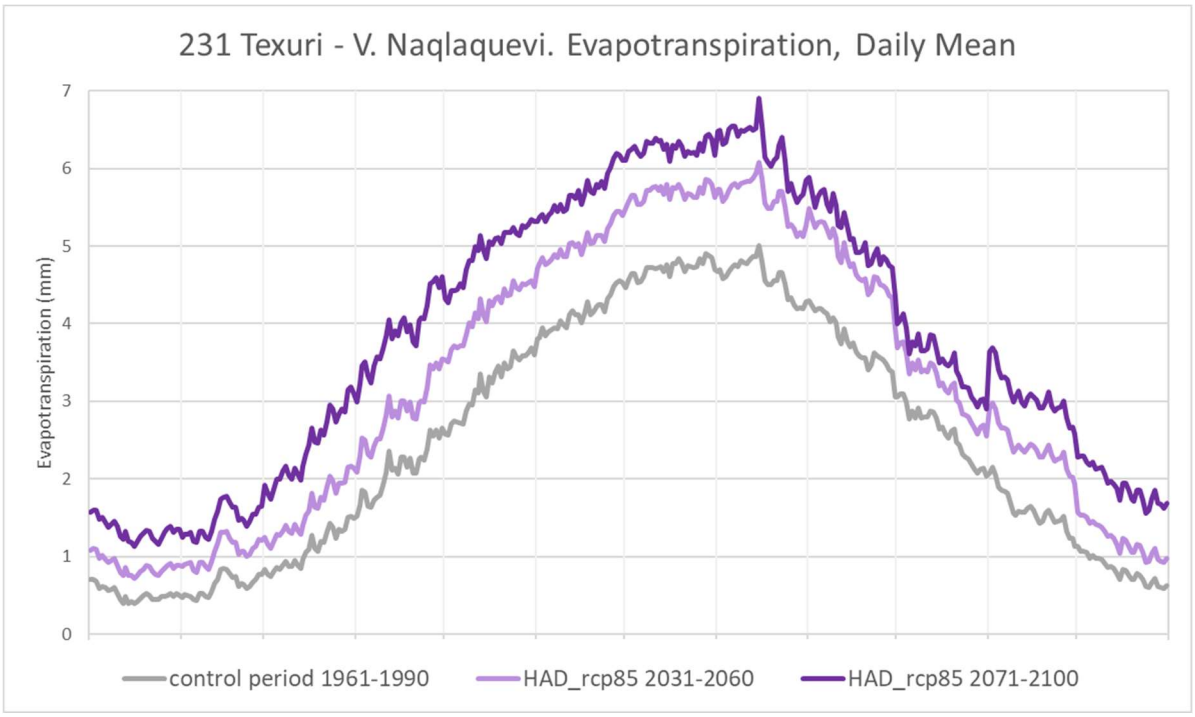

Figure A-84. Simulated daily mean evapotranspiration in the control period, 1961-1990 (grey line), the near future, 2031-2060 (light purple line) and the end of the century, 2071-2100 (dark purple line), according to the climate projection HAD, for the station 231 Texuri - V. Naqlaquevi.

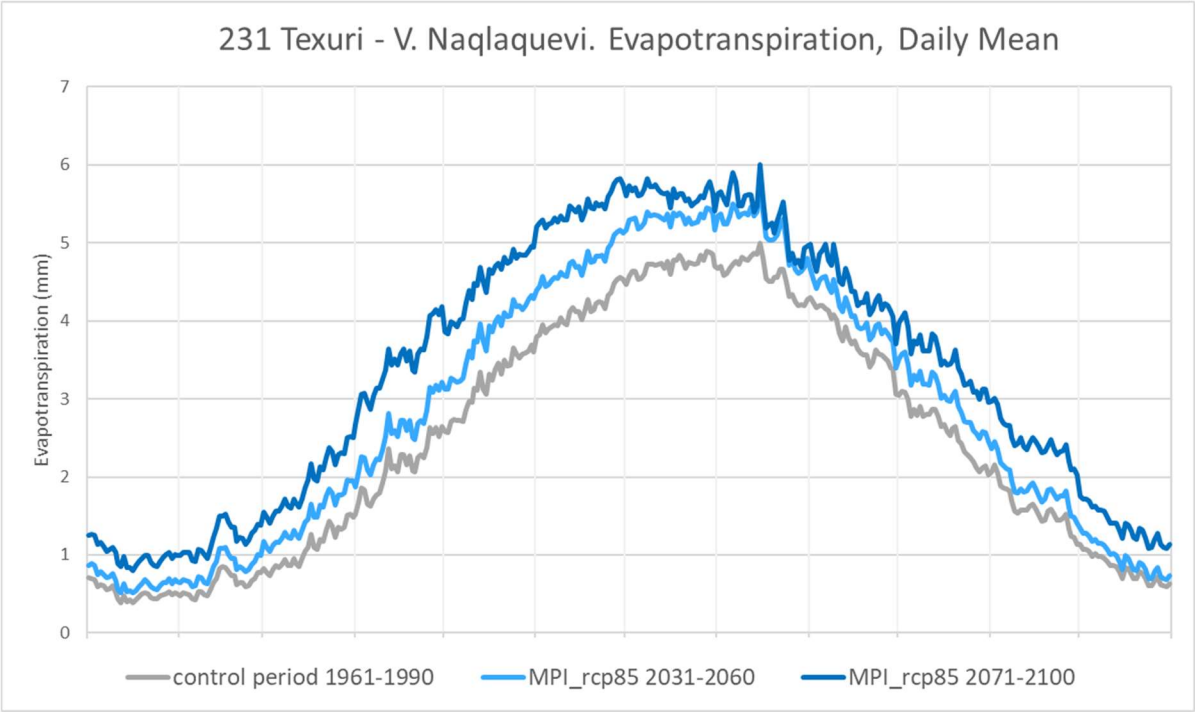

Figure A-85. Simulated daily mean evapotranspiration in the control period, 1961-1990 (grey line), the near future, 2031-2060 (light blue line) and the end of the century, 2071-2100 (dark blue line), according to the climate projection MPI, for the station 231 Texuri - V. Naqlaquevi.

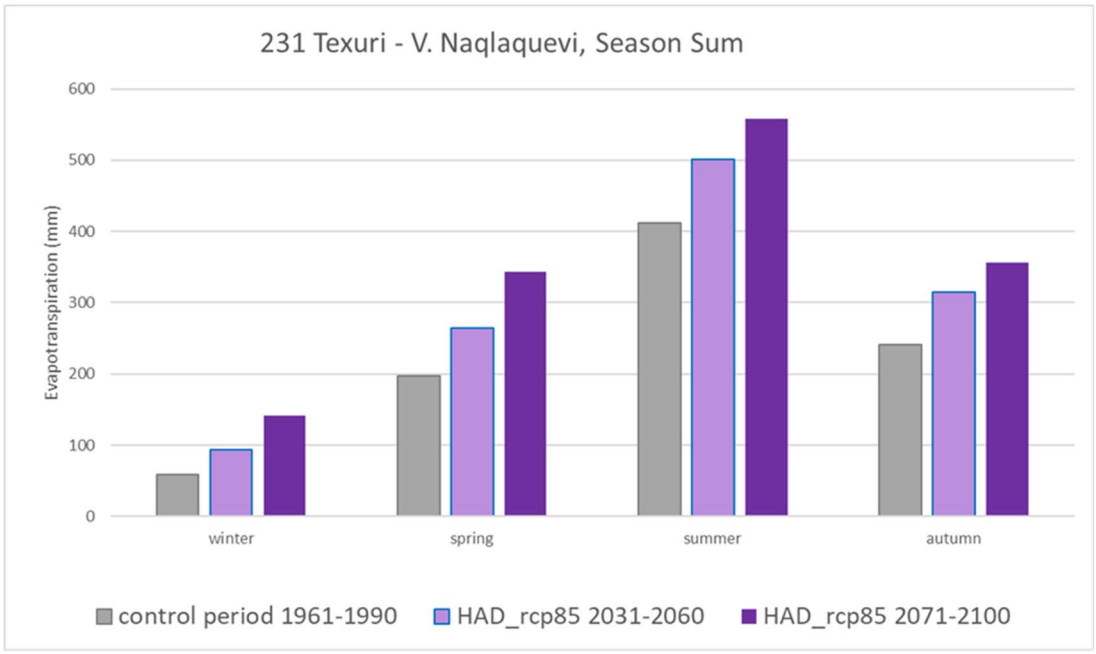

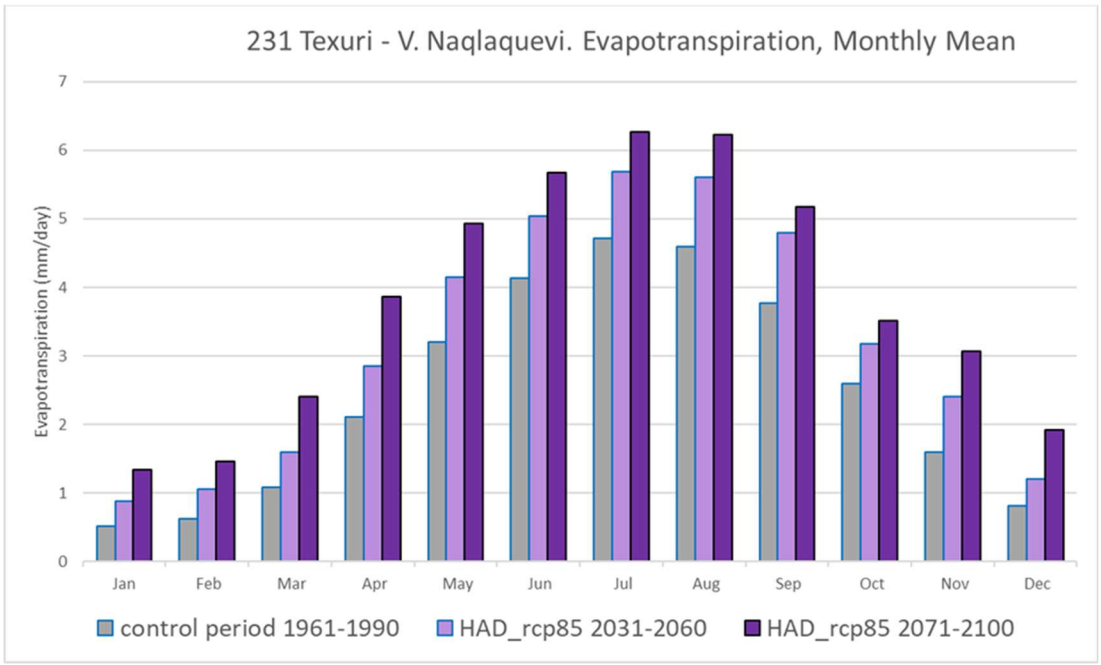

Figure A-86. Simulated season mean (top) and monthly mean (bottom) evapotranspiration in the control period, 1961-1990 (grey bars), the near future, 2031-2060 (light purple bars) and the end of the century, 2071-2100 (dark purple bars), according to the climate projection HAD for the station 231 Texuri - V. Naqlaquevi.

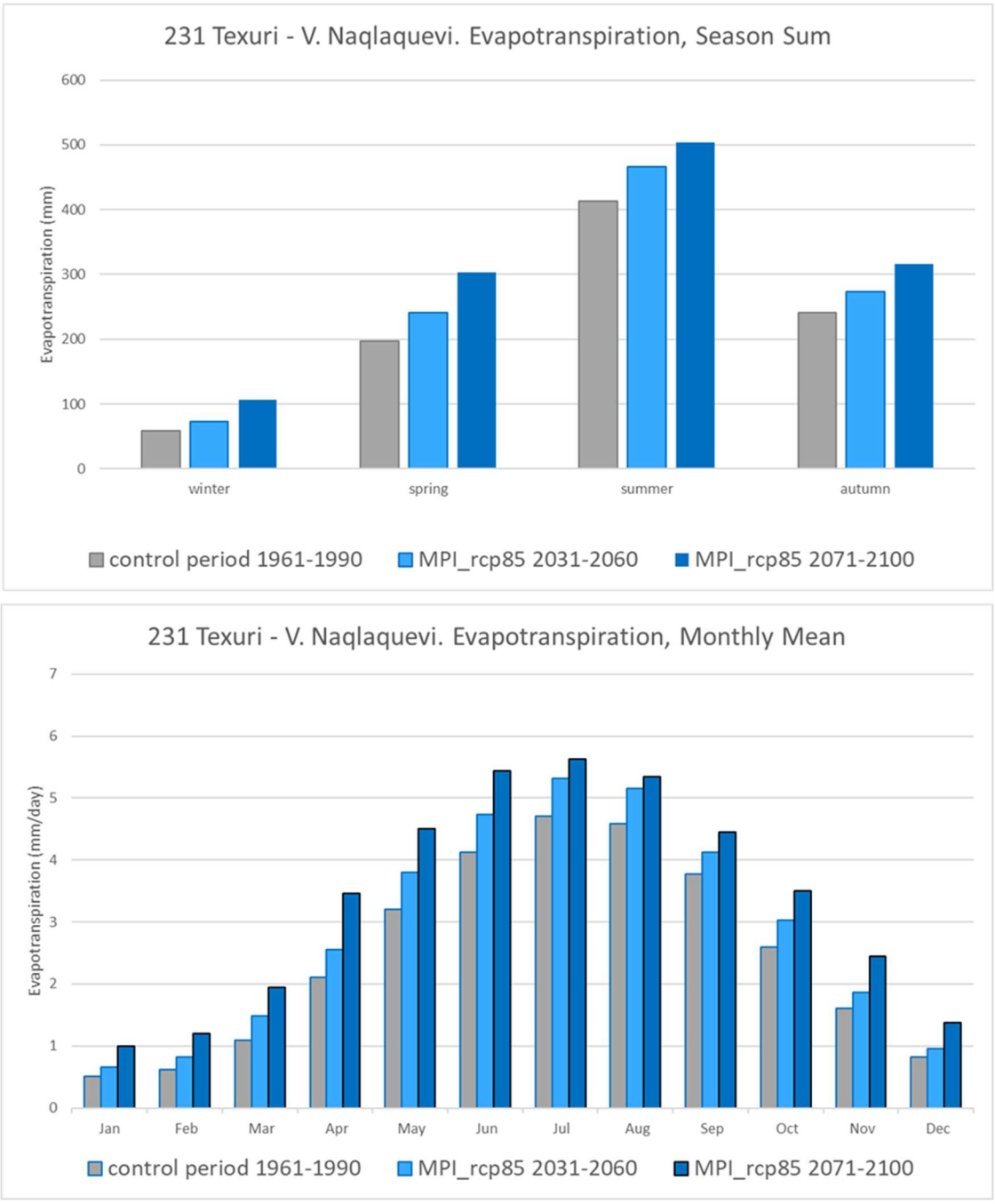

Figure A-87. Simulated season mean (top) and monthly mean (bottom) evapotranspiration in the control period, 1961-1990 (grey bars), the near future, 2031-2060 (light blue bars) and the end of the century, 2071-2100 (dark blue bars), according to the climate projection MPI, for the station 231 Texuri - V. Naqlaquevi.

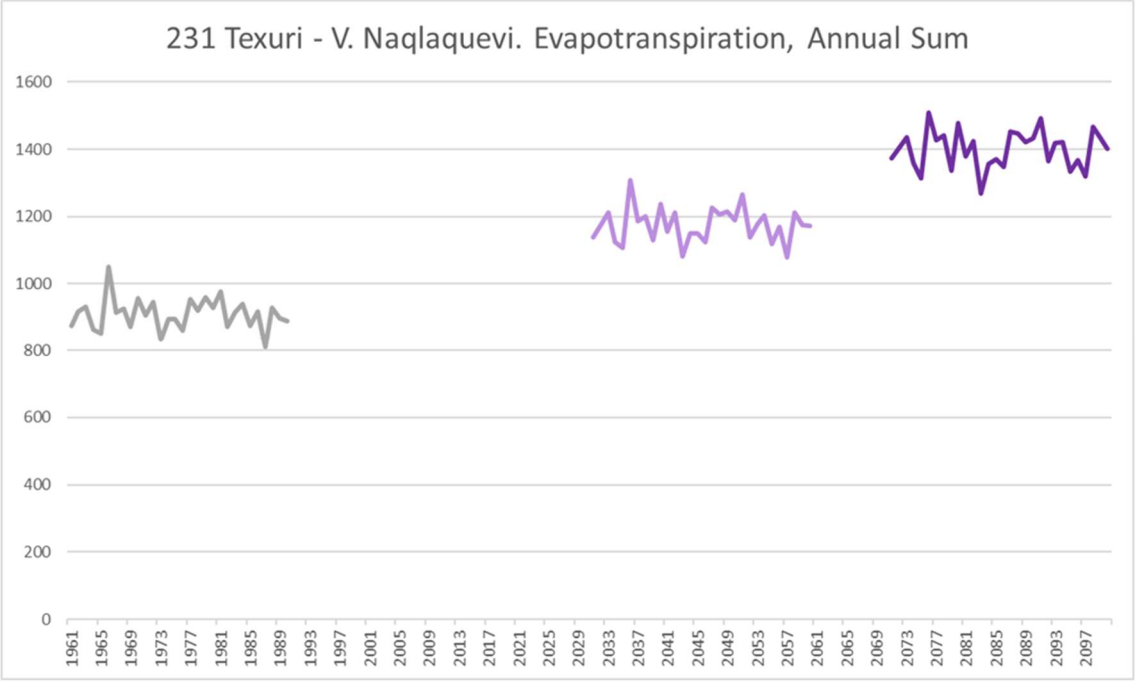

Figure A-88. Simulated annual evapotranspiration in the control period, 1961-1990 (grey line), the near future, 2031-2060 (light purple line) and the end of the century, 2071-2100 (dark purple line), according to the climate projection HAD, for the station 231 Texuri - V. Naqlaquevi.

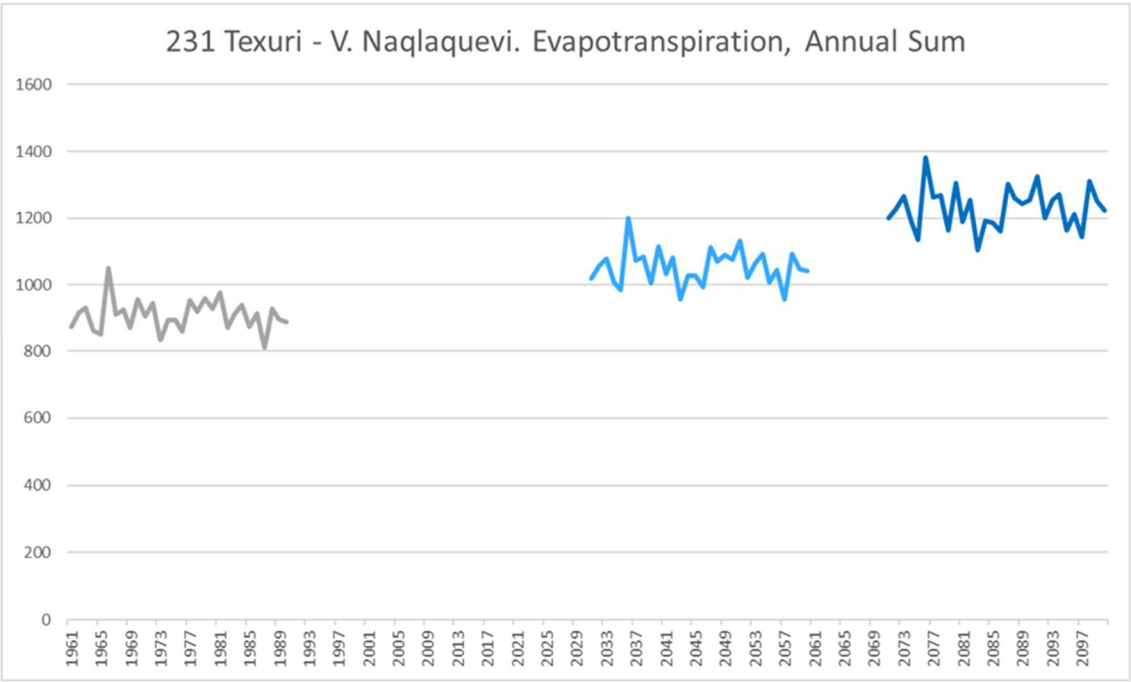

Figure A-89. Simulated annual evapotranspiration in the control period, 1961-1990 (grey line), the near future, 2031-2060 (light blue line) and the end of the century, 2071-2100 (dark blue line), according to the climate projection MPI, for the station 231 Texuri - V. Naqlaquevi.

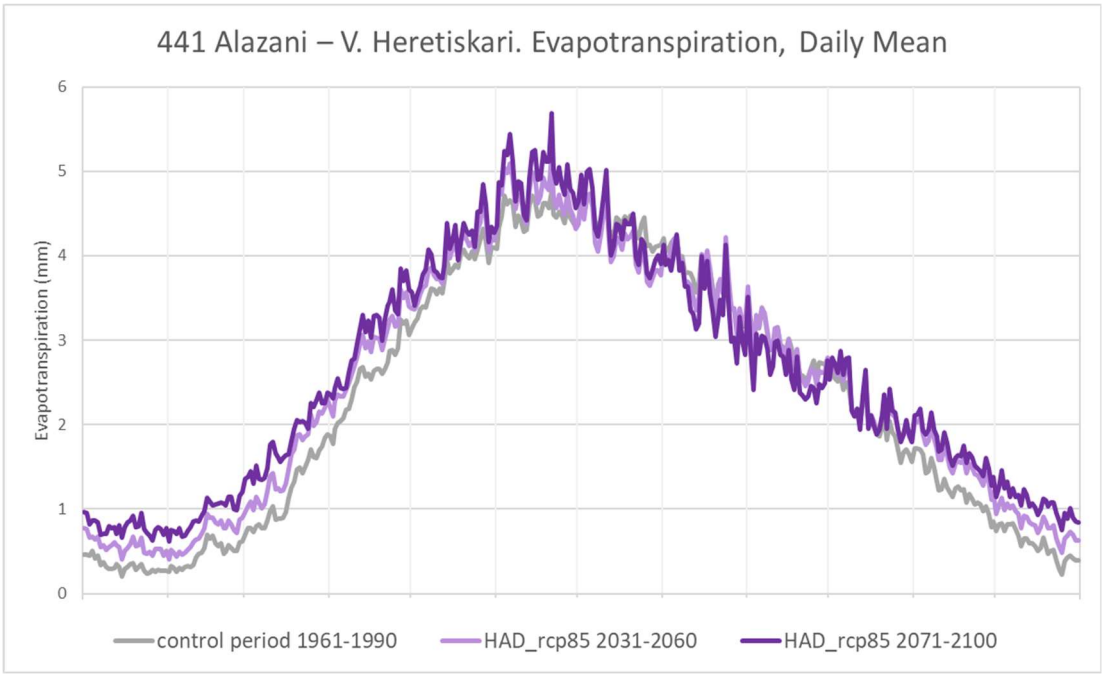

Figure A-90. Simulated daily mean evapotranspiration in the control period, 1961-1990 (grey line), the near future, 2031-2060 (light purple line) and the end of the century, 2071-2100 (dark purple line), according to the climate projection HAD, for the station 441 Alazani – V. Heretiskari.

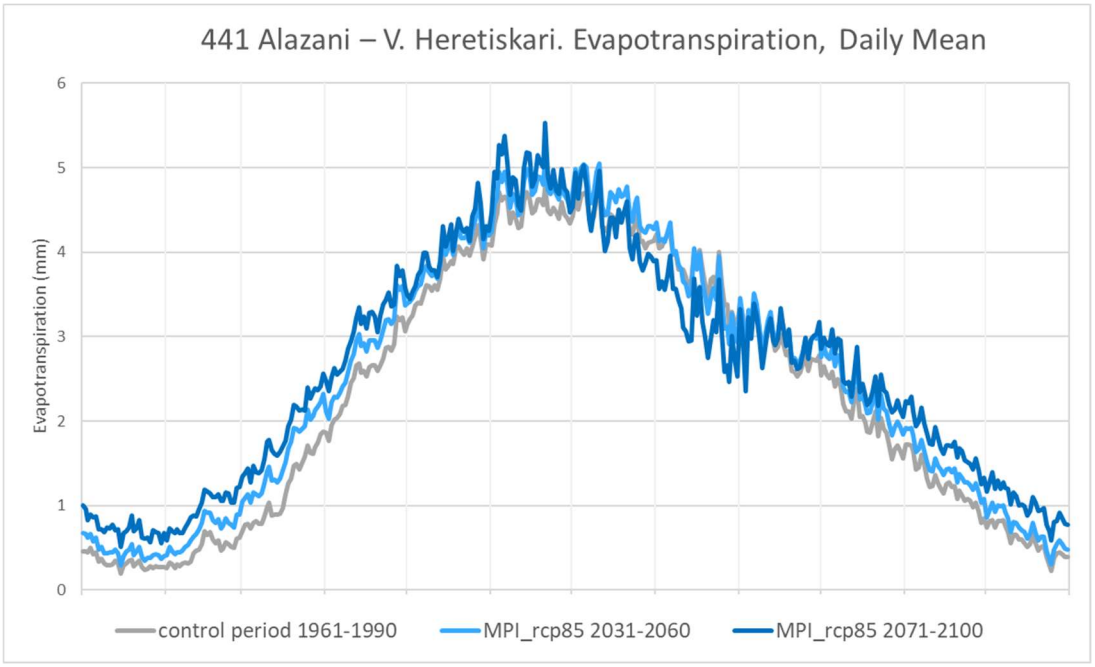

Figure A-91. Simulated daily mean evapotranspiration in the control period, 1961-1990 (grey line), the near future, 2031-2060 (light blue line) and the end of the century, 2071-2100 (dark blue line), according to the climate projection MPI, for the station 441 Alazani – V. Heretiskari

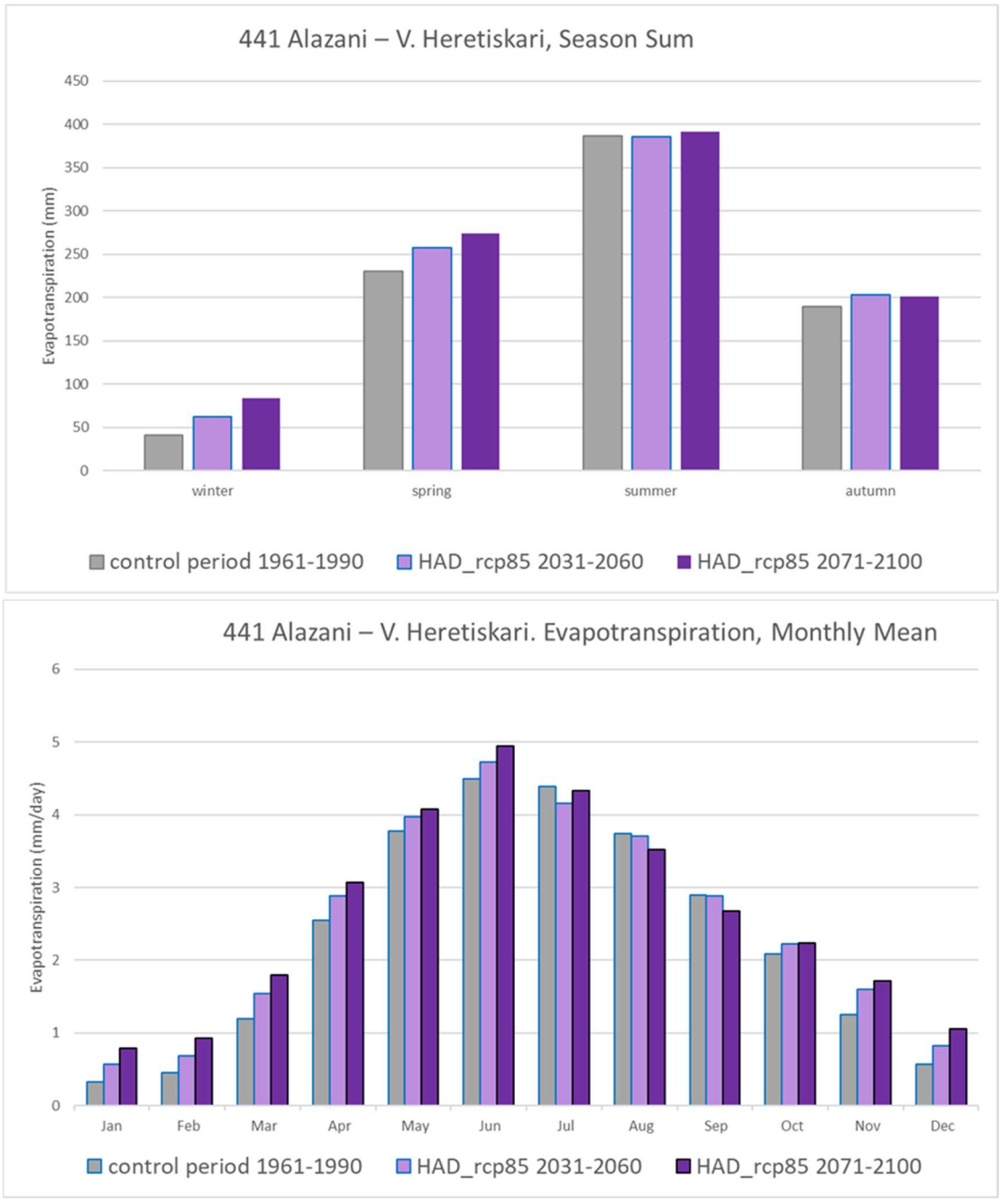

Figure A-92. Simulated season mean (top) and monthly mean (bottom) evapotranspiration in the control period, 1961-1990 (grey bars), the near future, 2031-2060 (light purple bars) and the end of the century, 2071-2100 (dark purple bars), according to the climate projection HAD, for the station 441 Alazani – V. Heretiskari.

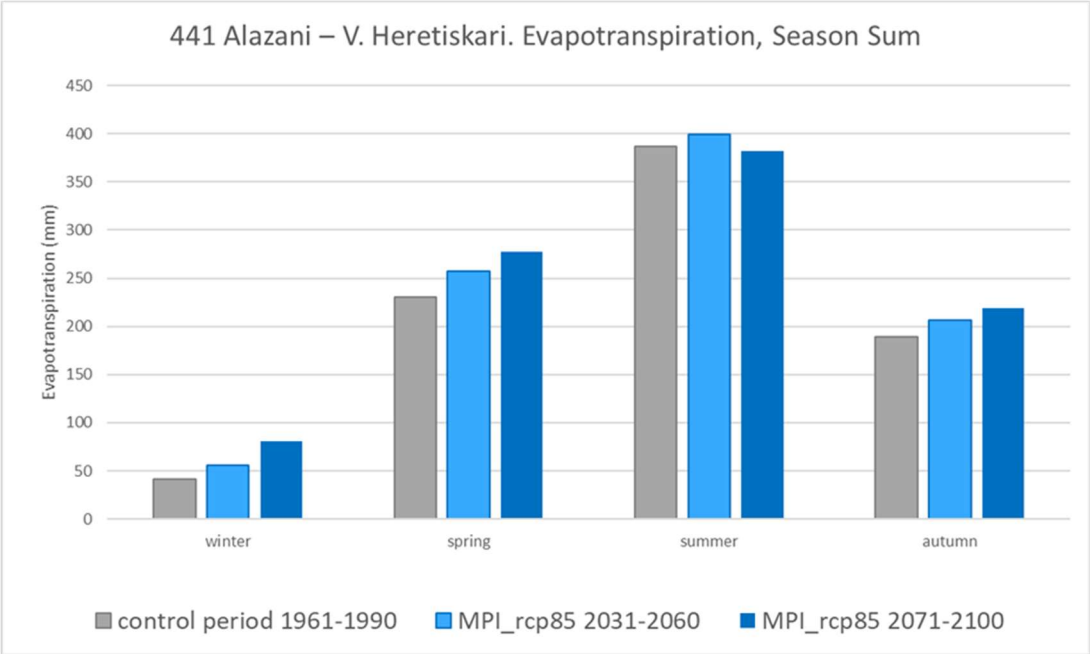

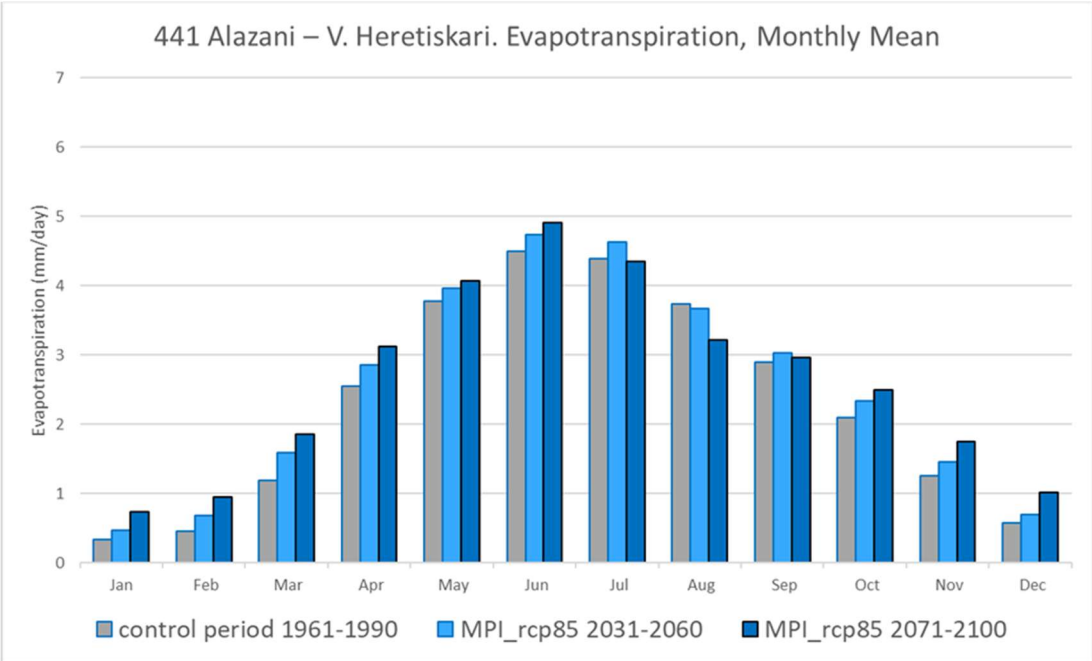

Figure A-93. Simulated season mean (top) and monthly mean (bottom) evapotranspiration in the control period, 1961-1990 (grey bars), the near future, 2031-2060 (light blue bars) and the end of the century, 2071-2100 (dark blue bars), according to the climate projection MPI, for the station 441 Alazani – V. Heretiskari.

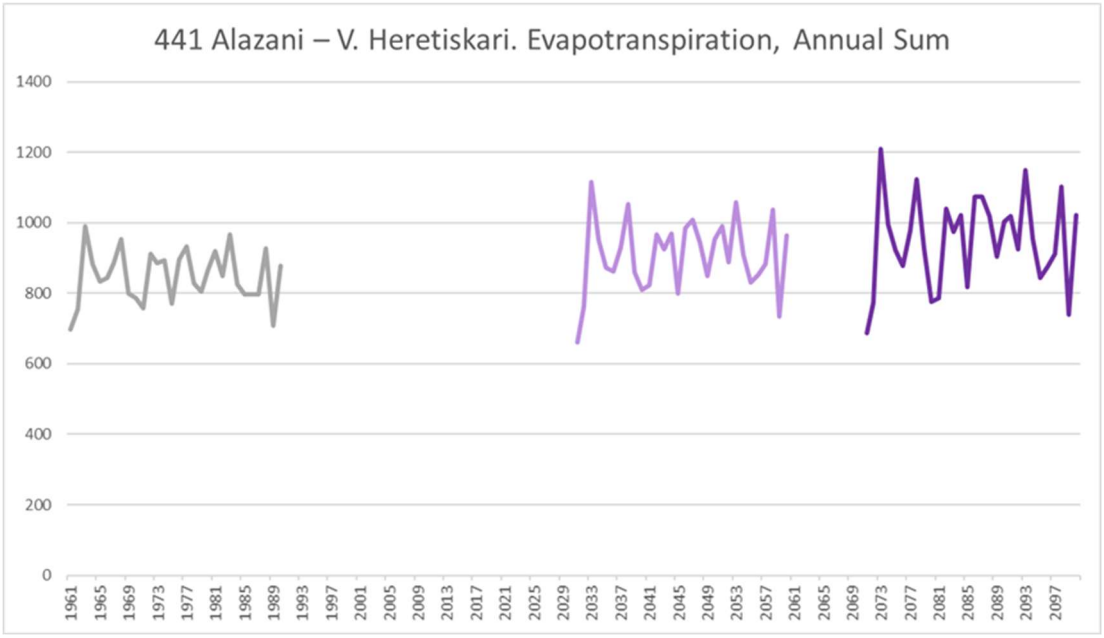

Figure A-94. Simulated annual evapotranspiration in the control period, 1961-1990 (grey line), the near future, 2031-2060 (light purple line) and the end of the century, 2071-2100 (dark purple line), according to the climate projection HAD, for the station 441 Alazani – V. Heretiskari.

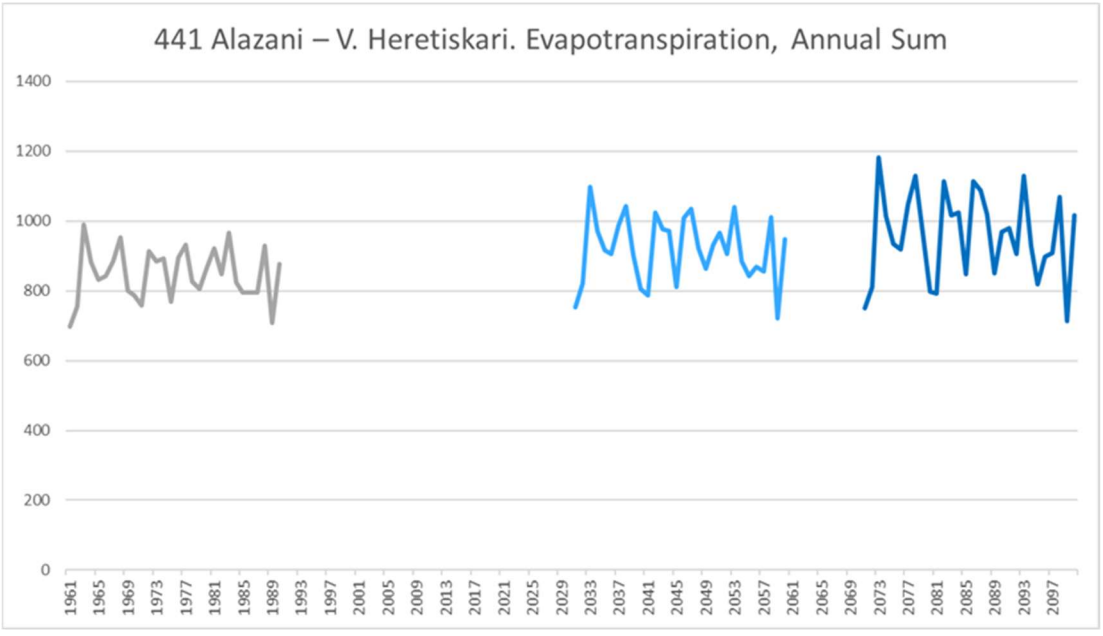

Figure A-95. Simulated annual evapotranspiration in the control period, 1961-1990 (grey line), the near future, 2031-2060 (light blue line) and the end of the century, 2071-2100 (dark blue line), according to the climate projection MPI, for the station 441 Alazani – V. Heretiskari.

Streamflow

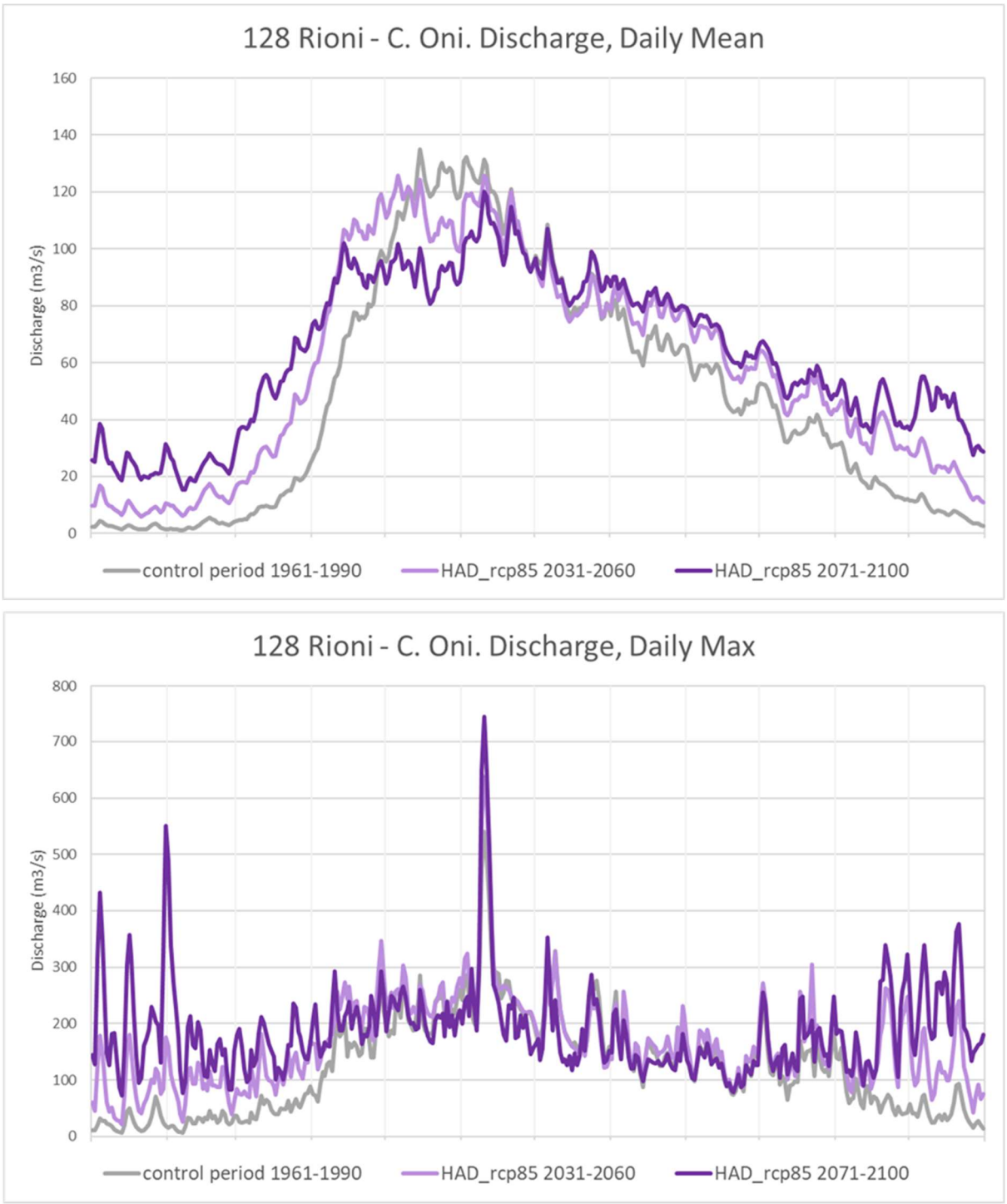

Figure A-96. Simulated daily mean streamflow (top) and daily maximum streamflow in the control period, 1961-1990 (grey line), the near future, 2031-2060 (light purple line) and the end of the century, 2071-2100 (dark purple line), according to the climate projection HAD and the high emission scenario, for the station 128 Rioni - C. Oni.

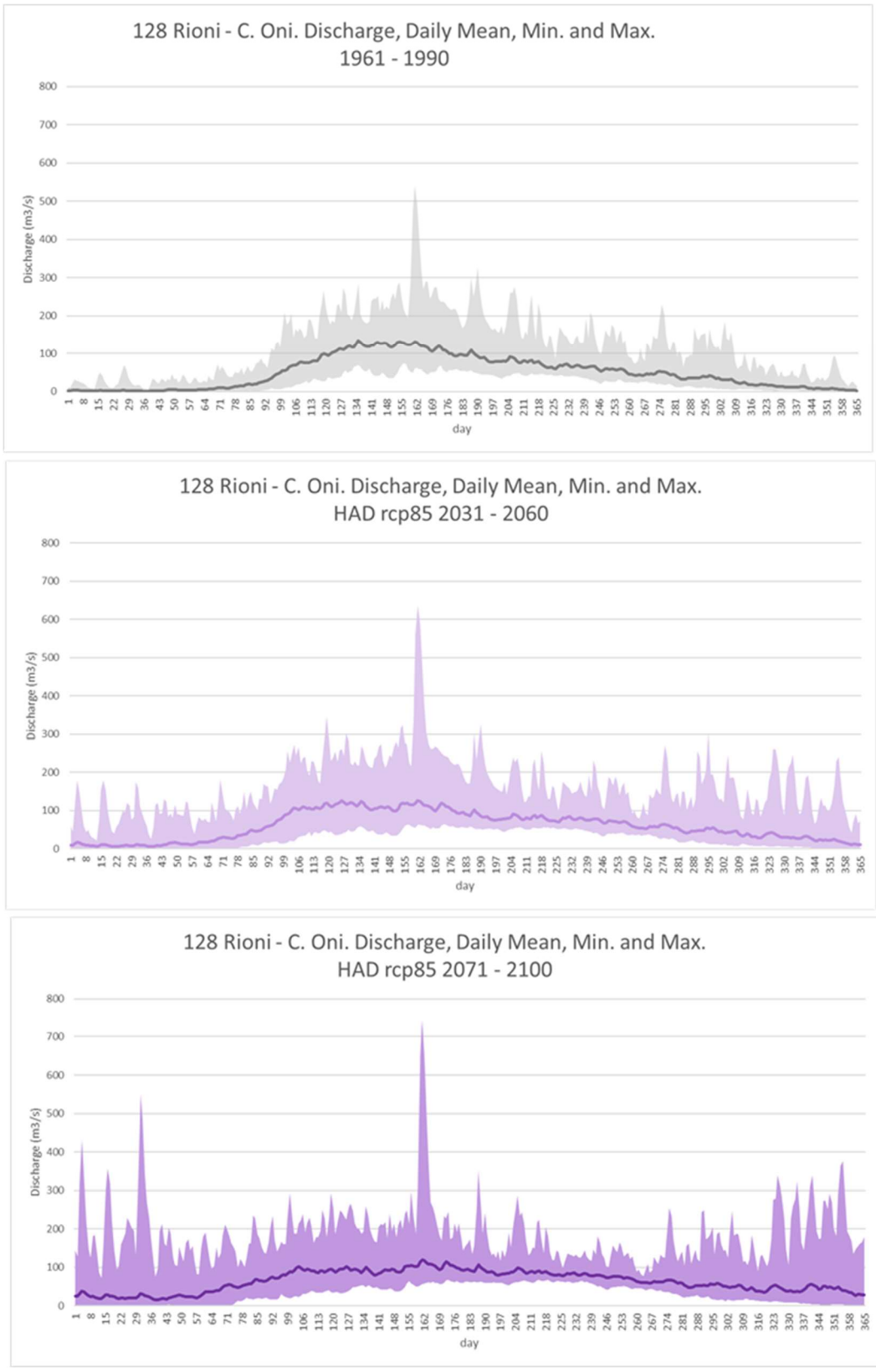

Figure A-97. Simulated daily minimum, mean and maximum streamflow in the control period, 1961-1990 (grey colours), the near future, 2031-2060 (light purple colours) and the end of the century, 2071-2100 (dark purple colours), according to the climate projection HAD and the high emission scenario, for the station 128 Rioni - C. Oni.

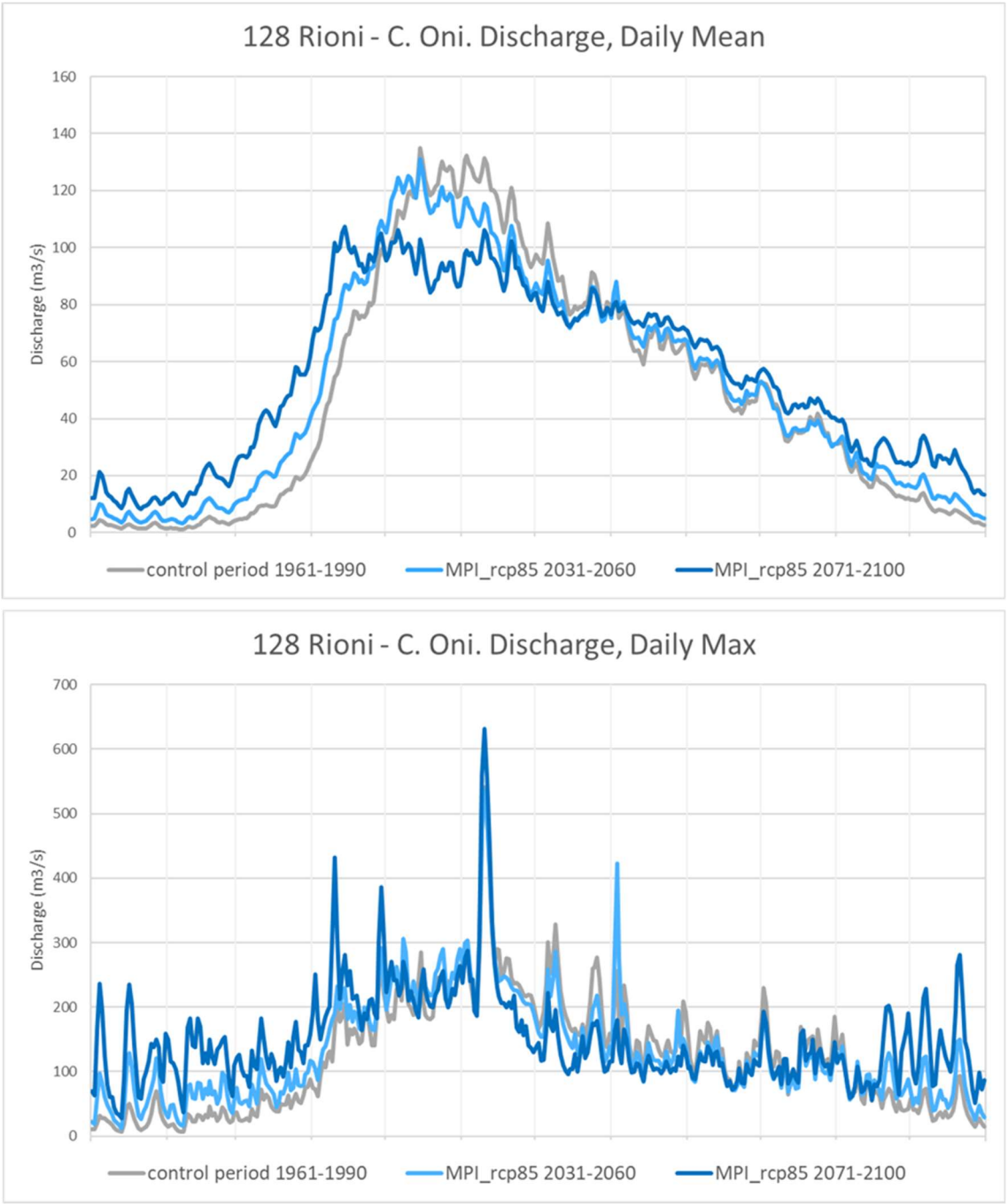

Figure A-98. Simulated daily mean streamflow (top) and daily maximum streamflow in the control period, 1961-1990 (grey line), the near future, 2031-2060 (light blue line) and the end of the century, 2071-2100 (dark blue line), according to the climate projection MPI and the high emission scenario, for the station 128 Rioni - C. Oni.

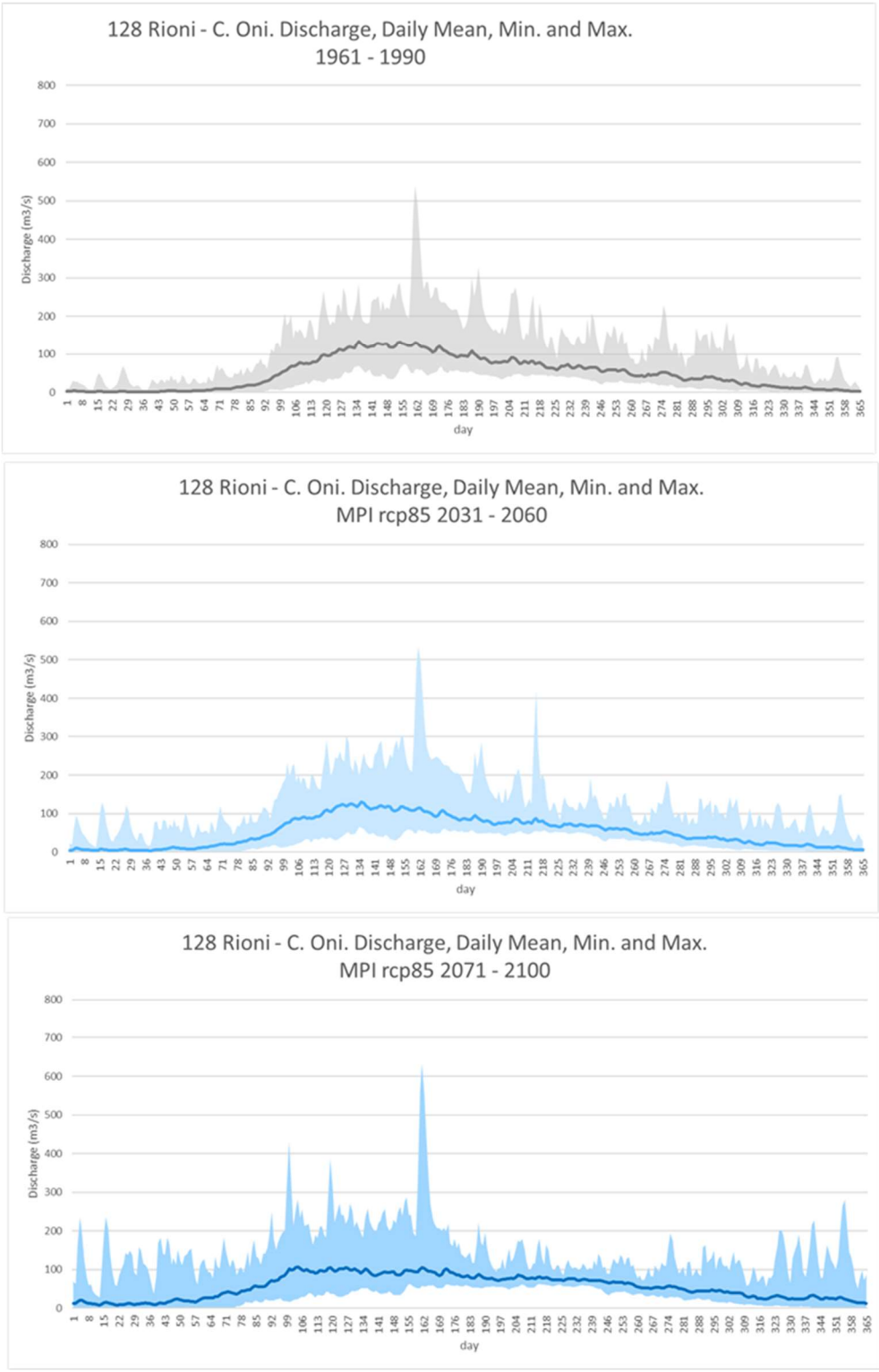

Figure A-99. Simulated daily minimum, mean and maximum streamflow in the control period, 1961-1990 (grey colours), the near future, 2031-2060 (light purple colours) and the end of the century, 2071-2100 (dark purple colours), according to the climate projection MPI and the high emission scenario, for the station 128 Rioni - C. Oni.

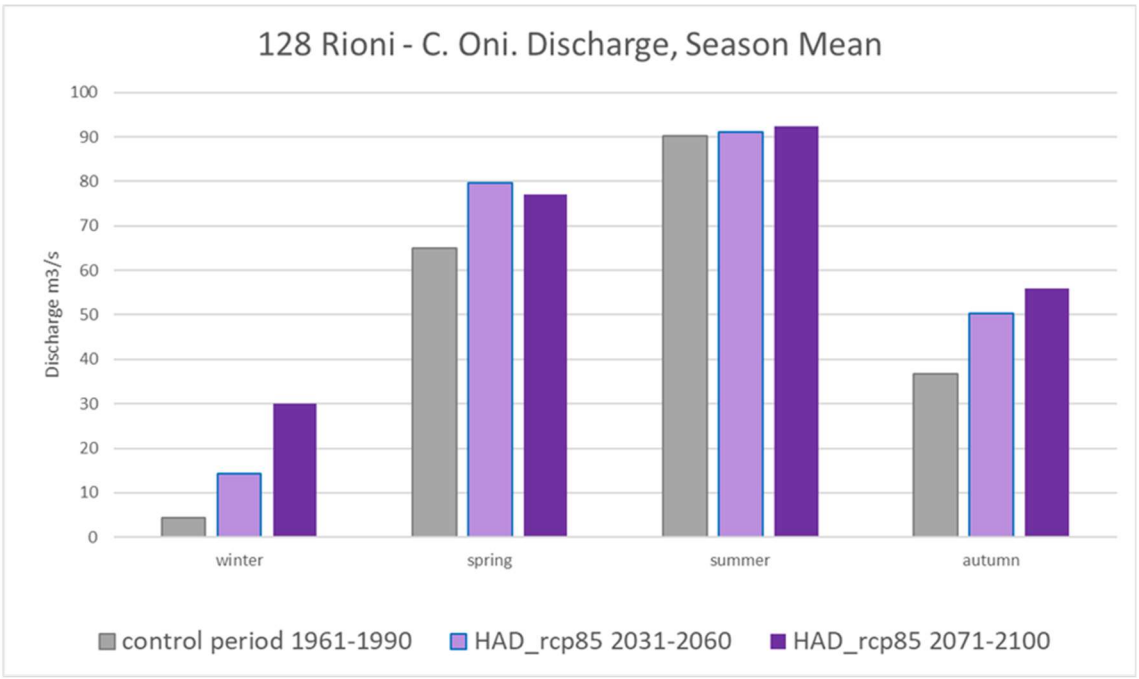

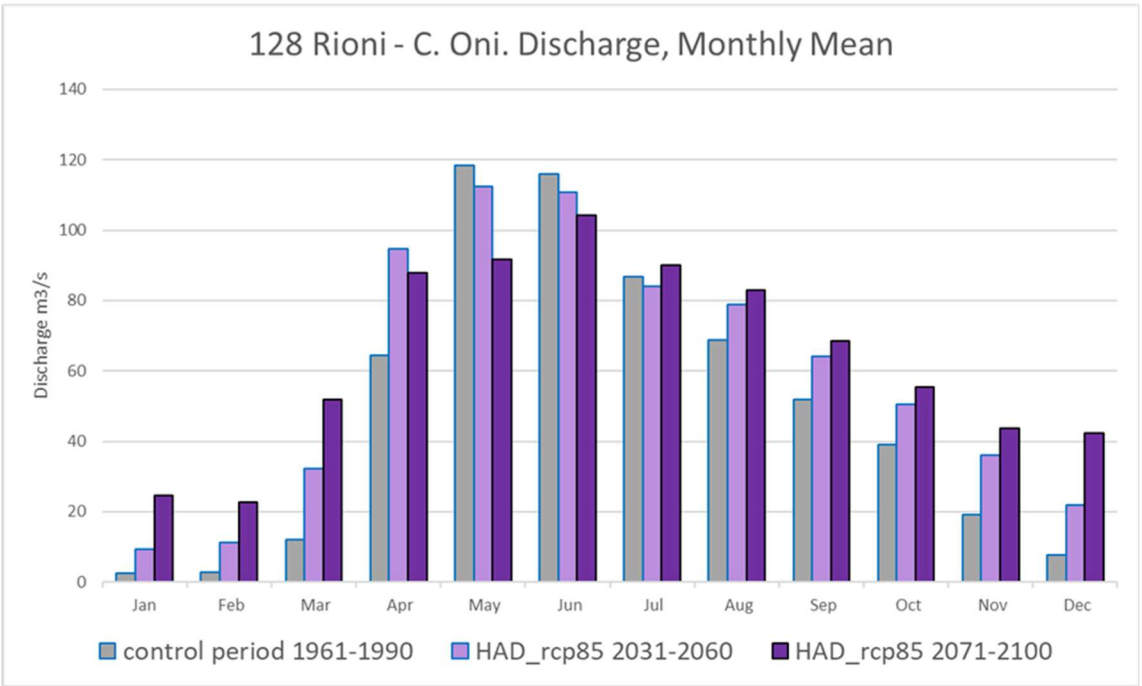

Figure A-100. Simulated season mean (top) and monthly mean (bottom) streamflow in the control period, 1961-1990 (grey bars), the near future, 2031-2060 (light purple bars) and the end of the century, 2071-2100 (dark purple bars), according to the climate projection HAD and the high emission scenario, for the station 128 Rioni - C. Oni.

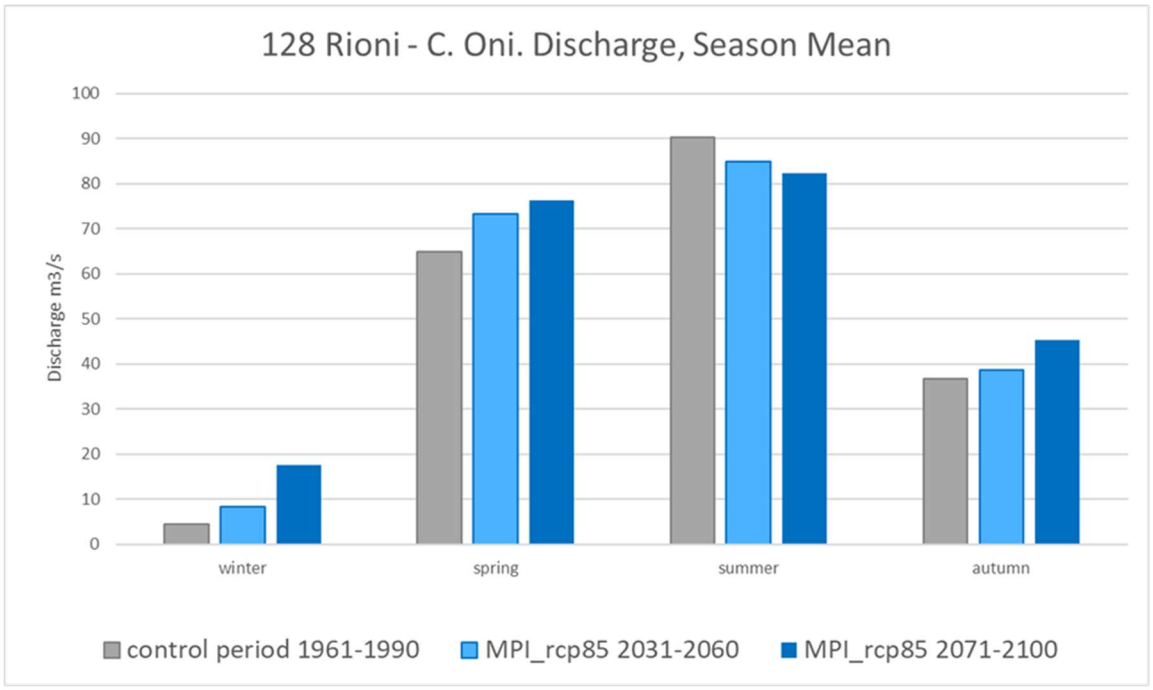

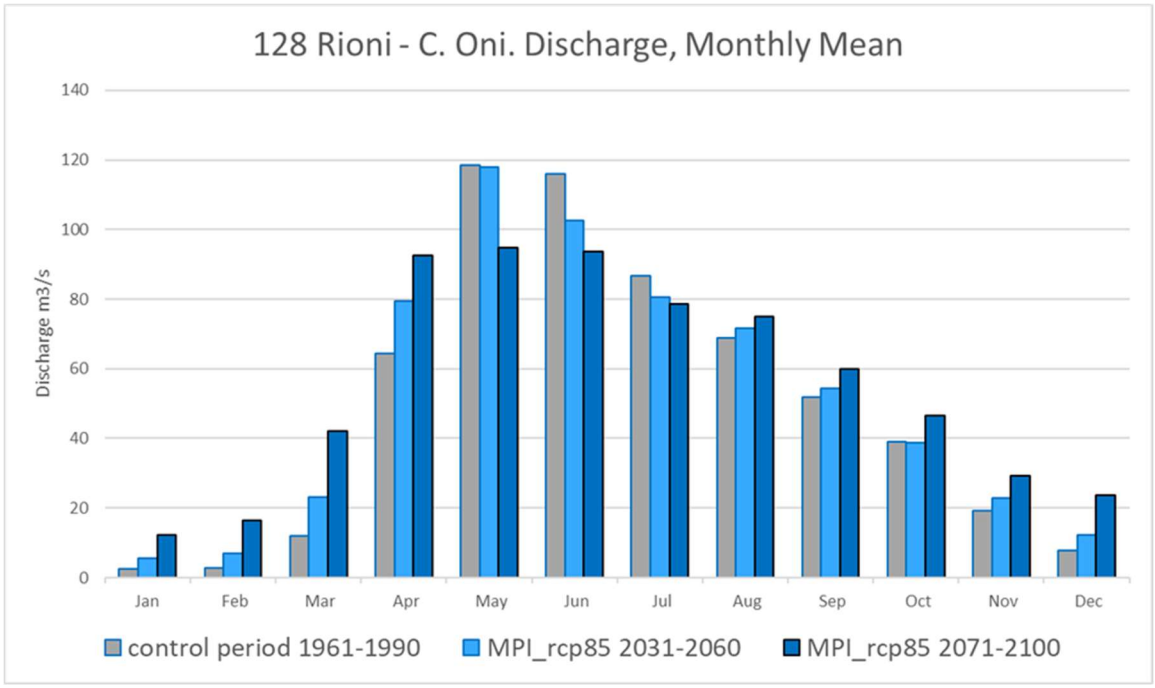

Figure A-101. Simulated season mean (top) and monthly mean (bottom) streamflow in the control period, 1961-1990 (grey bars), the near future, 2031-2060 (light blue bars) and the end of the century, 2071-2100 (dark blue bars), according to the climate projection MPI and the high emission scenario, for the station 128 Rioni - C. Oni.

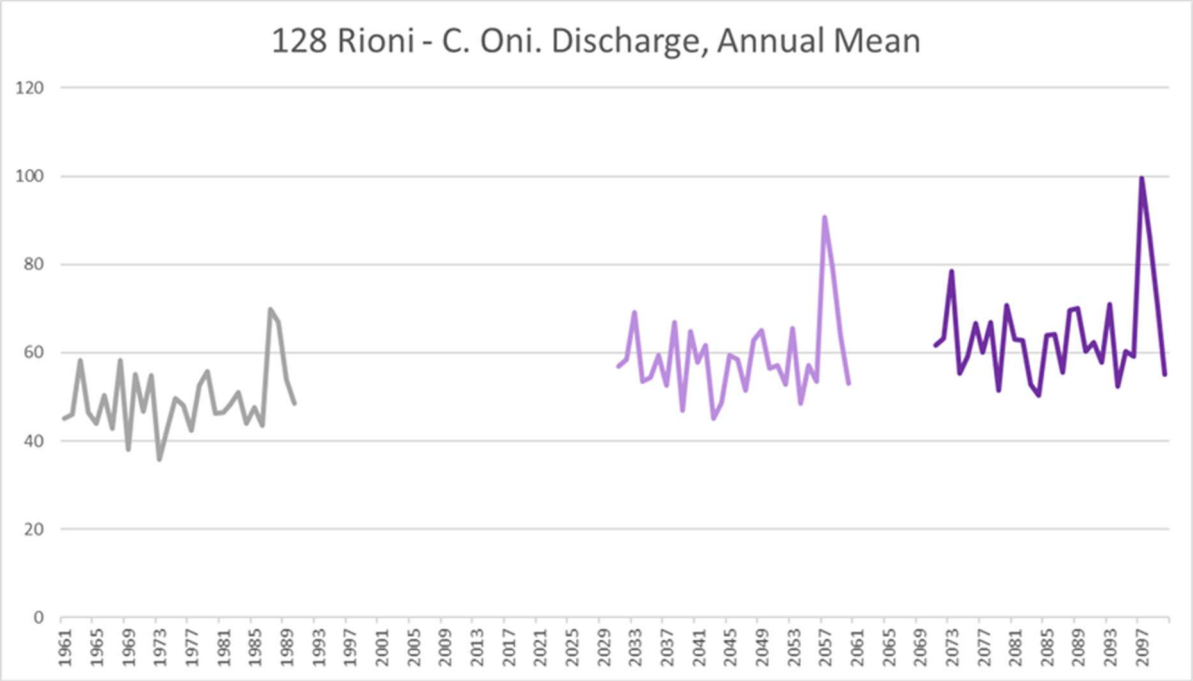

Figure A-102. Simulated annual streamflow in the control period, 1961-1990 (grey line), the near future, 2031-2060 (light purple line) and the end of the century, 2071-2100 (dark purple line), according to the climate projection HAD and the high emission scenario, for the station 128 Rioni - C. Oni.

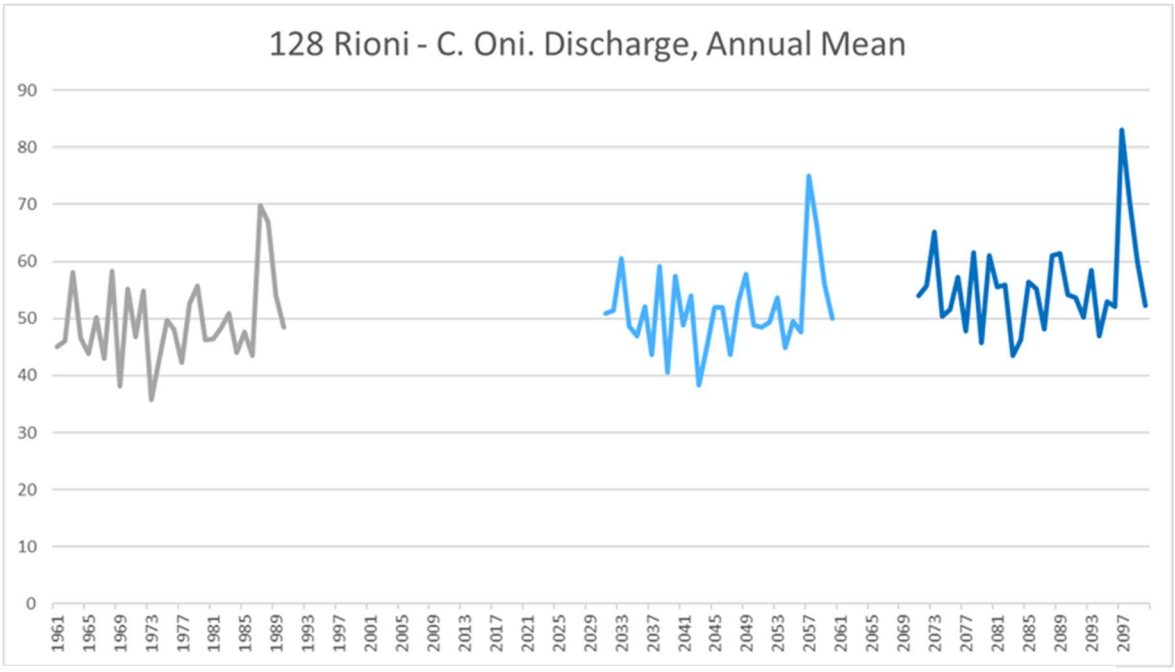

Figure A-103. Simulated annual streamflow in the control period, 1961-1990 (grey line), the near future, 2031-2060 (light purple line) and the end of the century, 2071-2100 (dark purple line), according to the climate projection HAD and the high emission scenario, for the station 128 Rioni - C. Oni.

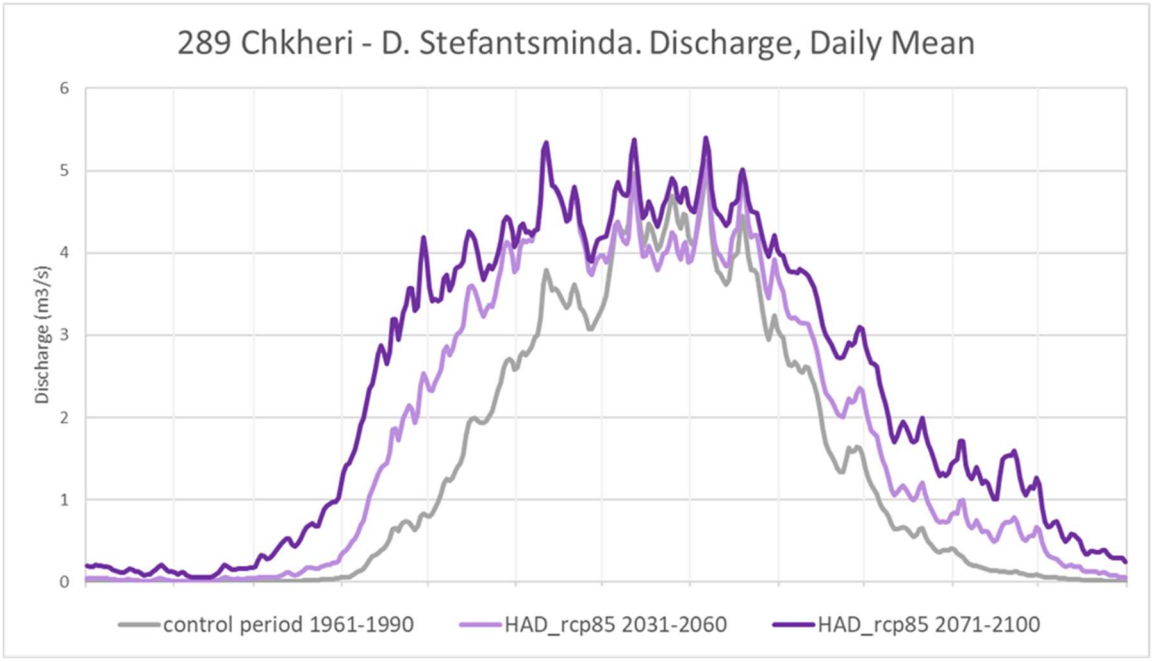

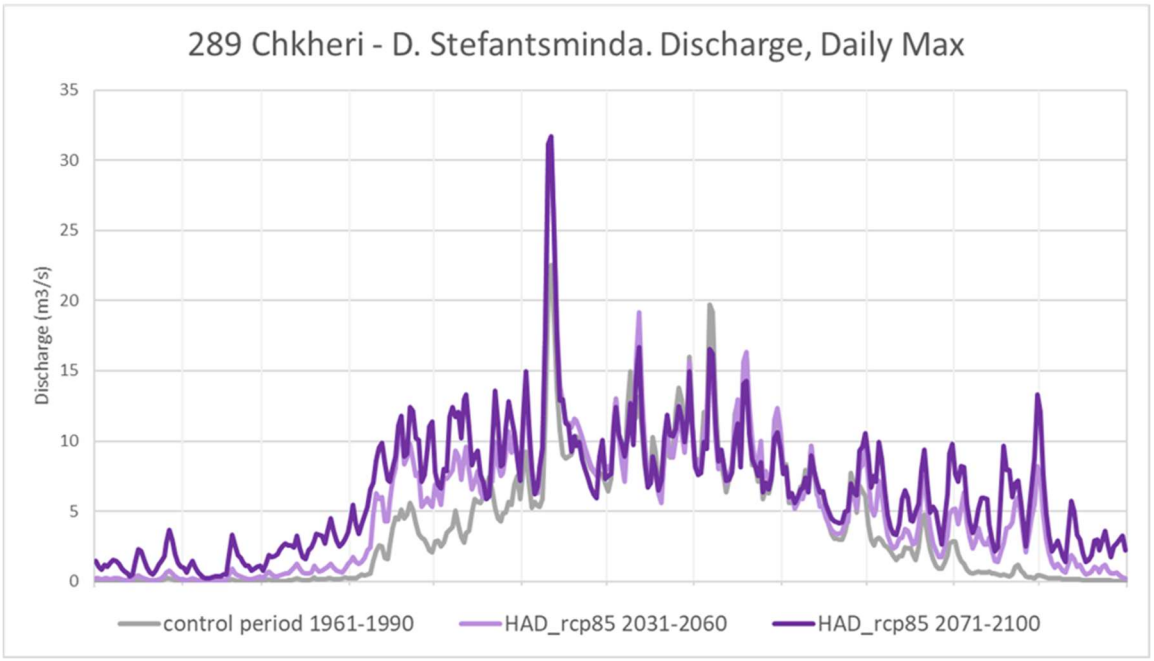

Figure A-104. Simulated daily mean streamflow (top) and daily maximum streamflow in the control period, 1961-1990 (grey line), the near future, 2031-2060 (light purple line) and the end of the century, 2071-2100 (dark purple line), according to the climate projection HAD and the high emission scenario, for the station 289 Chkheri - D. Stefantsminda.

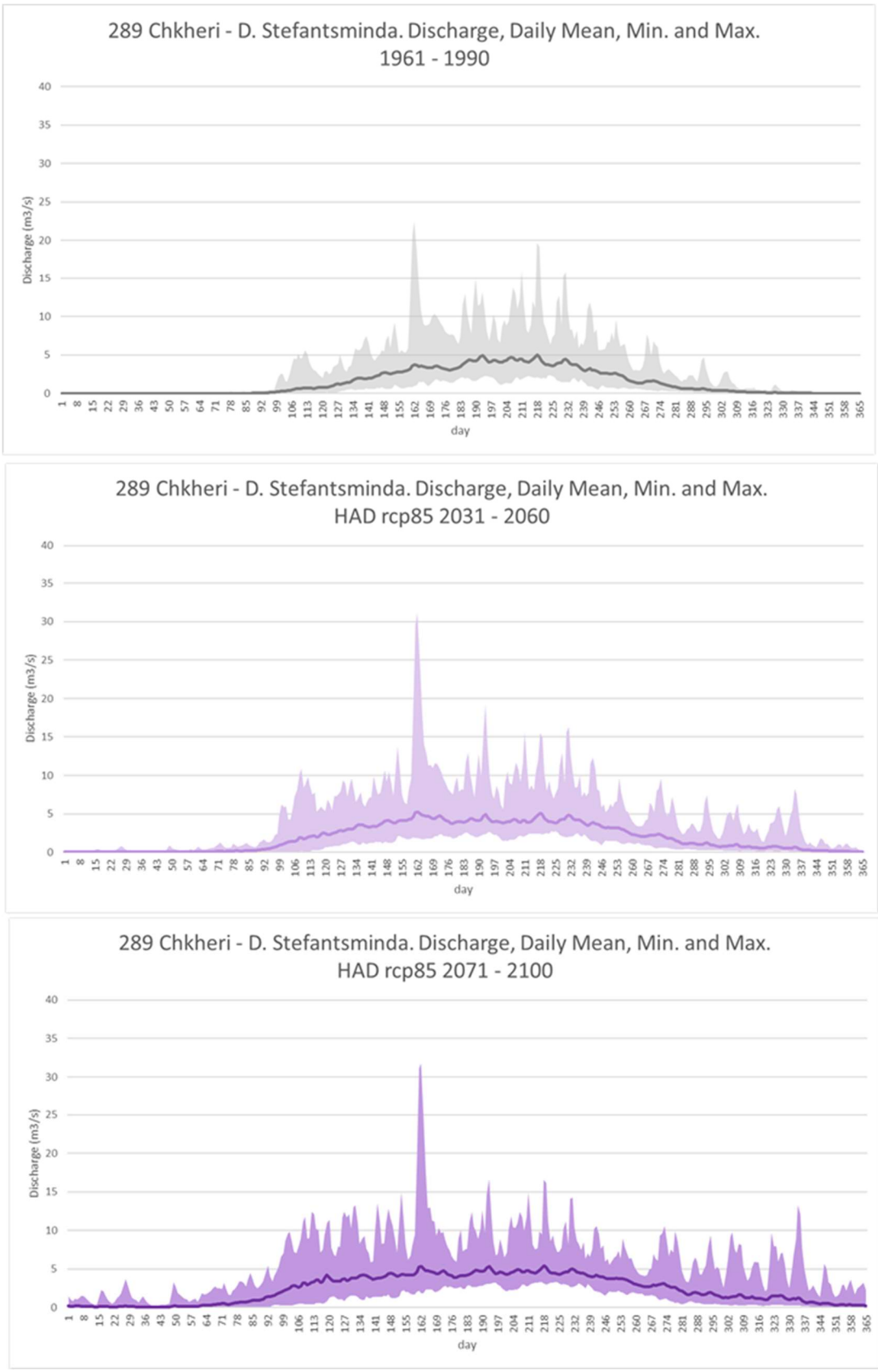

Figure A-105. Simulated daily minimum, mean and maximum streamflow in the control period, 1961-1990 (grey colours), the near future, 2031-2060 (light purple colours) and the end of the century, 2071-2100 (dark purple colours), according to the climate projection HAD and the high emission scenario, for the station 289 Chkheri - D. Stefantsminda.

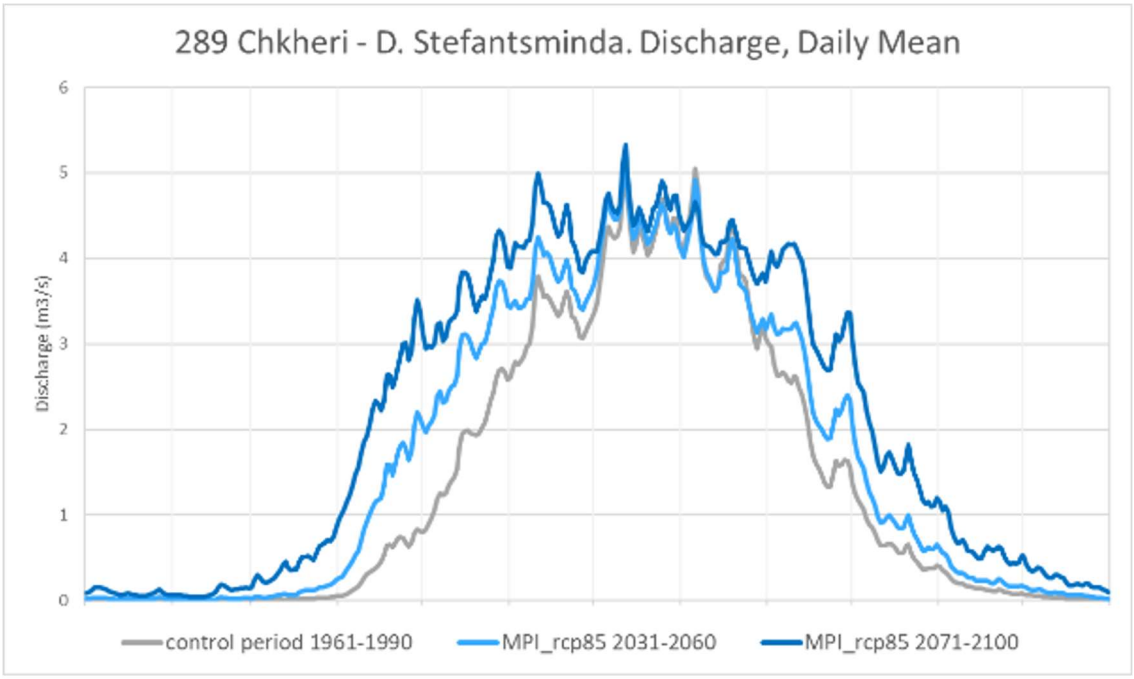

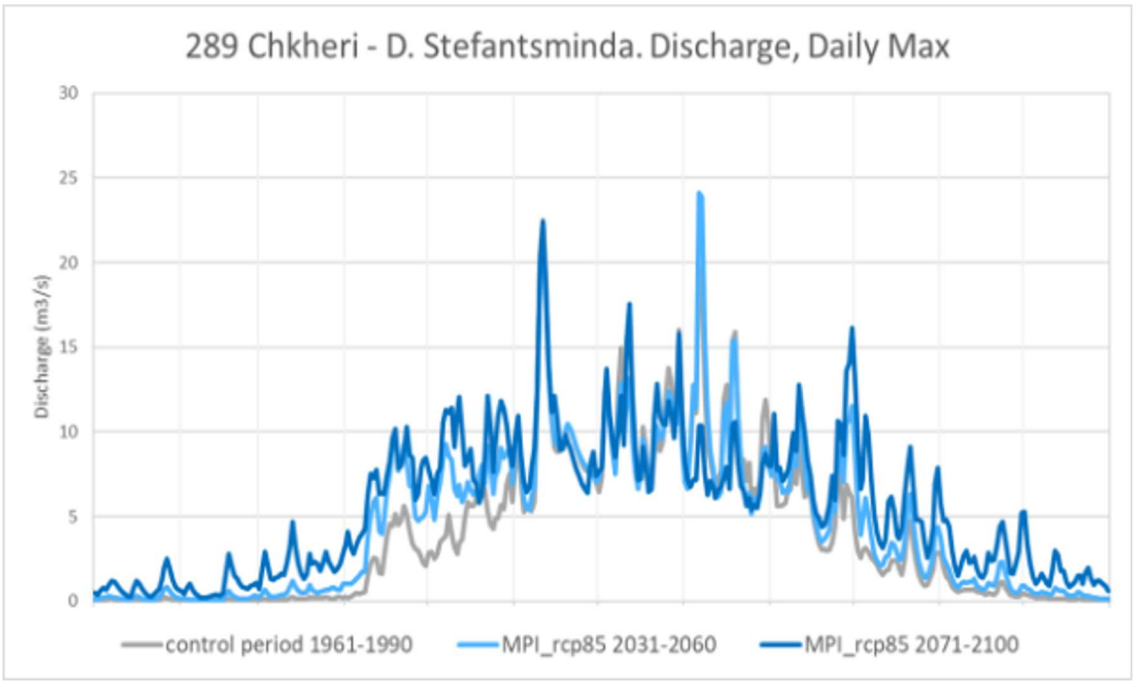

Figure A-106. Simulated daily mean streamflow (top) and daily maximum streamflow in the control period, 1961-1990 (grey line), the near future, 2031-2060 (light blue line) and the end of the century, 2071-2100 (dark blue line), according to the climate projection MPI and the high emission scenario, for the station 289 Chkheri - D. Stefantsminda.

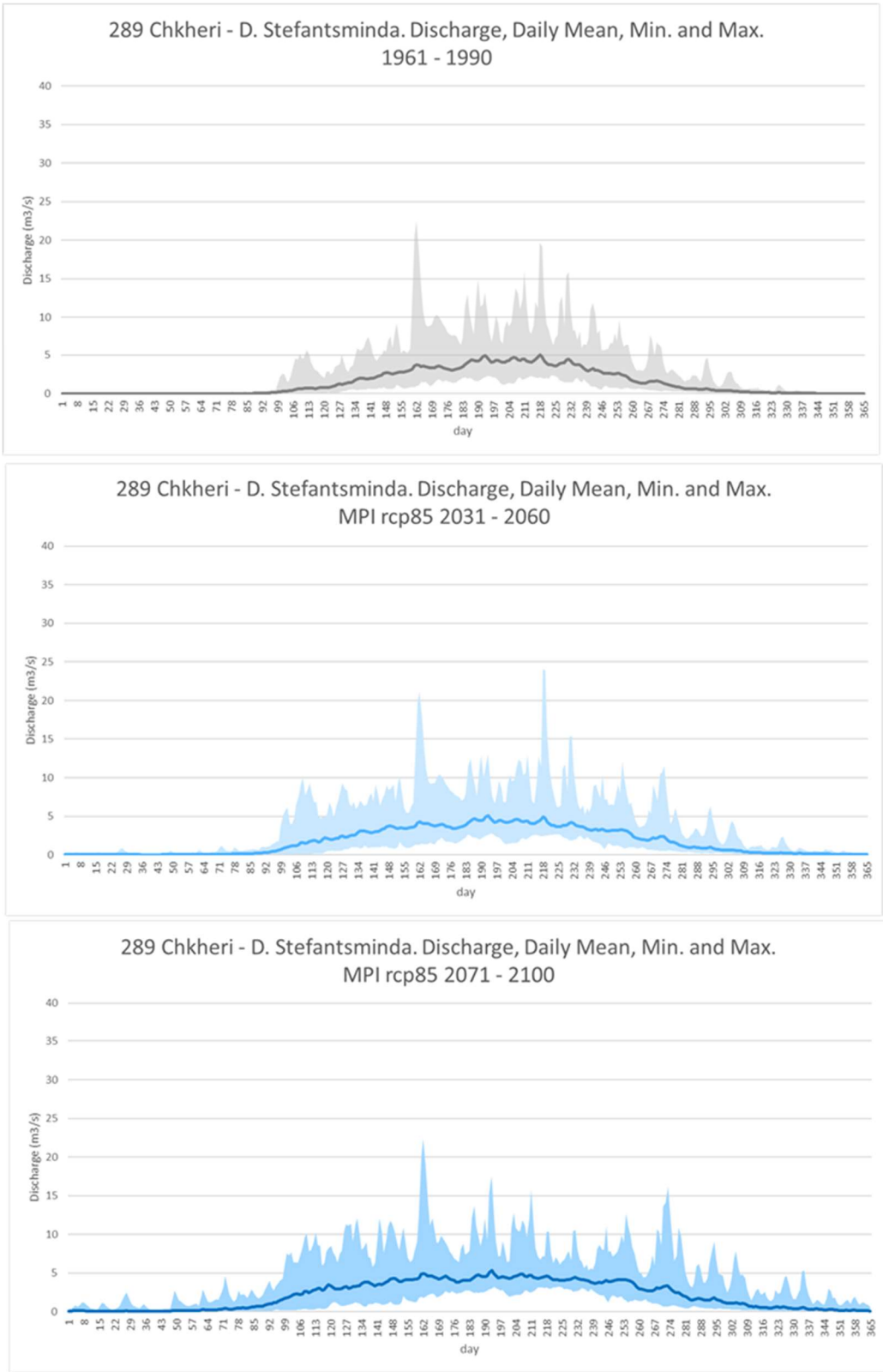

Figure A-107. Simulated daily minimum, mean and maximum streamflow in the control period, 1961-1990 (grey colours), the near future, 2031-2060 (light blue colours) and the end of the century, 2071-2100 (dark blue colours), according to the climate projection MPI and the high emission scenario, for the station 289 Chkheri - D. Stefantsminda.

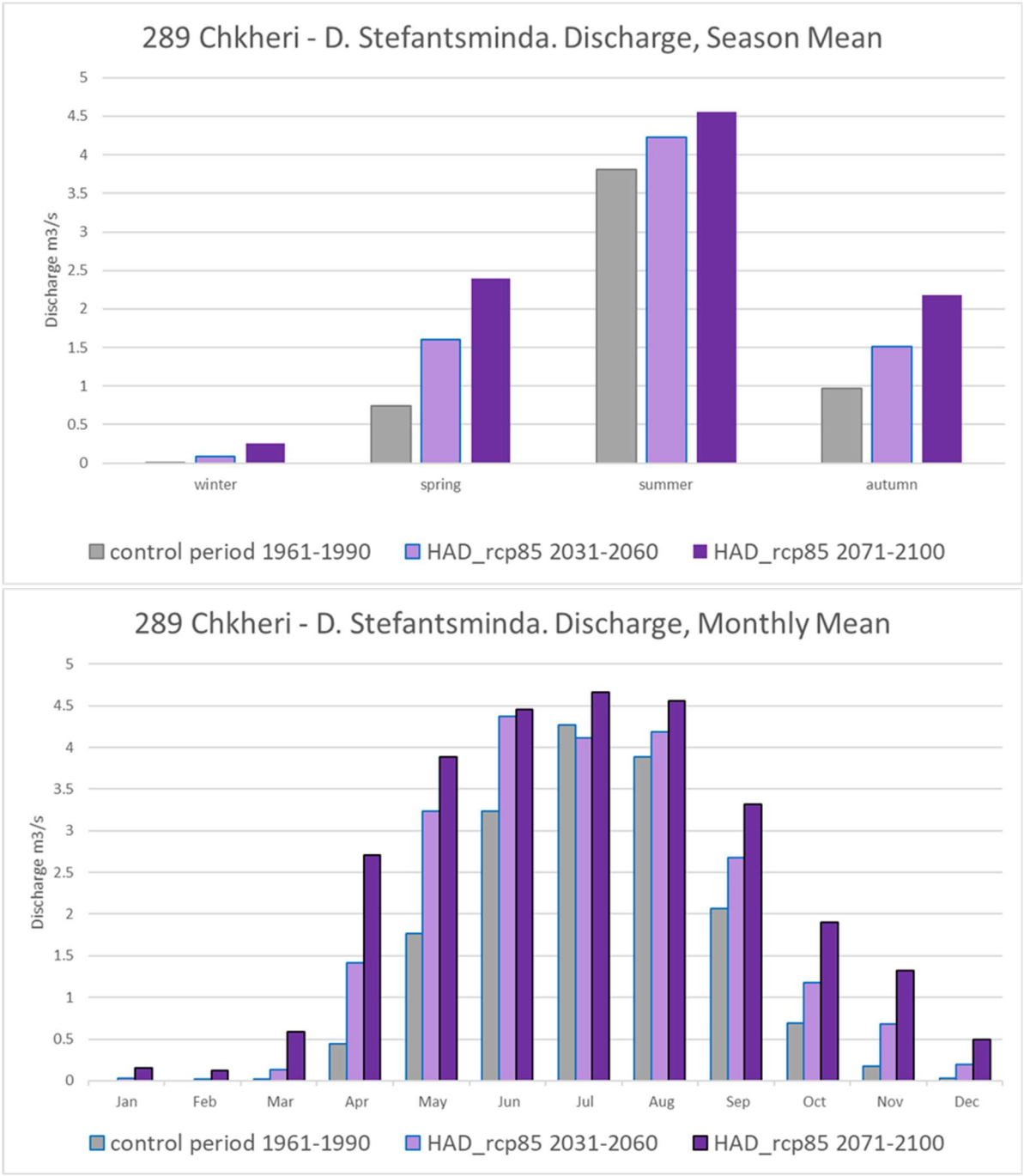

Figure A-108. Simulated season mean (top) and monthly mean (bottom) streamflow in the control period, 1961-1990 (grey bars), the near future, 2031-2060 (light purple bars) and the end of the century, 2071-2100 (dark purple bars), according to the climate projection HAD and the high emission scenario, for the station 289 Chkheri - D. Stefantsminda.

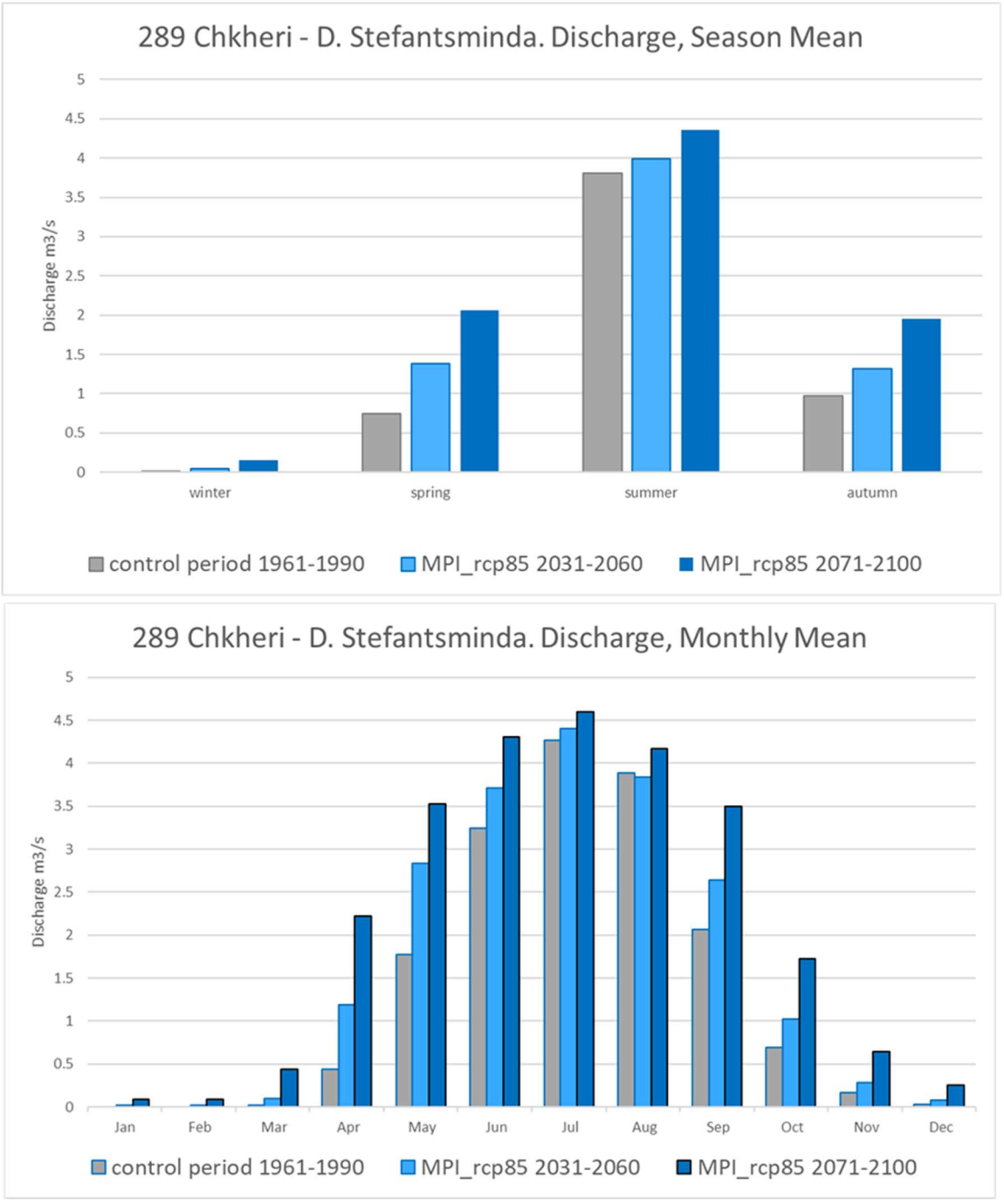

Figure A-109. Simulated season mean (top) and monthly mean (bottom) streamflow in the control period, 1961-1990 (grey bars), the near future, 2031-2060 (light blue bars) and the end of the century, 2071-2100 (dark blue bars), according to the climate projection MPI and the high emission scenario, for the station 289 Chkheri - D. Stefantsminda.

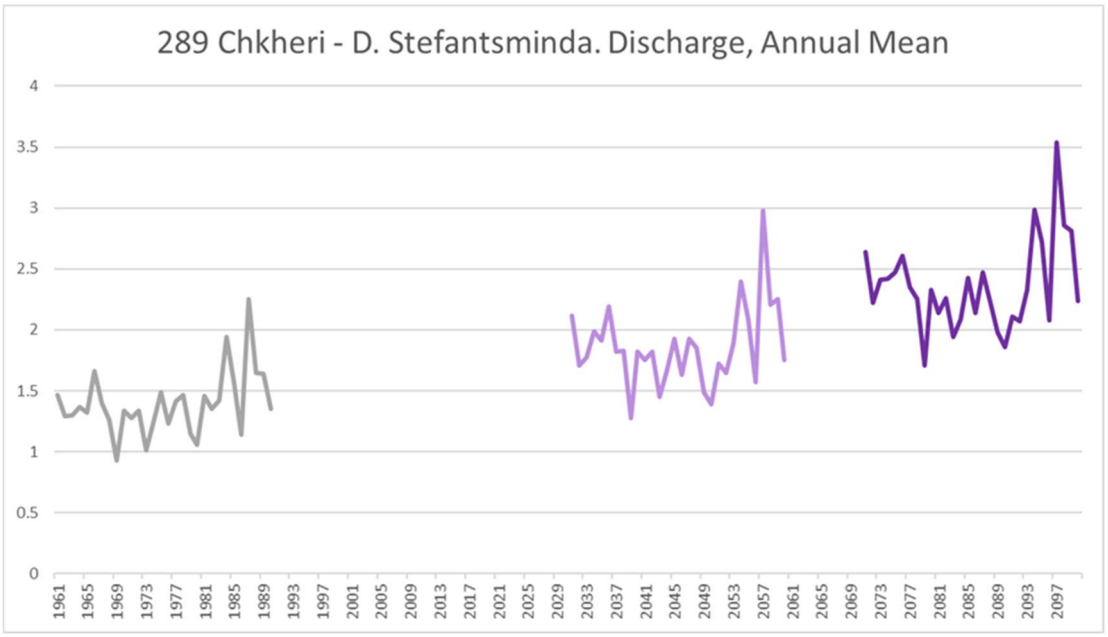

Figure A-110. Simulated annual streamflow in the control period, 1961-1990 (grey line), the near future, 2031-2060 (light purple line) and the end of the century, 2071-2100 (dark purple line), according to the climate projection HAD and the high emission scenario, for the station 289 Chkheri - D. Stefantsminda.

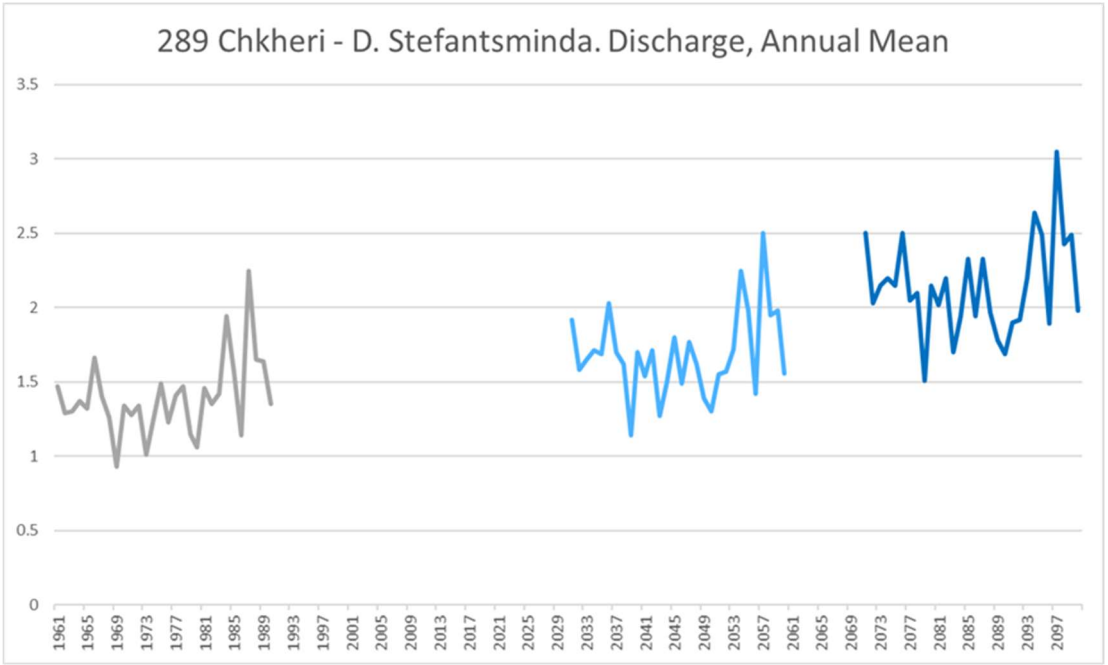

Figure A-111. Simulated annual streamflow in the control period, 1961-1990 (grey line), the near future, 2031-2060 (light blue line) and the end of the century, 2071-2100 (dark blue line), according to the climate projection MPI and the high emission scenario, for the station 289 Chkheri - D. Stefantsminda.

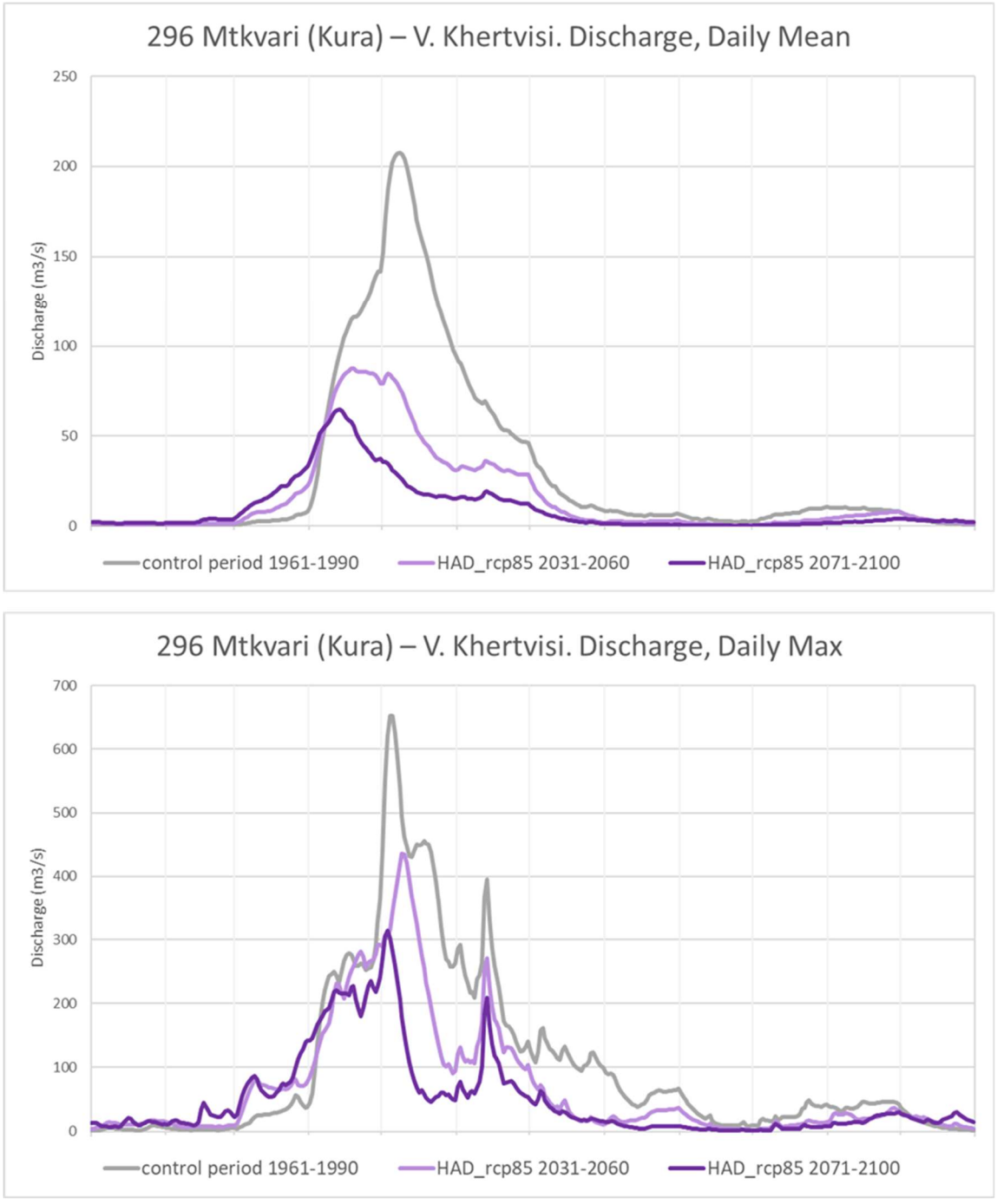

Figure A-112. Simulated daily mean streamflow (top) and daily maximum streamflow in the control period, 1961-1990 (grey line), the near future, 2031-2060 (light purple line) and the end of the century, 2071-2100 (dark purple line), according to the climate projection HAD and the high emission scenario, for the station 296 Mtkvari (Kura) – V. Khertvisi.

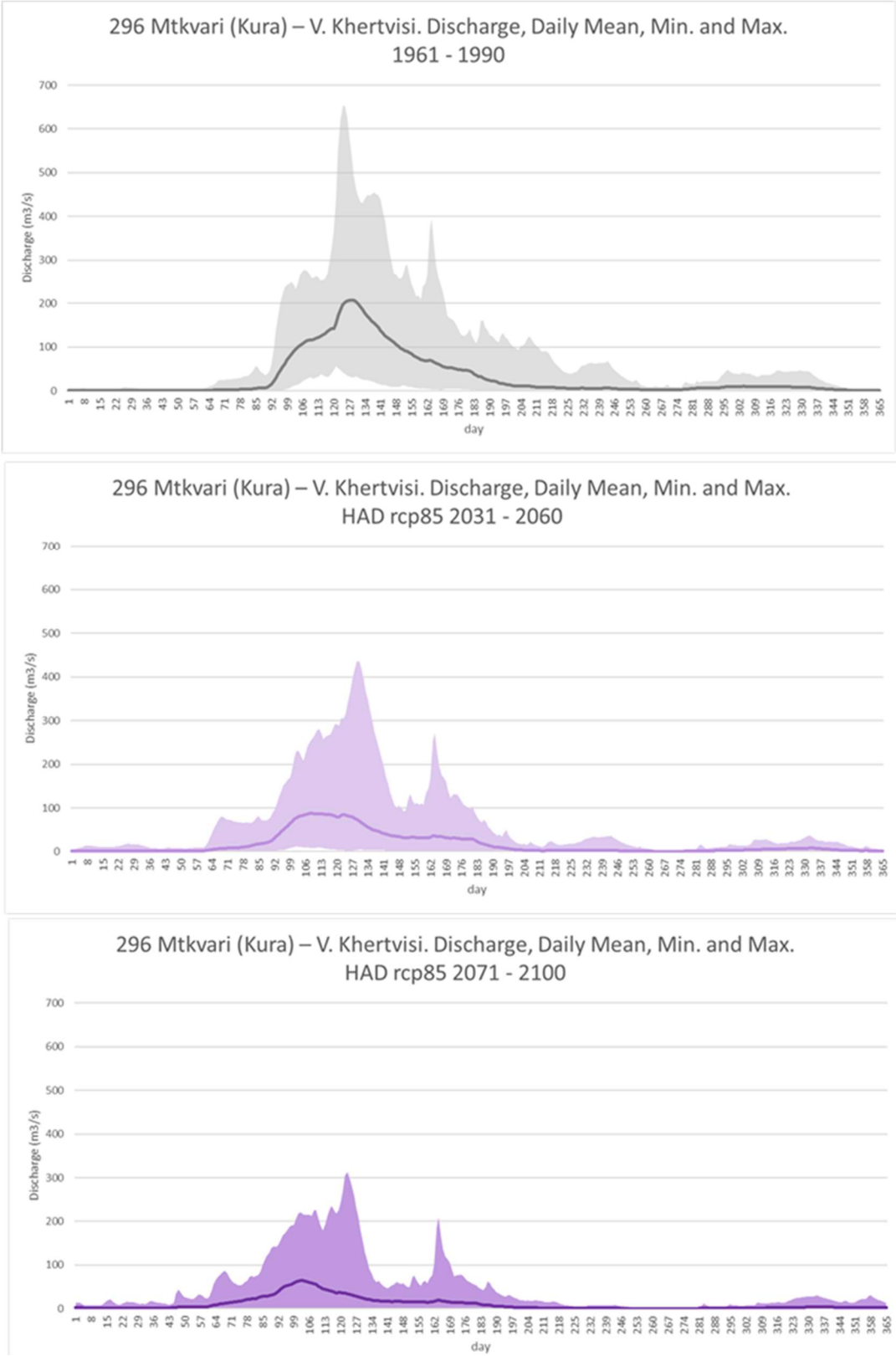

Figure A-113. Simulated daily minimum, mean and maximum streamflow in the control period, 1961-1990 (grey colours), the near future, 2031-2060 (light purple colours) and the end of the century, 2071-2100 (dark purple colours), according to the climate projection HAD and the high emission scenario, for the station 296 Mtkvari (Kura) – V. Khertvisi.

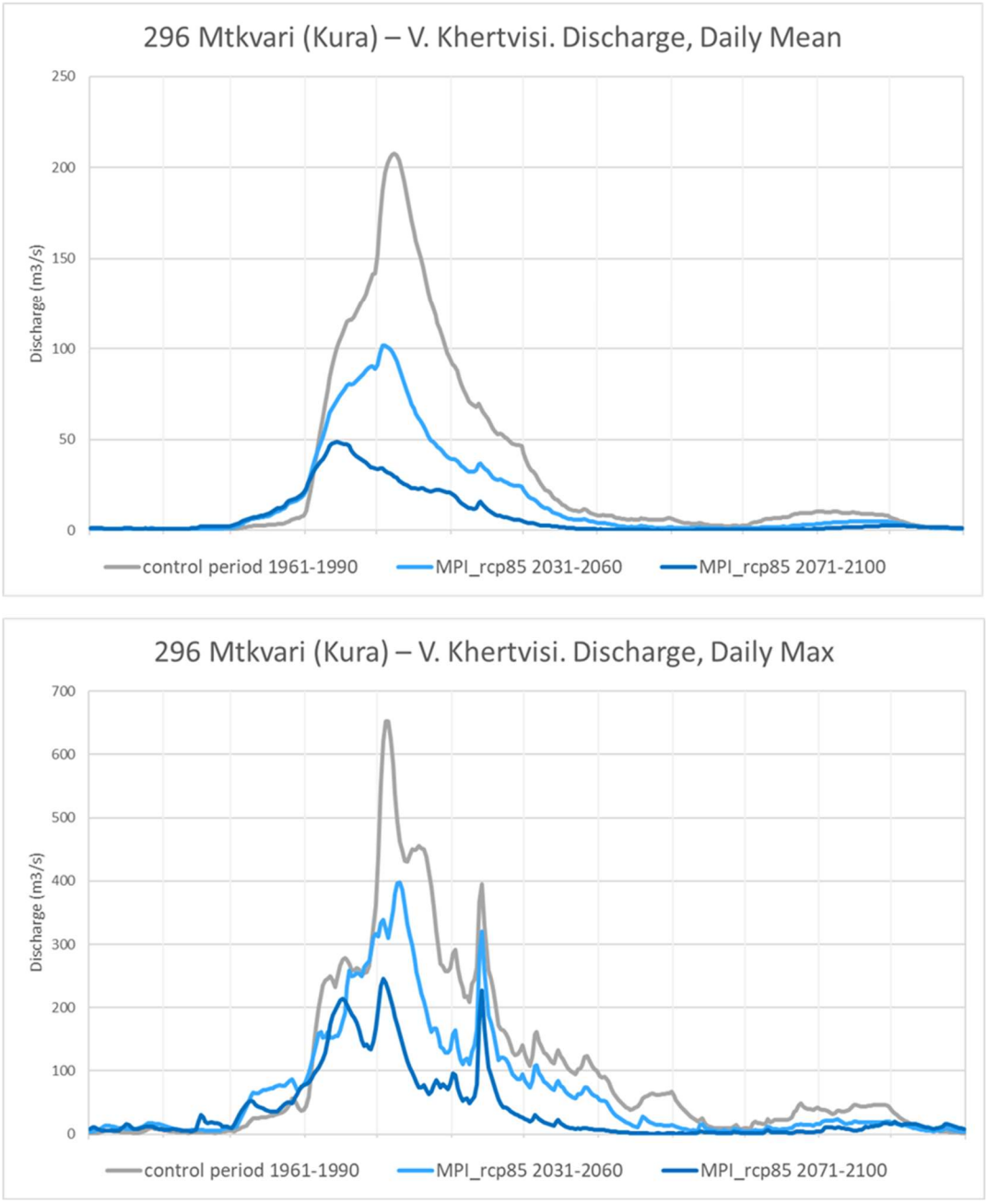

Figure A-114. Simulated daily mean streamflow (top) and daily maximum streamflow in the control period, 1961-1990 (grey line), the near future, 2031-2060 (light blue line) and the end of the century, 2071-2100 (dark blue line), according to the climate projection MPI and the high emission scenario, for the station 296 Mtkvari (Kura) – V. Khertvisi.

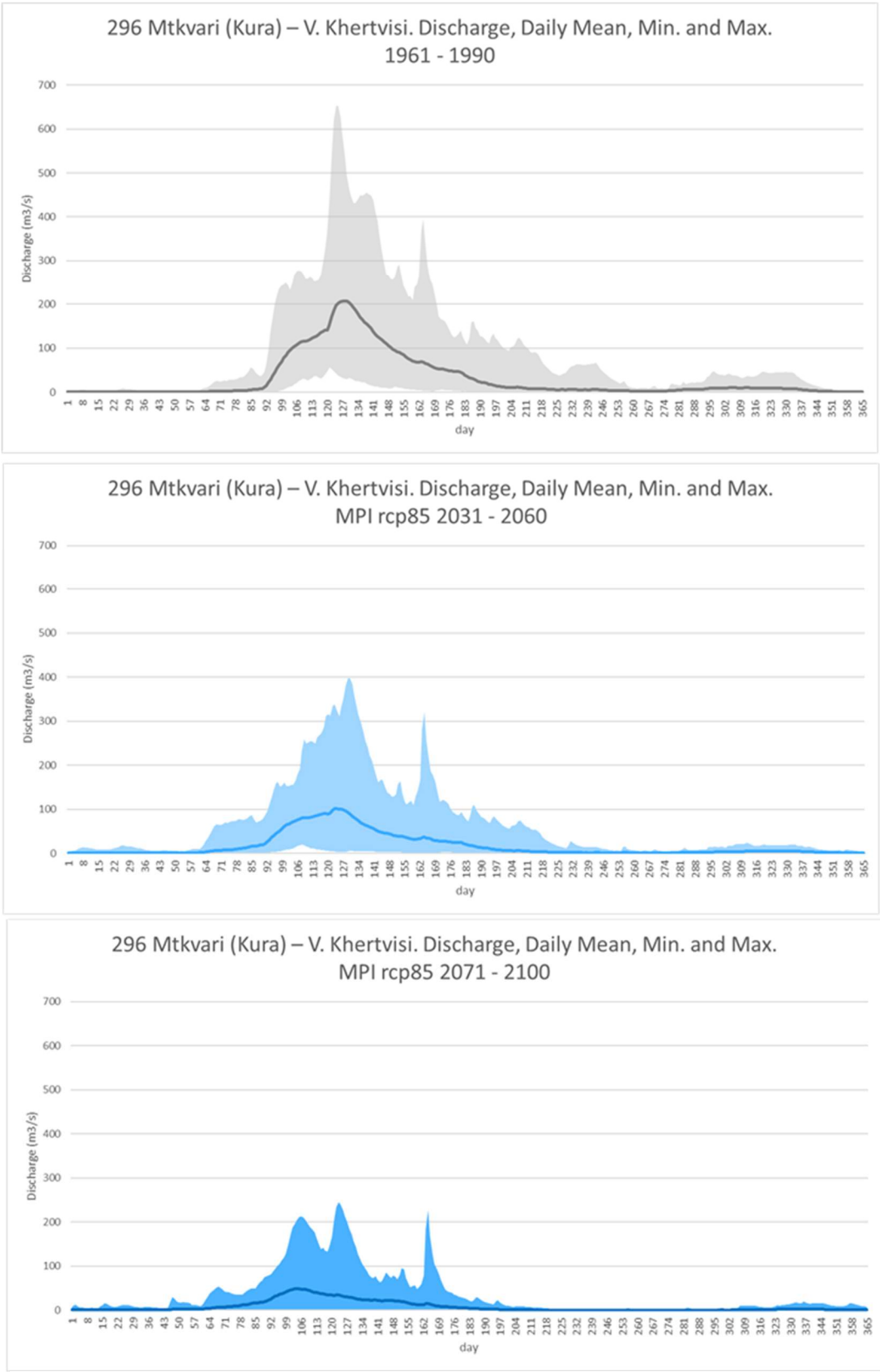

Figure A-115. Simulated daily minimum, mean and maximum streamflow in the control period, 1961-1990 (grey colours), the near future, 2031-2060 (light blue colours) and the end of the century, 2071-2100 (dark blue colours), according to the climate projection MPI and the high emission scenario, for the station 296 Mtkvari (Kura) – V. Khertvisi.

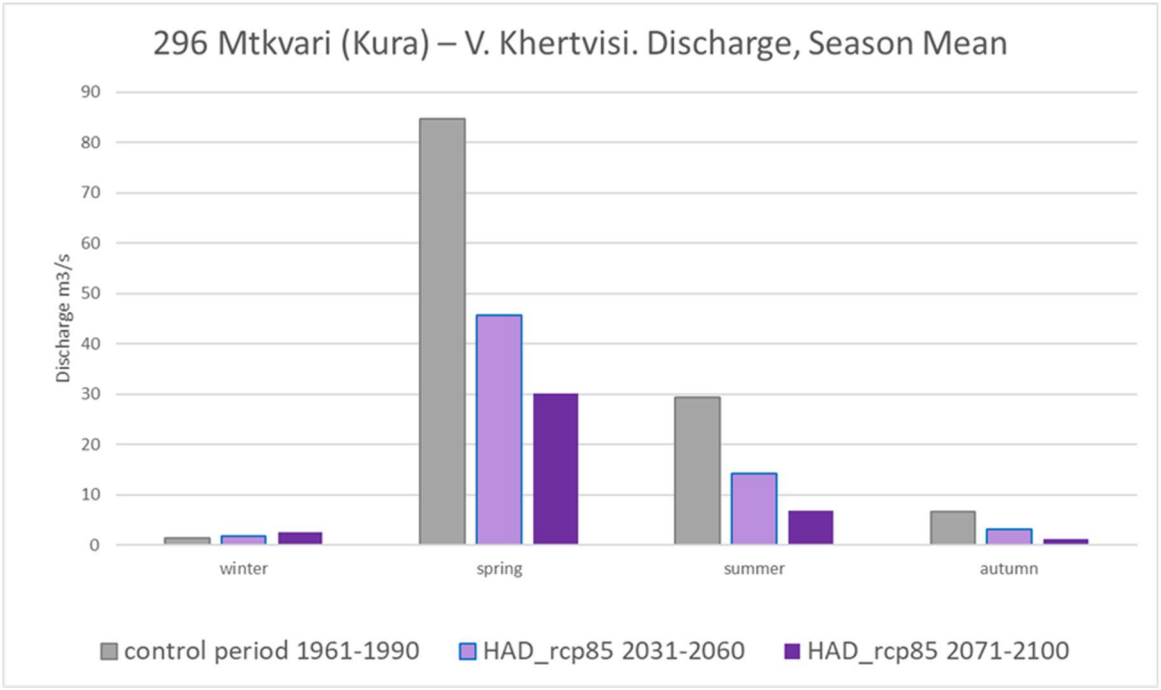

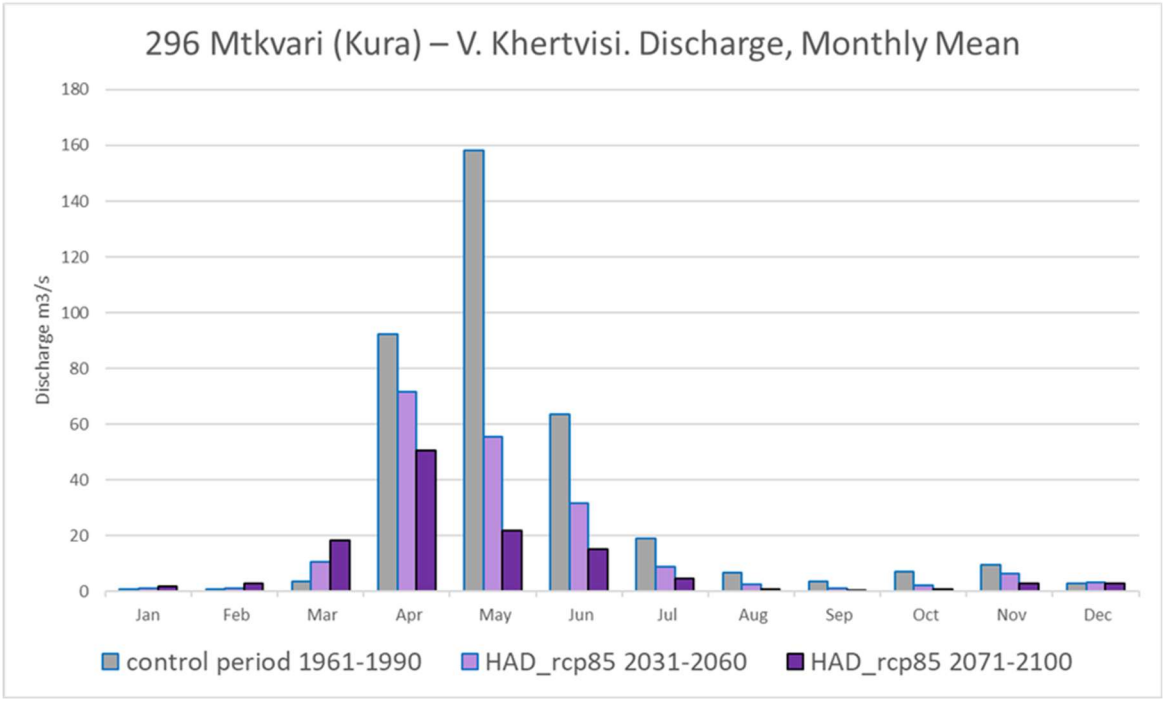

Figure A-116. Simulated season mean (top) and monthly mean (bottom) streamflow in the control period, 1961-1990 (grey bars), the near future, 2031-2060 (light purple bars) and the end of the century, 2071-2100 (dark purple bars), according to the climate projection HAD and the high emission scenario, for the station 296 Mtkvari (Kura) – V. Khertvisi.

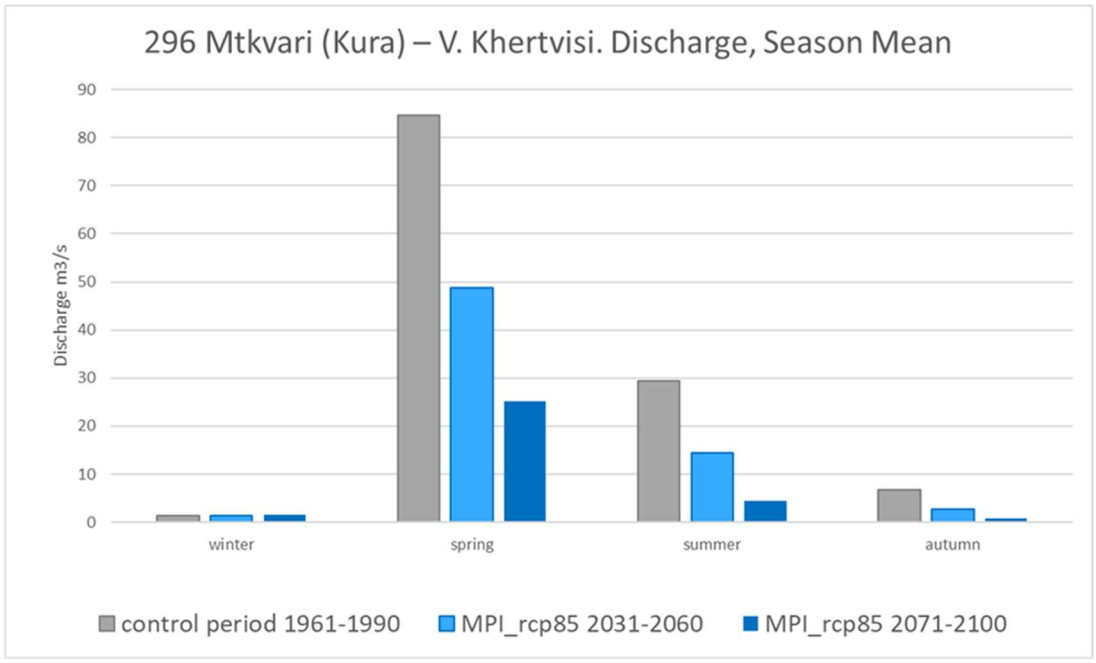

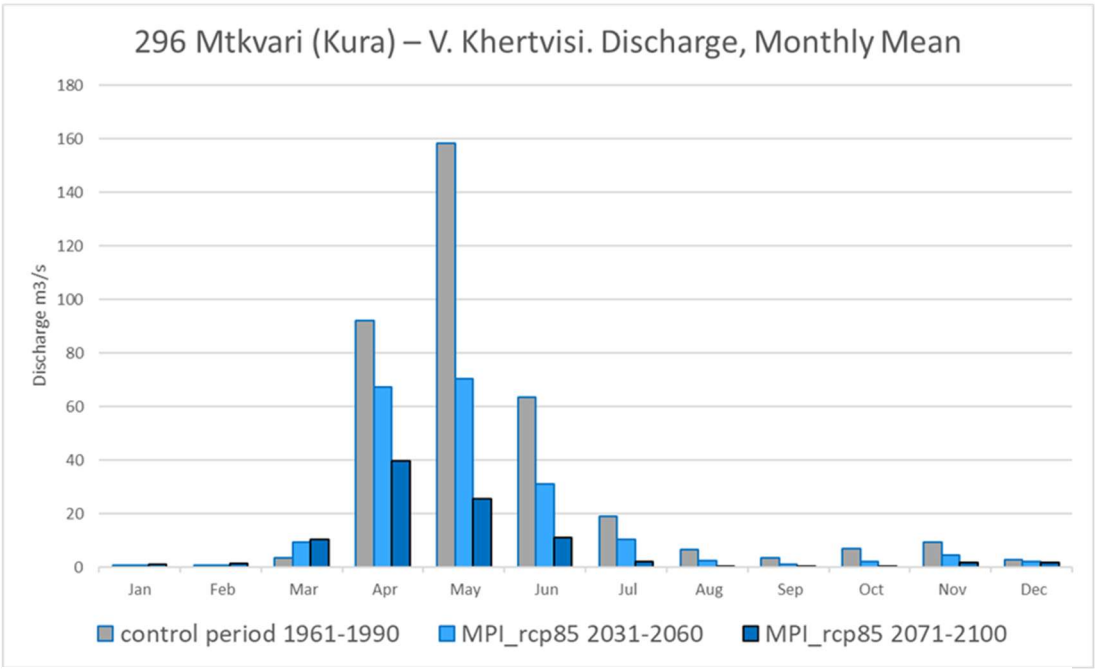

Figure A-117. Simulated season mean (top) and monthly mean (bottom) streamflow in the control period, 1961-1990 (grey bars), the near future, 2031-2060 (light blue bars) and the end of the century, 2071-2100 (dark blue bars), according to the climate projection HAD and the high emission scenario, for the station 296 Mtkvari (Kura) – V. Khertvisi.

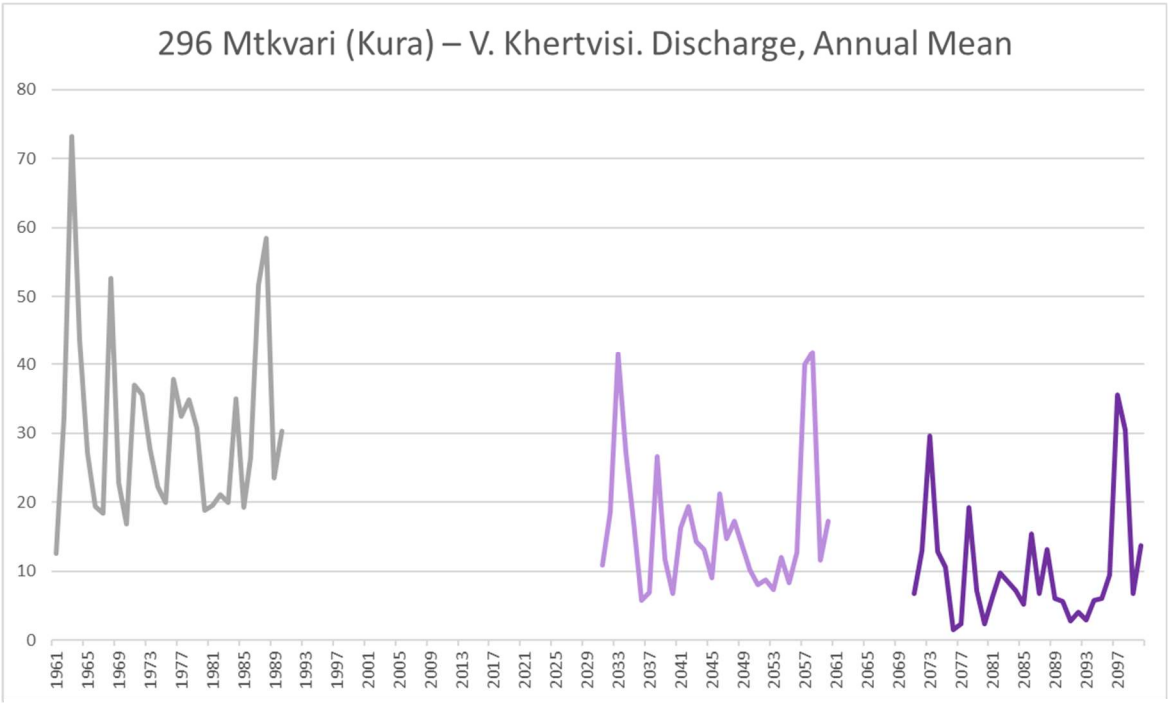

Figure A-118. Simulated annual streamflow in the control period, 1961-1990 (grey line), the near future, 2031-2060 (light purple line) and the end of the century, 2071-2100 (dark purple line), according to the climate projection HAD and the high emission scenario, for the station 296 Mtkvari (Kura) – V. Khertvisi.

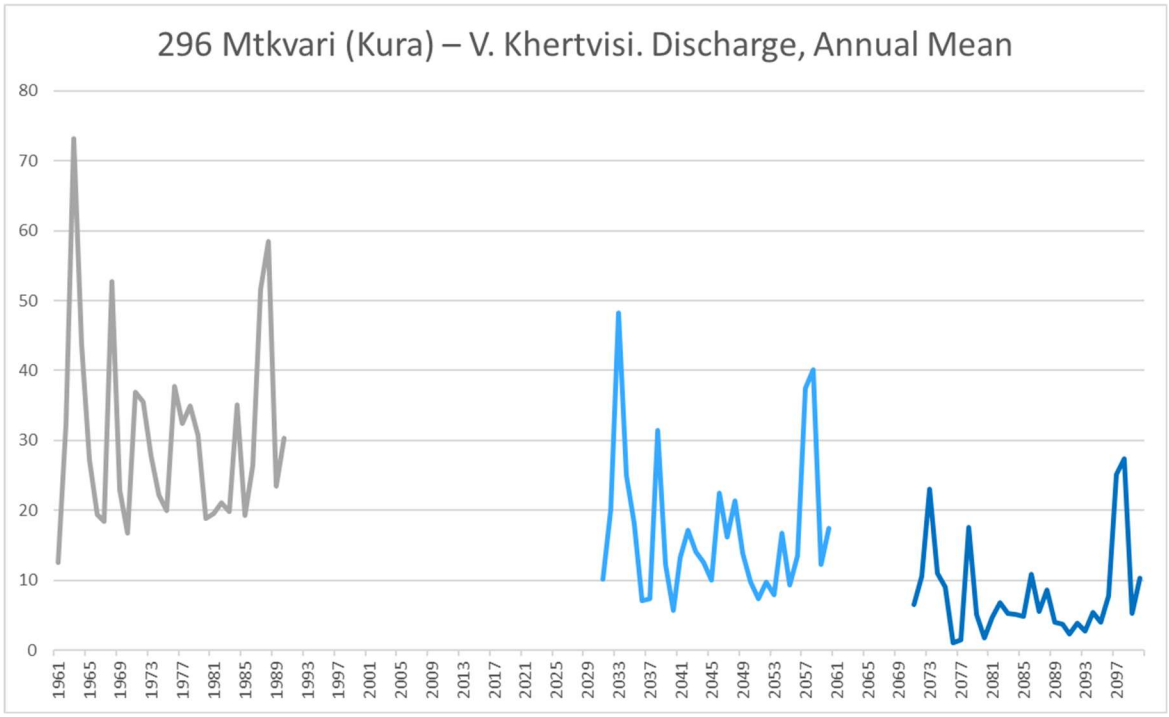

Figure A-119. Simulated annual streamflow in the control period, 1961-1990 (grey line), the near future, 2031-2060 (light blue line) and the end of the century, 2071-2100 (dark blue line), according to the climate projection MPI and the high emission scenario, for the station 296 Mtkvari (Kura) – V. Khertvisi.

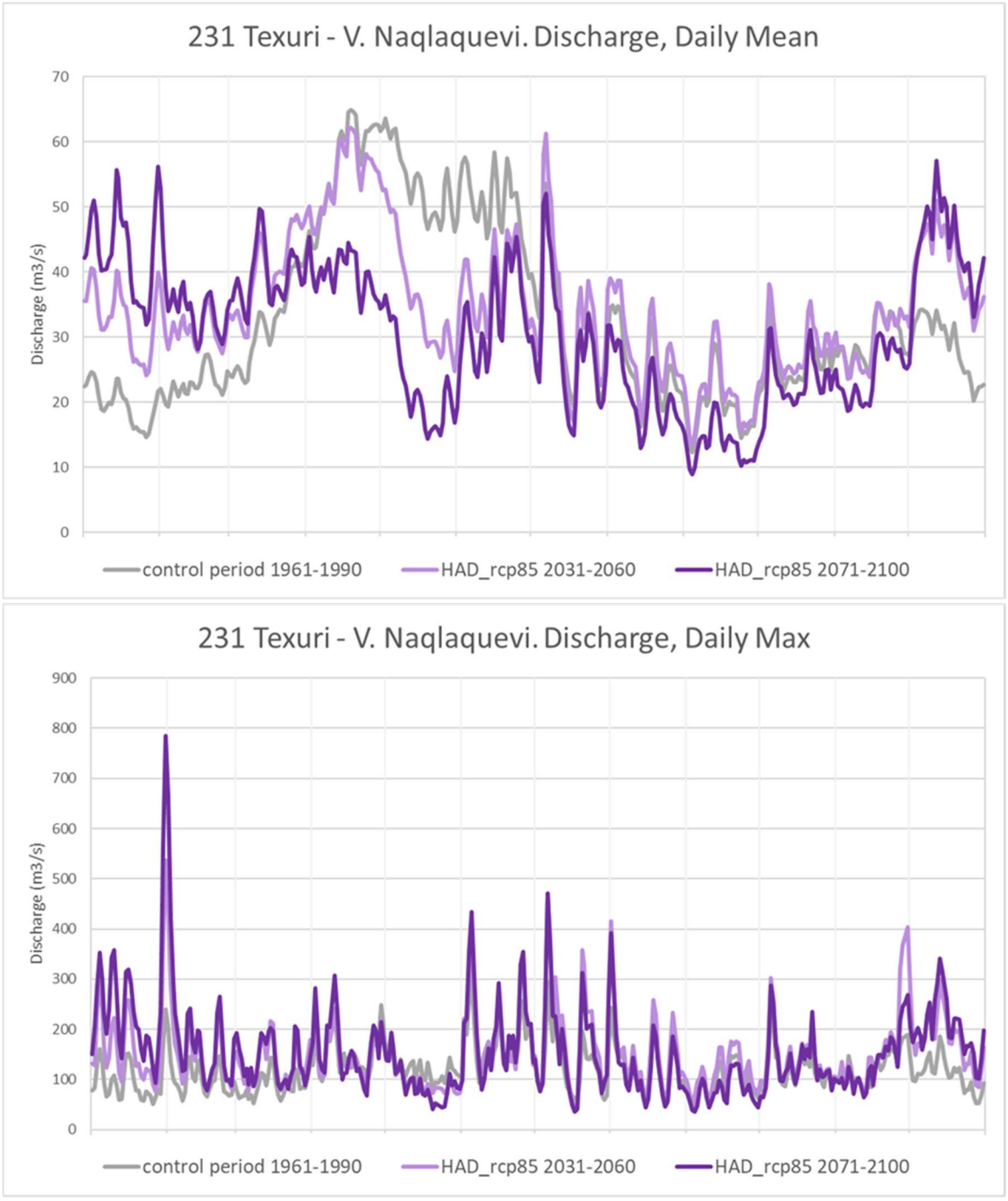

Figure A-120. Simulated daily mean streamflow (top) and daily maximum streamflow in the control period, 1961-1990 (grey line), the near future, 2031-2060 (light purple line) and the end of the century, 2071-2100 (dark purple line), according to the climate projection HAD and the high emission scenario, for the station 231 Texuri - V. Naqlaquevi.

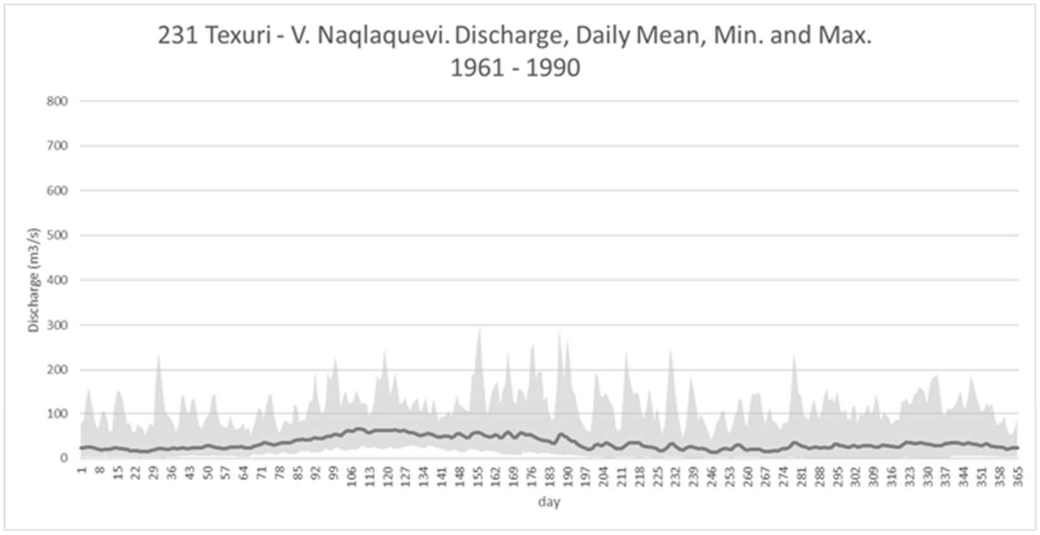

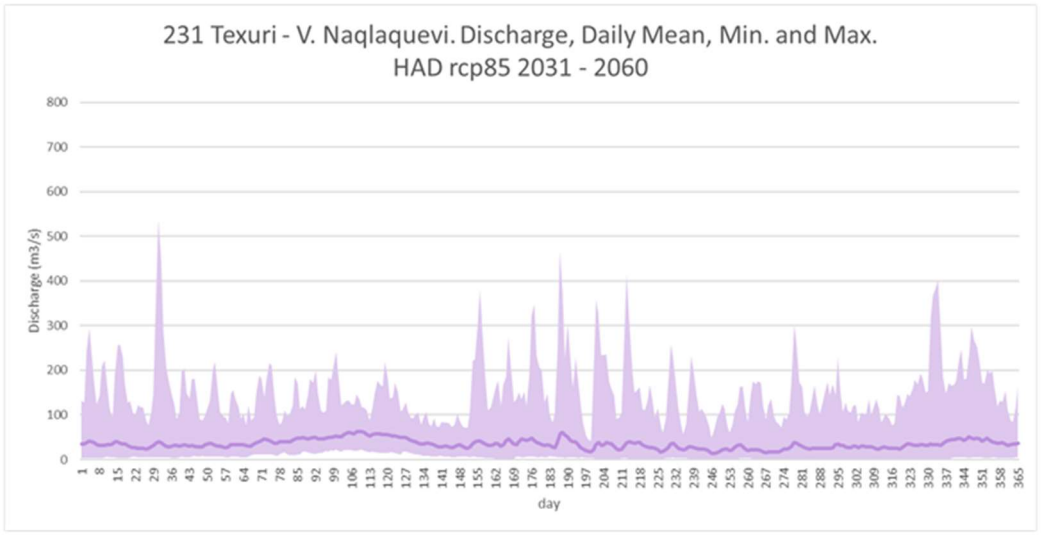

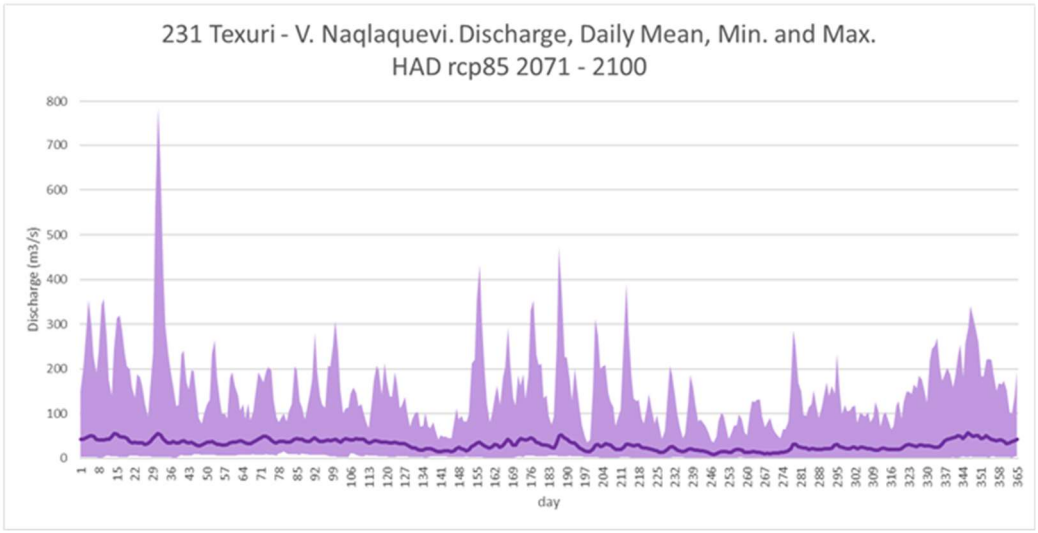

Figure A-121. Simulated daily minimum, mean and maximum streamflow in the control period, 1961-1990 (grey colours), the near future, 2031-2060 (light purple colours) and the end of the century, 2071-2100 (dark purple colours), according to the climate projection HAD and the high emission scenario, for the station 231 Texuri - V. Naqlaquevi.

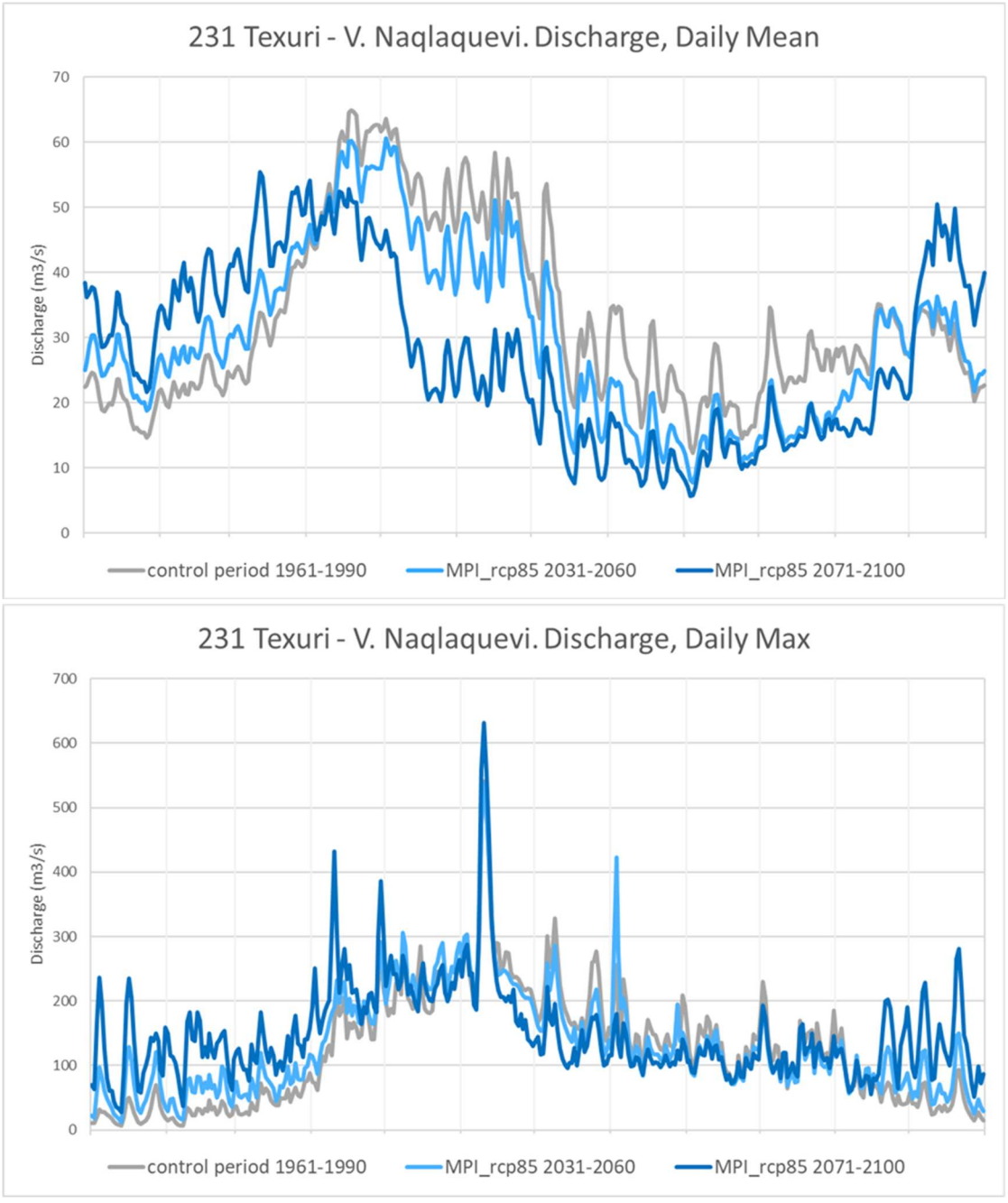

Figure A-122. Simulated daily mean streamflow (top) and daily maximum streamflow in the control period, 1961-1990 (grey line), the near future, 2031-2060 (light blue line) and the end of the century, 2071-2100 (dark blue line), according to the climate projection MPI and the high emission scenario, for the station 231 Texuri - V. Naqlaquevi.

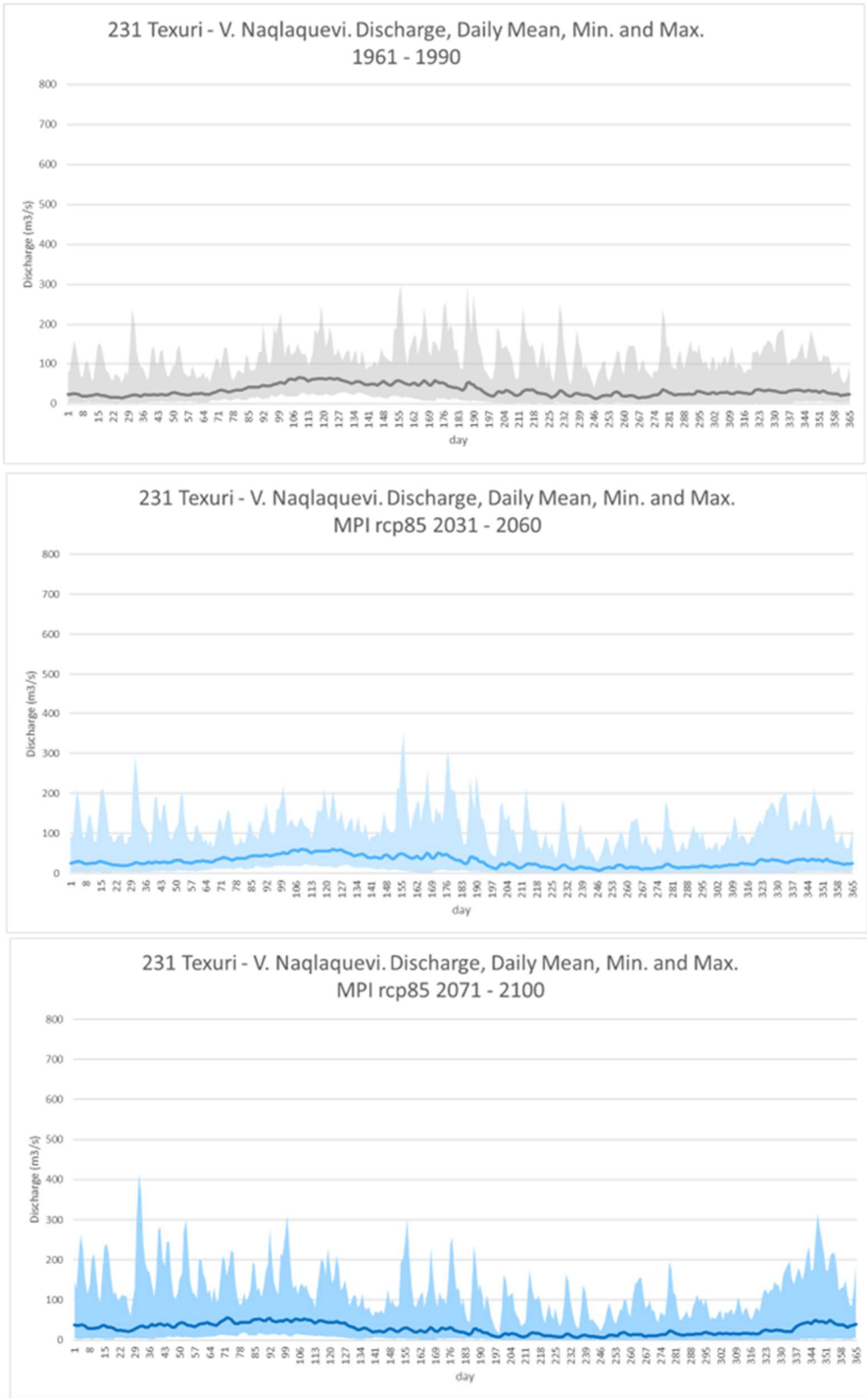

Figure A-123. Simulated daily minimum, mean and maximum streamflow in the control period, 1961-1990 (grey colours), the near future, 2031-2060 (light blue colours) and the end of the century, 2071-2100 (dark blue colours), according to the climate projection MPI and the high emission scenario, for the station 231 Texuri - V. Naqlaquevi.

Figure A-124. Simulated season mean (top) and monthly mean (bottom) streamflow in the control period, 1961-1990 (grey bars), the near future, 2031-2060 (light purple bars) and the end of the century, 2071-2100 (dark purple bars), according to the climate projection HAD and the high emission scenario, for the station 231 Texuri - V. Naqlaquevi.

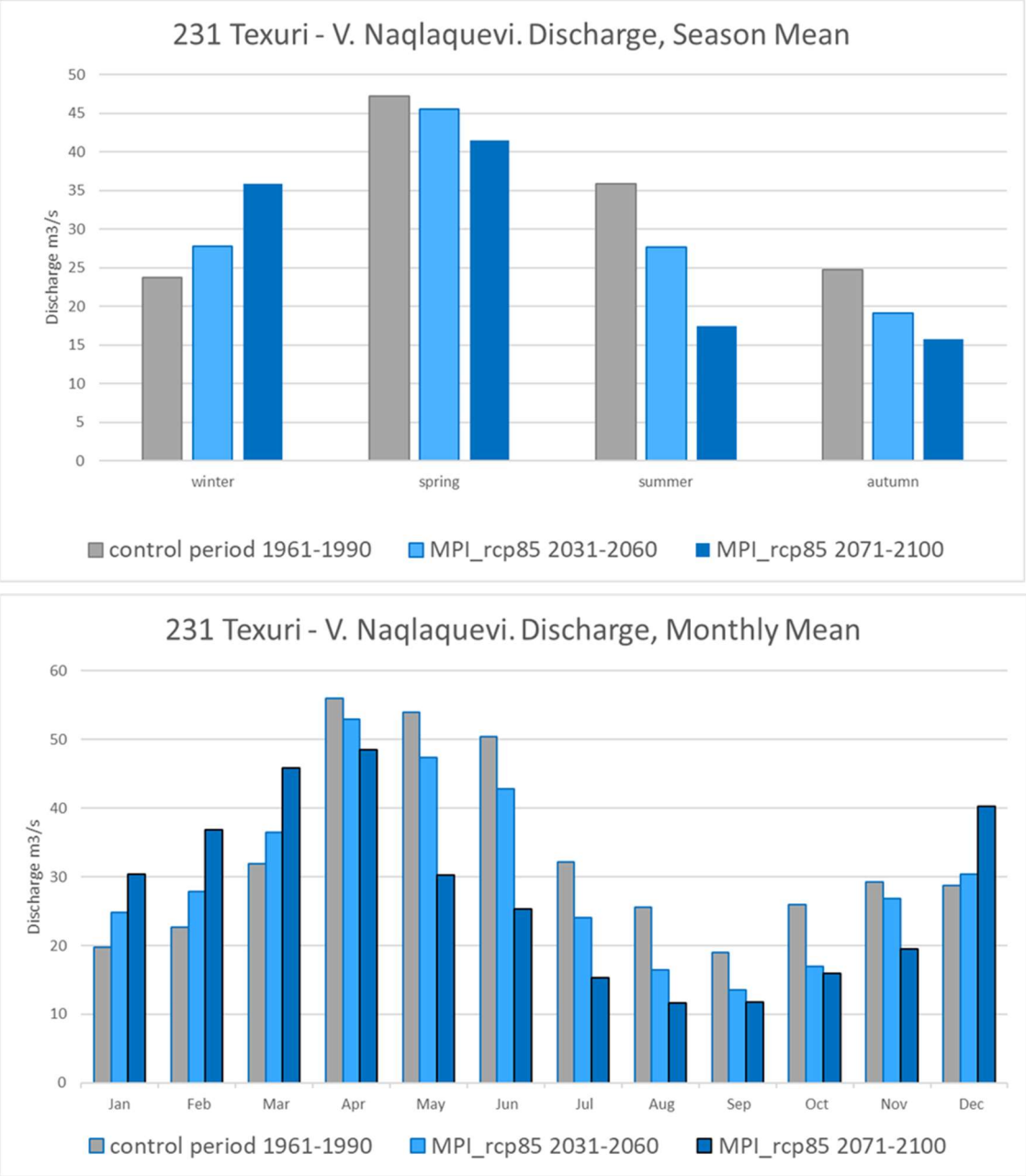

Figure A-125. Simulated season mean (top) and monthly mean (bottom) streamflow in the control period, 1961-1990 (grey bars), the near future, 2031-2060 (light blue bars) and the end of the century, 2071-2100 (dark blue bars), according to the climate projection HAD and the high emission scenario, for the station 231 Texuri - V. Naqlaquevi.

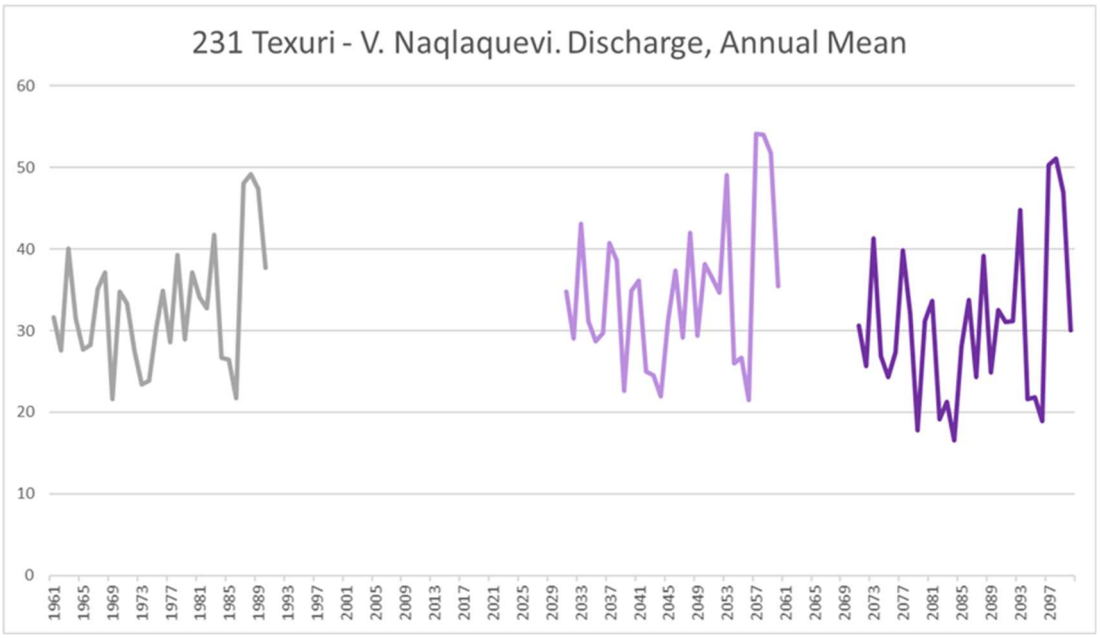

Figure A-126. Simulated annual streamflow in the control period, 1961-1990 (grey line), the near future, 2031-2060 (light purple line) and the end of the century, 2071-2100 (dark purple line), according to the climate projection HAD and the high emission scenario, for the station 231 Texuri - V. Naqlaquevi.

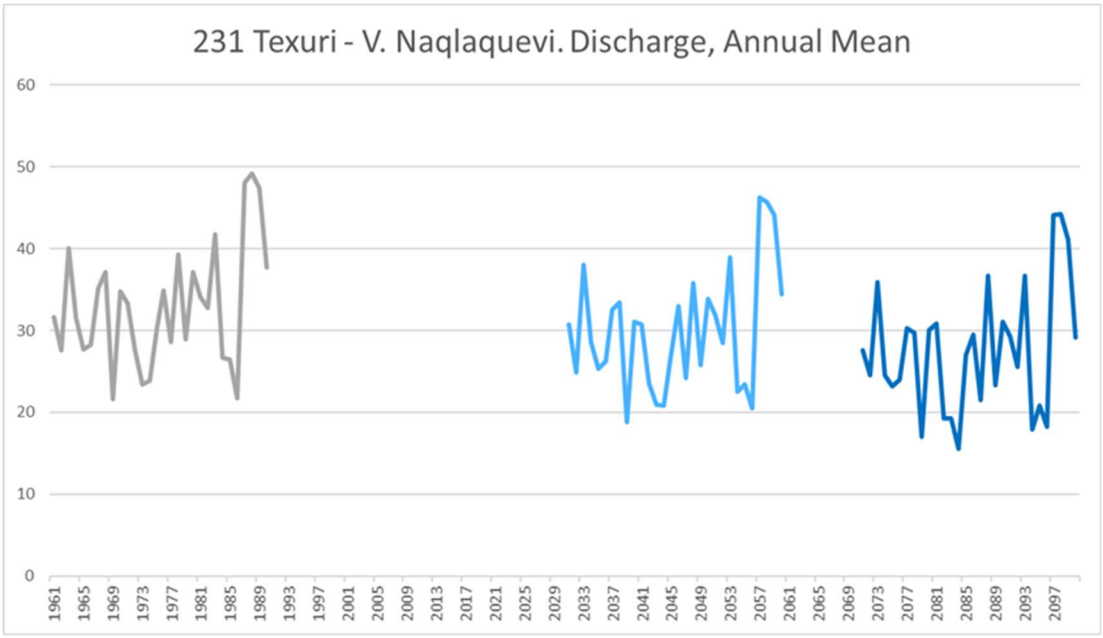

Figure 127. Simulated annual streamflow in the control period, 1961-1990 (grey line), the near future, 2031-2060 (light blue line) and the end of the century, 2071-2100 (dark blue line), according to the climate projection MPI and the high emission scenario, for the station 231 Texuri - V. Naqlaquevi.

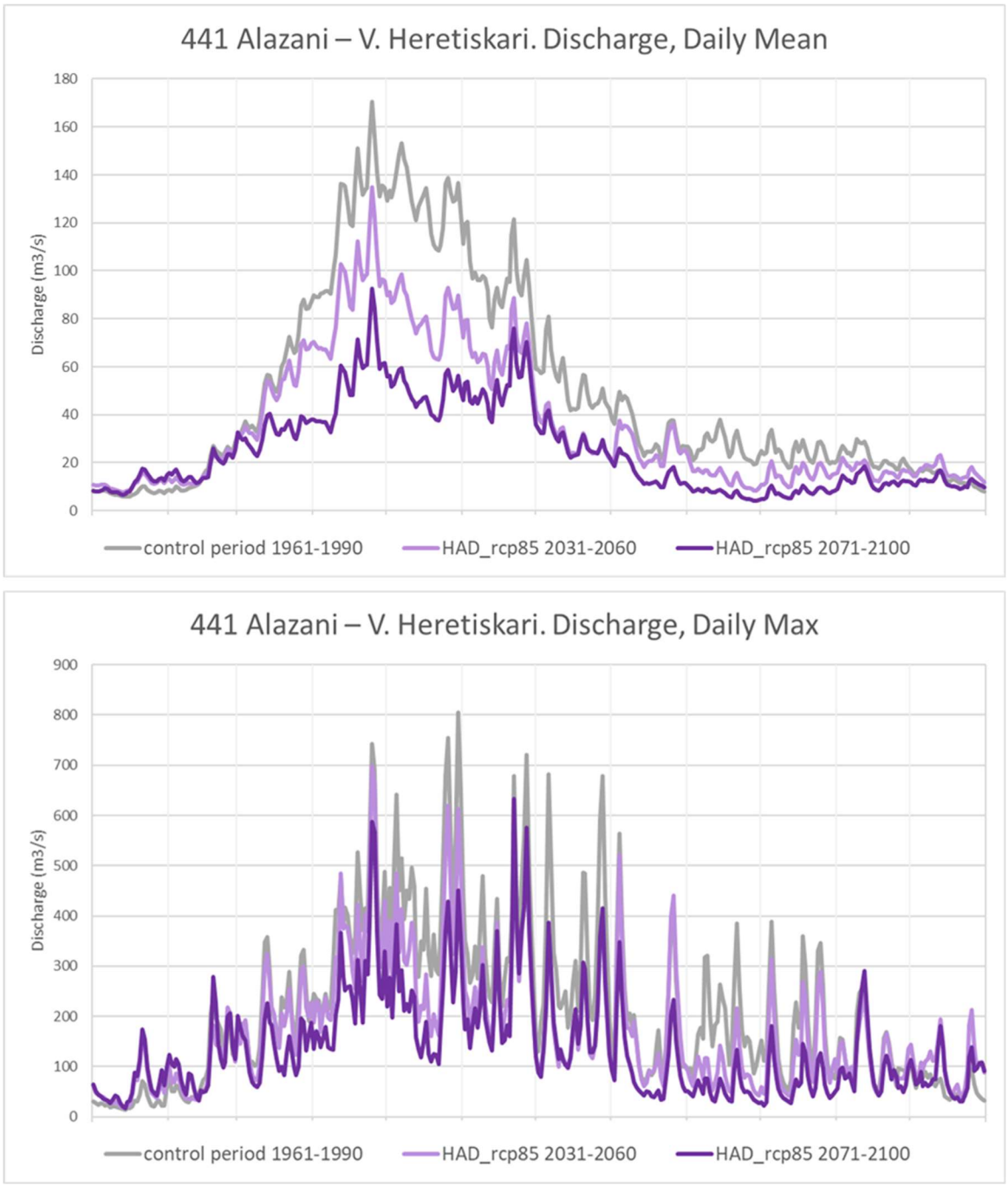

Figure A-128. Simulated daily mean streamflow (top) and daily maximum streamflow in the control period, 1961-1990 (grey line), the near future, 2031-2060 (light purple line) and the end of the century, 2071-2100 (dark purple line), according to the climate projection HAD and the high emission scenario, for the station 441 Alazani – V. Heretiskari.

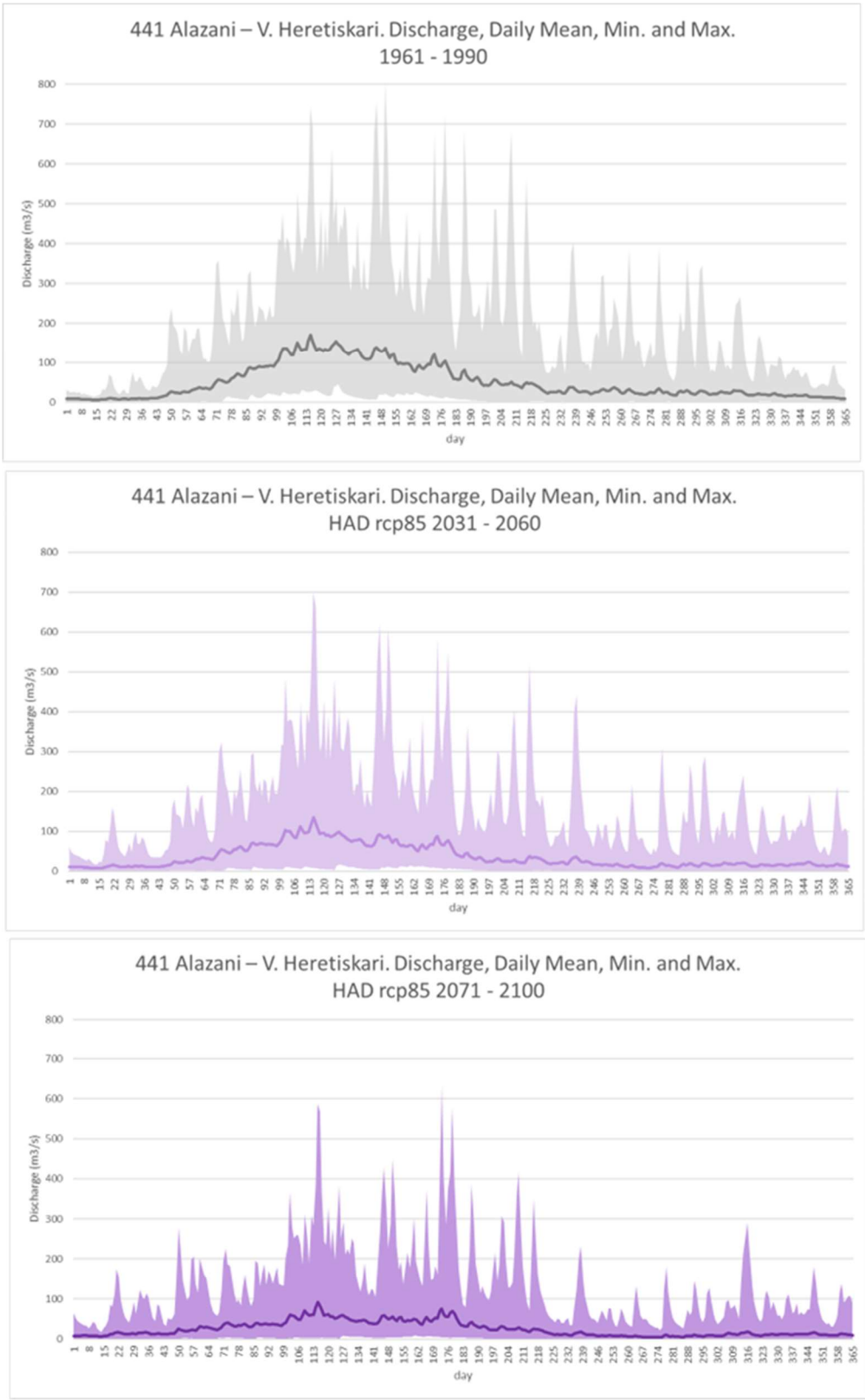

Figure A-129. Simulated daily minimum, mean and maximum streamflow in the control period, 1961-1990 (grey colours), the near future, 2031-2060 (light purple colours) and the end of the century, 2071-2100 (dark purple colours), according to the climate projection HAD and the high emission scenario, for the station 441 Alazani – V. Heretiskari.

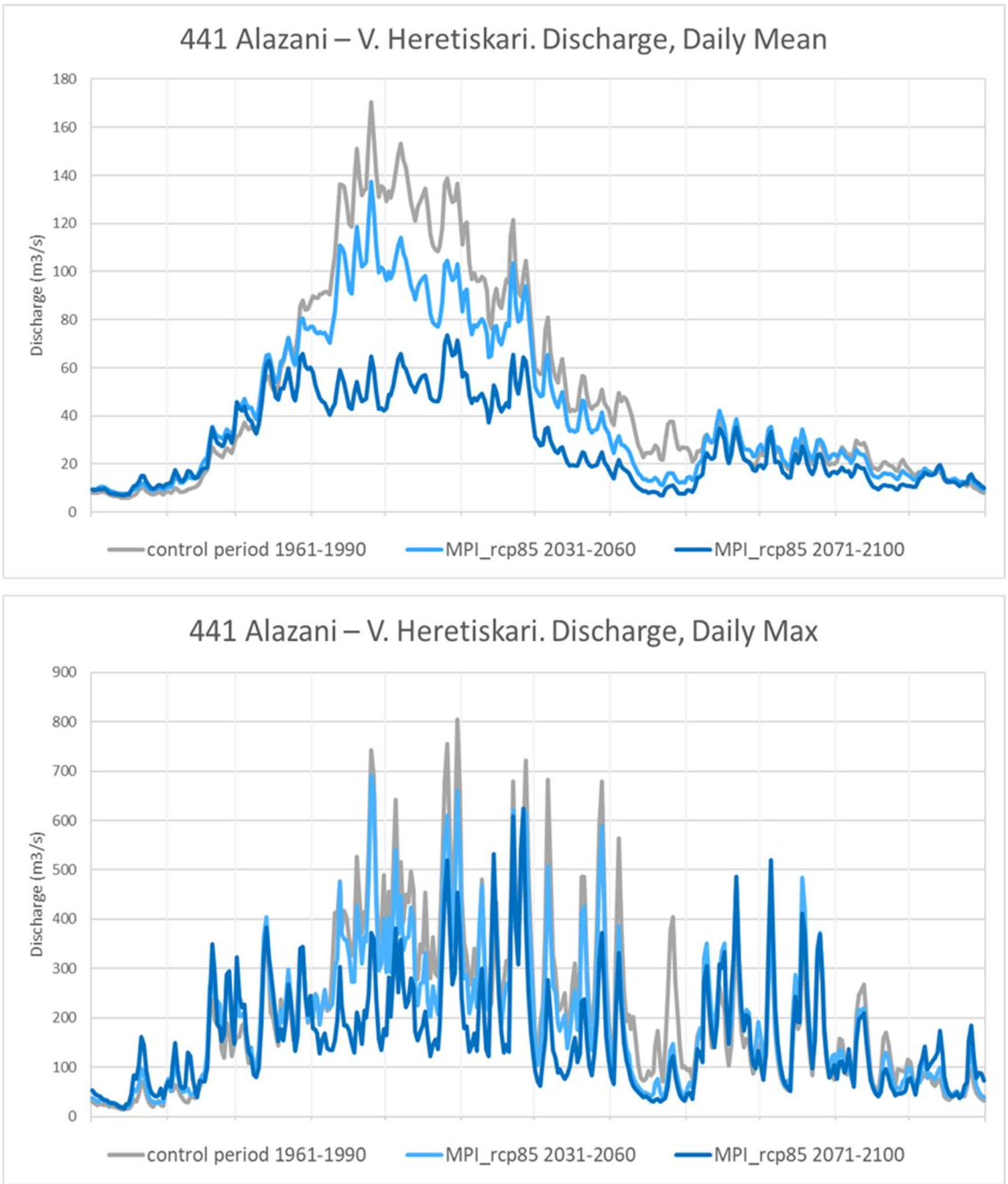

Figure A.130. Simulated daily mean streamflow (top) and daily maximum streamflow in the control period, 1961-1990 (grey line), the near future, 2031-2060 (light blue line) and the end of the century, 2071-2100 (dark blue line), according to the climate projection MPI and the high emission scenario, for the station 441 Alazani – V. Heretiskari.

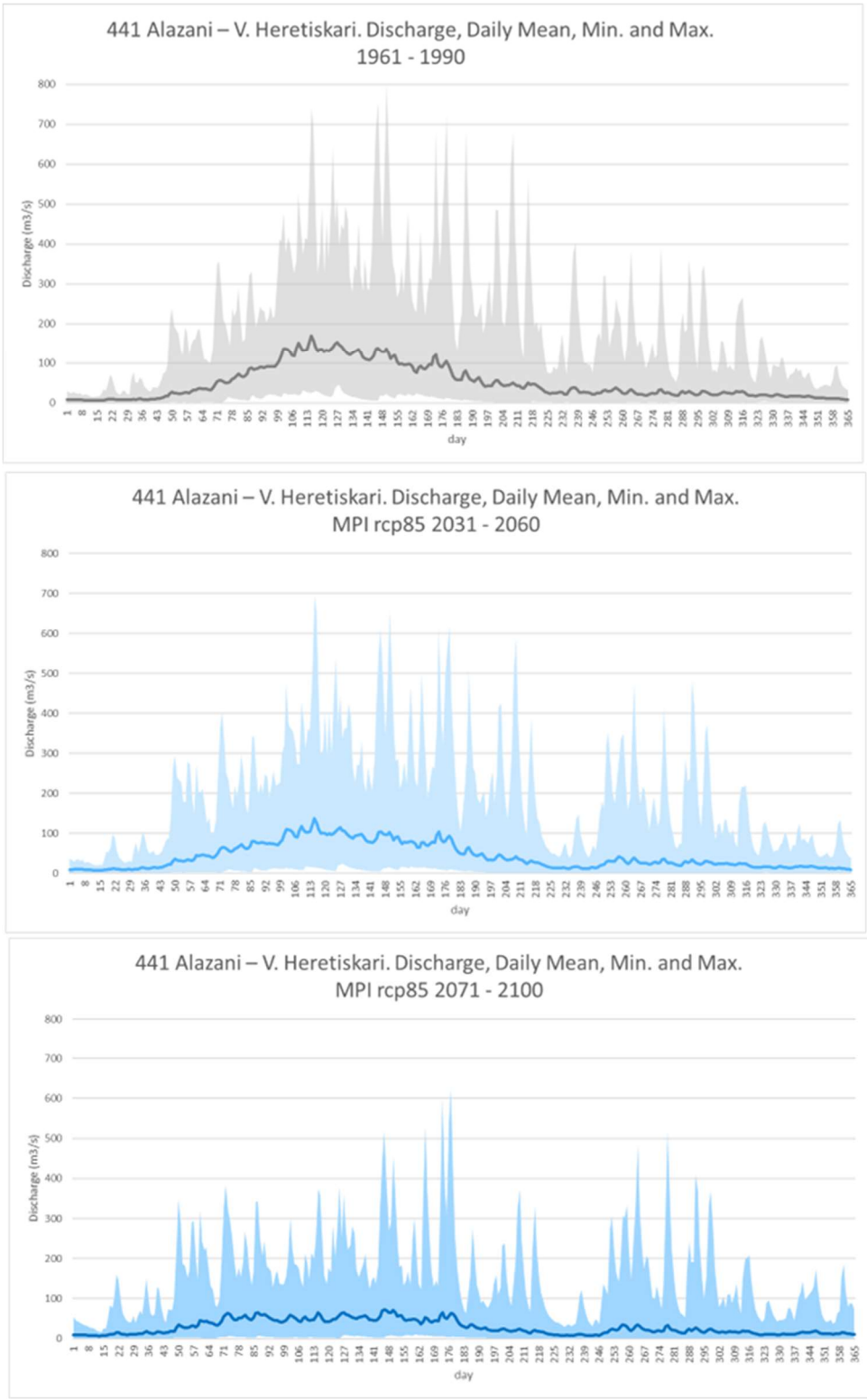

Figure A-131. Simulated daily minimum, mean and maximum streamflow in the control period, 1961-1990 (grey colours), the near future, 2031-2060 (light blue colours) and the end of the century, 2071-2100 (dark blue colours), according to the climate projection MPI and the high emission scenario, for the station 441 Alazani – V. Heretiskari.

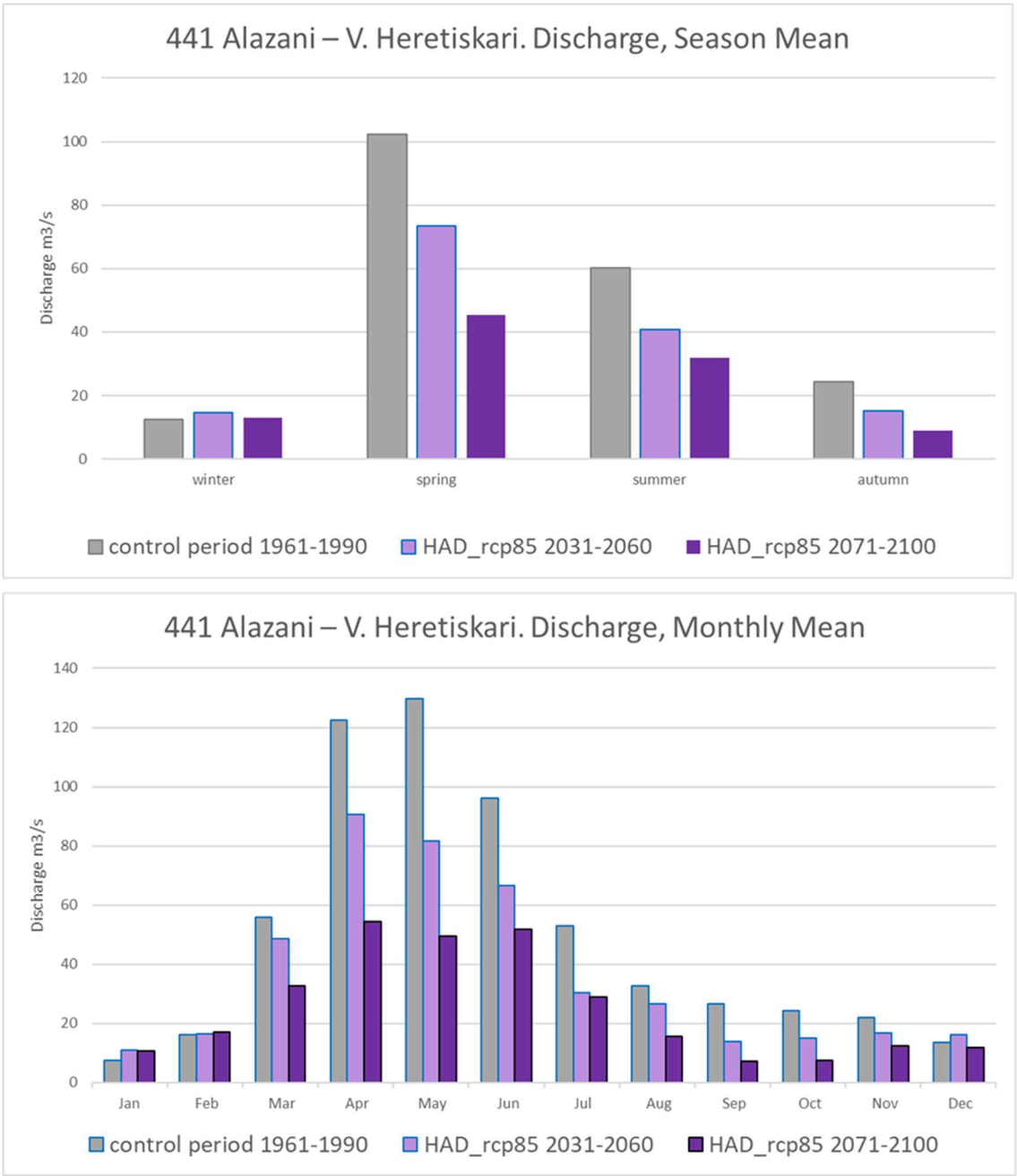

Figure A-132. Simulated season mean (top) and monthly mean (bottom) streamflow in the control period, 1961-1990 (grey bars), the near future, 2031-2060 (light purple bars) and the end of the century, 2071-2100 (dark purple bars), according to the climate projection HAD and the high emission scenario, for the station 441 Alazani – V. Heretiskari.

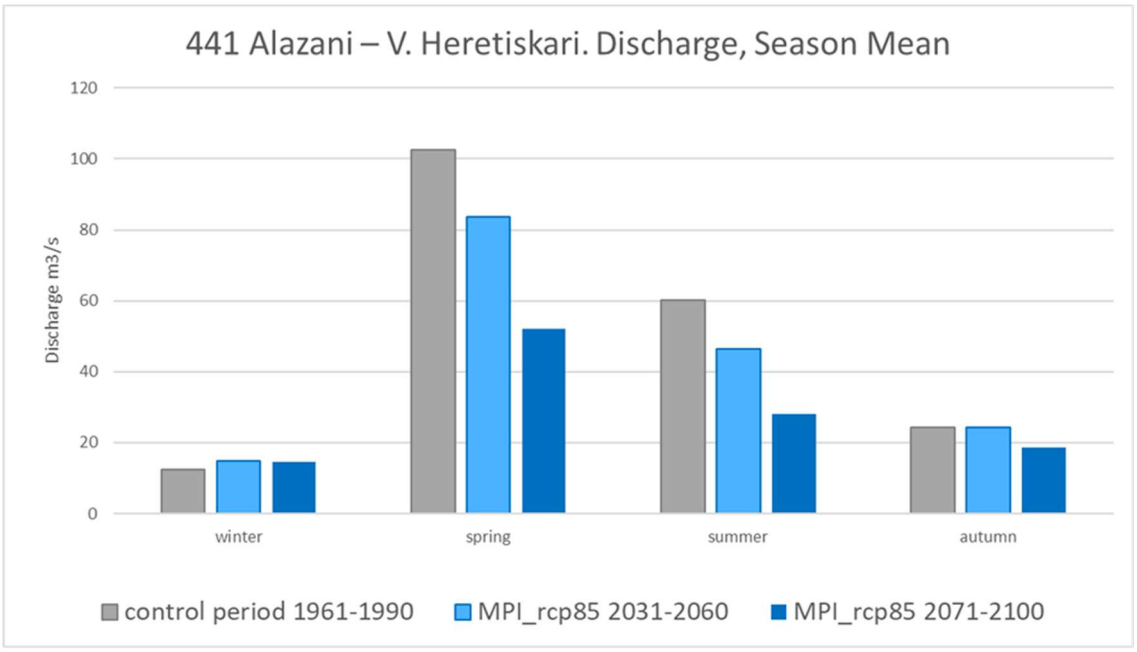

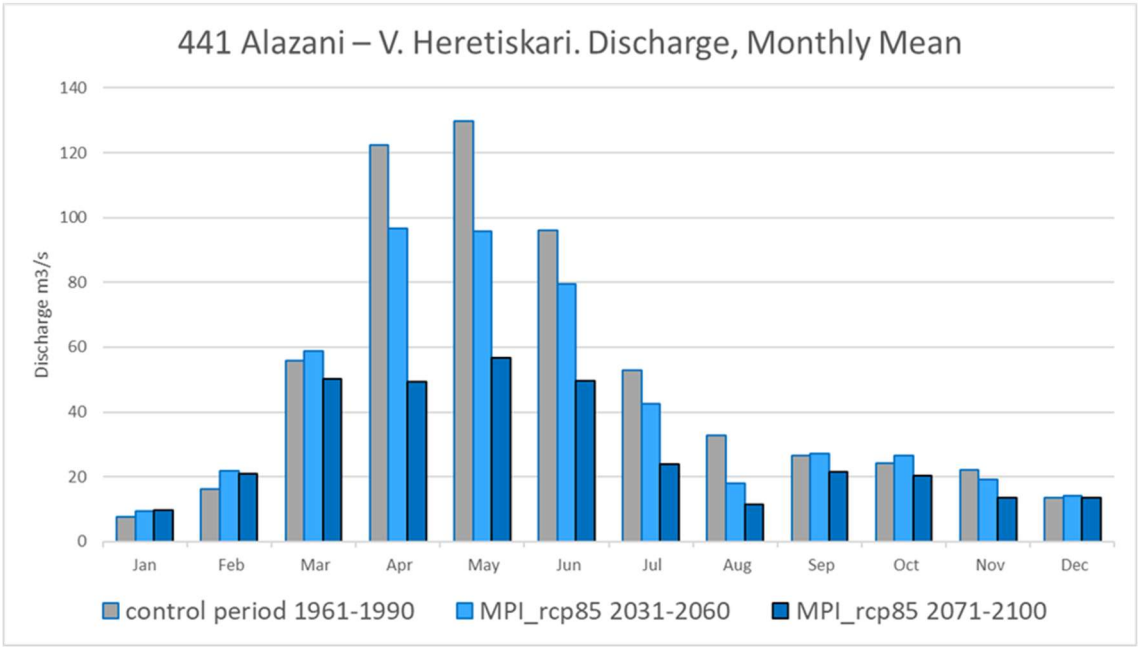

Figure A-133. Simulated season mean (top) and monthly mean (bottom) streamflow in the control period, 1961-1990 (grey bars), the near future, 2031-2060 (light blue bars) and the end of the century, 2071-2100 (dark blue bars), according to the climate projection HAD and the high emission scenario, for the station 441 Alazani – V. Heretiskari.

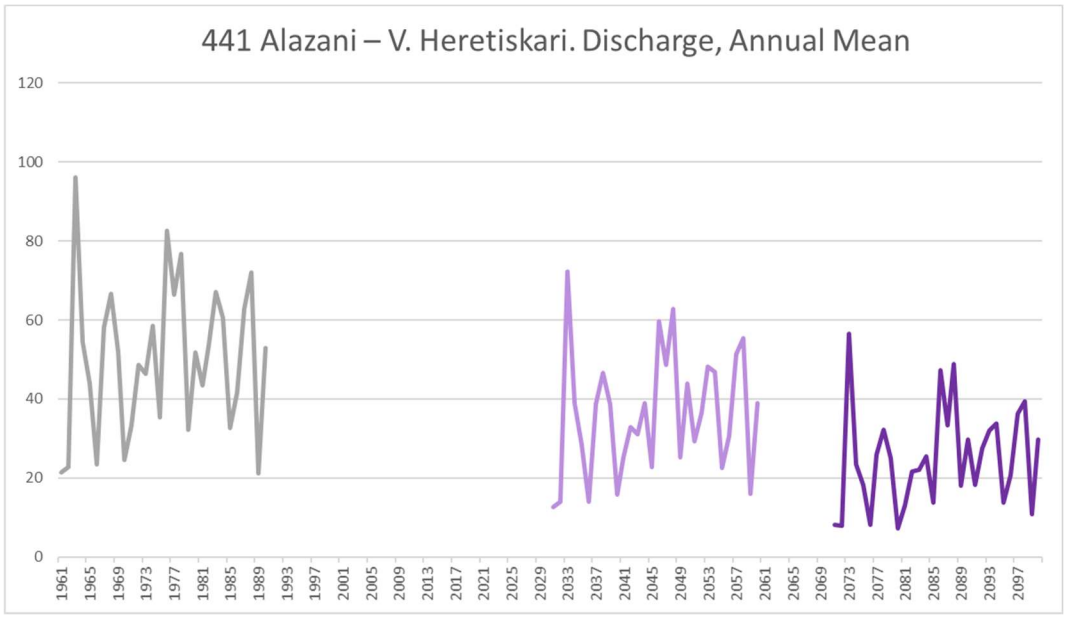

Figure A-134. Simulated annual streamflow in the control period, 1961-1990 (grey line), the near future, 2031-2060 (light purple line) and the end of the century, 2071-2100 (dark purple line), according to the climate projection HAD and the high emission scenario, for the station 441 Alazani – V. Heretiskari.

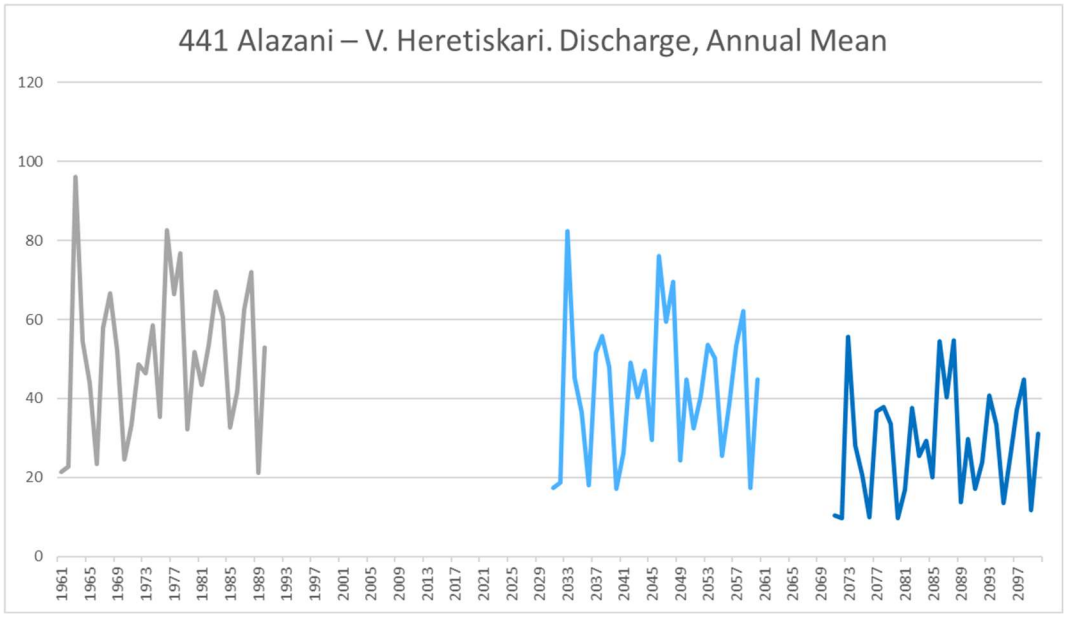

Figure A-135. Simulated annual streamflow in the control period, 1961-1990 (grey line), the near future, 2031-2060 (light blue line) and the end of the century, 2071-2100 (dark blue line), according to the climate projection MPI and the high emission scenario, for the station 441 Alazani – V. Heretiskari.

Snow water equivalent

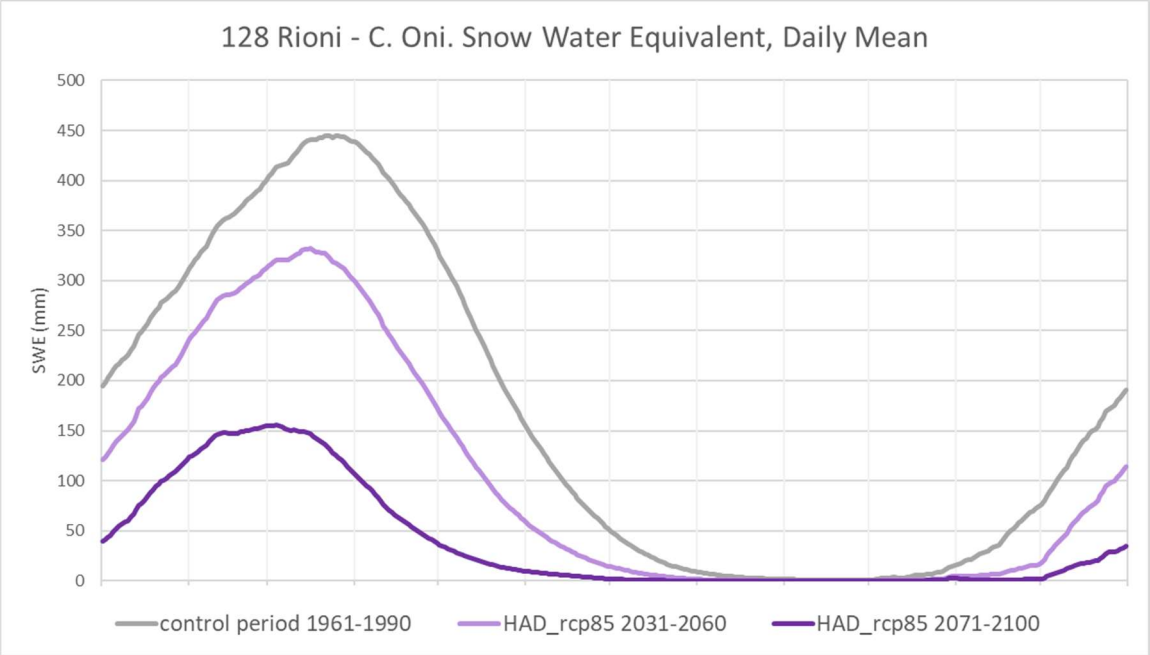

Figure A-136. Daily mean snow water equivalent in the control period, 1961-1990 (grey line), the near future, 2031-2060 (light purple line) and the end of the century, 2071-2100 (dark purple line), according to the climate projection HAD and the high emission scenario, for the station 128 Rioni - C. Oni.

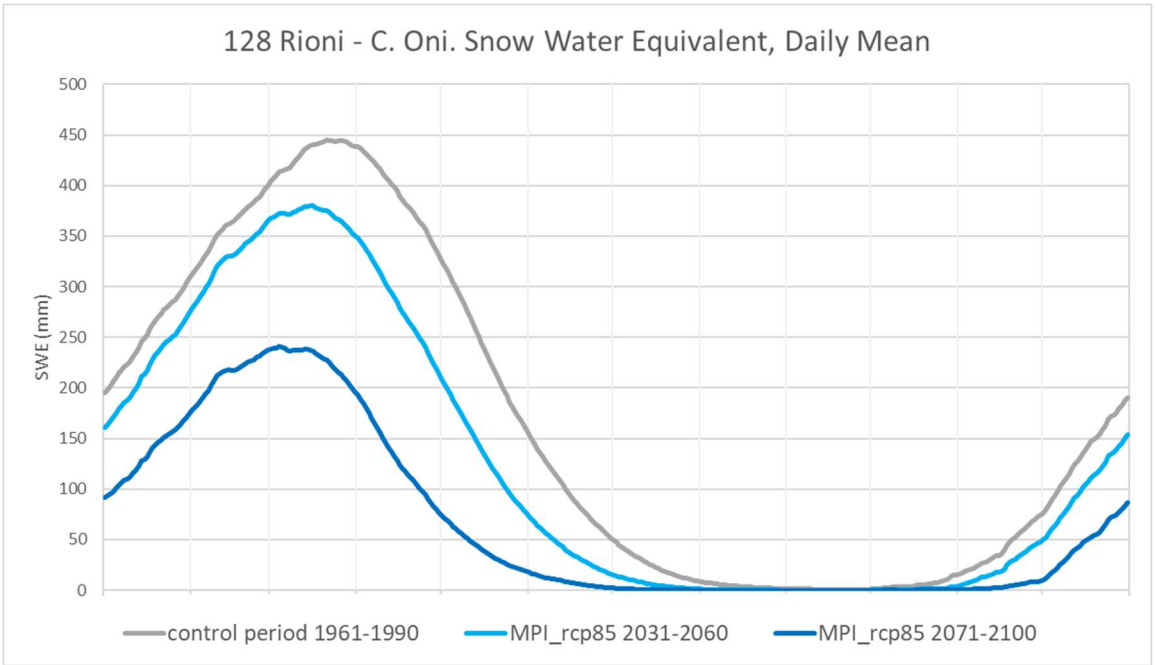

Figure A-137. Daily mean snow water equivalent in the control period, 1961-1990 (grey line), the near future, 2031-2060 (light blue line) and the end of the century, 2071-2100 (dark blue line), according to the climate projection MPI and the high emission scenario, for the station 128 Rioni - C. Oni.

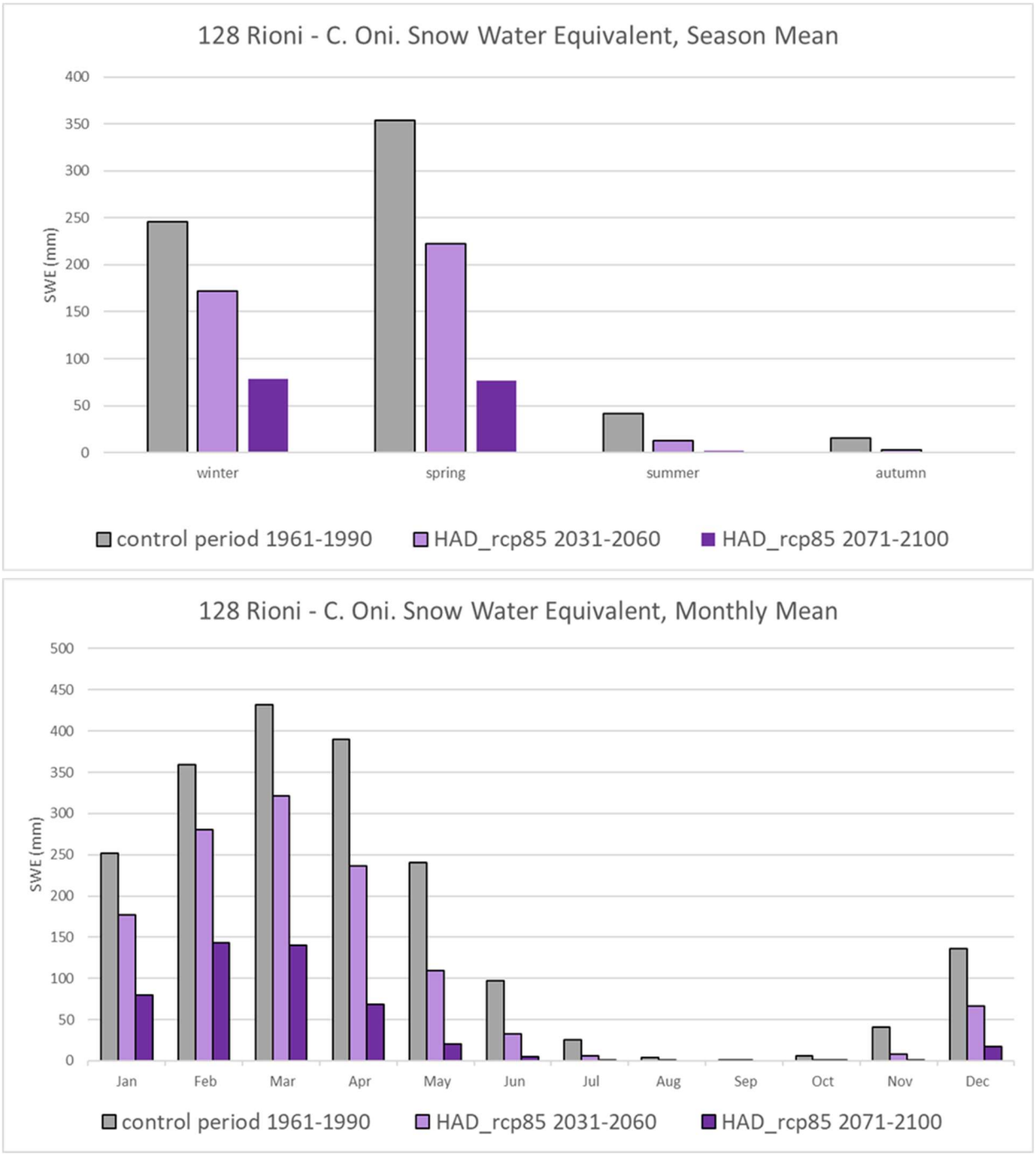

Figure A-138. Season mean (top) and monthly mean (bottom) snow water equivalent in the control period, 1961-1990 (grey bars), the near future, 2031-2060 (light purple bars) and the end of the century, 2071-2100 (dark purple bars), according to the climate projection HAD and the high emission scenario, for the station 128 Rioni - C. Oni.

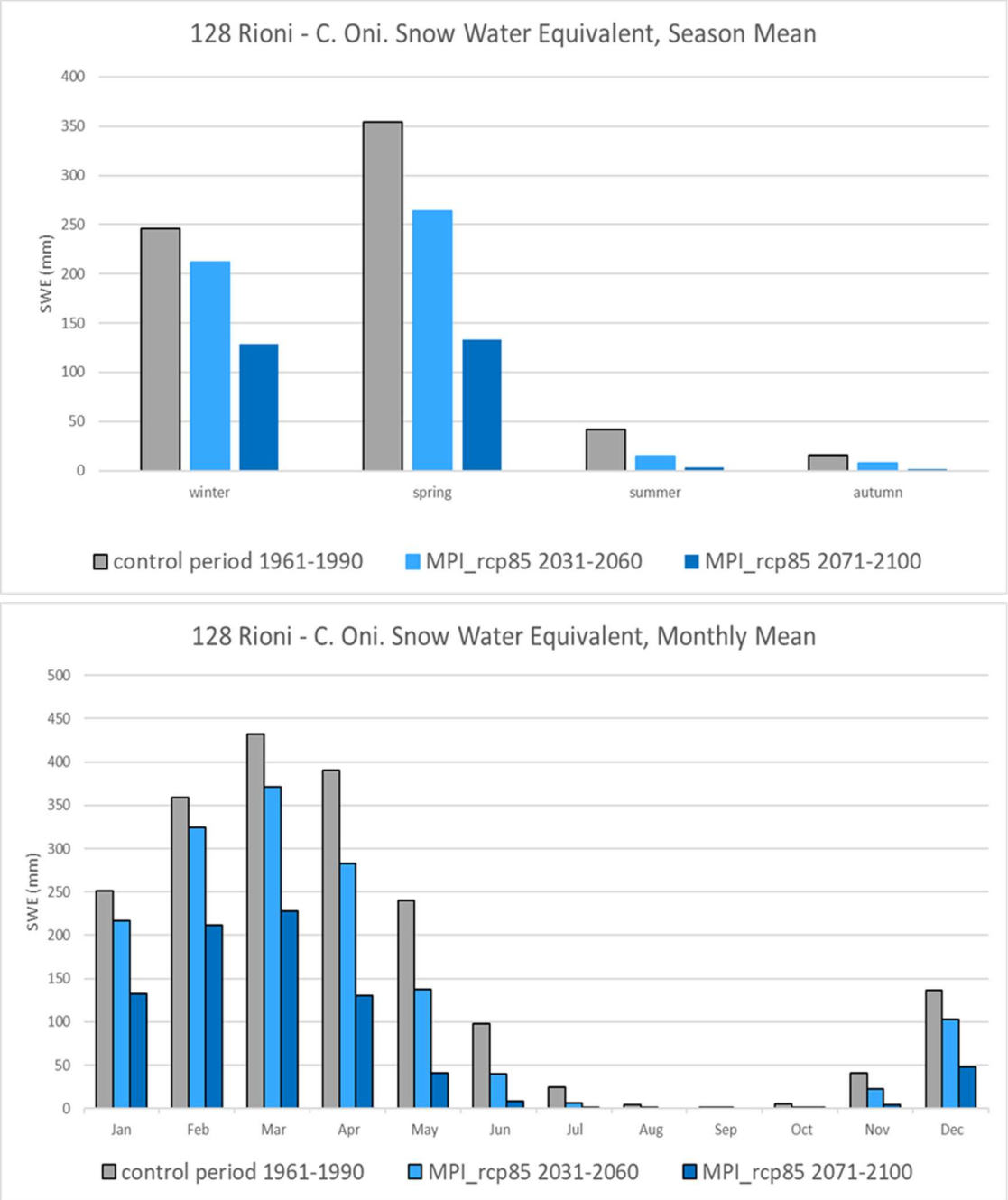

Figure A-139. Season mean (top) and monthly mean (bottom) snow water equivalent in the control period, 1961-1990 (grey bars), the near future, 2031-2060 (light blue bars) and the end of the century, 2071-2100 (dark blue bars), according to the climate projection MPI and the high emission scenario, for the station 128 Rioni - C. Oni.

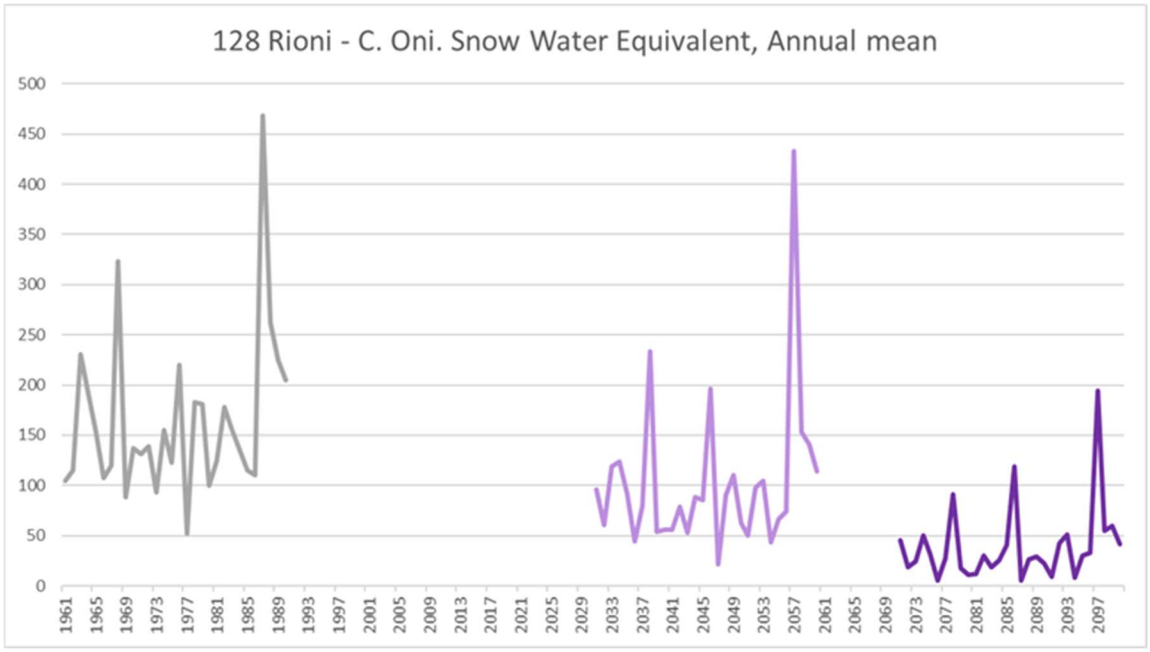

Figure A-140. Annual mean snow water equivalent in the control period, 1961-1990 (grey line), the near future, 2031-2060 (light purple line) and the end of the century, 2071-2100 (dark purple line), according to the climate projection HAD and the high emission scenario, for the station 128 Rioni - C. Oni.

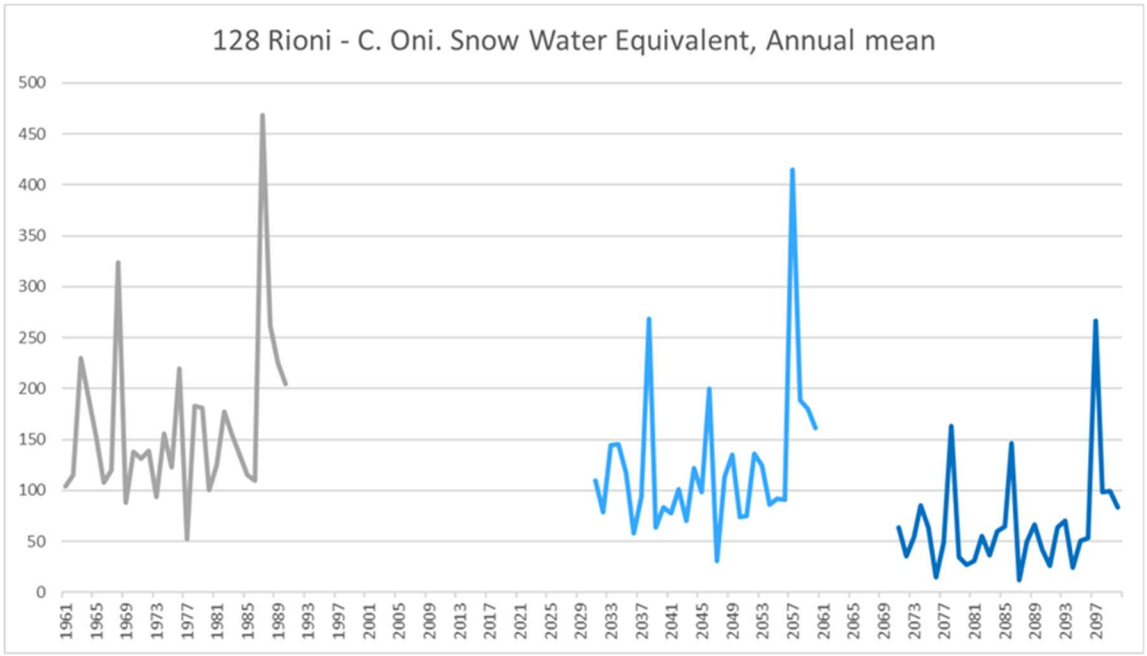

Figure A-141. Annual mean snow water equivalent in the control period, 1961-1990 (grey line), the near future, 2031-2060 (light blue line) and the end of the century, 2071-2100 (dark blue line), according to the climate projection MPI and the high emission scenario, for the station 128 Rioni - C. Oni.

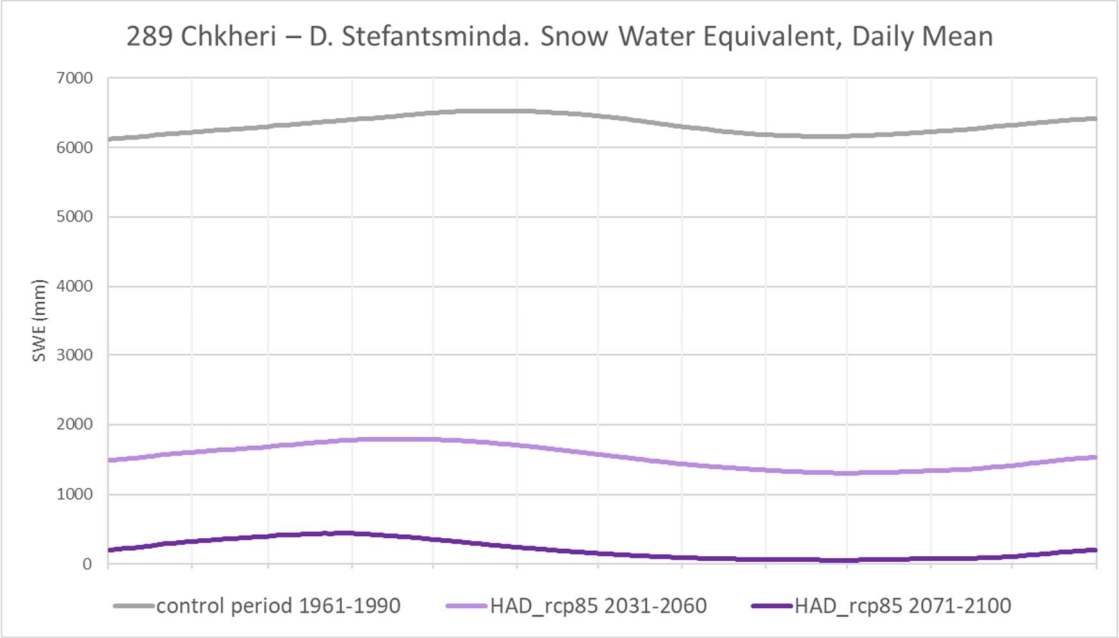

Figure A-142. Daily mean snow water equivalent in the control period, 1961-1990 (grey line), the near future, 2031-2060 (light purple line) and the end of the century, 2071-2100 (dark purple line), according to the climate projection HAD and the high emission scenario, for the station 289 Chkheri – D. Stefantsminda.

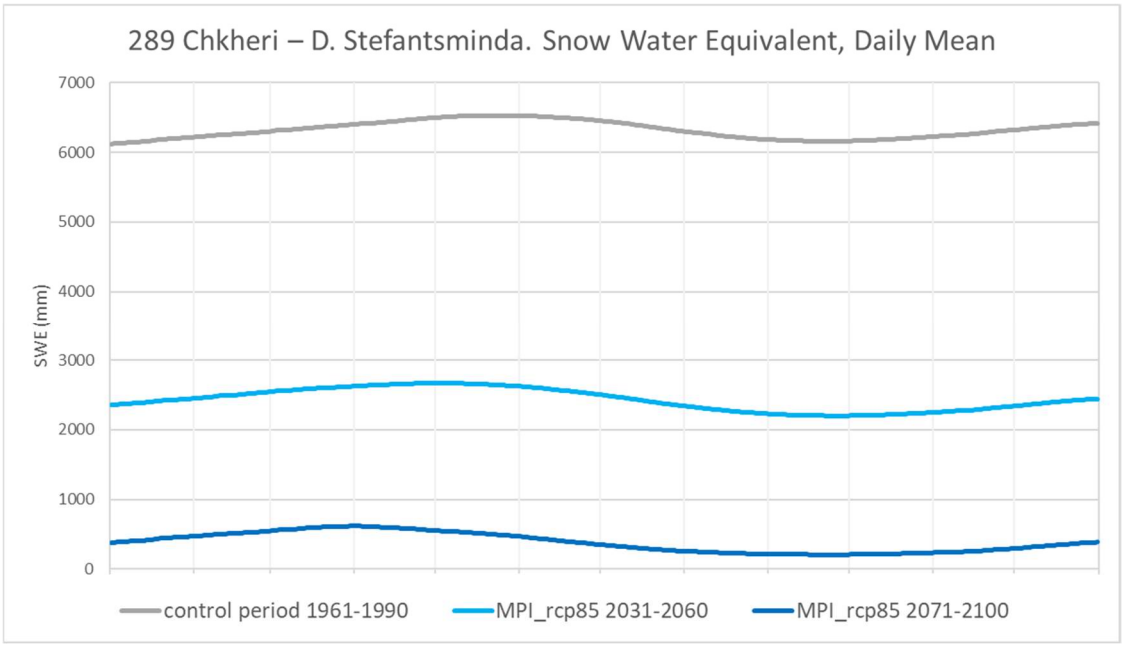

Figure A-143. Daily mean snow water equivalent in the control period, 1961-1990 (grey line), the near future, 2031-2060 (light blue line) and the end of the century, 2071-2100 (dark blue line), according to the climate projection MPI and the high emission scenario, for the station 289 Chkheri – D. Stefantsminda.

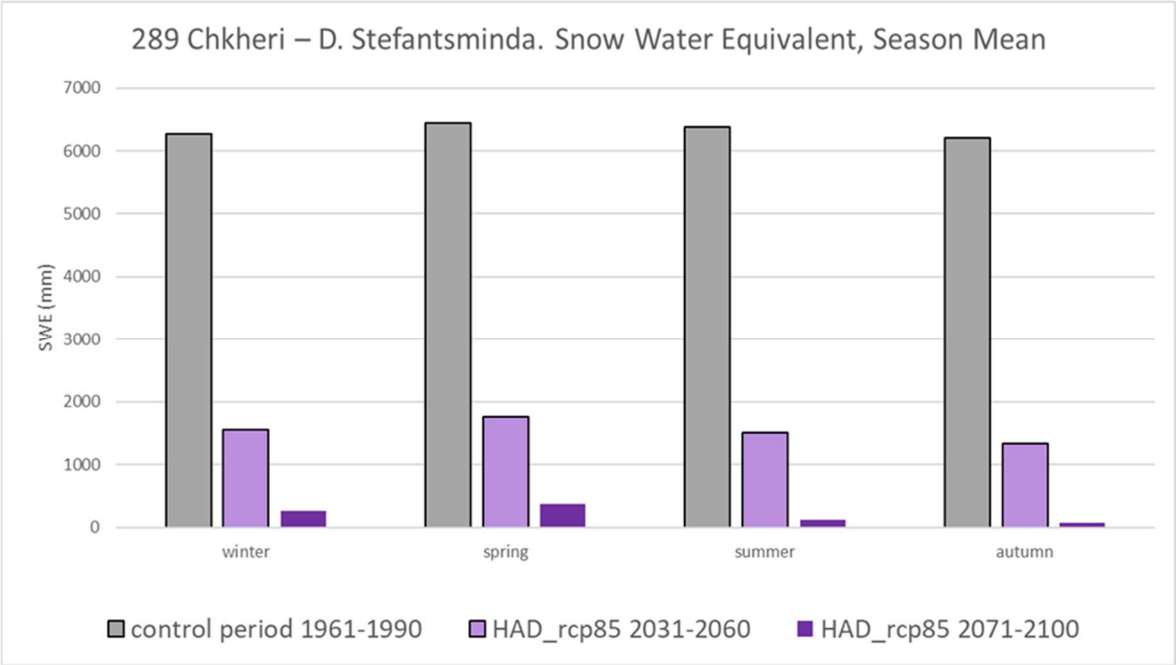

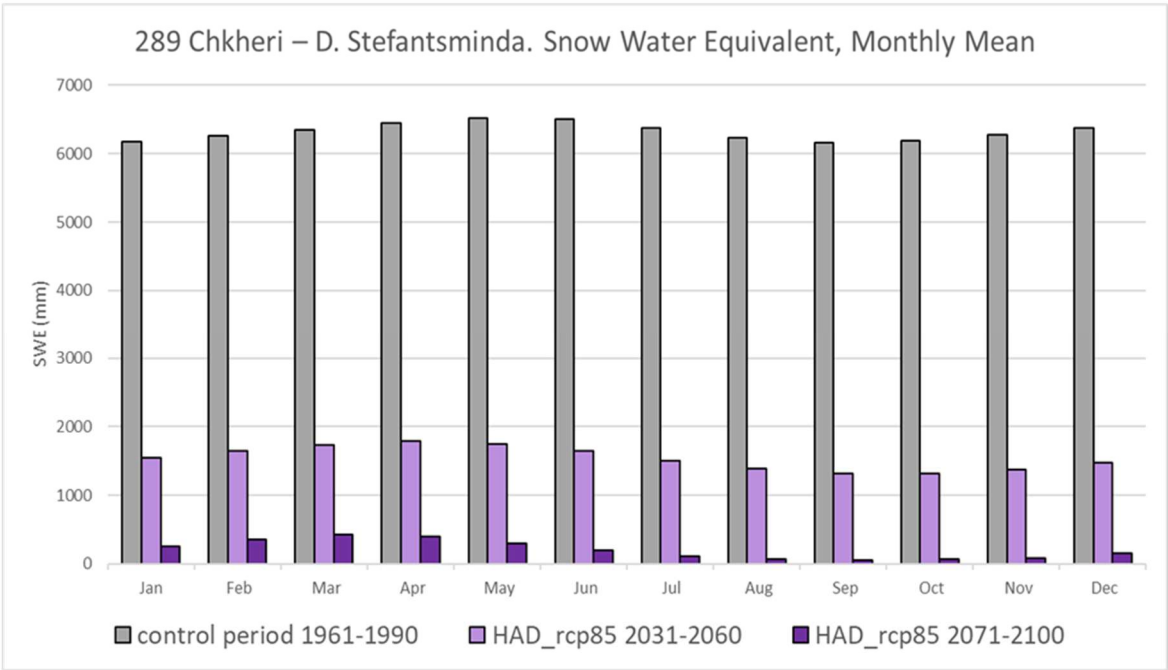

Figure A-144. Season mean (top) and monthly mean (bottom) snow water equivalent in the control period, 1961-1990 (grey bars), the near future, 2031-2060 (light purple bars) and the end of the century, 2071-2100 (dark purple bars), according to the climate projection HAD and the high emission scenario, for the station 289 Chkheri – D. Stefantsminda.

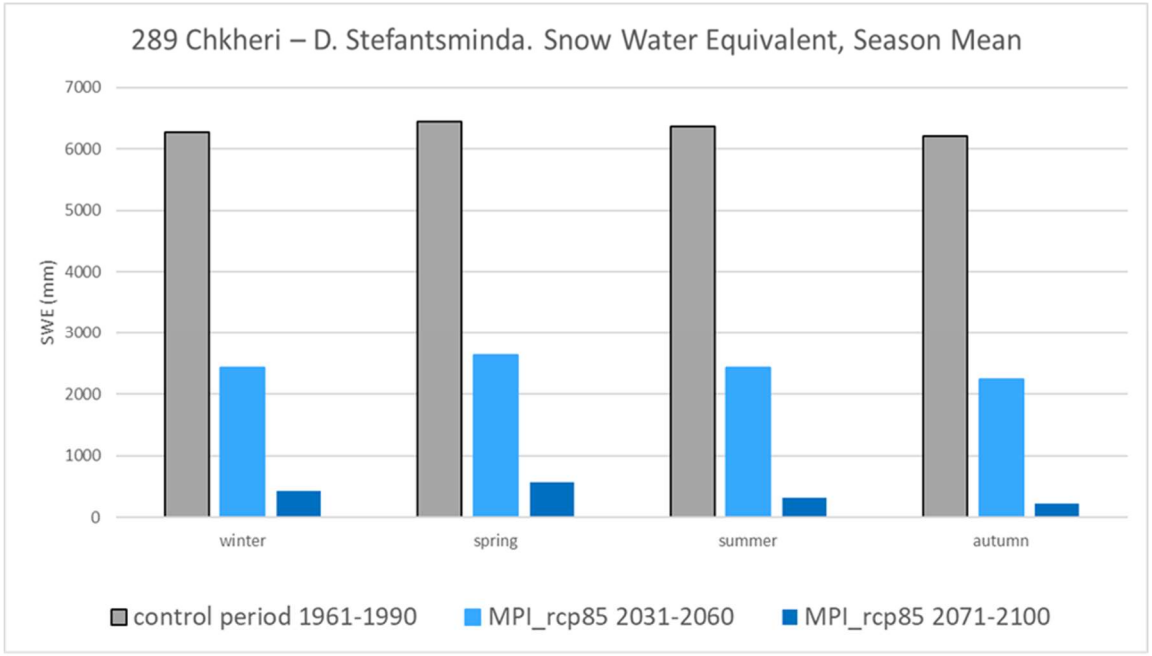

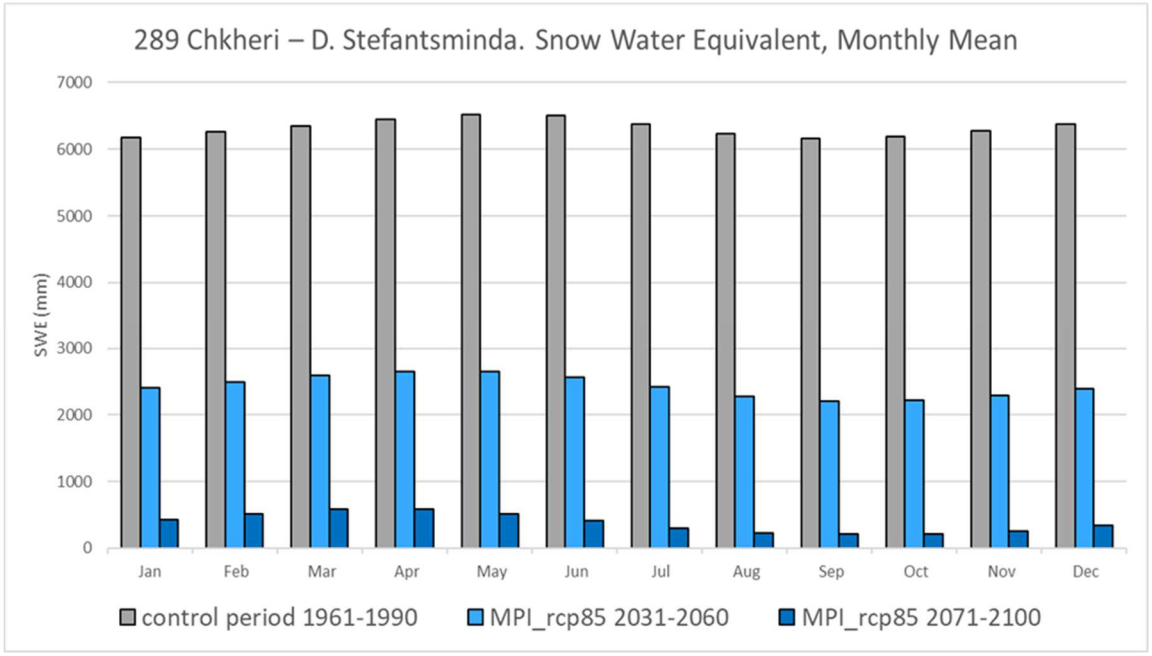

Figure A-145. Season mean (top) and monthly mean (bottom) snow water equivalent in the control period, 1961-1990 (grey bars), the near future, 2031-2060 (light purple bars) and the end of the century, 2071-2100 (dark purple bars), according to the climate projection HAD and the high emission scenario, for the station 289 Chkheri – D. Stefantsminda.

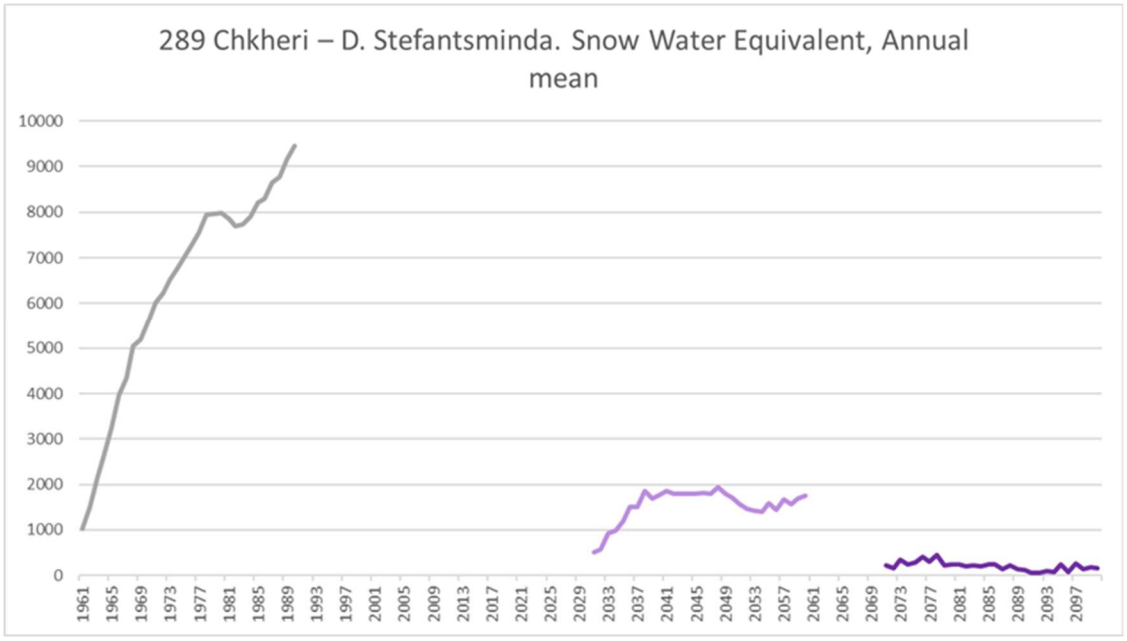

Figure A-146. Annual mean snow water equivalent in the control period, 1961-1990 (grey line), the near future, 2031-2060 (light purple line) and the end of the century, 2071-2100 (dark purple line), according to the climate projection HAD and the high emission scenario, for the station 289 Chkheri – D. Stefantsminda.

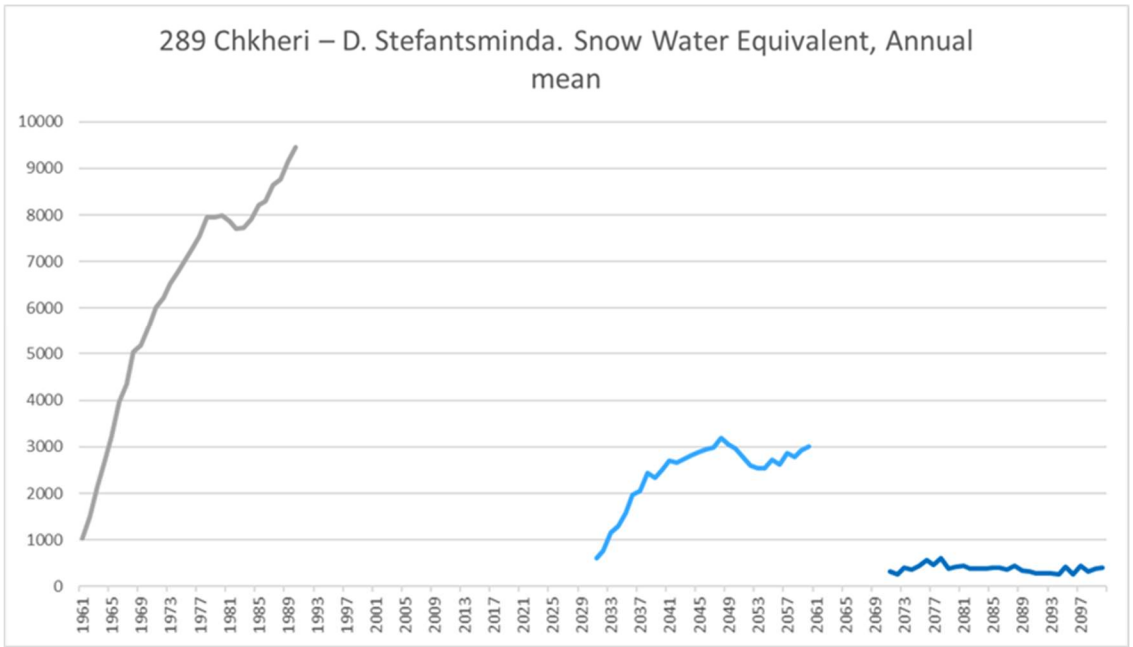

Figure 147. Annual mean snow water equivalent in the control period, 1961-1990 (grey line), the near future, 2031-2060 (light blue line) and the end of the century, 2071-2100 (dark blue line), according to the climate projection MPI and the high emission scenario, for the station 289 Chkheri – D. Stefantsminda.

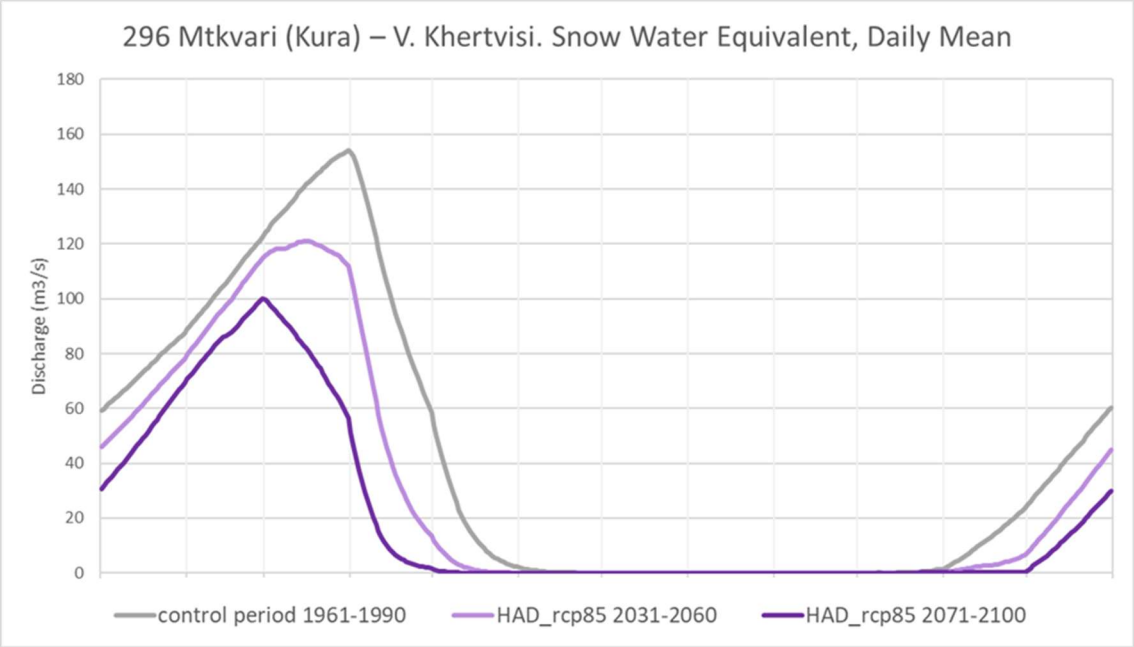

Figure A-148. Daily mean snow water equivalent in the control period, 1961-1990 (grey line), the near future, 2031-2060 (light purple line) and the end of the century, 2071-2100 (dark purple line), according to the climate projection HAD and the high emission scenario, for the station 296 Mtkvari (Kura) – V. Khertvisi.

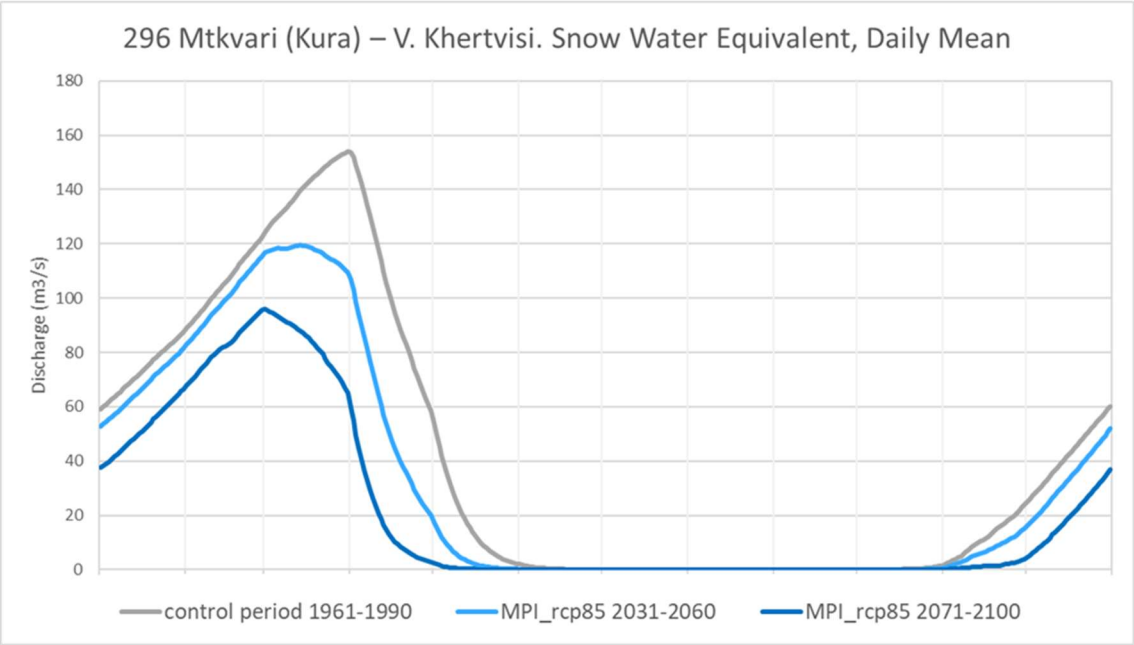

Figure A-149. Daily mean snow water equivalent in the control period, 1961-1990 (grey line), the near future, 2031-2060 (light blue line) and the end of the century, 2071-2100 (dark blue line), according to the climate projection MPI and the high emission scenario, for the station 296 Mtkvari (Kura) – V. Khertvisi.

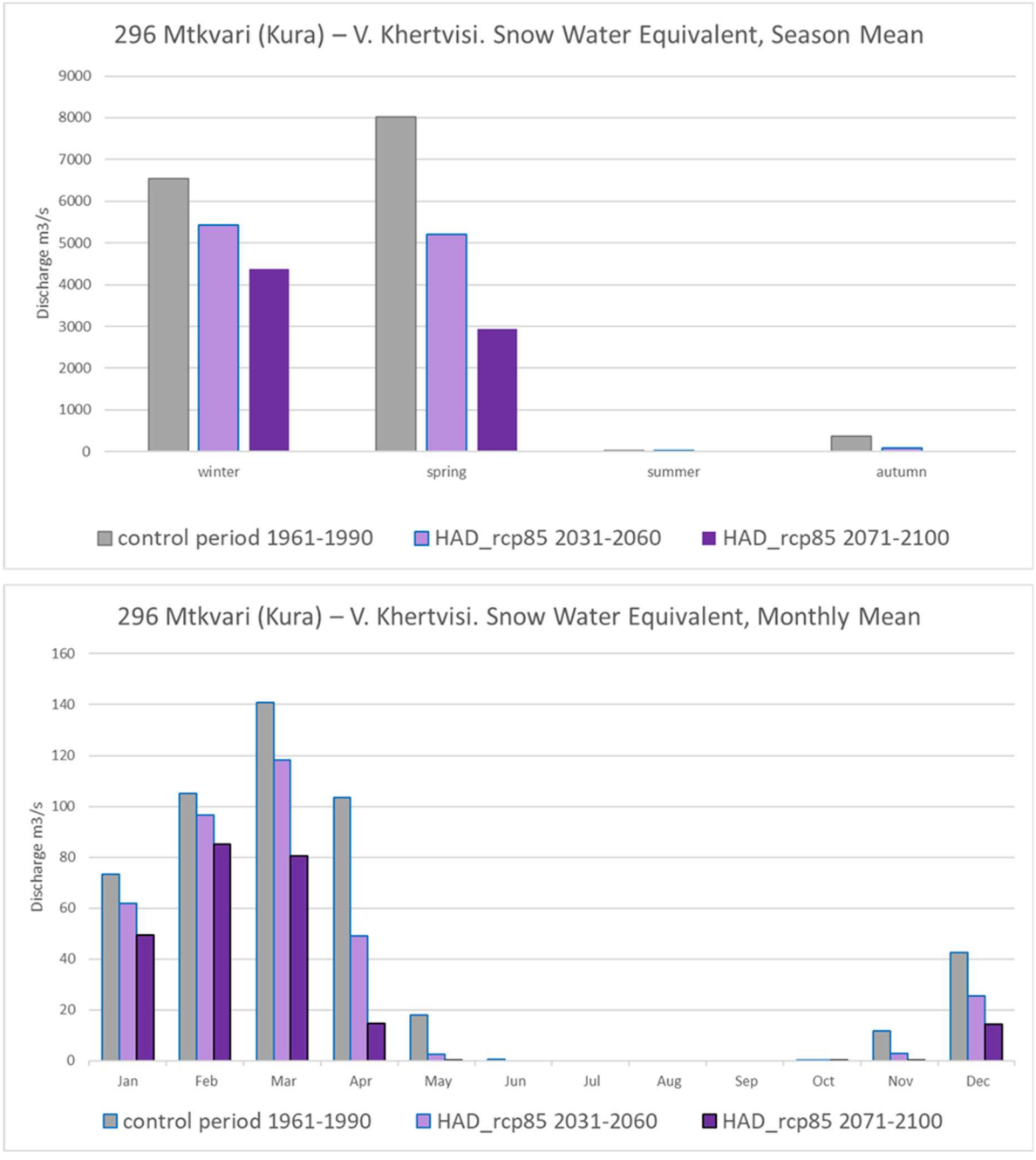

Figure A-150. Season mean (top) and monthly mean (bottom) snow water equivalent in the control period, 1961-1990 (grey bars), the near future, 2031-2060 (light purple bars) and the end of the century, 2071-2100 (dark purple bars), according to the climate projection HAD and the high emission scenario, for the station 296 Mtkvari (Kura) – V. Khertvisi.

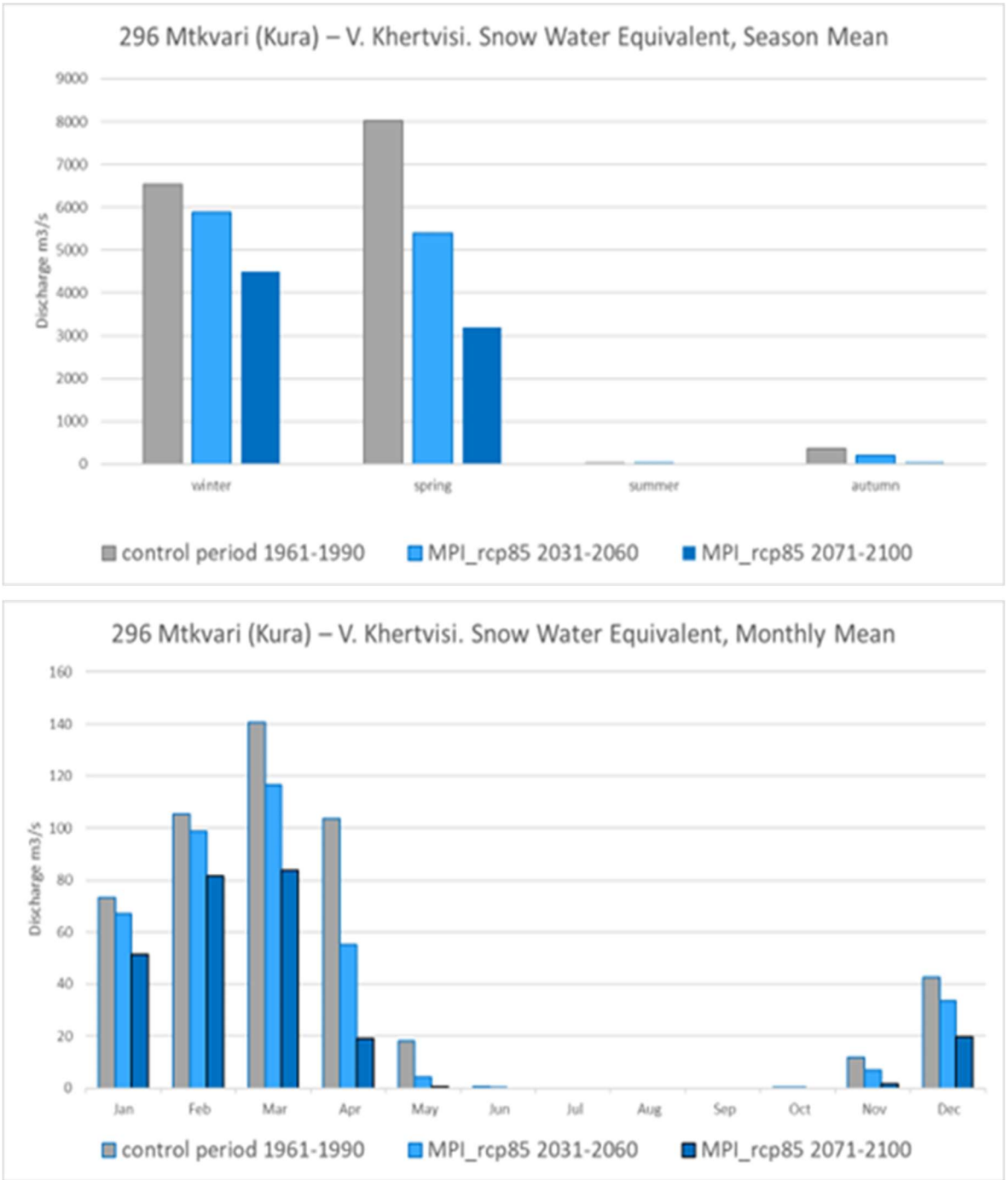

Figure A-151. Season mean (top) and monthly mean (bottom) snow water equivalent in the control period, 1961-1990 (grey bars), the near future, 2031-2060 (light blue bars) and the end of the century, 2071-2100 (dark blue bars), according to the climate projection MPI and the high emission scenario, for the station 296 Mtkvari (Kura) – V. Khertvisi.

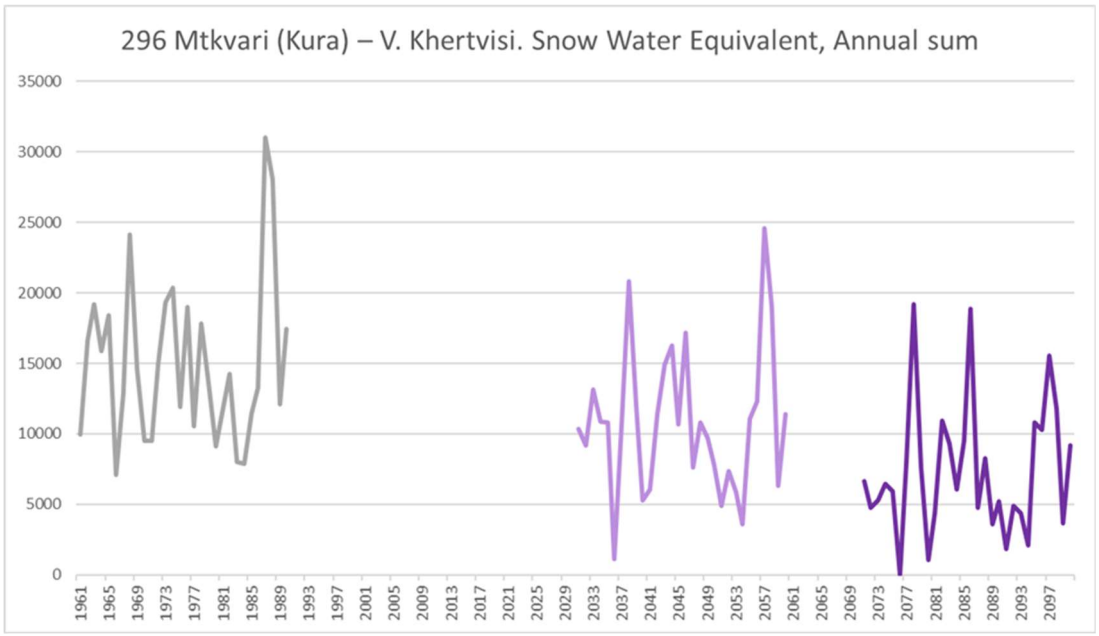

Figure A-152. Annual mean snow water equivalent in the control period, 1961-1990 (grey line), the near future, 2031-2060 (light purple line) and the end of the century, 2071-2100 (dark purple line), according to the climate projection HAD and the high emission scenario, for the station 296 Mtkvari (Kura) – V. Khertvisi.

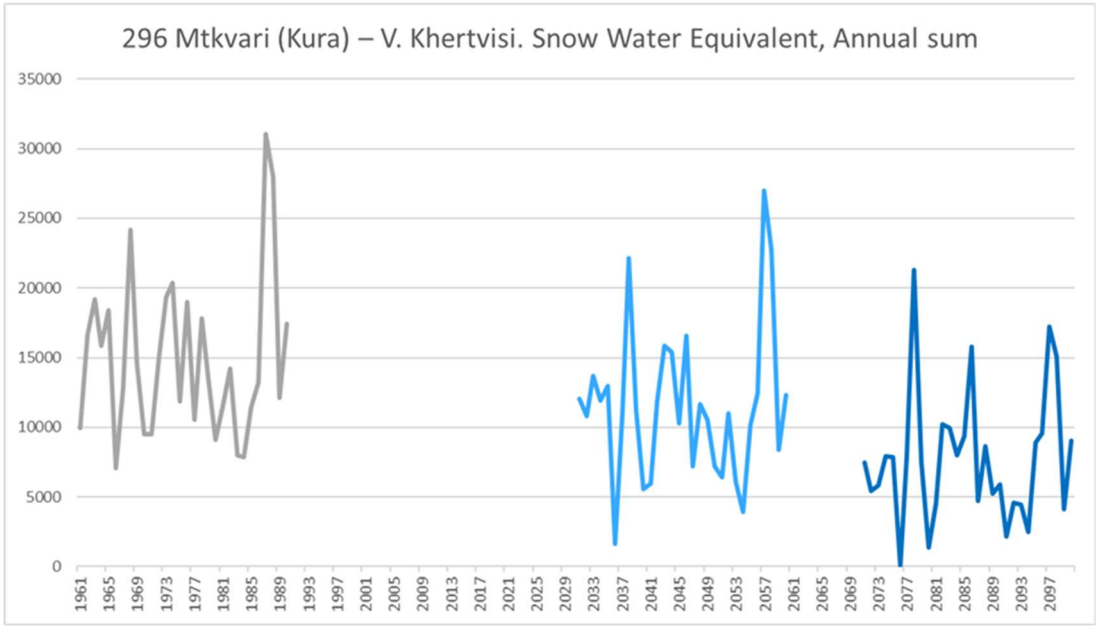

Figure A-153. Annual mean snow water equivalent in the control period, 1961-1990 (grey line), the near future, 2031-2060 (light blue line) and the end of the century, 2071-2100 (dark blue line), according to the climate projection MPI and the high emission scenario, for the station 296 Mtkvari (Kura) – V. Khertvisi.

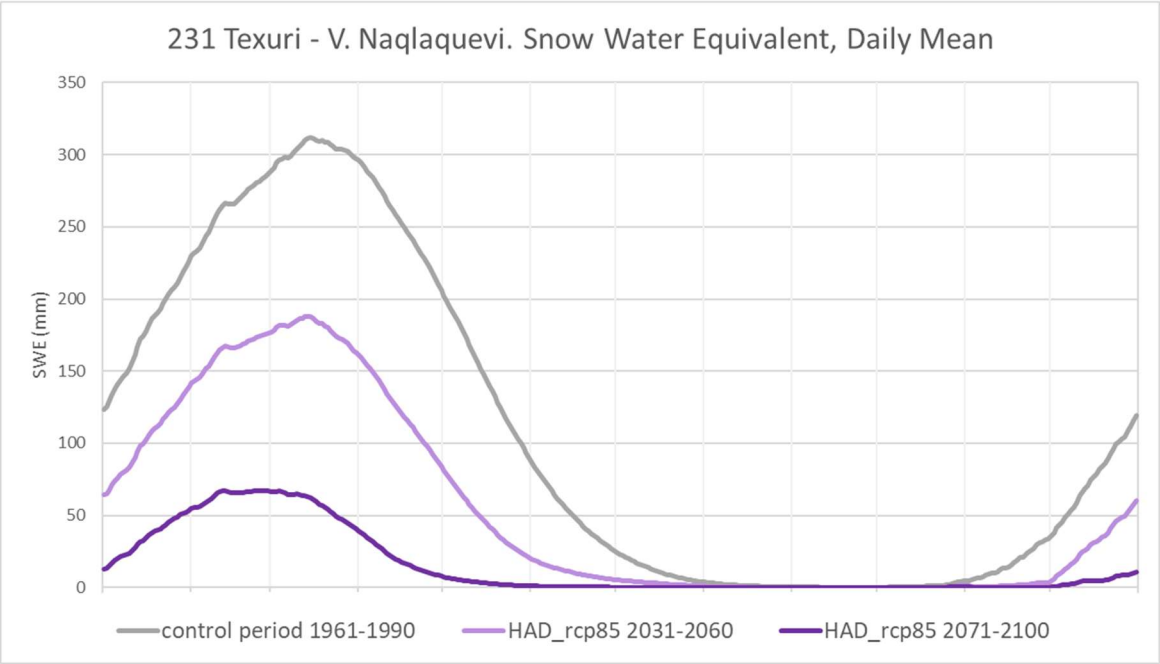

Figure A-154. Daily mean snow water equivalent in the control period, 1961-1990 (grey line), the near future, 2031-2060 (light purple line) and the end of the century, 2071-2100 (dark purple line), according to the climate projection HAD and the high emission scenario, for the station 231 Texuri - V. Naqlaquevi.

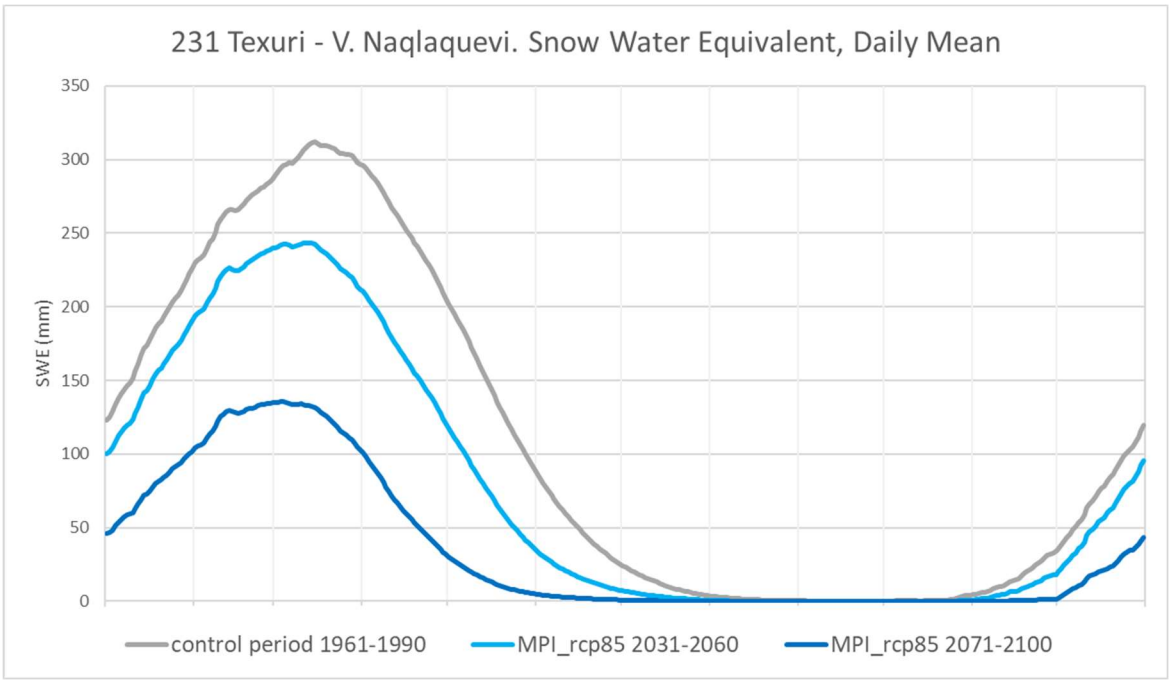

Figure A-155. Daily snow water equivalent in the control period, 1961-1990 (grey line), the near future, 2031-2060 (light blue line) and the end of the century, 2071-2100 (dark blue line), according to the climate projection MPI and the high emission scenario, for the station 231 Texuri - V. Naqlaquevi.

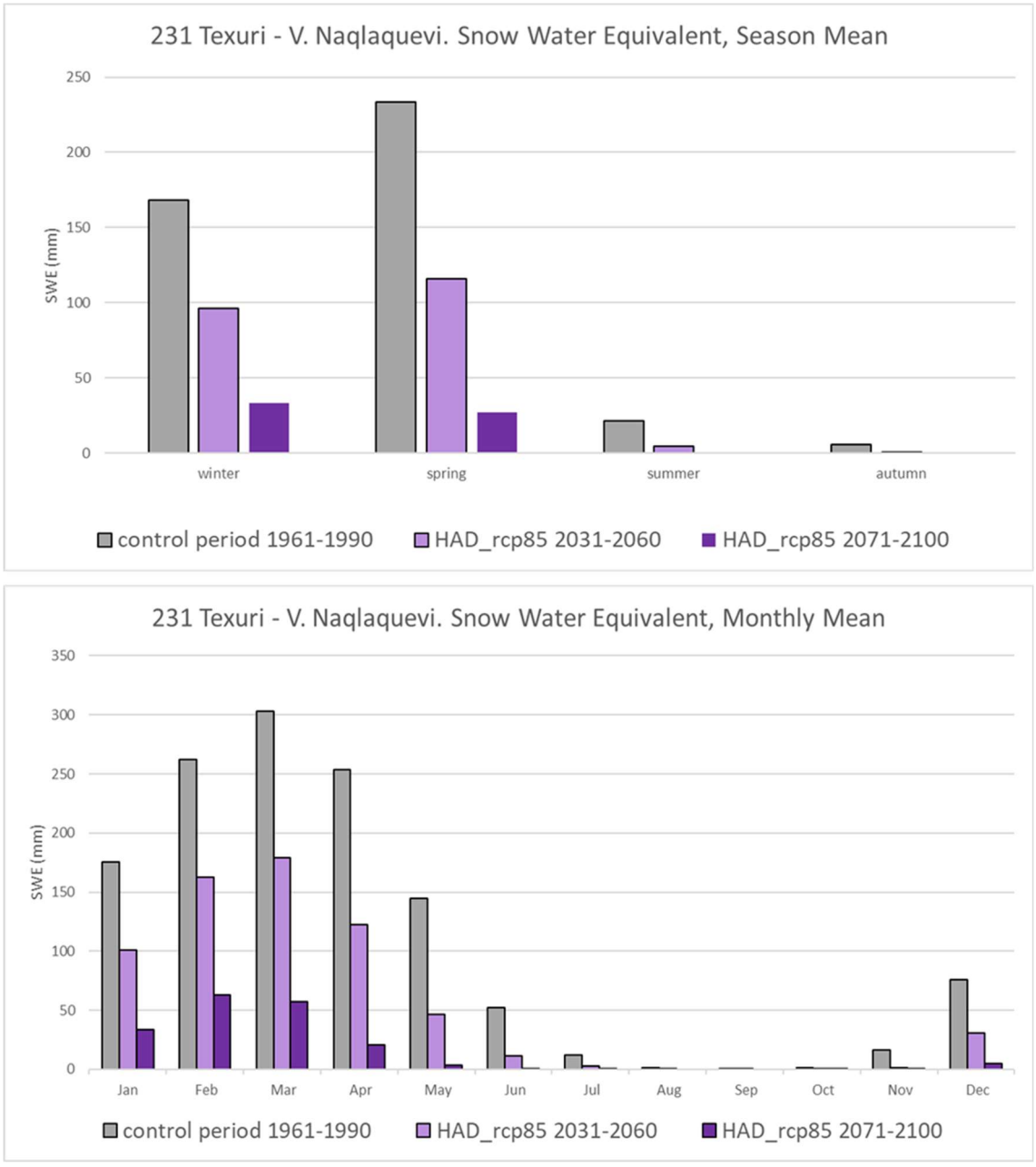

Figure A-156. Season mean (top) and monthly mean (bottom) snow water equivalent in the control period, 1961-1990 (grey bars), the near future, 2031-2060 (light purple bars) and the end of the century, 2071-2100 (dark purple bars), according to the climate projection HAD and the high emission scenario, for the station 231 Texuri - V. Naqlaquevi.

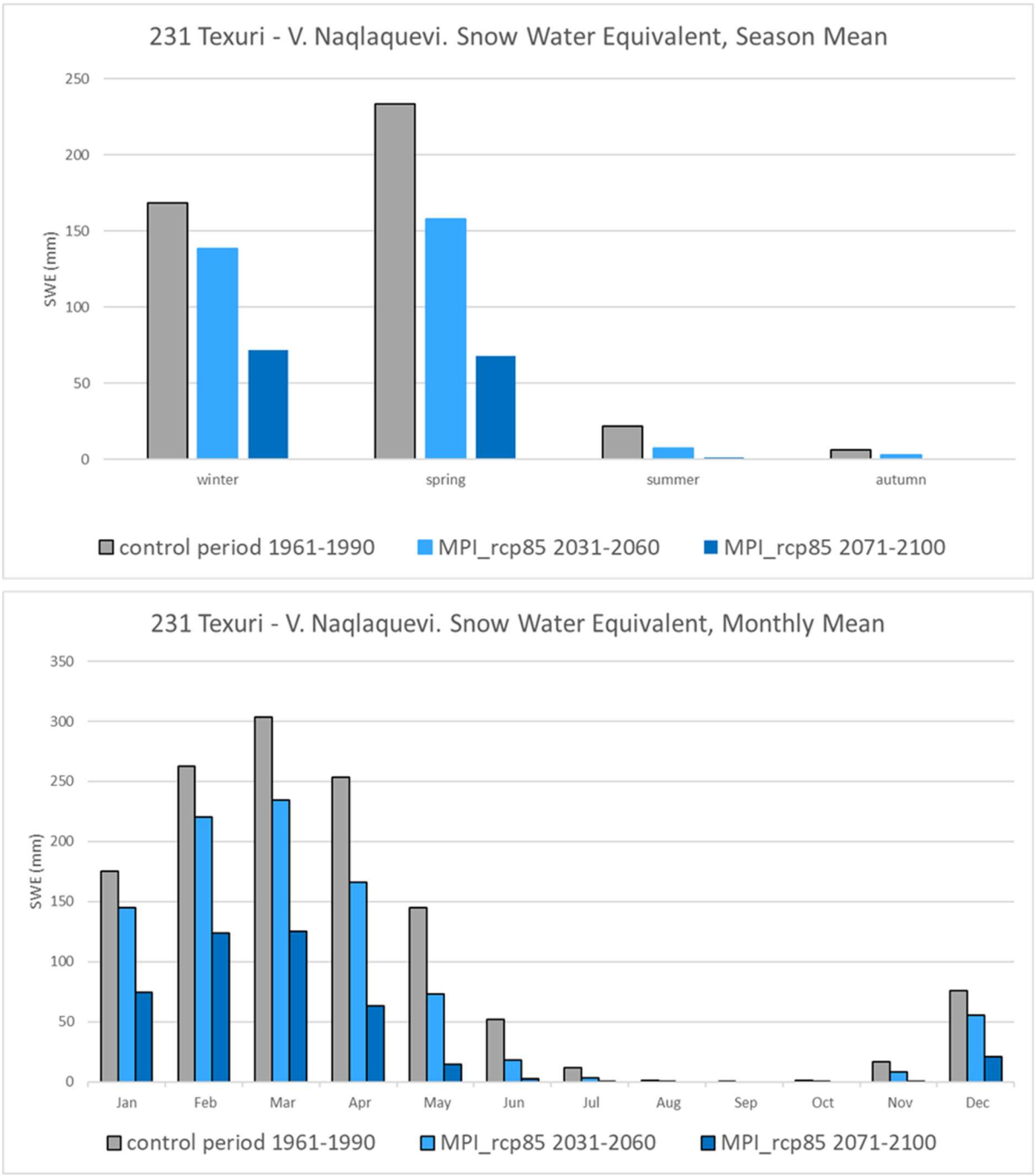

Figure A-157. Season mean (top) and monthly mean (bottom) snow water equivalent in the control period, 1961-1990 (grey bars), the near future, 2031-2060 (light blue bars) and the end of the century, 2071-2100 (dark blue bars), according to the climate projection MPI and the high emission scenario, for the station 231 Texuri - V. Naqlaquevi.

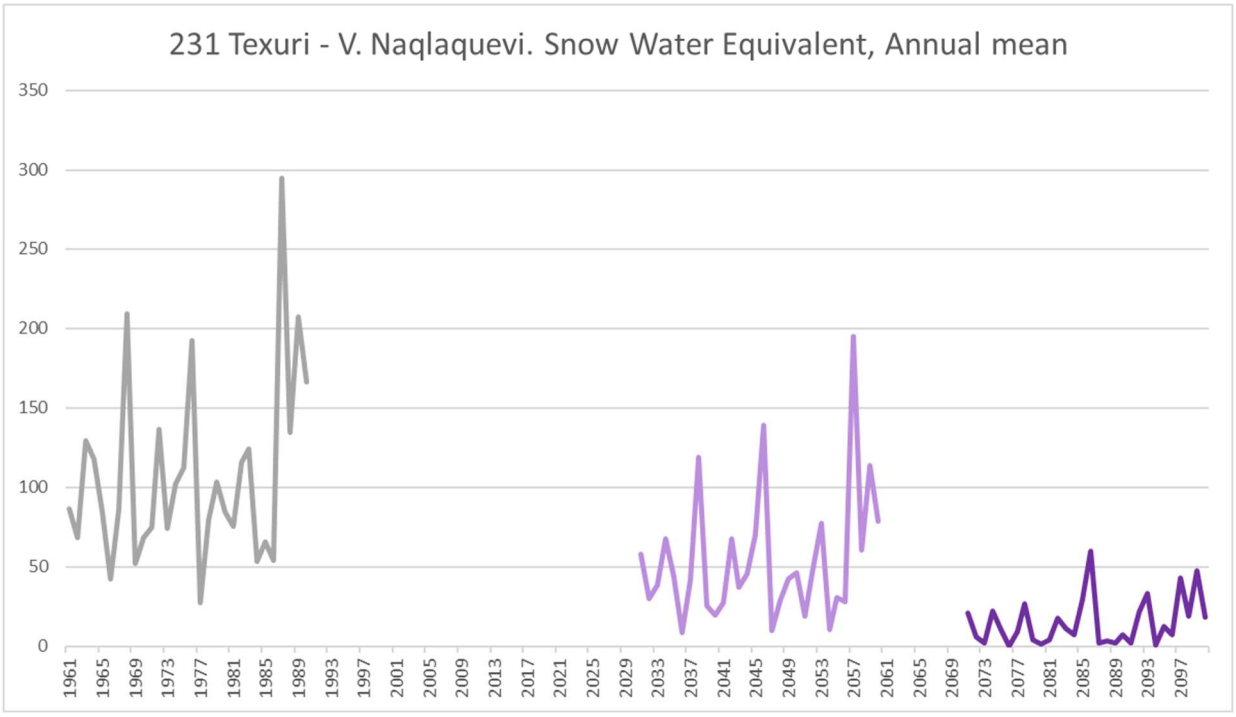

Figure A-158. Annual mean snow water equivalent in the control period, 1961-1990 (grey line), the near future, 2031-2060 (light purple line) and the end of the century, 2071-2100 (dark purple line), according to the climate projection HAD and the high emission scenario, for the station 231 Texuri - V. Naqlaquevi

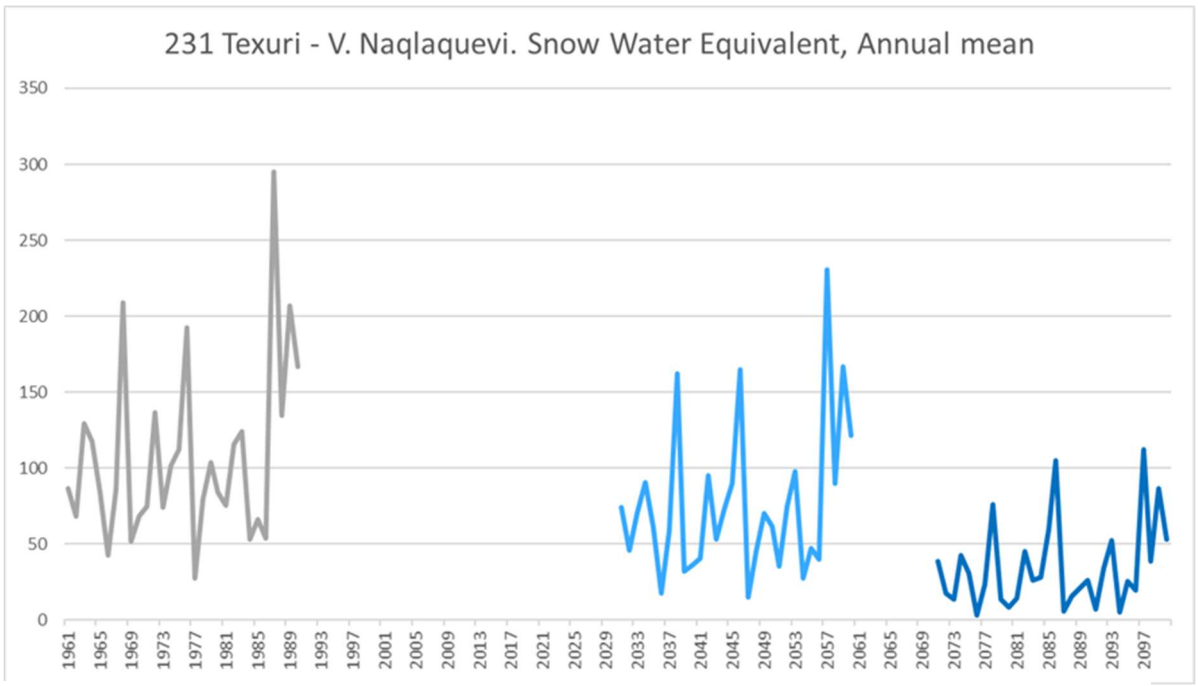

Figure A-159. Annual mean snow water equivalent in the control period, 1961-1990 (grey line), the near future, 2031-2060 (light blue line) and the end of the century, 2071-2100 (dark blue line), according to the climate projection MPI and the high emission scenario, for the station 231 Texuri - V. Naqlaquevi

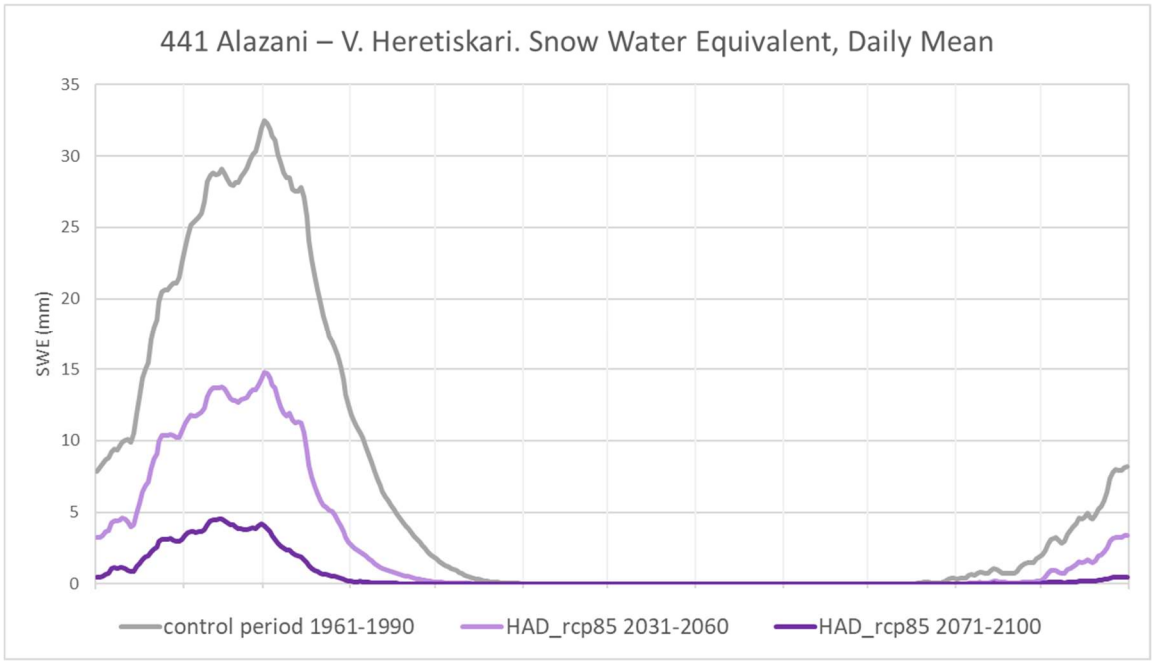

Figure A-160. Daily mean snow water equivalent in the control period, 1961-1990 (grey line), the near future, 2031-2060 (light purple line) and the end of the century, 2071-2100 (dark purple line), according to the climate projection HAD and the high emission scenario, for the station 441 Alazani – V. Heretiskari.

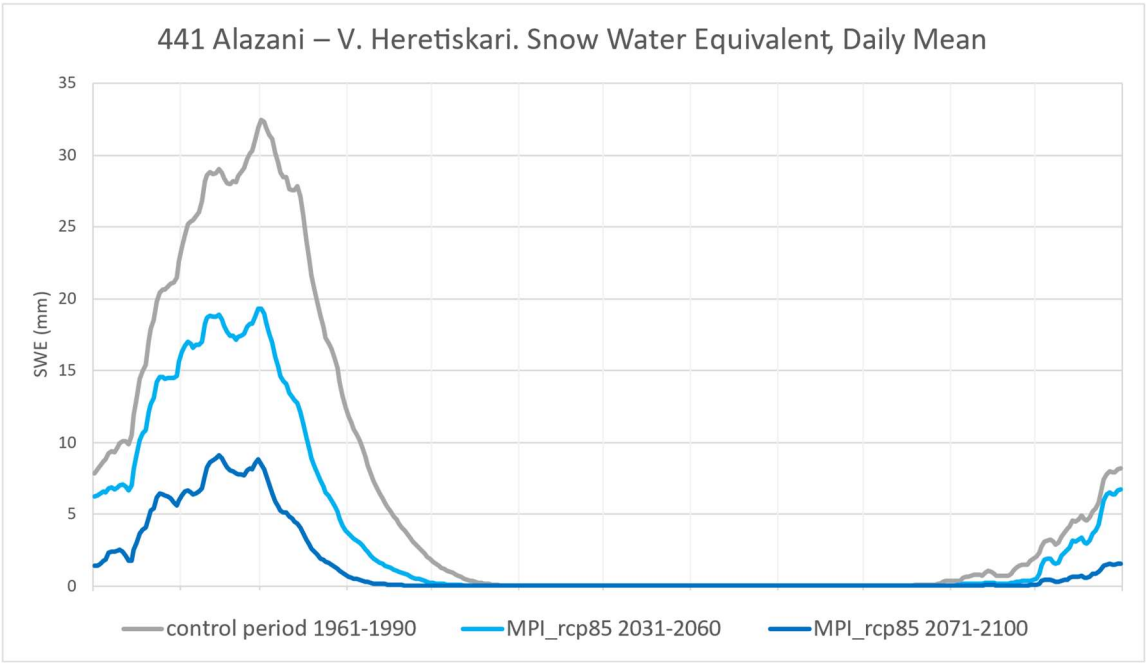

Figure A-161. Daily mean snow water equivalent in the control period, 1961-1990 (grey line), the near future, 2031-2060 (light blue line) and the end of the century, 2071-2100 (dark blue line), according to the climate projection MPI and the high emission scenario, for the station 441 Alazani – V. Heretiskari.

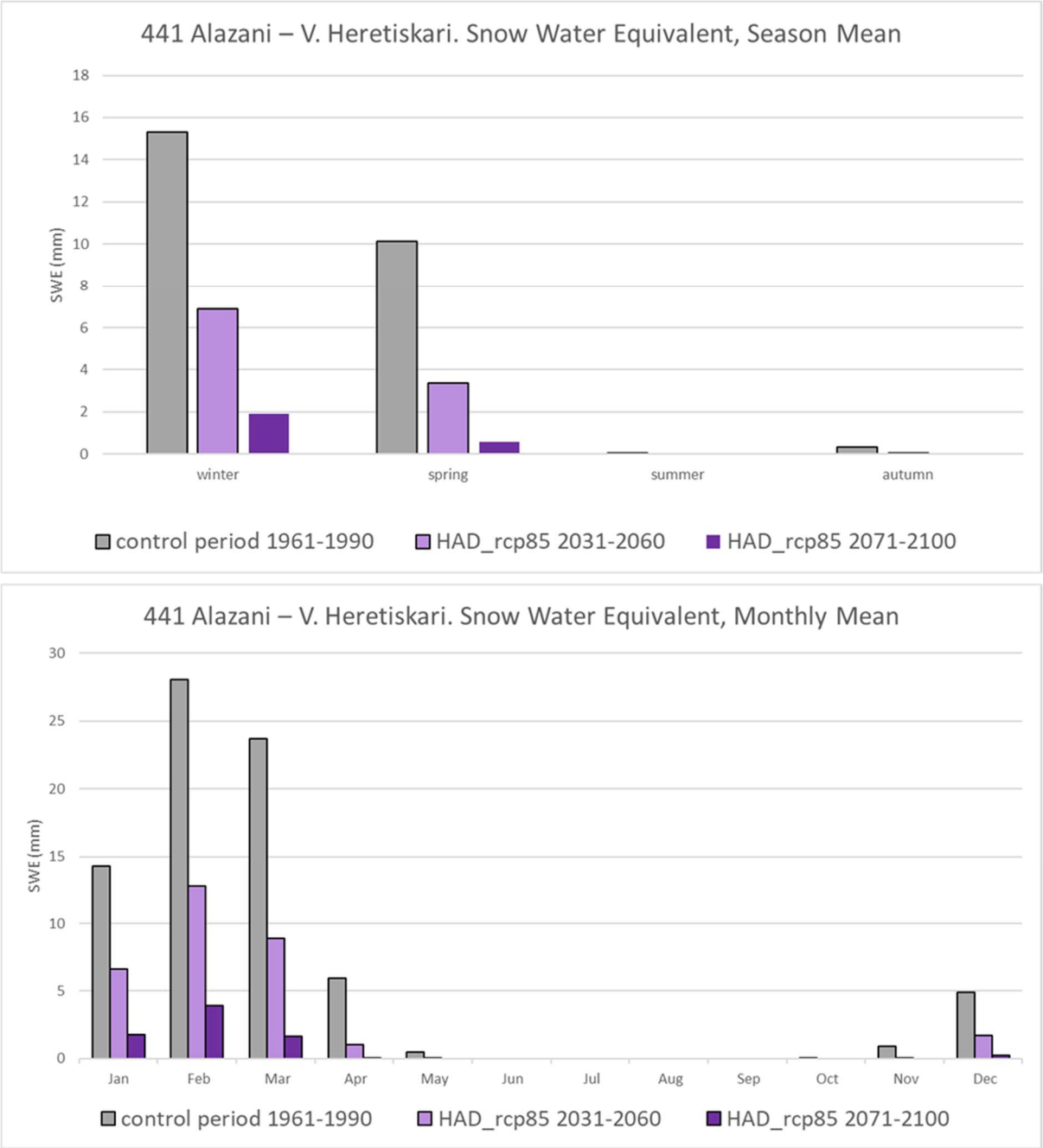

Figure A-162. Season mean (top) and monthly mean (bottom) snow water equivalent in the control period, 1961-1990 (grey bars), the near future, 2031-2060 (light purple bars) and the end of the century, 2071-2100 (dark purple bars), according to the climate projection HAD, for the station 441 Alazani – V. Heretiskari.

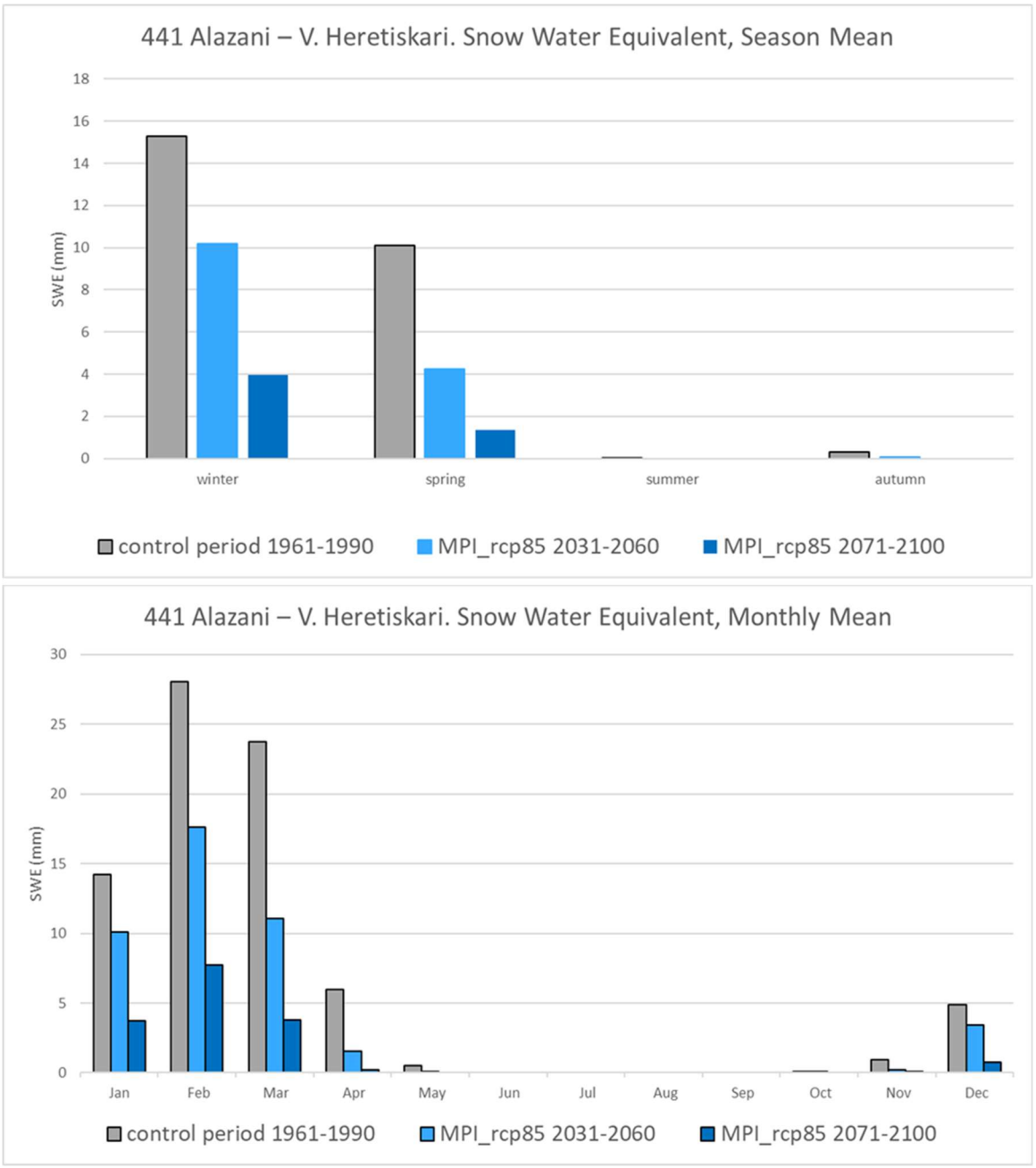

Figure A-163. Season mean (top) and monthly mean (bottom) snow water equivalent in the control period, 1961-1990 (grey bars), the near future, 2031-2060 (light blue bars) and the end of the century, 2071-2100 (dark blue bars), according to the climate projection MPI, for the station 441 Alazani – V. Heretiskari.

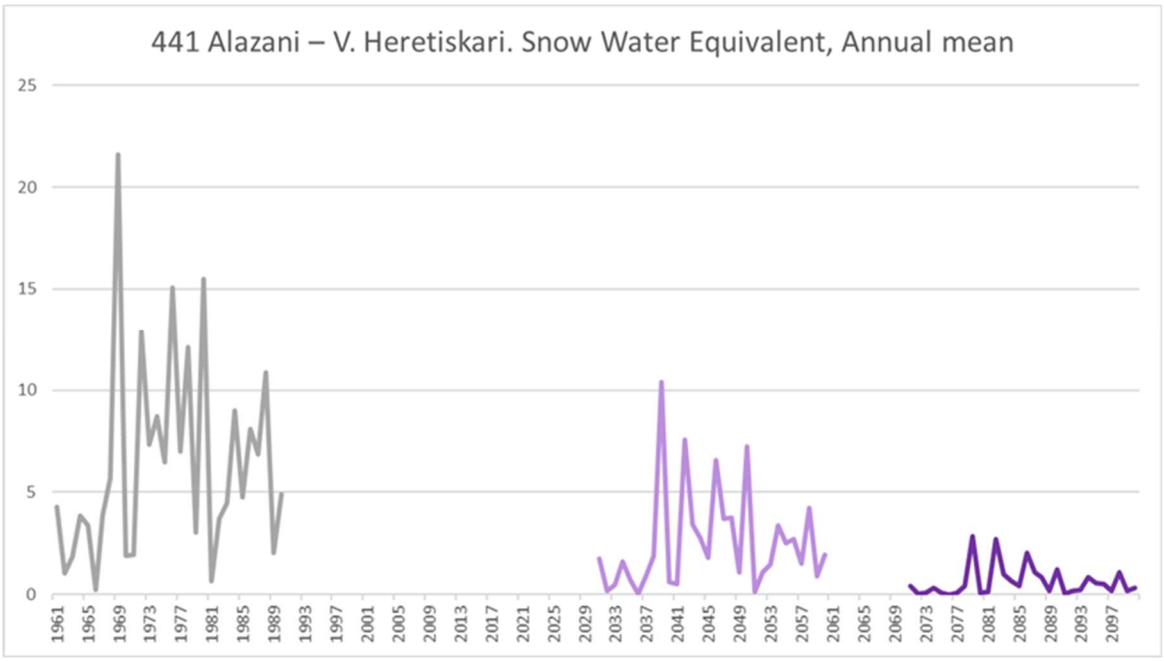

Figure A-164. Annual mean snow water equivalent in the control period, 1961-1990 (grey line), the near future, 2031-2060 (light purple line) and the end of the century, 2071-2100 (dark purple line), according to the climate projection HAD, for the station 441 Alazani – V. Heretiskari

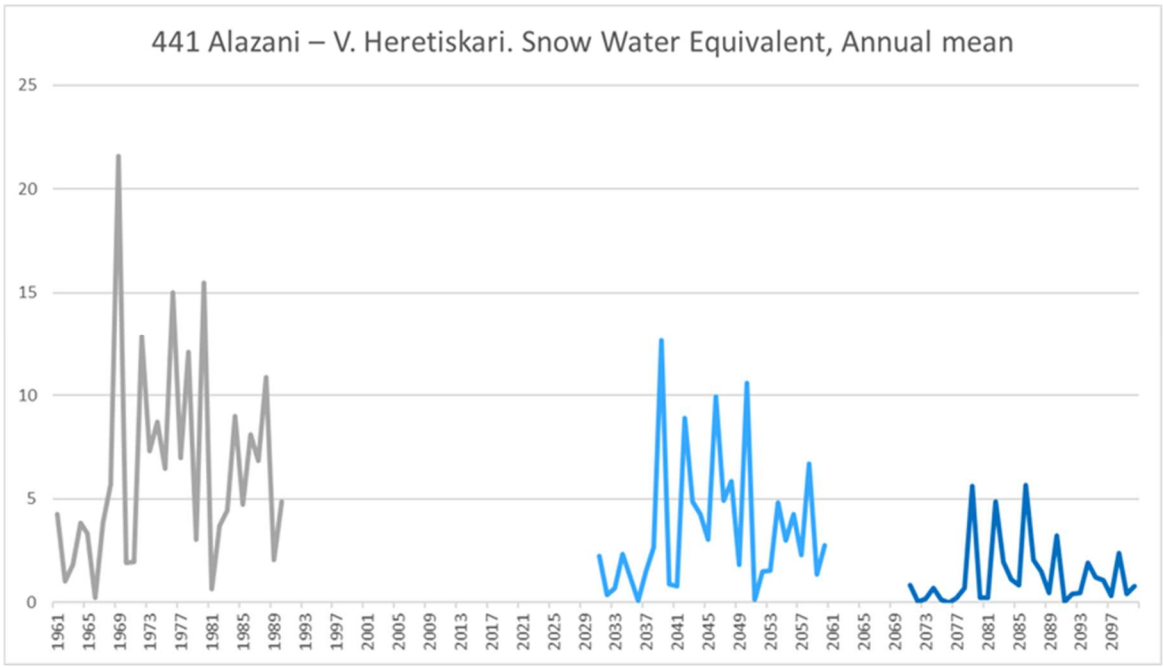

Figure A-165. Annual mean snow water equivalent in the control period, 1961-1990 (grey line), the near future, 2031-2060 (light blue line) the end of the century, 2071-2100 (dark blue line), according to the climate projection MPI, for the station 441 Alazani – V. Heretiskari

Water balance

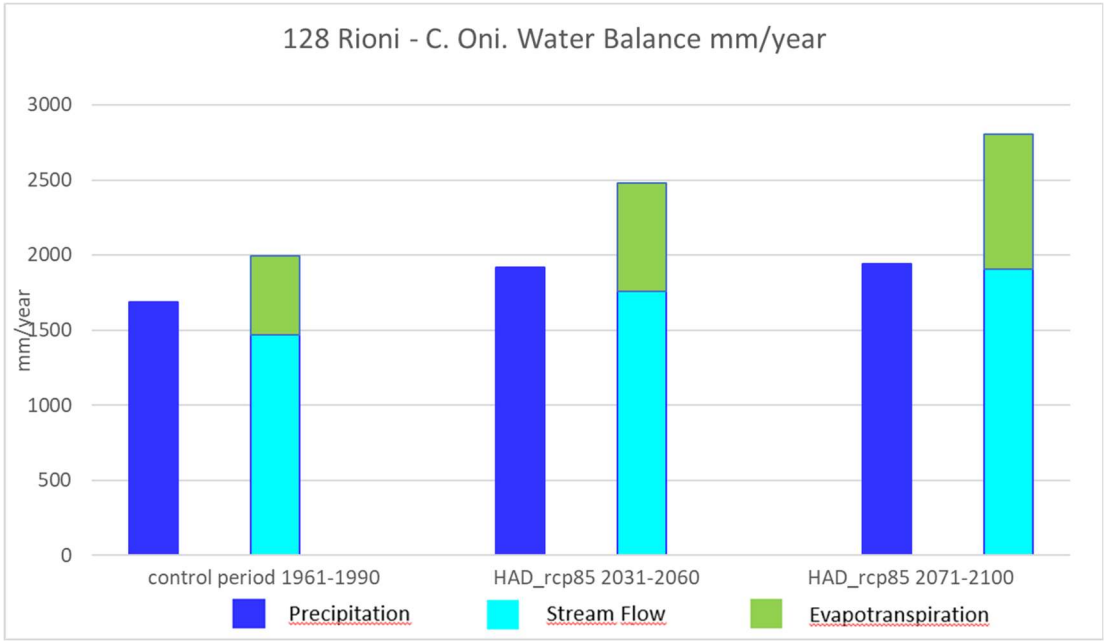

Figure A-166. Simulated water balance for basin upstream the station 128 Rioni - C. Oni, in the control period (to the left), the near future, 2031-2060 (in the middle) and the end of the century, 2071-2100 (to the right). Inflow to the basin is precipitation (blue bars) and outflow is evapotranspiration (green bars) and streamflow (turquoise bars). The projection HAD, and the high emission scenario is used.

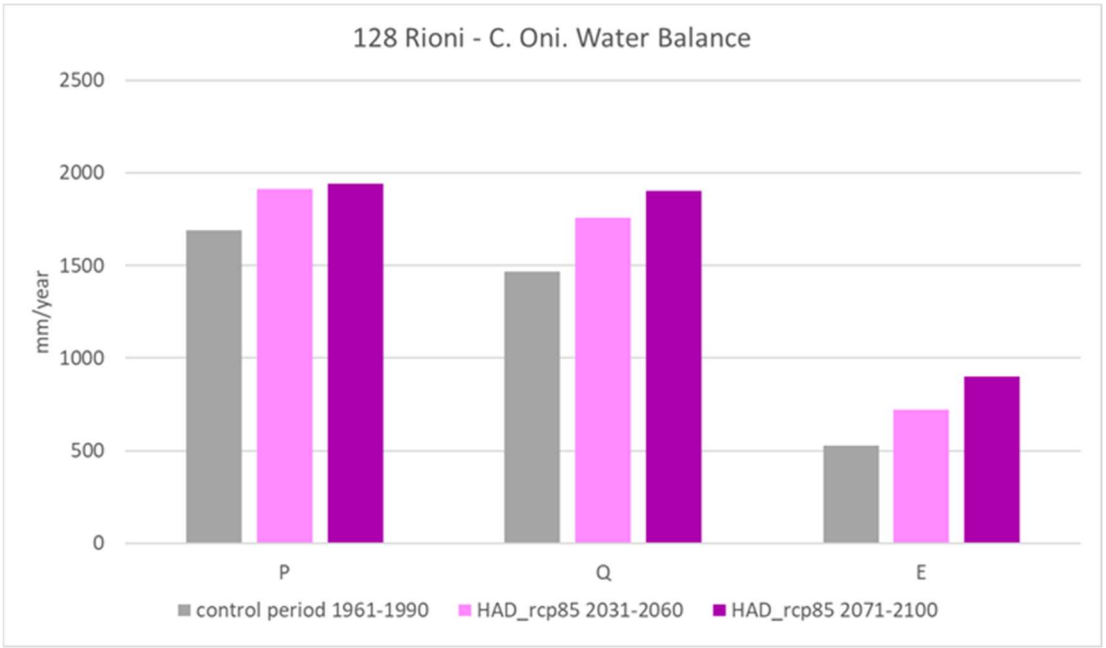

Figure A.167. Simulated water balance for basin upstream the station 128 Rioni - C. Oni, grouped according to the water balance element. The elements representing the control period are grey, those representing the near future, 2031-2060, are light purple, and those representing the end of the century, 2071 – 2100, are dark purple. The projection HAD, and the high emission scenario is used.

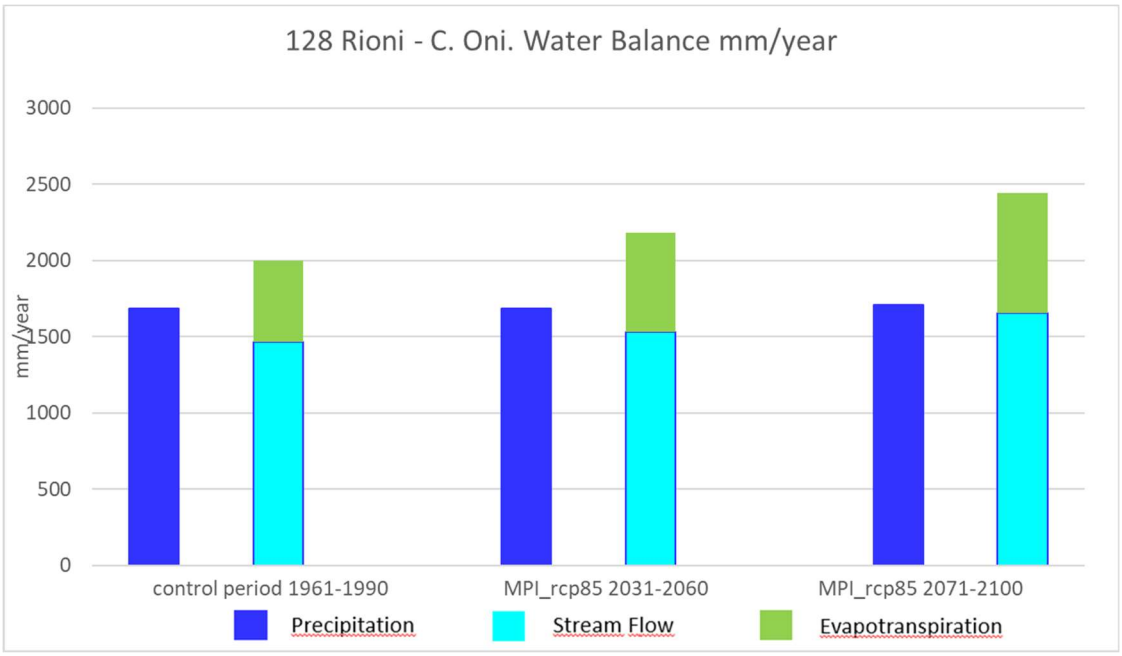

Figure A-168. Simulated water balance for basin upstream the station 128 Rioni - C. Oni, in the control period (to the left), the near future, 2031-2060 (in the middle) and the end of the century, 2071-2100 (to the right). Inflow to the basin is precipitation (blue bars) and outflow is evapotranspiration (green bars) and streamflow (turquoise bars). The projection MPI, and the high emission scenario is used.

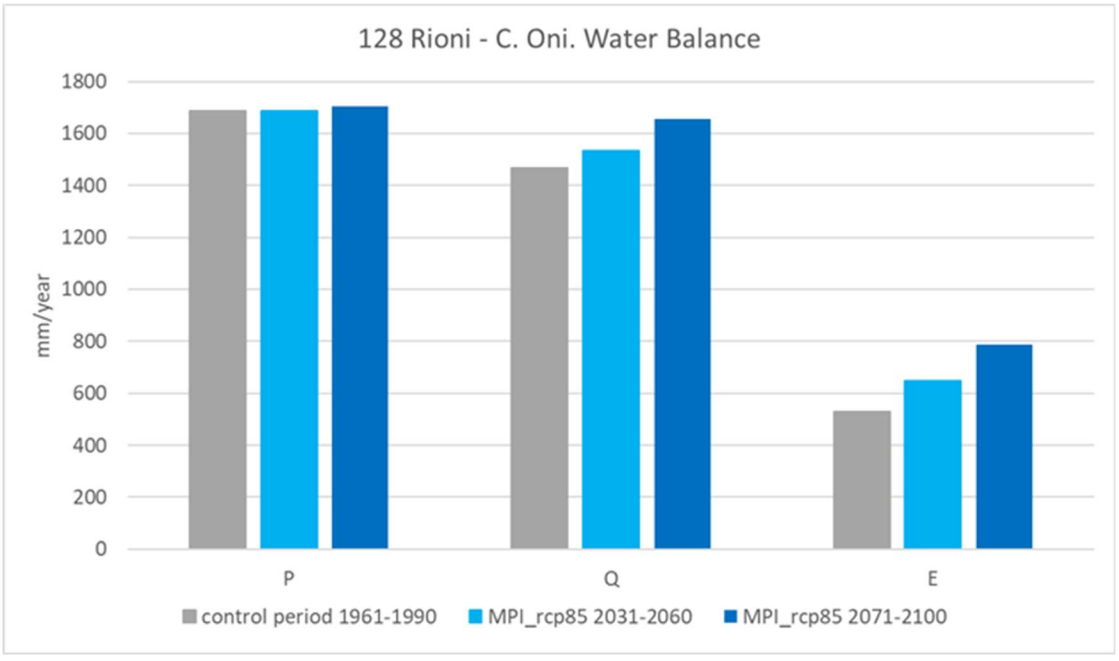

Figure A-169. Simulated water balance for basin upstream the station 128 Rioni - C. Oni, grouped according to the water balance element. The elements representing the control period are grey, those representing the near future, 2031-2060, are light blue, and those representing the end of the century are dark blue. The projection MPI, and the high emission scenario is used.

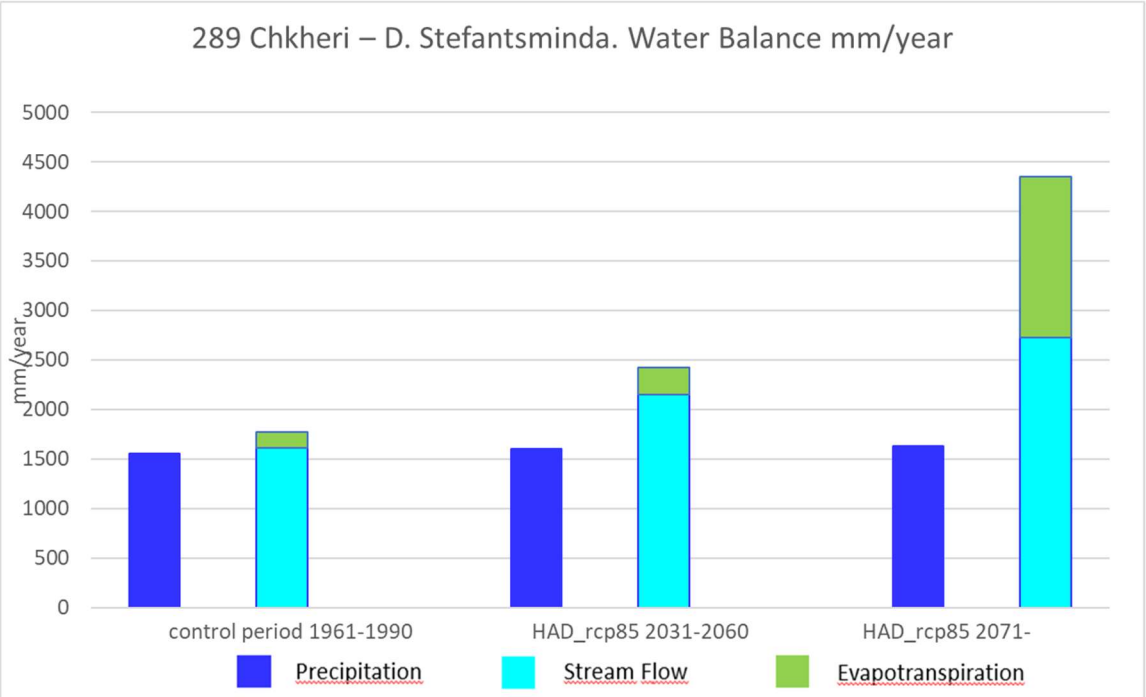

Figure A-170. Simulated water balance for basin upstream the station 289 Chkheri – D. Stefantsminda, in the control period (to the left), the near future, 2031-2060 (in the middle) and the end of the century, 2071-2100 (to the right). Inflow to the basin is precipitation (blue bars) and outflow is evapotranspiration (green bars) and streamflow (turquoise bars). The projection HAD, and the high emission scenario is used.

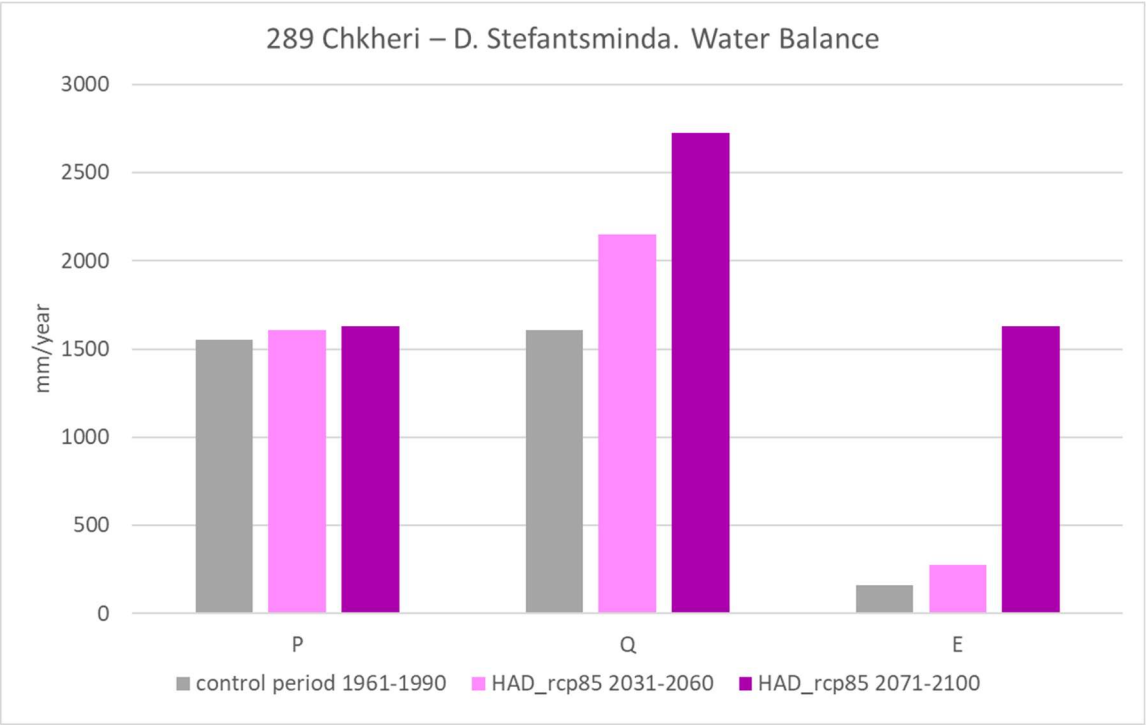

Figure A-171. Simulated water balance for basin upstream the station 289 Chkheri – D. Stefantsminda, grouped according to the water balance element. The elements representing the control period are grey, those representing the near future, 2031-2060, are light purple, and those representing the end of the century, 2071 – 2100, are dark purple. The projection HAD, and the high emission scenario is used.

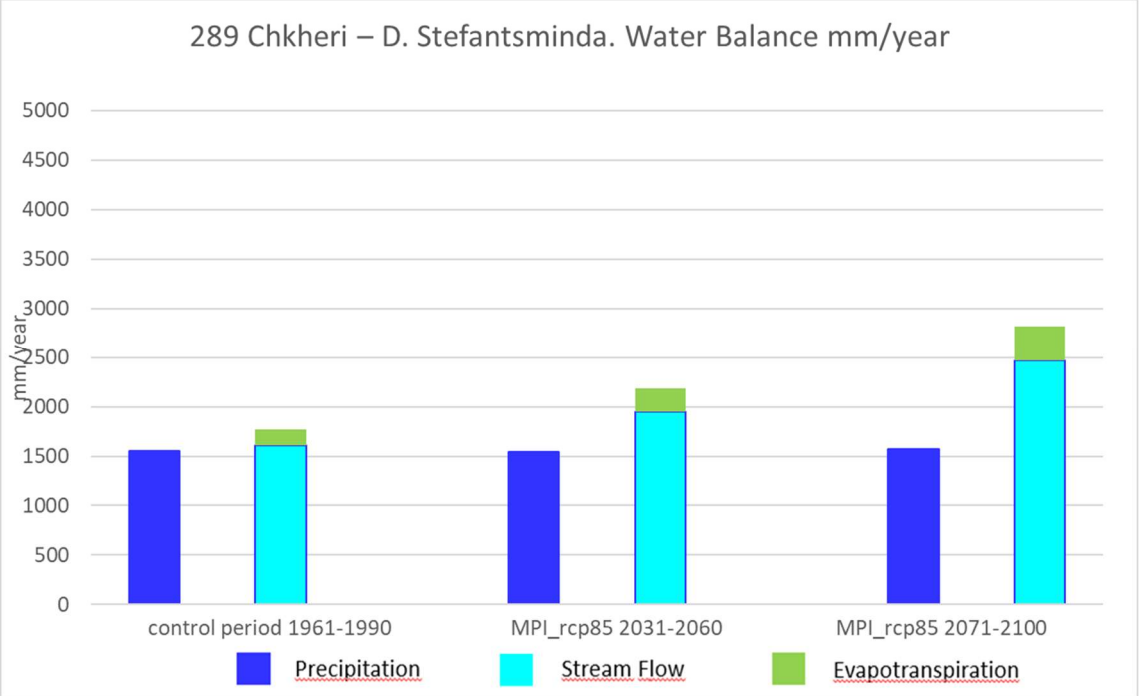

Figure A-172. Simulated water balance for basin upstream the station 289 Chkheri – D. Stefantsminda, in the control period (to the left), the near future, 2031-2060 (in the middle) and the end of the century, 2071-2100 (to the right). Inflow to the basin is precipitation (blue bars) and outflow is evapotranspiration (green bars) and streamflow (turquoise bars). The projection MPI, and the high emission scenario is used.

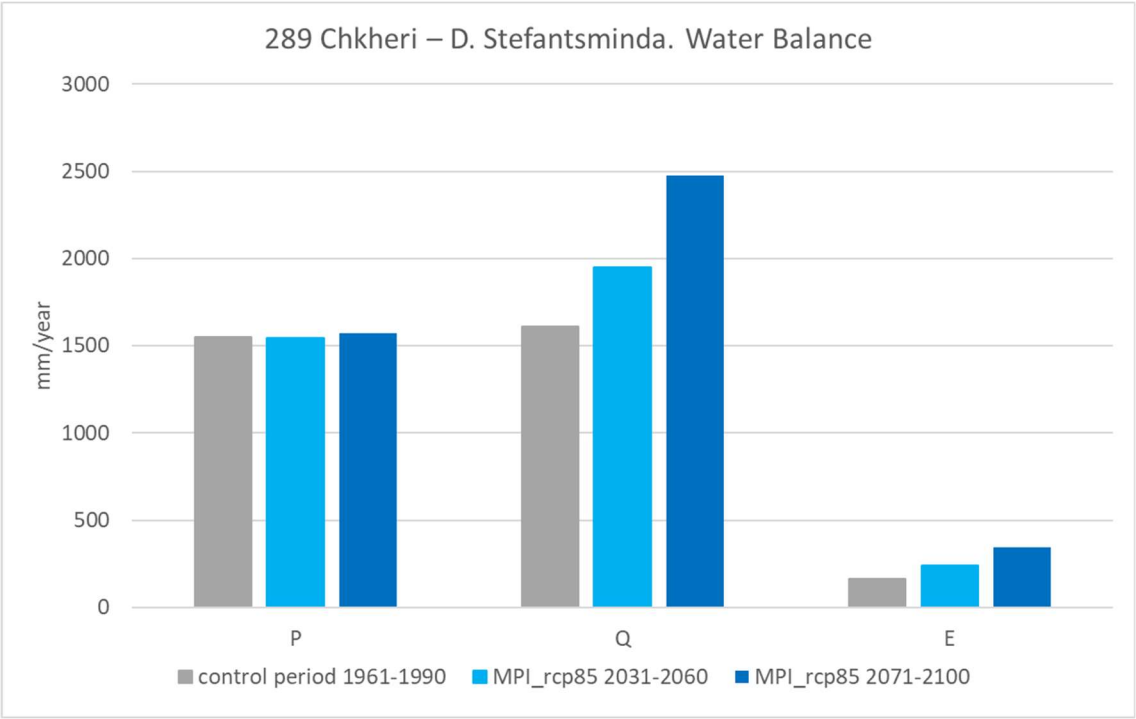

Figure A-173. Simulated water balance for basin upstream the station 289 Chkheri – D. Stefantsminda, grouped according to the water balance element. The elements representing the control period are grey, those representing the near future, 2031-2060, are light blue, and those representing the end of the century, 2071 – 2100, are dark blue. The projection MPI, and the high emission scenario is used.

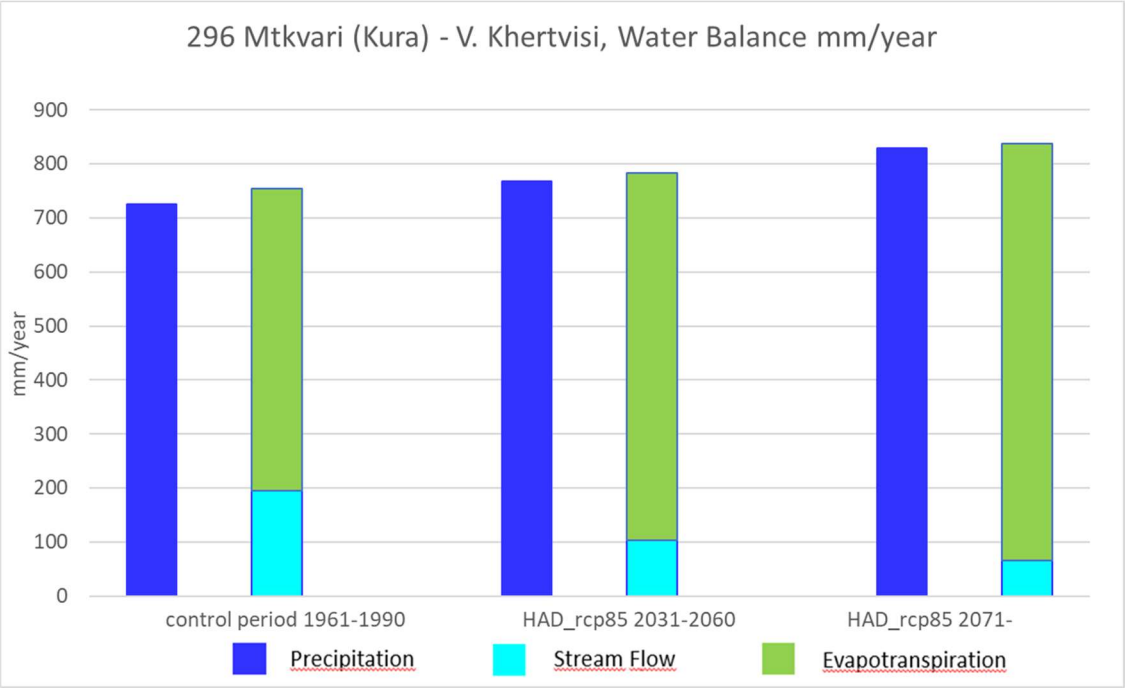

Figure A-174. Simulated water balance for basin upstream the station 296 Mtkvari (Kura) - V. Khertvisi, in the control period (to the left), the near future, 2031-2060 (in the middle) and the end of the century, 2071-2100 (to the right). Inflow to the basin is precipitation (blue bars) and outflow is evapotranspiration (green bars) and streamflow (turquoise bars). The projection HAD, and the high emission scenario is used.

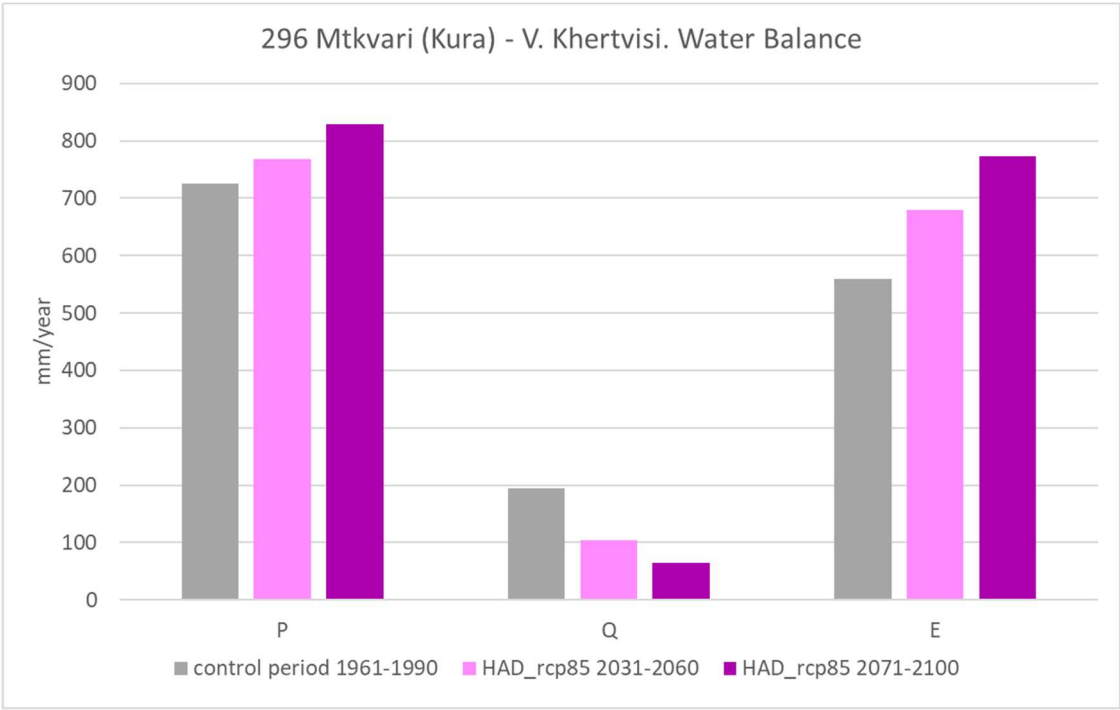

Figure A-175. Simulated water balance for basin upstream the station 296 Mtkvari (Kura) - V. Khertvisi, grouped according to the water balance element. The elements representing the control period are grey, those representing the near future, 2031-2060, are light purple, and those representing the end of the century, 2071 – 2100, are dark purple. The projection HAD, and the high emission scenario is used.

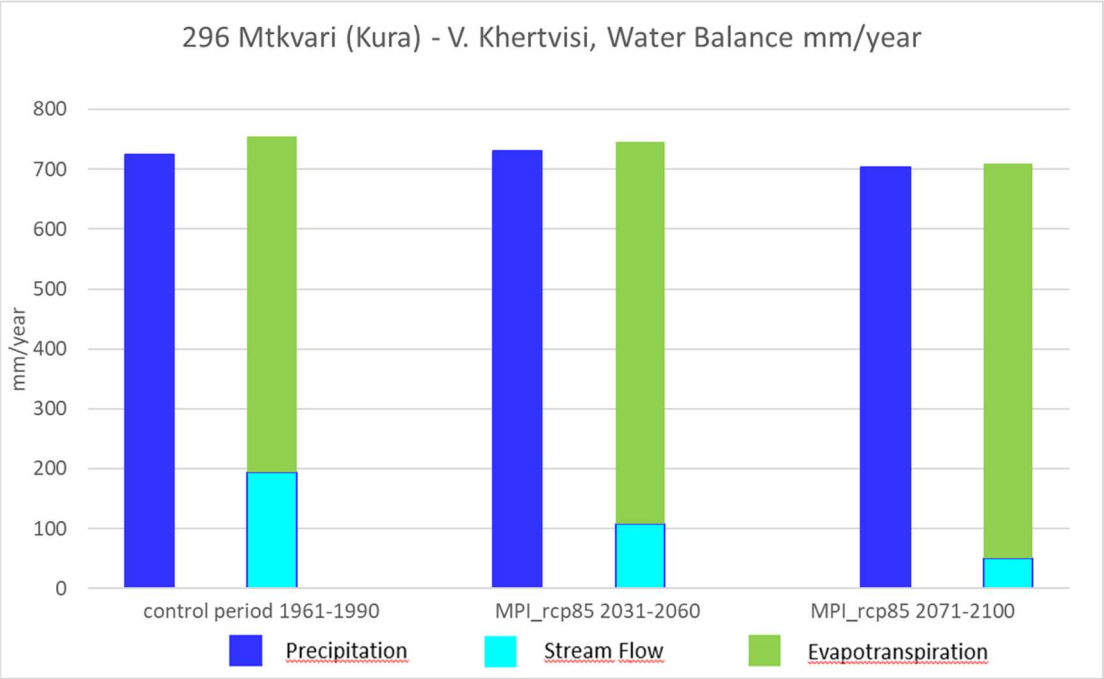

Figure A-176 . Simulated water balance for basin upstream the station 296 Mtkvari (Kura) - V. Khertvisi, in the control period (to the left), the near future, 2031-2060 (in the middle) and the end of the century, 2071-2100 (to the right). Inflow to the basin is precipitation (blue bars) and outflow is evapotranspiration (green bars) and streamflow (turquoise bars). The projection MPI, and the high emission scenario is used.

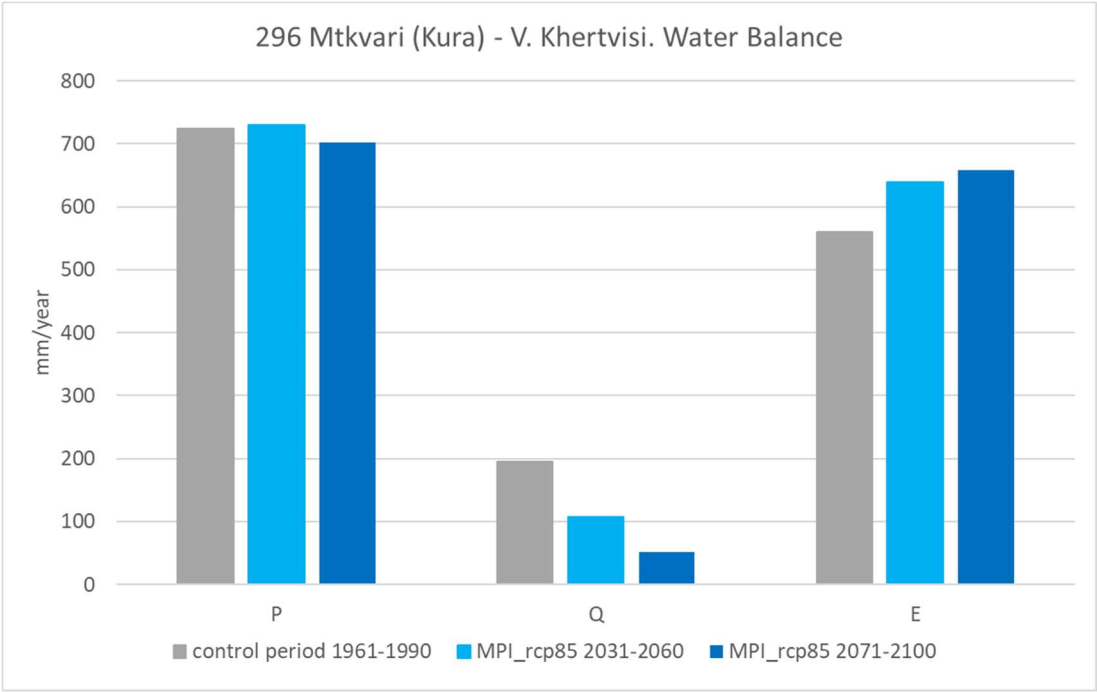

Figure A-177. Simulated water balance for basin upstream the station 296 Mtkvari (Kura) - V. Khertvisi, grouped according to the water balance element. The elements representing the control period are grey, those representing the near future, 2031-2060, are light blue, and those representing the end of the century, 2071 – 2100, are dark blue. The projection MPI, and the high emission scenario is used.

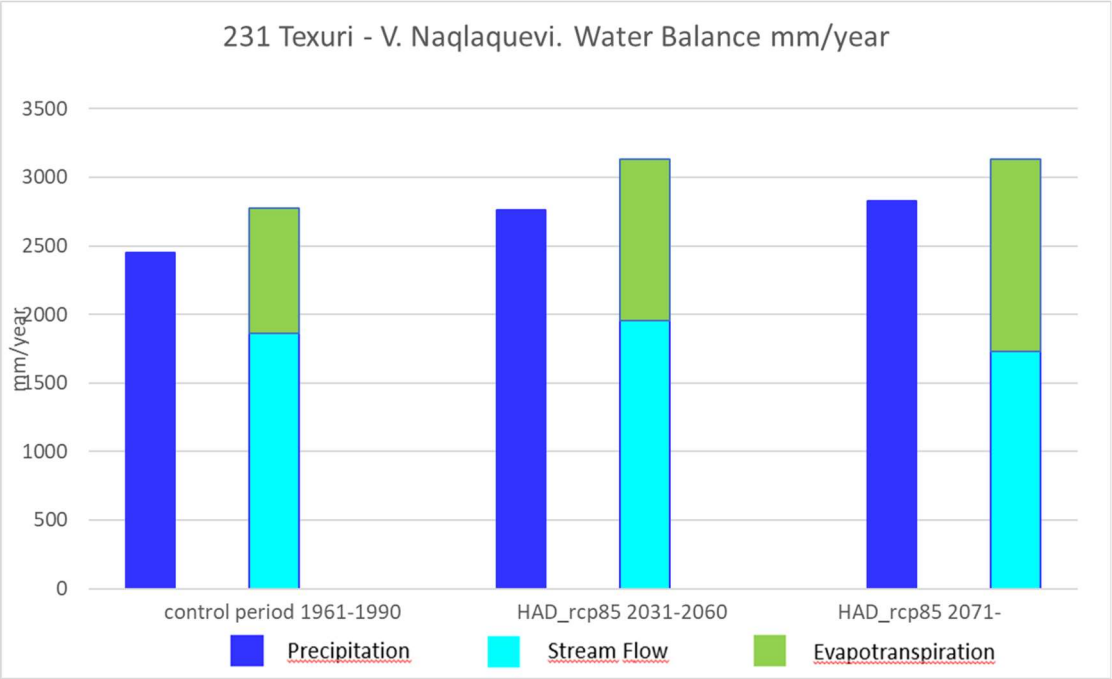

Figure A-178. Simulated water balance for basin upstream the station 231 Texuri - V. Naqlaquevi, in the control period (to the left), the near future, 2031-2060 (in the middle) and the end of the century, 2071-2100 (to the right). Inflow to the basin is precipitation (blue bars) and outflow is evapotranspiration (green bars) and streamflow (turquoise bars). The projection HAD, and the high emission scenario is used.

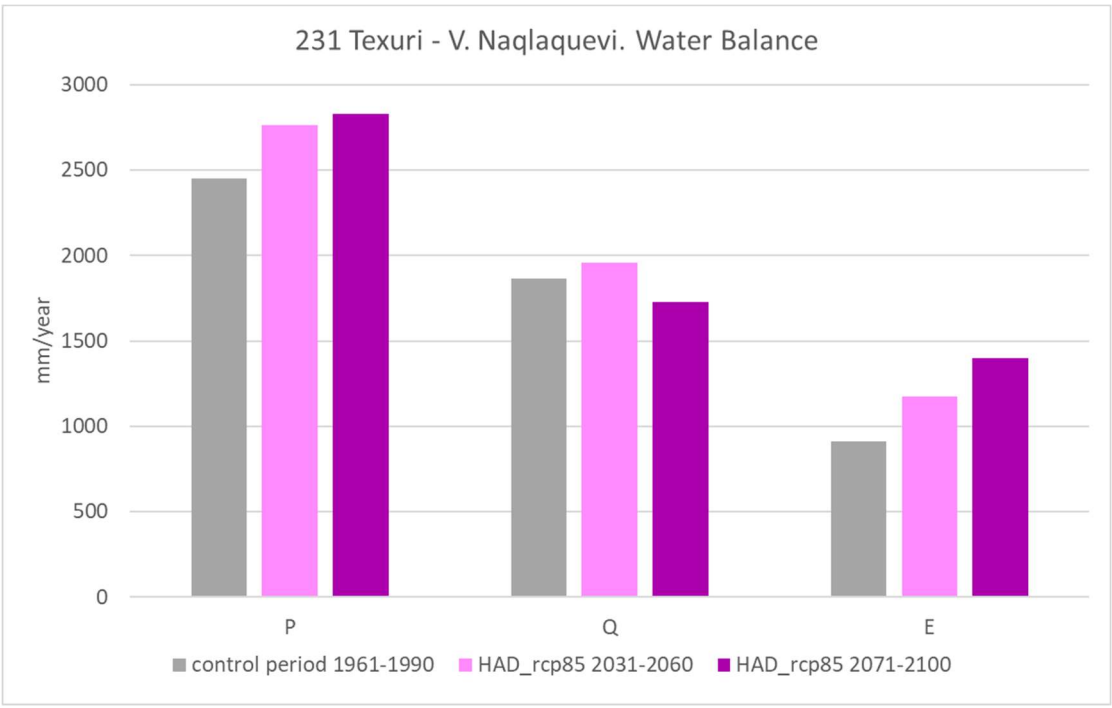

Figure A-179. Simulated water balance for basin upstream the station 231 Texuri - V. Naqlaquevi, grouped according to the water balance element. The elements representing the control period are grey, those representing the near future, 2031-2060, are light purple, and those representing the end of the century, 2071 – 2100, are dark purple. The projection HAD, and the high emission scenario is used.

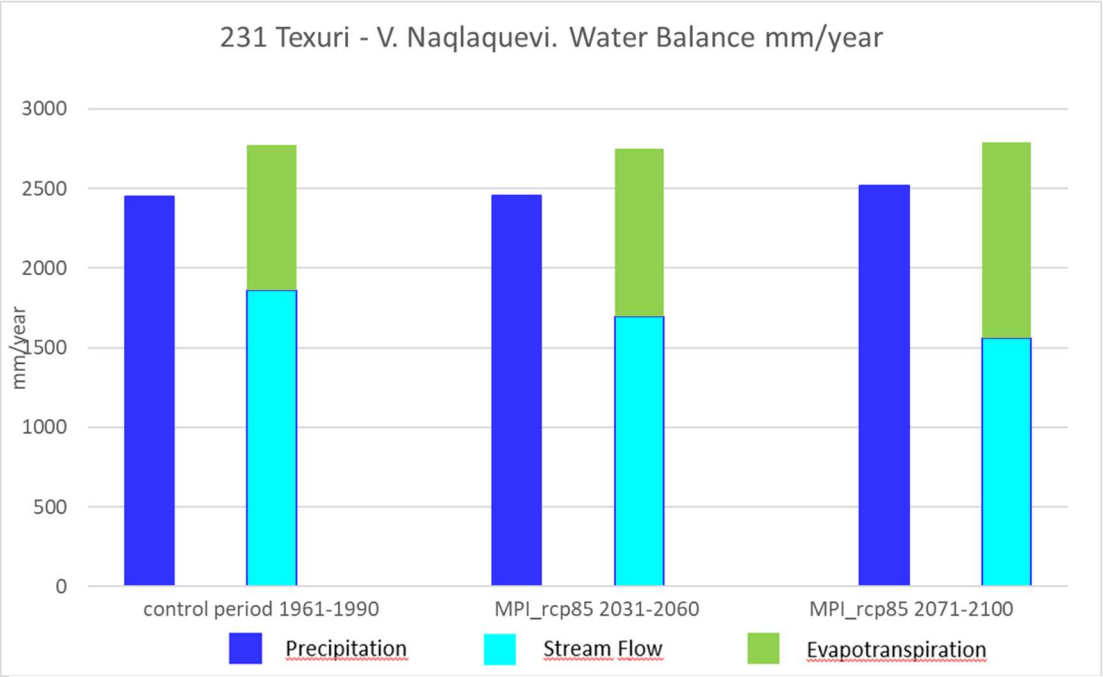

Figure A-180. Simulated water balance for basin upstream the station 231 Texuri - V. Naqlaquevi, in the control period (to the left), the near future, 2031-2060 (in the middle) and the end of the century, 2071-2100 (to the right). Inflow to the basin is precipitation (blue bars) and outflow is evapotranspiration (green bars) and streamflow (turquoise bars). The projection MPI, and the high emission scenario is used.

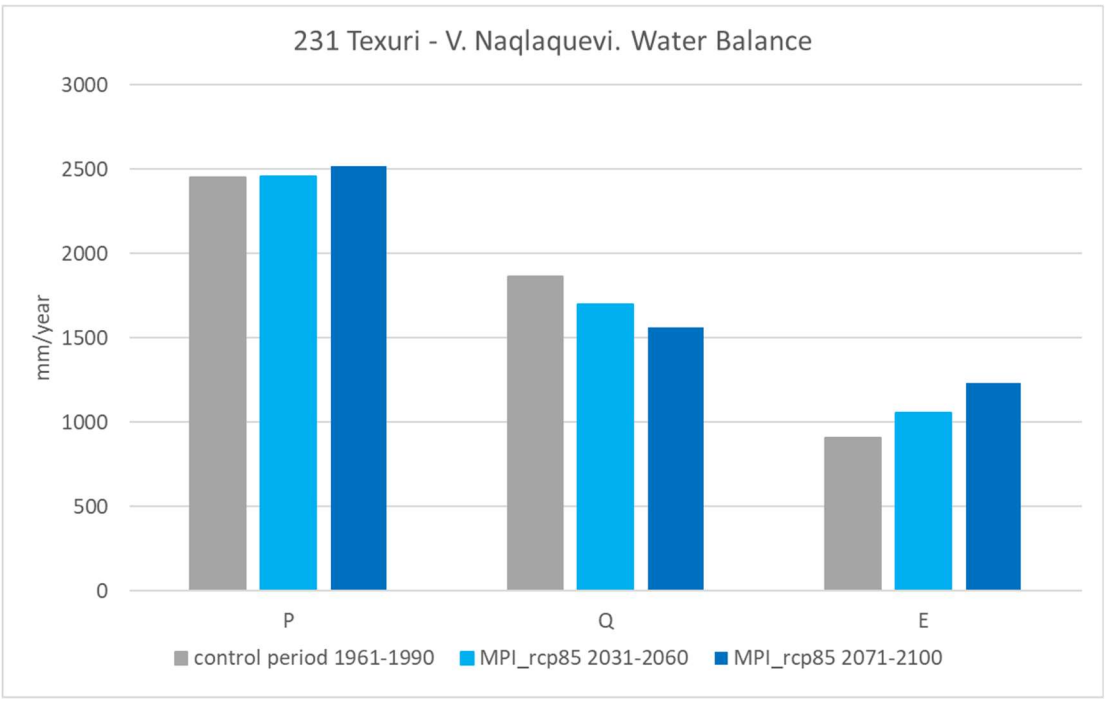

Figure A-181. Simulated water balance for basin upstream the station 231 Texuri - V. Naqlaquevi, grouped according to the water balance element. The elements representing the control period are grey, those representing the near future, 2031-2060, are light blue, and those representing the end of the century, 2071 – 2100, are dark blue. The projection MPI, and the high emission scenario is used.

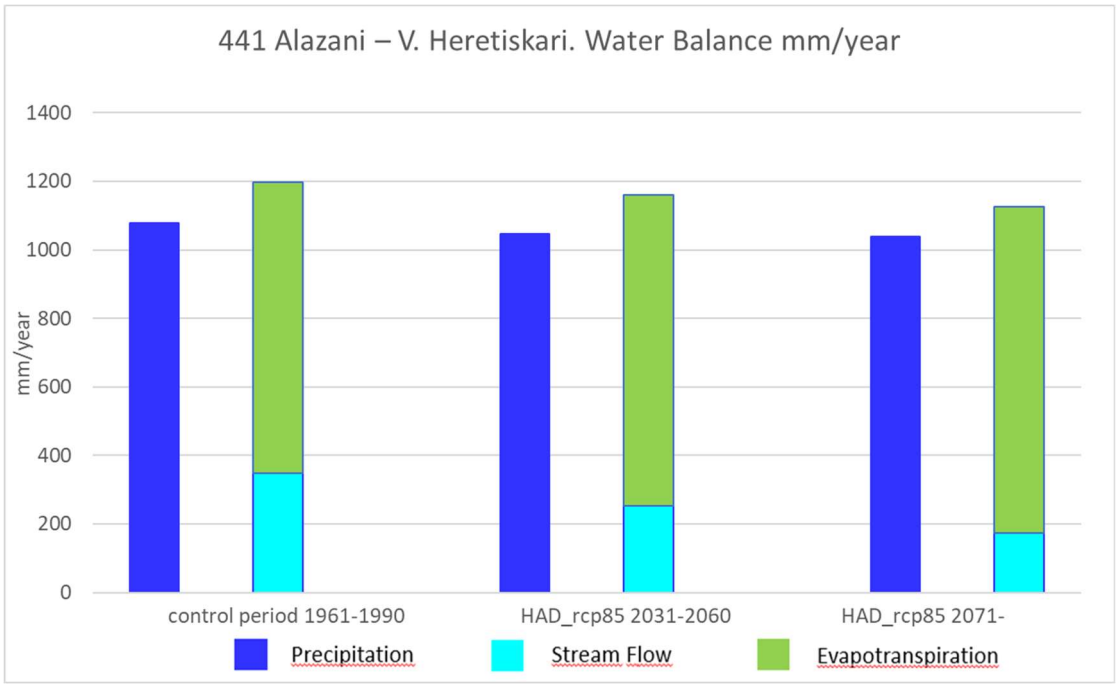

Figure A.182. Simulated water balance for basin upstream the station 441 Alazani – V. Heretiskari, in the control period (to the left), the near future, 2031-2060 (in the middle) and the end of the century, 2071-2100 (to the right). Inflow to the basin is precipitation (blue bars) and outflow is evapotranspiration (green bars) and streamflow (turquoise bars). The projection HAD, and the high emission scenario is used.

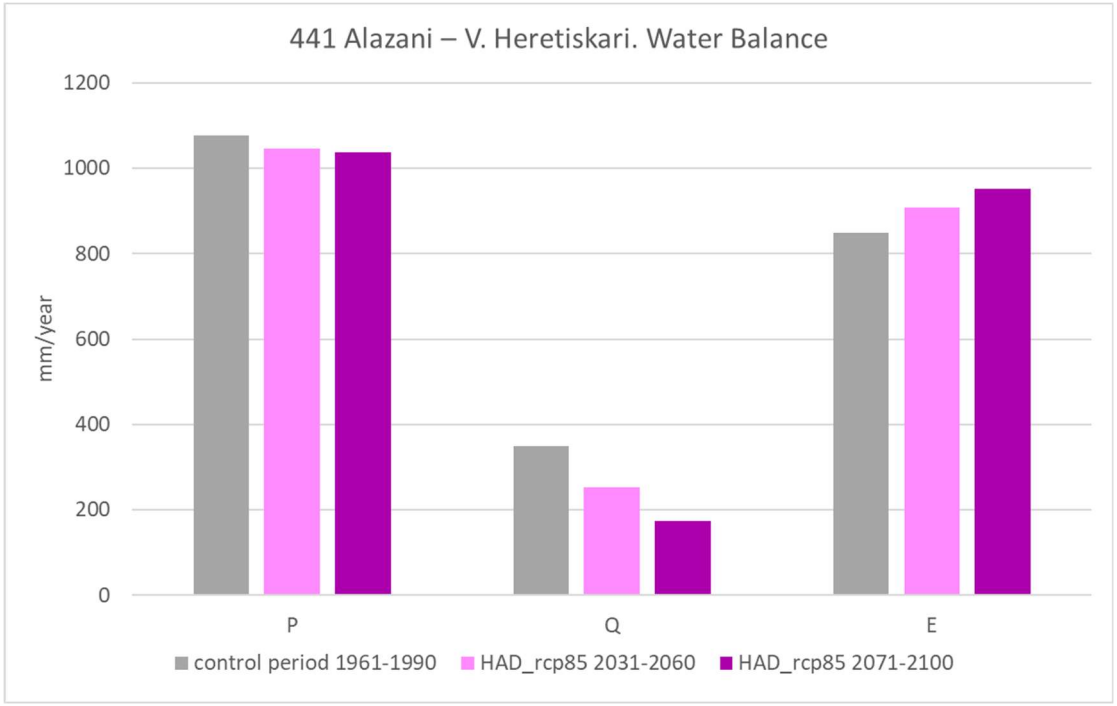

Figure A-183. Simulated water balance for basin upstream the station 441 Alazani – V. Heretiskari, grouped according to the water balance element. The elements representing the control period are grey, those representing the near future, 2031-2060, are light purple, and those representing the end of the century, 2071 – 2100, are dark purple. The projection HAD, and the high emission scenario is used.

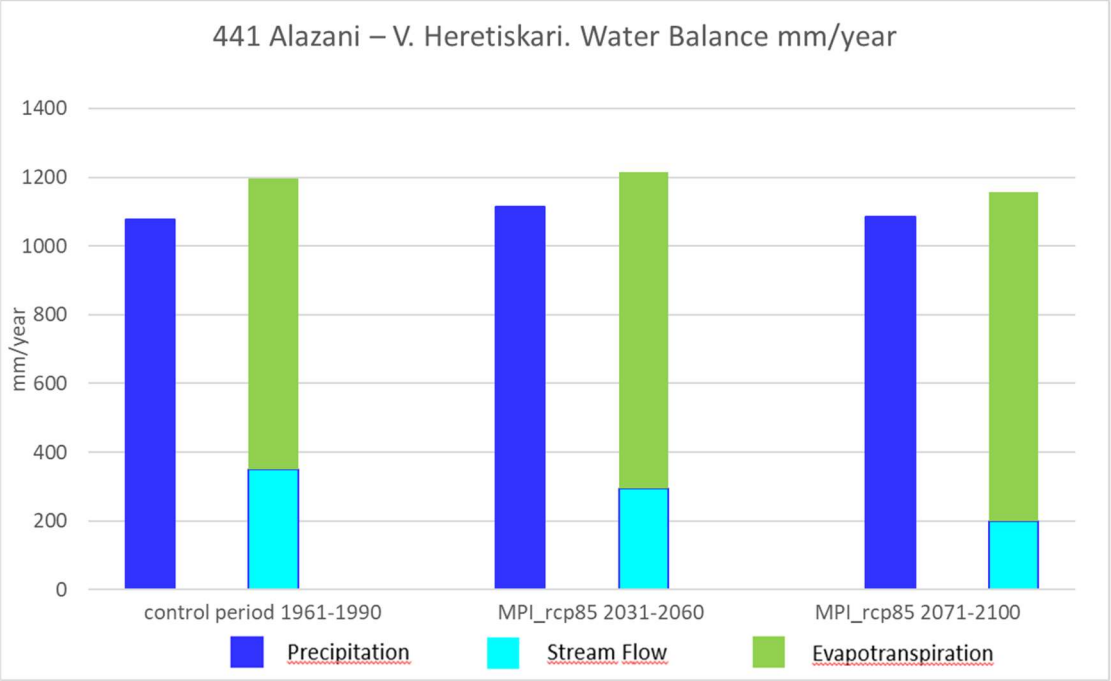

Figure A-184. Simulated water balance for basin upstream the station 441 Alazani – V. Heretiskari, in the control period (to the left), the near future, 2031-2060 (in the middle) and the end of the century, 2071-2100 (to the right). Inflow to the basin is precipitation (blue bars) and outflow is evapotranspiration (green bars) and streamflow (turquoise bars). The projection MPI, and the high emission scenario is used.

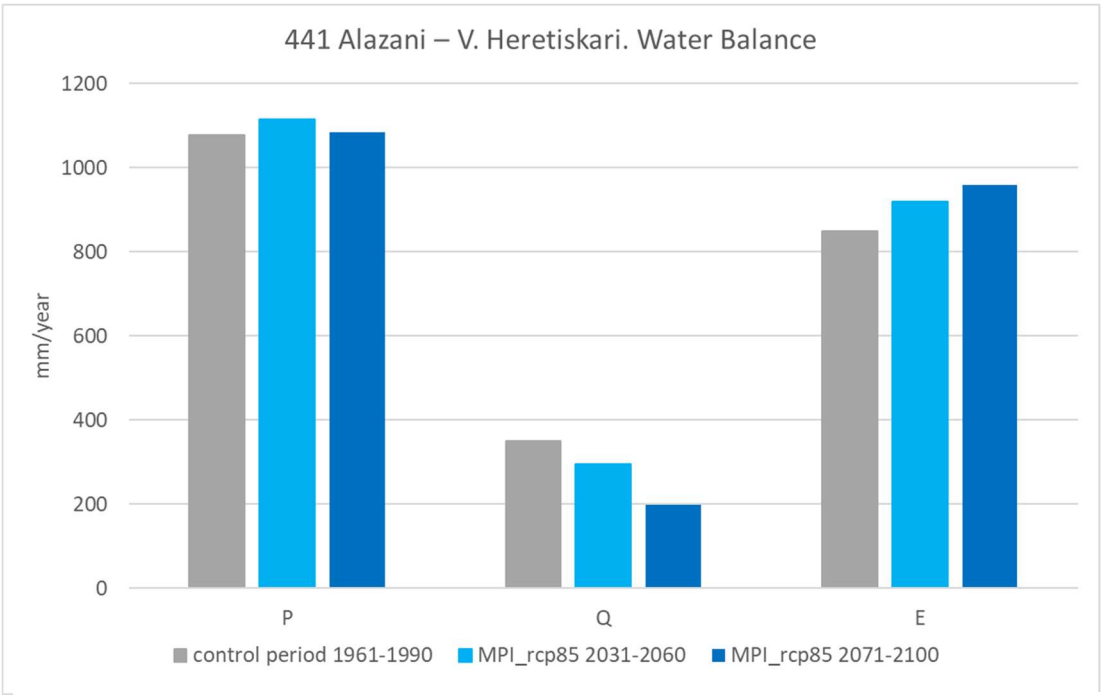

Figure A-185. Simulated water balance for basin upstream the station 441 Alazani – V. Heretiskari, grouped according to the water balance element. The elements representing the control period are grey, those representing the near future, 2031-2060, are light blue, and those representing the end of the century, 2071 – 2100, are dark blue. The projection MPI, and the high emission scenario is used.

Appendix B. Effects of climate change on the flood frequency curve for stream flow for selected climate projections, climate gas emission scenarios and stations.

Stations:

- 128 Rioni - C. Oni, zone 2, representing the Greater Caucasus region
- 289 Chkheri - D. Stefantsminda, zone 10, representing the Greater Caucasus region
- 296 Mtkvari (Kura) – V. Khertvisi, zone 9, representing the Lesser Caucasus region
- 231 Texuri - V. Naqlaquevi, zone 4, representing the Black Sea region
- 441 Alazani – V. Heretiskari, zone 14, representing the plains of eastern Georgia

The figures show the flow duration curve(black), sum lower (red) and the diversion capacity curve (green) for the selected catchments, based on hydrological model results for stream flow with precipitation and temperature input and time periods as indicated in the title. The annual discharge volumes that goes to flood loss, hydropower production potential, minimum water flow and low flow loss are indicated as areal fractions below the flow duration curve.

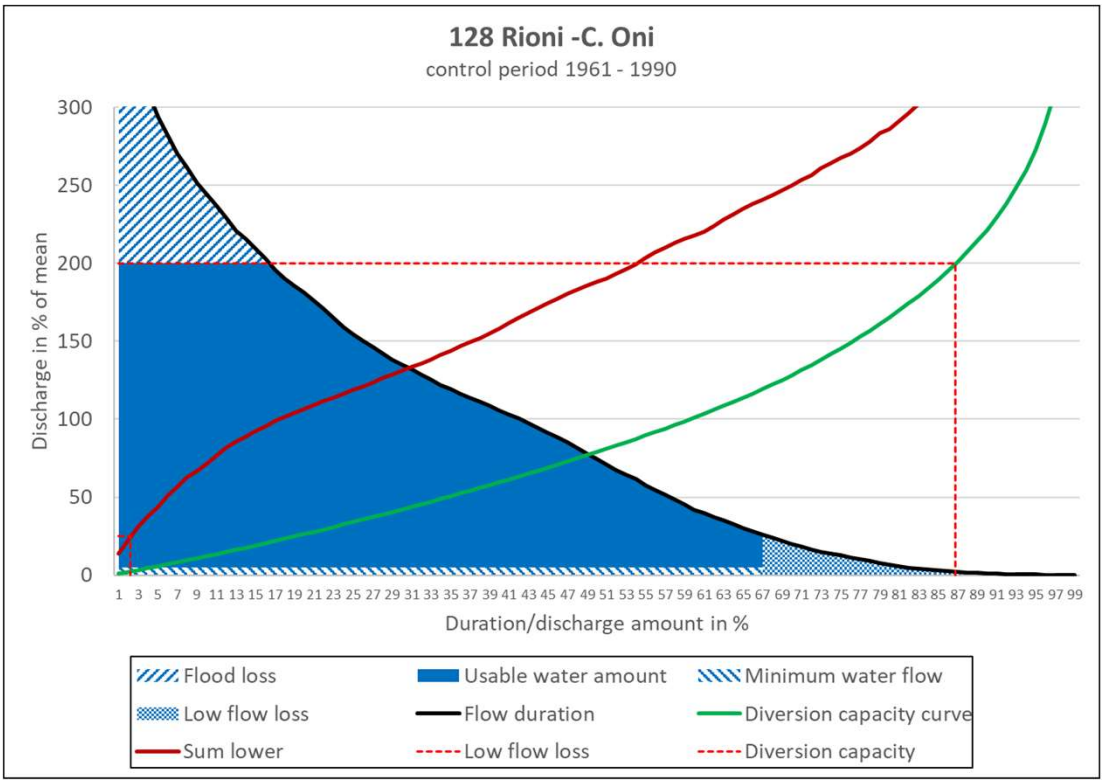
128 Rioni -C. Oni
control period 1961 - 1990
Discharge in % of mean
300
250
200
150
100
50
0
1 3 5 7 9 11 13 15 17 19 21 23 25 27 29 31 33 35 37 39 41 43 45 47 49 51 53 55 57 59 61 63 65 67 69 71 73 75 77 79 81 83 85 87 89 91 93 95 97 99
Duration/discharge amount in %
Flood loss
Usable water amount
Minimum water flow
Low flow loss
Flow duration
Diversion capacity curve
Sum lower
Low flow loss
Diversion capacity

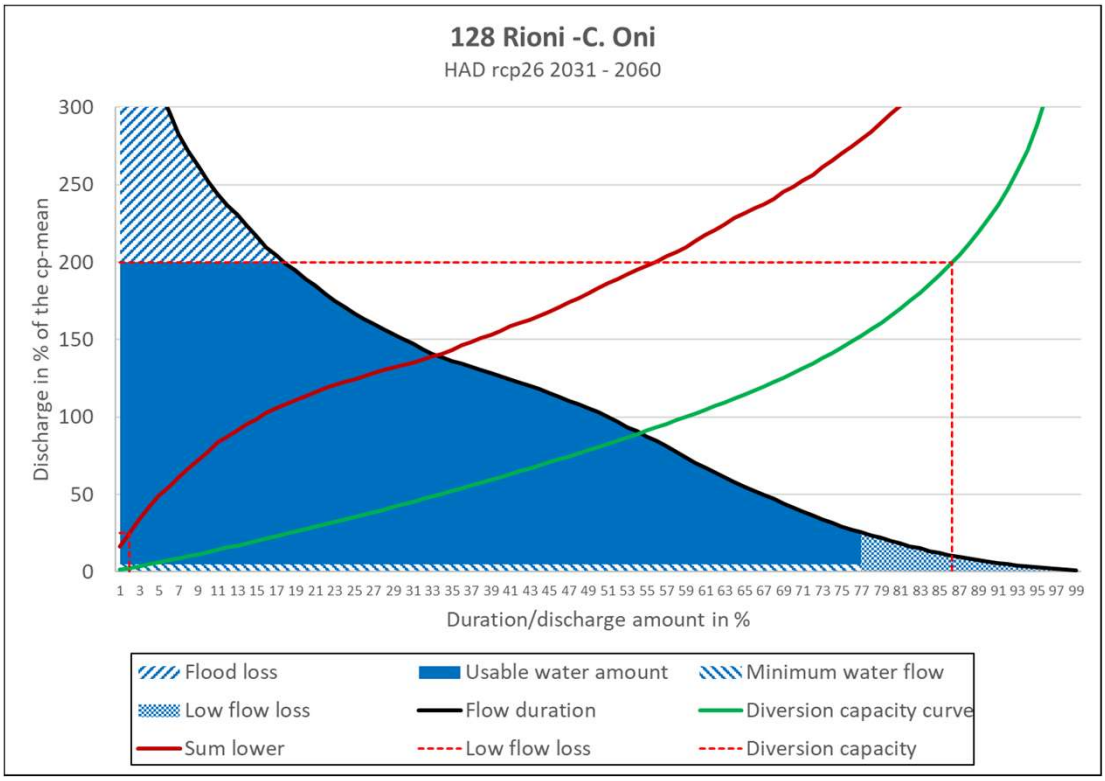
128 Rioni -C. Oni
HAD rcp26 2031 - 2060
Discharge in % of the cp-mean
300
250
200
150
100
50
0
1 3 5 7 9 11 13 15 17 19 21 23 25 27 29 31 33 35 37 39 41 43 45 47 49 51 53 55 57 59 61 63 65 67 69 71 73 75 77 79 81 83 85 87 89 91 93 95 97 99
Duration/discharge amount in %
Flood loss
Usable water amount
Minimum water flow
Low flow loss
Flow duration
Diversion capacity curve
Sum lower
Low flow loss
Diversion capacity

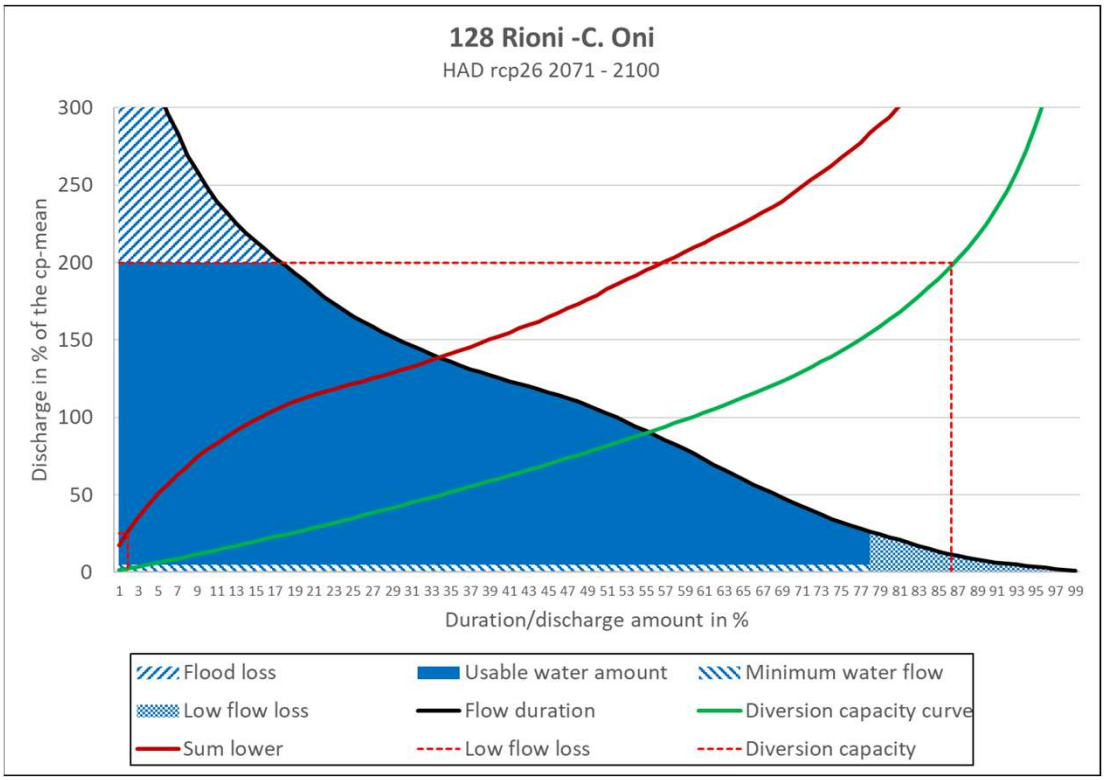
128 Rioni -C. Oni
HAD rcp26 2071 - 2100
Discharge in % of the cp-mean
300
250
200
150
100
50
0
1 3 5 7 9 11 13 15 17 19 21 23 25 27 29 31 33 35 37 39 41 43 45 47 49 51 53 55 57 59 61 63 65 67 69 71 73 75 77 79 81 83 85 87 89 91 93 95 97 99
Duration/discharge amount in %
Flood loss
Usable water amount
Minimum water flow
Low flow loss
Flow duration
Diversion capacity curve
Sum lower
Low flow loss
Diversion capacity

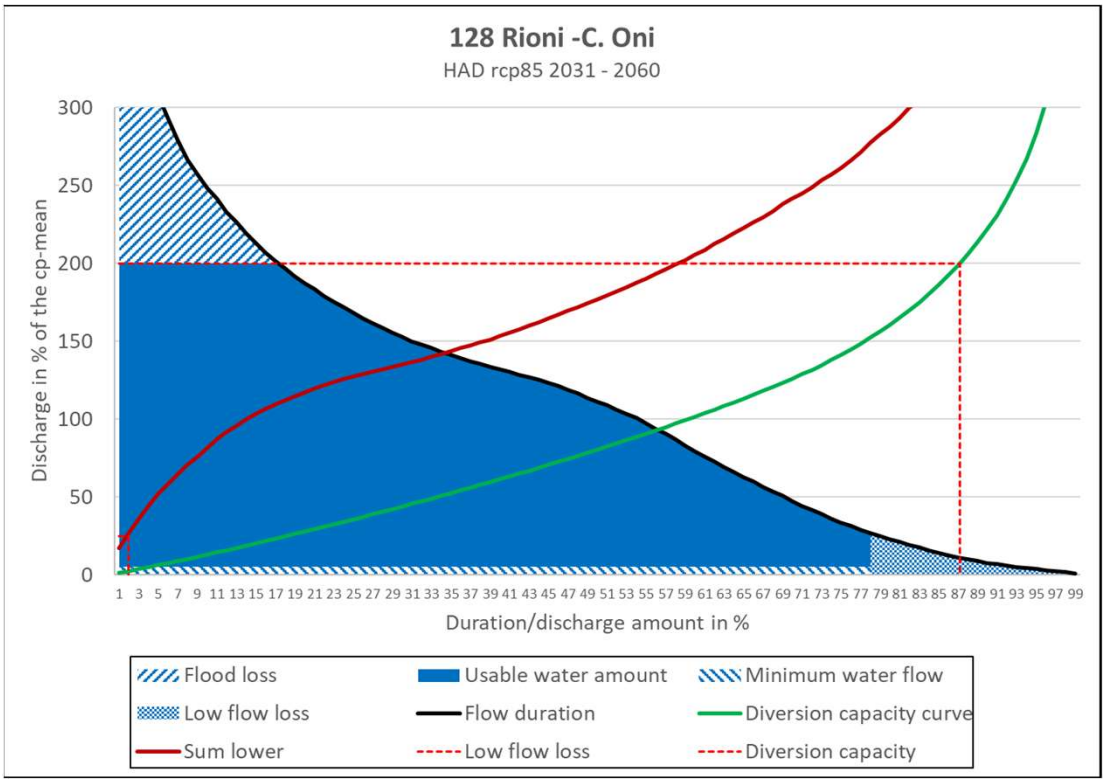
128 Rioni -C. Oni
HAD rcp85 2031 - 2060
Discharge in % of the cp-mean
300
250
200
150
100
50
0
1 3 5 7 9 11 13 15 17 19 21 23 25 27 29 31 33 35 37 39 41 43 45 47 49 51 53 55 57 59 61 63 65 67 69 71 73 75 77 79 81 83 85 87 89 91 93 95 97 99
Duration/discharge amount in %
Flood loss
Usable water amount
Minimum water flow
Low flow loss
Flow duration
Diversion capacity curve
Sum lower
Low flow loss
Diversion capacity

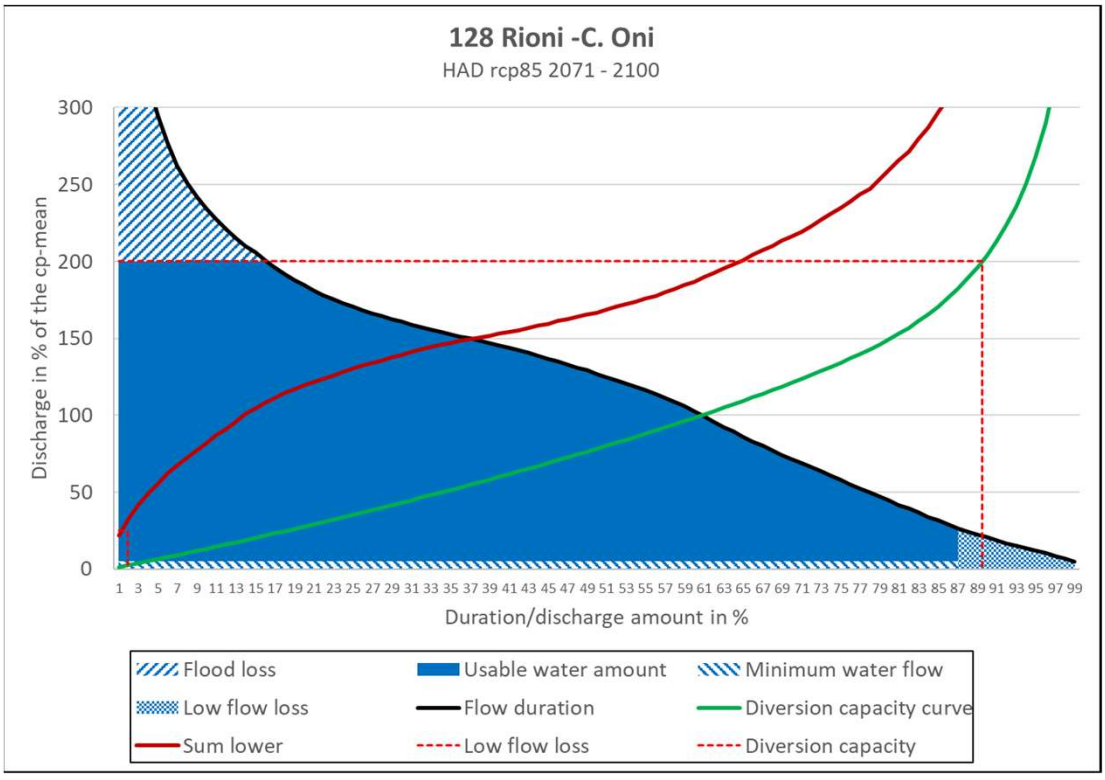
128 Rioni -C. Oni
HAD rcp85 2071 - 2100
Discharge in % of the cp-mean
300
250
200
150
100
50
0
1 3 5 7 9 11 13 15 17 19 21 23 25 27 29 31 33 35 37 39 41 43 45 47 49 51 53 55 57 59 61 63 65 67 69 71 73 75 77 79 81 83 85 87 89 91 93 95 97 99
Duration/discharge amount in %
Flood loss
Usable water amount
Minimum water flow
Low flow loss
Flow duration
Diversion capacity curve
Sum lower
Low flow loss
Diversion capacity

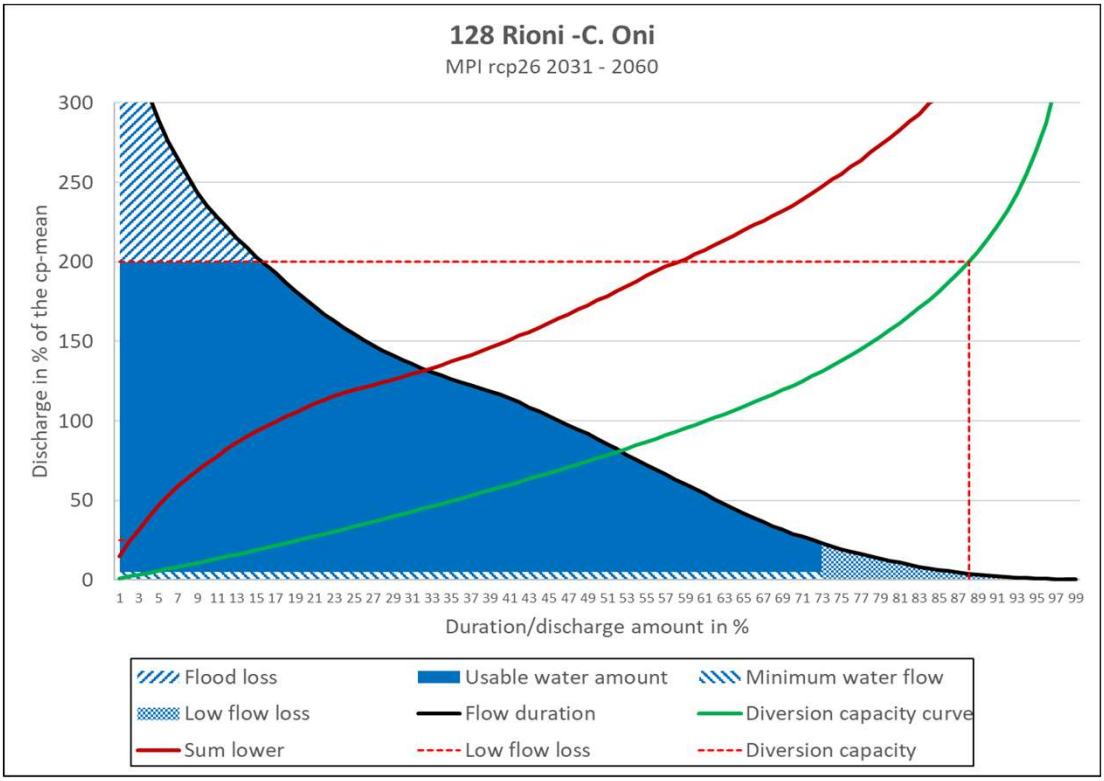
128 Rioni -C. Oni
MPI rcp26 2031 - 2060
Discharge in % of the cp-mean
300
250
200
150
100
50
0
1 3 5 7 9 11 13 15 17 19 21 23 25 27 29 31 33 35 37 39 41 43 45 47 49 51 53 55 57 59 61 63 65 67 69 71 73 75 77 79 81 83 85 87 89 91 93 95 97 99
Duration/discharge amount in %
Flood loss
Usable water amount
Minimum water flow
Low flow loss
Flow duration
Diversion capacity curve
Sum lower
Low flow loss
Diversion capacity

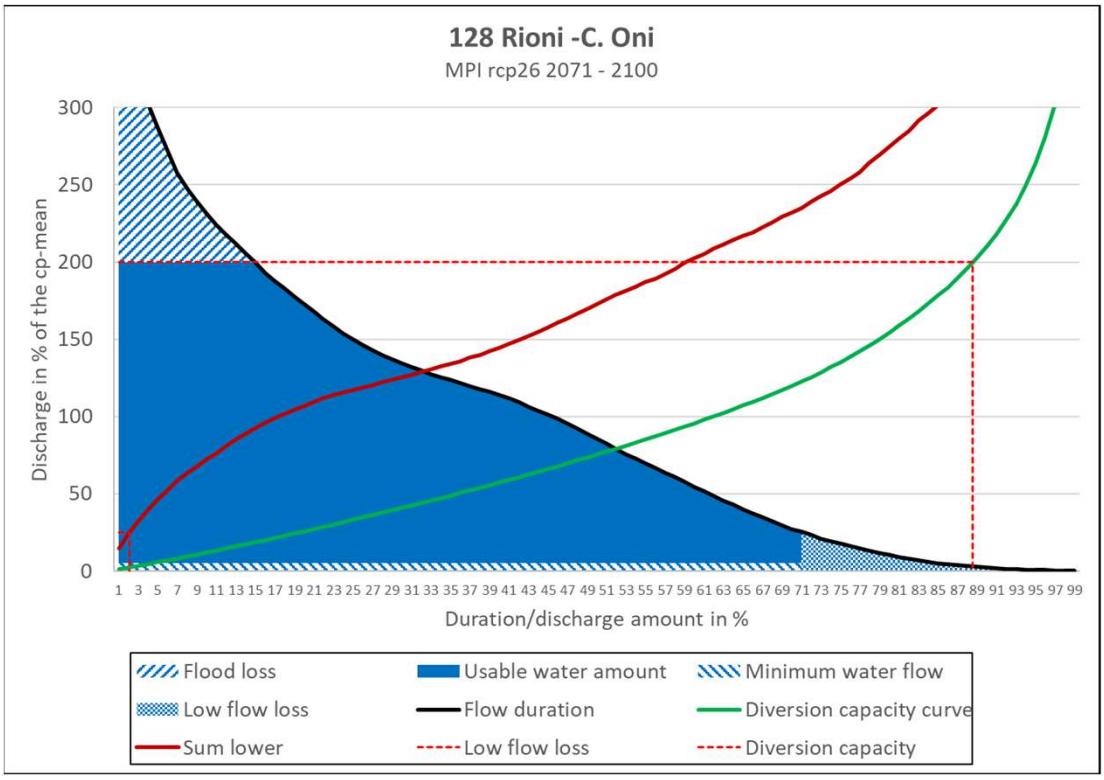
128 Rioni -C. Oni
MPI rcp26 2071 - 2100
Discharge in % of the cp-mean
300
250
200
150
100
50
0
1 3 5 7 9 11 13 15 17 19 21 23 25 27 29 31 33 35 37 39 41 43 45 47 49 51 53 55 57 59 61 63 65 67 69 71 73 75 77 79 81 83 85 87 89 91 93 95 97 99
Duration/discharge amount in %
Flood loss
Usable water amount
Minimum water flow
Low flow loss
Flow duration
Diversion capacity curve
Sum lower
Low flow loss
Diversion capacity

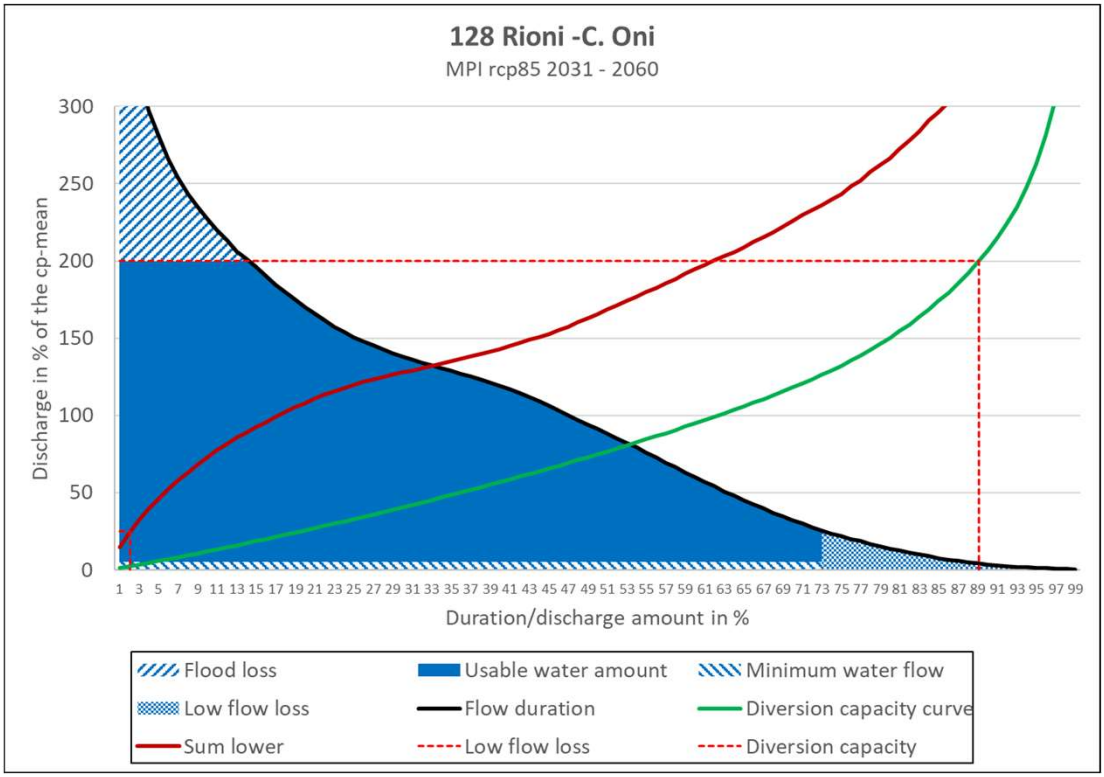
128 Rioni -C. Oni
MPI rcp85 2031 - 2060
Discharge in % of the cp-mean
300
250
200
150
100
50
0
1 3 5 7 9 11 13 15 17 19 21 23 25 27 29 31 33 35 37 39 41 43 45 47 49 51 53 55 57 59 61 63 65 67 69 71 73 75 77 79 81 83 85 87 89 91 93 95 97 99
Duration/discharge amount in %
Flood loss
Usable water amount
Minimum water flow
Low flow loss
Flow duration
Diversion capacity curve
Sum lower
Low flow loss
Diversion capacity

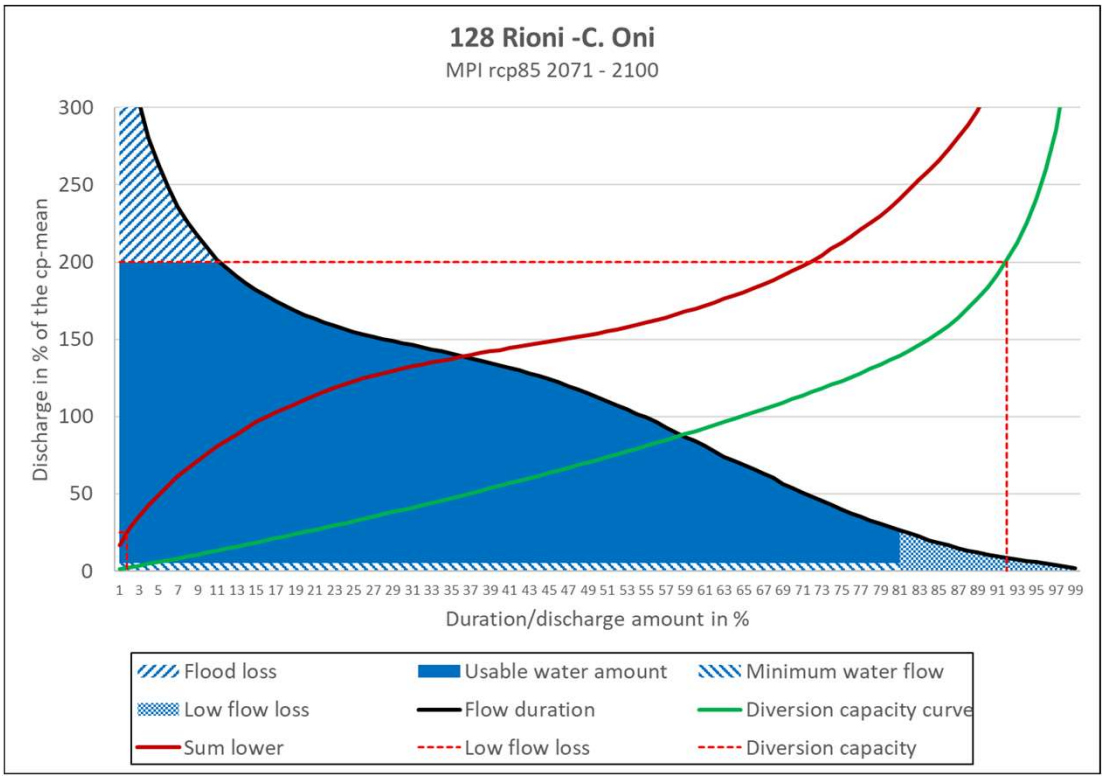
128 Rioni -C. Oni
MPI rcp85 2071 - 2100
Discharge in % of the cp-mean
300
250
200
150
100
50
0
1 3 5 7 9 11 13 15 17 19 21 23 25 27 29 31 33 35 37 39 41 43 45 47 49 51 53 55 57 59 61 63 65 67 69 71 73 75 77 79 81 83 85 87 89 91 93 95 97 99
Duration/discharge amount in %
Flood loss
Usable water amount
Minimum water flow
Low flow loss
Flow duration
Diversion capacity curve
Sum lower
Low flow loss
Diversion capacity

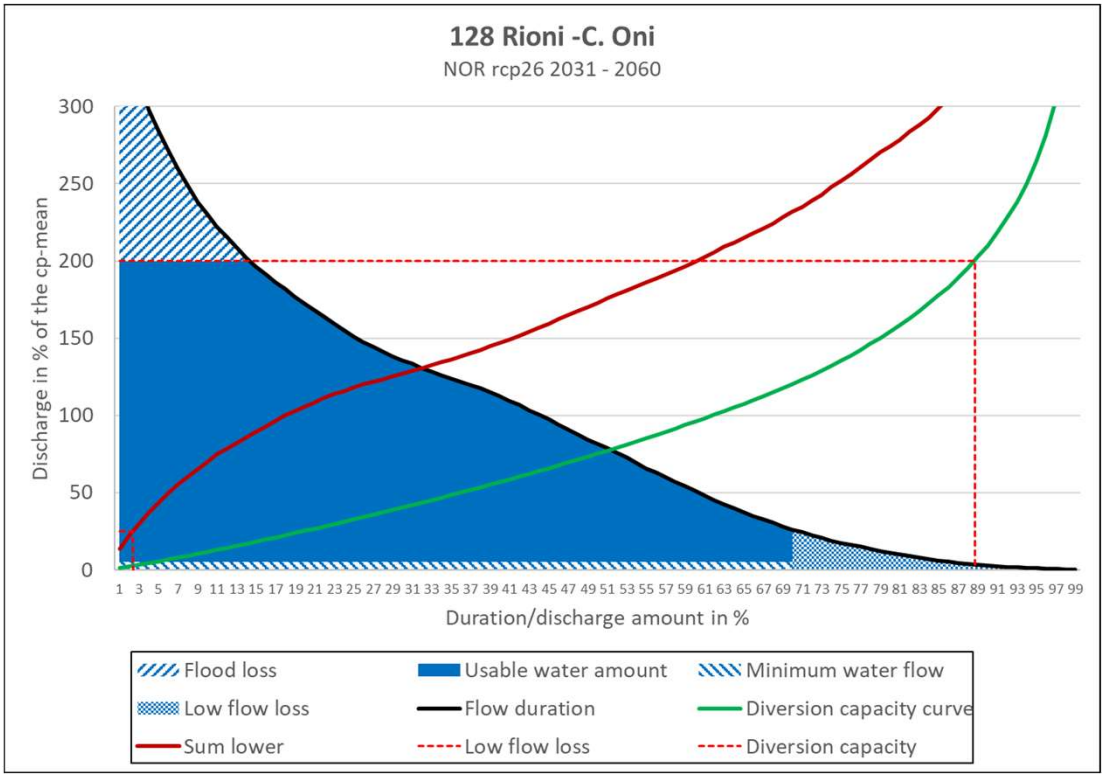
128 Rioni -C. Oni
NOR rcp26 2031 - 2060
Discharge in % of the cp-mean
300
250
200
150
100
50
0
1 3 5 7 9 11 13 15 17 19 21 23 25 27 29 31 33 35 37 39 41 43 45 47 49 51 53 55 57 59 61 63 65 67 69 71 73 75 77 79 81 83 85 87 89 91 93 95 97 99
Duration/discharge amount in %
Flood loss
Usable water amount
Minimum water flow
Low flow loss
Flow duration
Diversion capacity curve
Sum lower
Low flow loss
Diversion capacity

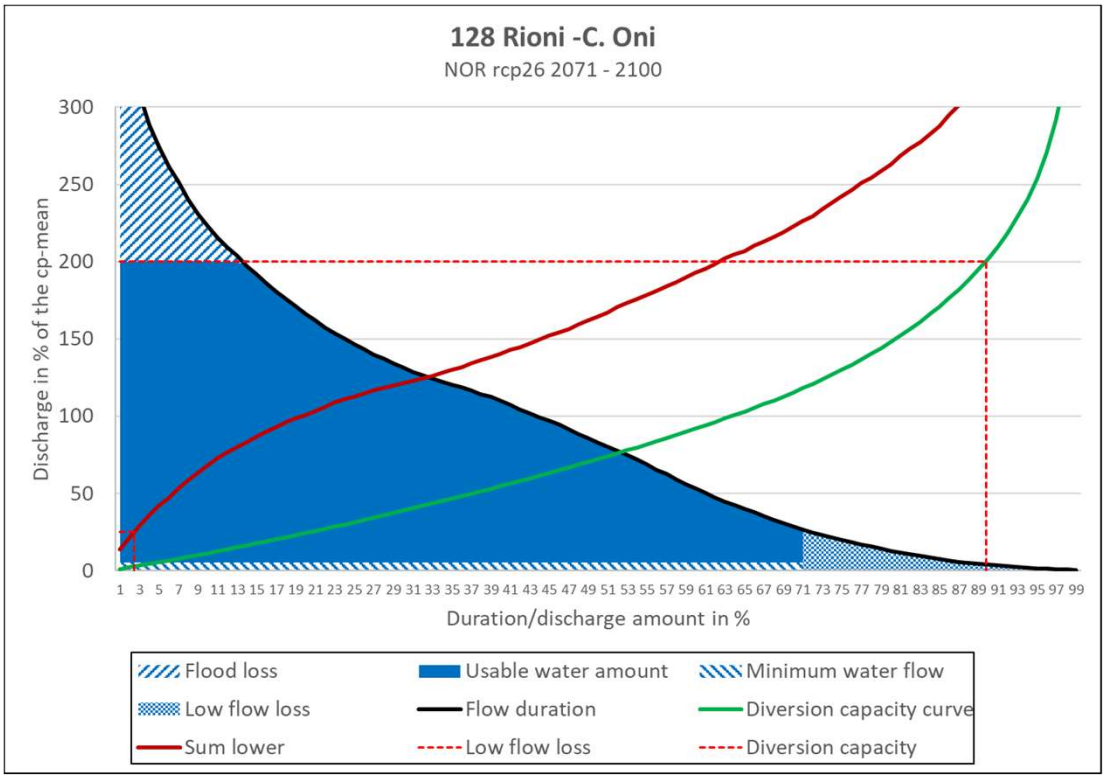
128 Rioni -C. Oni
NOR rcp26 2071 - 2100
Discharge in % of the cp-mean
300
250
200
150
100
50
0
1 3 5 7 9 11 13 15 17 19 21 23 25 27 29 31 33 35 37 39 41 43 45 47 49 51 53 55 57 59 61 63 65 67 69 71 73 75 77 79 81 83 85 87 89 91 93 95 97 99
Duration/discharge amount in %
Flood loss
Usable water amount
Minimum water flow
Low flow loss
Flow duration
Diversion capacity curve
Sum lower
Low flow loss
Diversion capacity

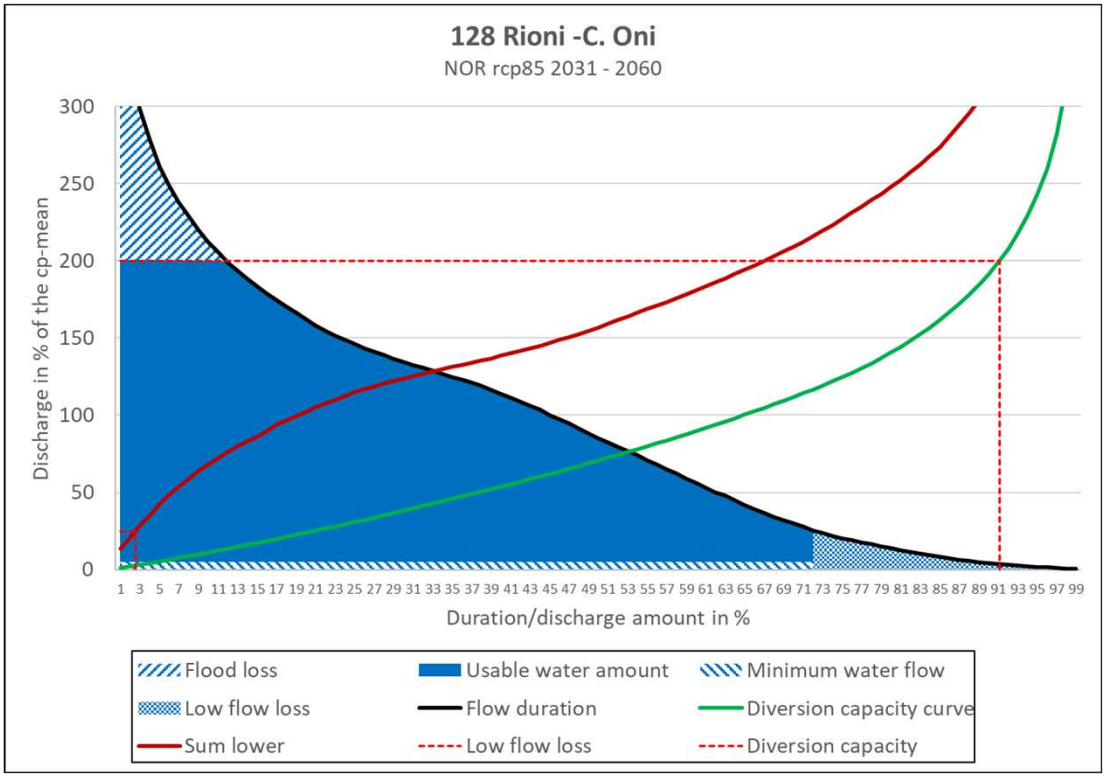
128 Rioni -C. Oni
NOR rcp85 2031 - 2060
Discharge in % of the cp-mean
300
250
200
150
100
50
0
1 3 5 7 9 11 13 15 17 19 21 23 25 27 29 31 33 35 37 39 41 43 45 47 49 51 53 55 57 59 61 63 65 67 69 71 73 75 77 79 81 83 85 87 89 91 93 95 97 99
Duration/discharge amount in %
Flood loss
Usable water amount
Minimum water flow
Low flow loss
Flow duration
Diversion capacity curve
Sum lower
Low flow loss
Diversion capacity

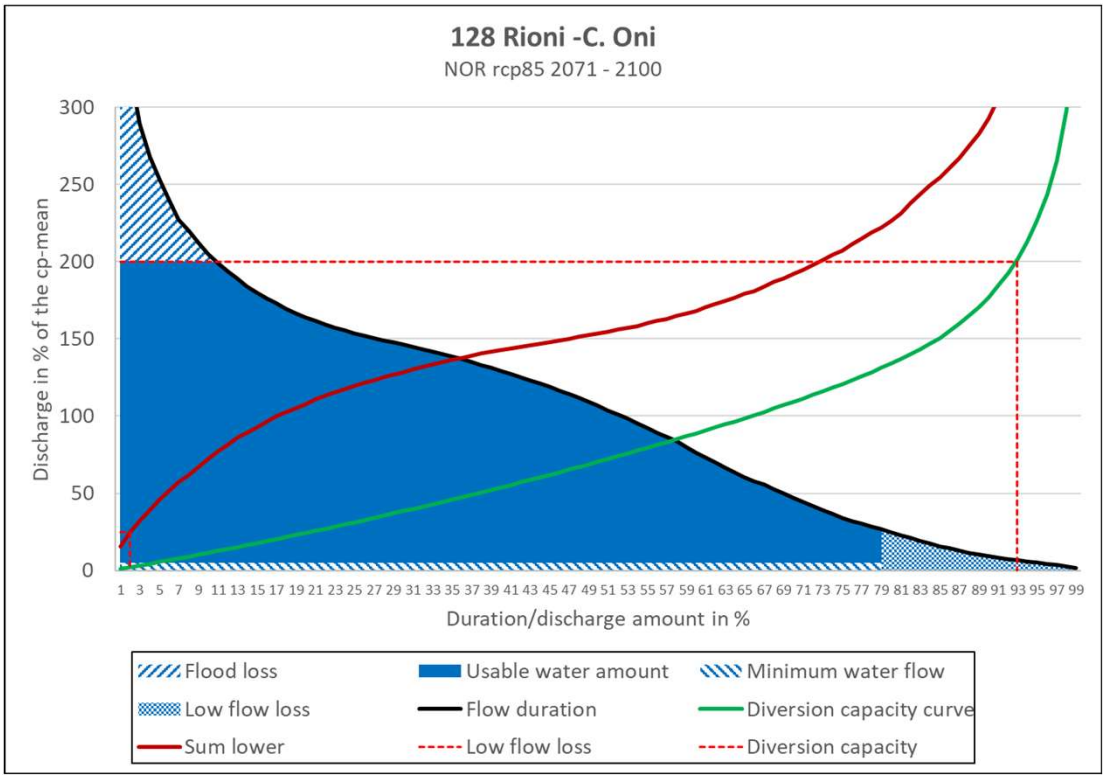
128 Rioni -C. Oni
NOR rcp85 2071 - 2100
Discharge in % of the cp-mean
300
250
200
150
100
50
0
1 3 5 7 9 11 13 15 17 19 21 23 25 27 29 31 33 35 37 39 41 43 45 47 49 51 53 55 57 59 61 63 65 67 69 71 73 75 77 79 81 83 85 87 89 91 93 95 97 99
Duration/discharge amount in %
Flood loss
Usable water amount
Minimum water flow
Low flow loss
Flow duration
Diversion capacity curve
Sum lower
Low flow loss
Diversion capacity

289 Chkheri – D. Stefantsminda

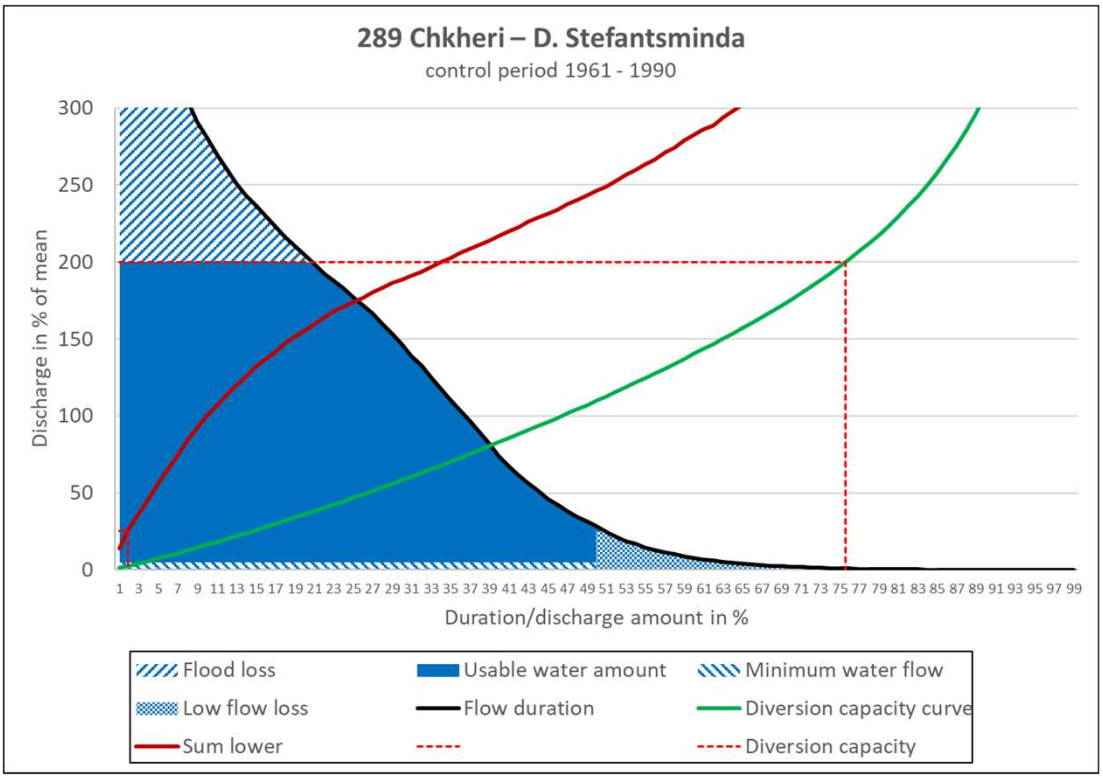

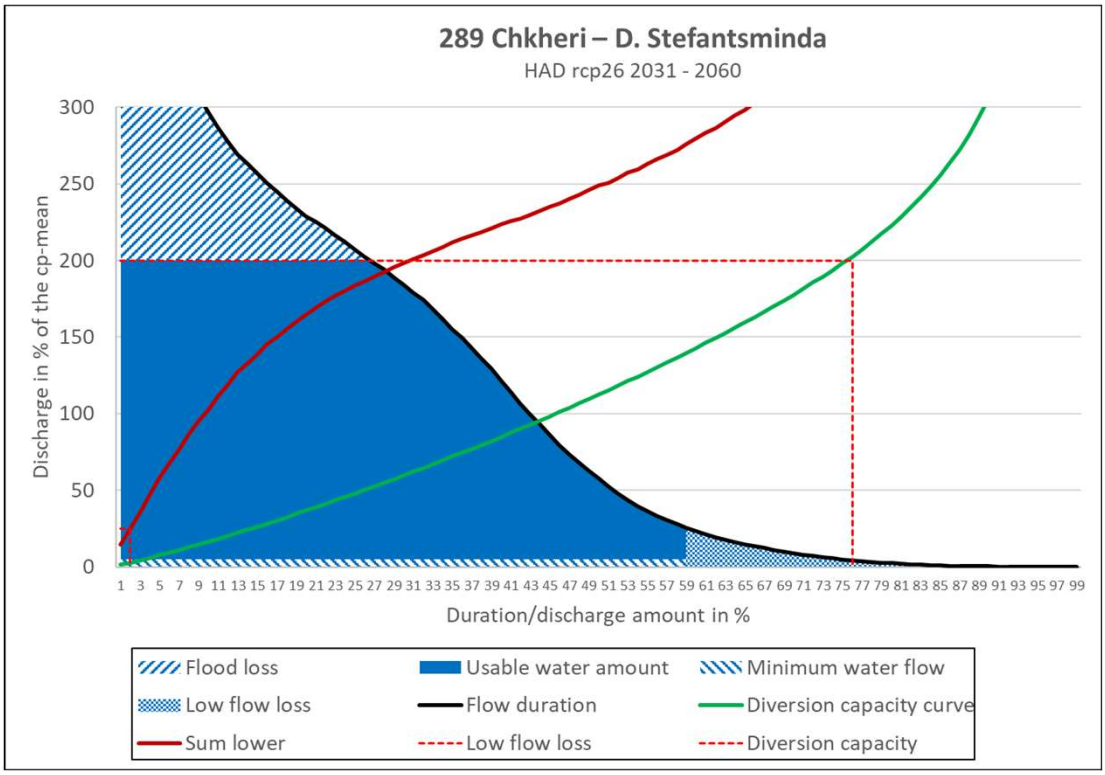
289 Chkheri – D. Stefantsminda
HAD rcp26 2031 - 2060
Discharge in % of the cp-mean
300
250
200
150
100
50
0
1 3 5 7 9 11 13 15 17 19 21 23 25 27 29 31 33 35 37 39 41 43 45 47 49 51 53 55 57 59 61 63 65 67 69 71 73 75 77 79 81 83 85 87 89 91 93 95 97 99
Duration/discharge amount in %
Flood loss
Usable water amount
Minimum water flow
Low flow loss
Flow duration
Diversion capacity curve
Sum lower
Low flow loss
Diversion capacity

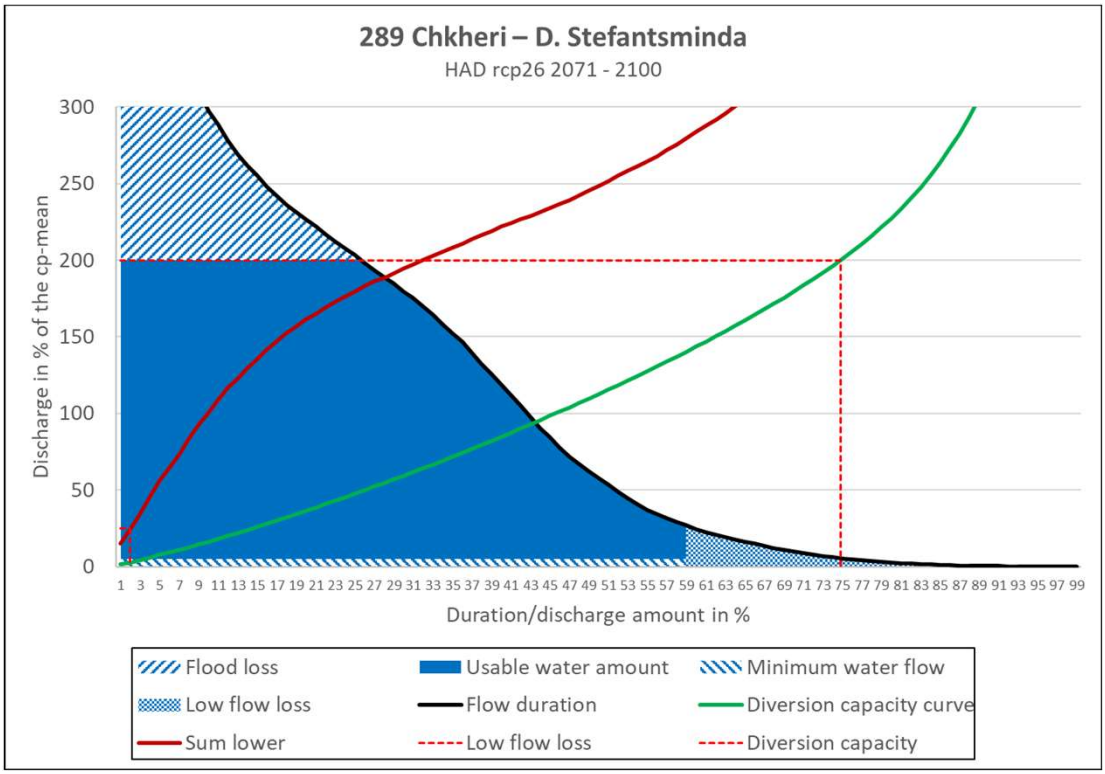
289 Chkheri – D. Stefantsminda
HAD rcp26 2071 - 2100
Discharge in % of the cp-mean
300
250
200
150
100
50
0
1 3 5 7 9 11 13 15 17 19 21 23 25 27 29 31 33 35 37 39 41 43 45 47 49 51 53 55 57 59 61 63 65 67 69 71 73 75 77 79 81 83 85 87 89 91 93 95 97 99
Duration/discharge amount in %
Flood loss
Usable water amount
Minimum water flow
Low flow loss
Flow duration
Diversion capacity curve
Sum lower
Low flow loss
Diversion capacity

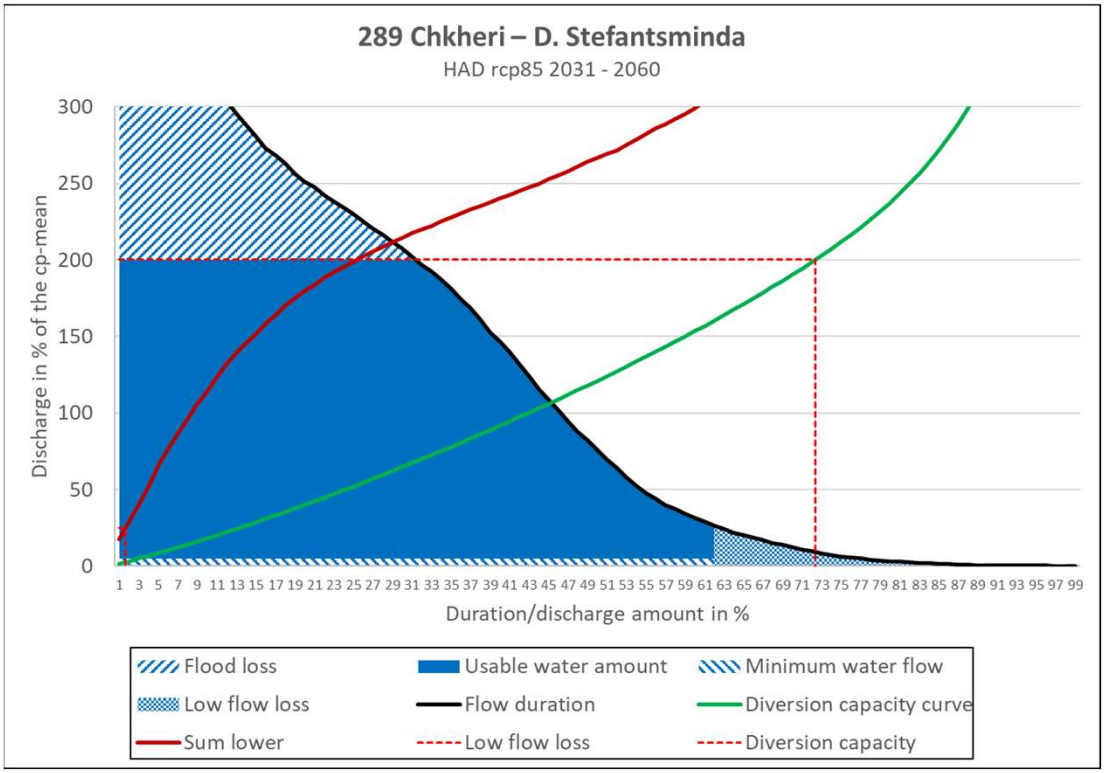
289 Chkheri – D. Stefantsminda
HAD rcp85 2031 - 2060
Discharge in % of the cp-mean
300
250
200
150
100
50
0
1 3 5 7 9 11 13 15 17 19 21 23 25 27 29 31 33 35 37 39 41 43 45 47 49 51 53 55 57 59 61 63 65 67 69 71 73 75 77 79 81 83 85 87 89 91 93 95 97 99
Duration/discharge amount in %
Flood loss
Usable water amount
Minimum water flow
Low flow loss
Flow duration
Diversion capacity curve
Sum lower
Low flow loss
Diversion capacity

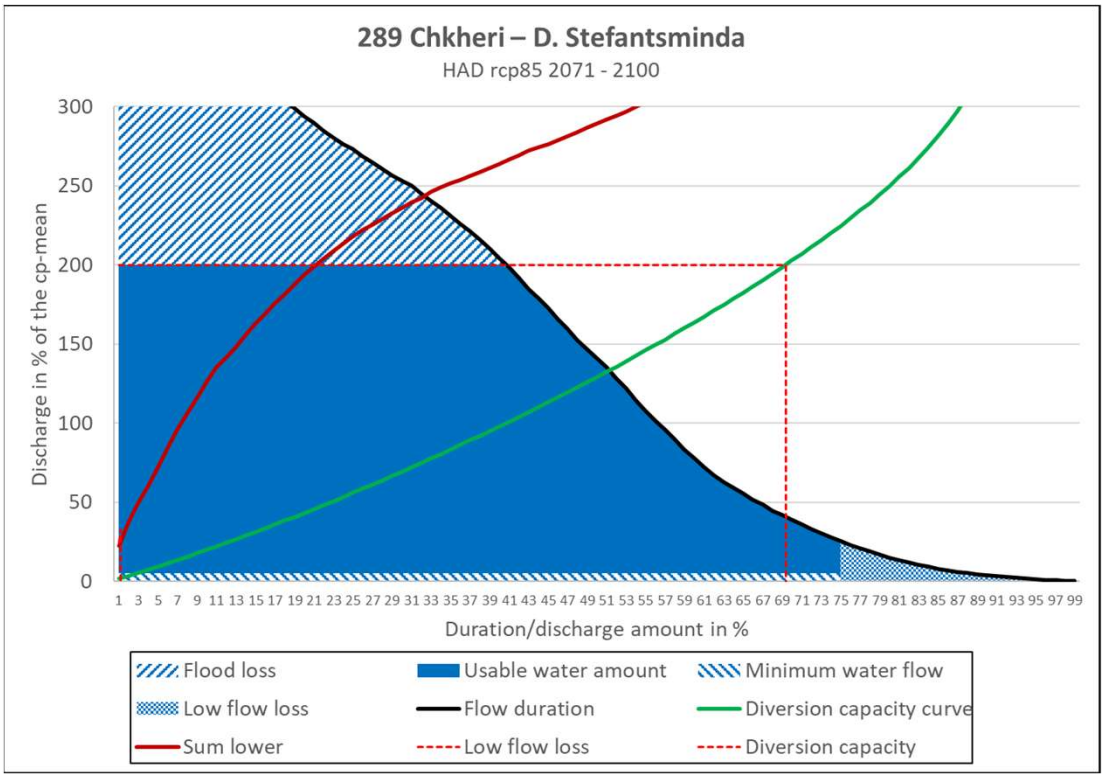
289 Chkheri – D. Stefantsminda
HAD rcp85 2071 - 2100
Discharge in % of the cp-mean
300
250
200
150
100
50
0
1 3 5 7 9 11 13 15 17 19 21 23 25 27 29 31 33 35 37 39 41 43 45 47 49 51 53 55 57 59 61 63 65 67 69 71 73 75 77 79 81 83 85 87 89 91 93 95 97 99
Duration/discharge amount in %
Flood loss
Usable water amount
Minimum water flow
Low flow loss
Flow duration
Diversion capacity curve
Sum lower
Low flow loss
Diversion capacity

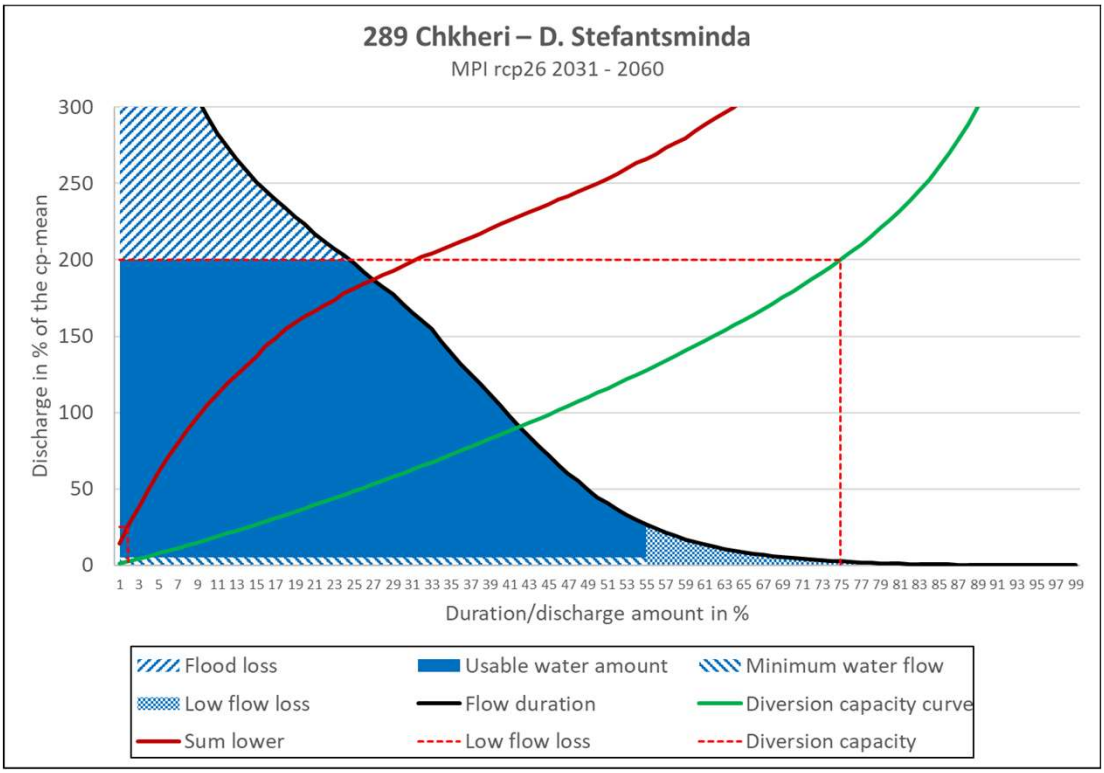
289 Chkheri – D. Stefantsminda
MPI rcp26 2031 - 2060
Discharge in % of the cp-mean
300
250
200
150
100
50
0
1 3 5 7 9 11 13 15 17 19 21 23 25 27 29 31 33 35 37 39 41 43 45 47 49 51 53 55 57 59 61 63 65 67 69 71 73 75 77 79 81 83 85 87 89 91 93 95 97 99
Duration/discharge amount in %
Flood loss
Usable water amount
Minimum water flow
Low flow loss
Flow duration
Diversion capacity curve
Sum lower
Low flow loss
Diversion capacity

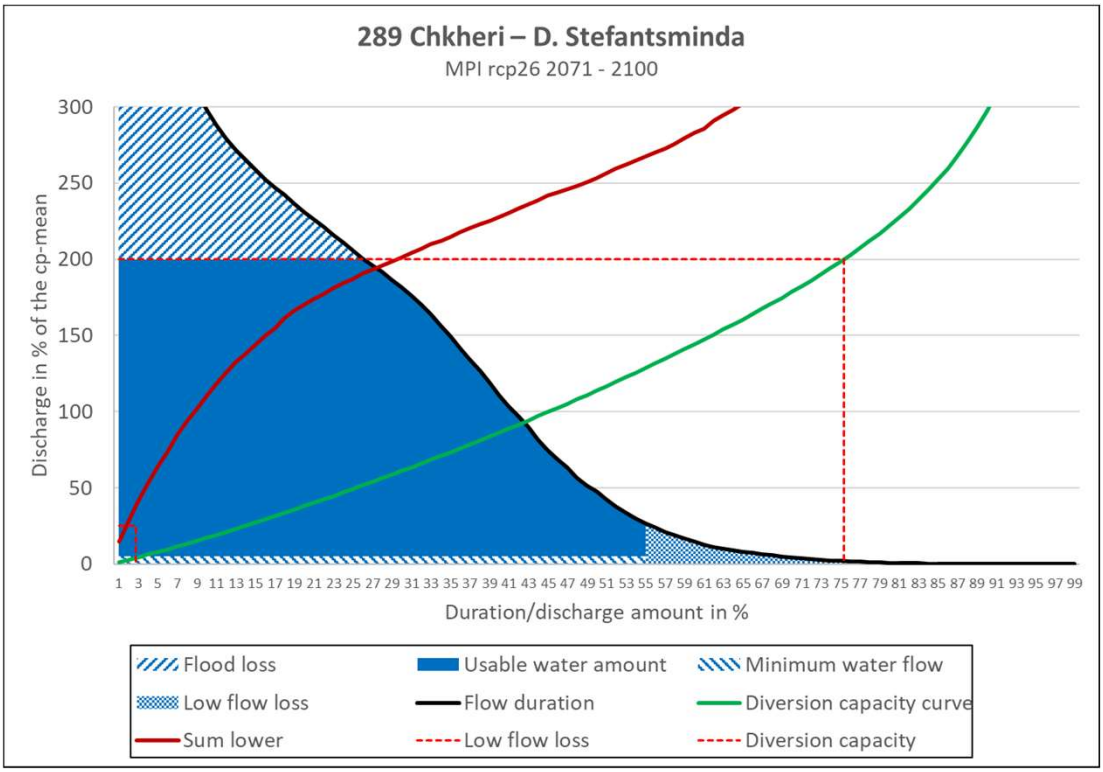
289 Chkheri – D. Stefantsminda
MPI rcp26 2071 - 2100
Discharge in % of the cp-mean
300
250
200
150
100
50
0
1 3 5 7 9 11 13 15 17 19 21 23 25 27 29 31 33 35 37 39 41 43 45 47 49 51 53 55 57 59 61 63 65 67 69 71 73 75 77 79 81 83 85 87 89 91 93 95 97 99
Duration/discharge amount in %
Flood loss
Usable water amount
Minimum water flow
Low flow loss
Flow duration
Diversion capacity curve
Sum lower
Low flow loss
Diversion capacity

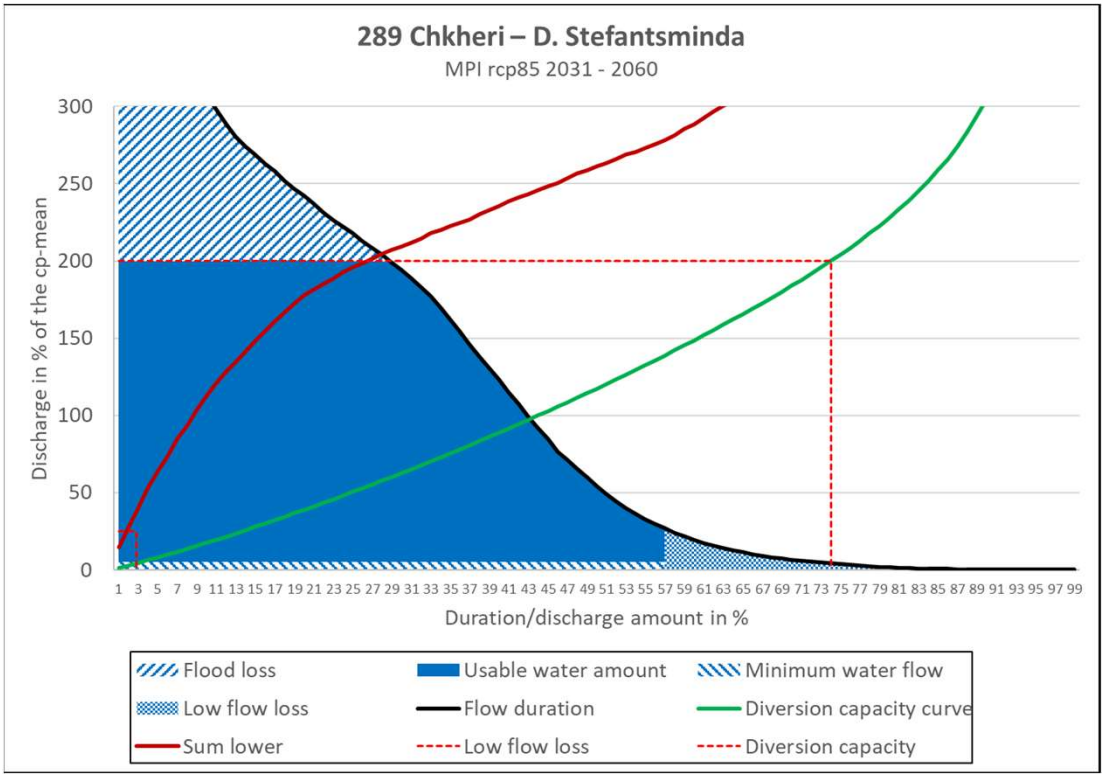
289 Chkheri – D. Stefantsminda
MPI rcp85 2031 - 2060
Discharge in % of the cp-mean
300
250
200
150
100
50
0
1 3 5 7 9 11 13 15 17 19 21 23 25 27 29 31 33 35 37 39 41 43 45 47 49 51 53 55 57 59 61 63 65 67 69 71 73 75 77 79 81 83 85 87 89 91 93 95 97 99
Duration/discharge amount in %
Flood loss
Usable water amount
Minimum water flow
Low flow loss
Flow duration
Diversion capacity curve
Sum lower
Low flow loss
Diversion capacity

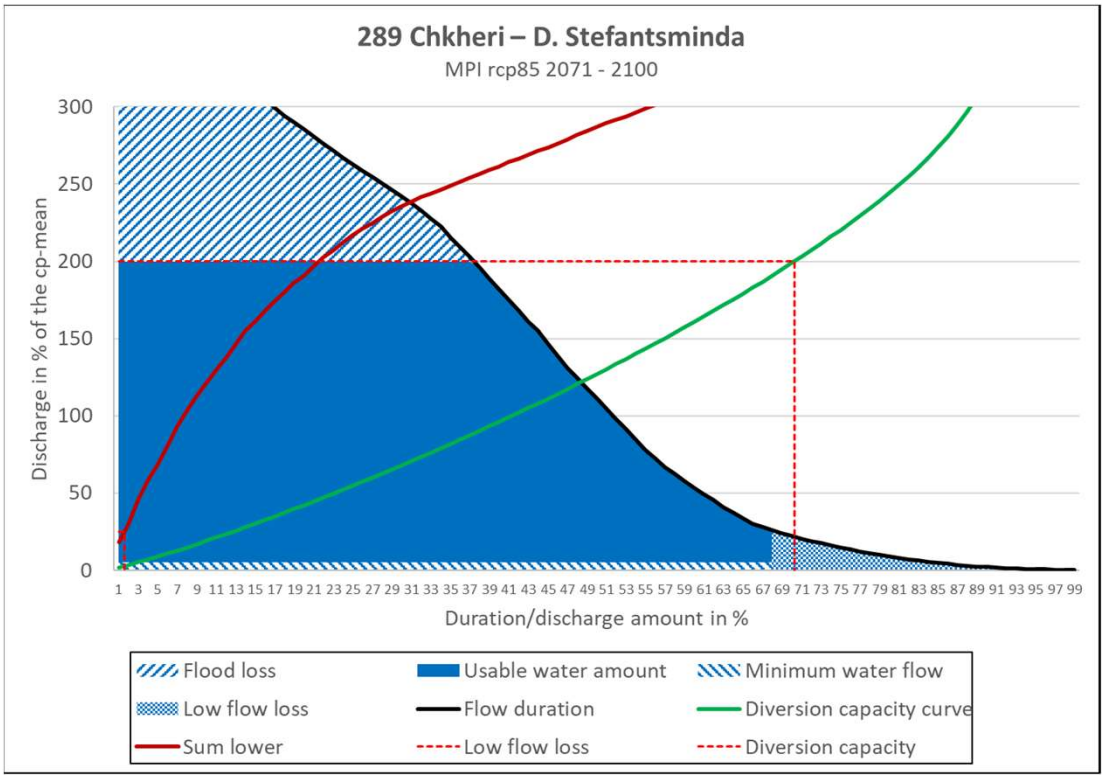
289 Chkheri – D. Stefantsminda
MPI rcp85 2071 - 2100
Discharge in % of the cp-mean
300
250
200
150
100
50
0
1 3 5 7 9 11 13 15 17 19 21 23 25 27 29 31 33 35 37 39 41 43 45 47 49 51 53 55 57 59 61 63 65 67 69 71 73 75 77 79 81 83 85 87 89 91 93 95 97 99
Duration/discharge amount in %
Flood loss
Usable water amount
Minimum water flow
Low flow loss
Flow duration
Diversion capacity curve
Sum lower
Low flow loss
Diversion capacity

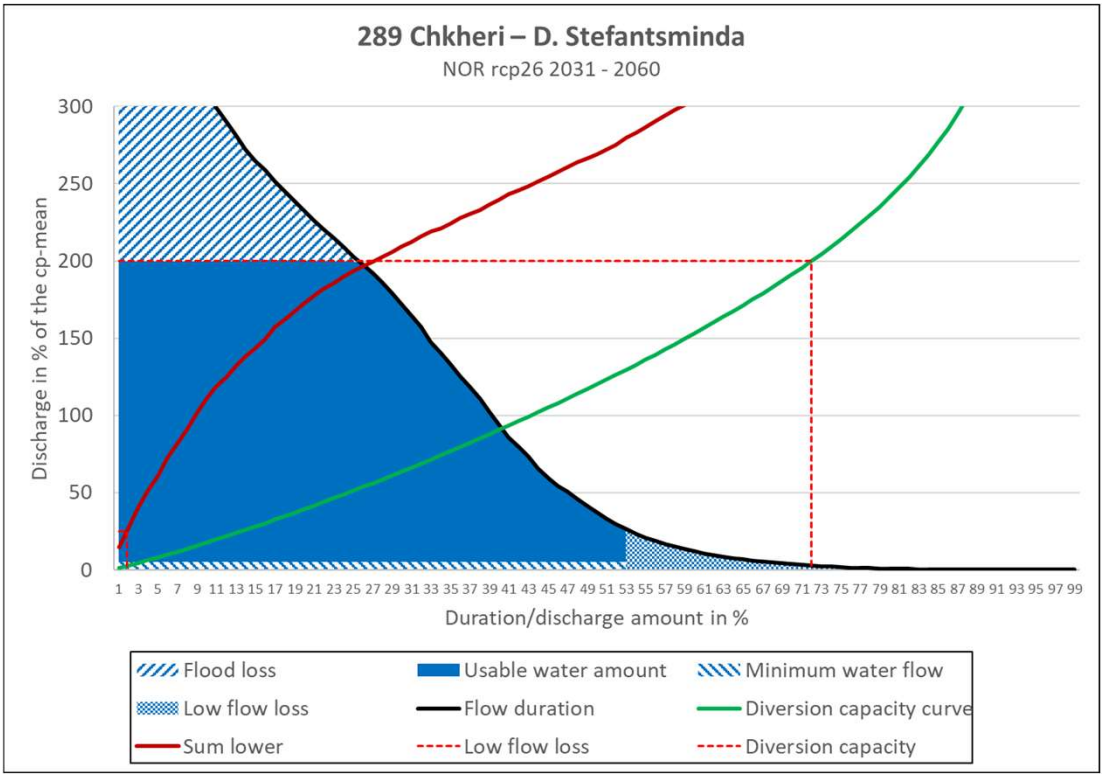
289 Chkheri – D. Stefantsminda
NOR rcp26 2031 - 2060
Discharge in % of the cp-mean
300
250
200
150
100
50
0
1 3 5 7 9 11 13 15 17 19 21 23 25 27 29 31 33 35 37 39 41 43 45 47 49 51 53 55 57 59 61 63 65 67 69 71 73 75 77 79 81 83 85 87 89 91 93 95 97 99
Duration/discharge amount in %
Flood loss
Usable water amount
Minimum water flow
Low flow loss
Flow duration
Diversion capacity curve
Sum lower
Low flow loss
Diversion capacity

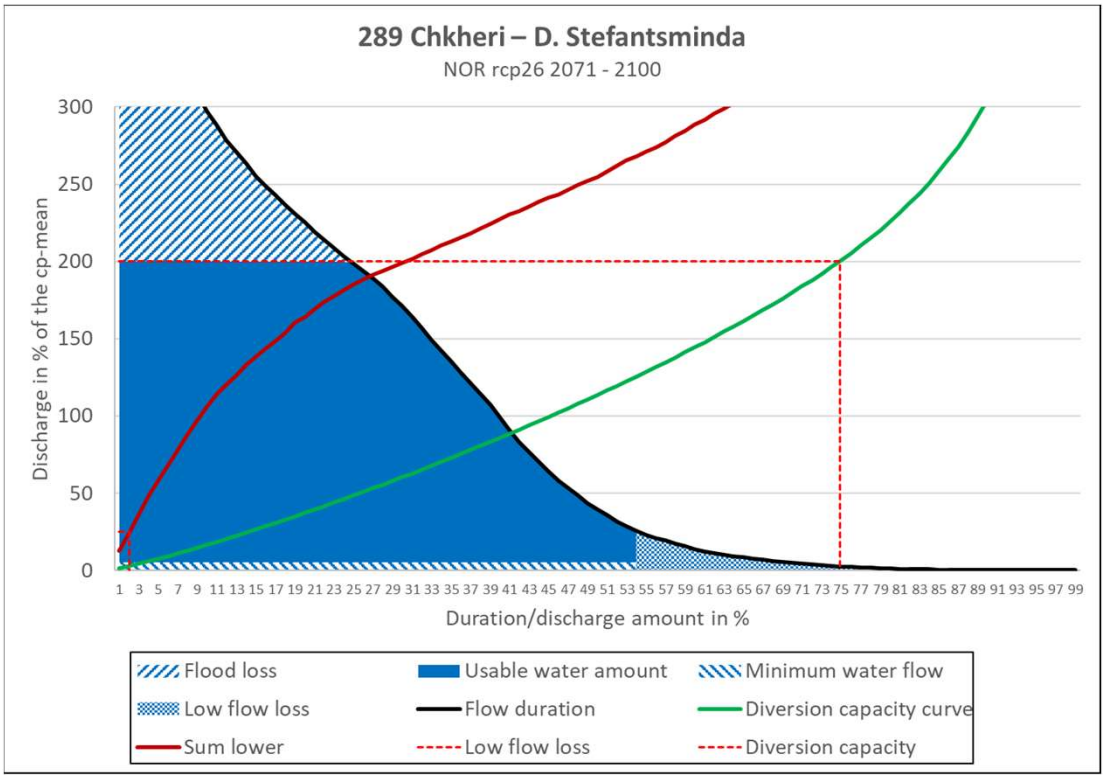
289 Chkheri – D. Stefantsminda
NOR rcp26 2071 - 2100
Discharge in % of the cp-mean
300
250
200
150
100
50
0
1 3 5 7 9 11 13 15 17 19 21 23 25 27 29 31 33 35 37 39 41 43 45 47 49 51 53 55 57 59 61 63 65 67 69 71 73 75 77 79 81 83 85 87 89 91 93 95 97 99
Duration/discharge amount in %
Flood loss
Usable water amount
Minimum water flow
Low flow loss
Flow duration
Diversion capacity curve
Sum lower
Low flow loss
Diversion capacity

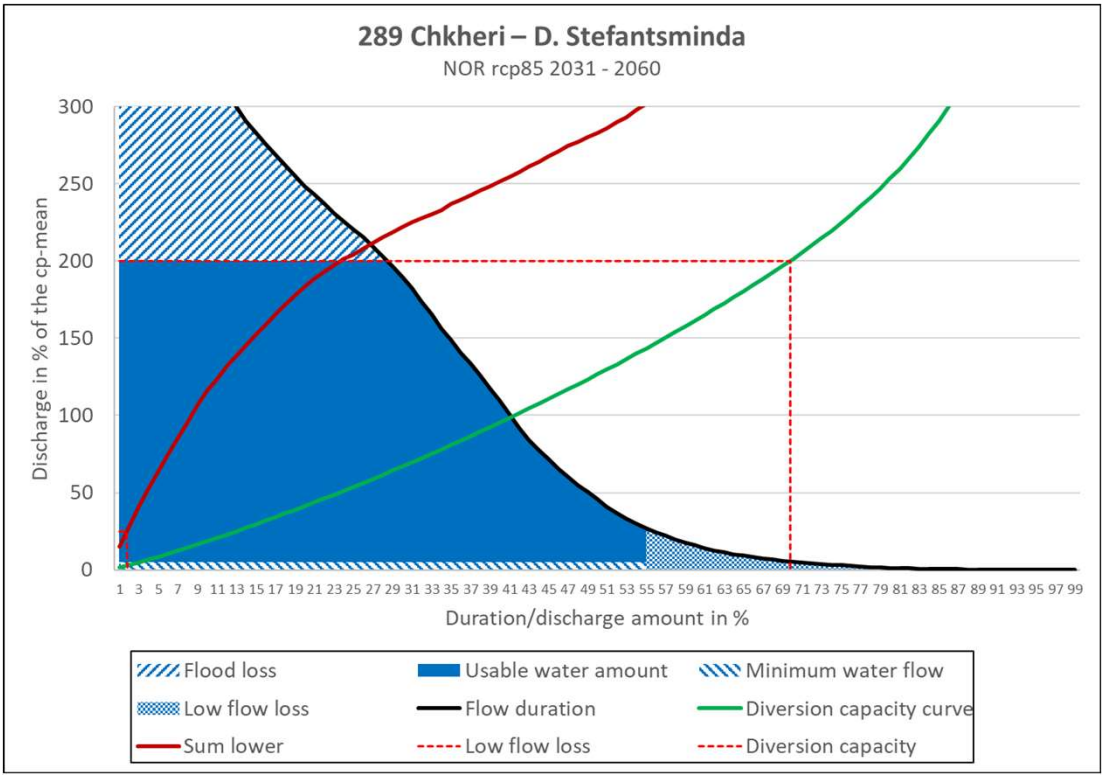
289 Chkheri – D. Stefantsminda
NOR rcp85 2031 - 2060
Discharge in % of the cp-mean
300
250
200
150
100
50
0
1 3 5 7 9 11 13 15 17 19 21 23 25 27 29 31 33 35 37 39 41 43 45 47 49 51 53 55 57 59 61 63 65 67 69 71 73 75 77 79 81 83 85 87 89 91 93 95 97 99
Duration/discharge amount in %
Flood loss
Usable water amount
Minimum water flow
Low flow loss
Flow duration
Diversion capacity curve
Sum lower
Low flow loss
Diversion capacity

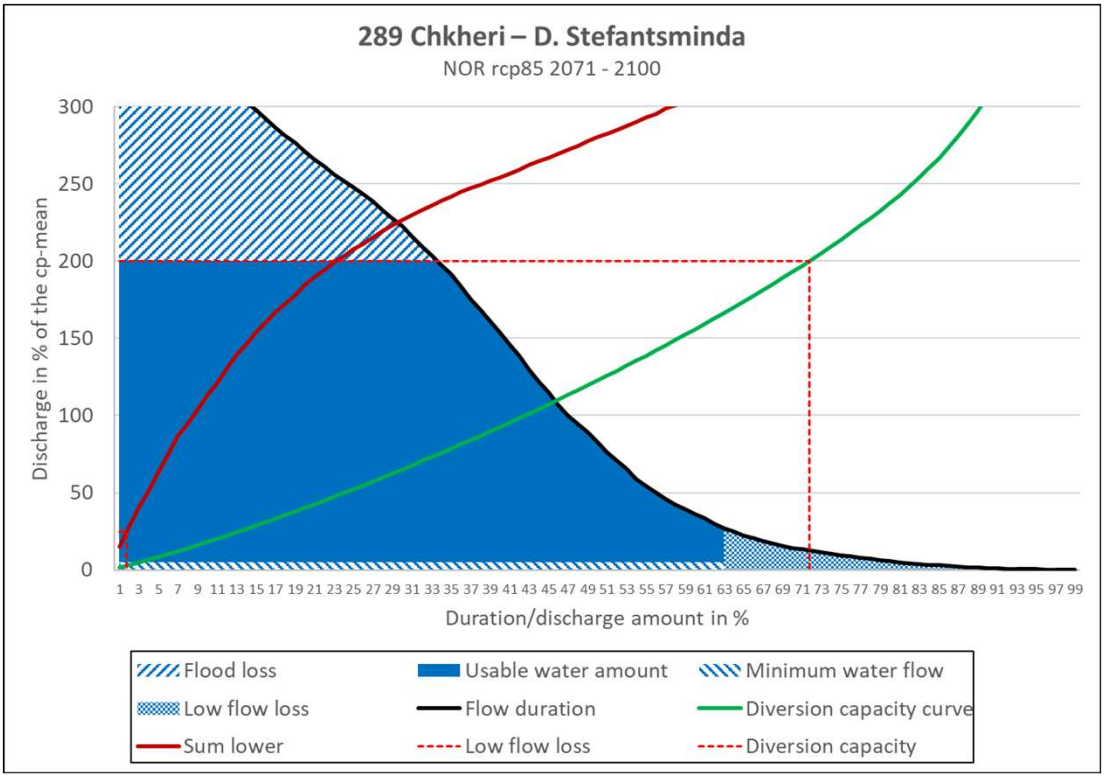
289 Chkheri – D. Stefantsminda
NOR rcp85 2071 - 2100
Discharge in % of the cp-mean
300
250
200
150
100
50
0
1 3 5 7 9 11 13 15 17 19 21 23 25 27 29 31 33 35 37 39 41 43 45 47 49 51 53 55 57 59 61 63 65 67 69 71 73 75 77 79 81 83 85 87 89 91 93 95 97 99
Duration/discharge amount in %
Flood loss
Usable water amount
Minimum water flow
Low flow loss
Flow duration
Diversion capacity curve
Sum lower
Low flow loss
Diversion capacity

296 Mtkvari (Kura) – V. Khertvisi

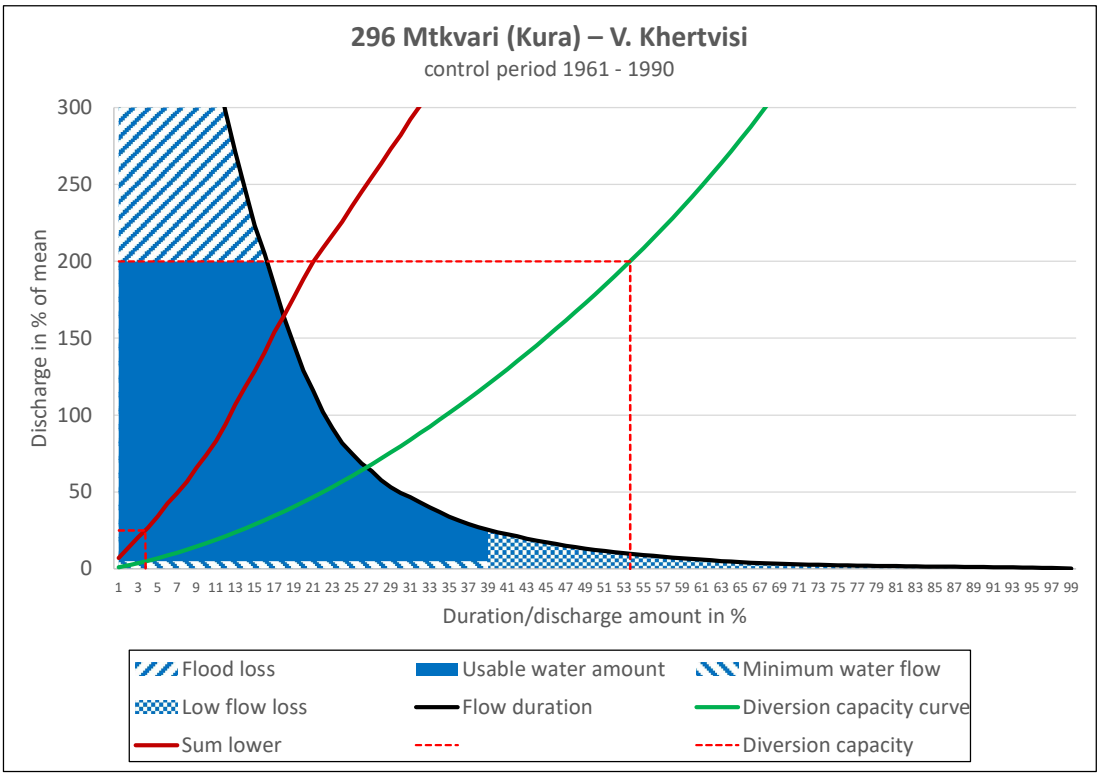

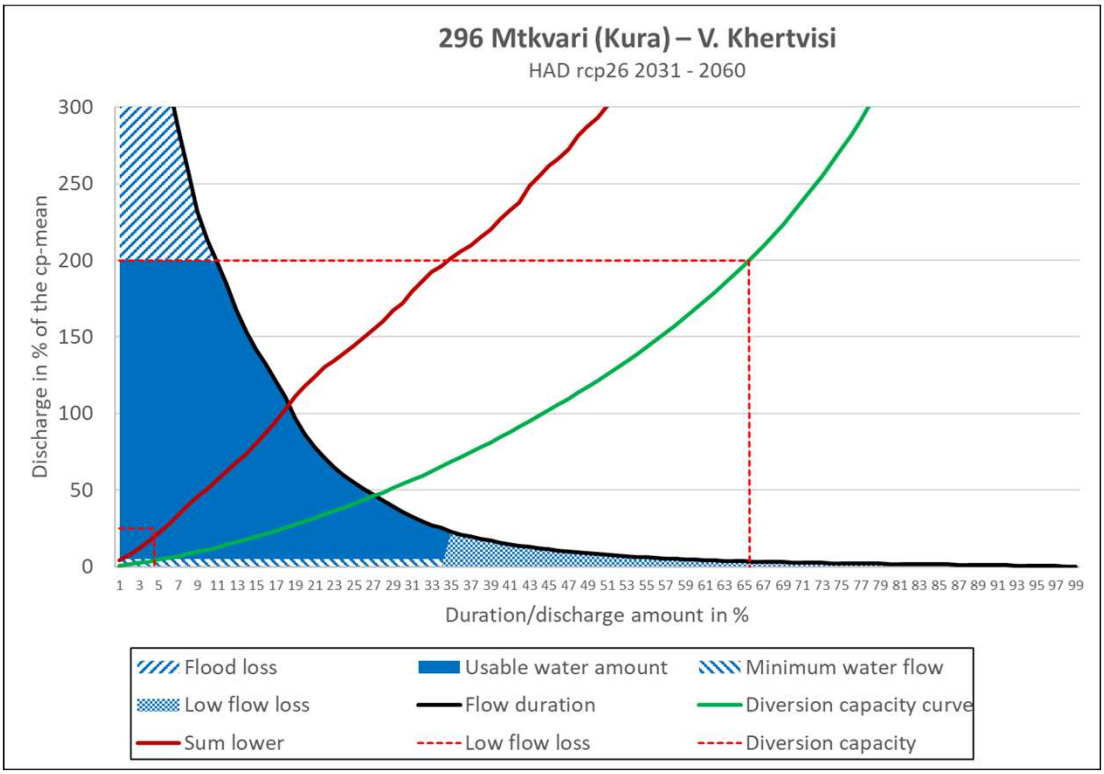
296 Mtkvari (Kura) – V. Khertvisi
HAD rcp26 2031 - 2060
Discharge in % of the cp-mean
300
250
200
150
100
50
0
1 3 5 7 9 11 13 15 17 19 21 23 25 27 29 31 33 35 37 39 41 43 45 47 49 51 53 55 57 59 61 63 65 67 69 71 73 75 77 79 81 83 85 87 89 91 93 95 97 99
Duration/discharge amount in %
Flood loss
Usable water amount
Minimum water flow
Low flow loss
Flow duration
Diversion capacity curve
Sum lower
Low flow loss
Diversion capacity

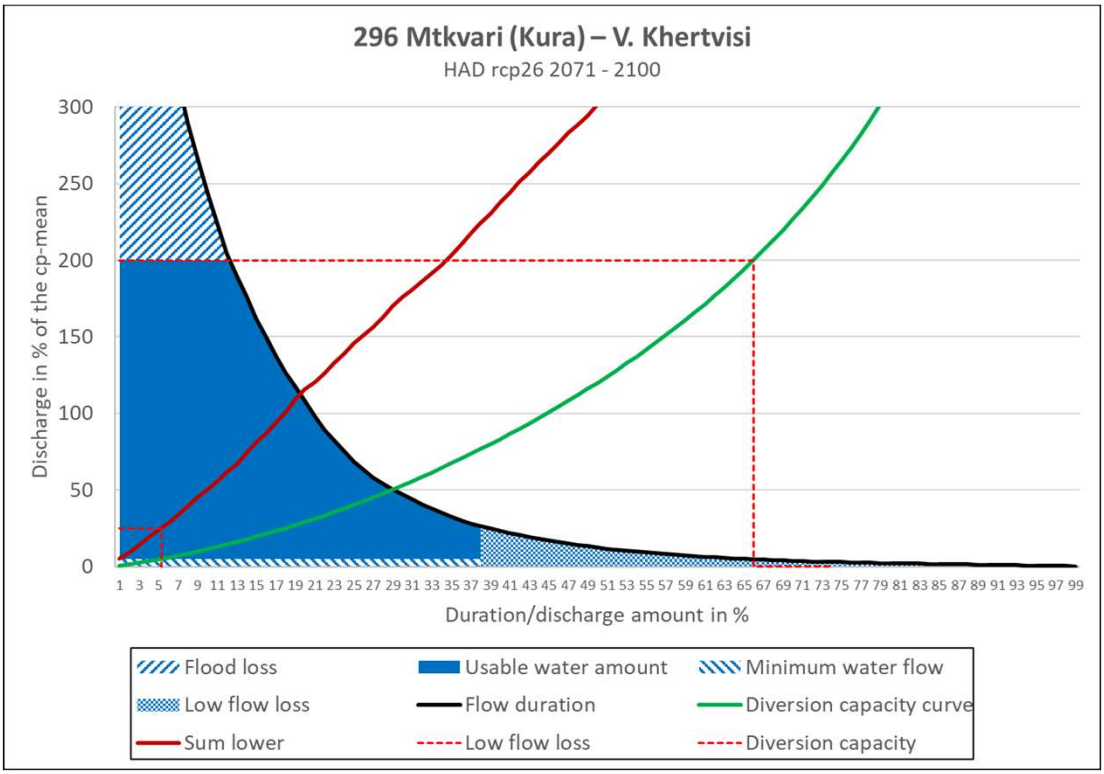
296 Mtkvari (Kura) – V. Khertvisi
HAD rcp26 2071 - 2100
Discharge in % of the cp-mean
300
250
200
150
100
50
0
1 3 5 7 9 11 13 15 17 19 21 23 25 27 29 31 33 35 37 39 41 43 45 47 49 51 53 55 57 59 61 63 65 67 69 71 73 75 77 79 81 83 85 87 89 91 93 95 97 99
Duration/discharge amount in %
Flood loss
Usable water amount
Minimum water flow
Low flow loss
Flow duration
Diversion capacity curve
Sum lower
Low flow loss
Diversion capacity

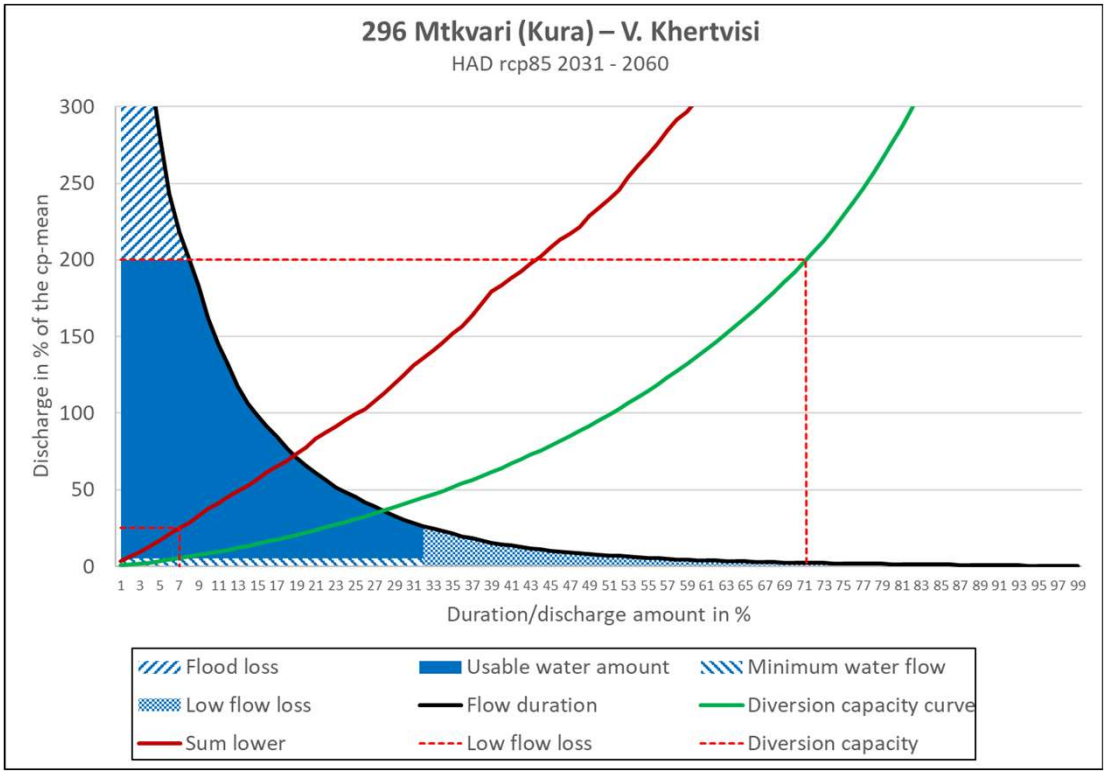
296 Mtkvari (Kura) – V. Khertvisi
HAD rcp85 2031 - 2060
Discharge in % of the cp-mean
300
250
200
150
100
50
0
1 3 5 7 9 11 13 15 17 19 21 23 25 27 29 31 33 35 37 39 41 43 45 47 49 51 53 55 57 59 61 63 65 67 69 71 73 75 77 79 81 83 85 87 89 91 93 95 97 99
Duration/discharge amount in %
Flood loss
Usable water amount
Minimum water flow
Low flow loss
Flow duration
Diversion capacity curve
Sum lower
Low flow loss
Diversion capacity

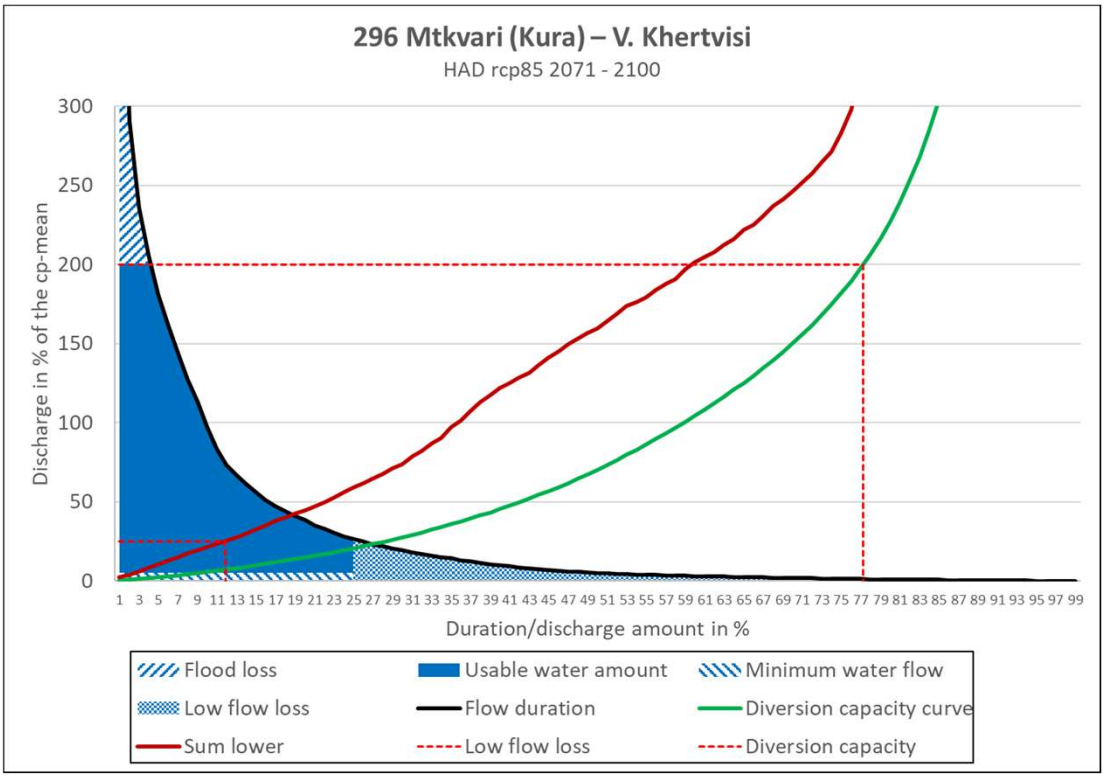
296 Mtkvari (Kura) – V. Khertvisi
HAD rcp85 2071 - 2100
Discharge in % of the cp-mean
300
250
200
150
100
50
0
1 3 5 7 9 11 13 15 17 19 21 23 25 27 29 31 33 35 37 39 41 43 45 47 49 51 53 55 57 59 61 63 65 67 69 71 73 75 77 79 81 83 85 87 89 91 93 95 97 99
Duration/discharge amount in %
Flood loss
Usable water amount
Minimum water flow
Low flow loss
Flow duration
Diversion capacity curve
Sum lower
Low flow loss
Diversion capacity

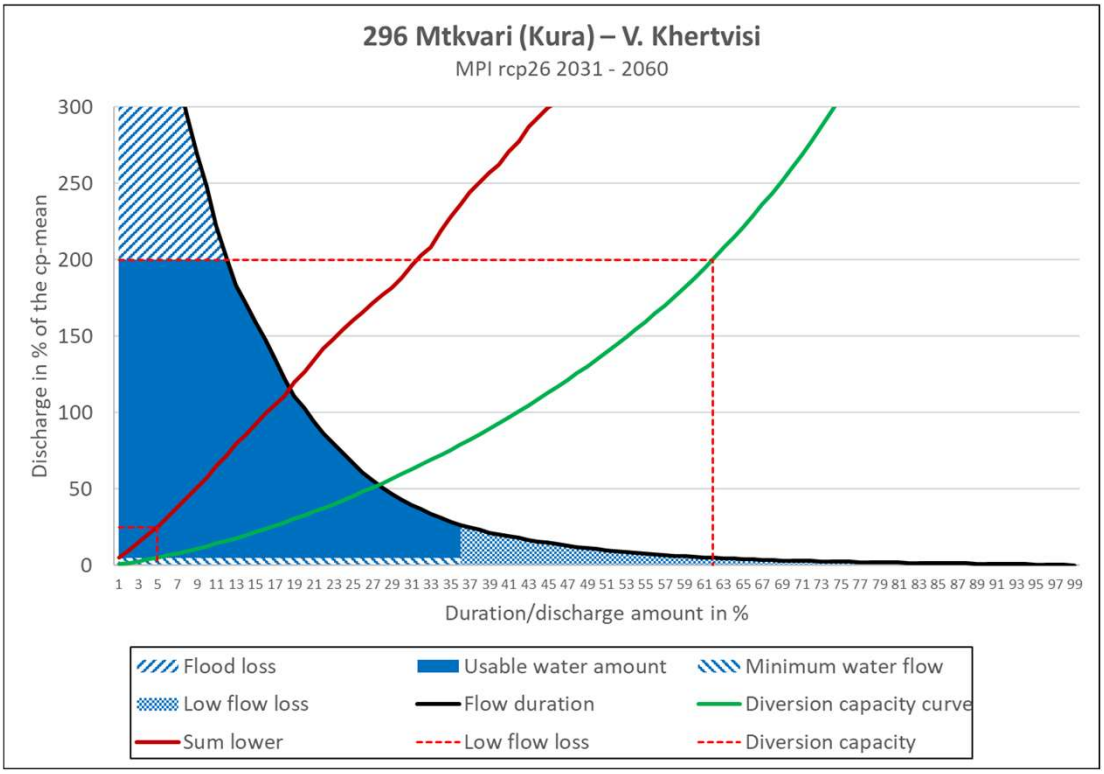
296 Mtkvari (Kura) – V. Khertvisi
MPI rcp26 2031 - 2060
Discharge in % of the cp-mean
300
250
200
150
100
50
0
1 3 5 7 9 11 13 15 17 19 21 23 25 27 29 31 33 35 37 39 41 43 45 47 49 51 53 55 57 59 61 63 65 67 69 71 73 75 77 79 81 83 85 87 89 91 93 95 97 99
Duration/discharge amount in %
Flood loss
Usable water amount
Minimum water flow
Low flow loss
Flow duration
Diversion capacity curve
Sum lower
Low flow loss
Diversion capacity

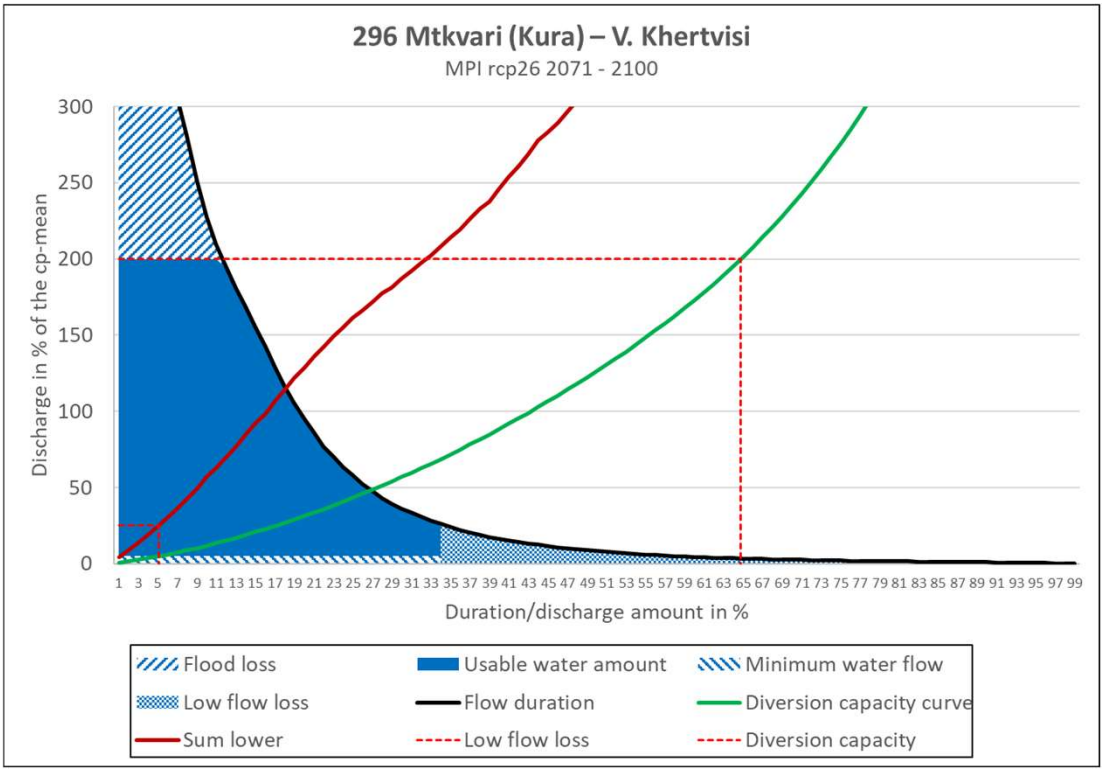
296 Mtkvari (Kura) – V. Khertvisi
MPI rcp26 2071 - 2100
Discharge in % of the cp-mean
300
250
200
150
100
50
0
1 3 5 7 9 11 13 15 17 19 21 23 25 27 29 31 33 35 37 39 41 43 45 47 49 51 53 55 57 59 61 63 65 67 69 71 73 75 77 79 81 83 85 87 89 91 93 95 97 99
Duration/discharge amount in %
Flood loss
Usable water amount
Minimum water flow
Low flow loss
Flow duration
Diversion capacity curve
Sum lower
Low flow loss
Diversion capacity

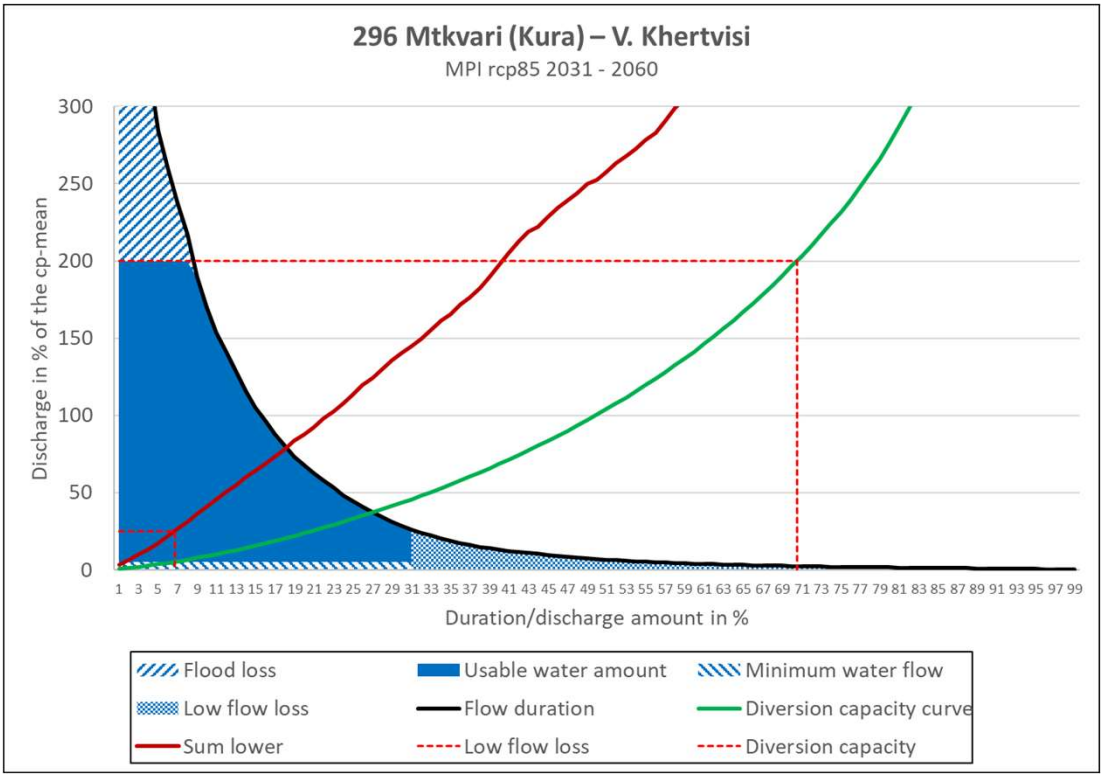
296 Mtkvari (Kura) – V. Khertvisi
MPI rcp85 2031 - 2060
Discharge in % of the cp-mean
300
250
200
150
100
50
0
1 3 5 7 9 11 13 15 17 19 21 23 25 27 29 31 33 35 37 39 41 43 45 47 49 51 53 55 57 59 61 63 65 67 69 71 73 75 77 79 81 83 85 87 89 91 93 95 97 99
Duration/discharge amount in %
Flood loss
Usable water amount
Minimum water flow
Low flow loss
Flow duration
Diversion capacity curve
Sum lower
Low flow loss
Diversion capacity

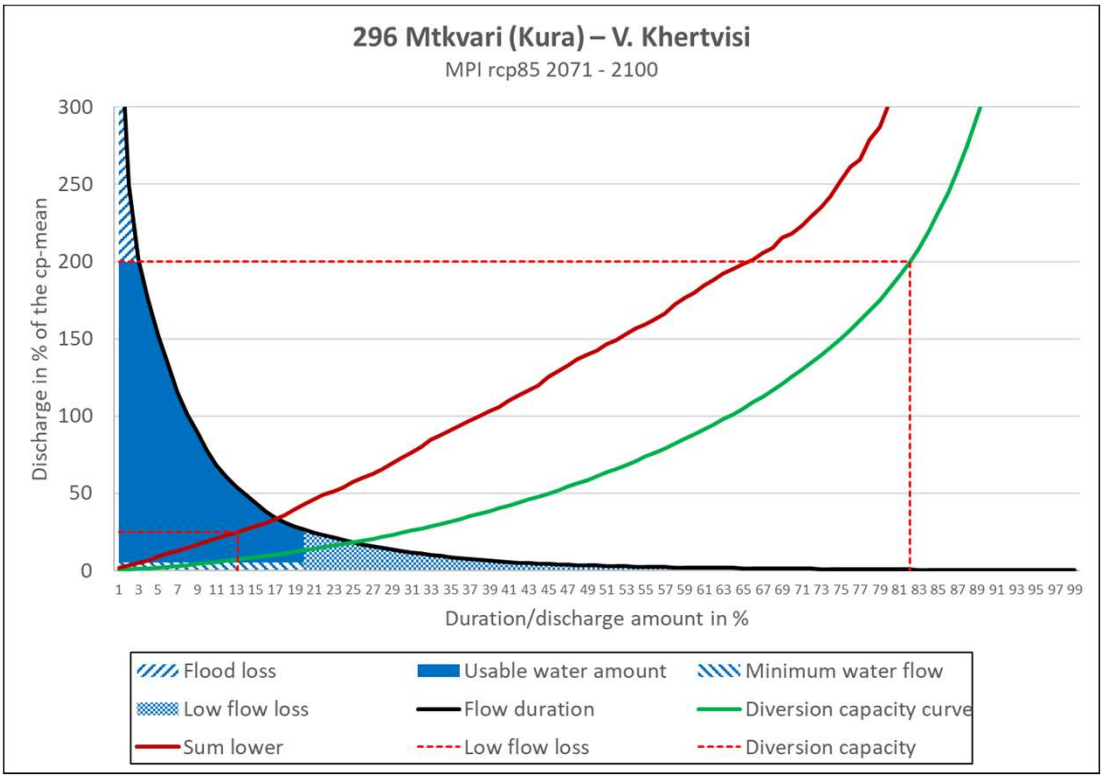
296 Mtkvari (Kura) – V. Khertvisi
MPI rcp85 2071 - 2100
Discharge in % of the cp-mean
300
250
200
150
100
50
0
1 3 5 7 9 11 13 15 17 19 21 23 25 27 29 31 33 35 37 39 41 43 45 47 49 51 53 55 57 59 61 63 65 67 69 71 73 75 77 79 81 83 85 87 89 91 93 95 97 99
Duration/discharge amount in %
Flood loss
Usable water amount
Minimum water flow
Low flow loss
Flow duration
Diversion capacity curve
Sum lower
Low flow loss
Diversion capacity

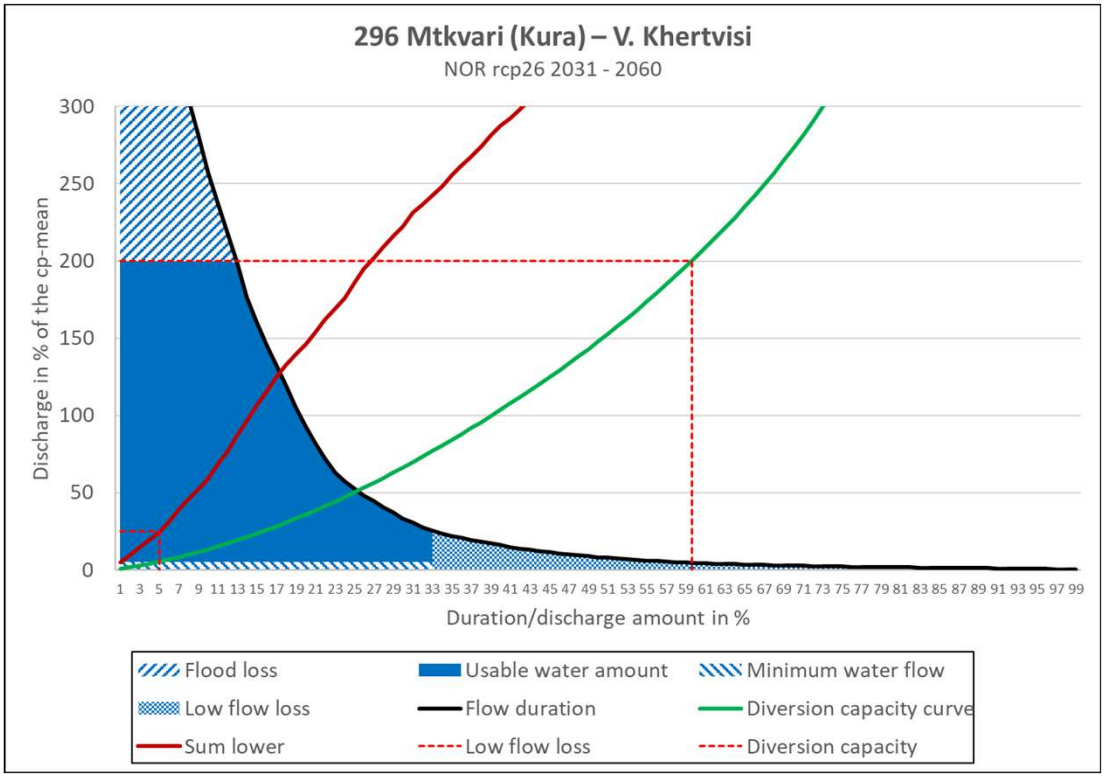
296 Mtkvari (Kura) – V. Khertvisi
NOR rcp26 2031 - 2060
Discharge in % of the cp-mean
300
250
200
150
100
50
0
1 3 5 7 9 11 13 15 17 19 21 23 25 27 29 31 33 35 37 39 41 43 45 47 49 51 53 55 57 59 61 63 65 67 69 71 73 75 77 79 81 83 85 87 89 91 93 95 97 99
Duration/discharge amount in %
Flood loss
Usable water amount
Minimum water flow
Low flow loss
Flow duration
Diversion capacity curve
Sum lower
Low flow loss
Diversion capacity

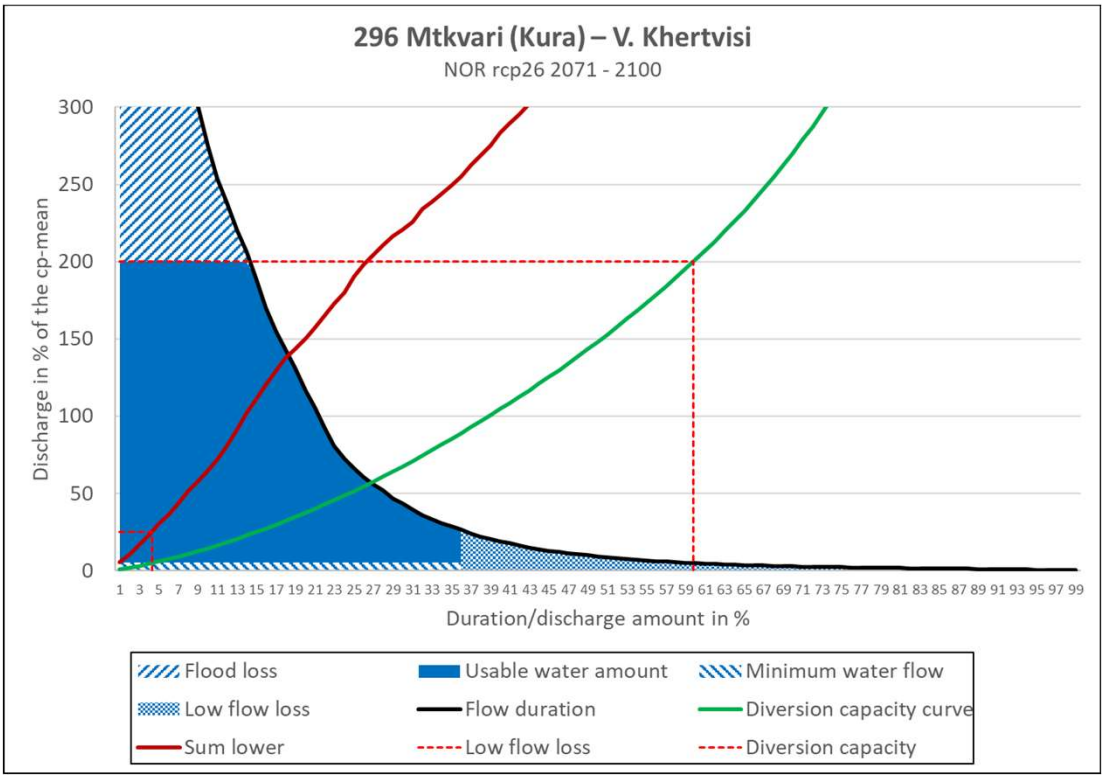
296 Mtkvari (Kura) – V. Khertvisi
NOR rcp26 2071 - 2100
Discharge in % of the cp-mean
300
250
200
150
100
50
0
1 3 5 7 9 11 13 15 17 19 21 23 25 27 29 31 33 35 37 39 41 43 45 47 49 51 53 55 57 59 61 63 65 67 69 71 73 75 77 79 81 83 85 87 89 91 93 95 97 99
Duration/discharge amount in %
Flood loss
Usable water amount
Minimum water flow
Low flow loss
Flow duration
Diversion capacity curve
Sum lower
Low flow loss
Diversion capacity

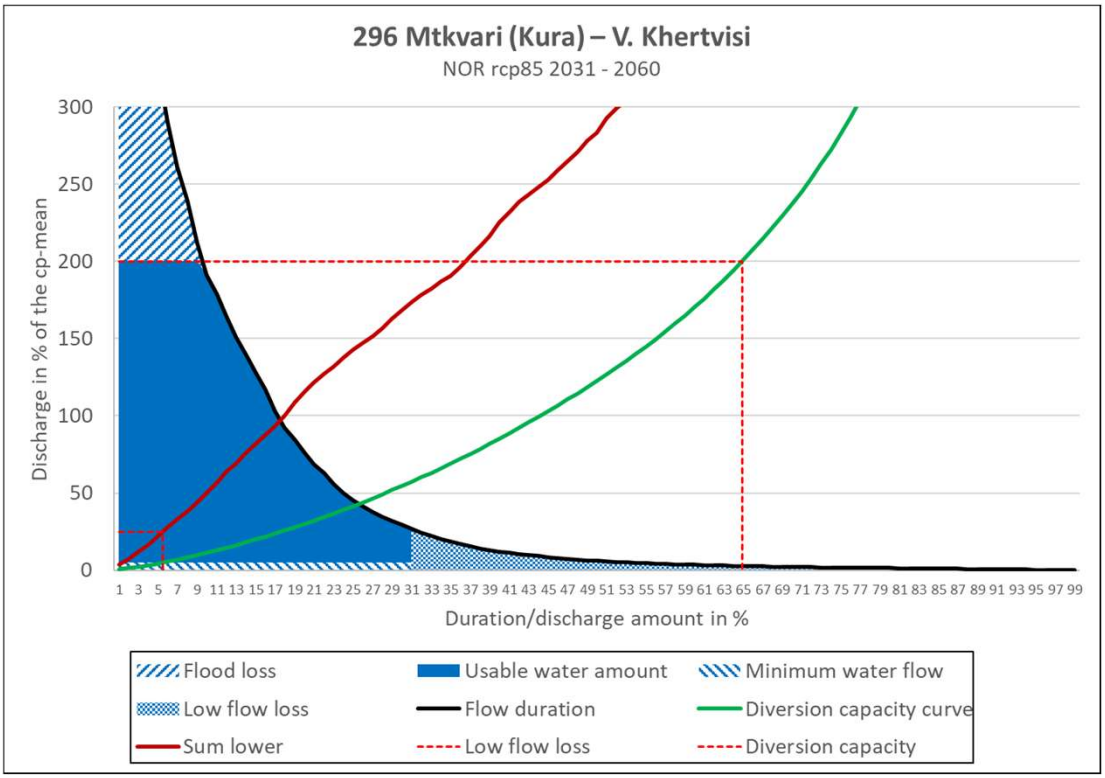
296 Mtkvari (Kura) – V. Khertvisi
NOR rcp85 2031 - 2060
Discharge in % of the cp-mean
300
250
200
150
100
50
0
1 3 5 7 9 11 13 15 17 19 21 23 25 27 29 31 33 35 37 39 41 43 45 47 49 51 53 55 57 59 61 63 65 67 69 71 73 75 77 79 81 83 85 87 89 91 93 95 97 99
Duration/discharge amount in %
Flood loss
Usable water amount
Minimum water flow
Low flow loss
Flow duration
Diversion capacity curve
Sum lower
Low flow loss
Diversion capacity

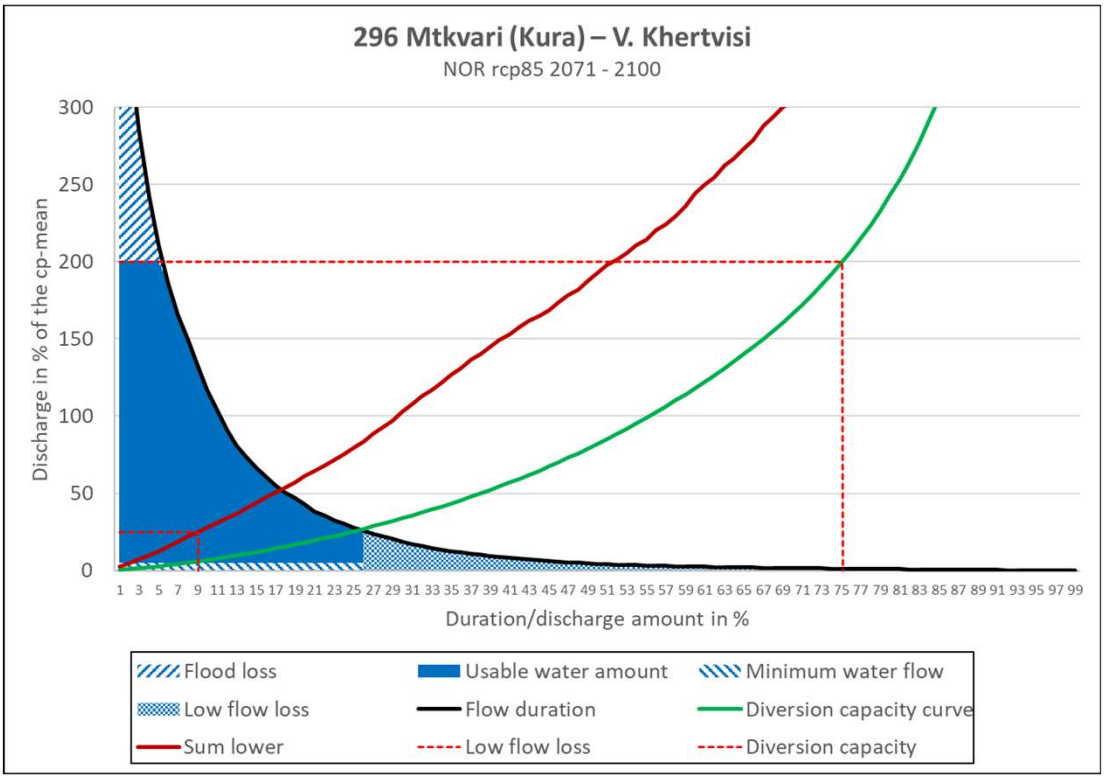
296 Mtkvari (Kura) – V. Khertvisi
NOR rcp85 2071 - 2100
Discharge in % of the cp-mean
300
250
200
150
100
50
0
1 3 5 7 9 11 13 15 17 19 21 23 25 27 29 31 33 35 37 39 41 43 45 47 49 51 53 55 57 59 61 63 65 67 69 71 73 75 77 79 81 83 85 87 89 91 93 95 97 99
Duration/discharge amount in %
Flood loss
Usable water amount
Minimum water flow
Low flow loss
Flow duration
Diversion capacity curve
Sum lower
Low flow loss
Diversion capacity

231 Texuri - V. Naqlaquevi

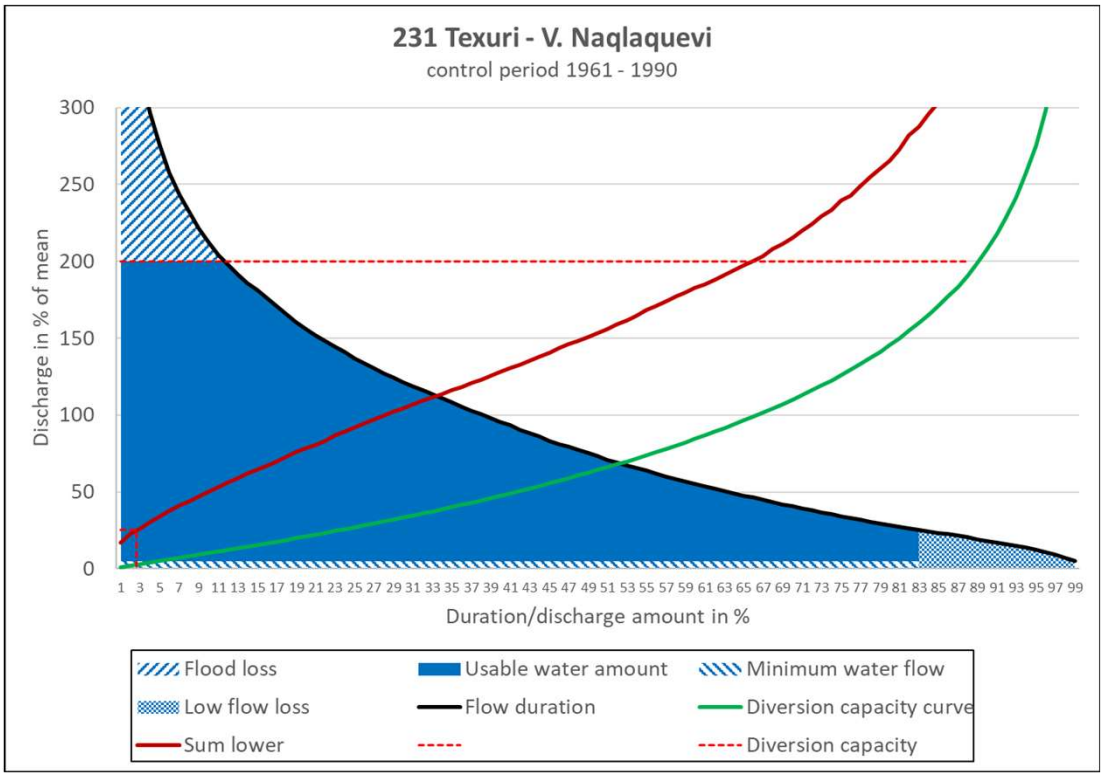

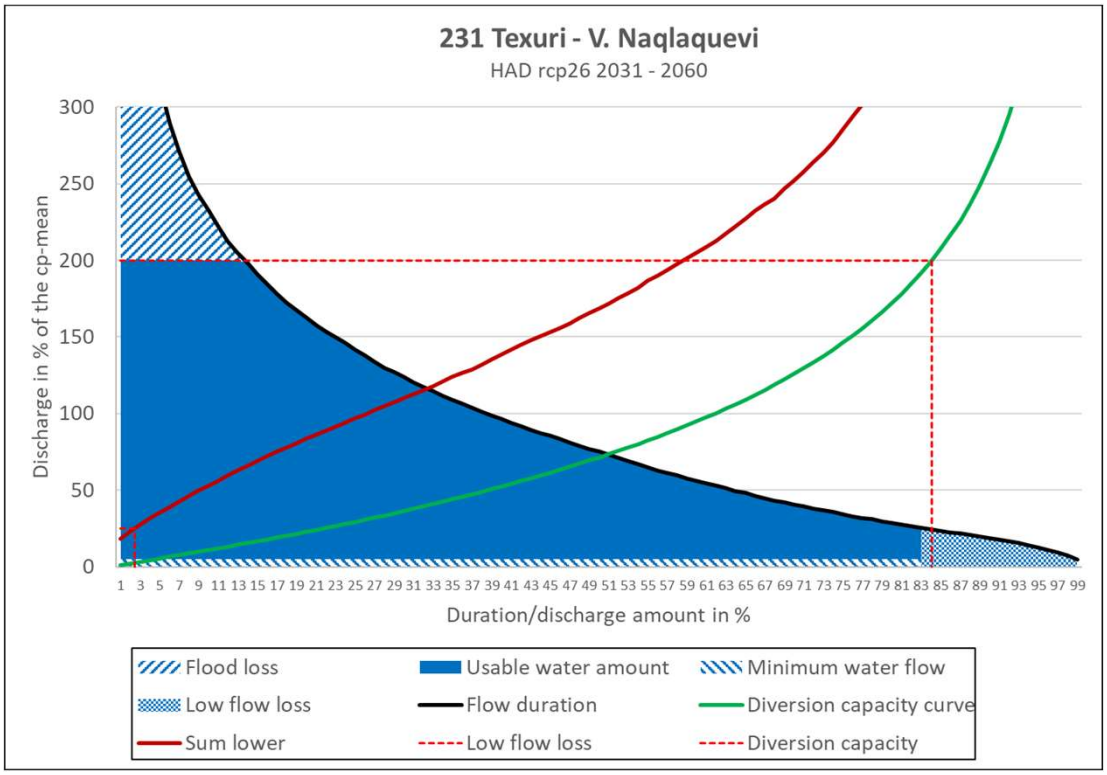
231 Texuri - V. Naqlaquevi
HAD rcp26 2031 - 2060
Discharge in % of the cp-mean
300
250
200
150
100
50
0
1 3 5 7 9 11 13 15 17 19 21 23 25 27 29 31 33 35 37 39 41 43 45 47 49 51 53 55 57 59 61 63 65 67 69 71 73 75 77 79 81 83 85 87 89 91 93 95 97 99
Duration/discharge amount in %
Flood loss
Usable water amount
Minimum water flow
Low flow loss
Flow duration
Diversion capacity curve
Sum lower
Low flow loss
Diversion capacity

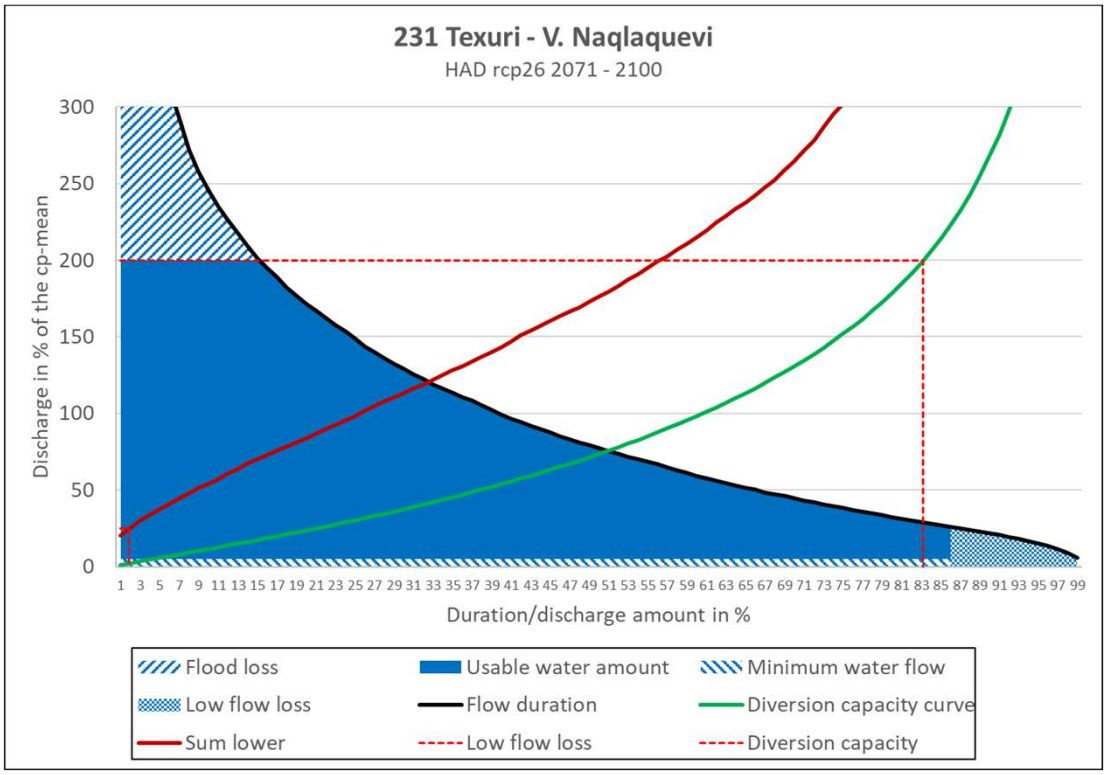
231 Texuri - V. Naqlaquevi
HAD rcp26 2071 - 2100
Discharge in % of the cp-mean
300
250
200
150
100
50
0
1 3 5 7 9 11 13 15 17 19 21 23 25 27 29 31 33 35 37 39 41 43 45 47 49 51 53 55 57 59 61 63 65 67 69 71 73 75 77 79 81 83 85 87 89 91 93 95 97 99
Duration/discharge amount in %
Flood loss
Usable water amount
Minimum water flow
Low flow loss
Flow duration
Diversion capacity curve
Sum lower
Low flow loss
Diversion capacity

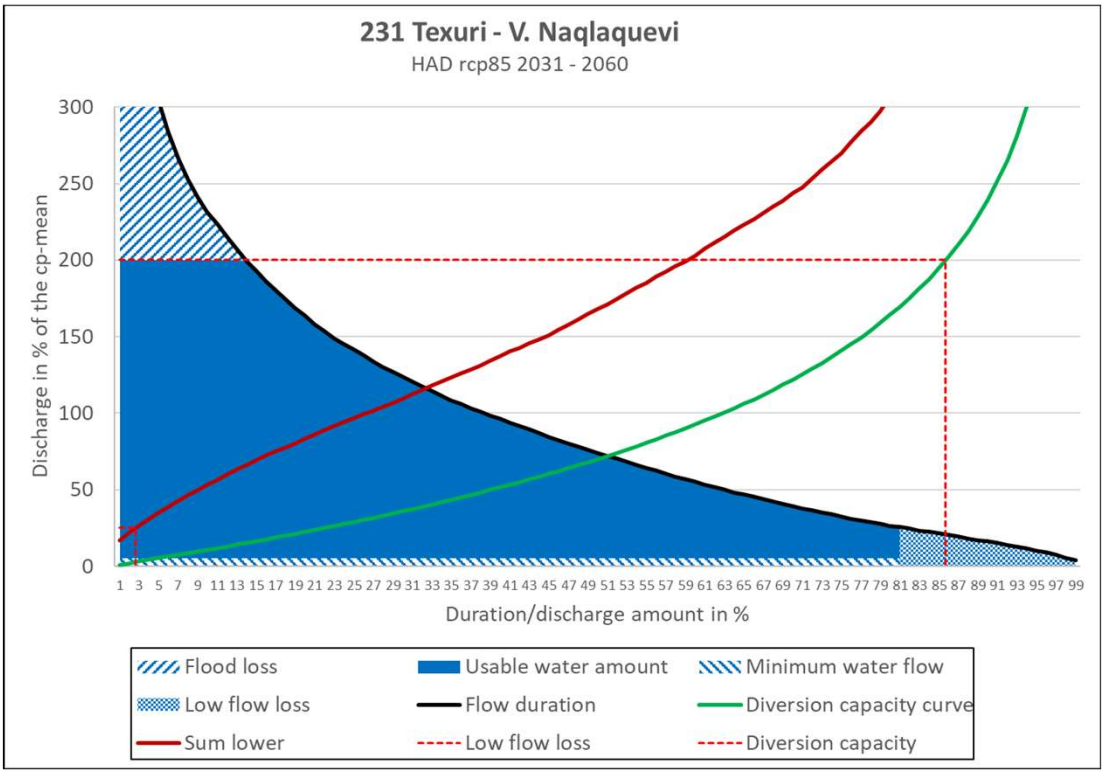
231 Texuri - V. Naqlaquevi
HAD rcp85 2031 - 2060
Discharge in % of the cp-mean
300
250
200
150
100
50
0
1 3 5 7 9 11 13 15 17 19 21 23 25 27 29 31 33 35 37 39 41 43 45 47 49 51 53 55 57 59 61 63 65 67 69 71 73 75 77 79 81 83 85 87 89 91 93 95 97 99
Duration/discharge amount in %
Flood loss
Usable water amount
Minimum water flow
Low flow loss
Flow duration
Diversion capacity curve
Sum lower
Low flow loss
Diversion capacity

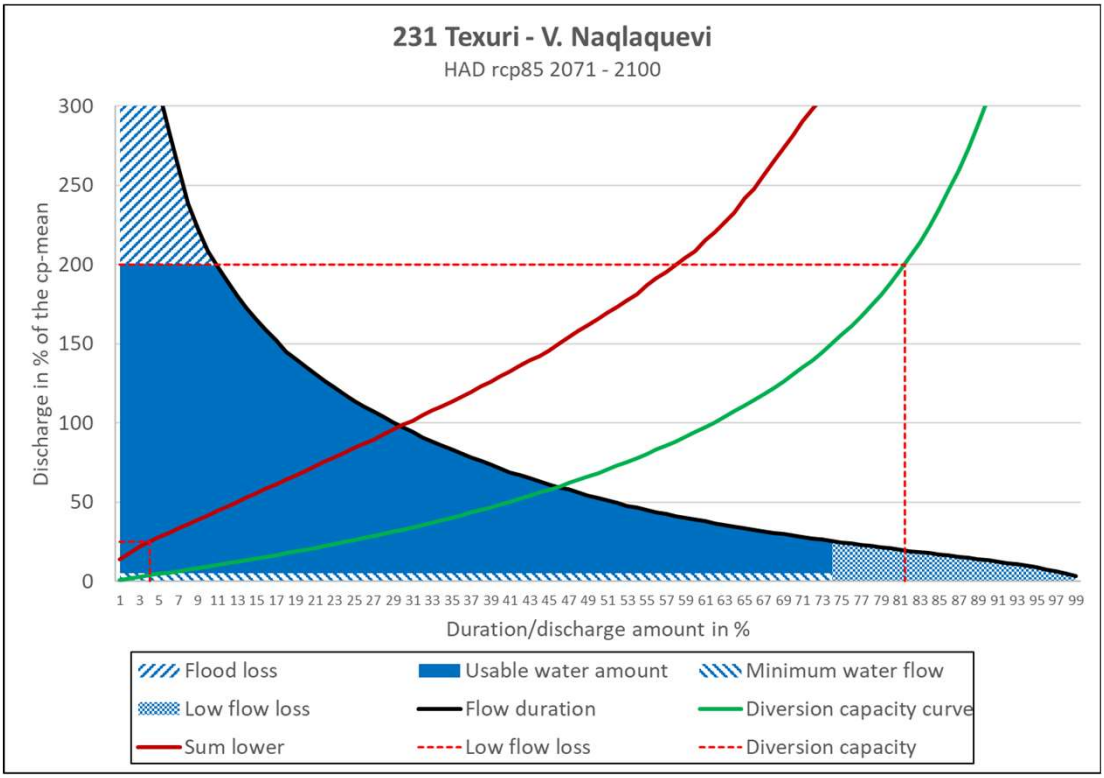
231 Texuri - V. Naqlaquevi
HAD rcp85 2071 - 2100
Discharge in % of the cp-mean
300
250
200
150
100
50
0
1 3 5 7 9 11 13 15 17 19 21 23 25 27 29 31 33 35 37 39 41 43 45 47 49 51 53 55 57 59 61 63 65 67 69 71 73 75 77 79 81 83 85 87 89 91 93 95 97 99
Duration/discharge amount in %
Flood loss
Usable water amount
Minimum water flow
Low flow loss
Flow duration
Diversion capacity curve
Sum lower
Low flow loss
Diversion capacity

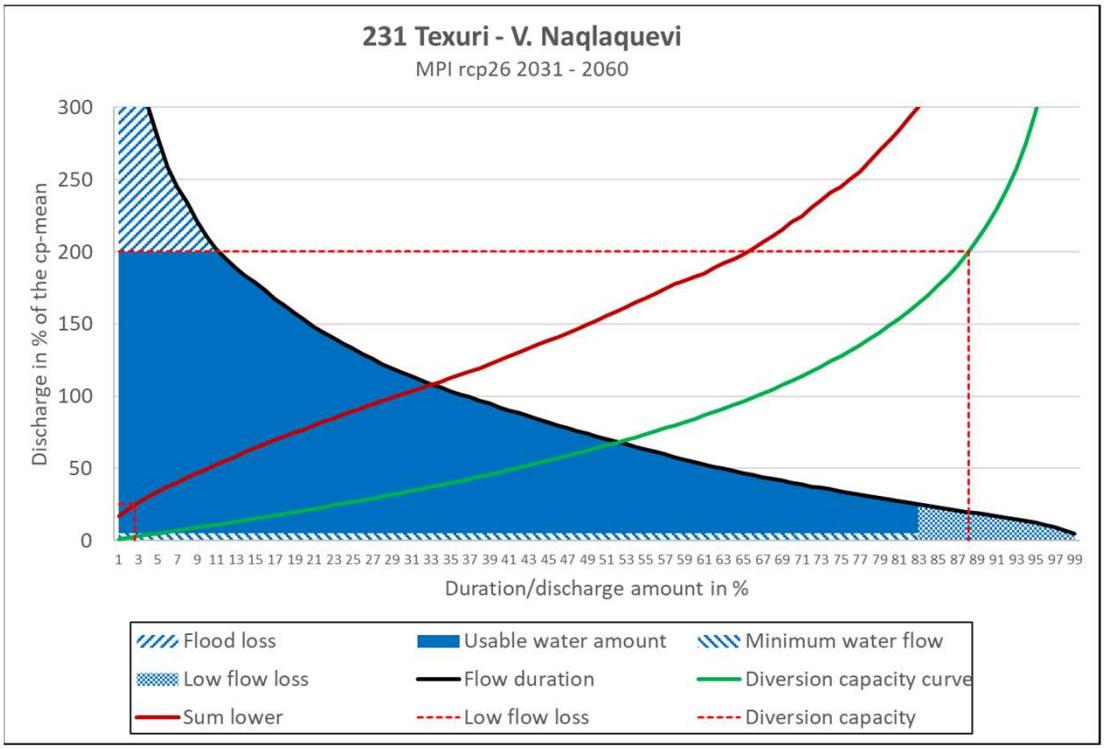
231 Texuri - V. Naqlaquevi
MPI rcp26 2031 - 2060
Discharge in % of the cp-mean
300
250
200
150
100
50
0
1 3 5 7 9 11 13 15 17 19 21 23 25 27 29 31 33 35 37 39 41 43 45 47 49 51 53 55 57 59 61 63 65 67 69 71 73 75 77 79 81 83 85 87 89 91 93 95 97 99
Duration/discharge amount in %
Flood loss
Usable water amount
Minimum water flow
Low flow loss
Flow duration
Diversion capacity curve
Sum lower
Low flow loss
Diversion capacity

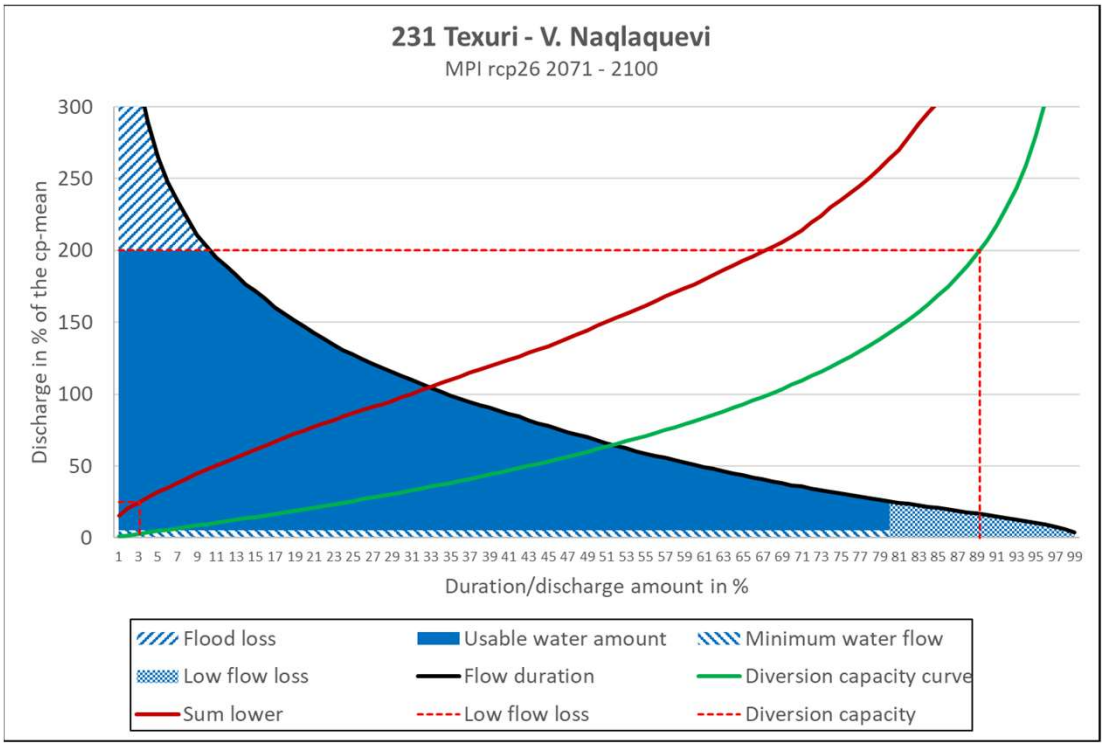
231 Texuri - V. Naqlaquevi
MPI rcp26 2071 - 2100
Discharge in % of the cp-mean
300
250
200
150
100
50
0
1 3 5 7 9 11 13 15 17 19 21 23 25 27 29 31 33 35 37 39 41 43 45 47 49 51 53 55 57 59 61 63 65 67 69 71 73 75 77 79 81 83 85 87 89 91 93 95 97 99
Duration/discharge amount in %
Flood loss
Usable water amount
Minimum water flow
Low flow loss
Flow duration
Diversion capacity curve
Sum lower
Low flow loss
Diversion capacity

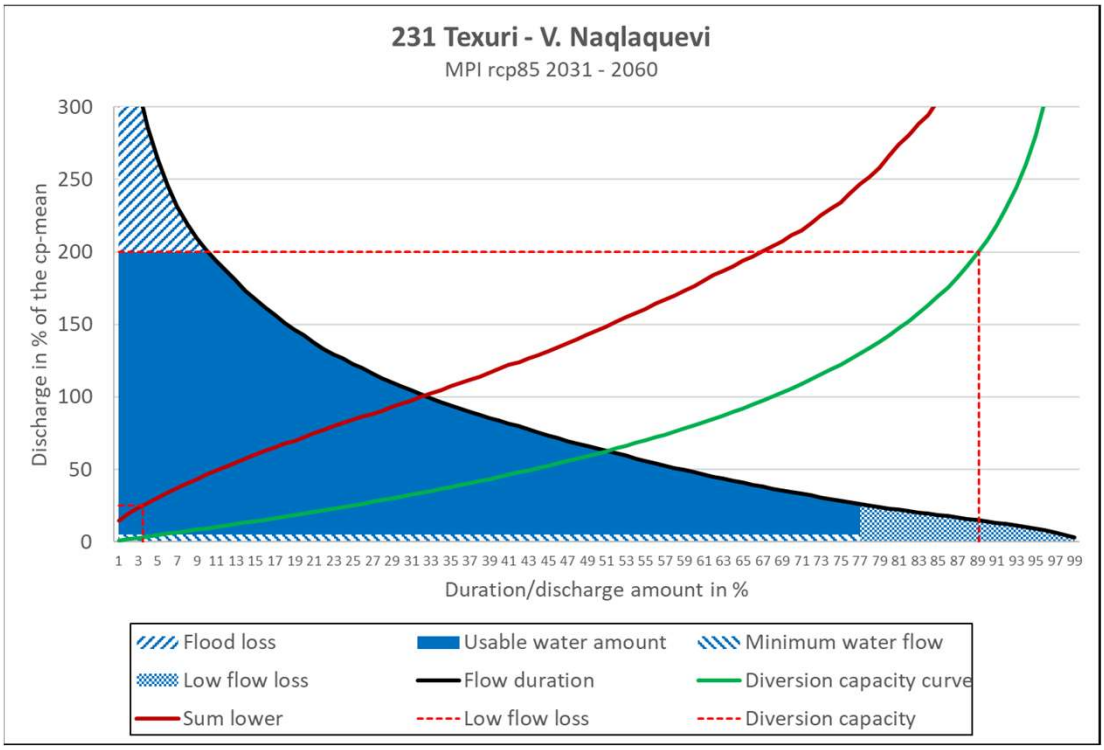
231 Texuri - V. Naqlaquevi
MPI rcp85 2031 - 2060
Discharge in % of the cp-mean
300
250
200
150
100
50
0
1 3 5 7 9 11 13 15 17 19 21 23 25 27 29 31 33 35 37 39 41 43 45 47 49 51 53 55 57 59 61 63 65 67 69 71 73 75 77 79 81 83 85 87 89 91 93 95 97 99
Duration/discharge amount in %
Flood loss
Usable water amount
Minimum water flow
Low flow loss
Flow duration
Diversion capacity curve
Sum lower
Low flow loss
Diversion capacity

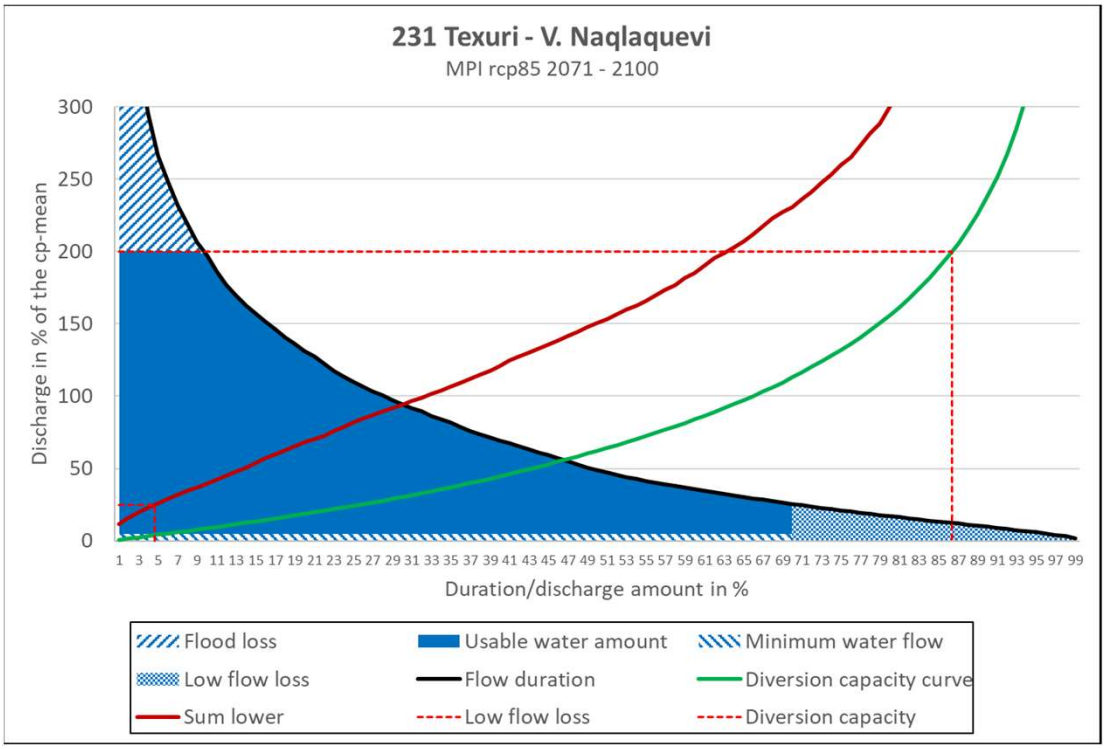
231 Texuri - V. Naqlaquevi
MPI rcp85 2071 - 2100
Discharge in % of the cp-mean
300
250
200
150
100
50
0
1 3 5 7 9 11 13 15 17 19 21 23 25 27 29 31 33 35 37 39 41 43 45 47 49 51 53 55 57 59 61 63 65 67 69 71 73 75 77 79 81 83 85 87 89 91 93 95 97 99
Duration/discharge amount in %
Flood loss
Usable water amount
Minimum water flow
Low flow loss
Flow duration
Diversion capacity curve
Sum lower
Low flow loss
Diversion capacity

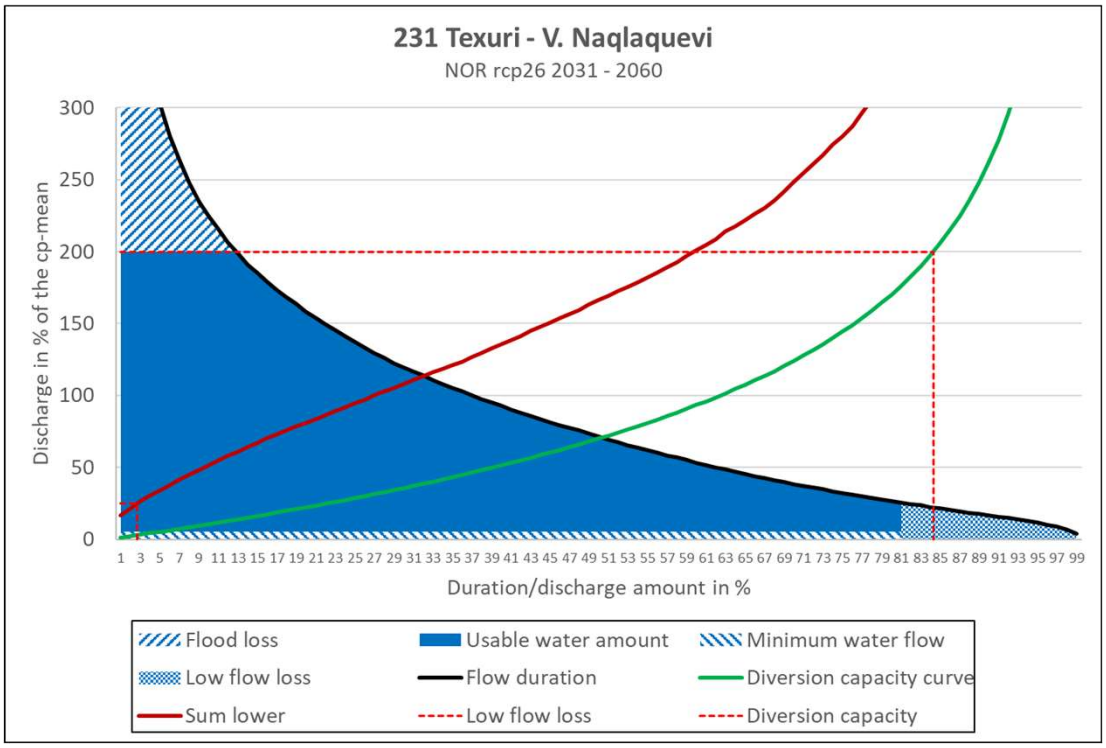
231 Texuri - V. Naqlaquevi
NOR rcp26 2031 - 2060
Discharge in % of the cp-mean
300
250
200
150
100
50
0
1 3 5 7 9 11 13 15 17 19 21 23 25 27 29 31 33 35 37 39 41 43 45 47 49 51 53 55 57 59 61 63 65 67 69 71 73 75 77 79 81 83 85 87 89 91 93 95 97 99
Duration/discharge amount in %
Flood loss
Usable water amount
Minimum water flow
Low flow loss
Flow duration
Diversion capacity curve
Sum lower
Low flow loss
Diversion capacity

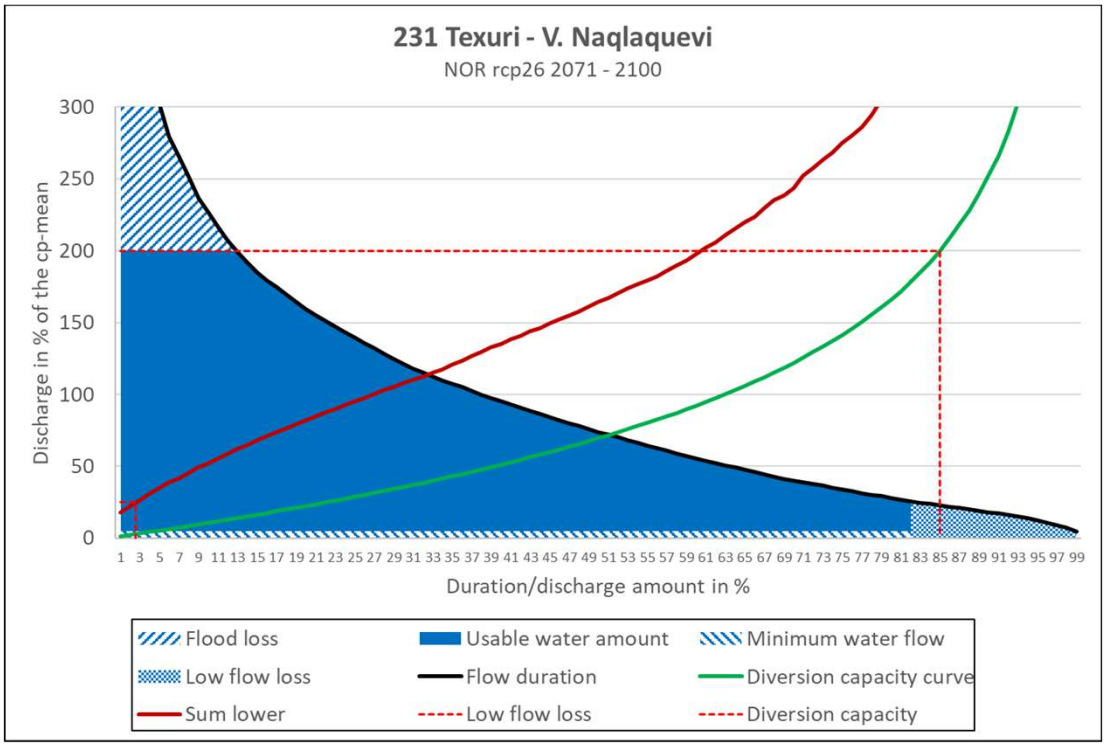
231 Texuri - V. Naqlaquevi
NOR rcp26 2071 - 2100
Discharge in % of the cp-mean
300
250
200
150
100
50
0
1 3 5 7 9 11 13 15 17 19 21 23 25 27 29 31 33 35 37 39 41 43 45 47 49 51 53 55 57 59 61 63 65 67 69 71 73 75 77 79 81 83 85 87 89 91 93 95 97 99
Duration/discharge amount in %
Flood loss
Usable water amount
Minimum water flow
Low flow loss
Flow duration
Diversion capacity curve
Sum lower
Low flow loss
Diversion capacity

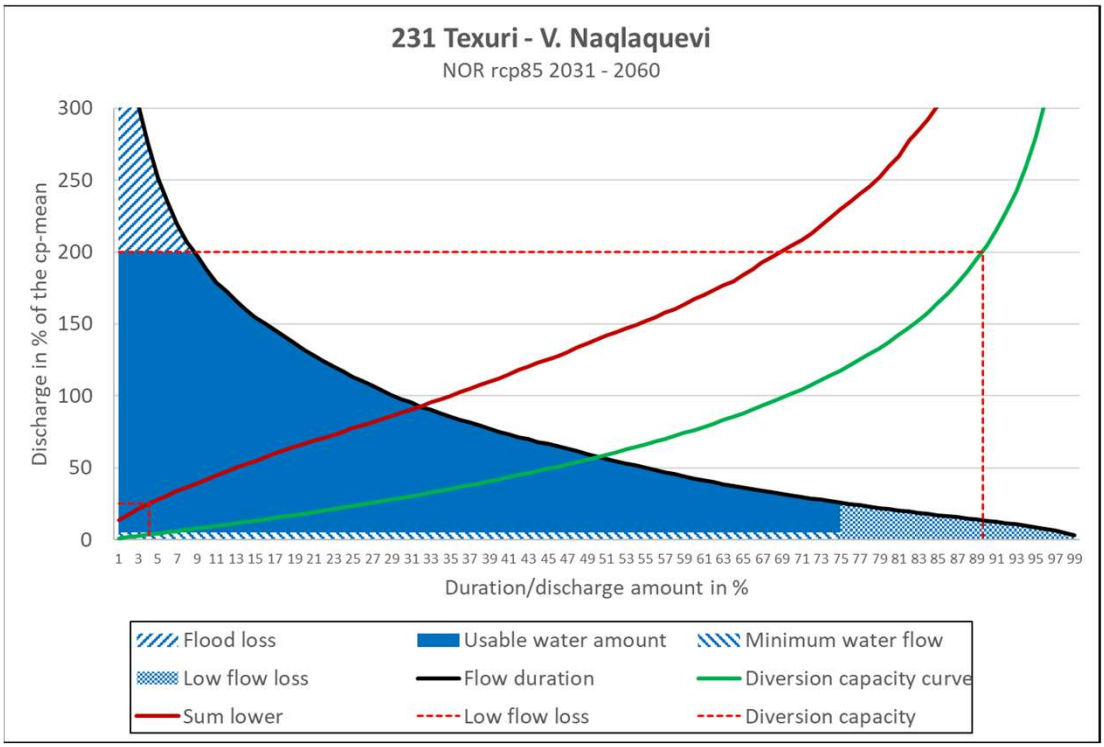
231 Texuri - V. Naqlaquevi
NOR rcp85 2031 - 2060
Discharge in % of the cp-mean
300
250
200
150
100
50
0
1 3 5 7 9 11 13 15 17 19 21 23 25 27 29 31 33 35 37 39 41 43 45 47 49 51 53 55 57 59 61 63 65 67 69 71 73 75 77 79 81 83 85 87 89 91 93 95 97 99
Duration/discharge amount in %
Flood loss
Usable water amount
Minimum water flow
Low flow loss
Flow duration
Diversion capacity curve
Sum lower
Low flow loss
Diversion capacity

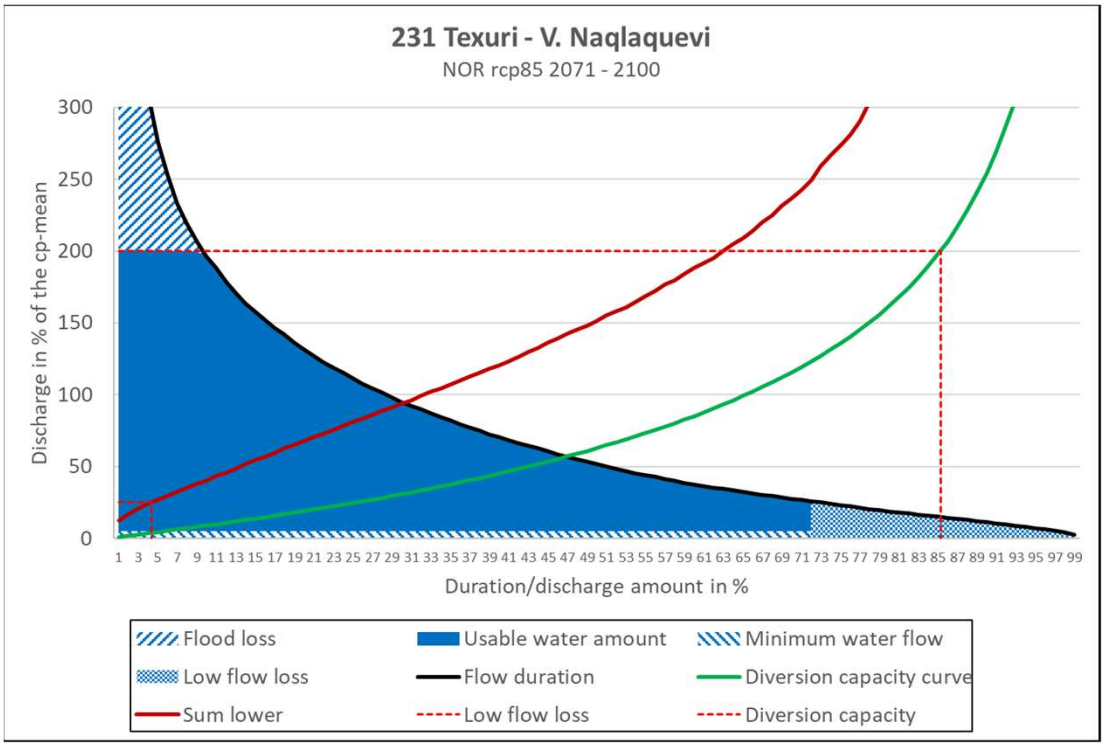
231 Texuri - V. Naqlaquevi
NOR rcp85 2071 - 2100
Discharge in % of the cp-mean
300
250
200
150
100
50
0
1 3 5 7 9 11 13 15 17 19 21 23 25 27 29 31 33 35 37 39 41 43 45 47 49 51 53 55 57 59 61 63 65 67 69 71 73 75 77 79 81 83 85 87 89 91 93 95 97 99
Duration/discharge amount in %
Flood loss
Usable water amount
Minimum water flow
Low flow loss
Flow duration
Diversion capacity curve
Sum lower
Low flow loss
Diversion capacity

441 Alazani - V. Heretiskari

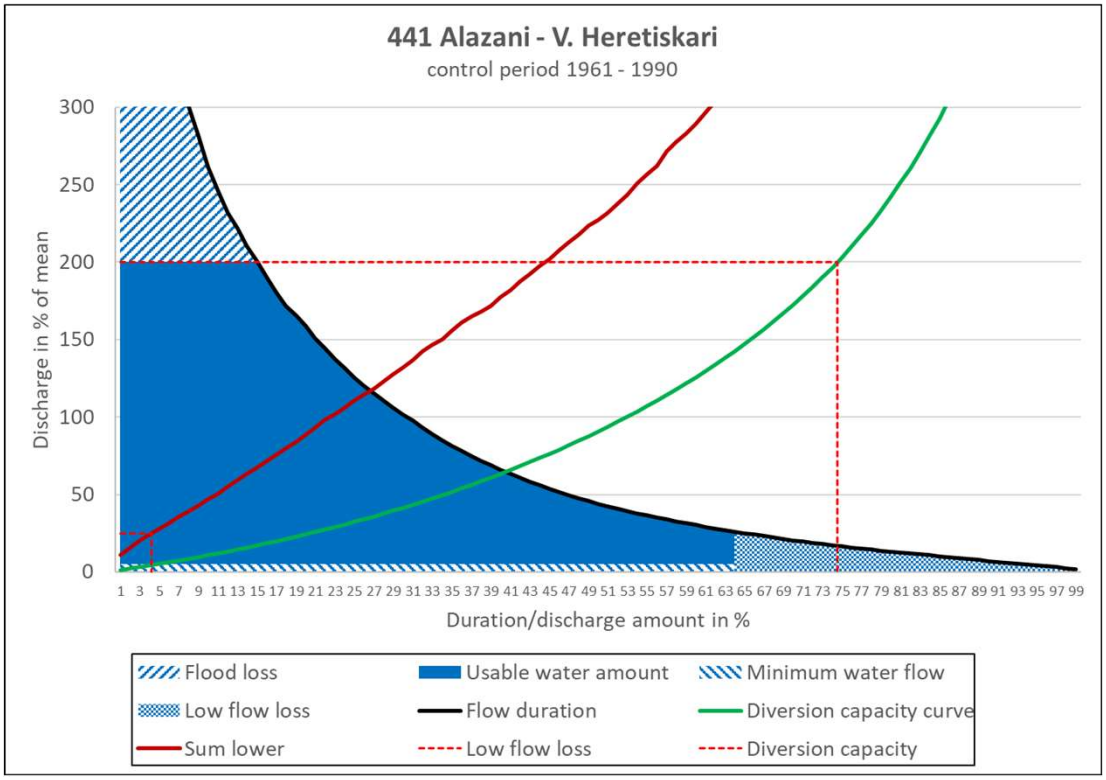

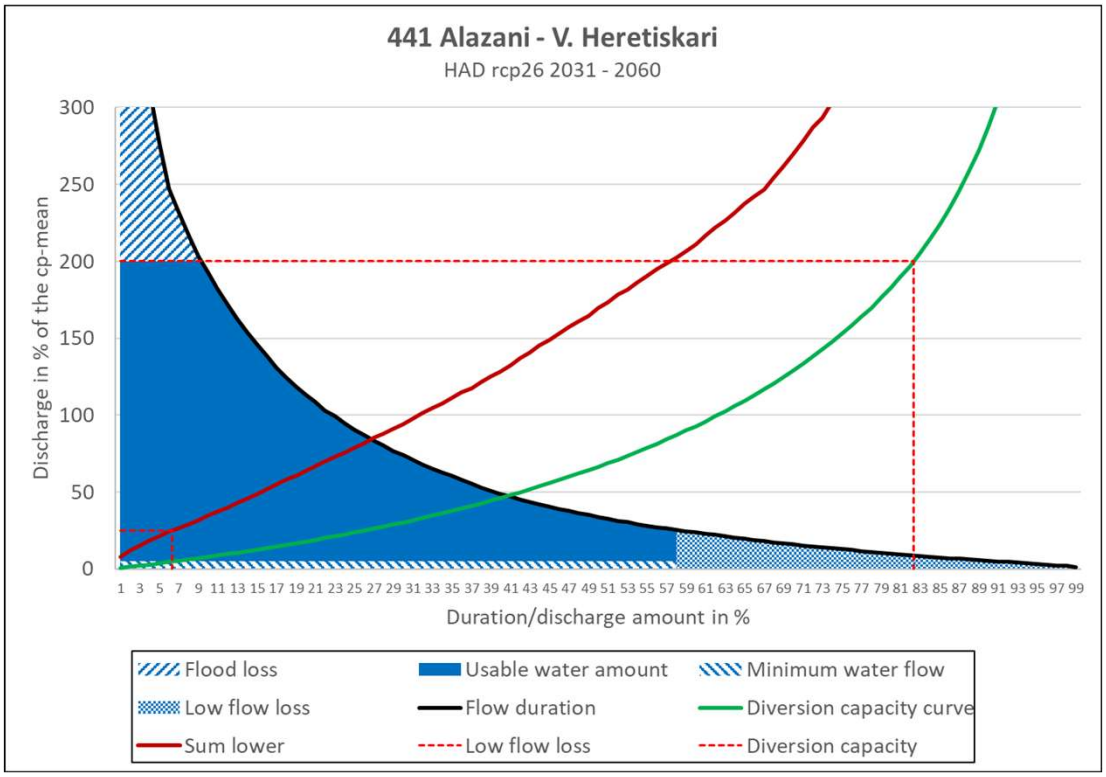
441 Alazani - V. Heretiskari
HAD rcp26 2031 - 2060
Discharge in % of the cp-mean
300
250
200
150
100
50
0
1 3 5 7 9 11 13 15 17 19 21 23 25 27 29 31 33 35 37 39 41 43 45 47 49 51 53 55 57 59 61 63 65 67 69 71 73 75 77 79 81 83 85 87 89 91 93 95 97 99
Duration/discharge amount in %
Flood loss
Usable water amount
Minimum water flow
Low flow loss
Flow duration
Diversion capacity curve
Sum lower
Low flow loss
Diversion capacity

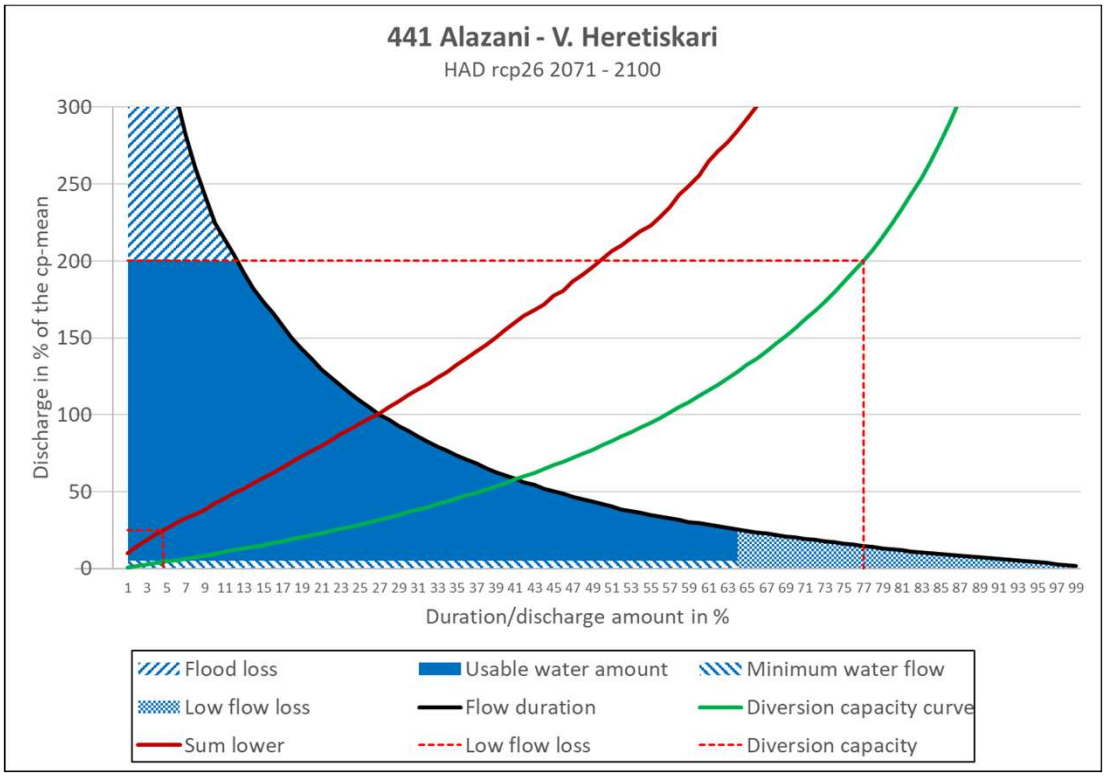
441 Alazani - V. Heretiskari
HAD rcp26 2071 - 2100
Discharge in % of the cp-mean
300
250
200
150
100
50
0
1 3 5 7 9 11 13 15 17 19 21 23 25 27 29 31 33 35 37 39 41 43 45 47 49 51 53 55 57 59 61 63 65 67 69 71 73 75 77 79 81 83 85 87 89 91 93 95 97 99
Duration/discharge amount in %
Flood loss
Usable water amount
Minimum water flow
Low flow loss
Flow duration
Diversion capacity curve
Sum lower
Low flow loss
Diversion capacity

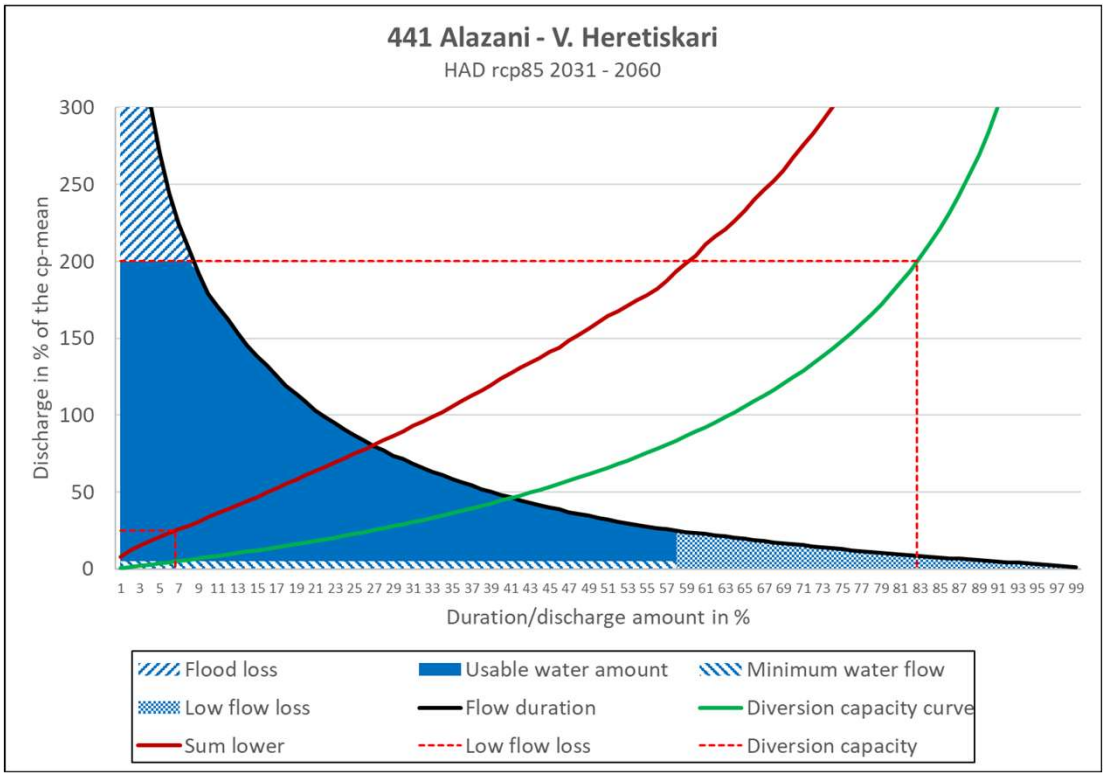
441 Alazani - V. Heretiskari
HAD rcp85 2031 - 2060
Discharge in % of the cp-mean
300
250
200
150
100
50
0
1 3 5 7 9 11 13 15 17 19 21 23 25 27 29 31 33 35 37 39 41 43 45 47 49 51 53 55 57 59 61 63 65 67 69 71 73 75 77 79 81 83 85 87 89 91 93 95 97 99
Duration/discharge amount in %
Flood loss
Usable water amount
Minimum water flow
Low flow loss
Flow duration
Diversion capacity curve
Sum lower
Low flow loss
Diversion capacity

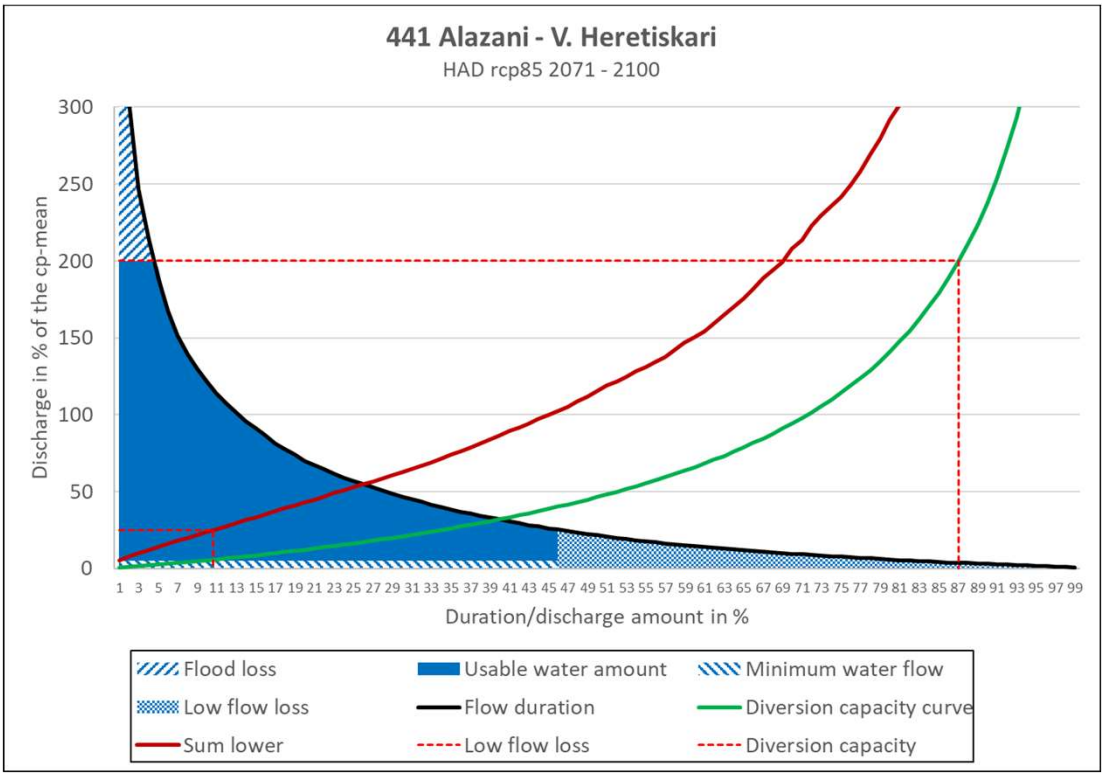
441 Alazani - V. Heretiskari
HAD rcp85 2071 - 2100
Discharge in % of the cp-mean
300
250
200
150
100
50
0
1 3 5 7 9 11 13 15 17 19 21 23 25 27 29 31 33 35 37 39 41 43 45 47 49 51 53 55 57 59 61 63 65 67 69 71 73 75 77 79 81 83 85 87 89 91 93 95 97 99
Duration/discharge amount in %
Flood loss
Usable water amount
Minimum water flow
Low flow loss
Flow duration
Diversion capacity curve
Sum lower
Low flow loss
Diversion capacity

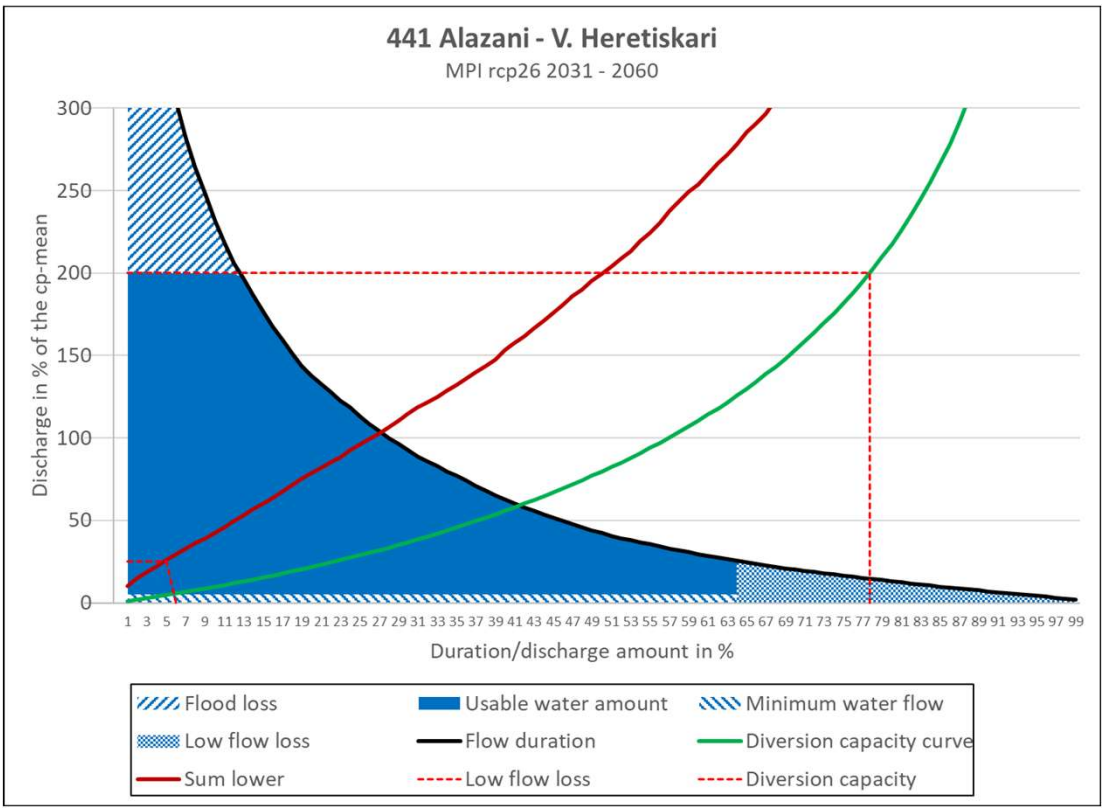
441 Alazani - V. Heretiskari
MPI rcp26 2031 - 2060
Discharge in % of the cp-mean
300
250
200
150
100
50
0
1 3 5 7 9 11 13 15 17 19 21 23 25 27 29 31 33 35 37 39 41 43 45 47 49 51 53 55 57 59 61 63 65 67 69 71 73 75 77 79 81 83 85 87 89 91 93 95 97 99
Duration/discharge amount in %
Flood loss
Usable water amount
Minimum water flow
Low flow loss
Flow duration
Diversion capacity curve
Sum lower
Low flow loss
Diversion capacity

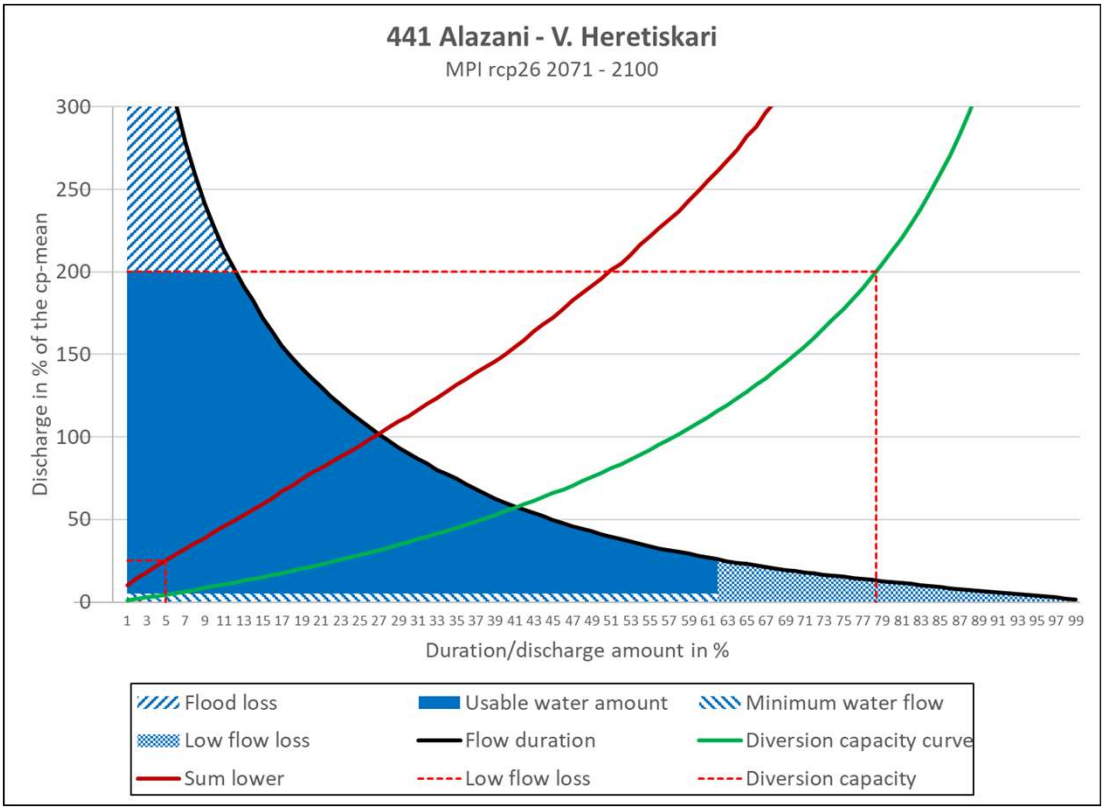
441 Alazani - V. Heretiskari
MPI rcp26 2071 - 2100
Discharge in % of the cp-mean
300
250
200
150
100
50
0
1 3 5 7 9 11 13 15 17 19 21 23 25 27 29 31 33 35 37 39 41 43 45 47 49 51 53 55 57 59 61 63 65 67 69 71 73 75 77 79 81 83 85 87 89 91 93 95 97 99
Duration/discharge amount in %
Flood loss
Usable water amount
Minimum water flow
Low flow loss
Flow duration
Diversion capacity curve
Sum lower
Low flow loss
Diversion capacity

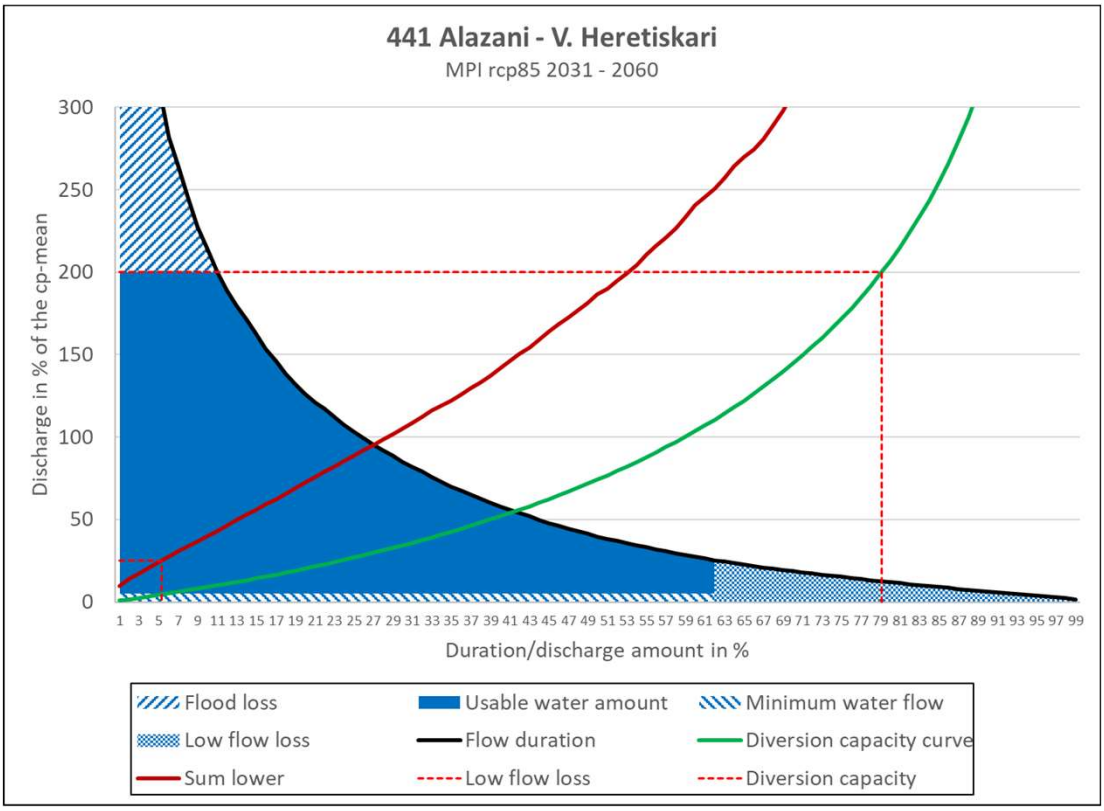
441 Alazani - V. Heretiskari
MPI rcp85 2031 - 2060
Discharge in % of the cp-mean
300
250
200
150
100
50
0
1 3 5 7 9 11 13 15 17 19 21 23 25 27 29 31 33 35 37 39 41 43 45 47 49 51 53 55 57 59 61 63 65 67 69 71 73 75 77 79 81 83 85 87 89 91 93 95 97 99
Duration/discharge amount in %
Flood loss
Usable water amount
Minimum water flow
Low flow loss
Flow duration
Diversion capacity curve
Sum lower
Low flow loss
Diversion capacity

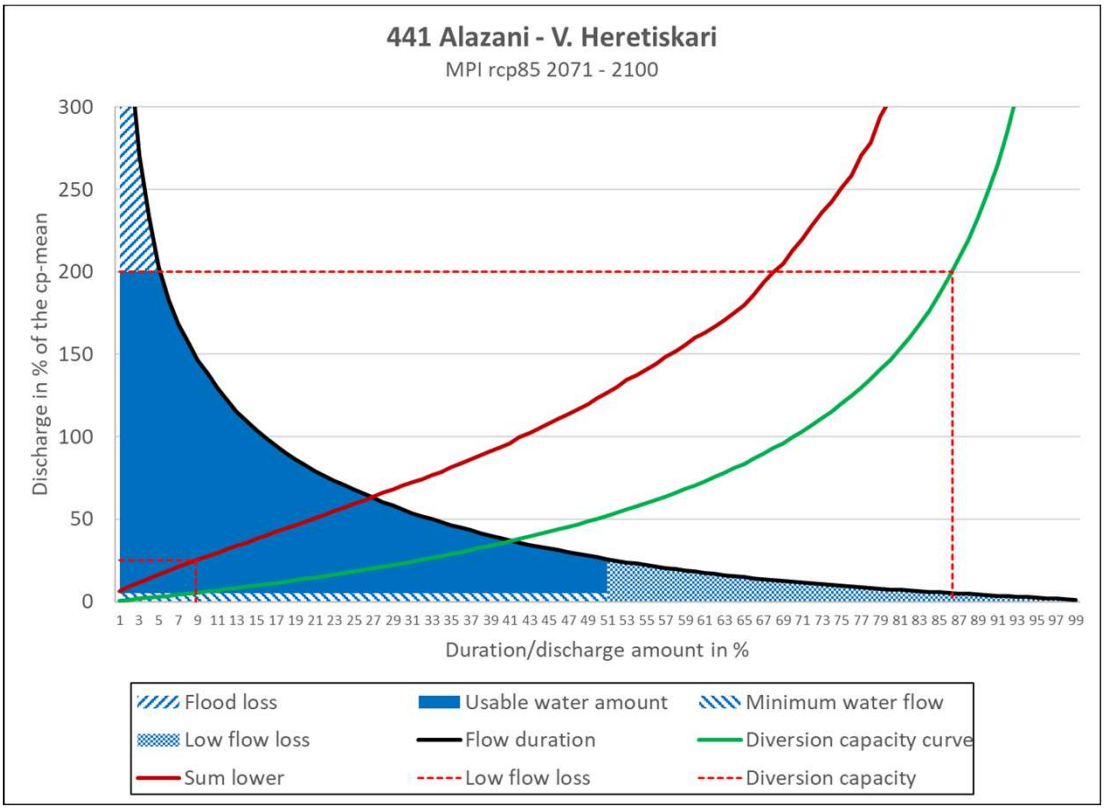
441 Alazani - V. Heretiskari
MPI rcp85 2071 - 2100
Discharge in % of the cp-mean
300
250
200
150
100
50
0
1 3 5 7 9 11 13 15 17 19 21 23 25 27 29 31 33 35 37 39 41 43 45 47 49 51 53 55 57 59 61 63 65 67 69 71 73 75 77 79 81 83 85 87 89 91 93 95 97 99
Duration/discharge amount in %
Flood loss
Usable water amount
Minimum water flow
Low flow loss
Flow duration
Diversion capacity curve
Sum lower
Low flow loss
Diversion capacity

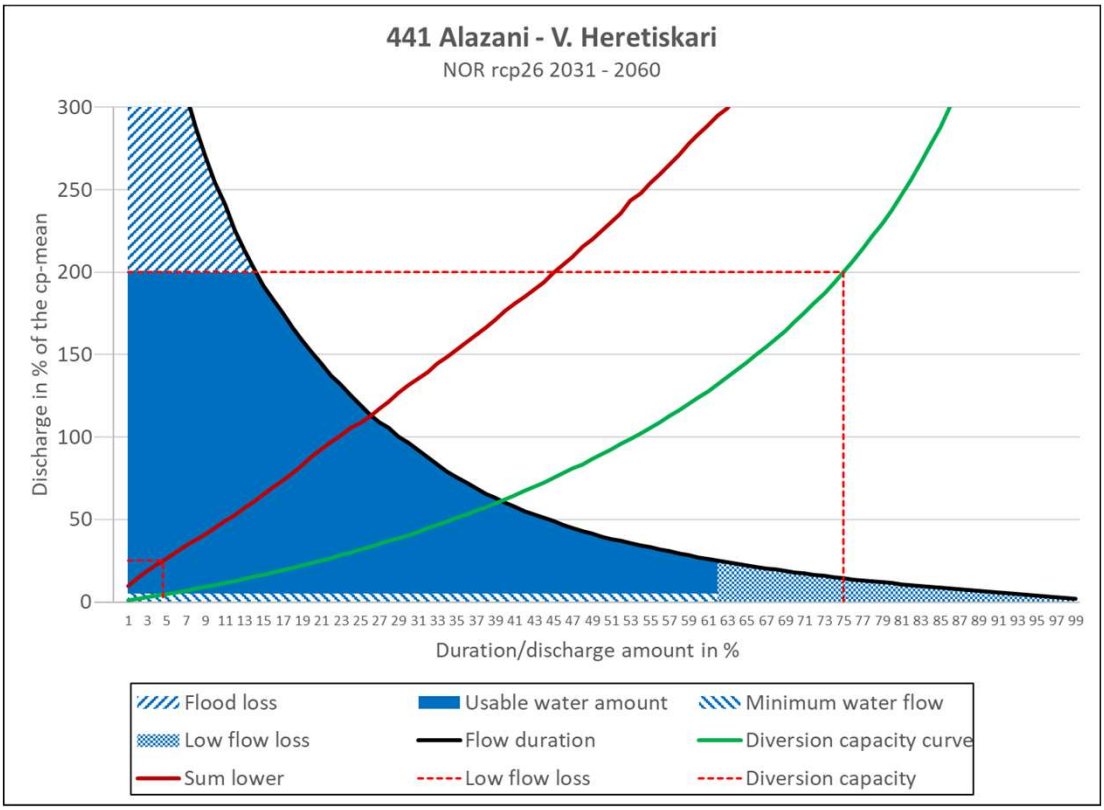
441 Alazani - V. Heretiskari
NOR rcp26 2031 - 2060
Discharge in % of the cp-mean
300
250
200
150
100
50
0
1 3 5 7 9 11 13 15 17 19 21 23 25 27 29 31 33 35 37 39 41 43 45 47 49 51 53 55 57 59 61 63 65 67 69 71 73 75 77 79 81 83 85 87 89 91 93 95 97 99
Duration/discharge amount in %
Flood loss
Usable water amount
Minimum water flow
Low flow loss
Flow duration
Diversion capacity curve
Sum lower
Low flow loss
Diversion capacity

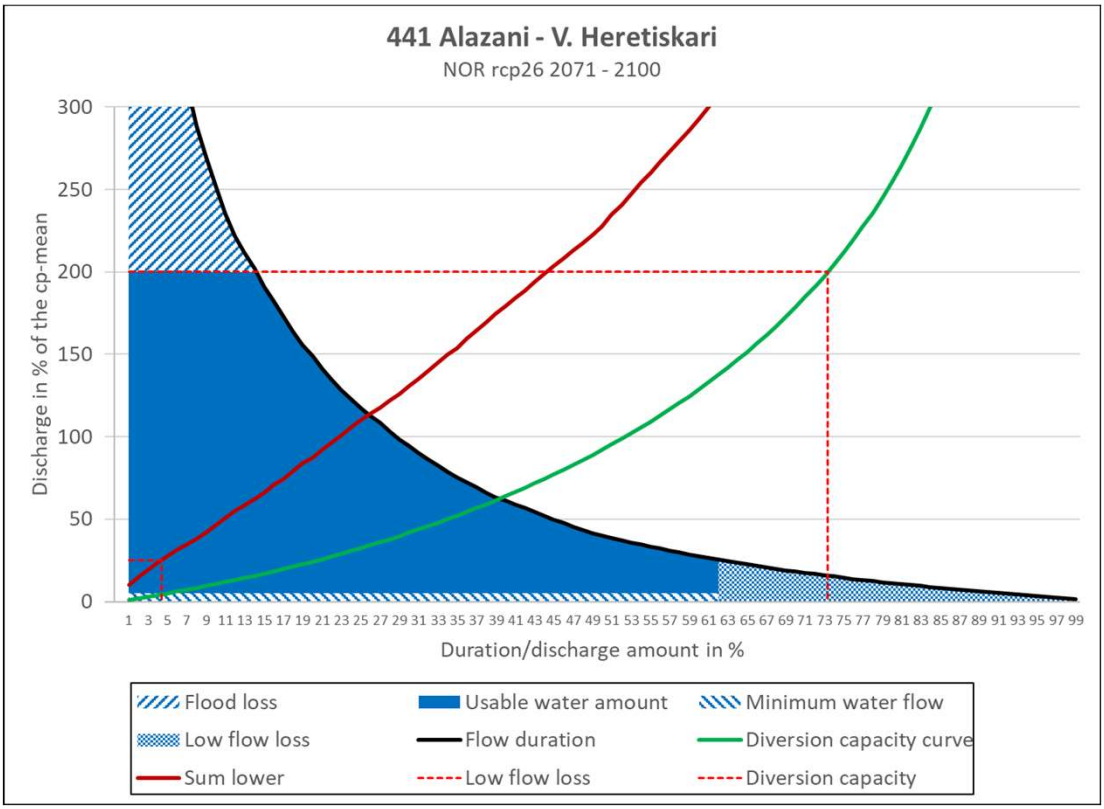
441 Alazani - V. Heretiskari
NOR rcp26 2071 - 2100
Discharge in % of the cp-mean
300
250
200
150
100
50
0
1 3 5 7 9 11 13 15 17 19 21 23 25 27 29 31 33 35 37 39 41 43 45 47 49 51 53 55 57 59 61 63 65 67 69 71 73 75 77 79 81 83 85 87 89 91 93 95 97 99
Duration/discharge amount in %
Flood loss
Usable water amount
Minimum water flow
Low flow loss
Flow duration
Diversion capacity curve
Sum lower
Low flow loss
Diversion capacity

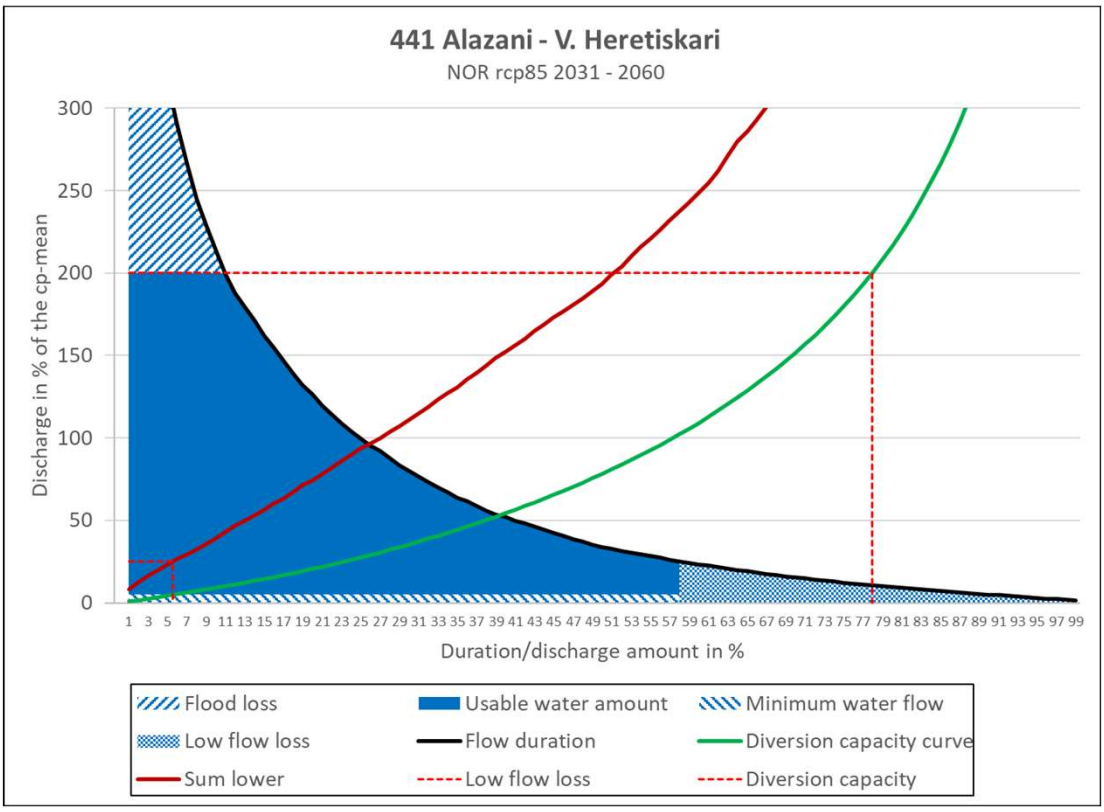
441 Alazani - V. Heretiskari
NOR rcp85 2031 - 2060
Discharge in % of the cp-mean
300
250
200
150
100
50
0
1 3 5 7 9 11 13 15 17 19 21 23 25 27 29 31 33 35 37 39 41 43 45 47 49 51 53 55 57 59 61 63 65 67 69 71 73 75 77 79 81 83 85 87 89 91 93 95 97 99
Duration/discharge amount in %
Flood loss
Usable water amount
Minimum water flow
Low flow loss
Flow duration
Diversion capacity curve
Sum lower
Low flow loss
Diversion capacity

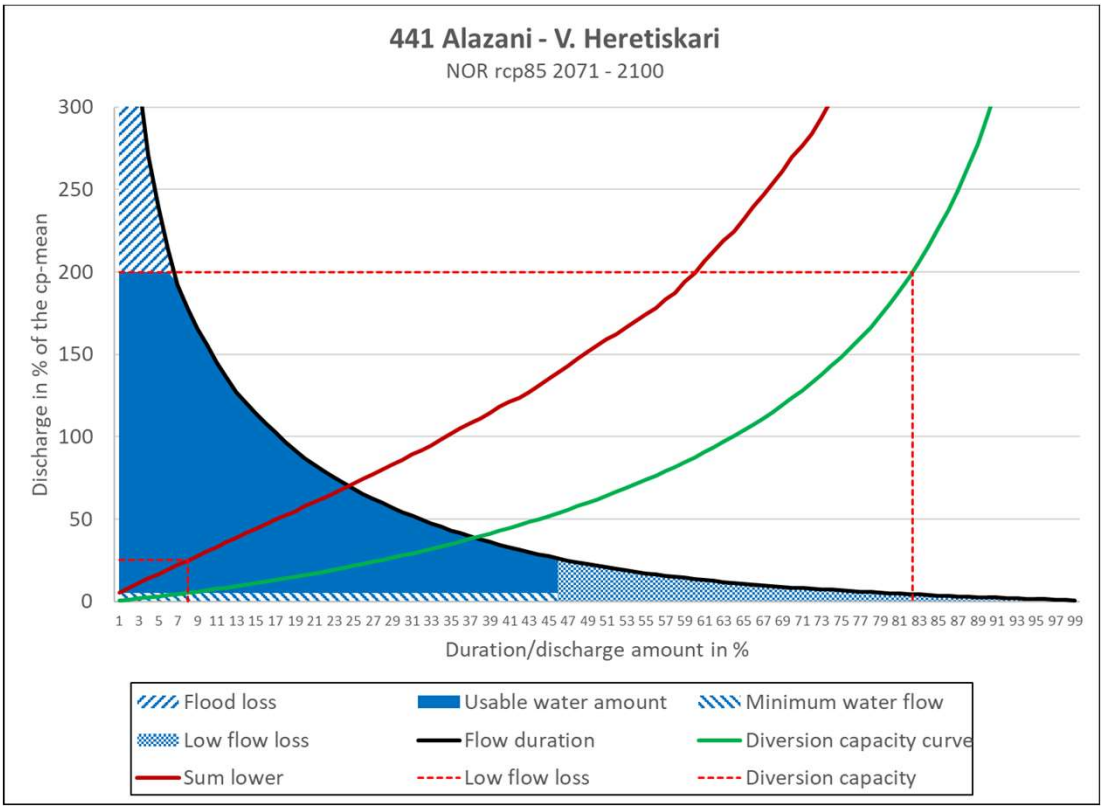
441 Alazani - V. Heretiskari
NOR rcp85 2071 - 2100
Discharge in % of the cp-mean
300
250
200
150
100
50
0
1 3 5 7 9 11 13 15 17 19 21 23 25 27 29 31 33 35 37 39 41 43 45 47 49 51 53 55 57 59 61 63 65 67 69 71 73 75 77 79 81 83 85 87 89 91 93 95 97 99
Duration/discharge amount in %
Flood loss
Usable water amount
Minimum water flow
Low flow loss
Flow duration
Diversion capacity curve
Sum lower
Low flow loss
Diversion capacity

NVE

Norges vassdrags- og energidirektorat

Middelthuns gate 29
Postboks 5091 Majorstuen
0301 Oslo
Telefon: (+47) 22 95 95 95